`Table of Contents

List of Figures

List of Tables

4.0 SOCIO-ECONOMIC. TERRESTRIAL AND PHYSICAL ENVIRONMENT SETTING

4.1 Onshore Environment

4.1.1 Socio-economic Environment

4.1.1.1 Community Physical Infrastructure and Services

In 2006, the Argentia area had approximately 3,500 occupied private dwellings. The majority (approximately 86 percent) of these dwellings was owned and approximately 14 percent were rented (Community Accounts no date). By 2011, the number of occupied private dwellings in the Argentia area had increased to approximately 4,500 (Statistics Canada 2012).

More people have moved into the Argentia area in recent years to take advantage of employment associated with projects such as the nickel processing plant in Long Harbour. There are also two major fabrication companies in the Argentia Industrial Park, employing between 150 to 200 people. As a result of this activity, housing sales have increased and it is becoming difficult to find housing to rent or buy in the Argentia area (Dooley 2011).

In 2007, there were 17 housing starts in Placentia and the surrounding area and in 2008, this number dropped to eight. In 2010, the number of housing starts rose to 19. There were 24 MLS sales in the area in 2007 and the average house price was $68,500. By 2010, the average house price increased to $78,352 and there were 27 MLS sales (C. Janes, pers. comm.). As of January 2012, there were approximately 25 homes for sale in the Argentia area, ranging in price from $40,000 to $399,000 (J. King, pers. comm.).

There are no data on vacancy rates in Placentia and the surrounding area, but there is a shortage of rental units because the majority currently house workers from the Long Harbour nickel processing plant. At the end of 2011, there were approximately 40 rental units in the area and fewer than five of these were vacant (J. King, pers. comm.).

According to the Mayor and Deputy Mayor of the Town of Placentia, residential development is a priority for the Town and there are a number of areas within the Placentia area that could be looked at for future residential development (Placentia Town Council 2011). Two areas in particular, in Dunville and southeastern Placentia, have been identified as possible areas for residential development and the Town of Placentia is looking for companies that may be interested in developing them. These two areas could accommodate up to 100 new homes (W. Hogan, pers. comm.).

A 500-person camp facility has been constructed in Long Harbour to house workers associated with the nickel processing plant construction. The camp was intended to provide those employees from outside the local area with an option to remain on site versus travelling long distances or attempting to secure accommodations locally. The camp was intended to help supplement the supply of local accommodations, which has had to respond to the increased demand since construction began at the facility (Newfoundland and Labrador Department of Natural Resources 2011). However, concern has been expressed that many employees have opted to live within the local

communities, rather than at the camp, creating increased demand for local housing. With construction of the nickel processing plant almost complete and the operations phase set to begin in 2013, it appears that the construction camp and the local community have been able to provide all of the required accommodations (Fitzpatrick 2012).

At the outset of nickel processing plant construction, the Town of Long Harbour-Mount Arlington Heights responded to an immediate demand for additional residential accommodation with the creation of a 28 unit mini-home development in 2010. A new 38-lot residential subdivision, called Middle Pond, is also under development in Long Harbour-Mount Arlington Heights. The sub-division could increase the number of homes in the town by just over 20 percent from current levels. A development strategy will be presented to the Town Council for approval and then the lots will be offered to the public for sale (Long Harbour Development Corporation 2011).

Social housing in the Argentia area is administered by Newfoundland and Labrador Housing Corporation (NLHC). In 2011, there were 126 social housing units in the Argentia area (Table 4-1). Almost 50 percent of these are owned, operated and maintained by NLHC and the majority (approximately 63 percent) of the units is located in Placentia. At least 95 percent of these homes are occupied and are generally only vacant while they are being prepared for new tenants (J. Bowering, pers. comm.).

Table 4-1 Social Housing Units, Argentia Area, 2011

Municipality	Direct Delivered	Rent Supplement	Affordable Housing	Community Based	Co-op	Total
Mitchell's Brook	4	0	0	0	0	4
Freshwater	9	0	0	0	0	9
Dunville	11	0	0	0	0	11
Jerseyside	4	0	0	0	0	4
Fox Harbour	1	0	0	0	0	1
Placentia	29	0	10	40	0	79
St. Bride's	0	0	0	14	0	14
Branch	2	0	0	0	0	2
Colinet	2	0	0	0	0	2
Total	62	0	10	54	0	126

Source: J. Bowering, pers. comm.
Direct Delivered: social housing units owned, operated and maintained by NLHC
Rent Supplement: rental properties owned and operated by private landlords. NLHC has agreement with landlords to subsidize the rent in some of these properties for eligible tenants with low incomes
Affordable Housing Initiatives: rental properties owned and operated by private sector groups, who agree to rent the properties to eligible tenants with low to moderate incomes
Community-Based Housing: rental properties owned and operated by non-profit volunteer boards for eligible tenants with low incomes
Co-operative Housing: social housing owned and operated by non-profit co-operatives

There is no emergency shelter for women or men in the Argentia area.

There are 13 hotels, motels and bed and breakfasts in the Argentia area. These provide more than 80 rooms in total (Newfoundland and Labrador Tourism 2012). There are also two campgrounds in the Argentia area. One of these is a recreational vehicle travel trailer park called Argentia Sunset Park, opened in 2007 by the AMA. The recreational vehicle park includes 40 lots and provides all of the necessary amenities for recreational

vehicle users, including water, sewer and a 30-amp electrical service (AMA no date). The other campground, Fitzgerald's Pond Park in Dunville, also offers 24 sites for campers and recreational vehicle users (Newfoundland and Labrador Tourism 2012).

There is potential for the WREP to affect housing in the Argentia area during the construction phase as a result of any related population increase. The Argentia area housing market has experienced some pressure associated with industrial development, primarily the Vale Long Harbour nickel processing plant. Residential development in the Town of Long Harbour-Mount Arlington Heights has increased to meet demand, and the Town of Placentia also has new construction ongoing and is considering increased residential development in response to existing demands.

It is unlikely that the WREP will put substantially increased pressure on housing in the Argentia area. Some of the WREP employees will come from the local area and already have their own accommodations, and a portion of the construction labour force currently working on the Vale facility will gain WREP employment, further reducing new WREP-related increases on demand for local housing. In addition, close to 90 percent of the nickel processing plant's construction workforce live outside of the Argentia area and commute to the WREP site on a daily basis, and a similar situation is expected with the WREP. Husky is investigating facilitating this by providing a free bus service to transport workers from selected pick-up points to the WREP site.

The relatively small number of construction workers who come from distant communities, such that they cannot commute on a daily basis, will require temporary accommodations in the vicinity of the WREP construction site. However, with the expected completion of the nickel processing plant construction in May 2013 (MacDonald 2012), the demand on the local housing market will ease before the 2014 start of CGS construction at Argentia, and while the WREP will contribute to the demand for local accommodations, it is likely that this will be absorbed by the housing market. However, Husky will continue to monitor the situation and, if required, the provision of additional housing for WREP construction workers could come from continued use of the nickel processing plant camp after that construction project has ended. In addition, Husky is looking into providing a free bus service to transport personnel to site.

4.1.1.2 Employment and Labour

Labour Requirements

Offshore development activity generates both direct and indirect employment opportunities. For the WREP, employment opportunities will be realized through construction of the graving dock at Argentia, construction of the CGS and, potentially, some components of the topsides facilities at existing fabrication yards. The location of engineering and management in the Province will provide opportunities for engineers and technicians, as well as other office support staff.

It is estimated that over 3.5 million hours of employment will take place in Newfoundland during the engineering and construction phase of the WREP. This includes FEED and detailed design, graving dock construction, CGS construction and WREP management. This estimate does not include subsea tie-in or marine works. A preliminary estimate of the Newfoundland hours (by National Occupational Classification (NOC)) associated with completion of the WREP (excluding FEED) is provided in Table 4-2.

Table 4-2 Estimated Person-hours (Full-time Equivalents) to Design Graving Dock and Construct Graving Dock and Concrete Gravity Structure by Quarter

NOC Code	Role	Qtr 3, 2012	Qtr 4, 2012	Qtr 1, 2013	Qtr 2, 2013	Qtr 3, 2013	Qtr 4, 2013	Qtr 1, 2014	Qtr 2, 2014	Qtr 3, 2014	Qtr 4, 2014	Qtr 1, 2015	Qtr 2, 2015	Qtr 3, 2015	Qtr 4, 2015	Qtr 1, 2016	Qtr 2, 2016	Qtr 3, 2016
Graving Dock Construction																		
0113	Purchasing Managers	0 (0)	0 (0)	0 (0)	97 (1)	971 (2)	873 (2)	788 (2)	0 (0)	0 (0)	0 (0)	0 (0)	0 (0)	0 (0)	0 (0)	0 (0)	0 (0)	0 (0)
0211	Engineering Managers	20 (1)	85 (1)	1229 (3)	773 (2)	4261 (9)	3836 (8)	3466 (7)	0 (0)	0 (0)	0 (0)	0 (0)	0 (0)	0 (0)	0 (0)	0 (0)	0 (0)	0 (0)
1221	Administrative Officers	0 (0)	0 (0)	0 (0)	97 (1)	971 (2)	873 (2)	788 (2)	0 (0)	0 (0)	0 (0)	0 (0)	0 (0)	0 (0)	0 (0)	0 (0)	0 (0)	0 (0)
1241	Administrative Assistance	0 (0)	0 (0)	0 (0)	291 (1)	2914 (6)	2619 (6)	2365 (5)	0 (0)	0 (0)	0 (0)	0 (0)	0 (0)	0 (0)	0 (0)	0 (0)	0 (0)	0 (0)
2131	Civil Engineers	130 (1)	426 (1)	426 (1)	1261 (3)	10833 (21)	9747 (19)	8802 (17)	0 (0)	0 (0)	0 (0)	0 (0)	0 (0)	0 (0)	0 (0)	0 (0)	0 (0)	0 (0)
2133	Electrical and Electronics Engineers	7 (1)	22 (1)	22 (1)	10 (1)	7 (1)	7 (1)	7 (1)	0 (0)	0 (0)	0 (0)	0 (0)	0 (0)	0 (0)	0 (0)	0 (0)	0 (0)	0 (0)
2134	Chemical Engineers	0 (0)	0 (0)	0 (0)	291 (1)	2914 (6)	2619 (6)	2365 (5)	0 (0)	0 (0)	0 (0)	0 (0)	0 (0)	0 (0)	0 (0)	0 (0)	0 (0)	0 (0)
2144	Geological Engineers	36 (1)	117 (1)	117 (1)	53 (1)	1864 (4)	1814 (4)	939 (2)	0 (0)	0 (0)	0 (0)	0 (0)	0 (0)	0 (0)	0 (0)	0 (0)	0 (0)	0 (0)
2151	Architects	18 (1)	59 (1)	59 (1)	27 (1)	20 (1)	20 (1)	18 (1)	0 (0)	0 (0)	0 (0)	0 (0)	0 (0)	0 (0)	0 (0)	0 (0)	0 (0)	0 (0)
2231	Civil Engineering Technologists and Technicians	9 (1)	29 (1)	29 (1)	13 (1)	10 (1)	10 (1)	9 (1)	0 (0)	0 (0)	0 (0)	0 (0)	0 (0)	0 (0)	0 (0)	0 (0)	0 (0)	0 (0)
2234	Construction Estimators	4 (1)	15 (1)	15 (1)	6 (1)	5 (1)	5 (1)	5 (1)	0 (0)	0 (0)	0 (0)	0 (0)	0 (0)	0 (0)	0 (0)	0 (0)	0 (0)	0 (0)
7205	General Foreman and Foreman for the following categories: Bricklayers and Allied Crafts - Concrete Finisher, Laborers - Trades Helpers (Formwork, Concrete, Slip, Accessway)	0 (0)	0 (0)	0 (0)	0 (0)	1559 (3)	1516 (3)	539 (2)	0 (0)	0 (0)	0 (0)	0 (0)	0 (0)	0 (0)	0 (0)	0 (0)	0 (0)	0 (0)
7302	General Foreman and Foreman for the following categories: Plant Operators (Crane Operator, Heavy Equipment Operator, Construction Equipment Operators [Stressing, Slip])	0 (0)	0 (0)	0 (0)	0 (0)	4157 (8)	4044 (8)	1436 (3)	0 (0)	0 (0)	0 (0)	0 (0)	0 (0)	0 (0)	0 (0)	0 (0)	0 (0)	0 (0)
7521	Journey Person and Apprentices for the following categories: Plant Operators (Heavy Equipment Operator, Construction Equipment Operators [Stressing, Slip])	0 (0)	0 (0)	0 (0)	0 (0)	34821 (67)	33873 (66)	12024 (24)	0 (0)	0 (0)	0 (0)	0 (0)	0 (0)	0 (0)	0 (0)	0 (0)	0 (0)	0 (0)
7611	Journey Person for the following categories: Laborers - Trades Helpers (Formwork, Concrete, Slip, Accessway)	0 (0)	0 (0)	0 (0)	192 (1)	13357 (26)	12852 (25)	5509 (11)	0 (0)	0 (0)	0 (0)	0 (0)	0 (0)	0 (0)	0 (0)	0 (0)	0 (0)	0 (0)
CGS Construction																		
0211	Engineering Managers	0 (0)	0 (0)	9192 (18)	11873 (23)	12256 (24)	7277 (14)	7088 (14)	8220 (16)	8319 (16)	7462 (15)	7807 (16)	8220 (16)	8319 (16)	7371 (15)	7999 (16)	7336 (15)	4456 (9)
1221	Administrative Officers	0 (0)	0 (0)	1838 (4)	2375 (5)	2451 (5)	1455 (3)	2123 (5)	2427 (5)	2455 (5)	2198 (5)	2301 (5)	2427 (5)	2455 (5)	2172 (5)	2357 (5)	2250 (5)	1485 (3)
1225	Purchasing Agents and Officers	0 (0)	0 (0)	0 (0)	0 (0)	0 (0)	0 (0)	2351 (5)	2612 (6)	2641 (6)	2354 (5)	2468 (5)	2612 (6)	2641 (6)	2325 (5)	2526 (5)	2612 (6)	1980 (4)
1241	Administrative Assistance	0 (0)	0 (0)	2758 (6)	3562 (7)	3677 (8)	2183 (5)	12292 (24)	13761 (27)	13916 (27)	12418 (24)	13018 (26)	13761 (27)	13916 (27)	12266 (24)	13323 (26)	13497 (26)	9902 (20)
2131	Civil Engineers	0 (0)	0 (0)	18178 (35)	24088 (47)	25538 (50)	14688 (29)	29266 (57)	32577 (63)	32944 (64)	29471 (57)	30841 (60)	32577 (63)	32944 (64)	29118 (56)	31561 (61)	31808 (62)	23151 (45)
2132	Mechanical Engineers	0 (0)	0 (0)	8259 (16)	11843 (23)	13522 (26)	7114 (14)	11046 (22)	12381 (24)	12534 (25)	11310 (22)	11783 (23)	12381 (24)	12534 (25)	11180 (22)	12067 (24)	10897 (21)	6403 (13)
2133	Electrical and Electronics Engineers	0 (0)	0 (0)	5933 (12)	8708 (17)	10141 (20)	5207 (11)	3063 (6)	3498 (7)	3552 (7)	3282 (7)	3377 (7)	3498 (7)	3552 (7)	3248 (7)	3464 (7)	2180 (5)	0 (0)
2134	Chemical Engineers	0 (0)	0 (0)	989 (2)	1451 (3)	1690 (4)	868 (2)	511 (1)	583 (2)	592 (2)	547 (2)	563 (2)	583 (2)	592 (2)	541 (2)	578 (2)	363 (1)	0 (0)
2141	Industrial and Manufacturing Engineers	0 (0)	0 (0)	4913 (10)	6564 (13)	7016 (14)	3996 (8)	1358 (3)	1666 (4)	1692 (4)	1550 (3)	1606 (4)	1666 (4)	1692 (4)	1533 (3)	1649 (4)	1038 (2)	0 (0)
2144	Geological Engineers	0 (0)	0 (0)	1902 (4)	2457 (5)	2536 (5)	1506 (3)	595 (2)	662 (2)	669 (2)	606 (2)	629 (2)	662 (2)	669 (2)	599 (2)	643 (2)	662 (2)	501 (1)
2145	Petroleum Engineers	0 (0)	0 (0)	2225 (5)	3266 (7)	3803 (8)	1953 (4)	1148 (3)	1312 (3)	1333 (3)	1231 (3)	1266 (3)	1312 (3)	1333 (3)	1219 (3)	1299 (3)	817 (2)	0 (0)
2147	Computer Engineers (Except Software Engineers and Designers)	0 (0)	0 (0)	494 (1)	726 (2)	845 (2)	434 (1)	255 (1)	291 (1)	296 (1)	273 (1)	282 (1)	291 (1)	296 (1)	271 (1)	288 (1)	182 (1)	0 (0)
2151	Architects	0 (0)	0 (0)	2802 (6)	3750 (8)	4015 (8)	2282 (5)	1027 (2)	1155 (3)	1170 (3)	1067 (3)	1104 (3)	1155 (3)	1170 (3)	1056 (3)	1129 (3)	989 (2)	544 (2)
2231	Civil Engineering Technologists and Technicians	0 (0)	0 (0)	4532 (9)	6289 (13)	6973 (14)	3801 (8)	12659 (25)	14107 (28)	14269 (28)	12776 (25)	13366 (26)	14107 (28)	14269 (28)	12624 (25)	13678 (27)	13557 (27)	9592 (19)
2234	Construction Estimators	0 (0)	0 (0)	1236 (3)	1596 (4)	1649 (4)	979 (2)	2631 (6)	2956 (6)	2990 (6)	2672 (6)	2798 (6)	2956 (6)	2990 (6)	2639 (6)	2864 (6)	2868 (6)	2064 (4)
2251	Architectural Technologists and Technicians	0 (0)	0 (0)	494 (1)	726 (2)	845 (2)	434 (1)	255 (1)	291 (1)	296 (1)	273 (1)	282 (1)	291 (1)	296 (1)	271 (1)	288 (1)	182 (1)	0 (0)
7201	Ironworkers - Rodman General Foreman & Foreman, Structural General Foreman & Foreman	0 (0)	0 (0)	0 (0)	0 (0)	0 (0)	0 (0)	522 (1)	9774 (19)	14371 (28)	9254 (18)	11320 (22)	13578 (27)	11742 (23)	4787 (10)	0 (0)	0 (0)	0 (0)

NOC Code	Role	Qtr 3, 2012	Qtr 4, 2012	Qtr 1, 2013	Qtr 2, 2013	Qtr 3, 2013	Qtr 4, 2013	Qtr 1, 2014	Qtr 2, 2014	Qtr 3, 2014	Qtr 4, 2014	Qtr 1, 2015	Qtr 2, 2015	Qtr 3, 2015	Qtr 4, 2015	Qtr 1, 2016	Qtr 2, 2016	Qtr 3, 2016
7203	Plumbers and Pipefitters - Pipefitters General Foreman & Apprentices	0 (0)	0 (0)	0 (0)	0 (0)	0 (0)	0 (0)	21 (1)	179 (1)	225 (1)	54 (1)	539 (2)	1503 (3)	1100 (3)	0 (0)	0 (0)	0 (0)	0 (0)
7204	General Foreman and Foreman for the following categories: Carpenters and Joiners - Scaffolder, Carpenter (Formwork, Stopends, Accessway)	0 (0)	0 (0)	0 (0)	0 (0)	0 (0)	0 (0)	57 (1)	1125 (3)	1966 (4)	1371 (3)	1659 (4)	1801 (4)	1406 (3)	508 (1)	0 (0)	0 (0)	0 (0)
7205	General Foreman and Foreman for the following categories: Bricklayers and Allied Crafts - Concrete Finisher, Laborers - Trades Helpers (Formwork, Concrete, Slip, Accessway)	0 (0)	0 (0)	0 (0)	0 (0)	0 (0)	0 (0)	1016 (2)	8428 (17)	11855 (23)	8480 (17)	11538 (23)	12715 (25)	12355 (24)	5353 (11)	763 (2)	789 (2)	598 (2)
7236	Ironworkers - Rodman Journey Person & Apprentices, Structural Journey Person & Apprentices & Journey Person (shop)	0 (0)	0 (0)	0 (0)	0 (0)	0 (0)	0 (0)	4896 (10)	186697 (360)	174400 (336)	86754 (167)	106120 (205)	127278 (245)	110093 (212)	44878 (87)	0 (0)	0 (0)	0 (0)
7252	Plumbers and Pipefitters - Pipefitters Journey Person & Apprentices	0 (0)	0 (0)	0 (0)	0 (0)	0 (0)	0 (0)	201 (1)	1677 (4)	2104 (5)	504 (1)	5048 (10)	14084 (28)	10313 (20)	0 (0)	0 (0)	0 (0)	0 (0)
7271	Journey Person and Apprentices for the following categories: Carpenters and Joiners - Scaffolder, Carpenter (Formwork, Stopends, Accessway)	0 (0)	0 (0)	0 (0)	0 (0)	0 (0)	0 (0)	665 (2)	13131 (26)	22953 (45)	16005 (31)	19360 (38)	21020 (41)	16413 (32)	5924 (12)	0 (0)	0 (0)	0 (0)
7302	General Foreman and Foreman for the following categories: Plant Operators (Crane Operator, Heavy Equipment Operator, Construction Equipment Operators [Stressing, Slip])	0 (0)	0 (0)	0 (0)	0 (0)	0 (0)	0 (0)	1801 (4)	2002 (4)	2024 (4)	1804 (4)	2172 (5)	2348 (5)	2374 (5)	1962 (4)	1936 (4)	2002 (4)	1518 (3)
7521	Journey Person and Apprentices for the following categories: Plant Operators (Heavy Equipment Operator, Construction Equipment Operators [Stressing, Slip])	0 (0)	0 (0)	0 (0)	0 (0)	0 (0)	0 (0)	15381 (30)	17090 (33)	17277 (34)	15399 (30)	18777 (37)	20333 (40)	20556 (40)	16899 (33)	16526 (32)	17090 (33)	12958 (25)
7611	Journey Person for the following categories: Laborers - Trades Helpers (Formwork, Concrete, Slip, Accessway)	0 (0)	0 (0)	0 (0)	0 (0)	0 (0)	0 (0)	13674 (27)	54120 (105)	72499 (140)	53490 (103)	70204 (136)	76985 (149)	75171 (145)	36714 (71)	12942 (25)	13383 (26)	10147 (20)

Please refer to Table 4-2, which outlines the skill sets required for the construction phase of the WREP. Based on this information, the Newfoundland and Labrador Department of Advanced Education and Skills can identify the qualifications, certifications and other requirements, including the need for, location and availability of related training opportunities associated with Husky's work force requirements.

A preliminary estimate of journey person/apprentice requirements is provided in Table 4-3. The information provided in Table 4-3 is based upon a Class IV estimate and represents the full resource requirement for the site based on a four-digit NOC. This estimate may not reflect the exact ratios that will be employed at the time of construction. The ratio used to calculate the required apprentices to journey persons is set according to collective agreements with unions. Where specifications did not exist, a reasonable ratio of apprentices to journey persons was assumed.

The construction phase of the WREP is going to require a wide range of skill sets. For graving dock construction, the types of skills that will be required include:

- Electrical trades
- Machinery and transportation equipment mechanics
- Crane operators, drillers and blasters
- Motor vehicle and transit drivers
- Heavy equipment operators
- Trades helpers and labourers.

CGS construction will require the following types of skills:

- Ironworkers
- Concrete finishers
- Electrical trades
- Plumbers, pipefitters and gas fitters
- Carpenters and cabinetmakers
- Machinery and transportation equipment mechanics
- Other mechanics and related repairers
- Crane operators, drillers and blasters
- Motor vehicle and transit drivers
- Heavy equipment operators
- Trades helpers and labourers.

Husky will provide quarterly reports to the Province during the construction phase, including information on the number of people employed by four-digit NOC code, the number of apprentices and journey persons, gender and residency of the workforce. During the operations phase, Husky will continue to report to the C-NLOPB quarterly on Canada-Newfoundland and Labrador Benefits associated with the WREP, including headcount by occupation type, residency and gender for Husky and its major contractors. Husky will also report annually to the C-NLOPB on the percentage of its workforce and that of its contractors that are comprised of the four designated groups: women; Aboriginal persons; persons with disabilities; and visible minorities.

Table 4-3 Estimated Number of Journey Persons and Apprentices

Area	NOC	Role	Worker Type	Qtr 3, 2013	Qtr 4, 2013	Qtr 1, 2014	Qtr 2, 2014	Qtr 3, 2014	Qtr 4, 2014	Qtr 1, 2015	Qtr 2, 2015	Qtr 3, 2015	Qtr 4, 2015	Qtr 1, 2016	Qtr 2, 2016	Qtr 3, 2016
Concrete Gravity Structure	7203	Plumbers and Pipefitters - Pipefitters General Foreman & Apprentices	Apprentices	0	0	0	0	0	0	1	3	2	0	0	0	0
Concrete Gravity Structure	7236	Ironworkers - Rodman Journey Person & Apprentices, Structural Journey Person & Apprentices & Journey Person (shop)	Journey Persons	0	0	8	287	268	133	163	196	169	69	0	0	0
Concrete Gravity Structure	7236	Ironworkers - Rodman Journey Person & Apprentices, Structural Journey Person & Apprentices & Journey Person (shop)	Apprentices	0	0	2	72	67	33	41	49	42	17	0	0	0
Concrete Gravity Structure	7252	Plumbers and Pipefitters - Pipefitters Journey Person & Apprentices	Journey Persons	0	0	0	3	3	1	8	22	16	0	0	0	0
Concrete Gravity Structure	7252	Plumbers and Pipefitters - Pipefitters Journey Persons & Apprentices	Apprentices	0	0	0	1	1	0	2	5	4	0	0	0	0
Concrete Gravity Structure	7271	Journey Persons and Apprentices for the following categories: Carpenters and Joiners - Scaffolder, Carpenter (Formwork, Stopends, Accessway)	Journey Persons	0	0	1	19	33	23	28	30	24	9	0	0	0
Concrete Gravity Structure	7271	Journey Person and Apprentices for the following categories: Carpenters and Joiners - Scaffolder, Carpenter (Formwork, Stopends, Accessway)	Apprentices	0	0	0	6	11	8	9	10	8	3	0	0	0
Concrete Gravity Structure	7521	Journey Person and Apprentices for the following categories: Plant Operators (Heavy Equipment Operator, Construction Equipment Operators [Stressing, Slip])	Journey Persons	0	0	24	26	27	24	29	31	32	26	25	26	20
Concrete Gravity Structure	7521	Journey Person and Apprentices for the following categories: Plant Operators (Heavy Equipment Operator, Construction Equipment Operators [Stressing, Slip])	Apprentices	0	0	6	7	7	6	7	8	8	6	6	7	5
Concrete Gravity Structure	7611	Journey Person for the following categories: Laborers - Trades Helpers (Formwork, Concrete, Slip, Accessway)	Journey Persons	0	0	26	104	139	103	135	148	145	71	25	26	20
Graving Dock	7521	Journey Person and Apprentices for the following categories: Plant Operators (Heavy Equipment Operator, Construction Equipment Operators [Stressing, Slip])	Journey Persons	54	52	18	0	0	0	0	0	0	0	0	0	0
Graving Dock	7521	Journey Person and Apprentices for the following categories: Plant Operators (Heavy Equipment Operator, Construction Equipment Operators [Stressing, Slip])	Apprentices	13	13	5	0	0	0	0	0	0	0	0	0	0
Graving Dock	7611	Journey Person for the following categories: Laborers - Trades Helpers (Formwork, Concrete, Slip, Accessway)	Journey Persons	26	25	11	0	0	0	0	0	0	0	0	0	0

Husky is developing a Diversity Plan for the WREP, which will be submitted to Women's Policy Office and Newfoundland and Labrador Department of Natural Resources. This plan will include strategies for women's employment and business access. The C-NLOPB has confirmed that the approved diversity plan for White Rose continues to meet the C-NLOPB's diversity plan guidelines and no amendments are required for the WREP. Husky is also submitting a White Rose Benefits Plan Amendment to the C-NLOPB, which will cover off the benefits related to the WREP.

Labour Capacity

The skill sets noted above were also required for construction of the nickel processing plant in Long Harbour. This construction program will be winding down when Husky anticipates start of graving dock construction. Therefore, there will be a pool of workers that can move from the Long Harbour site to the Argentia site.

Work on the Hebron project will also be getting underway in the same timeframe and that project will require some of the same skills sets required by Husky for CGS construction. However, the workforce that will be required for the WREP is substantially smaller than that required for both the Long Harbour and Hebron construction projects. Husky is confident that the required workers will be sourced through collaboration with its contractors and the relevant trade unions.

Husky, through its contractors (and their subcontractors), anticipates that elements of the workforce will be first sourced from the local area of Placentia/Long Harbour/ Whitbourne, based on hiring done for construction of the Vale nickel processing plant at Long Harbour. It is anticipated that additional work force would then be sourced from the wider Avalon Peninsula, Newfoundland and Labrador and the rest of Canada.

Based on experience at the Vale nickel processing plant project in Long Harbour, labour shortages in the following disciplines have been identified Canada-wide including Newfoundland and Labrador:

- Crane operators
- Surveyors
- Carpenters
- Brick layers (masons).

It is anticipated that with other large projects such as the Hebron project and Muskrat Falls being executed in the same timeframe, further local shortages of labour could occur in the following disciplines:

- Rebar placement
- Iron workers
- Cement finishers.

There may be training opportunities related to rebar placement as this occupation does not require an apprenticeship.

Husky presently is investigating strategies for recruitment and retention of the workforce through WREP completion.

Where specific skill development is required to meet WREP needs, Husky and its contractors and suppliers will work with educational institutions, industry and other stakeholders to facilitate the delivery of training to residents of Newfoundland and Labrador, including members of designated groups. Training may include regulatory/ safety, technical, competency and leadership training and will be delivered through various means, including on the job training and apprenticeships.

The construction phases is the phase in which WREP-related socio-economic effects are most likely to occur. However, while the main socio-economic effects will occur during construction, it should be noted that the scale of such activity for the WREP will be considerably smaller than for White Rose, Terra Nova or Hebron projects, let alone Hibernia. In total, the Hibernia construction phase saw approximately 41.5 million person-hours of work in Newfoundland and Labrador. The equivalent figures for Terra Nova and White Rose were 12.0 and 11.4 million person-hours, respectively. Preliminary estimates indicate that for the WHP, total employment generated by construction will be approximately 3.1 million person-hours (excluding FEED). This estimate includes construction of both the graving dock and the CGS component of the WHP. With construction-phases employment of 3.1 million person-hours (excluding FEED), labour requirements are less than 26 percent of the Terra Nova or White Rose requirements and less than 8 percent of that for Hibernia.

Similarly, for the Argentia area, the WREP is at a much smaller scale than the Long Harbour nickel processing plant. Construction phase employment at the Long Harbour project has been estimated at approximately 10 million person-hours, approximately six times more than the 3.1 million person-hours of construction-phase employment associated with the WHP. While the WREP will bring substantial economic benefits to the area, WREP effects are likely to be of much smaller magnitude than the Long Harbour project.

Given that these other projects have been highly beneficial to the economy, or, in the case of Hebron, is expected to generate positive economic effects, it is reasonable to expect that the WREP's effects will be similar, if smaller. As mentioned above, the majority of socio-economic WREP effects will occur during construction. The operations phase would see reduced effects, while still generating some benefits for employment and business.

4.1.1.3 Summary

With the WREP, Newfoundland and Labrador will continue to experience the socio-economic benefits of offshore petroleum development, which has remained the primary provincial economic driver since the 1990s. Following Husky's White Rose and North Amethyst projects, the WREP will continue to provide benefits to the province. While smaller in scale than the White Rose and Terra Nova projects, let alone Hibernia, the WREP represents another important step in the development of Newfoundland and Labrador's offshore oil and gas industry.

Benefits will be delivered according to Husky's approach to developing the WREP which will afford opportunities for local employment and business. The WREP will also contribute to forwarding the development of the oil and gas industry in the province, providing opportunities for further development of provincial expertise and capabilities in this economically important sector. Generating positive effects on employment and economy, the WREP will contribute to sustainable development in the province.

At the local scale, WREP-related benefits will be delivered to both the Argentia and St. John's areas. Construction-related employment and business opportunities will have direct economic benefits, while secondary multiplier benefits will also substantially benefit the economy. During operations, the WREP will continue to provide employment and contribute both direct and indirect benefits to the St. John's and provincial economies. While the WREP may lead to some increased demand on community services and infrastructure, it is not anticipated that any such increased demand will exceed the capacity of communities to respond. Furthermore, given the smaller scale of the WREP in relation to other successful projects, past experience indicates that these communities will be able to absorb any of the smaller demands that may result from the WREP.

4.1.2 Terrestrial Environment

Since the area is an exposed brownfield site, few terrestrial mammals are found on the Argentia Peninsula. Otter, muskrat and moose may be resident in the Argentia area, but not on the Argentia Peninsula (VBNC 2002). Furbearers located onshore near Argentia include small rodents such as rats and mice, meadow vole, snowshoe hare, mink, fox and masked shrew (ARG 1995; VBNC 2002). Rats, mice and meadow voles may be found on the Argentia Peninsula (VBNC 2002). Numerous species of birds inhabit the Argentia Peninsula. In summer, gannet, alcid and gull nesting and shearwater foraging communities characterize the inshore zone of Placentia Bay; a substantial waterfowl population occurs in the nearshore waters of Placentia Bay in the winter (VBNC 2002). No known species at risk reside, feed, stage or overwinter on the Argentia Peninsula (VBNC 2002).

There are numerous breeding pairs of Bald Eagle on Merasheen Island (Argentia Assessment Group et al. 1997). One of the deepwater mating sites being evaluated is west of Merasheen Island.

4.2 Nearshore Environment

4.2.1 Atmospheric Environment

4.2.1.1 Climate Overview

Placentia Bay, and its surrounding land areas, experiences a Maritime climate as its proximity to major storm tracks, the Atlantic Ocean and the Gulf Stream often lead to the occurrence of major weather events over the region throughout the year, specifically during the fall and winter. Wind direction is a critical component for determining the type of weather experienced across Newfoundland and Labrador, especially along the coasts.

The typical tracks that storms take over Atlantic Canada each year are shown in Figure 4-1. High and low pressure systems affecting Newfoundland and Labrador usually approach from the south or west, typically originating in central Canada or along the eastern seaboard of the United States. The most intense storms that affect eastern Newfoundland approach from the south and feed off the large temperature contrast (specifically from late fall through early spring) between eastern Canada, the Labrador Current and the Gulf Stream, which is present southeast of Newfoundland (Figure 4-2).

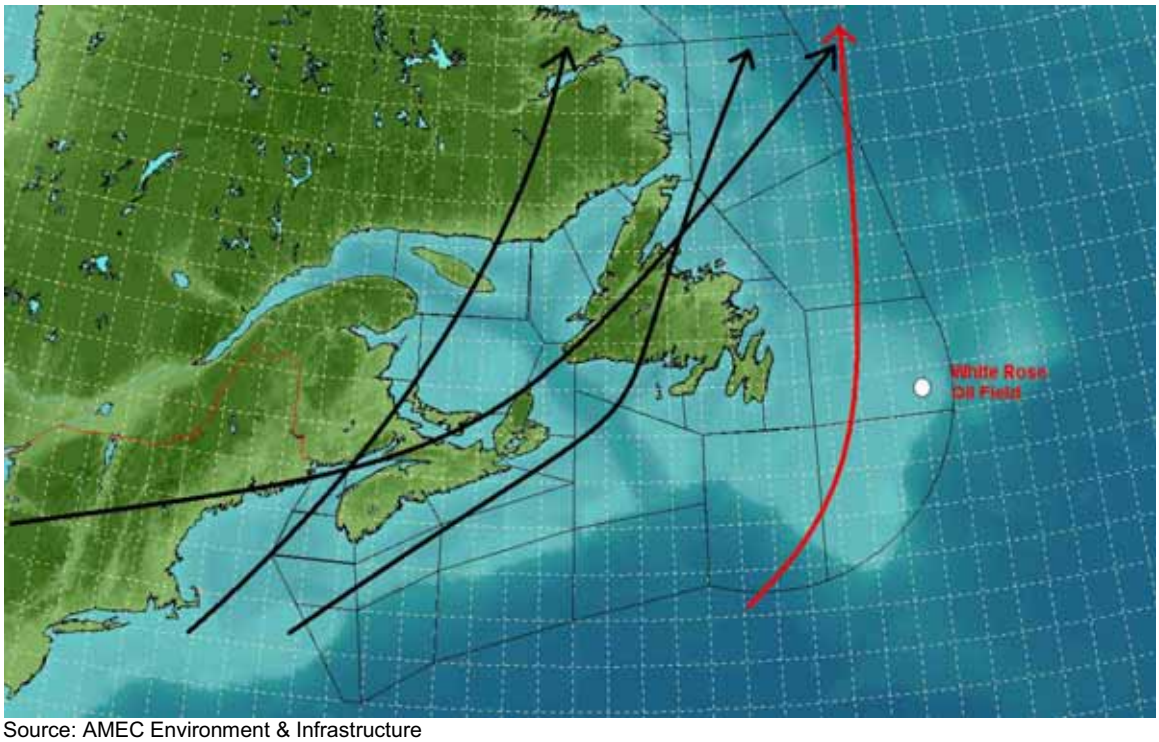

Source: AMEC Environment & Infrastructure

Figure 4-1 Predominant Storm Tracks Affecting Atlantic Canada

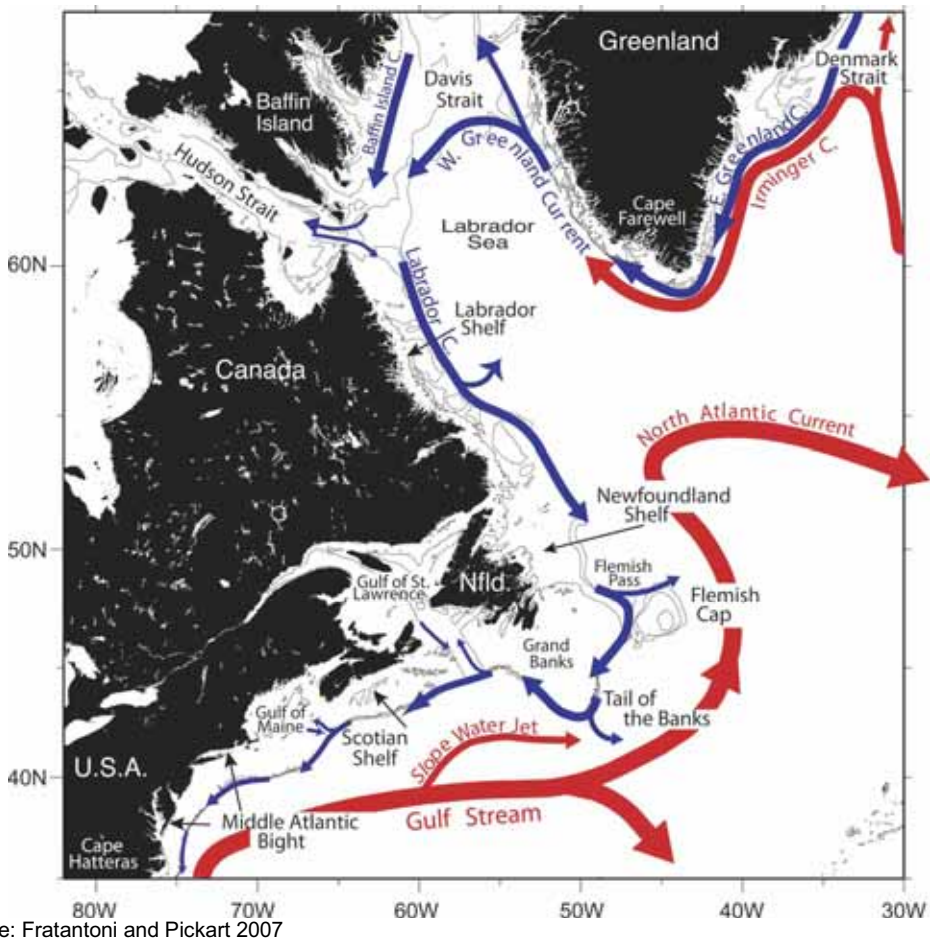

Source: Fratantoni and Pickart 2007
Note: The path of the shelfbreak jet (blue) and the warmer currents originating from the Gulf Stream (red) are shown

Figure 4-2 Surface Circulation Features in the Western North Atlantic

The most intense storms that affect Placentia Bay, with the exception of tropical storms and hurricanes, are experienced in the winter months, particularly those tracking east of the Island of Newfoundland. During the winter, these storms often produce winds gusts up to and exceeding 100 km/h and give substantial snowfall to eastern Newfoundland. Areas surrounding Placentia Bay typically receive the least amount of snowfall in the province due to the frequent occurrence of rain during winter storms. Ocean-effect snows, or snow squalls, often occur during the winter on the southern Avalon and Burin Peninsulas as cold westerly winds develop behind winter storms. These events have the ability to produce substantial, localized, snowfalls over regions in a short period of time.

The onset of spring is usually delayed by the prevalence of a cool polar air mass and low sea surface temperatures south of Newfoundland. The retreat of the polar front jet stream to the north, combined with the shift in prevailing wind direction to southwest, causes a change in the temperature patterns by mid-late June. Prolonged periods of fog and drizzle are common in the spring and early summer as warm air travels over the cold ocean water. In summer, the Maritime Tropical air mass from the south and the Maritime polar air mass from over the Labrador Current create varying temperatures from day to day. During the fall, southern Newfoundland tends to cool at a slow pace due to the delayed cooling of the ocean relative to land.

Atmospheric parameters for the Placentia Bay region were analyzed by using datasets from Environment Canada (land weather observation stations), MSC50 wind/wave hindcast model and SmartBay (wave buoys operated by the Marine Institute). These data sources are further described below. All of the applicable observation sites are shown in Figure 4-3.

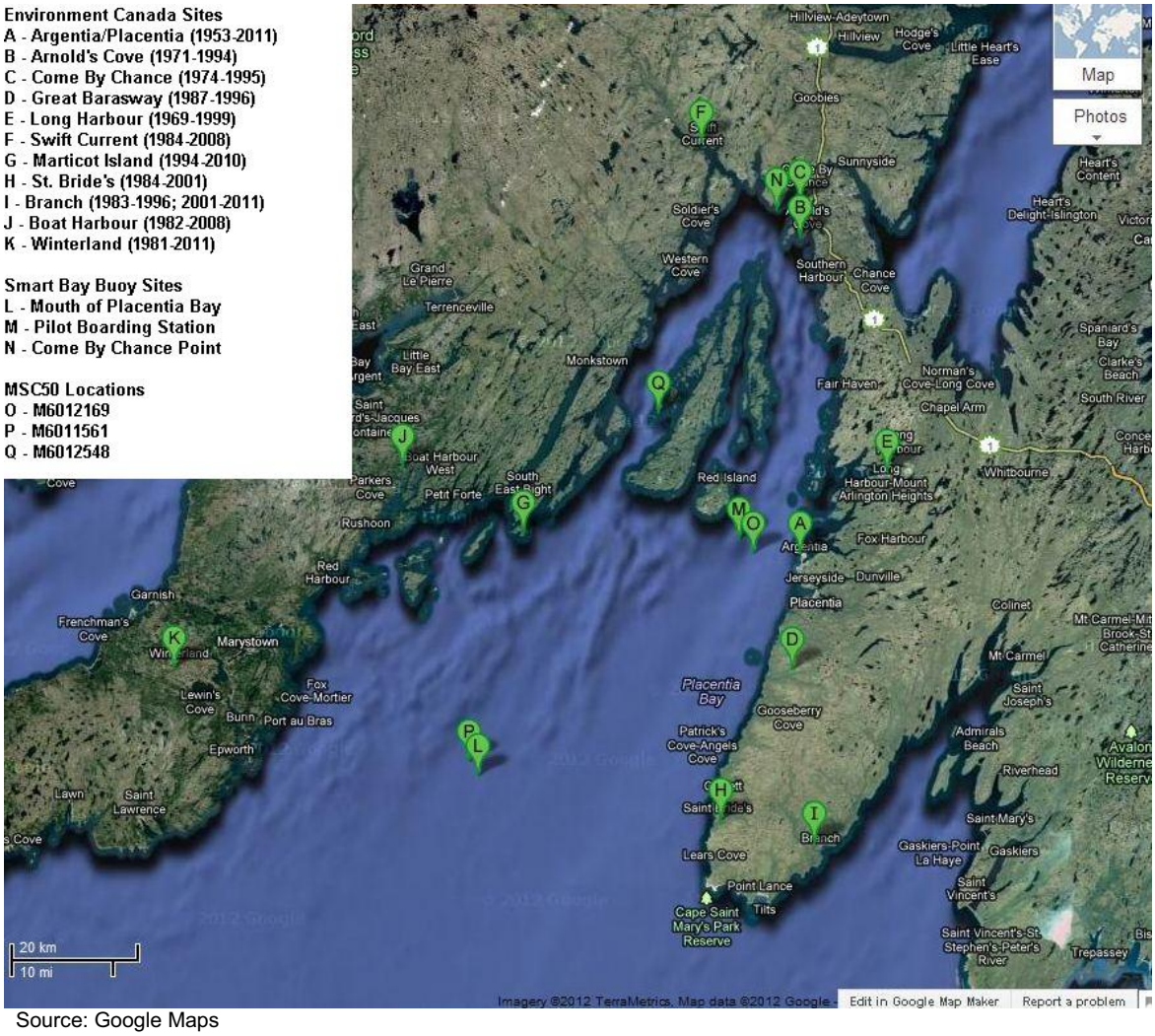

Source: Google Maps

Figure 4-3 Location of Nearshore Weather Stations

Eleven Environment Canada weather stations (Environment Canada 2012a) were used for determining air temperature, wind and precipitation statistics for the nearshore climatology of Placentia Bay. These stations, along with their years of record, are listed in Table 4-4. Many of these stations were operated by volunteer climate observers, who took measurements once per day and sent the collected information on to Environment Canada.

Table 4-4 List of Environment Canada Daily Weather Observation Sites

Site Location	Years of Record
Argentia and Placentia	Argentia: 1953-1970, 1976-2011; Placentia 1970-1975
Arnold's Cove	1971-1994
Boat Harbour	1982-2008
Branch	1983-1996; 2001-2011
Come By Chance	1974-1995
Great Barasway	1987-1996
Long Harbour	1969-1999
St. Bride's	1984-2001
Swift Current	1984-2008
Winterland	1981-2011
Source: Environment Canada 2012a	

Some weather stations operated by Environment Canada report on an hourly basis and, unless they are staffed at an airport, are typically automated sites that transmit data back to Environment Canada every hour. Data from the Argentia area were reported hourly by an observer from 1953 to 1986; therefore, reliable visibility and precipitation type information is available. An automated weather station has been reporting from Argentia since 1986 to the present day. A list of weather stations, which reported on an hourly basis, used in assessing the climatology of Placentia Bay, is presented in Table 4-5.

Table 4-5 List of Environment Canada Hourly Weather Observation Sites

Site Location	Years of Record
Argentia-Placentia	1953-2011 (Staffed Visibility/Precipitation through 1986)
Marticot Island	1994-2010
Winterland	1999-2011
Source: Environment Canada 2012a	

SmartBay, Placentia Bay, is an initiative of the School of Ocean Technology at Memorial University's Fisheries and Marine Institute, which began in 2006. The objective of the SmartBay project is to provide better decision making from a safety, efficiency, policy and environmental perspective for various industries, including fishery, oil and gas, marine transportation, recreational boaters and municipalities. Since its inception, three marine buoys have been deployed in Placentia Bay and real-time information from each location is updated on the publicly available website (SmartBay 2012).

Atmospheric data were also obtained for the study area (46.0°N to 48.0°N, 56.0°W to 53°W) from the International Comprehensive Ocean-Atmosphere Data Set (ICOADS) (Woodruff et al. 1998, 2005; Worley et al. 2005; ICOADS 2012), which consists of global marine (ship and rig) data observations from 1960 to 2011, compiled by the National Center for Atmospheric Research.

The following sections present monthly and annual statistics for air temperature, wind speed, wind direction, precipitation (type and amount) and visibility. Monthly estimates of vessel icing potential are also presented, based on calculations using air and sea surface temperature measurements.

4.2.1.2 Air Temperature

Monthly air temperature statistics were calculated for nearshore land sites using ICOADS data from 11 Environment Canada weather stations and across Placentia Bay. As expected, the air temperature values exhibit strong seasonal and diurnal variations, especially from land stations. The mean temperature of the 11 Environment Canada stations ranges from -4.3°C in February to 15.6°C in August. The coldest observed air temperature from land stations surrounding Placentia Bay is -29.5°C over northern sections of the Burin Peninsula, observed in both January and February. The warmest air temperature from these stations was 31.5°C in September. The maximum daily average temperature peaks in August at 19.5°C, while the coldest mean daily minimum of -8.3°C is observed in February. The monthly air temperature statistics for the Environment Canada weather sites surrounding Placentia Bay are plotted in Figure 4-4 and presented in Table 4-6.

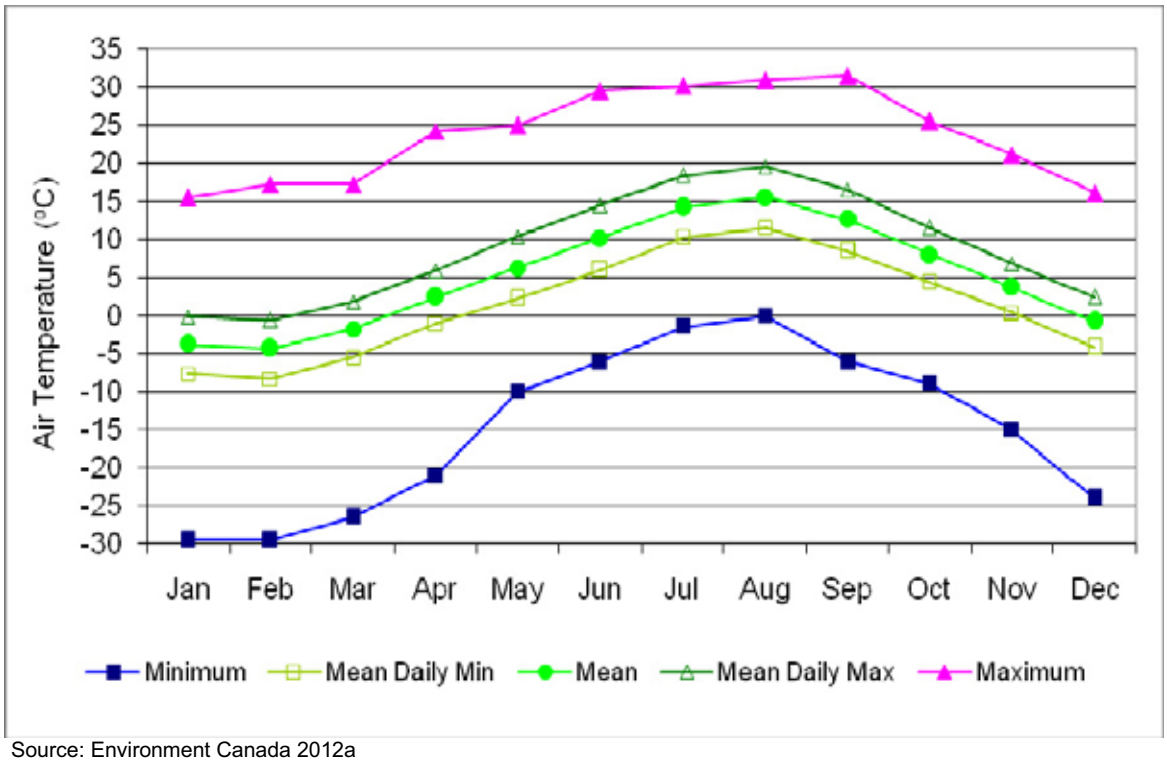

Source: Environment Canada 2012a

Figure 4-4 Monthly Air Temperature from Environment Canada Sites near Placentia Bay

Table 4-6 Monthly Air Temperature from Environment Canada Sites near Placentia Bay

Month	Mean (°C)	Max (°C)	Min (°C)	Mean Daily Max (°C)	Mean Daily Min (°C)
Jan	-3.8	15.5	-29.5	-0.2	-7.6
Feb	-4.3	17.2	-29.5	-0.6	-8.3
Mar	-1.7	17.2	-26.5	1.9	-5.5
Apr	2.5	24.2	-21.0	6.0	-1.0
May	6.3	25.0	-10.0	10.5	2.3
Jun	10.2	29.5	-6.0	14.5	6.1
Jul	14.3	30.2	-1.5	18.4	10.4
Aug	15.6	31.0	0.0	19.5	11.6
Sep	12.6	31.5	-6.0	16.5	8.5
Oct	8.1	25.5	-9.0	11.5	4.5
Nov	3.7	21.1	-15.0	6.9	0.4
Dec	-0.8	16.1	-24.0	2.4	-4.2
Source: Environment Canada 2012a					

Over Placentia Bay, air temperature variations are less pronounced due to the effects of the water. Maximum and minimum temperature values are typically less extreme than those over the nearby land mass. The mean temperature of the ICOADS data ranges from -1.6°C in February to 14.8°C in August. The coldest observed air temperature over Placentia Bay is -18.2°C in February, while the maximum air temperature was 25.2°C in August. The maximum daily average temperature peaks in August at 16.9°C, while the coldest mean daily minimum of -3.9°C is observed in February. Using ICOADS data, the air temperature statistics for Placentia Bay are plotted in Figure 4-5 and presented in Table 4-7.

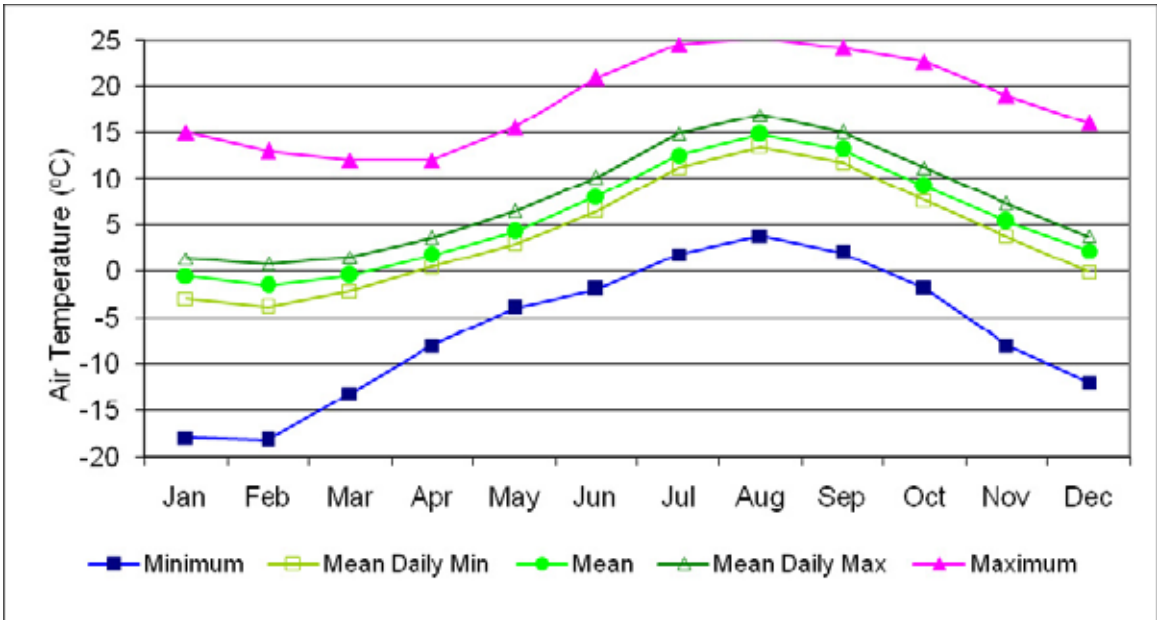

Source: ICOADS 2012

Figure 4-5 Monthly Air Temperature Statistics for Placentia Bay

Table 4-7 Monthly Air Temperature Statistics for Placentia Bay

Month	Mean (°C)	Max (°C)	Min (°C)	Mean Daily Max (°C)	Mean Daily Min (°C)
Jan	-0.6	15	-18	1.4	-3
Feb	-1.6	13	-18.2	0.8	-3.9
Mar	-0.4	12	-13.2	1.5	-2.2
Apr	1.7	12	-8	3.6	0.4
May	4.3	15.5	-4	6.4	2.9
Jun	8	20.9	-2	10.2	6.5
Jul	12.5	24.5	1.8	14.9	11.2
Aug	14.8	25.2	3.8	16.9	13.4
Sep	13.2	24.2	2	15.1	11.7
Oct	9.2	22.6	-1.8	11.2	7.7
Nov	5.4	19	-8	7.3	3.8
Dec	2.2	16	-12	3.8	-0.1
Source: ICOADS 2012					

4.2.1.3 Wind Climatology

Wind speed and direction statistics were derived using the MSC50 hindcast, which consists of hourly wind values for the period 1954 to 2010 inclusive, and Environment Canada weather stations, which reported hourly observations around Placentia Bay. Three data nodes were chosen from the MSC50 dataset for analysis as representative of the eastern, southern and northern parts of Placentia Bay. While the SmartBay buoys deployed in Placentia Bay have a brief observation period, their wind statistics were calculated to compare with those from the MSC50 dataset.

Wind and wave data were obtained from the MSC50 (MSC06min subset), wind and wave hindcast dataset. The MSC50 dataset represents the current best technology and the most comprehensive wind and wave database for eastern Canadian waters (Swail et al. 2006).

The dataset covers hourly wind and wave parameters, from 1954 to 2010, for the North Atlantic Ocean and includes consideration of period with sea ice coverage (Swail et al. 2006; Environment Canada 2011; Fisheries and Oceans Canada (DFO) 2012a). The MSC50 domain (MSC30S) covers the North Atlantic Ocean from approximately 80°W to 20°E and from 0°N to 80°N at 0.5° resolution (approximately 50 km); while the Eastern Canada Subset (MSC06min) covers from approximately 74°W to 42°W and from 40°N to 52°N at 0.1° resolution (approximately 10 km).

Hourly time-series (1954 to 2010) for the MSC06min subset were obtained from DFO (2012a).

Three node locations were selected to be representative of WREP activities in Placentia Bay:

- M6012169: Between Red Island and Argentia, 47.3°N, 54.1°W, for WREP activities near Argentia
- M6012548: Between Isle Valen and Merasheen Island, 47.5°N, 54.3°W, for a potential deep-water mating site in that part of the bay
- M6011561: Mouth of Placentia Bay, 47.0°N, 54.7°W, for tow-out from Placentia Bay to the Grand Banks

Average and maximum wind speeds between all three MSC50 data points were very similar for each month; therefore an overall average of all three locations was used to represent these nodes. The monthly and annual mean and maximum wind speeds for Placentia Bay are presented in Tables 4-8 and 4-9 Both SmartBay buoys recorded their maximum wind in September; both were observed the same afternoon as Hurricane Igor tracked just east of Newfoundland on September 21, 2010. The minimum mean speed occurs in the summer months, while the maximum peaks in the winter (January-February).

Table 4-8 Monthly and Annual Mean Wind Speed over Placentia Bay

Month	MSC50 Average (m/s)	SmartBay (Mouth of Bay) (m/s)	SmartBay (Pilot Boarding Station) (m/s)
Jan	10.6	9.4	8.4
Feb	10.0	9.5	9.2
Mar	9.3	9.0	8.9
Apr	8.0	6.9	7.6
May	6.3	5.8	5.9
Jun	5.7	5.4	5.6
Jul	5.4	5.4	5.8
Aug	6.0	5.8	5.5
Sep	7.2	6.8	7.5
Oct	8.6	7.5	7.6
Nov	9.4	8.0	7.5
Dec	10.4	9.0	8.0
Annual	8.1	7.4	7.3
Source: DFO 2012a; SmartBay 2012			

Table 4-9 Monthly and Annual Maximum Wind Speed over Placentia Bay

Month	MSC50 (m/s)	SmartBay (Mouth of Bay) (m/s)	SmartBay (Pilot Boarding Station) (m/s)
Jan	25.7	19.5	21.7
Feb	27.0	20.2	22
Mar	27.9	18.5	20.2
Apr	20.9	18.8	19.4
May	22.6	15.7	14.5
Jun	20.1	16.4	16
Jul	22.8	16.7	17.2
Aug	26.3	20.3	16.4
Sep	29.5	25.5	25.5
Oct	28.4	20.5	20.8
Nov	25.1	17.8	18.8
Dec	25.8	21.6	20.2
Annual	29.5	25.5	25.5
Source: DFO 2012a; SmartBay 2012			

Wind data from the SmartBay buoys are of a considerably shorter period of time than the MSC50 gridded data. Weather information is only available since 2007 for the buoy located at the mouth of Placentia Bay, while measurements from the pilot boarding station, just west of Argentia, began in 2010. Since the SmartBay program has only been running for a short period, the buoy data have not sampled a substantial amount of storms; hence, a lower range of maximum wind speeds will have been recorded. While the monthly averages are quite comparable between the MSC50 and SmartBay datasets (differences typically between 1 and 2 m/s), the maximum wind speeds from the SmartBay buoys show speeds of 5 to 8 m/s lower than the MSC50 because they have not sampled as many years of events (Figure 4-6).

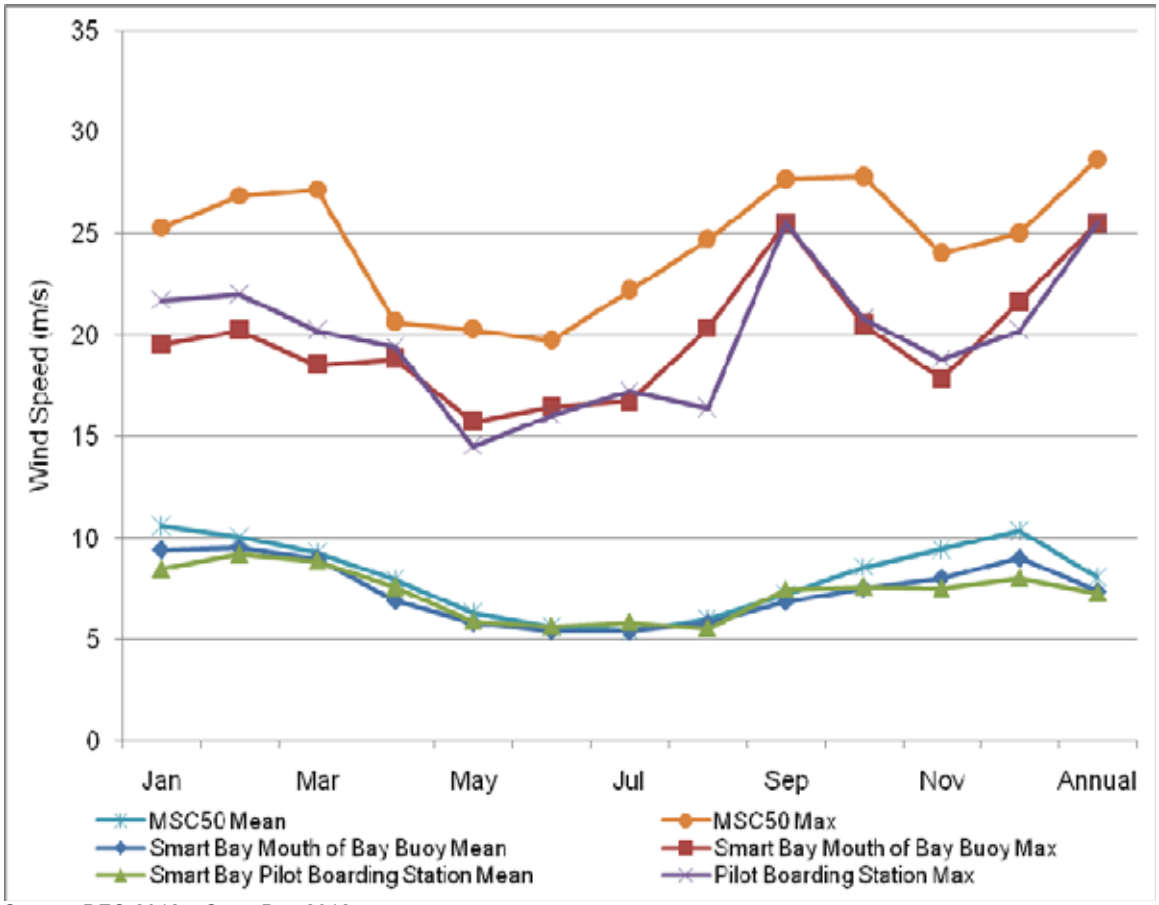

Source: DFO 2012a; SmartBay 2012

Figure 4-6 Monthly Average and Maximum Wind Speed Statistics for Placentia Bay

The monthly statistics of mean wind speed, most frequent wind direction, maximum wind speed and direction of maximum speed for the three MSC50 node locations are presented in Tables 4-10 to 4-12. The average wind speed (m/s) is nearly identical between the three locations; therefore, an average of the nodes was used when comparing with the SmartBay buoy data in Tables 4-8 and 4-9. The maximum average wind speed occurs in January, while the minimum is in July. The most frequent wind direction is southwesterly for all sites. Slight differences exist with the maximum hourly wind speed between the three nodes, with the minimum occurring in either May or June and the maximum in September or October.

Table 4-10 Mean and Maximum Wind Parameters for MSC50 Node M6012169

Month	Average Hourly Wind Speed (m/s)	Most Frequent Wind Direction (from)	Max Hourly Wind Speed (m/s)	Direction of Max Hourly Speed
Jan	10.6	W	25.2	S
Feb	10.1	W	27.0	W
Mar	9.3	W	26.7	SW
Apr	8.0	W	20.7	NW
May	6.4	SW	19.3	N
Jun	5.7	SW	19.7	NW
Jul	5.4	SW	21.5	SW
Aug	6.0	SW	25.3	S
Sep	7.3	SW	29.5	SE
Oct	8.6	W	26.9	S
Nov	9.5	W	23.5	W
Dec	10.4	W	24.8	N
Annual	8.1	SW	29.5	SE
Source: DFO 2012a				

Table 4-11 Mean and Maximum Wind Parameters for MSC50 Node M6012548

Month	Average Hourly Wind Speed (m/s)	Most Frequent Wind Direction (from)	Max Hourly Wind Speed (m/s)	Direction of Max Hourly Speed (from)
Jan	10.6	W	24.9	S
Feb	9.9	W	26.8	NW
Mar	9.2	W	26.8	SW
Apr	7.9	W	20.3	NW
May	6.3	SW	18.9	N
Jun	5.7	SW	19.3	NW
Jul	5.4	SW	22.8	SW
Aug	6.0	SW	22.4	S
Sep	7.2	SW	26.9	NW
Oct	8.6	W	28.0	S
Nov	9.4	W	23.4	W
Dec	10.4	W	24.4	N
Annual	8.0	SW	28.0	S
Source: DFO 2012a				

Table 4-12 Mean and Maximum Wind Parameters for MSC50 Node M6011561

Month	Average Hourly Wind Speed (m/s)	Most Frequent Wind Direction (from)	Max Hourly Wind Speed (m/s)	Direction of Max Hourly Speed (from)
Jan	10.6	W	25.7	SW
Feb	10.1	W	26.7	NW
Mar	9.4	W	27.9	SW
Apr	8.0	W	20.9	NW
May	6.3	SW	22.6	E
Jun	5.6	SW	20.1	NW
Jul	5.4	SW	22.3	SW
Aug	6.0	SW	26.3	S
Sep	7.2	W	26.6	E
Oct	8.5	W	28.4	S
Nov	9.4	W	25.1	E
Dec	10.3	W	25.8	N
Annual	8.1	SW	28.4	S
Source: DFO 2012a				

Monthly, seasonal and annual wind roses were derived from the three MSC50 data nodes and are presented as Figures 4-7 to 4-15.

Hourly observations from three Environment Canada weather stations (Marticot Island, Argentia-Placentia and Winterland) were used to assess the typical wind conditions nearshore Placentia Bay. These three sites provide a broad regional summary of winds surrounding the region as they encompass the west, north and east sides of Placentia Bay. The lowest mean wind speeds are expected during the summer months (June-July), while the maximum occurs in the winter (January-February). The monthly and annual mean and maximum wind speeds for nearshore Placentia Bay are presented in Tables 4-13 and 4-14 and plotted in Figure 4-16.

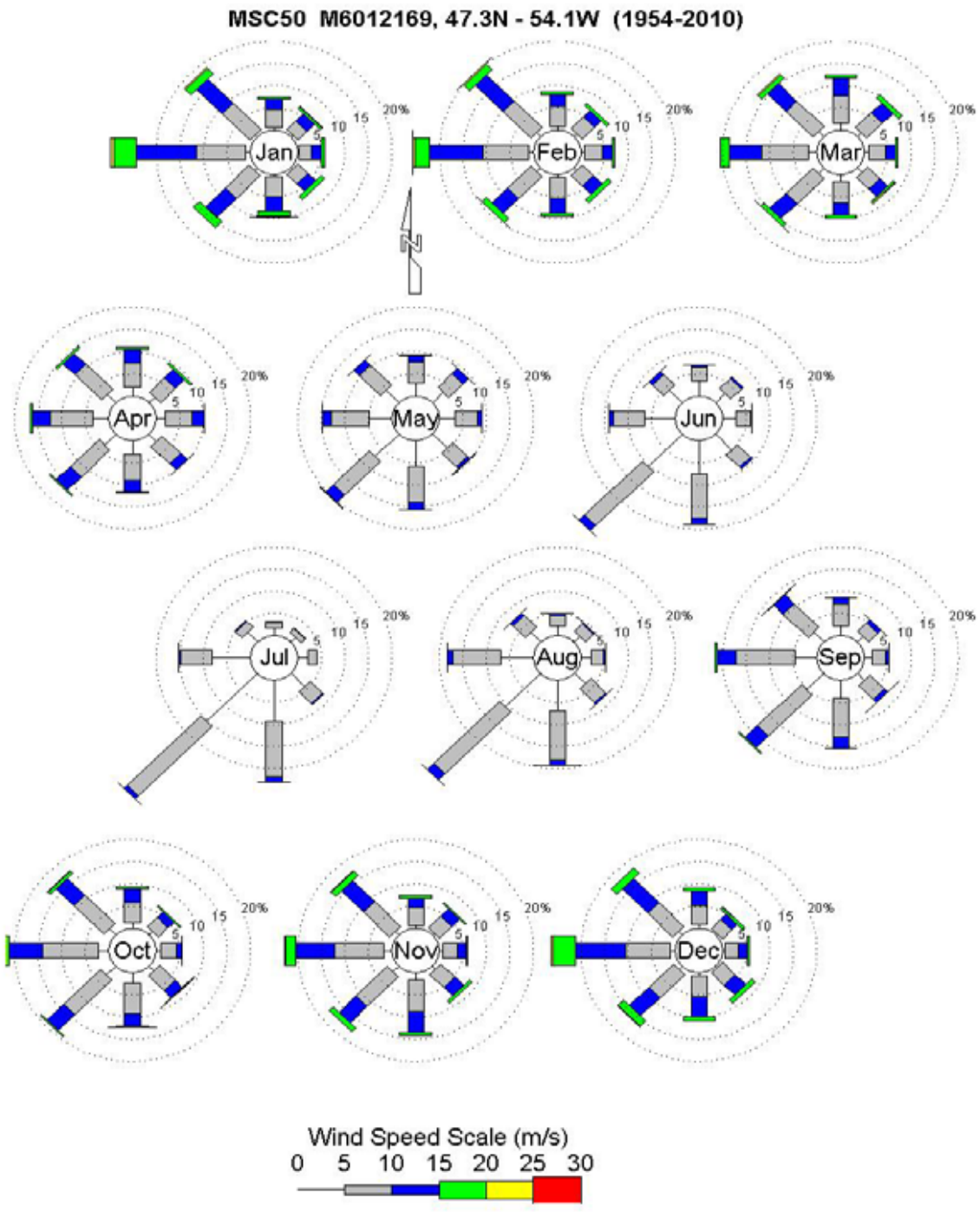

Source: DFO 2012a

Figure 4-7 Monthly Wind Roses for MSC50 node M6012169

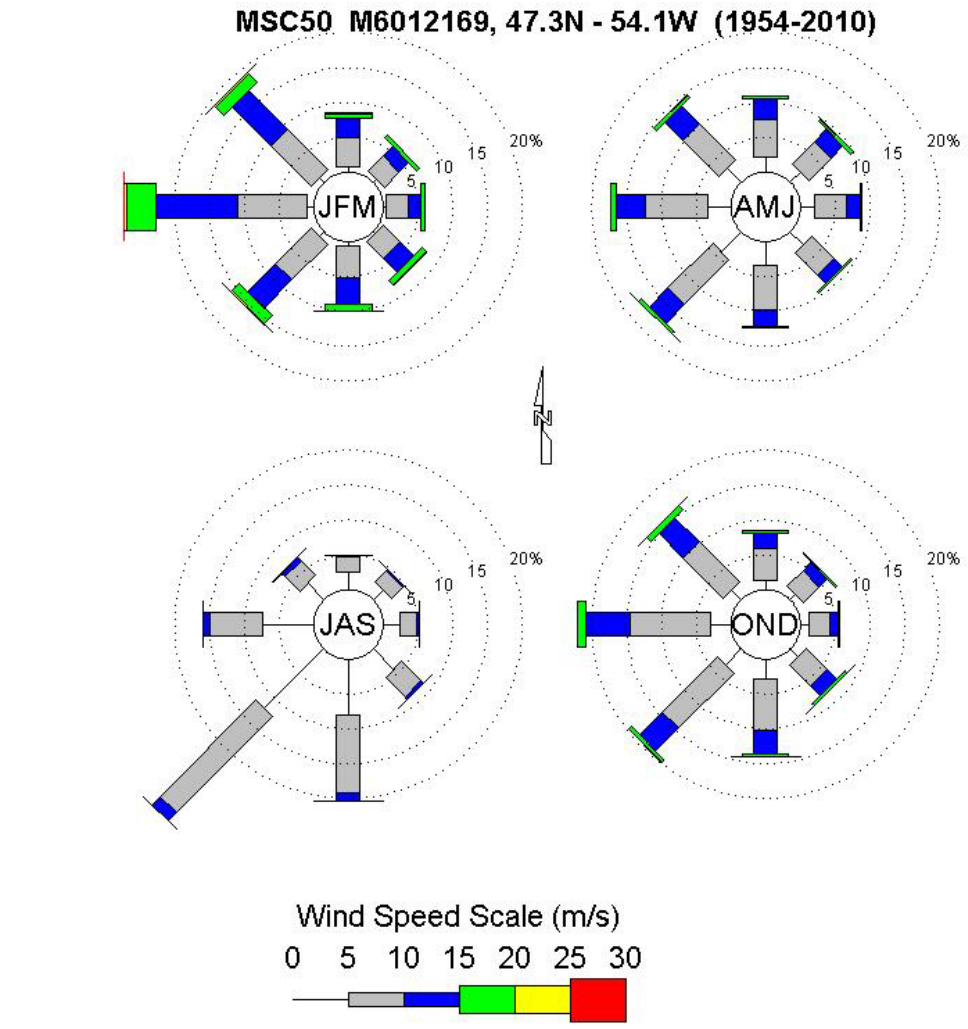

Source: DFO 2012a

Figure 4-8 Seasonal Wind Roses for MSC50 node M6012169

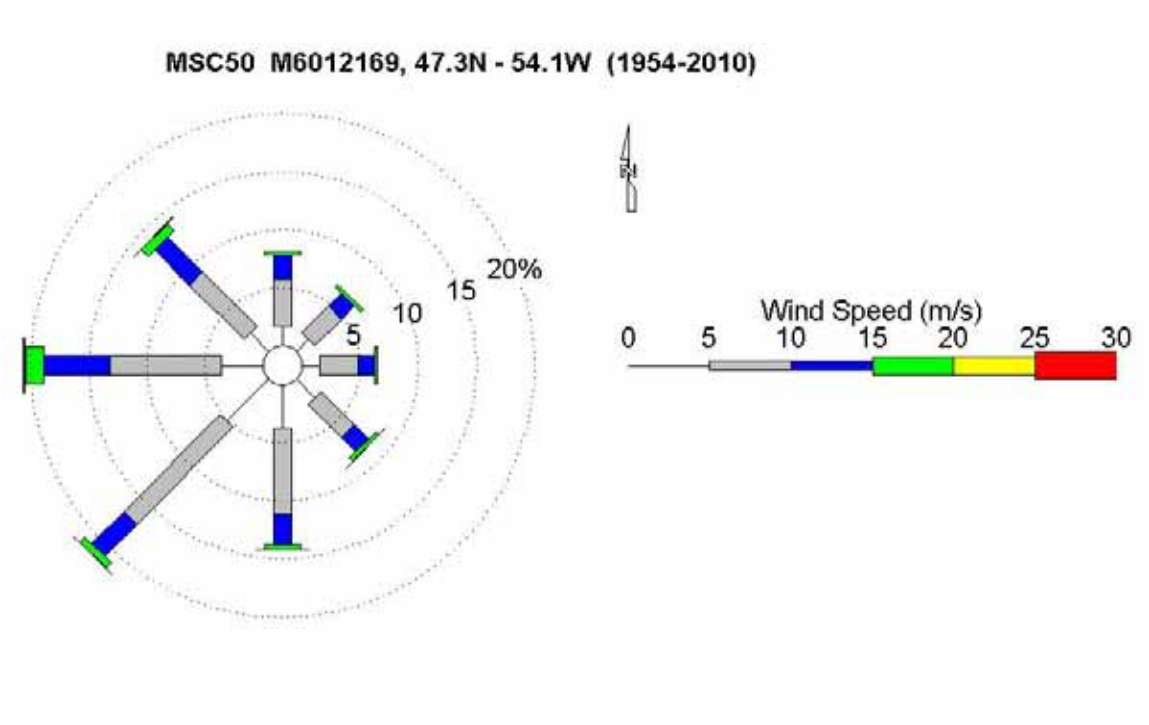

Source: DFO 2012a

Figure 4-9 Yearly Wind Rose for MSC50 node M6012169

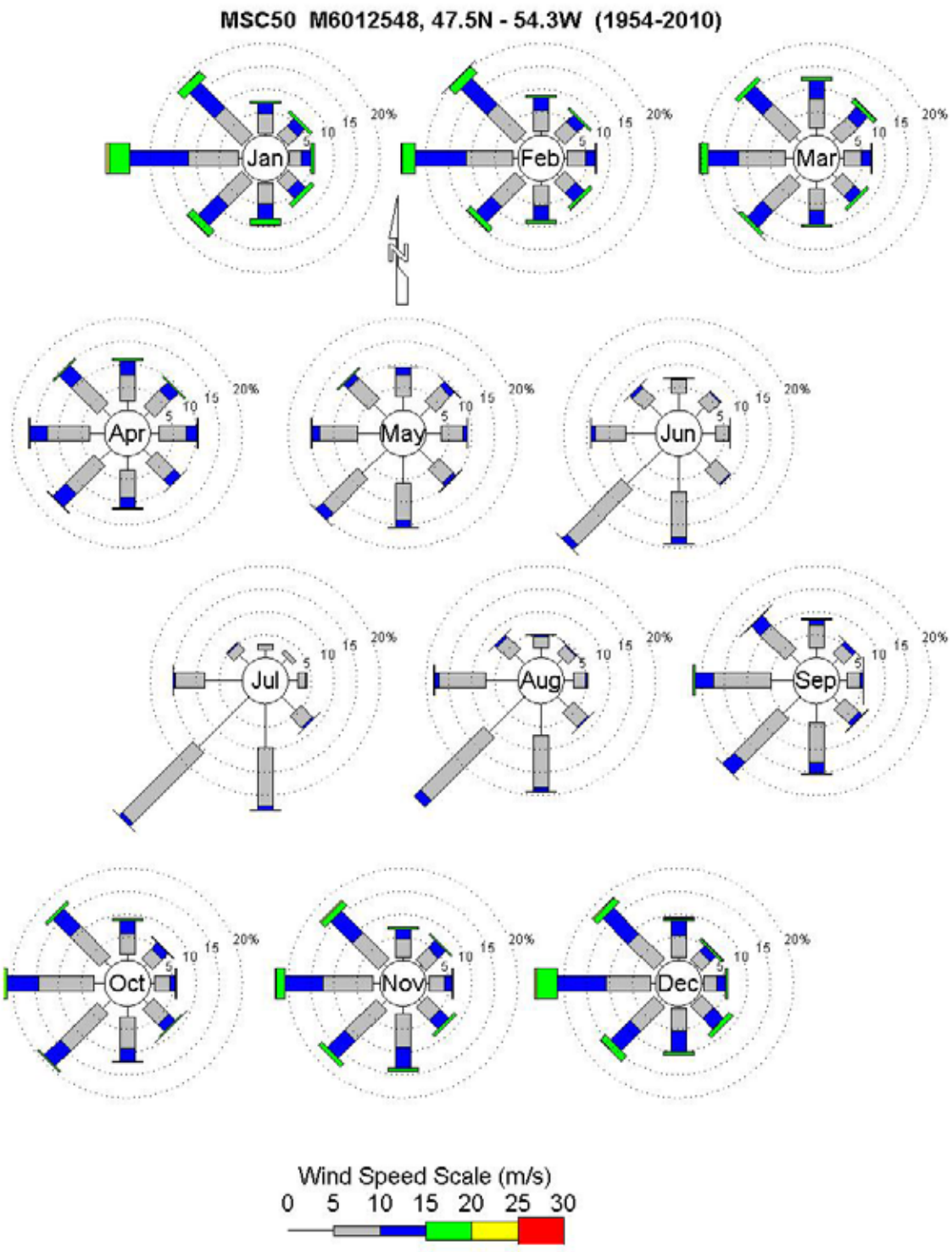

Source: DFO 2012a

Figure 4-10 Monthly Wind Roses for MSC50 node M6012148

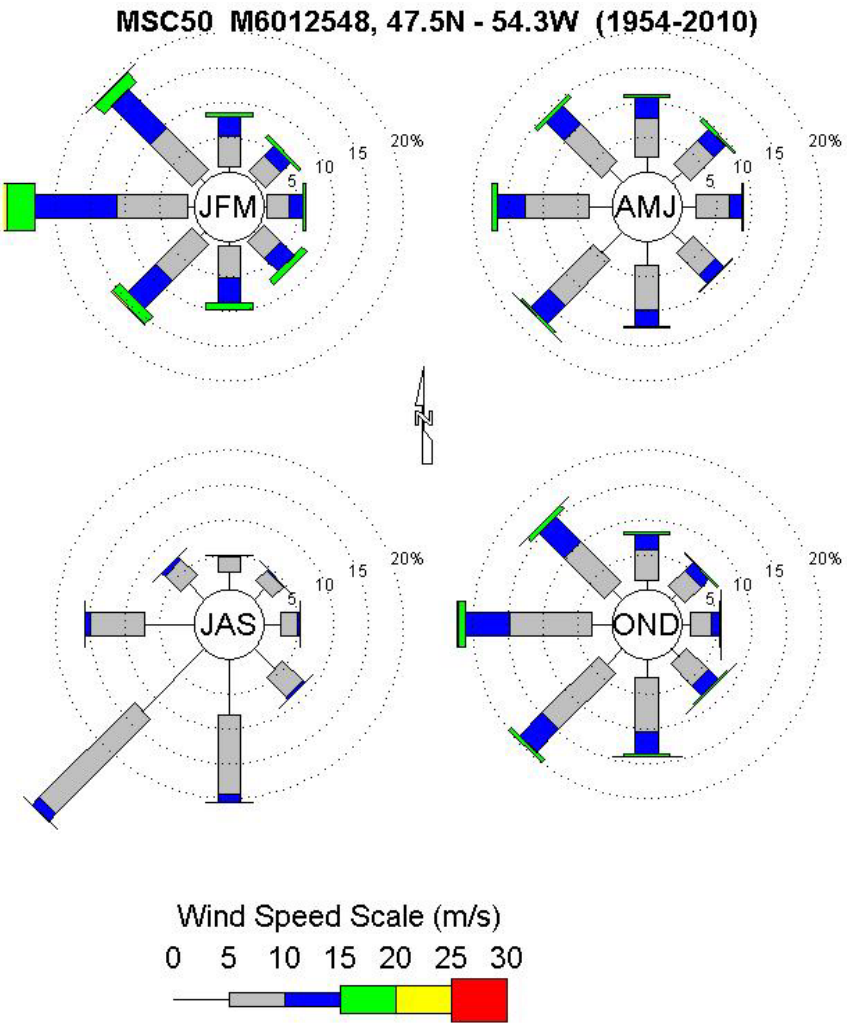

Source: DFO 2012a

Figure 4-11 Seasonal Wind Roses for MSC50 node M6012148

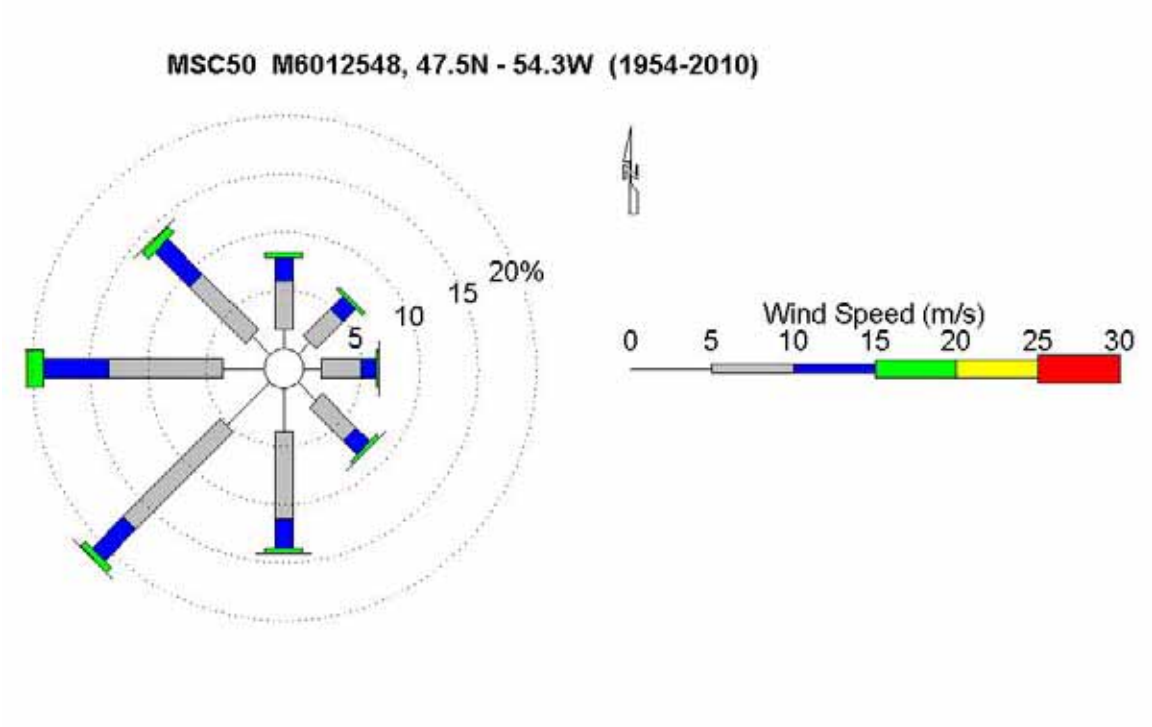

Source: DFO 2012a

Figure 4-12 Yearly Wind Rose for MSC50 node M6012148

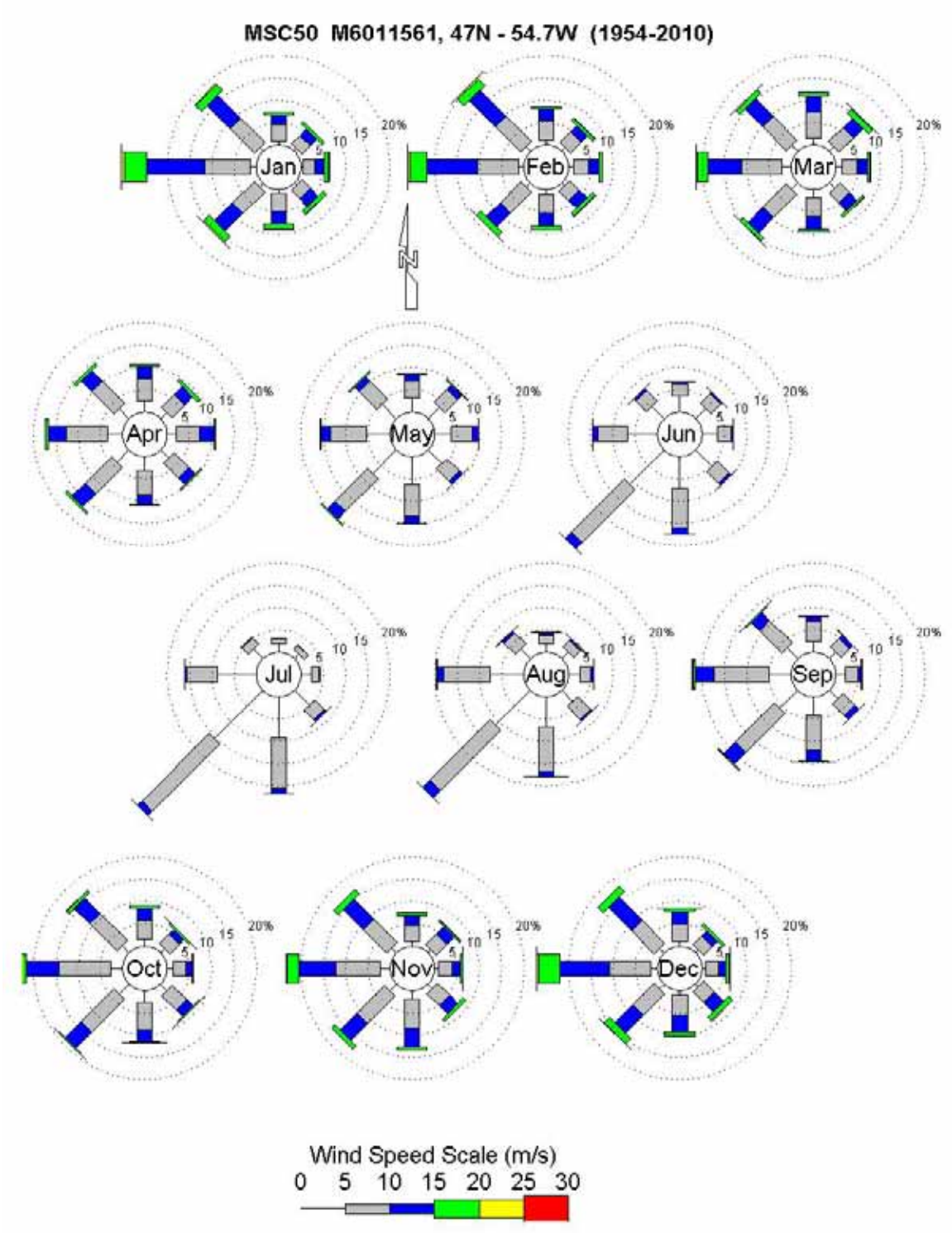

Source: DFO 2012a

Figure 4-13 Monthly Wind Roses for MSC50 node M6011561

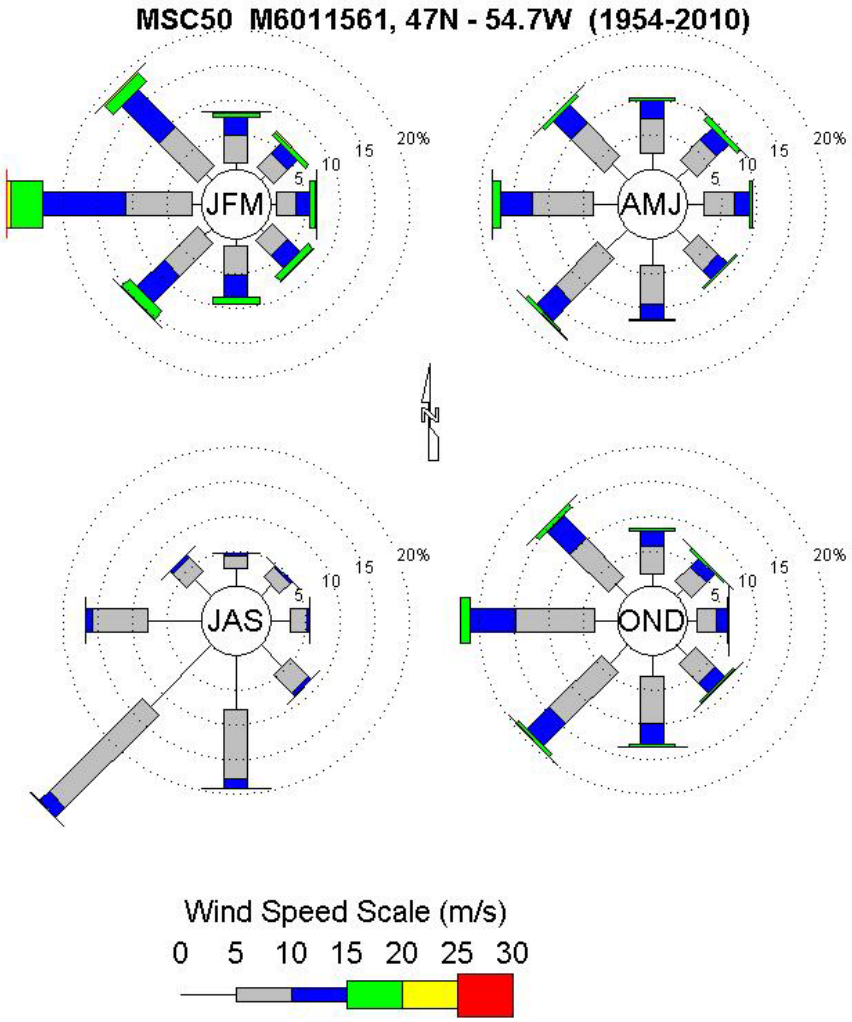

Source: DFO 2012a

Figure 4-14 Seasonal Wind Roses for MSC50 node M6011561

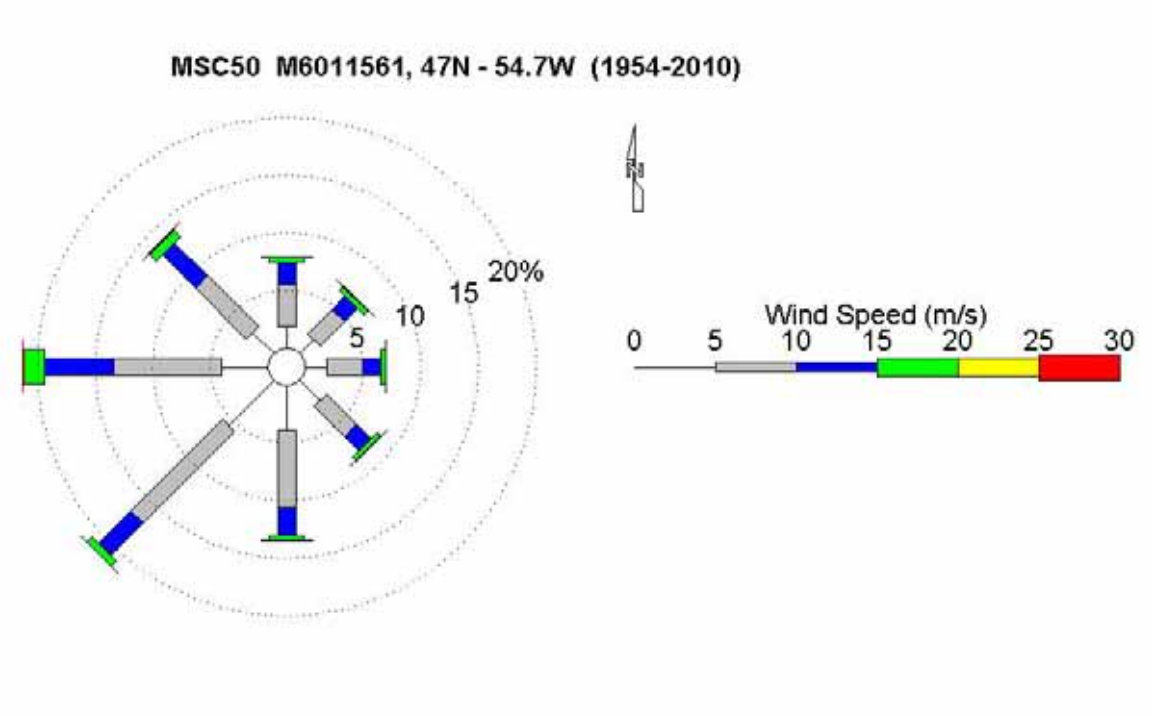

Source: DFO 2012a

Figure 4-15 Yearly Wind Rose for MSC50 node M6011561

Table 4-13 Monthly and Annual Mean Wind Speed Nearshore Placentia Bay

Month	Argentia-Placentia (m/s)	Marticot Island (m/s)	Winterland (m/s)
Jan	8.2	6.6	6.9
Feb	7.8	6.7	7.2
Mar	7.4	6.5	6.7
Apr	6.6	5.3	6.2
May	5.8	4.2	5.5
Jun	5.6	3.8	5.2
Jul	5.4	3.7	4.5
Aug	5.6	3.9	4.4
Sep	6.0	4.6	5.2
Oct	6.9	5.5	5.8
Nov	7.4	6.1	5.4
Dec	8.0	6.3	6.6
Annual	6.7	5.3	5.8
Source: Environment Canada 2012a			

Table 4-14 Monthly and Annual Maximum Wind Speed Nearshore Placentia Bay

Month	Argentia-Placentia (m/s)	Marticot Island (m/s)	Winterland (m/s)
Jan	30.3	26.4	25.3
Feb	30.8	28.3	27.2
Mar	24.2	31.9	22.2
Apr	25.8	27.2	22.2
May	23.3	25.8	23.6
Jun	20.6	18.6	18.1
Jul	21.7	20.6	19.4
Aug	22.2	22.2	20.6
Sep	26.4	29.7	25.3
Oct	28.6	27.8	22.8
Nov	28.1	25.8	20.6
Dec	30	27.2	25.8
Annual	30.8	31.9	27.2
Source: Environment Canada 2012a			

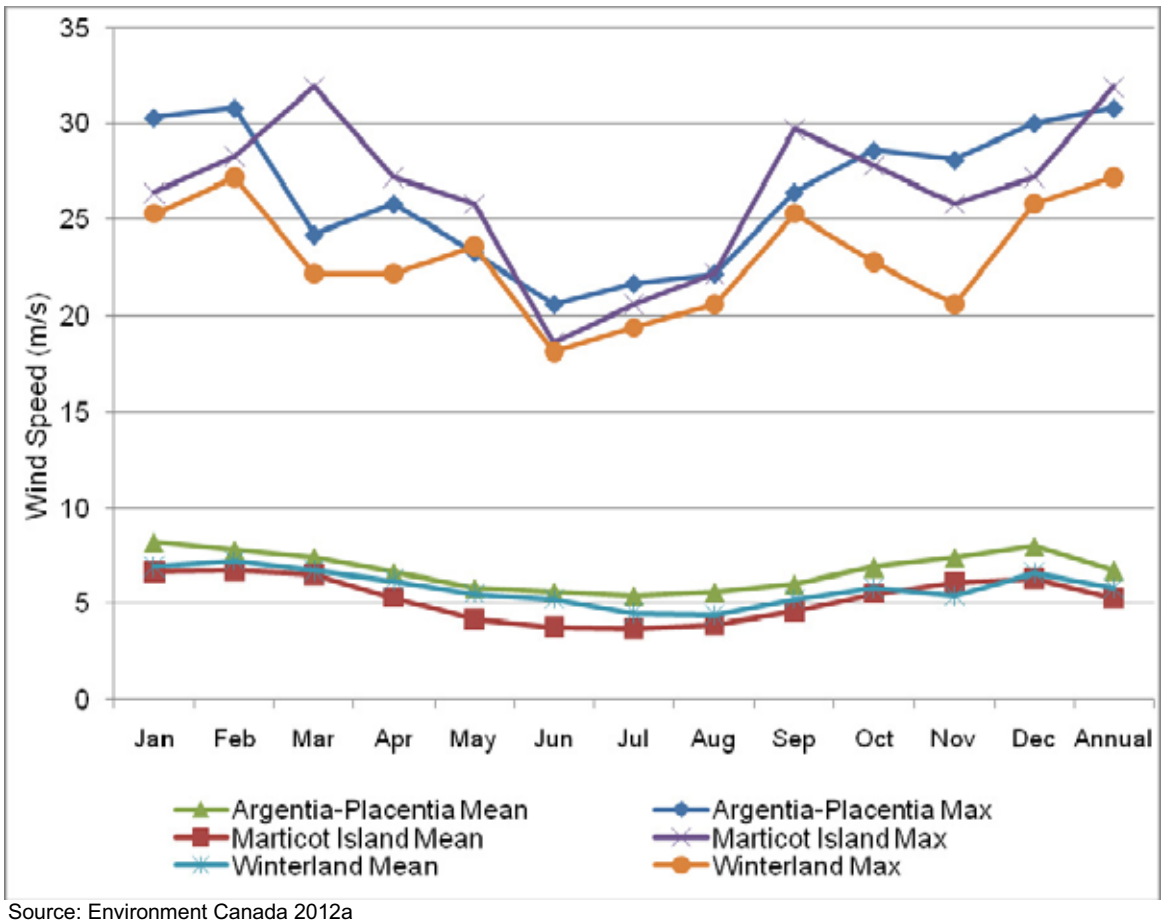

Source: Environment Canada 2012a

Figure 4-16 Monthly Average and Maximum Wind Speed for Nearshore Placentia Bay

4.2.1.4 Precipitation and Severe Weather

All of the Environment Canada sites used in the assessment of the Placentia Bay nearshore climatology, except Marticot Island, recorded precipitation amounts during their observation period, split between snowfall and rainfall values. While areas around Placentia Bay typically received the least amount of snowfall in Newfoundland and Labrador, annual averages can vary considerably across the region, depending on the year and type of weather events affecting the province. Typically, many storms during the winter track across the Island of Newfoundland, specifically Placentia Bay and the Avalon Peninsula, causing precipitation to frequently change over to rain. Strong Nor'easters, which track east of the Avalon Peninsula, tend to produce the most substantial snowfall and highest winds for eastern Newfoundland in the winter and typically occur, on average, a few times each year.

Another source of snowfall in the region is experienced when cold west-southwesterly winds behind departing low pressure systems initiate the development of ocean-effect snow squalls, which can occasionally become severe over the Burin and southern Avalon Peninsulas, particularly from December to March.

Using all available datasets for precipitation amounts near Placentia Bay, the average monthly rainfall and snowfall values were determined and the results are plotted in Figure 4-17 and presented in Table 4-15. Based on these results, the heaviest snowfall typically peaks in January, and then gradually diminishes through early May. Snow rarely occurs from June through September, with the first snowfall generally beginning mid to late October. On average, snow makes up only 10 to 15 percent of the total annual precipitation experienced around Placentia Bay.

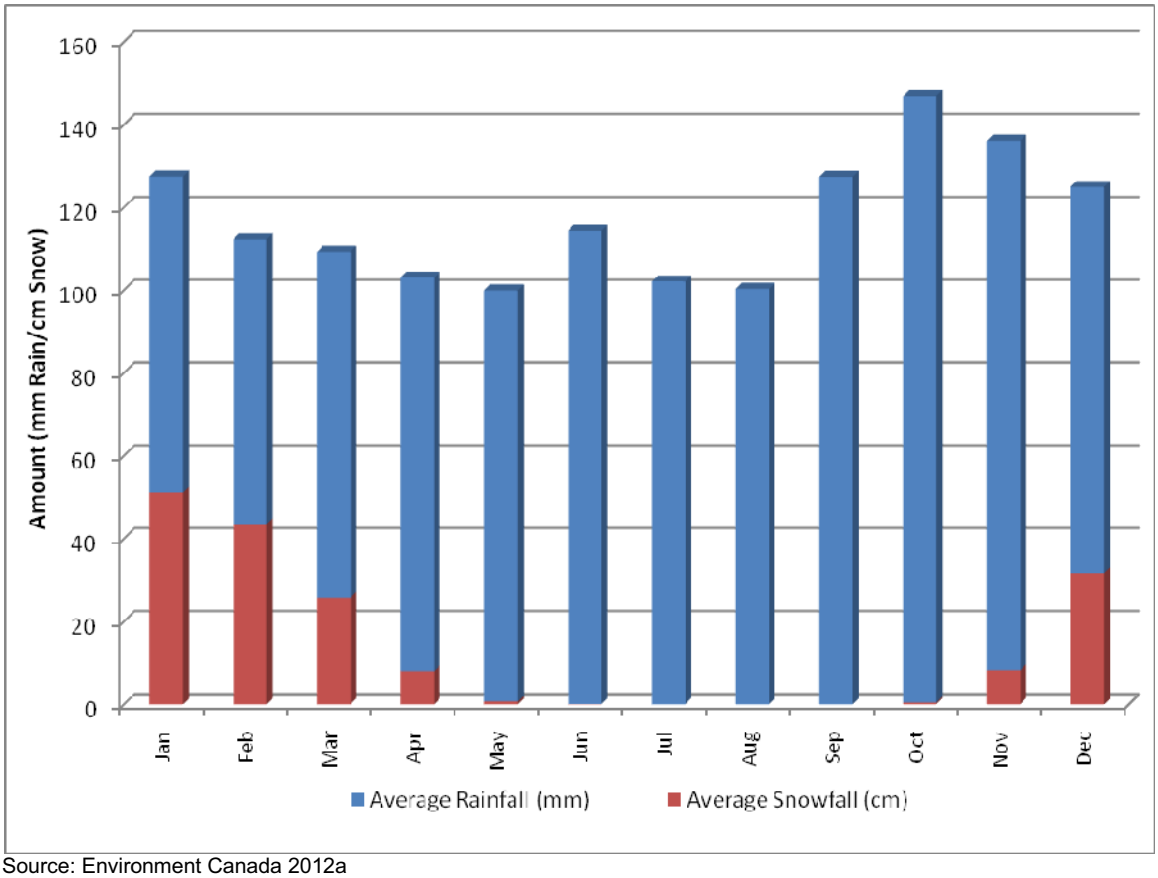

Source: Environment Canada 2012a

Figure 4-17 Average Monthly Snowfall and Rainfall Amounts for Nearshore Placentia Bay

Table 4-15 Average Monthly Snowfall and Rainfall Amounts for Nearshore Placentia Bay

Month	Rainfall (mm)	Snowfall (cm)	Total Precip (mm)
Jan	76.3	51.1	124.0
Feb	68.8	43.6	108.7
Mar	83.4	25.8	105.7
Apr	95.0	8.0	98.8
May	99.2	0.7	96.9
Jun	114.3	0.0	110.6
Jul	102.1	0.0	101.0
Aug	100.3	0.0	99.0
Sep	127.3	0.0	123.0
Oct	146.3	0.4	142.6
Nov	127.9	8.2	133.0
Dec	93.3	31.6	122.2
Annual	1234.3	169.4	1365.5

Source: Environment Canada 2012a

Monthly rainfall

In fall values typically average at least 90 mm, except during the winter months of January through March, when the peak snowfalls occur. On average, the rainiest season for Placentia Bay is in the fall months (September to November), when monthly rainfall is usually between 125 to 150 mm. An important contributor to these heavy rain amounts in the fall is the presence of tropical systems that track near or across Newfoundland, transporting copious amounts of tropical moisture to the region.

Daily total precipitation amounts (combination of rain and snow accumulations) from eight Environment Canada weather stations on the southwestern Avalon Peninsula and Burin Peninsula were assessed to determine the maximum recorded daily precipitation. Since each station has different periods of record, the maximum amount from all sites was extracted for each month to determine the possible daily rate. The results are plotted in Figure 4-18. The lowest maximum daily amounts have been measured in December and January, while the maximum was in July. This daily amount of nearly 190 mm was recorded in Argentia during Tropical Storm Chantal in 2007.

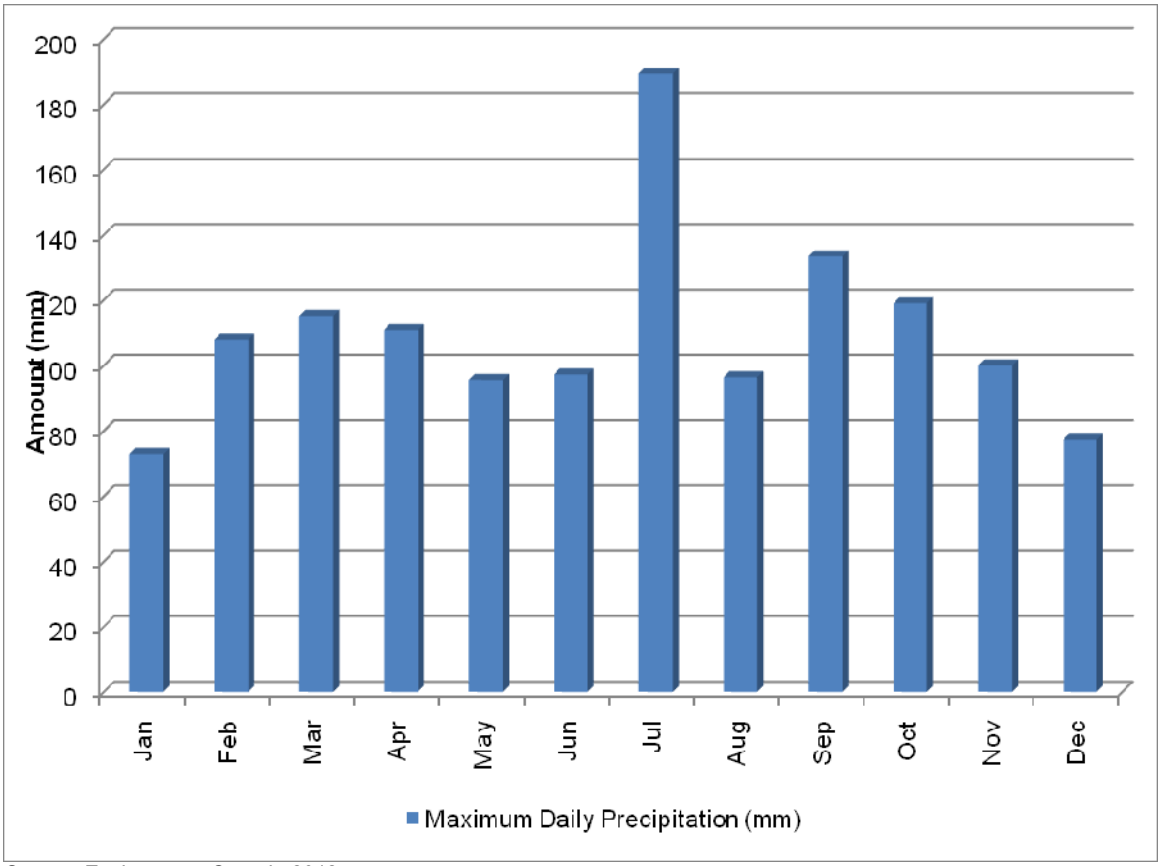

Source: Environment Canada 2012a

Figure 4-18 Maximum Daily Precipitation by Month

While eastern Newfoundland often receives the most freezing rain events in all of Canada (National Climate Data and Information Archive Weather Winners 2003), these occurrences are less frequent over Placentia Bay, as freezing precipitation typically occurs when north to northeasterly winds blow over the land (for example, areas of northeastern Newfoundland from St. John's to Twillingate). Occasionally through the winter months, warm fronts associated with low pressure systems sweep across Placentia Bay and often produce a period of freezing precipitation (freezing rain or freezing drizzle) during the transition from snow to rain.

The Environment Canada weather station in Argentia was staffed and reported each hour from 1953 to 1986; therefore, statistics were calculated on the average number of monthly and annual hours where each precipitation type was reported. Additionally, the average occurrence of thunderstorms for Argentia was determined. These results are shown in Table 4-16. Based on these calculations, freezing precipitation normally occurs 22 hours each year, with the peak occurrence reported in February and March.

Thunderstorm activity is rare in Newfoundland, especially in eastern sections, due to the cold ocean waters, but, on average, thunderstorms are observed six hours each year, with the most likely occurrence in the summer (July-August).

Table 4-16 Average Number of Hours Each Month and Year All Precipitation in Argentia

Month	Snow	Rain	Freezing Rain/ Drizzle	Ice Pellets/ Sleet	Thunderstorms
Jan	122.2	49.8	4.3	3.5	0.0
Feb	113.0	41.2	6.0	1.6	0.0
Mar	98.5	50.2	6.2	3.0	0.0
Apr	48.8	64.9	2.3	1.4	1.3
May	12.8	74.7	0.1	0.6	0.5
Jun	0.3	64.6	0.0	0.2	0.8
Jul	0.0	52.8	0.0	0.0	1.0
Aug	0.0	60.9	0.0	0.0	1.7
Sep	0.1	63.9	0.0	0.0	0.6
Oct	3.8	82.8	0.0	0.2	0.2
Nov	23.4	83.5	0.2	1.0	0.3
Dec	88.8	59.3	2.5	1.6	0.0
Annual	511.7	748.6	21.6	13.2	6.4
Source: Environment Canada 2012a					

The ICOADS database contains observations from Placentia Bay of all precipitation types, as well as thunderstorm occurrence, where each occurrence of a weather state is recorded as an event, but precipitation amounts are not available. The frequency of occurrence of the different precipitation types and thunderstorms has been calculated as a percentage of the total monthly and annual weather observations for the full recording period (1960 to 2011). The statistics are presented in Table 4-17 and plotted in Figure 4-19.

The most commonly observed precipitation types are rain and snow, while freezing precipitation occurs far less frequently. The monthly frequency of rain events is lowest in February (6.2 percent), correlating with the peak in snowfall occurrence (21.5 percent). Thunderstorms occur far less over Placentia Bay than the surrounding land area, but have the potential to occur throughout the year, particularly in the summer months. Hail is typically associated with thunderstorms, although some months show a higher frequency of hail than thunderstorms, likely due to observers inaccurately reporting ice pellets as hail (Figure 4-20).

Table 4-17 Frequency of Occurrence for Several Precipitation Types and Thunderstorms

Month	Rain/ Drizzle	Freezing Rain/ Drizzle	Rain/ Snow Mixed	Snow	Hail	Thunderstorm	Total
Jan	7.9	0.4	1.0	18.3	0.5	0.1	28.2
Feb	6.2	0.8	0.7	21.5	0.7	0.0	30.0
Mar	7.8	0.7	0.8	14.7	0.3	0.0	24.3
Apr	9.7	0.3	0.5	5.0	0.1	0.1	15.7
May	10.7	0.0	0.2	1.0	0.0	0.0	12.1
Jun	8.9	0.0	0.1	0.0	0.1	0.0	9.2
Jul	8.4	0.0	0.1	0.2	0.0	0.1	8.8
Aug	8.7	0.0	0.0	0.1	0.1	0.2	9.2
Sep	10.8	0.0	0.1	0.1	0.1	0.2	11.3
Oct	14.3	0.0	0.2	0.3	0.1	0.1	15.1
Nov	12.8	0.1	0.5	3.1	0.3	0.1	16.9
Dec	9.7	0.2	1.1	12.8	0.4	0.0	24.3
Annual	9.7	0.2	0.4	6.0	0.2	0.1	16.7
Source: ICOADS 2012							

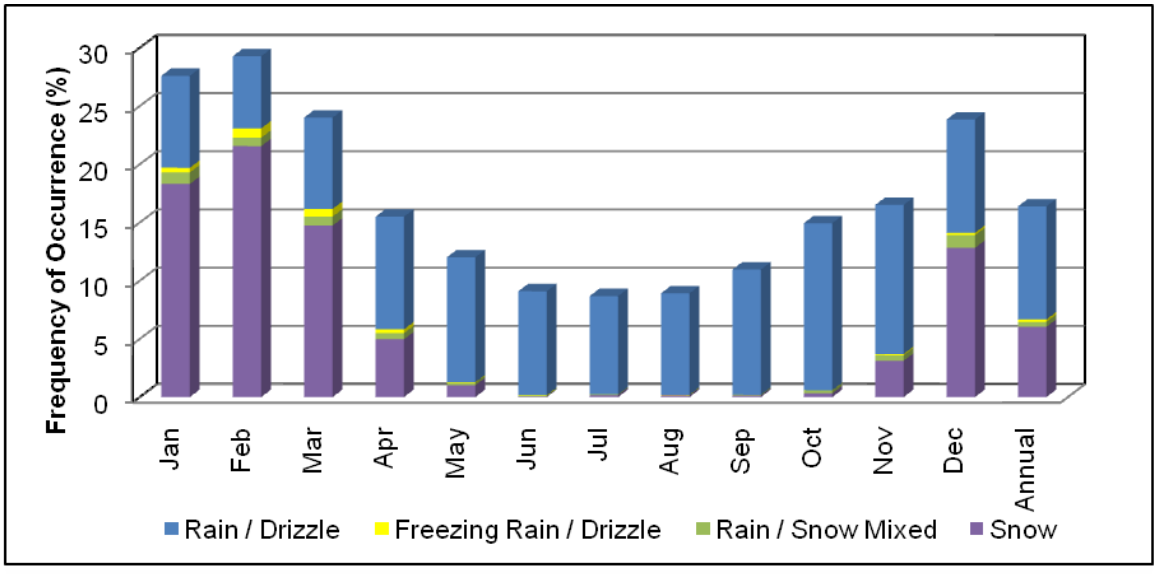

Source: ICOADS 2012

Figure 4-19 Frequency of Occurrence of Precipitation Types

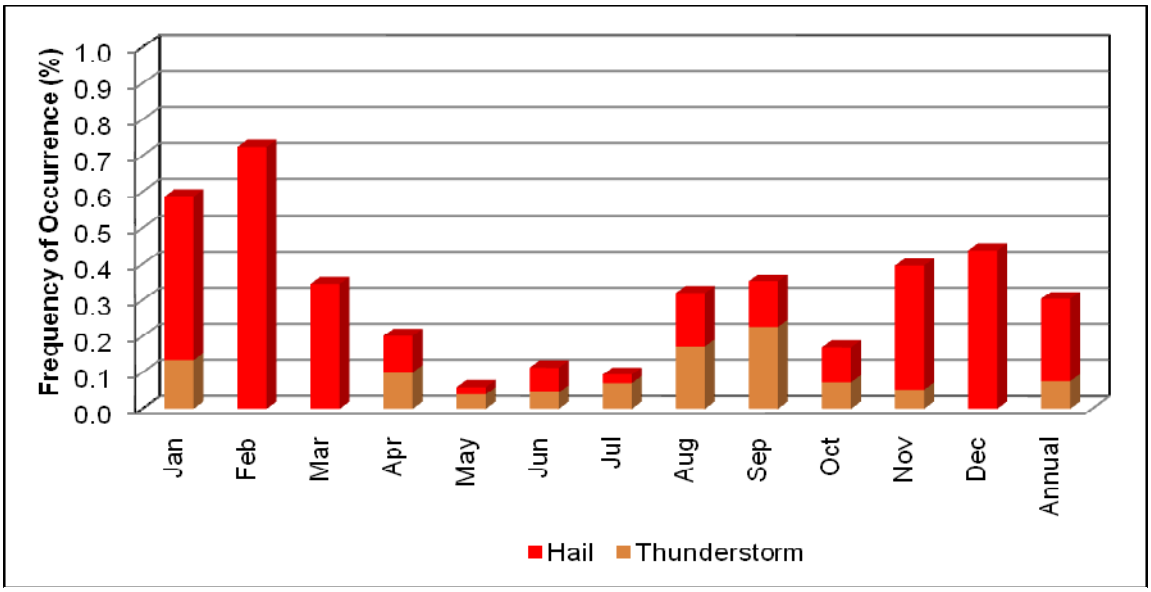

Source: ICOADS 2012

Figure 4-20 Frequency of Occurrence of Hail and Thunderstorms

4.2.1.5 Visibility

Visibility in Placentia Bay can be affected by daylight hours, blowing snow and precipitation, but the most important contributor to reduced visibility is fog and mist. There are several processes that cause fog to develop, but the most common in Placentia Bay is advection fog. This type of fog develops when warm air moves over the colder water, causing condensation to take place. Because the water does not warm as quickly as land, fog is less frequent over areas surrounding Placentia Bay, but it is a regular occurrence, especially in the spring and summer as the fog moves onshore from the bay. The most common wind direction causing fog over Placentia Bay is from southeast to southwest, which funnels warmer air over the region.

Visibility observations were available from Environment Canada stations in Argentia (1953 to 1986) and Winterland (1999 to 2011). As expected, low visibility occurs far less frequently in Winterland, as the location is inland over the Burin Peninsula and is not exposed to an onshore flow when winds originate from the south and southwest.

In Argentia, the highest frequency of good (greater than 10 km) visibility occurs in the fall, when the land/water temperature contrast is least pronounced and snow has yet to begin. Meanwhile, the greatest occurrence of reduced visibilities occurs during the late spring and early summer, when fog often dominates the south coast of Newfoundland with the land/water temperature contrast at its highest. At this time of year, southwesterly winds often bring warm air masses over the region, while the ocean waters have warmed only marginally. This leads to frequent extensive fog banks. Poor visibility conditions (less than 2 km) increase through the spring and peak in July, when it is observed over 30 percent of the time. Conversely, reduced visibility in the winter and early spring can sometimes be attributed to fog and mist, but is typically associated with snow and blowing snow. Visibility observations from Argentia have been classified as

very poor (less than 0.5 km), poor (greater than or equal to 0.5 km and less than 2.0 km), fair (greater than or equal to 2.0 km and less than 10.0 km) or good (greater than 10 km). The monthly and annual frequencies of occurrence of each visibility classification for Argentia are presented in Table 4-18 and plotted in Figure 4-21.

Table 4-18 Frequency of Good, Fair, Poor and Very Poor Visibility States for Argentia

Month	Total % of Visibility >10 km	Total % of Visibility Between 2 to 10 km	Total % of Visibility Between 0.5 to 2 km	Total % of Visibility <0.5 km
Jan	68.9	22.9	6.0	2.2
Feb	69.4	22.1	6.2	2.3
Mar	67.6	23.4	6.1	2.9
Apr	67.6	23.5	5.3	3.6
May	64.8	21.1	7.2	6.9
Jun	55.7	20.6	10.9	12.8
Jul	48.2	21.4	14.3	16.1
Aug	62.1	19.6	9.6	8.8
Sep	73.6	16.5	5.0	5.0
Oct	76.4	16.9	3.5	3.2
Nov	77.7	17.5	2.9	1.9
Dec	74.8	18.8	4.6	1.8
Annual	67.2	20.4	6.8	5.6
Source: Environment Canada 2012a				

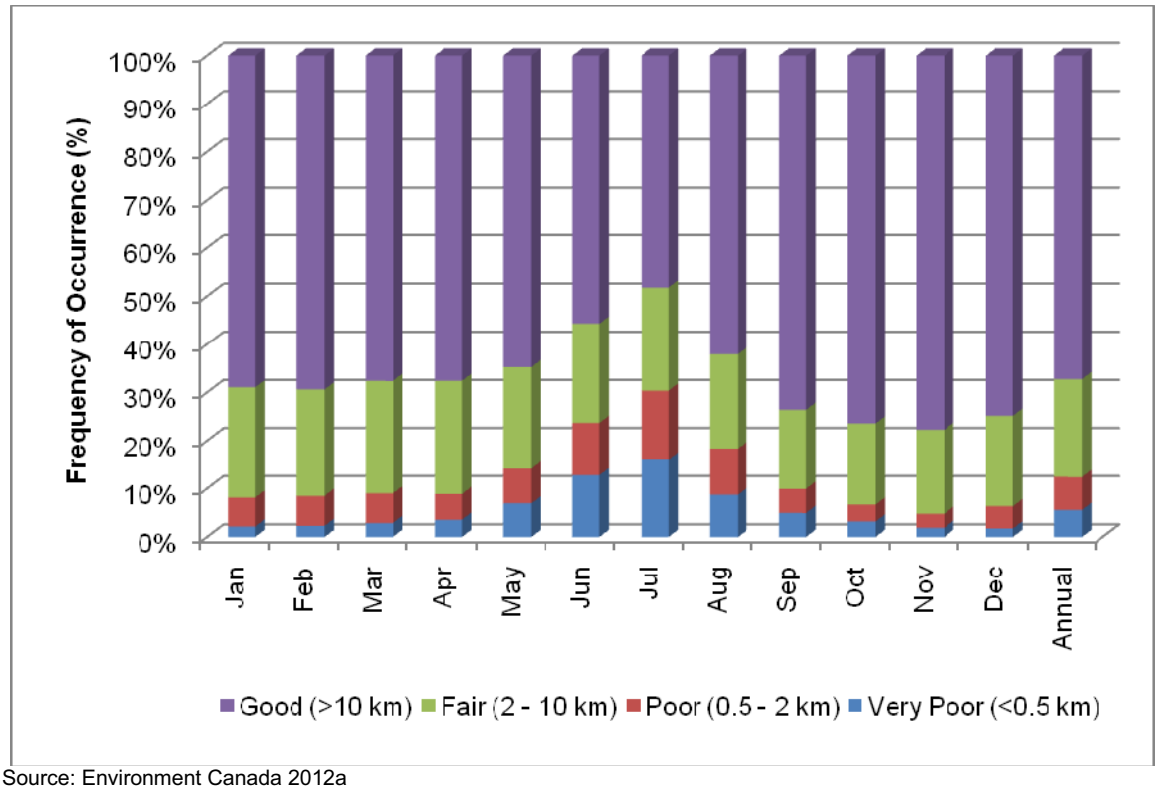

Source: Environment Canada 2012a

Figure 4-21 Frequency of Good, Fair, Poor and Very Poor Visibility States for Argentia

Visibility data in Winterland display different results than those just across Placentia Bay, in Argentia, due to various reasons. With its inland location and being less exposed to fog banks coming onshore with warm south to southwesterly winds, fog is substantially less prevalent in eastern sections of the Burin Peninsula. Additionally, ocean-effect snow squalls occur more frequently over the Burin Peninsula in the winter months, leading to higher rates of reduced visibility in the winter than over the southwestern Avalon Peninsula.

In Winterland, as with Argentia, the highest frequency of good visibility occurs in the fall, when fog is less prevalent and snow has yet to begin. Meanwhile, the greatest occurrence of fair and poor visibilities occurs during the winter months. Very poor visibility reaches its peak in July as dense fog surrounding the Burin Peninsula eventually engulfs the region. The monthly and annual frequencies of occurrence of each visibility classification for Winterland are presented in Table 4-19 and plotted in Figure 4-22.

Table 4-19 Frequency of Good, Fair, Poor and Very Poor Visibility States for Winterland

Month	Total % of Visibility >10 km	Total % of Visibility Between 2 to 10 km	Total % of Visibility Between 0.5 to 2 km	Total % of Visibility <0.5 km
Jan	68.5	19.3	10.0	2.1
Feb	64.2	19.8	12.2	3.8
Mar	76.2	16.1	5.9	1.7
Apr	77.3	14.4	5.7	2.6
May	79.1	13.9	4.5	2.6
Jun	76.9	14.3	5.9	2.9
Jul	70.2	18.1	6.6	5.0
Aug	78.2	16.0	3.6	2.2
Sep	81.3	13.5	3.1	2.1
Oct	81.6	14.4	2.6	1.4
Nov	79.2	15.0	4.1	1.7
Dec	73.2	18.6	6.7	1.5
Annual	75.5	16.1	5.9	2.5
Source: Environment Canada 2012a				

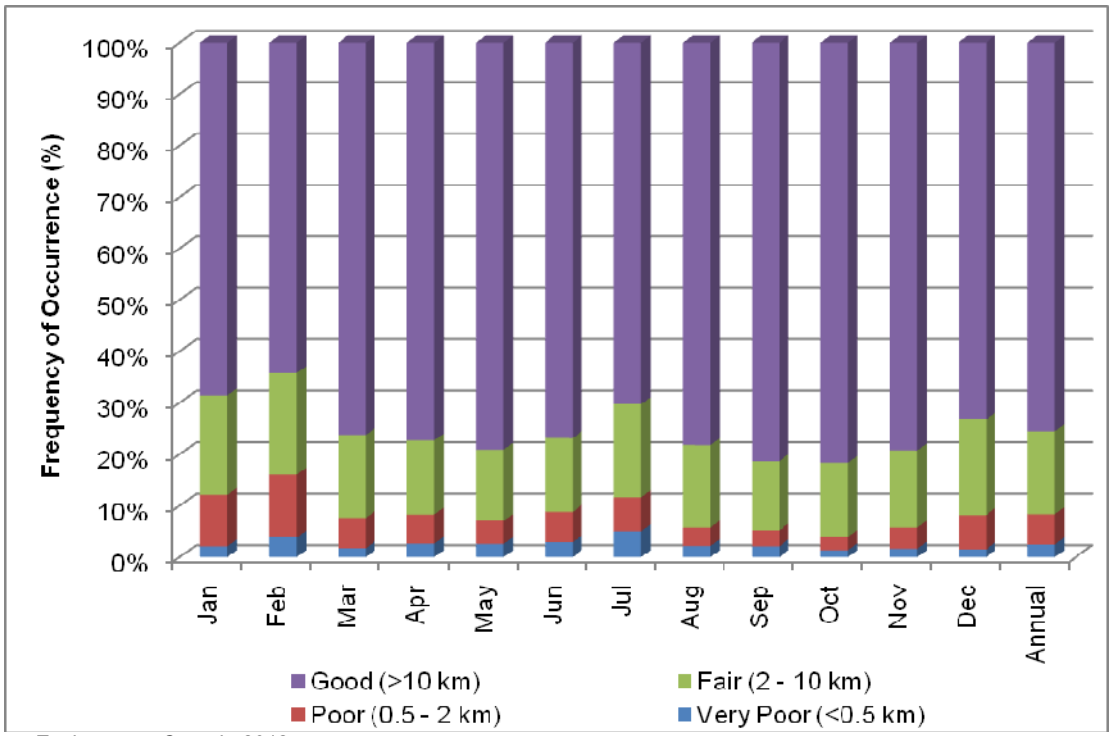

Source: Environment Canada 2012a

Figure 4-22 Frequency of Good, Fair, Poor and Very Poor Visibility States for Winterland

Visibility observations from the ICOADS dataset were assessed for Placentia Bay. As expected, the frequency of reduced visibilities (poor and very poor) is substantially higher over the open waters of the bay, than over the nearshore area. The peak of reduced visibility occurs in the summer (July), when poor/very poor conditions are experienced 36.5 percent of the time. During the fall months, good visibility is observed more frequently, between 55 and 60 percent of the time. The monthly and annual frequencies of occurrence of each visibility state is presented in Table 4-20 and plotted in Figure 4-23.

Table 4-20 Frequency of Good, Fair, Poor and Very Poor Visibility States

Month	Total % of Visibility >10 km	Total % of Visibility Between 2 to 10 km	Total % of Visibility Between 0.5 to 2 km	Total % of Visibility <0.5 km
Jan	44.5	44.5	7.3	3.7
Feb	41.5	47.0	7.3	4.1
Mar	44.4	43.4	7.2	5.0
Apr	43.8	36.7	8.4	11.1
May	43.2	33.0	8.5	15.3
Jun	37.8	29.9	10.1	22.2
Jul	33.4	30.2	9.3	27.2
Aug	45.0	30.2	8.6	16.2
Sep	57.4	30.2	5.3	7.1
Oct	58.3	33.7	4.0	4.0
Nov	56.5	35.2	4.0	4.3
Dec	50.9	41.7	4.5	2.9
Annual	46.4	36.2	7.1	10.3
Source: ICOADS 2012				

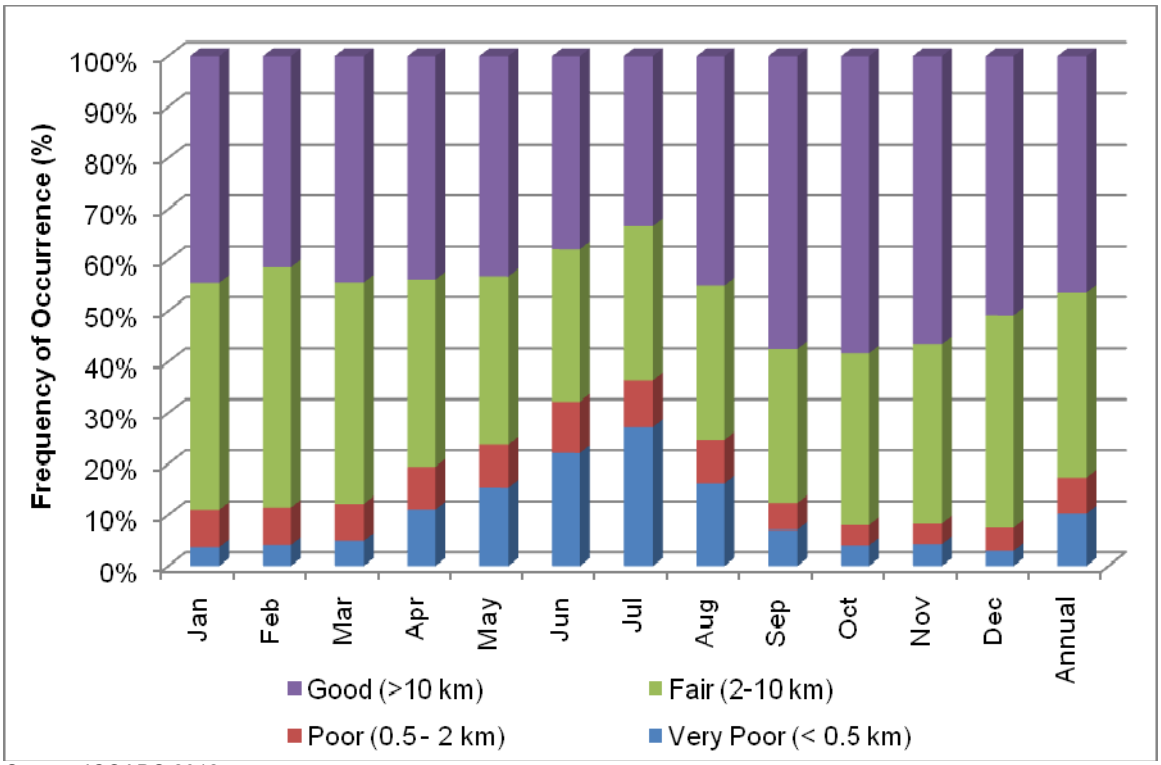

Source: ICOADS 2012

Figure 4-23 Frequency of Good, Fair, Poor and Very Poor Visibility States

4.2.1.6 Vessel Icing Potential

The formation of vessel icing, also known as freezing spray, is a marine weather phenomenon produced by the combination of several parameters, including air temperature, sea surface temperature, wind speed, wave height and precipitation.

Standardized algorithms were developed by Overland (1990) for the prediction of sea spray vessel icing. These algorithms were based primarily on reports from vessels that were 20 to 75 m in length and the heat balance equation of an icing surface. The algorithm presented by Overland (1990) is:

$$PPR = V_a (T_f - T_a) / 1 + 0.3 (T_w - T_f)$$

where,

PPR = Icing Predictor

Va = Wind Speed (m/s)

Tf = Freezing point of seawater (typically -1.7°C or -1.8°C)

Ta = Air temperature (°C)

Tw = Sea surface temperature (°C)

There are four classes of vessel icing severity, based on the rate (cm/h), as shown in Table 4-21.

Table 4-21 Vessel Icing Class and Rate

PPR	<0	0 to 22.4	22.4 to 53.3	53.3 to 83.0	>83.0
Icing Class	None	Light	Moderate	Heavy	Extreme
Icing Rates (cm/h)	0	<0.7	0.7 to 2.0	2.0 to 4.0	>4.0
Source: Overland 1990					

The algorithm has been used to derive an estimate of icing potential in the Placentia Bay area by using air and sea temperatures, plus wind speed data from ICOADS (1960 to 2011). The results have been sorted into the four vessel icing classes listed in Table 4-21 and are presented in monthly and annual frequencies of occurrence in Figure 4-24. Vessel icing is expected to occur between late November and early April, with the maximum frequency of 35 percent occurring in February. During February, extreme icing rates are expected 1.2 percent of the time, heavy icing 2.2 percent, moderate icing 7.5 percent and light icing nearly 24 percent of the time.

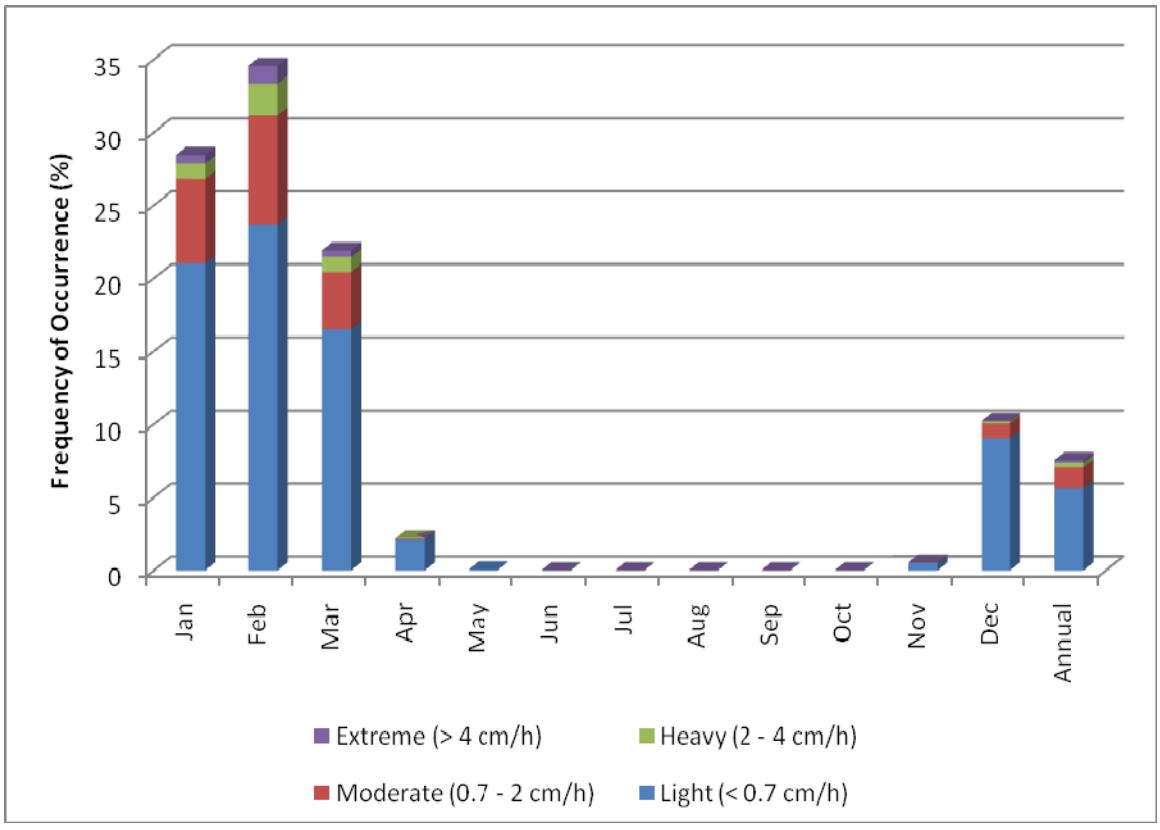

Source: ICOADS 2012.

Figure 4-24 Frequency of Occurrence of Vessel Icing Potential in Placentia Bay

4.2.1.7 Tropical Systems

While hurricanes making landfall in Newfoundland are rare, tropical systems, whether they are weakened hurricanes, tropical storms or post-tropical (extra tropical) storms, affect Newfoundland and Labrador, on average, once or twice each year. Hurricanes and tropical systems feed off warm ocean waters south of the Gulf Stream. Since Placentia Bay lies north of the Gulf Stream, tropical systems tend to weaken considerably once they approach Newfoundland and Labrador due to the colder water temperatures. On occasion, tropical storms and hurricanes maintain their strength or weaken slowly as they approach Newfoundland for various reasons. Two important possibilities for stronger tropical systems affecting Newfoundland are the forward speed of the system and sea surface temperature anomalies. If the tropical storm/hurricane is travelling at a higher than average speed, the system does not have time to weaken, despite the cooler waters entering its core. Additionally, if sea surface temperatures south of Newfoundland are warmer than average, especially late in the summer and early fall, the storm is able to survive slightly longer as it approaches Atlantic Canada.

Historical tropical system tracks were reviewed from National Hurricane Center (NHC) (2012) and the Canadian Hurricane Centre (CHC) (2012) data from 1954 to 2011 to determine the number of tropical systems that have tracked near, or across, Newfoundland and Labrador. The results are presented in Table 4-22 and plotted in Figure 4-25.

Table 4-22 Tropical Systems Affecting Newfoundland and Labrador by Decade

Decade	Number of Tropical Systems
1954-1959	7
1960-1969	13
1970-1979	13
1980-1989	9
1990-1999	14
2000-2009	23
2010-2011	5
Source: CHC 2012; NHC 2012	

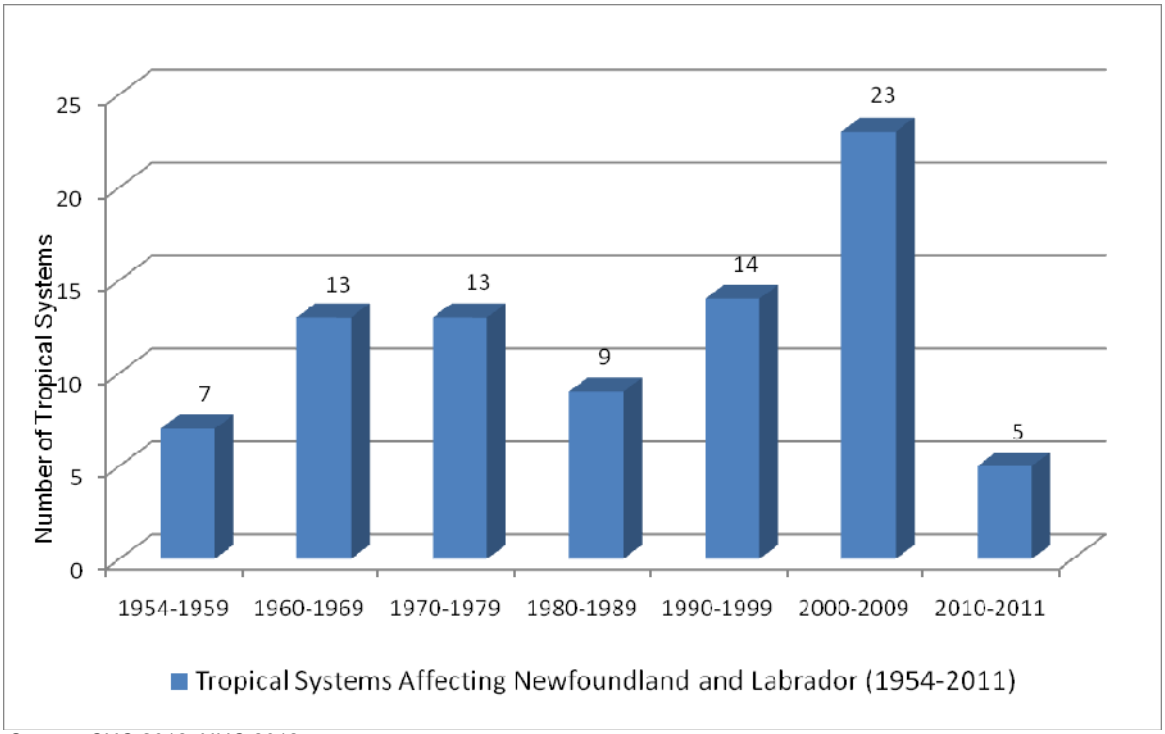

Source: CHC 2012; NHC 2012

Figure 4-25 Number of Tropical Systems Affecting Newfoundland-Labrador by Decade

Tropical systems can affect Newfoundland anytime during the Atlantic hurricane season (June 1 to November 30), but the most activity generally occurs in the fall season (September and October). One of the main reasons for the increased activity during this time of year is the shift of the Bermuda High to the east, allowing systems over the Caribbean to track northward towards Atlantic Canada. The Bermuda High is a dominant ridge of high pressure over the Atlantic typically centred near Bermuda, which guides weather systems over the southern Atlantic Ocean towards the southeastern United States, and provides the dominant southwesterly flow to eastern Canada during the summer. The sea surface temperatures south of Newfoundland typically reach their peak in late September, allowing systems that approach from the south to maintain their strength as they track towards Newfoundland. The number of tropical systems that have affected Newfoundland and Labrador, by month, from 1954 to 2011, are plotted in Figure 4-26.

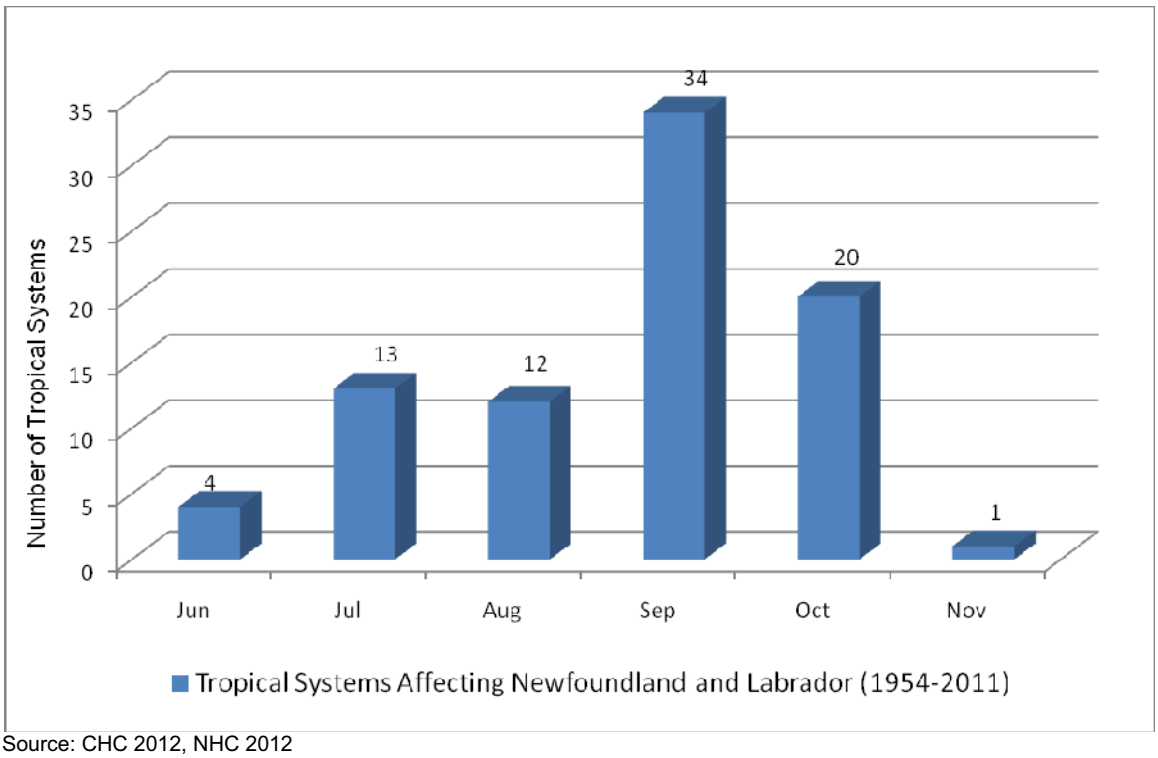

Source: CHC 2012, NHC 2012

Figure 4-26 Number of Tropical Systems Affecting Newfoundland-Labrador by Month

Tropical storms, in any form, and hurricanes rarely make landfall in Newfoundland, but many track across the marine districts around Atlantic Canada, including Placentia Bay. All tropical systems that have tracked through the Environment Canada South Coast marine district (which encompasses Placentia Bay) since 1954 are displayed in Figure 4-27. Additionally, the frequency of tropical storms tracking over Placentia Bay, by decade and month, are plotted as Figures 4-28 and 4-29. As noted above, there is an apparent discernible trend in the number of tropical systems that have tracked across southeastern Newfoundland since 2000. From 1954 to 1999, there were 11 tropical systems that tracked through Placentia Bay. Since 2000 through 2011, 12 storms have moved across Placentia Bay, averaging one per year.

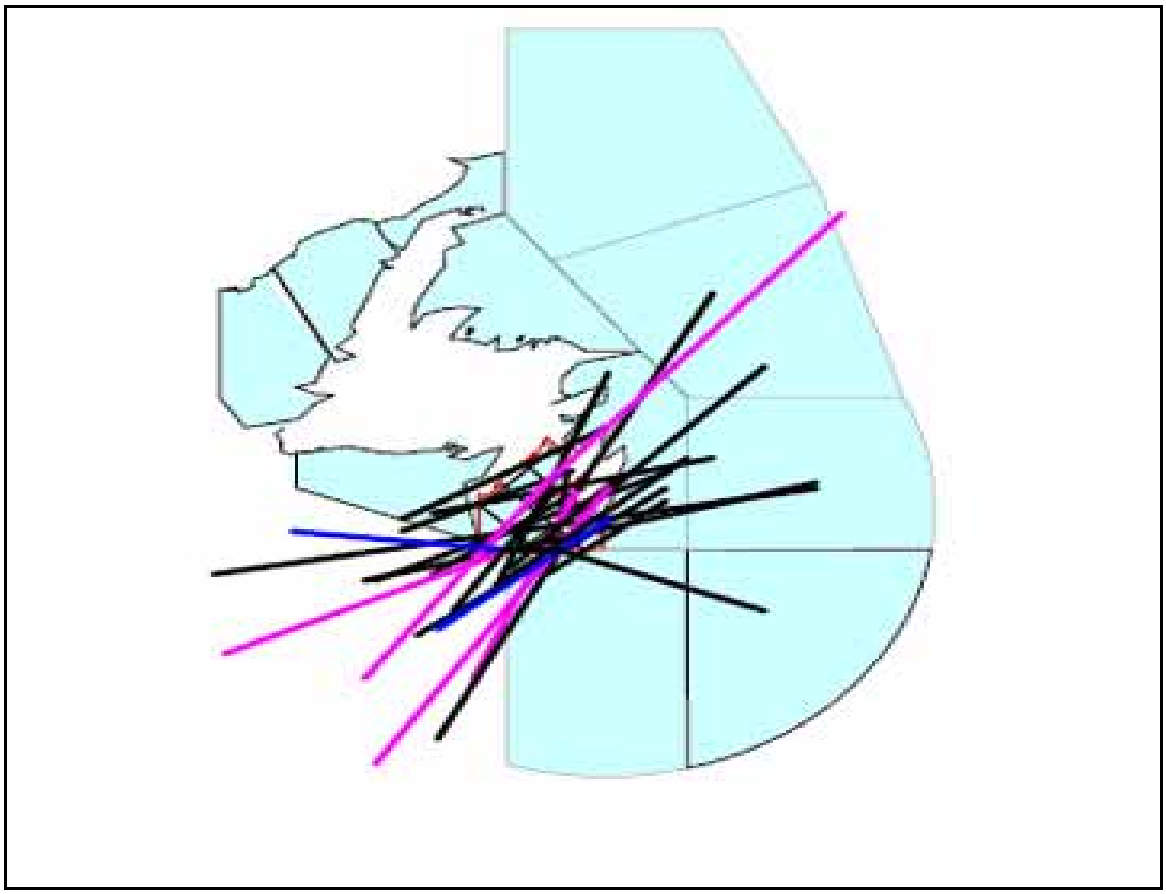

Source: CHC 2012
Note: Track colours: Magenta - hurricanes category 1; Blue - tropical storms; Black - storm transitioned to extra-tropical

Figure 4-27 Historical Tropical Tracks in Environment Canada, South Coast Marine Area

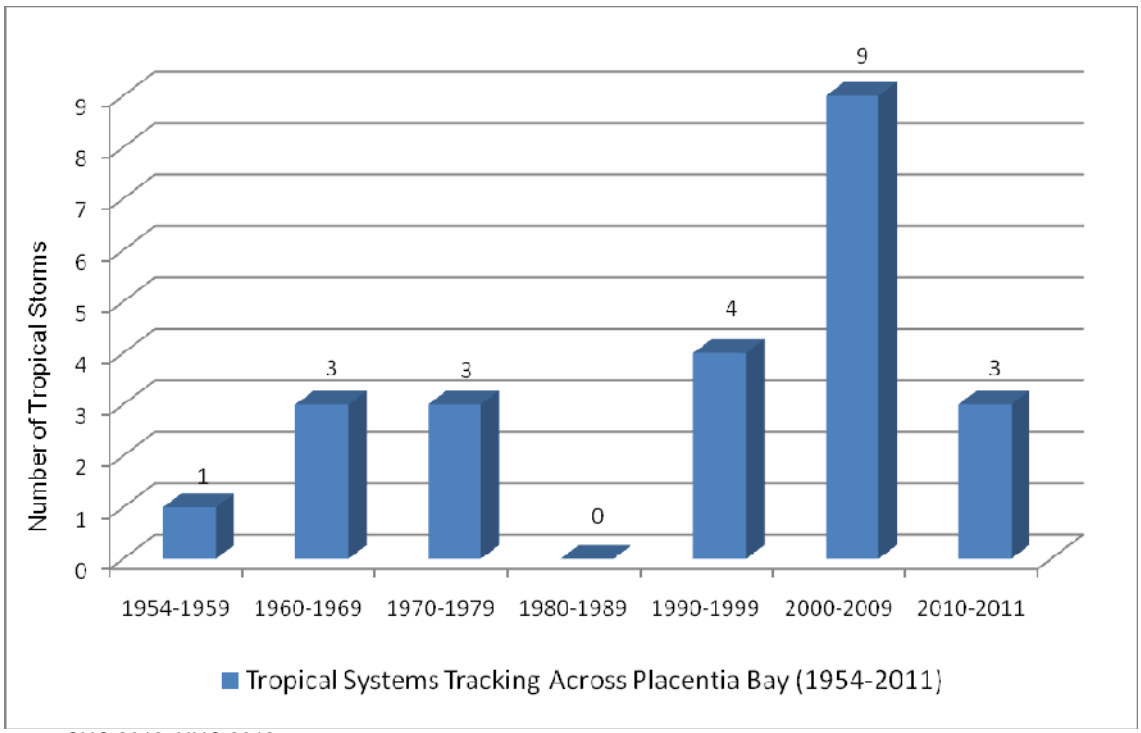

Source: CHC 2012; NHC 2012

Figure 4-28 Number of Tropical Systems Tracking Across Placentia Bay by Decade

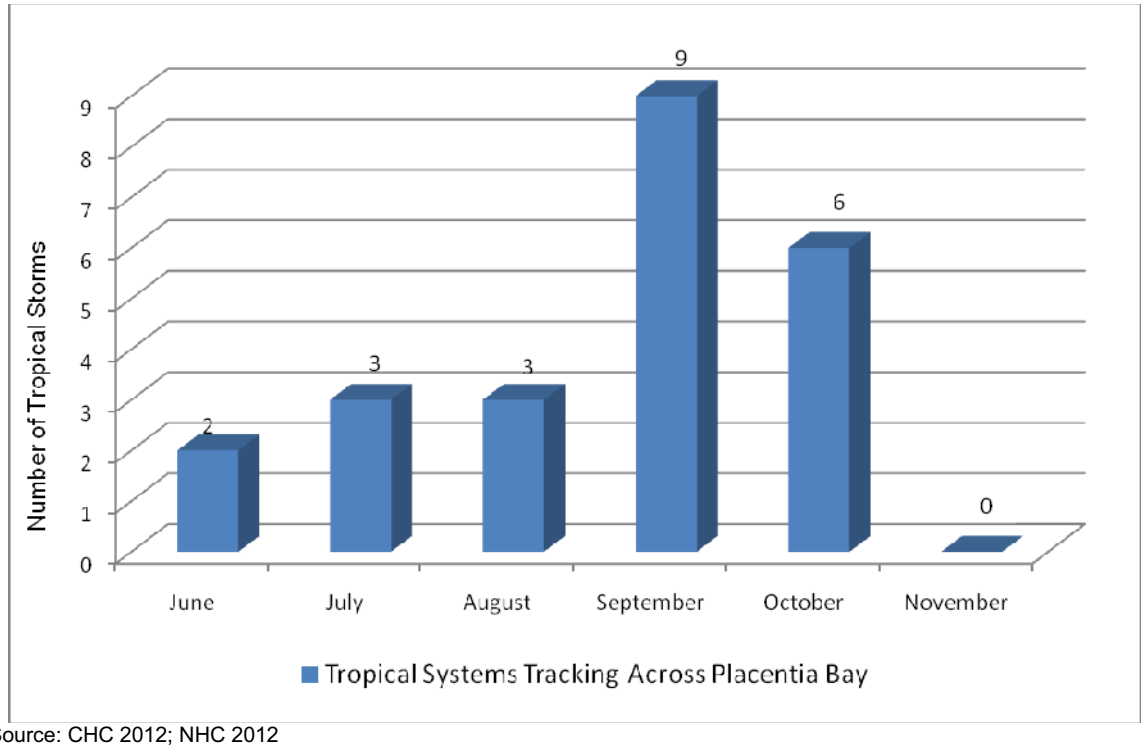

Source: CHC 2012; NHC 2012

Figure 4-29 Number of Tropical Systems Tracking Across Placentia Bay by Month

There have been many notable tropical storms and hurricanes that have affected Placentia Bay. The most recent storm was Hurricane Igor, which tracked just east of the Avalon Peninsula in September 2010. Igor caused major destruction to eastern Newfoundland, specifically over the Burin and Bonavista Peninsulas, where rainfall amounts exceeded 200 mm and winds gusted well in excess of 100 km/h throughout the region. Typically with tropical systems, the strongest winds associated with the low are on the east side of low's centre, as the wind speeds are enhanced by the forward motion of the storm. The heaviest rainfall is typically located in the northwest quadrant of the low, so systems, like Igor, tracking just east of the Avalon Peninsula, will give considerable rainfall to eastern Newfoundland, including areas near Placentia Bay. A selection of the most severe tropical systems to affect Placentia Bay is provided below, along with a summary of the storm's track and weather statistics.

Tropical Storm Ana (July 1985)

Ana developed near Bermuda mid-July, 1985 and developed into a tropical storm, making landfall near Grand Bank, on the Burin Peninsula, early in the morning of July 19, with maximum sustained winds of 102 km/h, and then quickly became extratropical as it tracked across Placentia Bay and the northern Avalon Peninsula. The Burin Peninsula was hit the hardest, with strong winds and heavy rainfall, generally between 60 to 100 mm for all regions surrounding Placentia Bay.

Hurricane Luis (September 1995)

The 1995 Atlantic hurricane season is tied for the third most active season in recorded history, only behind the 1993 and 2005 seasons. 1995 was also a busy season for tropical systems affecting Newfoundland, as a total of four storms tracked near the province, making it the third most active season between 1954 and 2011.

Luis originated off the West African coast on August 27, 1995, and rapidly strengthened to a Category 4 hurricane (Saffir Simpson Scale) on August 31. Luis tracked near the Caribbean early in September, and then veered northwards towards Atlantic Canada, making landfall as a Category 1 hurricane over the southwestern Avalon Peninsula (just south of Argentia) early on September 11. Winds gusted over 100 km/h over the southwestern Avalon and coastal regions of the Burin Peninsula, while rainfall amounts of 75 to 150 mm were observed in the region. Notable rainfall totals include:

- 143.6 mm in Boat Harbour, on the Burin Peninsula
- 150.8 mm in Red Harbour, on the Burin Peninsula
- 133.6 mm in Salt Pond, on the Burin Peninsula
- 133.0 mm in Winterland, on the Burin Peninsula
- 130.2 mm in Garnish, on the Burin Peninsula
- 78.0 mm in Long Harbour, near Argentia.

Extratropical Storm Earl (September 1998)

Earl developed over the Gulf of Mexico late on August 31, 1998, making landfall as a Category 2 hurricane in Florida on September 2. As Earl moved over the Atlantic Ocean and tracked northeastward over cooler waters, it became extratropical and intensified due to a strong baroclinic zone (strong temperature contrast) and made landfall over the extreme southwestern Avalon Peninsula (near St. Bride's) late in the evening of September 5, and then quickly moved away from Newfoundland the following day. While the heaviest rainfall was observed over central Newfoundland, amounts of 25 to 50 mm were recorded over the Burin and southwestern Avalon Peninsulas. Wind gusts in excess of 100 km/h were reported along coastal sections of the Avalon, and four consecutive hours of 70 to 80 km/h sustained winds were recorded at weather stations in both Argentia and Marticot Island early in the morning of September 6.

Tropical Storm Gert (September 1999)

Gert formed off the west coast of Africa on September 11, 1999, becoming a hurricane just two days later as it tracked to the west. Gert veered to the northeast, passing east of Bermuda, then went just east of the Avalon Peninsula as a tropical storm late on September 22, producing wave heights up to 23.6 m just offshore of the Avalon Peninsula. In St. Bride's, on the southwestern Avalon Peninsula, large waves damaged a wharf and multiple boats. Gert did not exhibit the often observed post-tropical rain pattern, as the rain was to the right of the storm, instead of the left (west) side.

Strong winds from Gert were observed across southeastern Newfoundland, starting late on September 22, with sustained winds reaching 90 km/h in St. Lawrence, on the Burin Peninsula.

Hurricane Michael (October 2000)

Michael began on October 15, 2000, east of Florida and entered Canadian waters as a Category 1 hurricane on October 19, making landfall just west of Harbour Breton, Newfoundland and Labrador, and quickly transitioned to a post-tropical storm afterwards. While the heaviest rainfall occurred over western Newfoundland, very strong winds were reported over southeastern Newfoundland. A sample of wind observations is provided below:

- Sustained winds briefly reached 100 km/h at Marticot Island early in the morning of October 20; sustained winds were above 60 km/h for 18 hours straight
- Peak sustained winds of 96 km/h at St. Lawrence, on the Burin Peninsula, on the evening of October 19; sustained winds were above 50 km/h for 33 hours straight; the station reported a peak gust of 172 km/h
- Peak sustained winds of 126 km/h at Sagona Island, west of the Burin Peninsula, on the evening of October 19; sustained winds were above 100 km/h for 3 hours straight and above 65 km/h for 29 hours straight; the station reported a peak gust of 150 km/h.

Tropical Storm Chantal (August 2007)

Chantal was a short-lived tropical storm in the North Atlantic Ocean, developing on July 31, 2007, between Bermuda and Cape Cod. Chantal underwent extratropical transition early on August 1 and tracked over the extreme southeastern Avalon later that day. While the strongest winds remained offshore of Newfoundland, torrential rains affected the Avalon and Burin Peninsulas, causing substantial damage from flooding. Rainfall totals recorded were as high as 200 mm in Argentia and 190 mm in Whitbourne.

Hurricane Igor (September 2010)

Igor formed off Africa on September 8, 2010, and generally moved westward, attaining hurricane status on September 12. Igor briefly reached Category 5 status early on September 15, when maximum winds reached 250 km/h over the open Atlantic Ocean. Igor tracked just west of Bermuda on September 20, and then rapidly accelerated northeastward towards Newfoundland (Figure 4-30). On the same day, an intense frontal system over Newfoundland became stationary, pulling moisture and heavy rainfall from Igor over the province. Igor re-intensified early on September 21 and tracked just east of the Avalon Peninsula as a Category 1 hurricane later that day.

Very strong winds and excessive rainfall fell over much of eastern Newfoundland, with well over 200 mm falling over the Burin and Bonavista Peninsulas. A large swath of 100+ mm rainfall occurred over all of eastern Newfoundland. Sustained hurricane-force winds (120 to 130 km/h) were recorded over much of eastern Newfoundland and gusts peaked between 150 to 170 km/h. Below is a sample of wind and rainfall statistics from Hurricane Igor:

- Sagona Island: 113 km/h sustained winds; 163 km/h gust
- Argentia: 132 km/h gust
- St. Lawrence: 124 km/h
- Winterland: 111 km/h
- St. Lawrence: 238 mm
- St. Pierre/Miquelon: 160 mm.

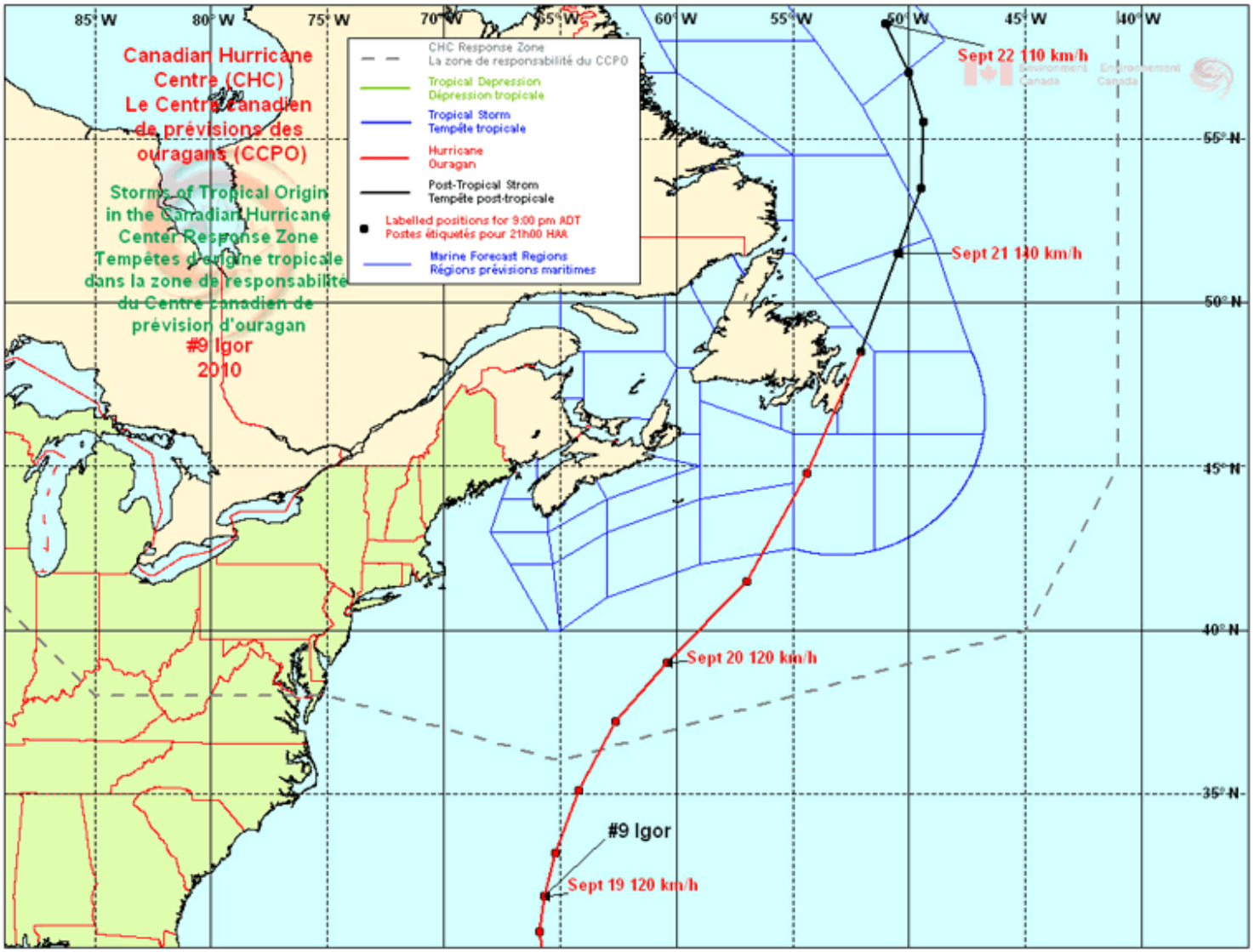

Source: CHC 2012

Figure 4-30 Track of Hurricane Igor

4.2.2 Oceanic Environment

4.2.2.1 Bathymetry

Placentia Bay is a major embayment of the south coast of the Island of Newfoundland, bounded on the west by the Burin Peninsula and on the east by the Avalon Peninsula. The axis of the bay lies in a north-northeasterly direction, with its opening to the Atlantic Ocean at the southwest. The bay faces onto the western reaches of the Grand Banks of Newfoundland. The opening at the mouth of the bay is approximately 87 km wide, with a depth at the middle of approximately 240 m, shoaling toward the shore. The distance from the mouth of the bay at Cape St. Mary's to the head of the bay at Come By Chance, along the eastern shore, is approximately 105 km, and along the western shore from Ferryland Head to Come By Chance is approximately 143 km.

While the bay does not have a sill across its mouth, the bathymetry immediately outside the bay rises up on its western side, squeezing the main channel and restricting the exchange between the deeper water within the bay and the outside ocean water (Davidson et al. 1984).

Placentia Bay contains numerous islands and shoals. The eastern half of the bay is characterized by a well-defined channel, Eastern Channel, and shipping lane, with depths of typically 200 m, which runs from the mouth of the bay almost to the head of the bay. The western half of Placentia Bay is characterized by numerous banks, shoals and reefs. The top end of the bay contains several islands, the largest being Merasheen Island, Long Island and Red Island. Because of the orientation of its mouth, Placentia Bay is exposed to winds, waves and currents propagating in from the Atlantic Ocean.

The central portion of the bay, including WREP areas of interest at Argentia, and potential deep-water mating sites west and east of Merasheen Island (Husky 2012a), is shown in an electronic navigation chart excerpt in Figure 4-31. This shows depth contours in metres, and soundings in metres and decimetres:

- At Argentia, depths to the northeast are in the 10 to 18 m range; within approximately 2 km of the shore to the east, depths are approximately 20 m: within approximately 5 km depths exceed 100 m
- Between Merasheen Island and Red Island, depths exceed 100 m, with soundings of 152 and 163 m
- Between Isle Valen and Merasheen Island, depths exceed 200 m, with several soundings of approximately 350 m.

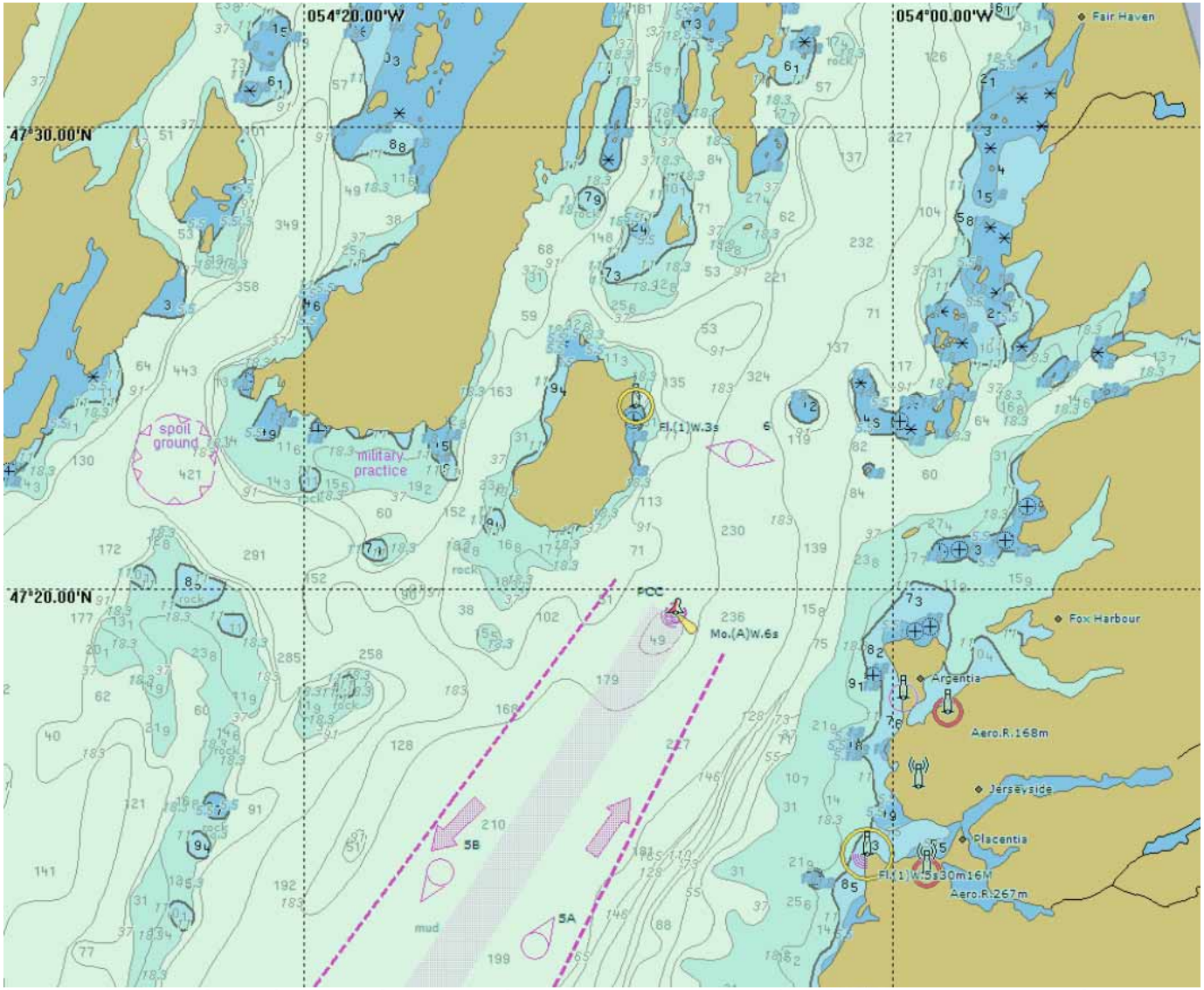

Source: Canadian Hydrographic Service Chart, 4016, Saint-Pierre to St. John's, Electronic Navigation Chart CA276274, ed. update 6.0, 05-Sep-2008

Figure 4-31 Placentia Bay Bathymetry for White Rose Extension Project Locations Argentia, Red Island, Merasheen Island, Isle Valen

4.2.2.2 Waves

Characterizations of normal and extreme wave conditions are available from two primary sources: the multi-year MSC50 wave hindcast; and SmartBay wave measurements within Placentia Bay.

MSC50

Wave data were obtained from the MSC50 (MSC06min subset), wind and wave hindcast dataset (Swail et al. 2006). The MSC50 dataset represents the state of the art and most comprehensive wind and wave database for Eastern Canada waters.

The dataset covers hourly wind and wave parameters, from 1954 to 2010, for the North Atlantic Ocean and includes consideration of periods with sea ice coverage (Swail et al. 2006; Environment Canada 2011; DFO 2012b). The MSC50 domain (MSC30S) covers the North Atlantic Ocean from approximately 80°W to 20°E and from 0°N to 80°N at 0.5° resolution (approximately 50 km); while the Eastern Canada Subset (MSC06min) covers from approximately 74°W to 42°W and from 40°N to 52°N at 0.1° resolution (approximately 10 km).

Hourly time series (1954 to 2010) for the MSC06min subset were obtained from DFO (2012a).

Three nodes locations were selected as follows to characterize wave conditions in Placentia Bay and to be representative of WREP activities (Figure 4-32):

- M6012169: Between Red Island and Argentia, 47.3°N, 54.1°W, water depth of 216 m, for WREP activities near Argentia
- M6012548: Between Isle Valen and Merasheen Island, 47.5°N, 54.3°W, water depth of 75 m, near a potential deepwater site in that part of the bay (the other potential site is between Red Island and Merasheen Island)
- M6011561: Mouth of Placentia Bay, 47.0°N, 54.7°W, water depth of 244 m, for tow-out from Placentia Bay to the Grand Banks.

MSC50 wave parameters include significant wave height (Hs) and spectral peak wave period (Tp)[1]. The Hs is calculated as four times the square root of the total variance (spectral definition of Hs). The Tp is the inverse of the frequency at which the wave energy spectrum has its peak.

Monthly wave height and wave period statistics, followed by frequency of occurrence of wave period for different wave height ranges, and a set of monthly, seasonal and annual wave height roses, are presented, each time reporting each of the three MSC50 nodes. Seasonal mean and 99th percentile wave heights are also presented. A comparison, of mean and maximum wave statistics, is provided for the three 57-year MSC50 nodes and three (albeit much shorter record) SmartBay buoy measurements. Time series figures are presented to compare MSC50 hindcast and SmartBay measurement waves.

[1] MSC50 parameters include wind speed, wind direction, Hs, Tp , wave direction, wave spread and spectral moments

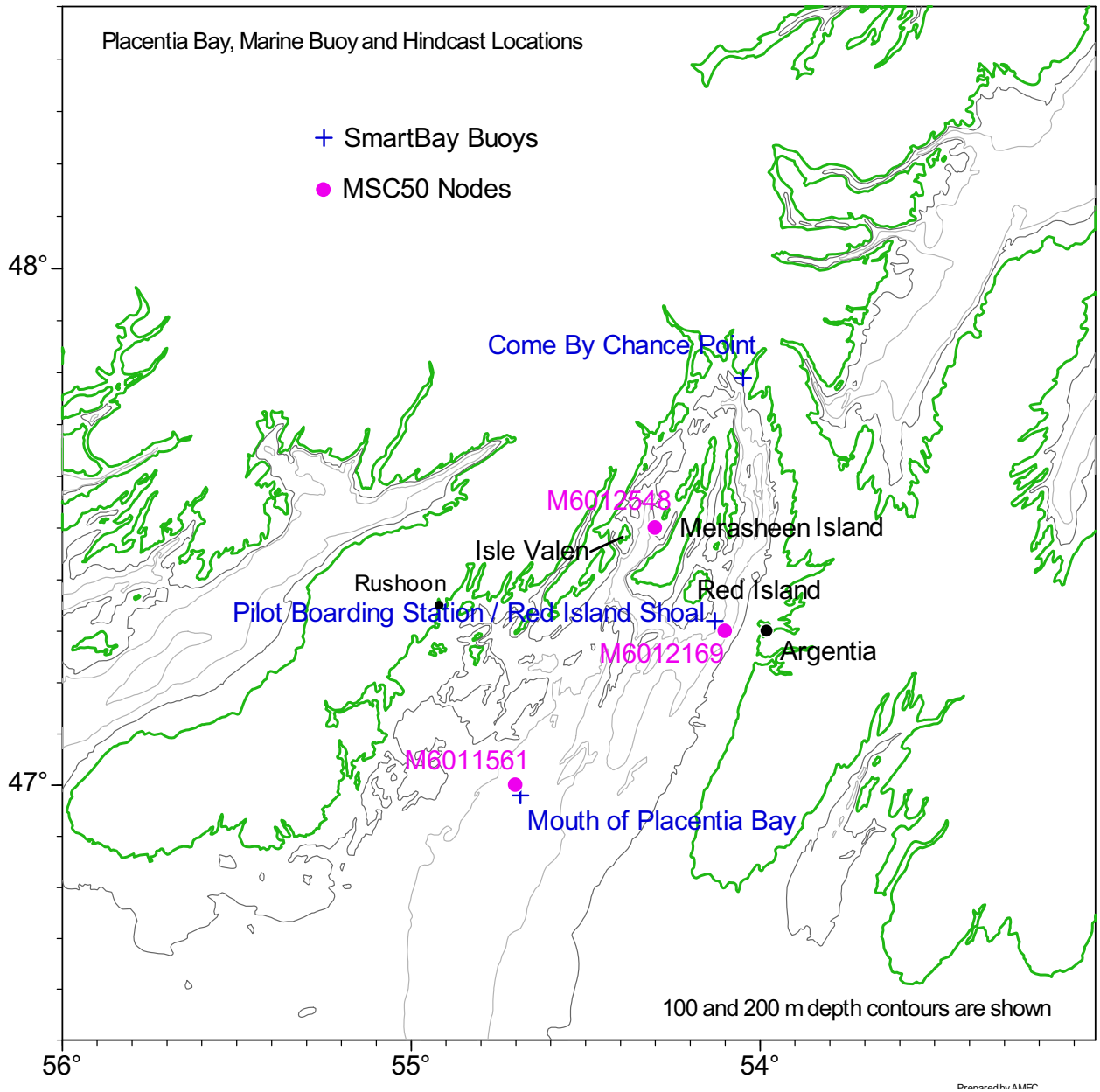

Figure 4-32 Wave Data Source Locations, Placentia Bay

SmartBay

SmartBay, Placentia Bay[2] (SmartBay 2012) is an initiative of the Centre for Applied Ocean Technology, the applied research arm of Memorial University's Marine Institute's School of Ocean Technology, developed and operated with industry team partners.

Initially funded in 2006 under the federal government's Ocean Action Plan, SmartBay has also received critical ongoing financial and in-kind support from the Newfoundland and Labrador Department of Innovation Trade and Rural Development, Atlantic Canada Opportunities Agency, the Marine Institute of Memorial University and the Canadian Coast Guard (CCG), and substantial in-kind support from its industry partners.

One of the key benefits of SmartBay is the availability of met-ocean information, resulting in better operational decisions minimizing the potential of an incident, and improved emergency response time for real or simulated events. Three buoys, measuring waves, currents, wind and air pressure, air temperature, sea temperature and salinity, are strategically located throughout Placentia Bay (Figure 4-32):

- Pilot Boarding Station / Red Island Shoal, 47.3°N, 54.1°W, water depth of 216 m
- Mouth of Placentia Bay, 47.3°N, 54.1°W, water depth of 244 m
- Come By Chance Point, 47.3°N, 54.1°W, water depth of 75 m.

The Come Bay Chance Point buoy is a 1.7 m AXYS met-ocean buoy, the other two are 3 m AXYS met-ocean buoys. Monthly wave statistics for the three Placentia Bay buoys are presented, together with the MSC50 comparisons noted above.

Monthly Wave Statistics

Monthly and annual Hs and Tp statistics for the three MSC50 node locations are presented in Tables 4-23 to 4-25 for near Red Island, near Isle Valen, and mouth of Placentia Bay, respectively.

Wave heights in Placentia Bay are lowest in the spring and summer, and largest in the winter. Minimum monthly mean Hs values range from 0.2 m in June and July at the Isle Valen location, to 1.3 m from May through August at the mouth of Placentia Bay. Near Red Island, monthly means from April through September are 1.0 m or less. Maximum monthly mean Hs range from 1.6 m in December near Red Island to 2.4 m, also in December, at the mouth of Placentia Bay. With its location sheltered from the open ocean to the south, monthly mean Hs near Isle Valen do not exceed 0.6 m (December and January).

[2] http://www.smartbay.ca/ SmartBay is owned and operated by the Fisheries and Marine Institute of Memorial University of Newfoundland. The vision of SmartBay is "to provide simple access by all stakeholders to data and information in support of effective management and sustainable development of coastal ocean areas and the safety and security of life at sea".

Table 4-23 Monthly and Annual Wave Statistics, MSC50 node M6012169, near Red Island

	Significant Wave Height, Hs (m)			Peak Wave Period, Tp (s)		
Month	**Mean**	**Maximum**	**Most Frequent Direction (from)**	**Mean**	**Maximum**	**Associated with Maximum Hs**
Jan	1.5	7.6	SW	6.3	17.7	14.0
Feb	1.4	7.7	SW	6.2	18.9	14.1
Mar	1.1	8.2	SW	5.8	17.5	14.3
Apr	1.0	4.4	SW	6.2	17.3	11.8
May	0.9	4.8	SW	6.6	17.4	11.0
Jun	0.9	4.2	SW	6.8	17.4	10.0
Jul	0.9	5.2	SW	6.9	17.2	10.8
Aug	0.9	6.1	SW	6.6	15.6	14.2
Sep	1.0	6.4	SW	6.6	18.9	12.0
Oct	1.2	7.0	SW	6.4	17.7	13.0
Nov	1.4	6.0	SW	6.7	17.1	11.8
Dec	1.6	7.4	SW	7.0	18.8	14.0
Annual	1.2	8.2	SW	6.5	18.9	14.3
Source: DFO 2012a						

Table 4-24 Monthly and Annual Wave Statistics, MSC50 node M6012548, near Isle Valen

	Significant Wave Height, Hs (m)			Peak Wave Period, Tp (s)		
Month	**Mean**	**Maximum**	**Most Frequent Direction (from)**	**Mean**	**Maximum**	**Associated with Maximum Hs**
Jan	0.6	2.1	W	4.2	20.4	14.3
Feb	0.5	2.2	W	4.0	19.4	14.4
Mar	0.4	2.3	W	3.6	17.4	14.5
Apr	0.4	1.3	SW	3.2	17.3	4.6
May	0.3	1.3	SW	2,5	17.3	4.4
Jun	0.2	1.3	SW	2.3	17.6	4.7
Jul	0.2	1.4	SW	2.1	17.6	12.2
Aug	0.3	1.5	SW	2.5	21.0	4.6
Sep	0.4	1.8	SW	3.5	18.4	14.5
Oct	0.5	2.2	W	3.4	17.6	14.3
Nov	0.5	1.6	W	3.8	20.5	12.2
Dec	0.6	2.1	W	4.4	19.6	14.4
Annual	0.4	2.3	SW	3.3	21.0	14.5
Source: DFO 2012a						

Table 4-25 Monthly and Annual Wave Statistics, MSC50 node M6011561, Mouth of Placentia Bay

	Significant Wave Height, Hs (m)			Peak Wave Period, Tp (s)		
Month	**Mean**	**Maximum**	**Most Frequent Direction (from)**	**Mean**	**Maximum**	**Associated with Maximum Hs**
Jan	2.1	9.8	SW	7.3	19.2	14.3
Feb	2.0	10.5	SW	7.3	19.1	14.2
Mar	1.8	10.9	SW	7.1	17.3	14.4
Apr	1.6	6.3	SW	7.2	17.2	11.9
May	1.3	6.7	SW	7.2	17.5	13.8
Jun	1.3	6.1	SW	7.3	17.4	13.9
Jul	1.3	6.7	SW	7.3	16.8	11.7
Aug	1.3	9.3	SW	7.2	17.3	14.1
Sep	1.5	9.4	SW	7.6	17.4	14.6
Oct	1.8	10.1	SW	7.3	18.8	13.1
Nov	2.0	8.2	SW	7.7	18.7	13.2
Dec	2.4	9.8	SW	8.2	18.9	14.1
Annual	1.7	10.9	SW	7.4	19.2	14.4
Source: DFO 2012a						

Near Red Island, maximum Hs ranges from 4.2 m in June to 8.2 m in March. At the mouth of Placentia Bay location, maximum Hs ranges from 6.1 m in June to 10.9 m in March. Monthly maximum Hs values near Isle Valen are 2.3 m (March) or less in all months. Due to its sheltered location, wave conditions in Argentia Harbour would be considerably less than the open water, Red Island values.

Waves are most frequently from the southwest. This is true for all months of the year near Red Island and for the mouth of Placentia Bay. Only in the fall and winter for Isle Valen are waves instead most frequently from the west.

The largest waves are also generally from the southwest. The exception is at the mouth of Placentia Bay, where in late spring to early summer, and in fall, the largest waves are from the open Atlantic Ocean to the south. The southwest pattern near Isle Valen deviates in April (maximum waves from the northeast) and August and September (maximum waves from the south).

The monthly mean Tp ranges from 2.1 s in summer near Isle Valen to 8.2 s in December at the mouth of Placentia Bay. The annual mean Tp value ranges from 3.3 s near Isle Valen to 6.5 s near Red Island, and 7.4 s for the mouth of Placentia Bay. Monthly maximum Tp ranges from 15.6 s in August (Red Island) to 21 s (Isle Valen) from spring until early fall. The large periods reported for near Isle Valen are due to occasions when there is little local wind wave energy (for that sheltered location), and hence very small

amplitude (e.g., less than 5 cm), but very long period swell present from the open ocean (e.g., South Atlantic Ocean, which ends up “dominating” locally).

Comparisons of mean and maximum Hs and Tp for the three MSC50 node locations are presented in Figures 4-33 and 4-34.

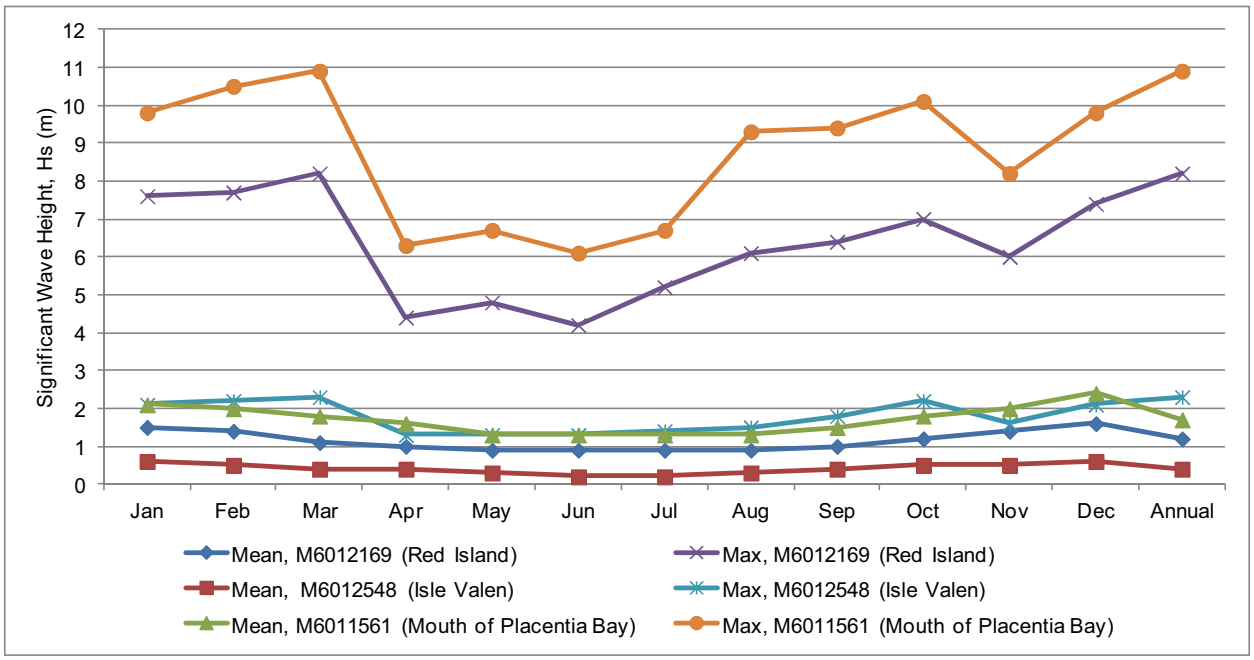

Source: DFO 2012a

Figure 4-33 Monthly Mean and Maximum Significant Wave Height, Placentia Bay

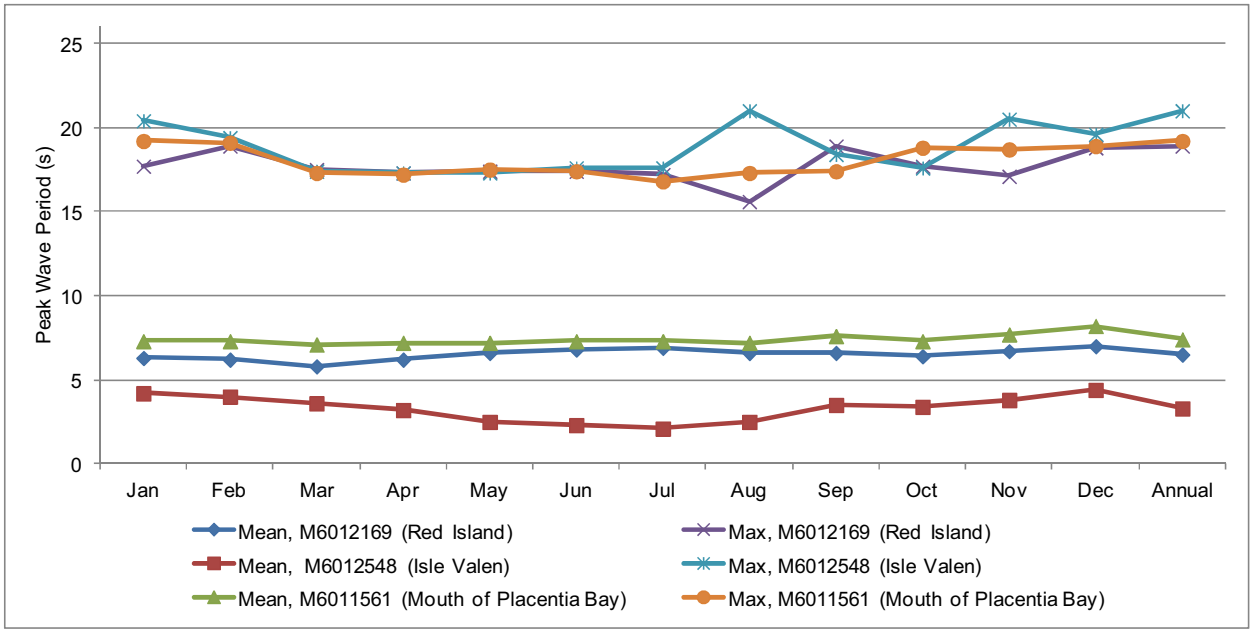

Source: DFO 2012a

Figure 4-34 Monthly Mean and Maximum Peak Wave Period, Placentia Bay

Peak Wave Period as a function of Significant Wave Height

Histograms of the percent occurrence of Tp for different wave height ranges are presented in Figures 4-35 to 4-37 for near Red Island, near Isle Valen and mouth of Placentia Bay respectively. Note that due to the much lower range of wave heights seen near Isle Valen, a different scale for Hs is used in Figure 4-36.

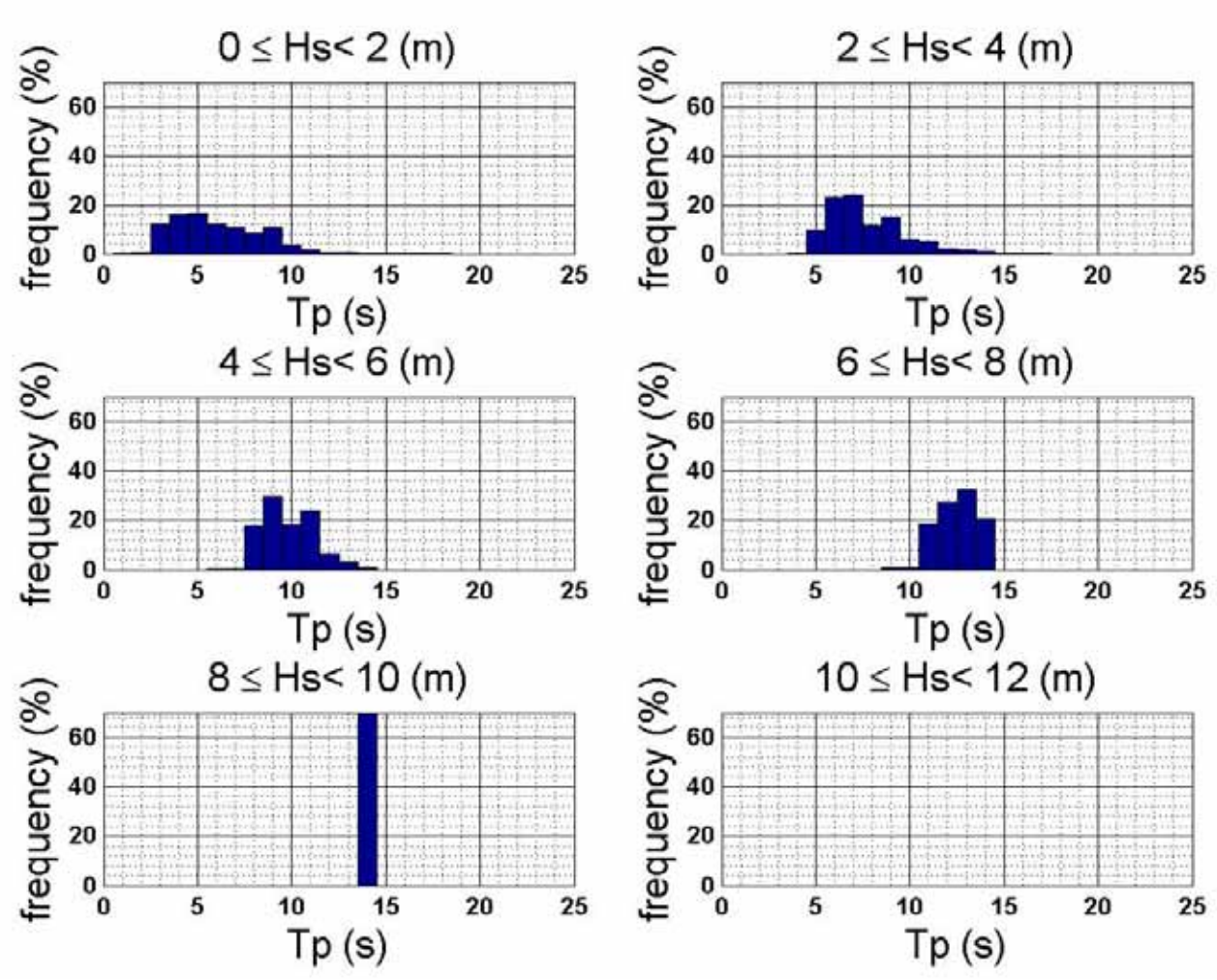

Source: DFO 2012a

Figure 4-35 Frequency of Occurrence of Peak Wave Period as a function of Significant Wave Height for MSC50 node M6012169, near Red Island

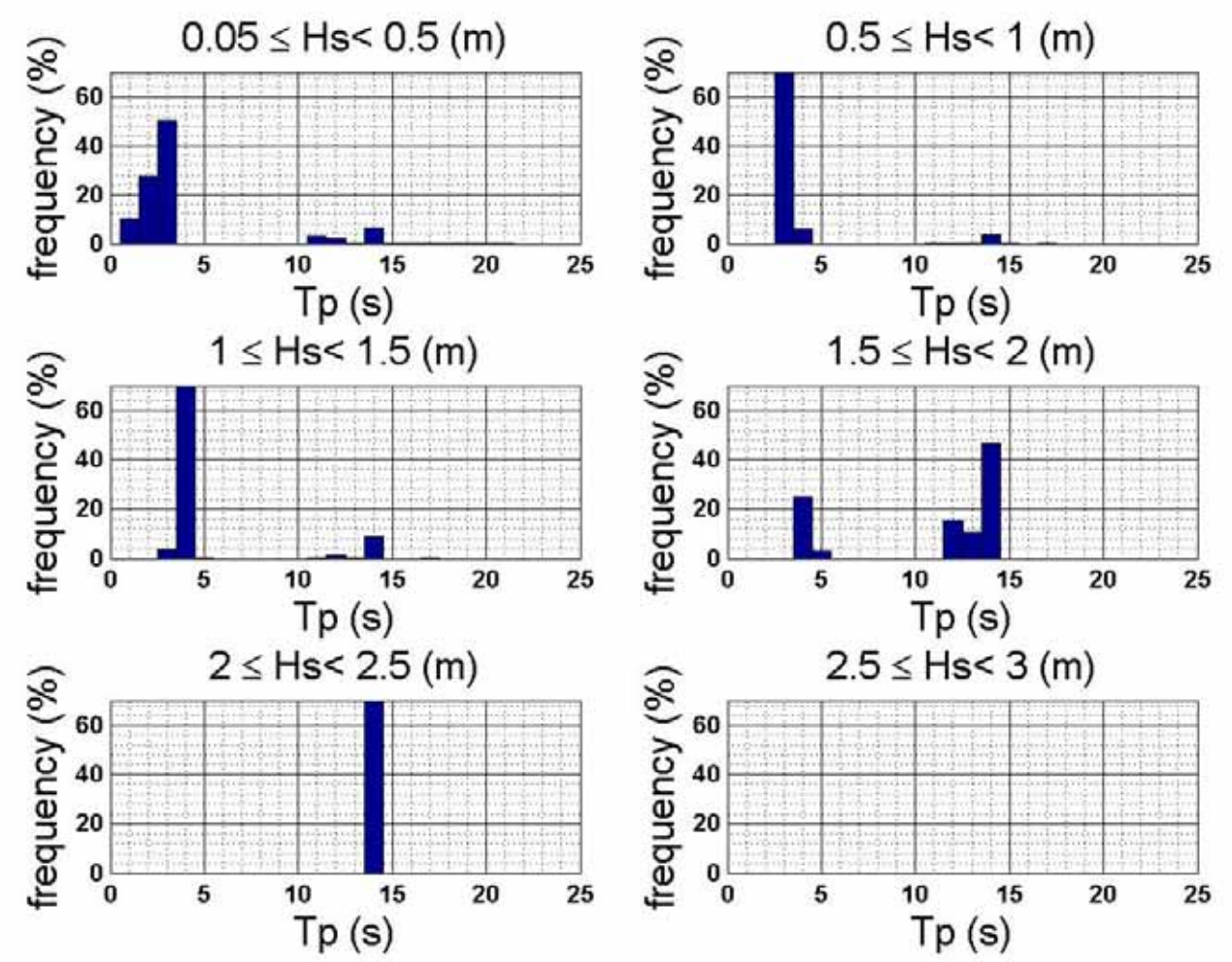

Source: DFO 2012a

Figure 4-36 Frequency of Occurrence of Peak Wave Period as a function of Significant Wave Height for MSC50 node M6012548, near Isle Valen

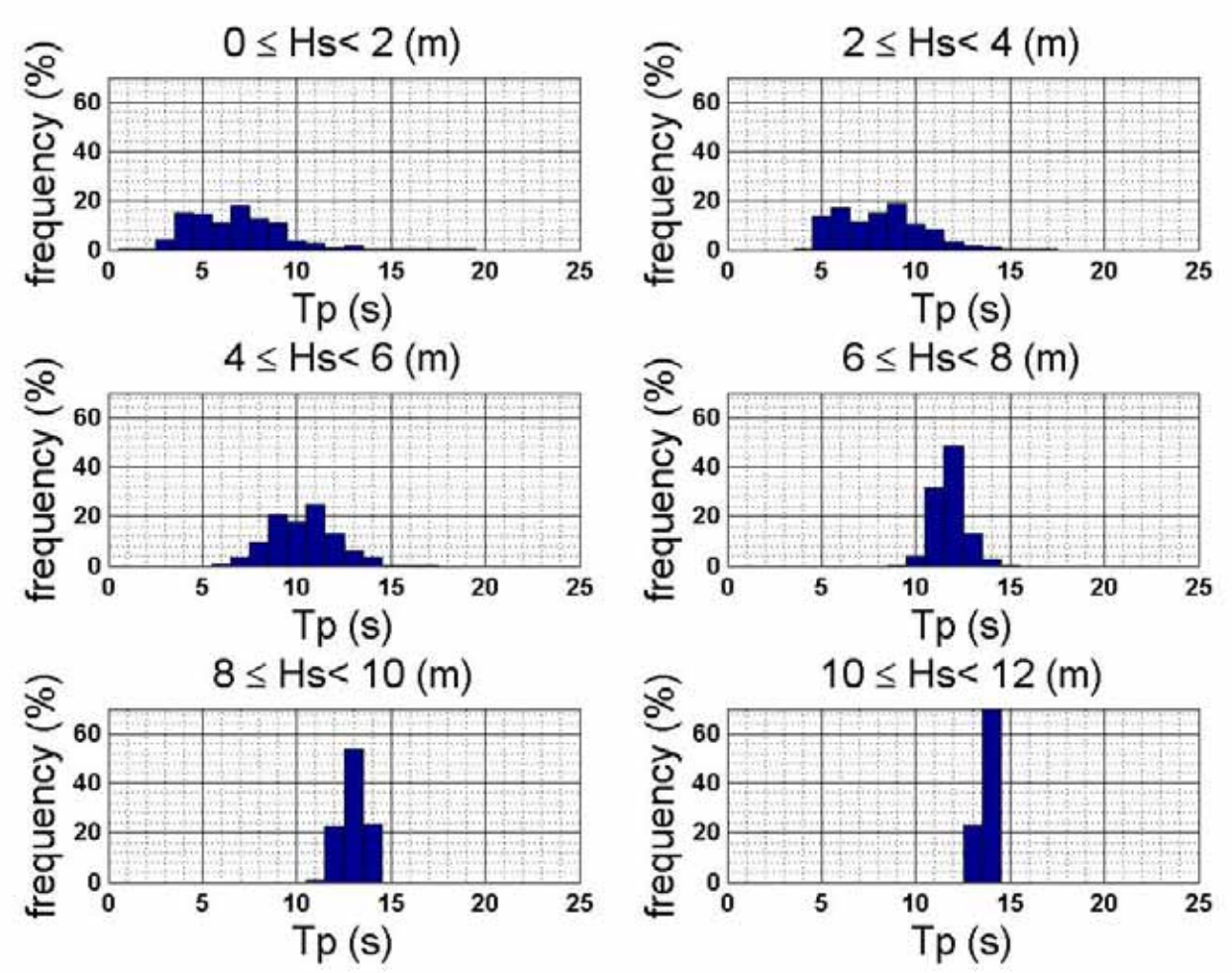

Source: DFO 2012a

Figure 4-37 Frequency of Occurrence of Peak Wave Period as a function of Significant Wave Height for MSC50 node M6011561, Mouth of Placentia Bay

For waves near Red Island (Figure 4-35) less than 2 m (which occurs 88 percent of the time annually), Tp is most frequently 4 or 5 s. For waves in the 2 m to just less than 4 m range (which occurs 11 percent annually) Tp is most frequently 6 or 7 s. Waves in the 6 to 8 m range most frequently have associated Tp of 12 or 13 s.

For the mouth of Placentia Bay (Figure 4-37), waves are 2 m or less 70 percent of the time annually, and between 2 and 4 m for 26 percent of the time. For larger waves, in the 8 to 10 m range (which occurs 0.04 percent of the time annually), Tp are 13 s for 50 percent of the time.

Wave Roses

Monthly, seasonal and annual wave roses for the three Placentia Bay MSC50 node locations are presented in Figures 4-38 to 4-46. Each wave rose indicates the directional distribution of waves, their frequency of occurrence and the corresponding wave magnitudes. For example in January, 36 percent of waves are from the southwest while less than 3 percent are from the east; 20 percent of waves from the west are 2 m or less while 1.6 percent of waves from the southwest are between 4 and 6 m (Figure 4-38). Note that due to the much lower range of wave heights seen near Isle Valen, a different scale for Hs is used in the roses. The seasonal characterizations are: winter (Janunary to March, or JFM in the rose), spring (April to June), summer (July to September) and fall (October to December).

For Red Island, nearest Argentia, waves are from the southwest 56 percent of the time annually. The next most frequent direction is from the west at 19 percent. Twelve percent of waves are greater than 2 m (7 of the 12 percent being from the southwest). The southwest direction dominates through the spring and summer; in the fall, consistent with the change in wind direction, there are more waves from the west.

A seasonal comparison for most frequent wave directions and waves over the 2 m threshold is shown in Table 4-26.

Table 4-26 Wave Rose Summary, MSC50 node M6012169, near Red Island

Season	Most Frequent Directions (from)	Waves Greater than 2 m
Winter	37% from SW; 27% from W	21%; 11% of these are from SW; 9% from W
Spring	64% from SW; 12% from W	5%; 4% of these are from SW; 1% from W
Summer	76% from SW; 1 % from W	4%; 3% of these are from SW; 1% from W
Fall	44% from SW; 26% from W	19%; 11% of these are from SW; 8% from W
Source: DFO 2012a		

For the Isle Valen location (Figures 4-41 to 4-43), waves are still most frequent from the southwest generally throughout the year, although with a slightly greater occurrence of waves from the west – particularly in the fall and winter, south and north. Annually, 25 percent of the time waves are from the southwest, 21 percent are from west, 15 percent from the south and 14 percent from the north. At this location, waves greater than 1 m occur less than 4 percent of the time, annually. This amount is 6 to 8 percent in the fall and winter and less than 1 percent in the spring and summer.

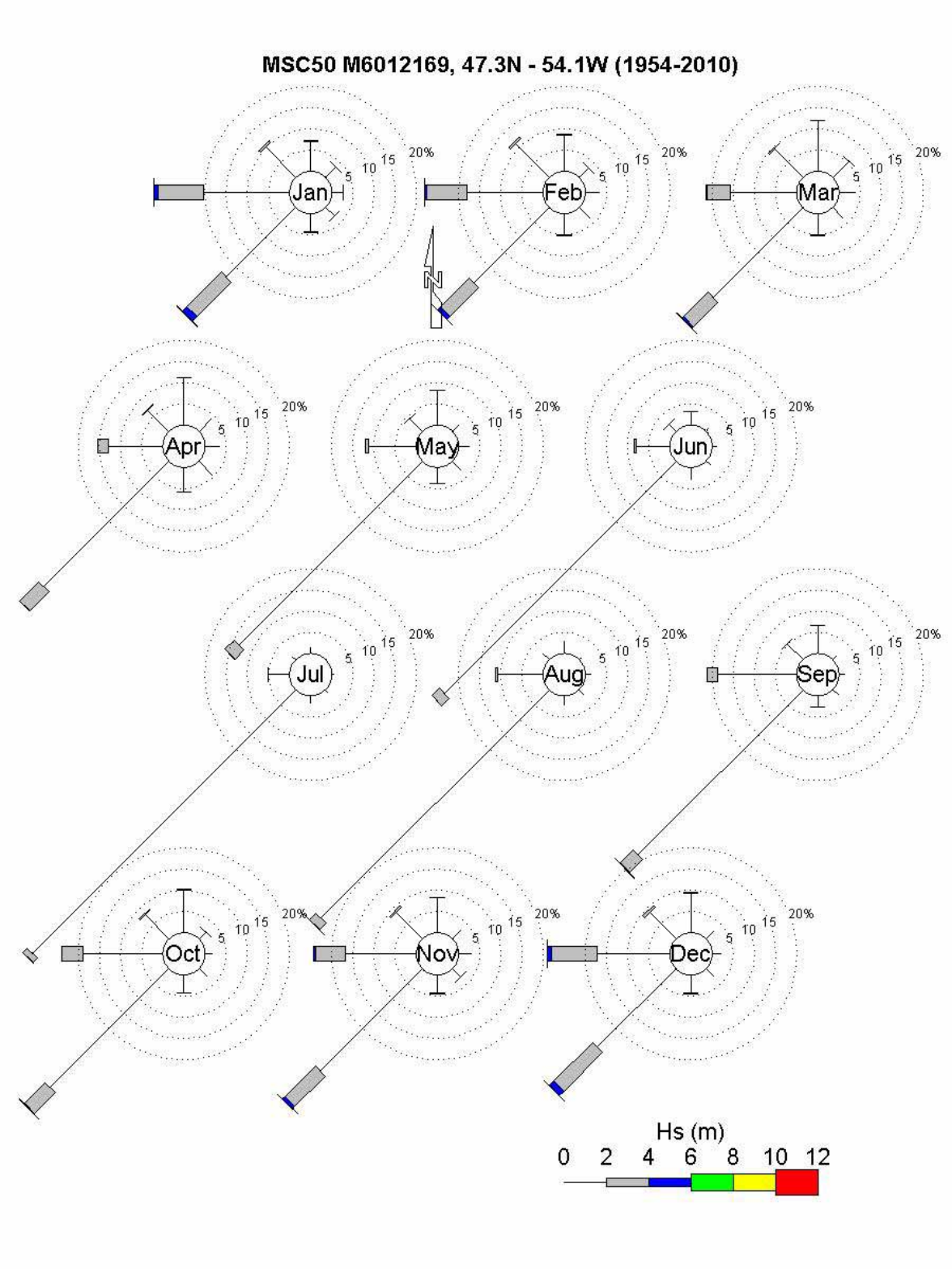

Source: DFO 2012ba

Figure 4-38 Monthly Wave Roses for MSC50 node M6012169, near Red Island

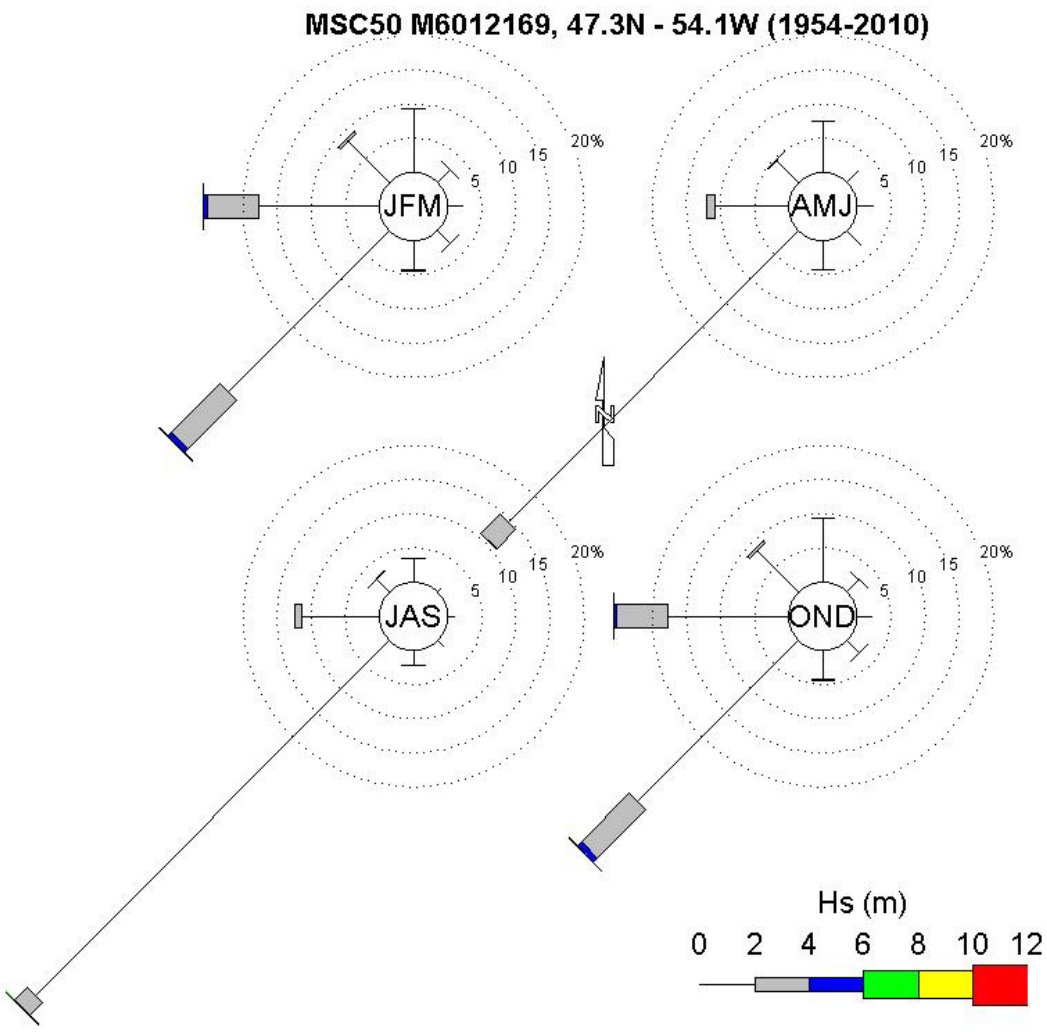

Source: DFO 2012a

Figure 4-39 Seasonal Wave Roses for MSC50 node M6012169, near Red Island

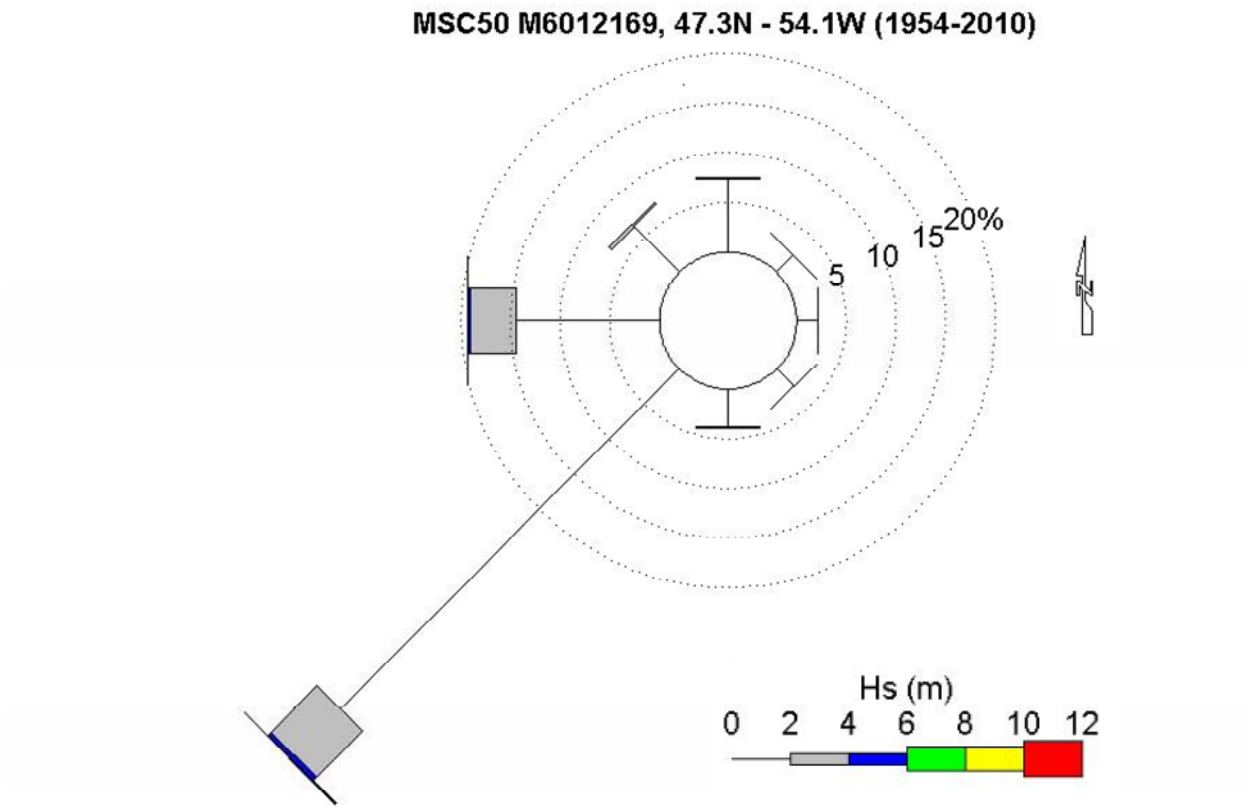

Source: DFO 2012a

Figure 4-40 Yearly Wave Rose for MSC50 node M6012169, near Red Island

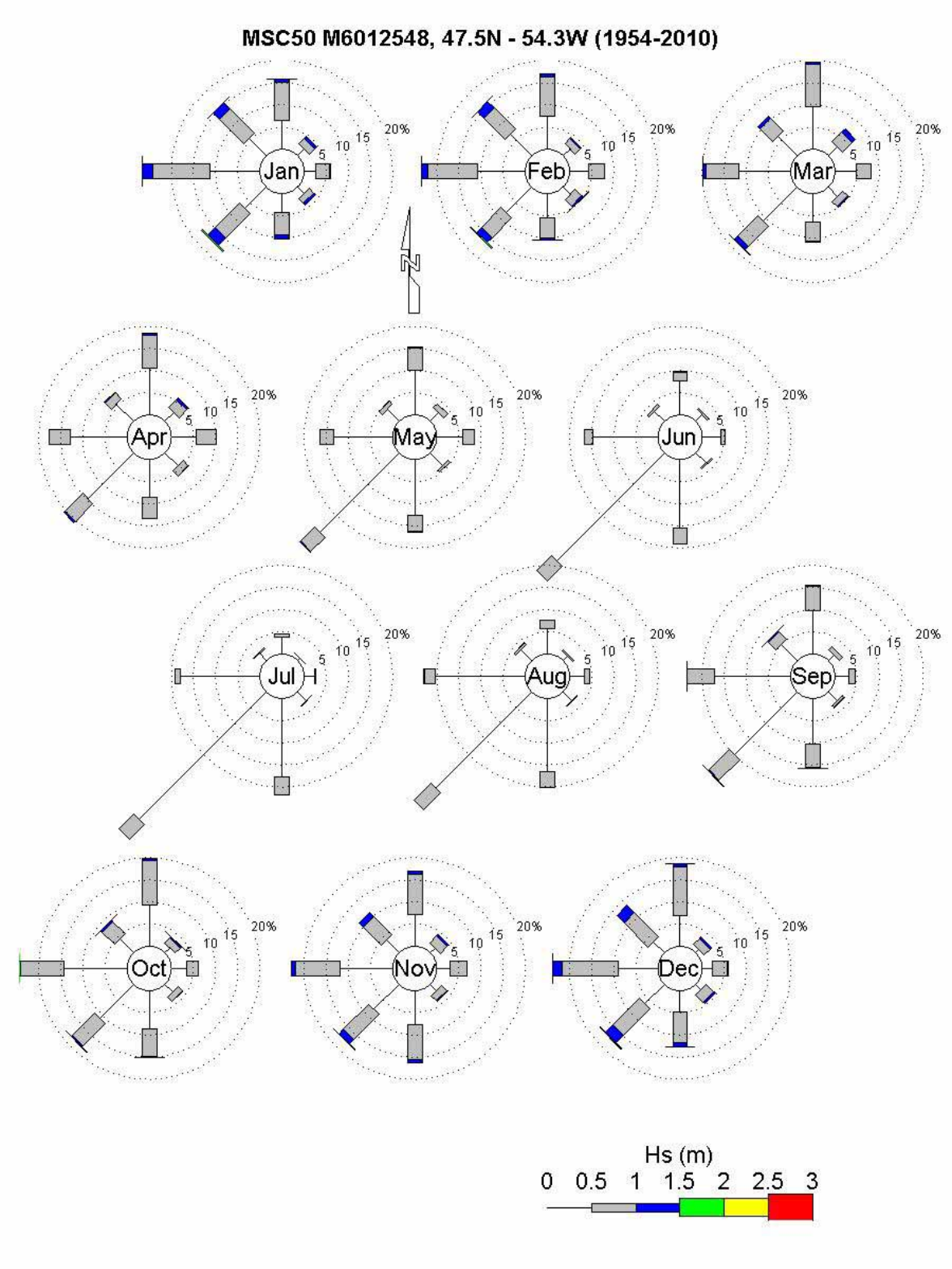

Source: DFO 2012a

Figure 4-41 Monthly Wave Roses for MSC50 node M6012148, near Isle Valen

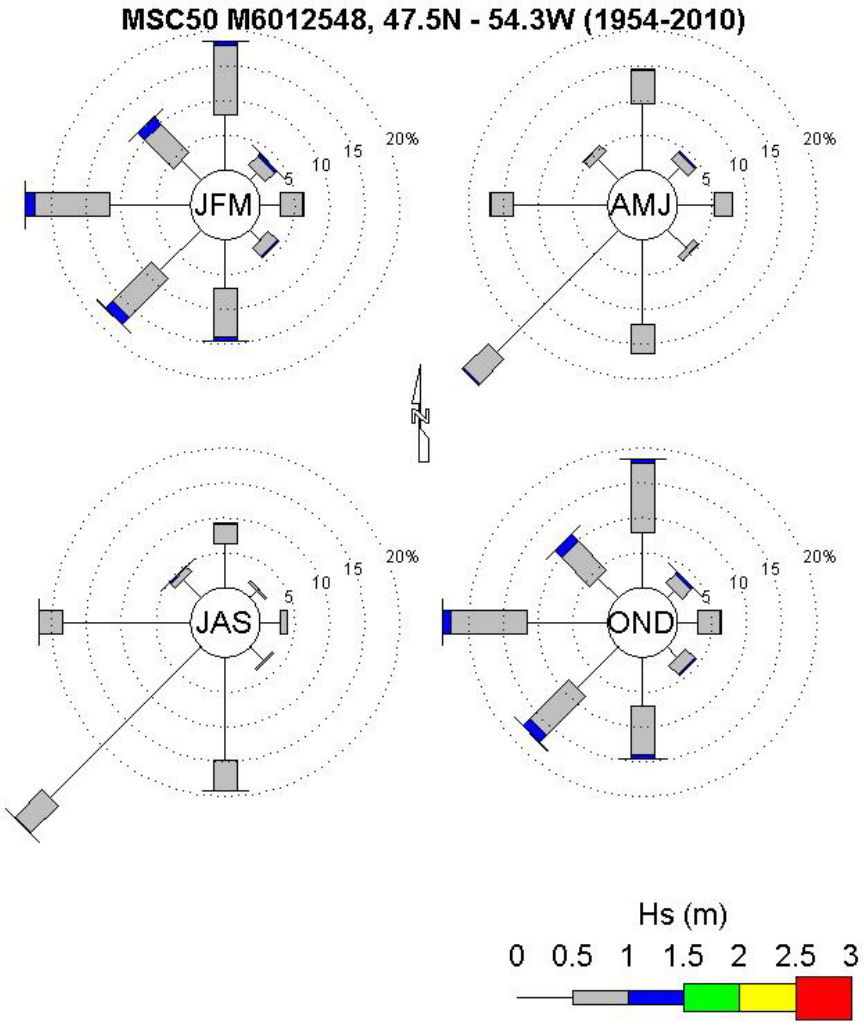

Source: DFO 2012a

Figure 4-42 Seasonal Wave Roses for MSC50 node M6012148, near Isle Valen

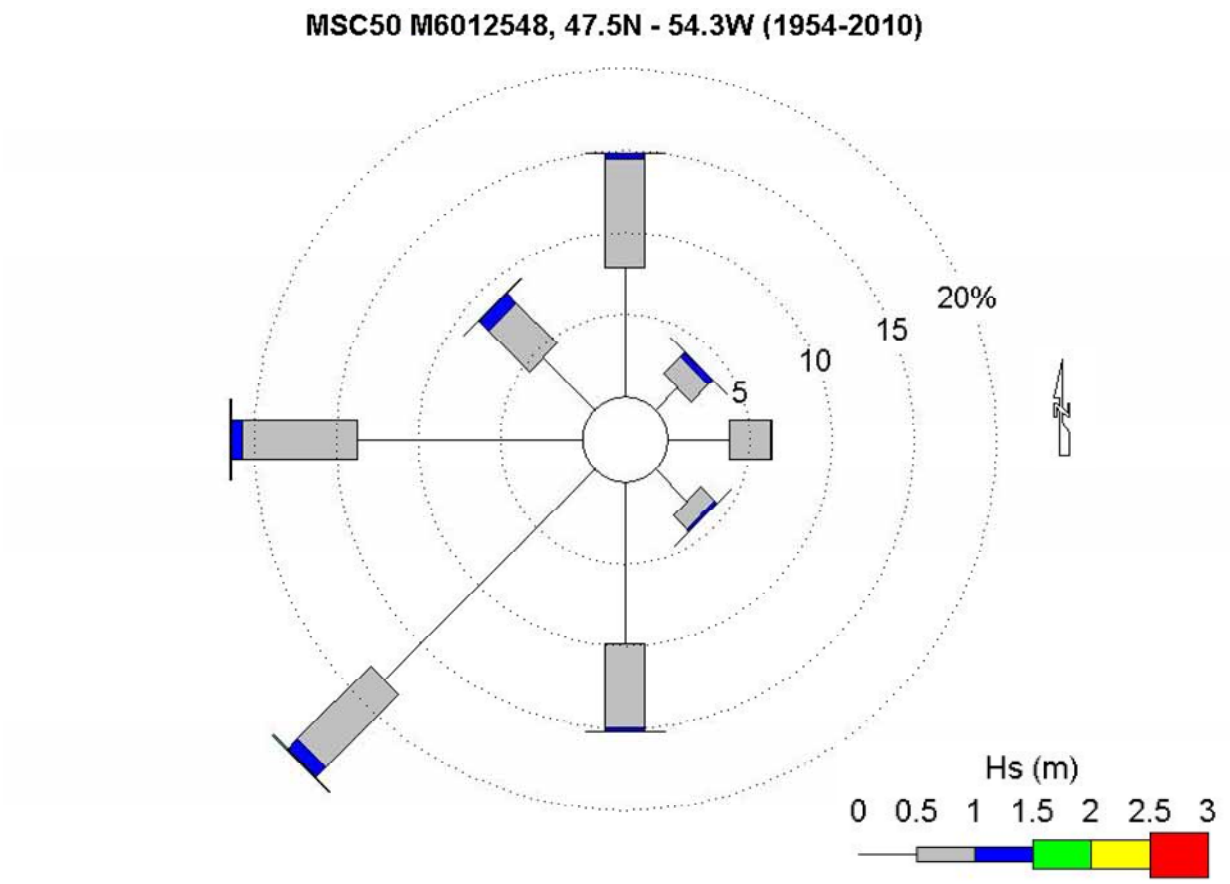

Source: DFO 2012a

Figure 4-43 Yearly Wave Rose for MSC50 node M6012148, near Isle Valen

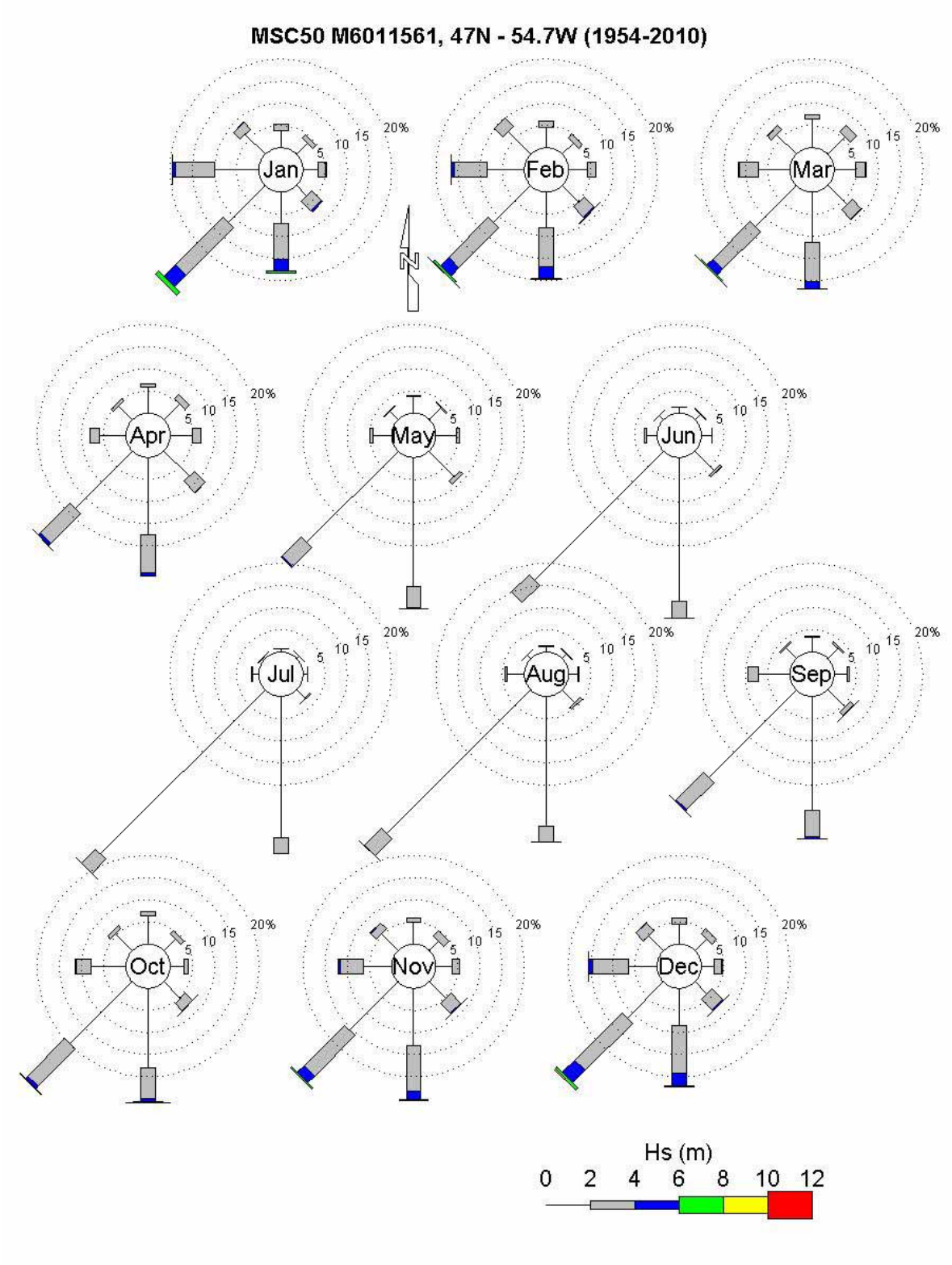

Source: DFO 2012a

Figure 4-44 Monthly Wave Roses for MSC50 node M6011561, Mouth of Placentia Bay

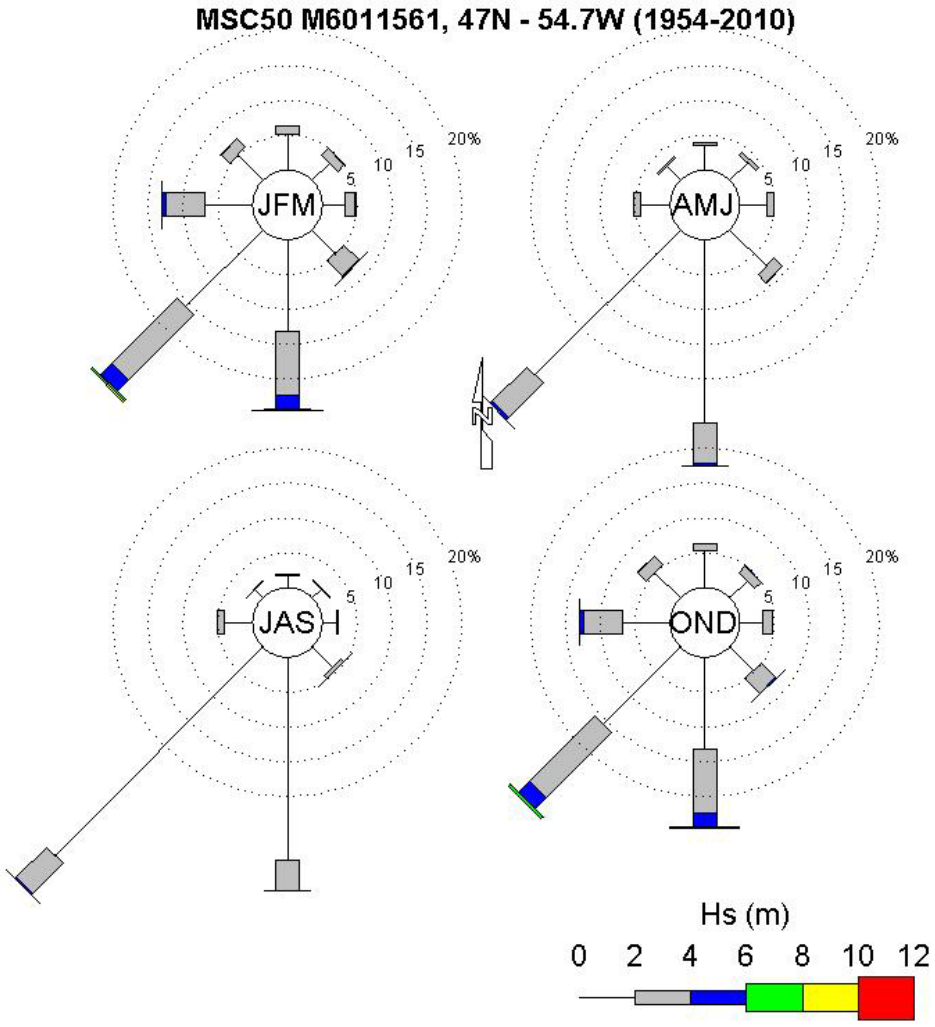

Source: DFO 2012a

Figure 4-45 Seasonal Wave Roses for MSC50 node M6011561, Mouth of Placentia Bay

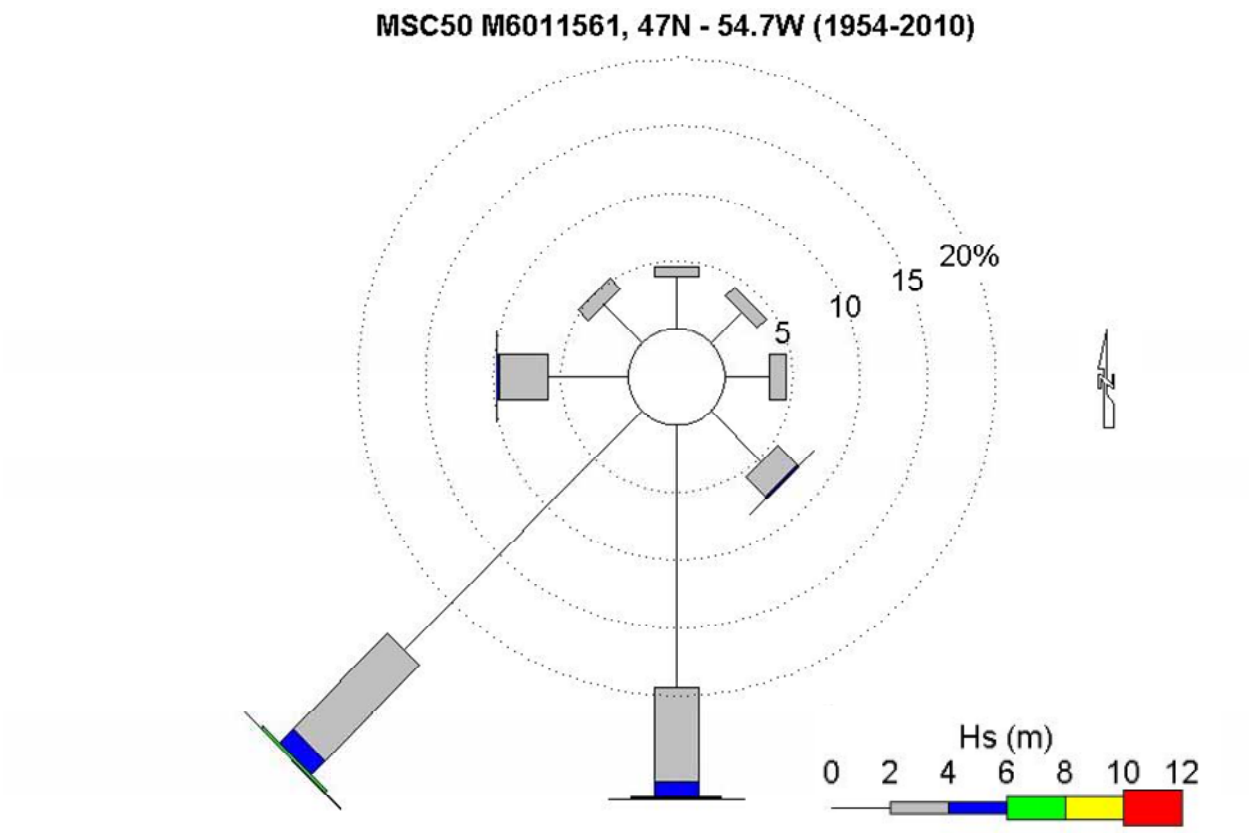

Source: DFO 2012a

Figure 4-46 Yearly Wave Rose for MSC50 node M6011561, Mouth of Placentia Bay

A seasonal comparison for most frequent wave directions and waves over a 1 m threshold is shown in Table 4-27.

Table 4-27 Wave Rose Summary, MSC50 node M6012548, near Isle Valen

Season	Most Frequent Directions (from)	Waves Greater than 1 m
Winter	23% from W; 17% each from N and SW	8%; approximately 2% each from the W and SW
Spring	30% from SW; 17% from W; 16% from S	<1% mostly from the SW and N
Summer	36% from SW; 22% from W	<1% mostly from the SW and NW
Fall	23% from W; 18% each from N and SW	6%; mostly from the SW through NW
Source: DFO 2012a		

For the mouth of Placentia Bay, waves are annually from the southwest 37 percent of the time, 28 percent from the south, and less than ten percent from other directions. Thirty percent of waves are greater than 2 m, annually. Waves are 4 m or greater 3 percent annually; in spring and summer waves are 4 m or greater less than 1 percent each, while in fall and winter they are greater than 2 m 5 and 7 percent, respectively.

A seasonal comparison for most frequent wave directions and waves over the 2 m threshold is shown in Table 4-28.

Table 4-28 Wave Rose Summary, MSC50 node M6011561, Mouth of Placentia Bay

Season	Most Frequent Directions (from)	Waves Greater than 2 m
Winter	29% from SW; 20% from S	35%; 16% of these are from SW; 11% from S
Spring	37% from SW; 32% from S	18%; 7% of these are from SW; 6% from S
Summer	48% from SW; 34% from S	13%; 6% of these are from SW; 4% from S
Fall	32% from SW; 24% from S	42%; 16% of these are from SW; 11% from S
Source: DFO 2012a		

Comparison of MSC50 Wave Hindcast and SmartBay Wave Measurements

As noted in Section 4.2.1, measurements from the SmartBay buoys are of considerably shorter record length than the 57-year MSC50 hindcast. Data have been measured since the beginning of 2007 for the Mouth of Placentia Bay buoy, while measurements from the Pilot Boarding Station and Come By Chance Point buoys exist since July 2010. Several measurement gaps also exist due to buoy maintenance[3]. As such, the SmartBay measurements have not yet captured the range of conditions that can be experienced in the bay, particularly maximum values. Nevertheless, the buoy measurements do provide a validation of the MSC50 hindcast, as illustrated for two three-month periods in Figures 4-47 and 4-48 for the Pilot Boarding Station and Mouth of Placentia Bay locations. The comparison between measurement and hindcast values is excellent at both locations.

A summary of monthly and annual mean and maximum Hs values for the three buoys is presented in Table 4-29, with statistics through December 2011. At the Pilot Boarding Station, near Red Island, the largest waves measured to date are from October 2011: a maximum Hs value of 7.5 m; and associated maximum wave height of 12.3 m. The largest waves measured by SmartBay at the mouth of the bay were measured in January 2007: a maximum Hs value of 9.1 m, and associated maximum wave height of 13.6 m. Waves at the head of the bay, from the Come By Chance Point buoy, are small, ranging from 0.2 to 0.5 m on average each month, with monthly maximum Hs values ranging 0.9 m in August to 2.8 m in December.

[3] A high-level summary only: Mouth of Placentia Bay: currents commence Jun 2007, gaps Jan-Jun 2008, Oct 2008 to Mar 2009, no wind Dec 2009 to Jun 2010, no waves Mar to Oct 2010; Pilot Boarding Station: several gaps Aug 2010, currents end early Nov 2011; Come By Chance Point: gap from late Jun to early Sep 2010:

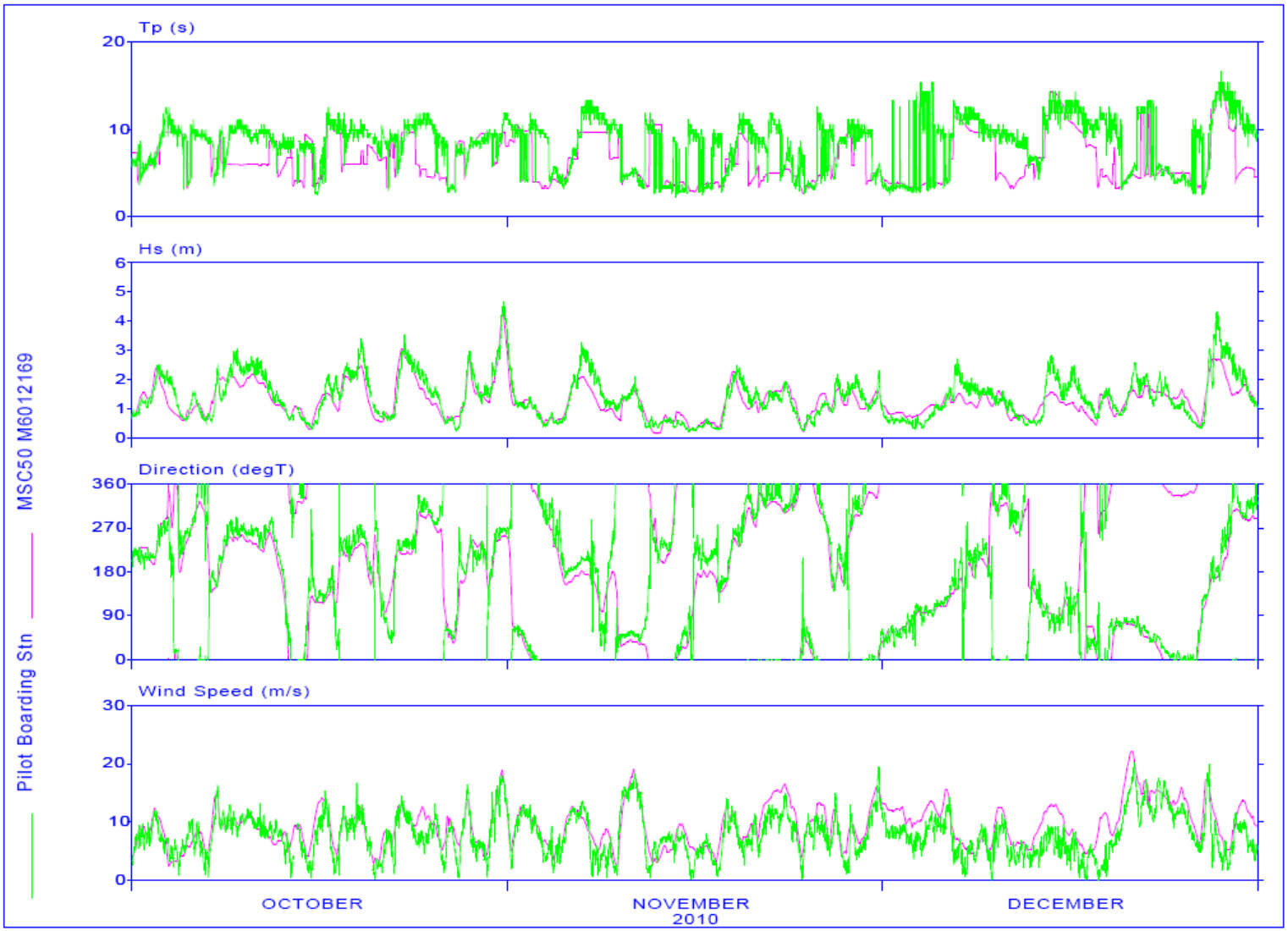

Source: SmartBay 2012

Figure 4-47 Wind and Wave Comparison, MSC50 (Near Argentia) and SmartBay (Pilot Boarding Station)

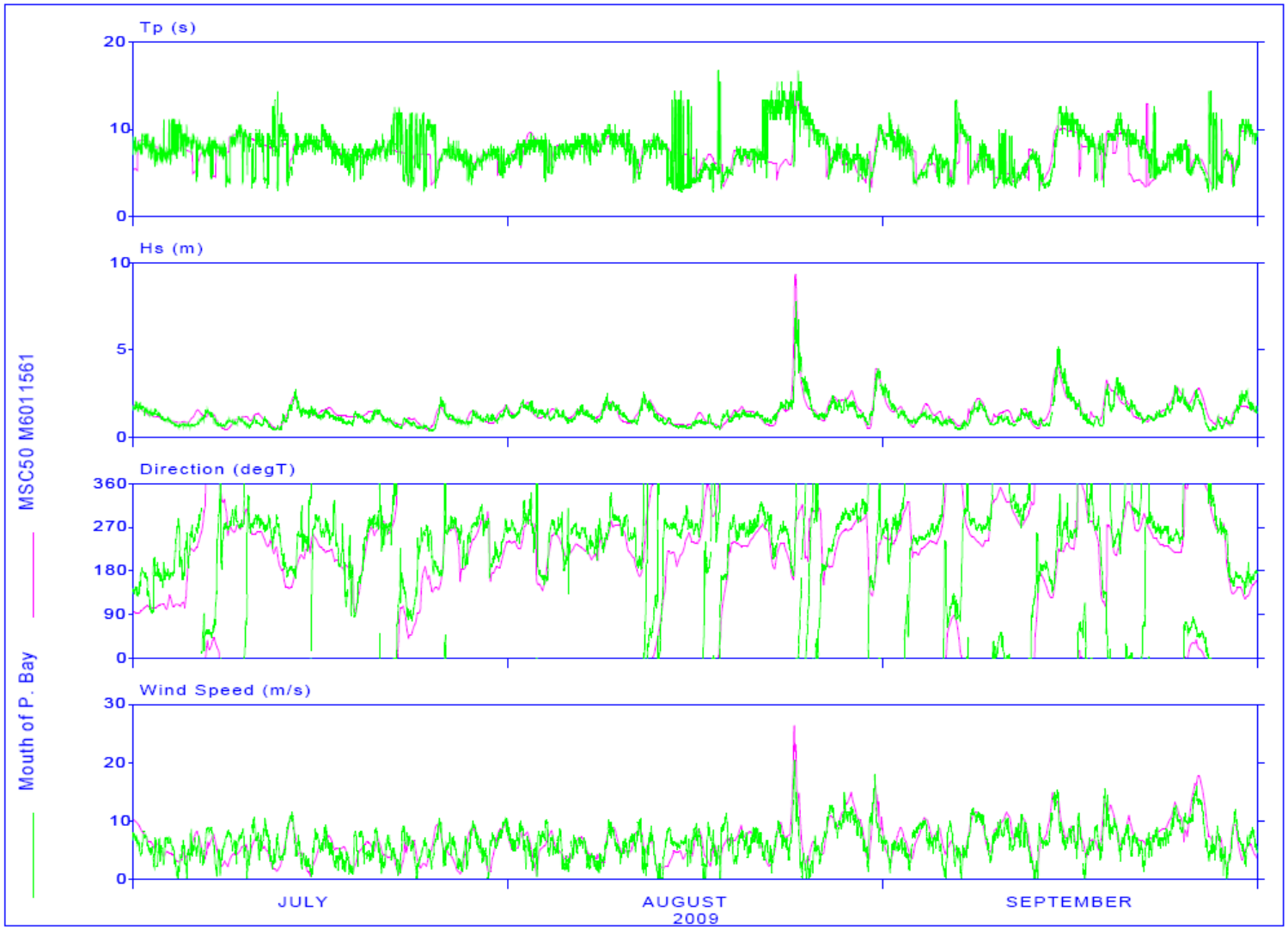

Source: SmartBay 2012

Figure 4-48 Wind and Wave Comparison, MSC50 and SmartBay, Mouth of Placentia Bay

Table 4-29 Monthly and Annual Wave Statistics, SmartBay Buoys

	Pilot Boarding Station		Mouth of Placentia Bay		Come By Chance Point	
Month	**Mean (m)**	**Maximum (m)**	**Mean (m)**	**Maximum (m)**	**Mean (m)**	**Maximum (m)**
Jan	1.7	5.6	2.4	9.1	0.4	1.7
Feb	1.8	5.8	2.5	7.7	0.5	2.7
Mar	1.5	3.8	1.8	5.8	0.5	1.7
Apr	1.7	6.1	1.9	6.9	0.5	2.1
May	0.6	1.9	1.3	4.4	0.2	1.0
Jun	0.7	2.6	1.2	4.1	0.5	1.6
Jul	1.0	6.4	1.3	5.7	0.4	1.6
Aug	0.8	2.6	1.3	7.8	0.2	0.9
Sep	1.2	4.0	1.4	5.2	0.4	1.9
Oct	1.5	7.5	1.6	7.9	0.5	2.1
Nov	1.7	4.4	2.0	6.1	0.4	2.1
Dec	1.3	4.7	2.4	8.0	0.4	2.8
Annual	1.3	7.5	1.7	9.1	0.4	2.8
Source: SmartBay 2012						

Since the SmartBay program has only been running since 2006, the buoy data have not sampled a substantial amount of storms; hence, a lower range of maximum wind speeds will have been encountered.

While the monthly averages are quite comparable between the MSC50 and SmartBay datasets (differences typically between 1 and 2 m/s), the maximum wind speeds from the SmartBay buoys show speeds of 5 to 8 m/s lower than the MSC50.

4.2.2.3 Tsunamis

Tsunamis are long-period gravity waves generated in a body of water by an impulsive disturbance that vertically displaces the water column. Earthquakes, landslides, volcanic eruptions and even explosions or the impact of cosmic bodies such as meteorites can generate tsunamis. The resulting wave energy spreads outwards across the ocean at high speed. Tsunami occurrences in Canada are rare, with the Pacific Coast at greatest risk due to the high occurrence of earthquake and landslide activity in the Pacific Ocean. Their occurrence can result in major damage and loss of life.

Tsunamis generated by earthquakes generally originate from what is referred to as far-field sources; they are sometimes called teletsunamis. Tsunamis resulting from the deformation of the sea floor caused by an earthquake can travel far, while tsunamis generated by other mechanisms generally dissipate quickly, only affecting areas close to the source. Not all earthquakes generate tsunamis (DFO 2008a).

For Newfoundland and the Grand Banks, the most relevant far-field sources are the Azores-Gibraltar Ridge zone, the Mid-Atlantic Ridge and the north side of the Caribbean Arc. Tsunamis generated by other mechanisms generally originate from near-field sources such as the Laurentian Channel, origin of the 1929 Grand Banks tsunami.

A potential near-field source for the construction site at Argentia would be a substantial landslide in Placentia Bay or on the Grand Banks. There are four instances of probable or confirmed tsunamis in Newfoundland:

- Probable tsunami: November 1, 1755. “Probable result of Lisbon earthquake. Emptied Bonavista harbour and 10 minutes later water returned and overflowed parts of the community.” (Newfoundland and Labrador Heritage 2000).
- Probable tsunami: September 24, 1848. “Teletsunami from unknown source location. The tsunami was observed in southern Labrador from Fishing Ships Harbour to St. John's. No earthquake was recorded on that day, so it is likely that this was a landslide-induced tsunami, or possibly from an offshore earthquake, although none was recorded.” (National Geophysical Data Center 2009).
- Probable tsunami: June 27, 1864. “An earthquake off the southwestern coast of the Avalon Peninsula caused a local tsunami at Saint Shotts.” (National Geophysical Data Center 2009).
- Confirmed tsunami: November 18, 1929. An earthquake of magnitude 7.2 occurred approximately 250 km south of Newfoundland along the southern edge of the Grand Banks, at 5:02 PM local time. "The earthquake triggered a large submarine slump (an estimated volume of 200 cubic km of material was moved on the Laurentian slope) which ruptured 12 transatlantic cables in multiple places, and generated a tsunami. The tsunami was recorded along the eastern seaboard as far south as South Carolina and across the Atlantic Ocean in Portugal." Approximately 2.5 hours after the earthquake, tsunami waves struck the Burin in three main pulses, causing the local sea level to rise between 2 and 7 m, with waters as high as 13 m in some bays on the Burin. The tsunami claimed 28 lives and destroyed or moved many buildings.” (Natural Resources Canada, 2008; National Geophysical Data Center 2009).

The location of the 1929 Grand Banks tsunami event in the Laurentian Channel is shown in Figure 4-49, as is the location of 32 of the 45 associated tsunami runups (purple crosses), primarily on the Burin Peninsula, and the 1864 Saint Shotts tsunami event (green square).

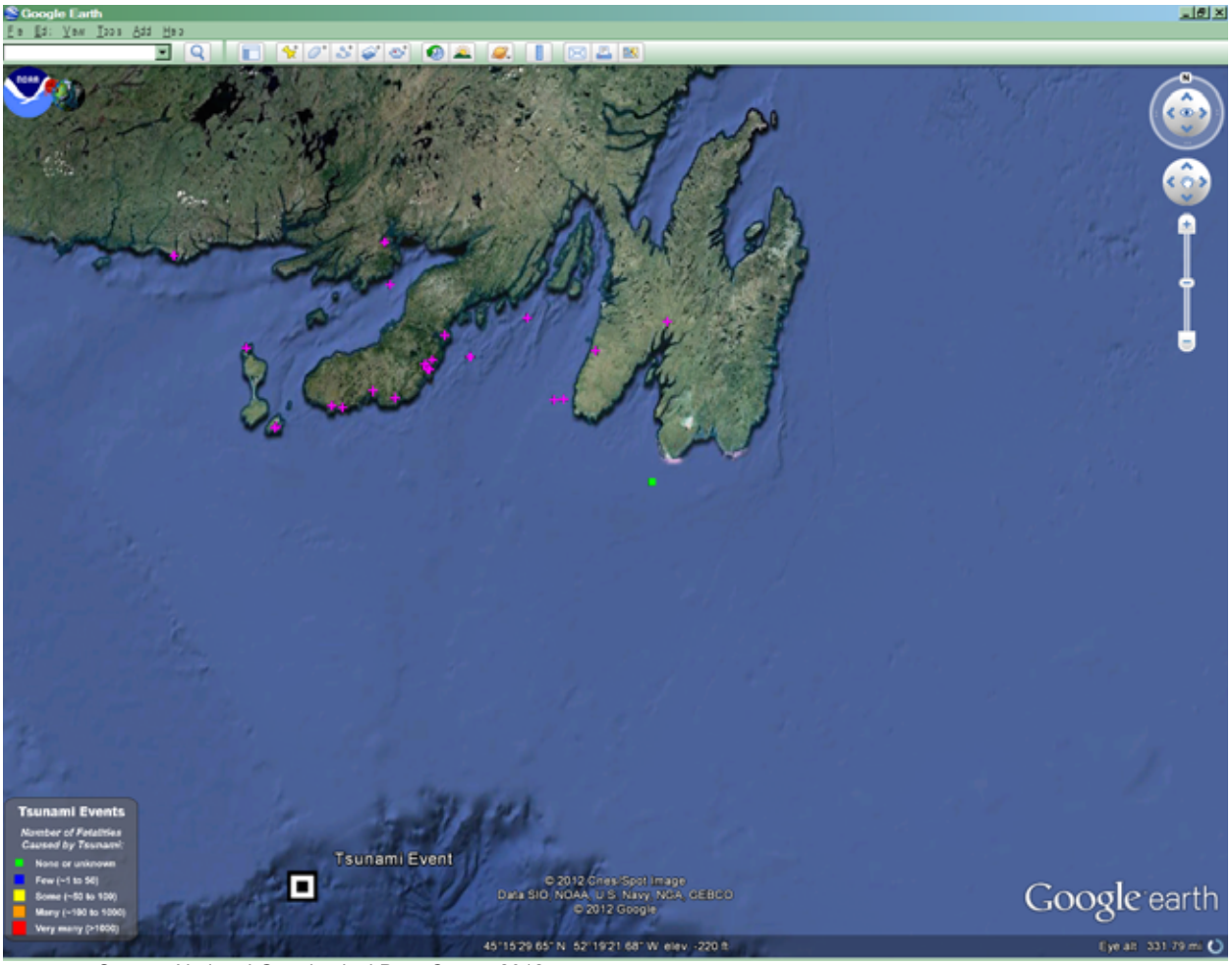

Source: National Geophysical Data Center 2012

Figure 4-49 Newfoundland Tsunami Events and Runups

The geological stability of the region is illustrated in Figure 4-50 where a high relative hazard is shown near the site of the 1929 Laurentian Slope earthquake (Magnitude 7.2). Otherwise, the region shows low to moderate relative hazard, and historically only small earthquakes typically of Magnitude 3 or 4 occur (Figure 4-51). It has been found that, in general, earthquakes of about Magnitude 6.5 or greater are necessary to induce offsets and rupture lengths sufficient to generate a tsunami (Gonzalez et al. 2007).

Tsunamis are an infrequent event in Atlantic Canada. Given the historical record of probable or confirmed tsunamis in Newfoundland noted above, and the historical record of earthquakes of tsunamigenic potential in the Atlantic region, over these periods on the order of 300 to 400 years, one might therefore estimate a tsunami return period on the order of 50 to 100 years, or longer for a destructive tsunami like the 1929 event.

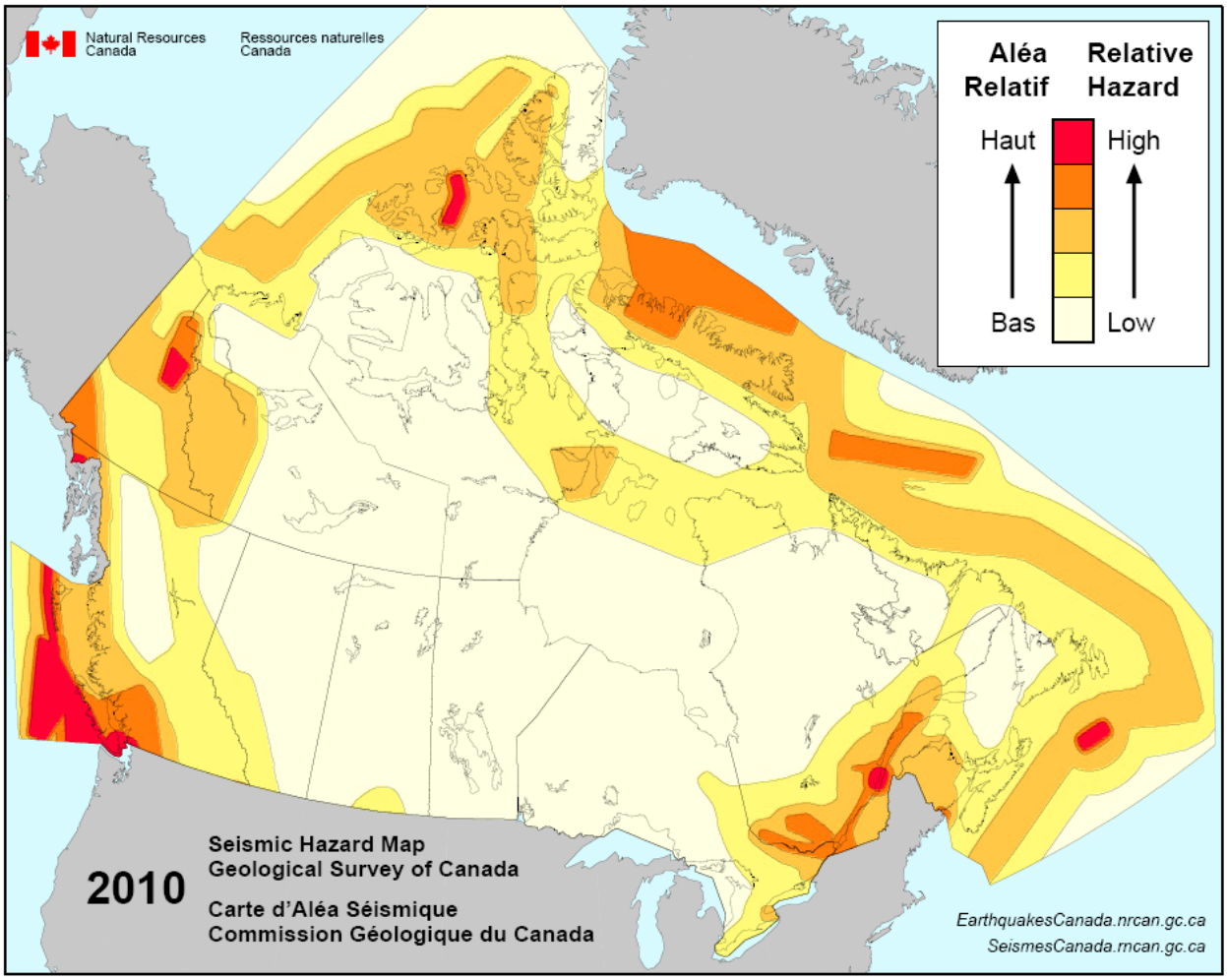

Source: Natural Resources Canada 2011a

Figure 4-50 Simplified Seismic Hazard Map for Canada

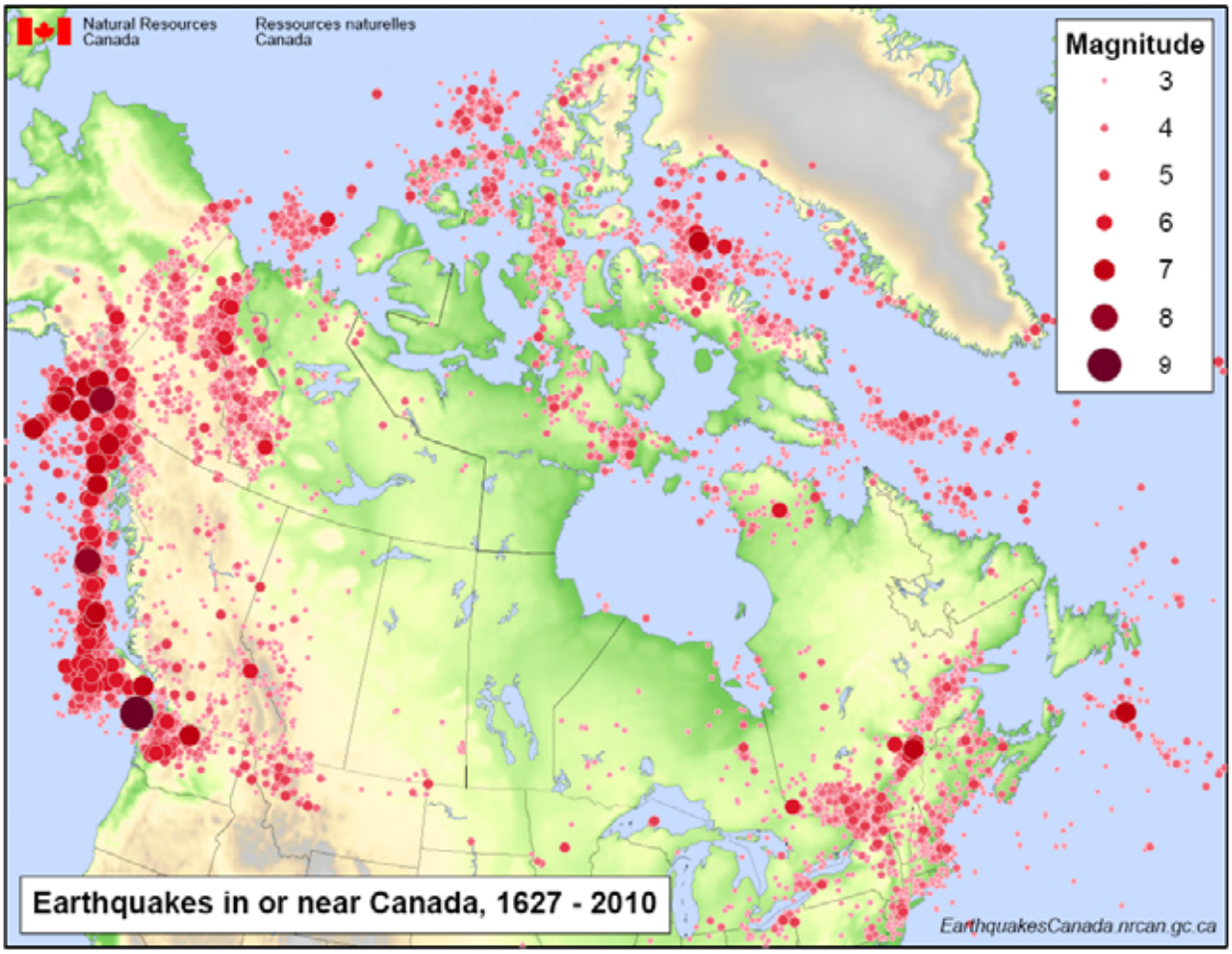

Source: Natural Resources Canada 2011b

Figure 4-51 Earthquakes in or near Canada, 1627-2010

4.2.2.4 Currents

Studies of circulation in Placentia Bay (e.g., Lawrence et al. 1973; Seaconsult 1988, 1989; Hart et al. 1999; Douglas et al. 2000) describe a general cyclonic circulation during spring and summer, with waters entering by the eastern shore and leaving by the western shore, forming a counter-clockwise open gyre in the bay.

Mean speeds are generally weak and range from 8 to 18 cm/s at the surface (in the top approximately 20 m) and from 3 to 7 cm/s at sub-surface (approximately 45 to 55 m). Bottom currents in the deepest part of the bay and the channel were published only once (April to June 1998), in the western and eastern shore, at 180 and 110 m water depth, respectively. They show barely measurable currents on the order of a few cm/s (Hart et al. 1999). Little correlation was found between the wind stress and the observed currents at any depth (Seaconsult 1989; Douglas et al. 2000).

Possible evidence of a counter-current on the edge of the east slope of the main channel in Placentia Bay has been described in the study by Seaconsult (1989), but hasn't been confirmed in the studies by Hart et al. (1999) or Douglas et al. (2000).

A general circulation modelling study has also been performed for the Newfoundland Shelf (Han 2005) and is thought to give a reasonable estimate of the current seasonality at the entrance of the bay (G. Han, pers. comm.). The results of this study are presented in Figure 4-52 and are in good agreement with available measurements (surface currents approximately 10 cm/s, mid-depth currents approximately 5 cm/s and bottom currents approximately 2 cm/s).

The results show the seasonality of the general circulation, with stronger inshore currents present during fall and weaker currents present during spring and summer, which seem to be associated with the inshore Labrador Current (G. Han, pers. comm.).

Ocean Currents: Measurements

The SmartBay buoys have provided current measurement at the Come By Chance Point and Pilot Boarding Station locations since July 2010, and at the Mouth of Placentia Bay location since June 2007 (albeit with some data gaps as noted Section 4.2.2.2, Footnote 3). Current meters are located approximately 0.5 m below the sea surface.

A summary of monthly mean and 95 percent upper limit surface current speeds for the three buoys is presented in Table 4-30, with statistics through December 2011 (November 2011 for the Mouth of Placentia Bay). Currents are light at the head of the bay: at Come By Chance Point mean surface currents are approximately 8 cm/s most months and 95 percent upper limit speeds range from 11 cm/s in July to 23 cm/s in September. Currents are measurably larger at the Pilot Boarding Station location near Argentia; mean currents of approximately 22 cm/s, with 95 percent upper limit speeds ranging from 33 cm/s in December to 48 cm/s in September. The largest currents from the buoys are at the mouth of Placentia Bay: mean currents range from 19 cm/s in June and July to 29 cm/s in November, with 95 percent upper limit speeds ranging from 135 cm/s in February to 178 cm/s in November. The annual 95 percent upper limit current speed at the mouth of Placentia Bay buoy is 59 cm/s.

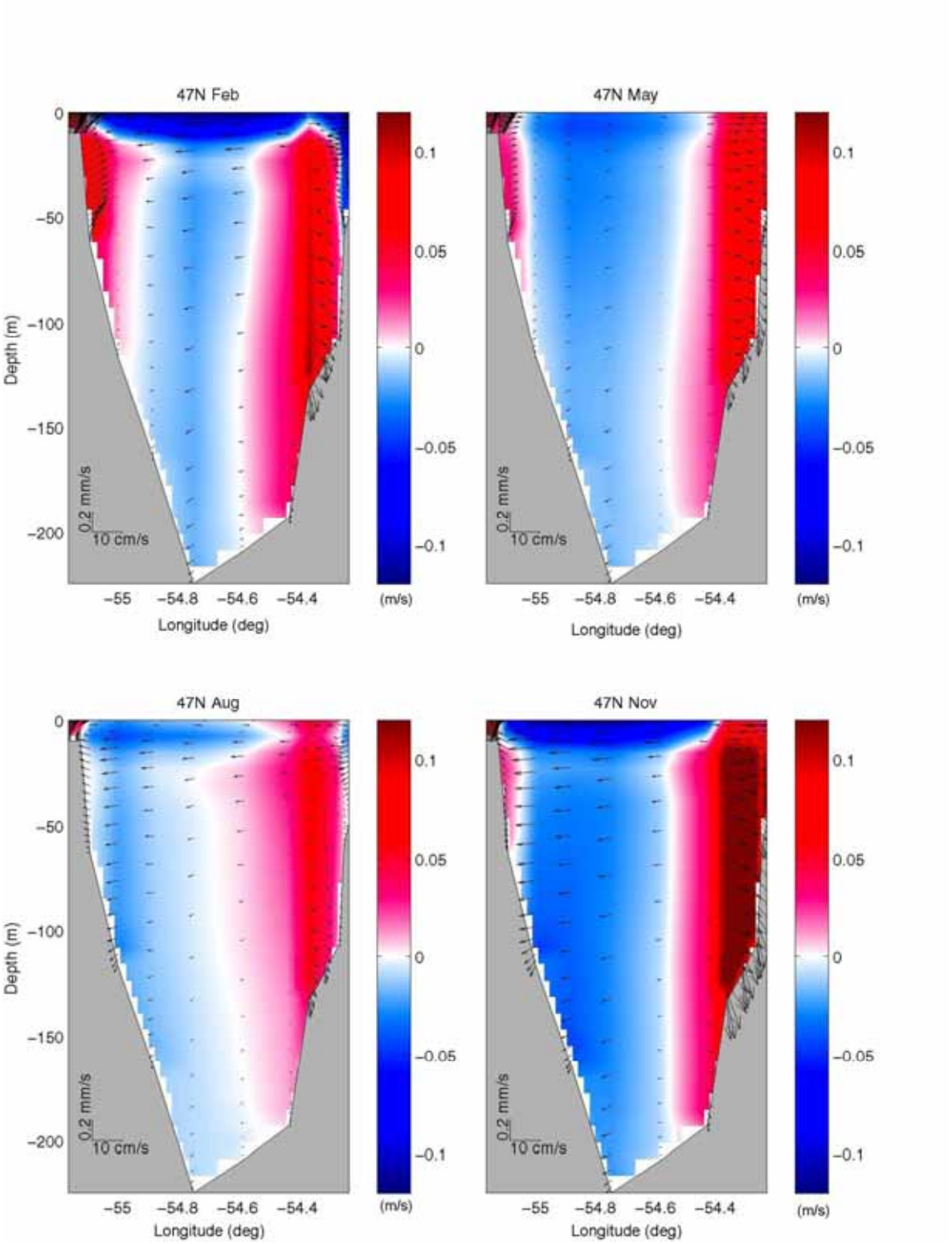

Source: G. Han, pers. comm.
Note: positive, red, indicates currents to the north; negative, blue, indicates currents to the south

Figure 4-52 Seasonal Current Profiles West-to-East, along 47°N, Entrance of Placentia Bay

Table 4-30 Monthly Surface Current Statistics, SmartBay Buoys

Month	Pilot Boarding Station		Mouth of Placentia Bay		Come By Chance Point	
	Mean (cm/s)	95% Upper Limit (cm/s)	Mean (cm/s)	95% Upper Limit (cm/s)	Mean (cm/s)	95% Upper Limit (cm/s)
Jan	20	39	27	51	8	16
Feb	20	41	25	48	8	17
Mar	21	39	24	52	10	20
Apr	18	34	22	53	9	20
May	20	40	23	61	8	17
Jun	19	37	19	54	9	19
Jul	21	45	19	49	3	11
Aug	23	45	23	63	8	17
Sep	26	48	26	69	9	23
Oct	25	45	28	71	8	19
Nov	22	46	29	72	7	17
Dec	15	33	24	46	8	18
Annual	22	43	24	59	8	18
Source: SmartBay 2012						

Example three month plots of wind, current, and waves for the three SmartBay buoy are presented in Figures 4-53 to 4-55 for illustration of the normal current speeds measured, as well as some of the larger current events found in the record. Current and wind directions are shown in the same panel, with current direction “to”.

A three-month period in late summer-early fall 2010 at the Come By Chance Point buoy is shown in Figure 4-53. The largest measured currents from the SmartBay record at this location are 70 cm/s on September 22, in contrast to the mean September current speed of 9 cm/s.

A three-month period in fall 2010 at the Pilot Boarding Station buoy is shown in Figure 4-54. The high current speed event takes place on September 13, with a maximum measured current speed of 97 cm/s and average speed of 70 cm/s over the 24 hours around this peak. A similar event took place in November, with maximum current speeds of 94 cm/s measured on November 11, and speeds averaging 55 cm/s over the two days around this event. These are the largest measured currents in the Pilot Boarding Station SmartBay buoy record. The mean November current speed is 22 cm/s.

A three-month period in late summer 2009 at the mouth of Placentia Bay Station buoy is shown in Figure 4-55. Currents average 65 cm/s. On the morning of August 24, the current reaches a maximum speed of 90 cm/s. This is in contrast to the previous day, in which speeds averaged 10 cm/s; the August mean current speed is 23 cm/s.

Source: SmartBay 2012

Figure 4-53 SmartBay, Come By Chance Point, Wind, Current, Waves, Aug-Oct 2010

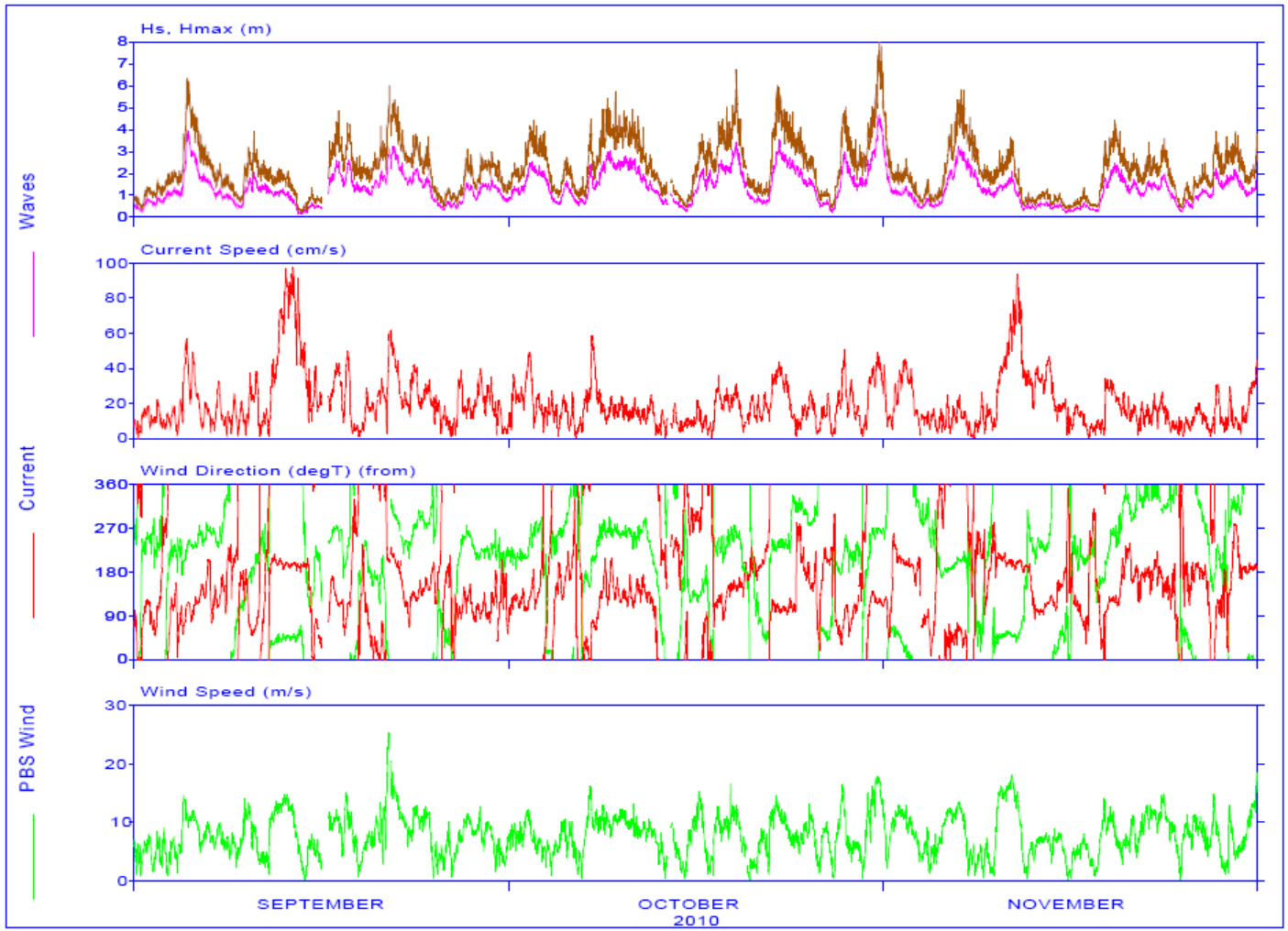

Source: SmartBay 2012

Figure 4-54 SmartBay, Pilot Boarding Station, Wind, Current, Waves, Sep-Nov 2010

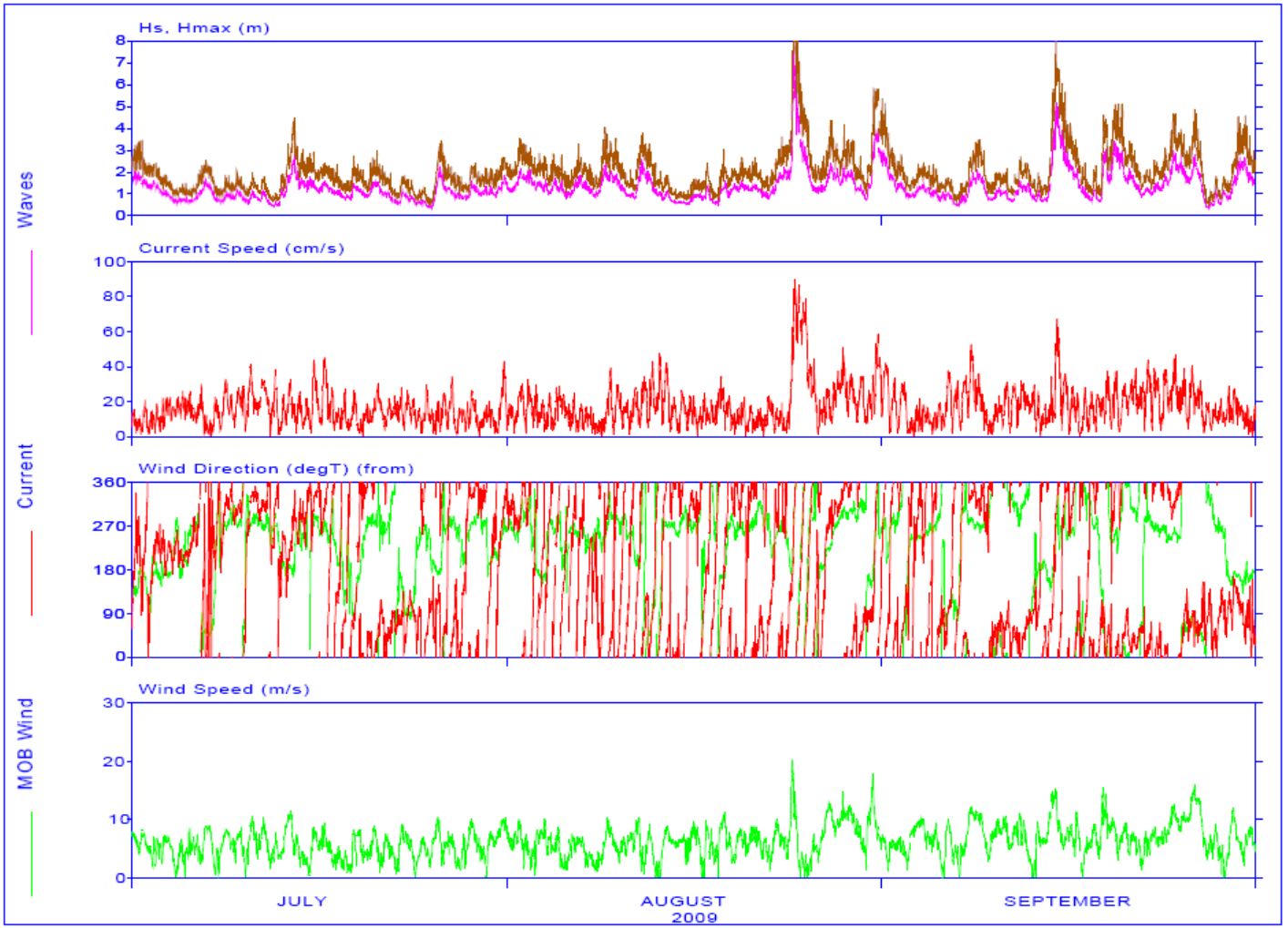

Source: SmartBay 2012

Figure 4-55 SmartBay, Mouth of Placentia Bay, Wind, Current, Waves, Jul-Sep 2009

Ocean Currents: Regional Modelling

DFO has developed a three-dimensional (3-D) circulation model based on a finite-volume coastal ocean model (FVCOM) to simulate temperature, currents and stratification. The model is forced, at the lateral open boundaries, with five leading tidal constituents and non-tidal sea surface elevation and at the surface with wind and heat flux. The open boundary temperature, salinity and non-tidal sea levels are derived from a larger-scale shelf model. Simulated tides agree well with tide-gauge data, and non-tidal currents show reasonable agreement with moored measurements (Ma et al. 2011).

The model realistically simulates many features of the bay, including the evolution of stratification from spring to fall, the cyclonic circulation in the outer bay and late-spring upwelling on the western side of the outer bay (Ma et al. 2011).

Tidal currents are light in Placentia Bay. Tidal ellipses, for the M2 and K1 tidal constituents, are presented in Figure 4-56. Observations are shown in red; the 100 and 200 m depth contours are shown. Tidal currents are approximately 2 to 5 cm/s near Argentia.

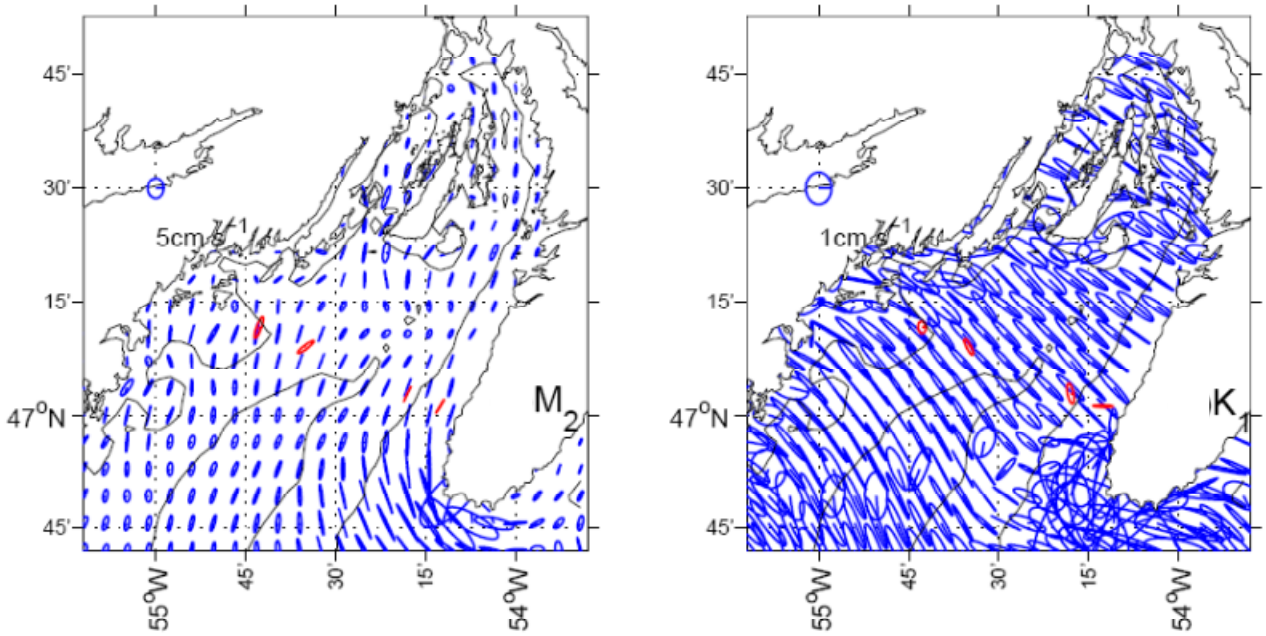

Source: Ma et al., 2011

Figure 4-56 Near-surface M2 and K1 Near-Surface Currents, Placentia Bay

Seasonal outputs of monthly-mean near-surface climatology for Placentia Bay, from the DFO FVCOM model (Ma et al. 2011), were obtained from DFO (G. Han, pers. comm.). These finite element grid points (approximately 40,000 for each month) were then sub-sampled to a rectangular grid with spacing of 0.05° (or 3', approximately every 3.8 km at latitude 47.5°N). The four seasonal maps (February, May, August, November) are shown in Figures 4-57 to 4-60.

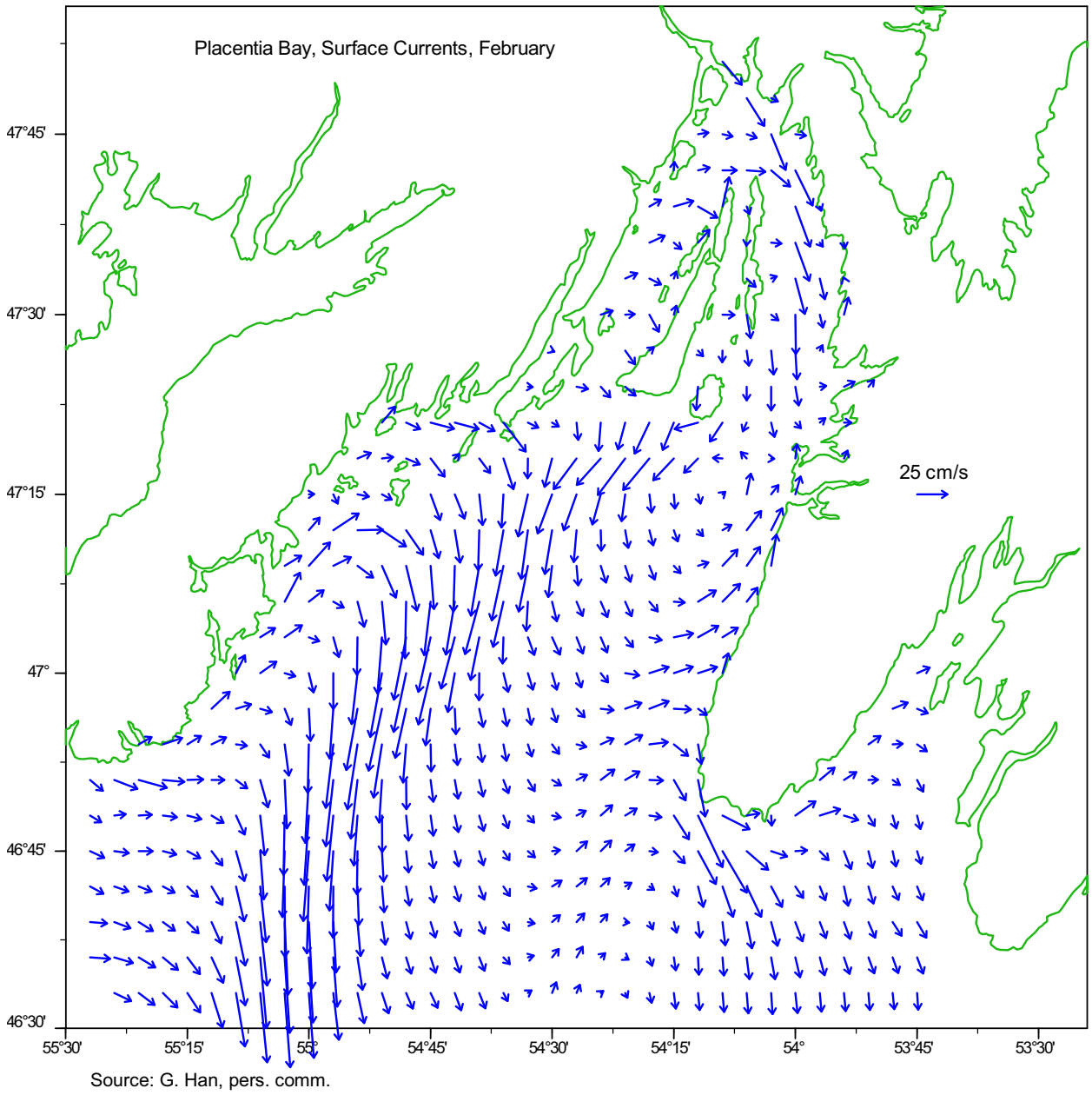

Figure 4-57 February Mean Near-Surface Currents, Placentia Bay

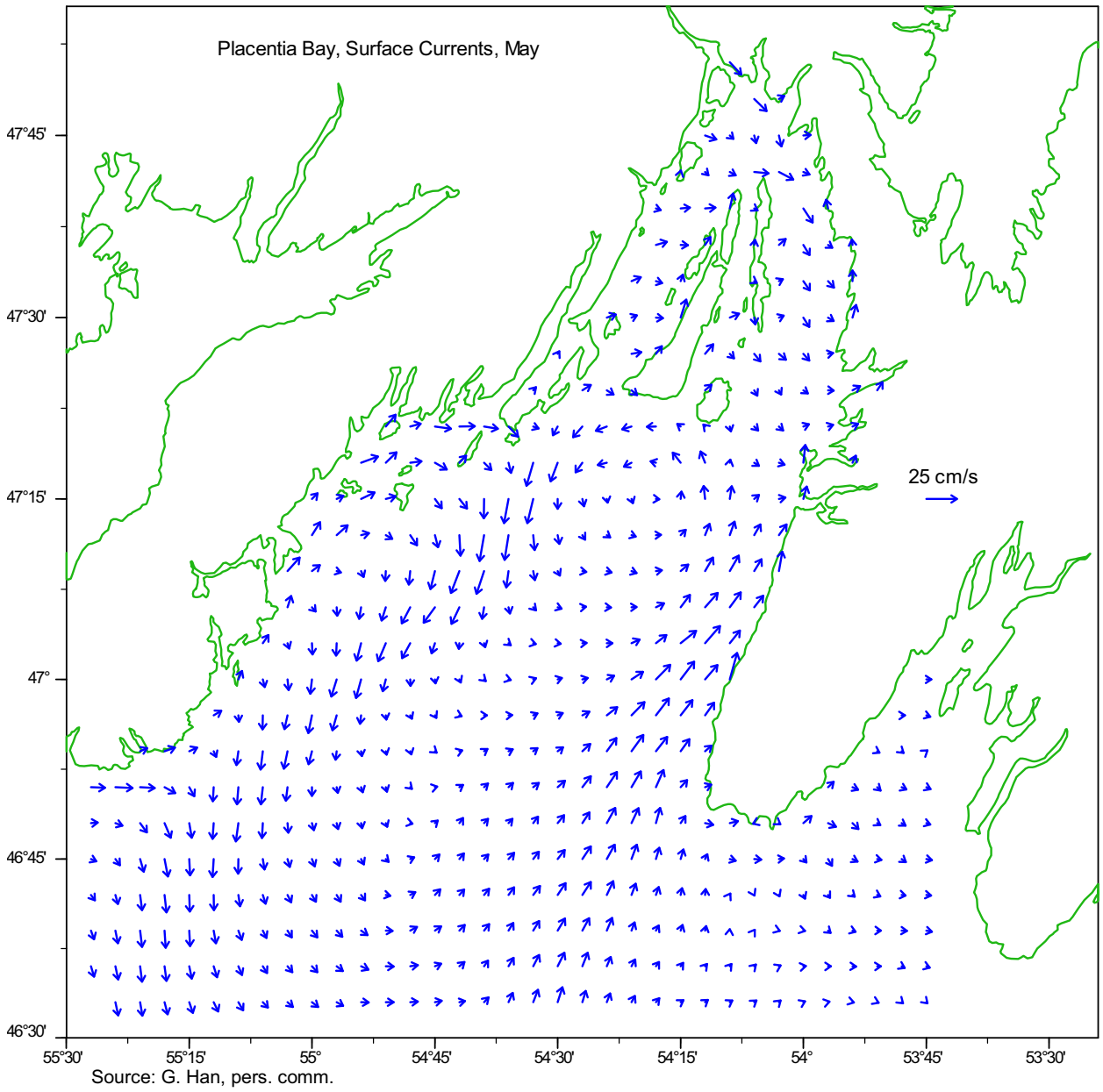

Source: G. Han, pers. comm.

Figure 4-58 May Mean Near-Surface Currents, Placentia Bay

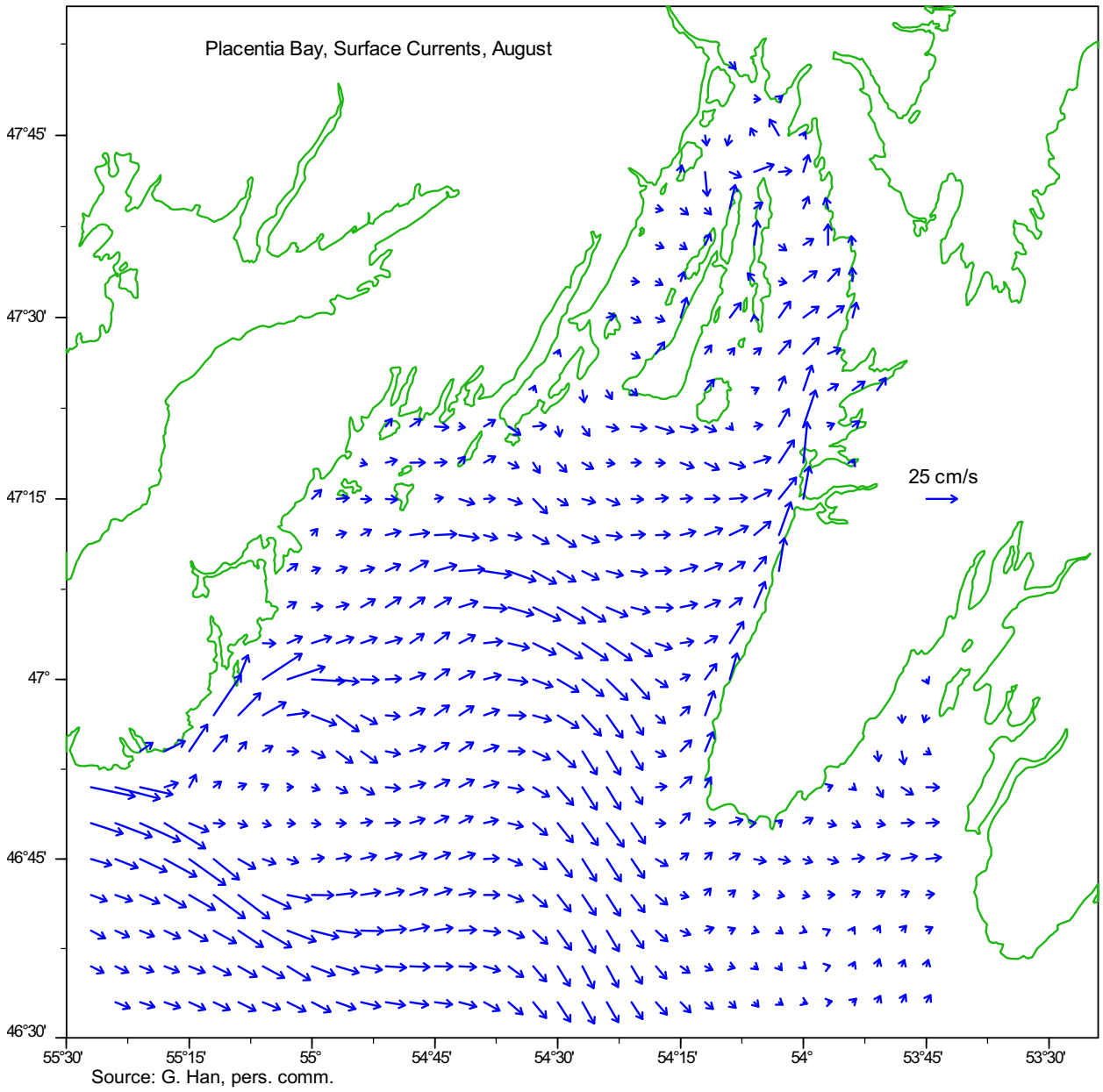

Figure 4-59 August Mean Near-Surface Currents, Placentia Bay

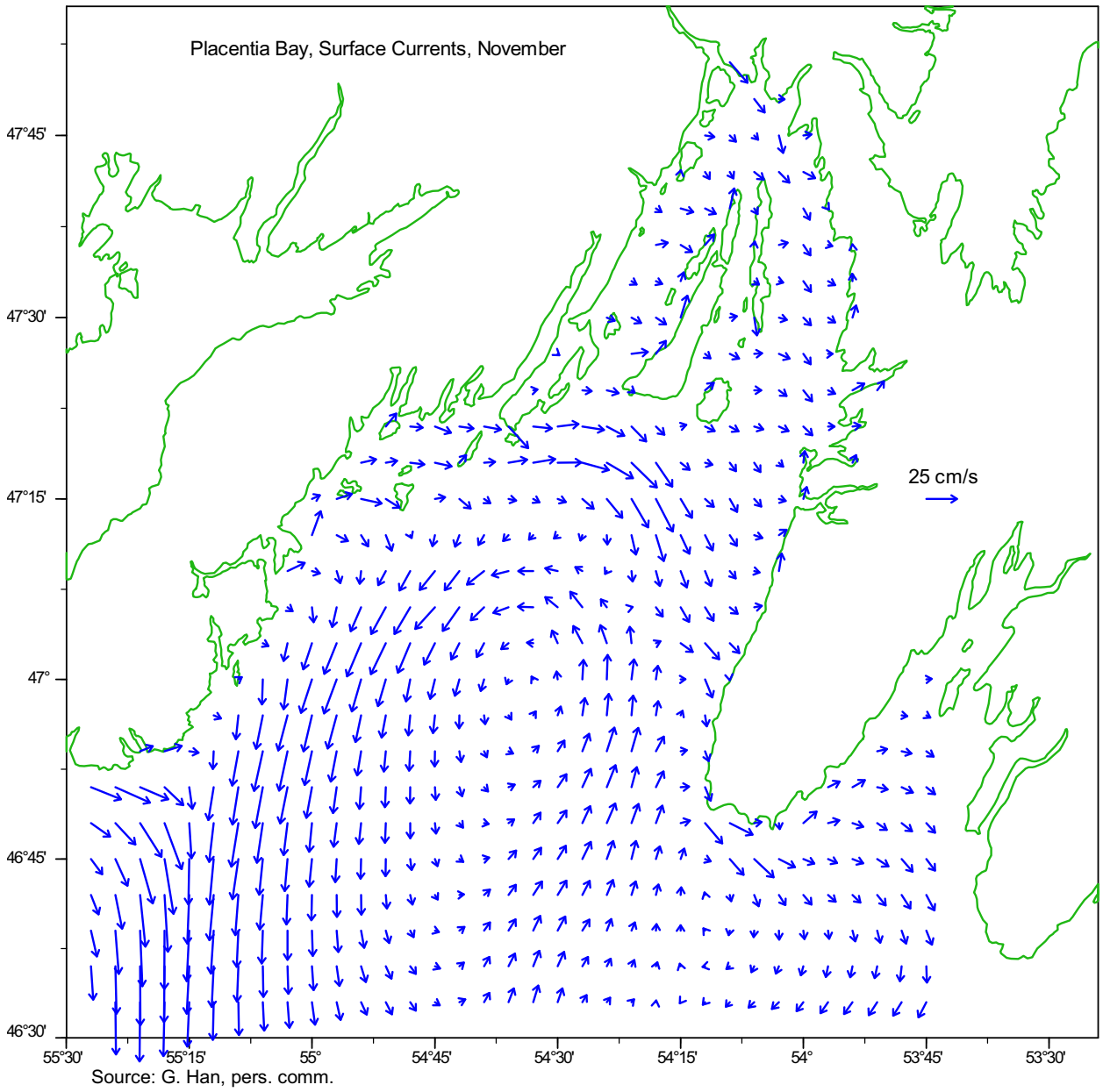

Figure 4-60 November Mean Near-Surface Currents, Placentia Bay

Mean and maximum currents, derived from the FVCOM model outputs, are noted in Table 4-31. Mean speeds over the bay are approximately 10 cm/s, slightly greater in the winter and slightly less in spring. The strongest mean currents, up to 70 cm/s, occur on the western side of the bay in winter and fall.

Table 4-31 Monthly-Mean Near-Surface Currents, Placentia Bay

Month	Mean Current Speed (cm/s)	Maximum Current Speed (cm/s)	Direction of Maximum Current (to)
Feb	12	66	ESE
May	7	63	ESE
Aug	9	46	E
Nov	9	70	ESE

Near Argentia, the mean flow is light in February, May and November, less than 10 cm/s. In February, a counter-clockwise gyre sits just west of Argentia Peninsula. While associated currents are light near Argentia, southerly currents up to approximately 30 cm/s occur to the north, and northerly currents up to approximately 25 cm/s occur to the south. The strongest currents occur up the Eastern Channel in August, up to 20 to 30 cm/s, in a northerly direction.

4.2.2.5 Tides, Storm Surges

Tides

Tides in Placentia Bay are primarily semi-diurnal, with two highs and two lows every 24 to 25 hours. Tidal ranges for Argentia, Come By Chance at the head of Placentia Bay and Burin, on the Burin Peninsula on the western shore of the bay, are presented in Table 4-32. Normal and extreme tidal elevations for Argentia are presented in Table 4-33. For orientation, the relation between tidal surfaces (e.g., Mean Water Level, Higher High Water, Mean Tide, Higher High Water, Large Tide), charting datums, and physical features are illustrated in Figure 4-61.

Table 4-32 Tidal Range, Placentia Bay

	Argentia	Come By Chance	Burin
Mean Tide Range (m)	1.6	1.6	1.5
Large Tide range (m)	2.4	2.5	2.2
Source: DFO 2012b			

Table 4-33 Normal and Extreme Tidal Levels, Argentia

	Argentia
Mean Water Level (m)	1.4
Higher High Water, Mean Tide (m)	2.3
Higher High Water, Large Tide (m)	2.6
Lower Low Water, Mean Tide (m)	0.7
Lower Low Water, Large Tide (m)	0.2
Recorded Extreme, Higher High Water (m)	3.4
Recorded Extreme, Lower Low Water (m)	-0.4
Source: DFO 2012b	

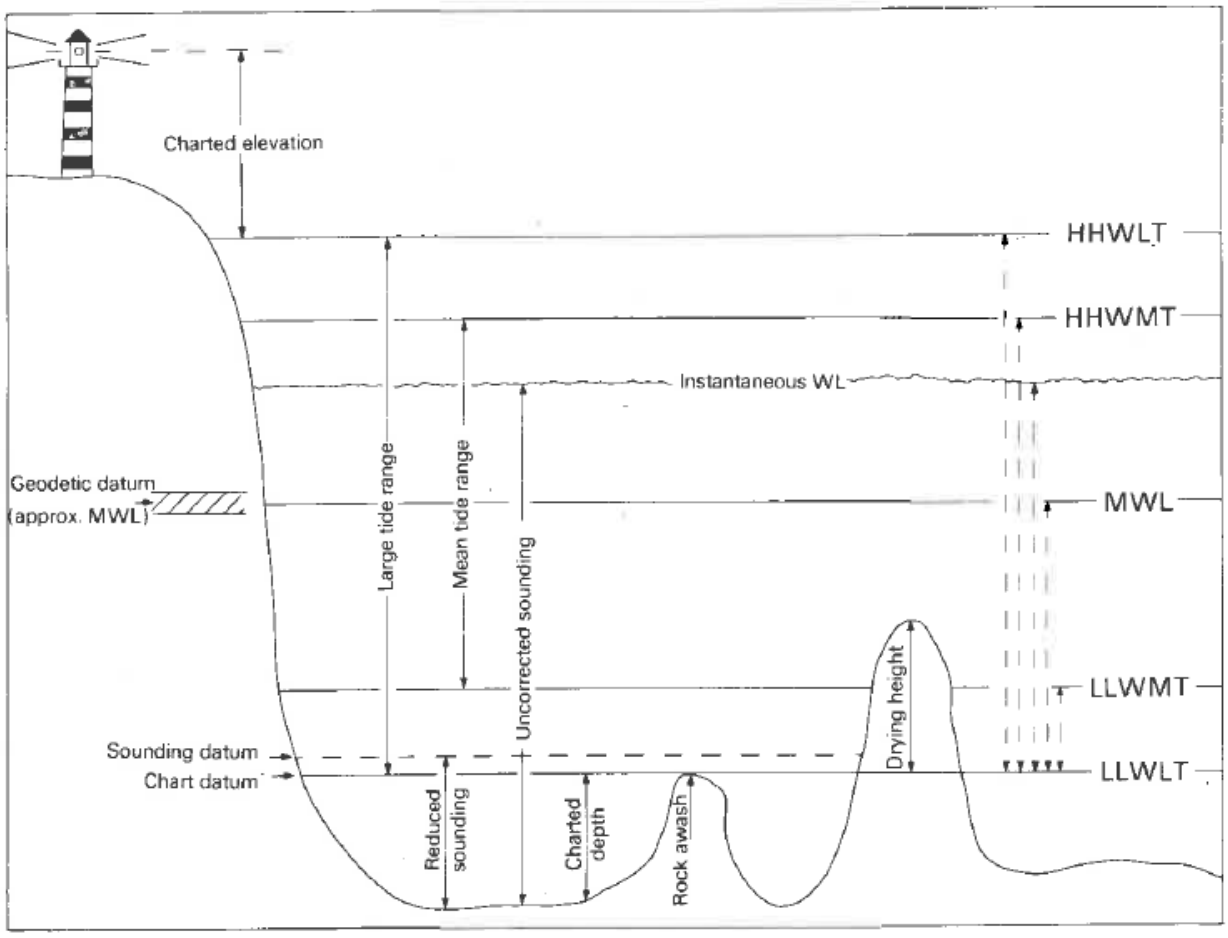

Source: Forrester 1983

Figure 4-61 Relation between Tidal Surfaces, Charting Datums and Physical Features

Co-tidal charts of the water surface elevation amplitude and phase of the strongest tidal components, the M2 principal semi-diurnal lunar characteristic of the tide, and K1 luni-solar diurnal characteristic of the tide, are shown in Figure 4-62. The charts indicate that for the semi-diurnal tide, the surface elevation amplitude is approximately 0.6 m (a tidal range of 1.2 m) at the mouth of bay, slightly higher, approximately 0.65 cm, towards the head of the bay. The tidal signal propagates from northeast to southwest, taking approximately a quarter-hour to traverse the bay. The diurnal tide propagates from the south, with an amplitude of approximately 0.05 m.

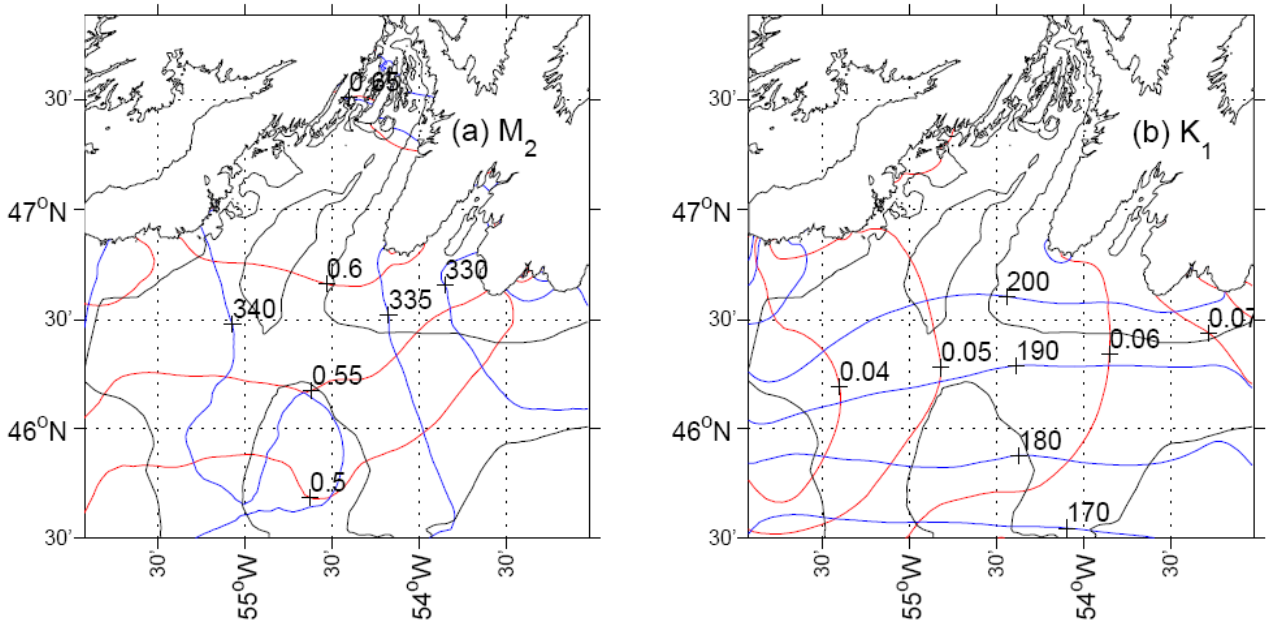

Source: Ma et al. 2011
Note: co-amplitude (red) and co-phase (blue)

Figure 4-62 Co-Tidal Chart of M2 (a) and K1 (b)

Storm Surge

The upper portion of Placentia Bay, particularly from Rushoon on the Burin Peninsula to near Placentia on the Avalon Peninsula is susceptible to frequent storm surges and seiches (due to the bay's wedge-shaped geometry and large islands at the head of the bay) (Bowyer 1995).

Storm surge or wind setup, associated with very low pressure storm systems passing through the region and strong winds blowing over the water surface, results in high water levels that can cause severe flooding for low-lying coastal regions.

Seiches are another phenomenon caused by both atmospheric pressure and wind-induced sea level changes. The seiche effect can be described as the return flow of water from one side of the bay (or lake or other enclosed water body) with an elevated level to the side with a depressed end. This process can result in oscillations of water levels similar to the sloshing action that occurs in an enclosed tank of water. During seiche effects, any given shoreline location may experience alternate periods of elevated

and depressed levels over a period of several hours, with the initial seiche levels being at much lower elevations than the original wind setup.

These hazards are further illustrated, in qualitative terms, in the Natural Resources Canada, Atlas of Canada, Natural Hazards Storm Surge interactive map, which shows the location of storm surge risk (both severity or consequences and frequency) in Canada (Figure 4-63)[4]. This indicates a high hazard (medium frequency, high severity) for the town of Placentia, given its low elevation.

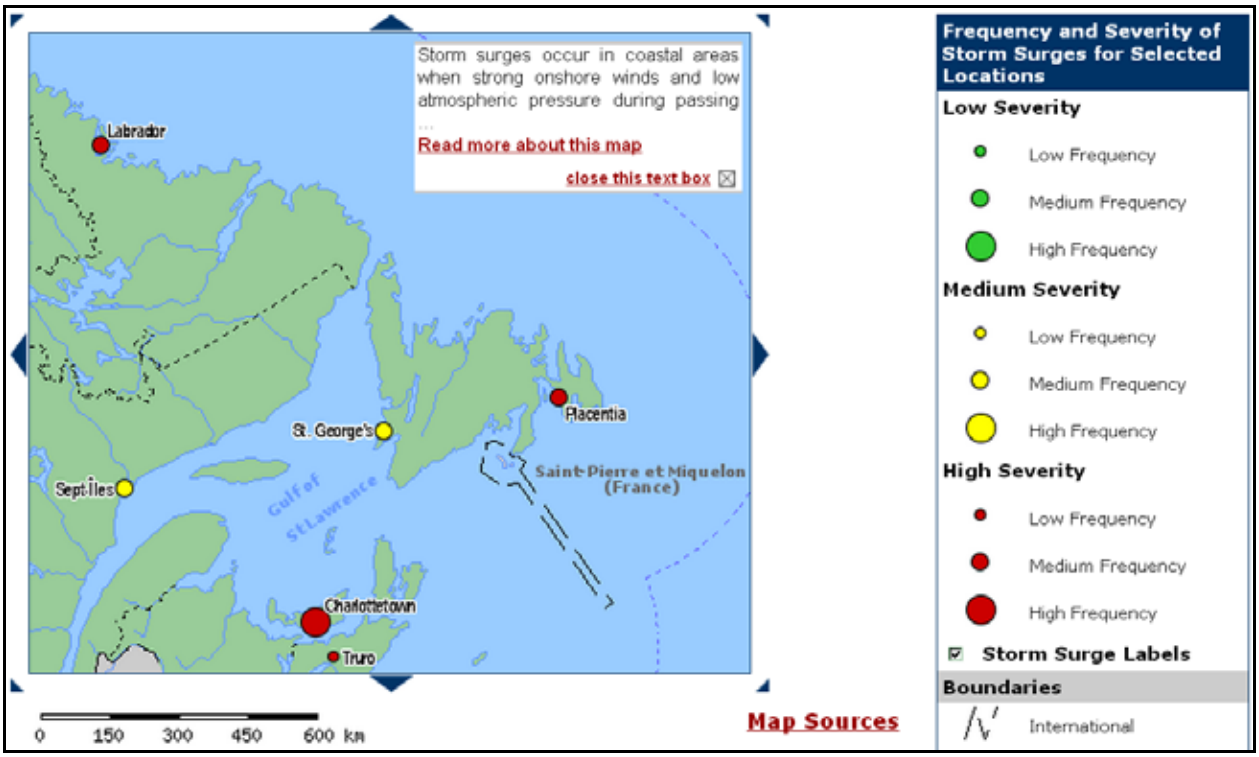

Source: Natural Resources Canada 2008
Note: The map shows a qualitative estimate of storm-surge hazard and the data shown are for illustrative purposes only and should not be used for local storm-surge hazard management.

Figure 4-63 The Atlas of Canada: Storm Surge Hazard Map, Newfoundland

An estimate of 0.8 m for probable maximum storm surge can be made from inspection of the 40-year return period hindcast values by Bernier and Thompson (2006), as illustrated in Figure 4-64.

[4] Each dot symbol on the map indicates a representative storm surge site. The site may represent a few to several hundred kilometres of shoreline. The size of the dots reflects frequency, not area covered. On this map, a low frequency means one surge every few years, a medium frequency indicates one surge every year and a high frequency represents several surges every year. Low severity corresponds to some flooding or erosion during large surges, with minor resulting damage. Medium severity indicates moderate flooding or erosion during large surges, with moderate damage. High severity means extensive flooding or severe erosion during large surges, with significant damage http://atlas.nrcan.gc.ca/site/english/maps/environment/naturalhazards/storm_surge/storm_surge/1

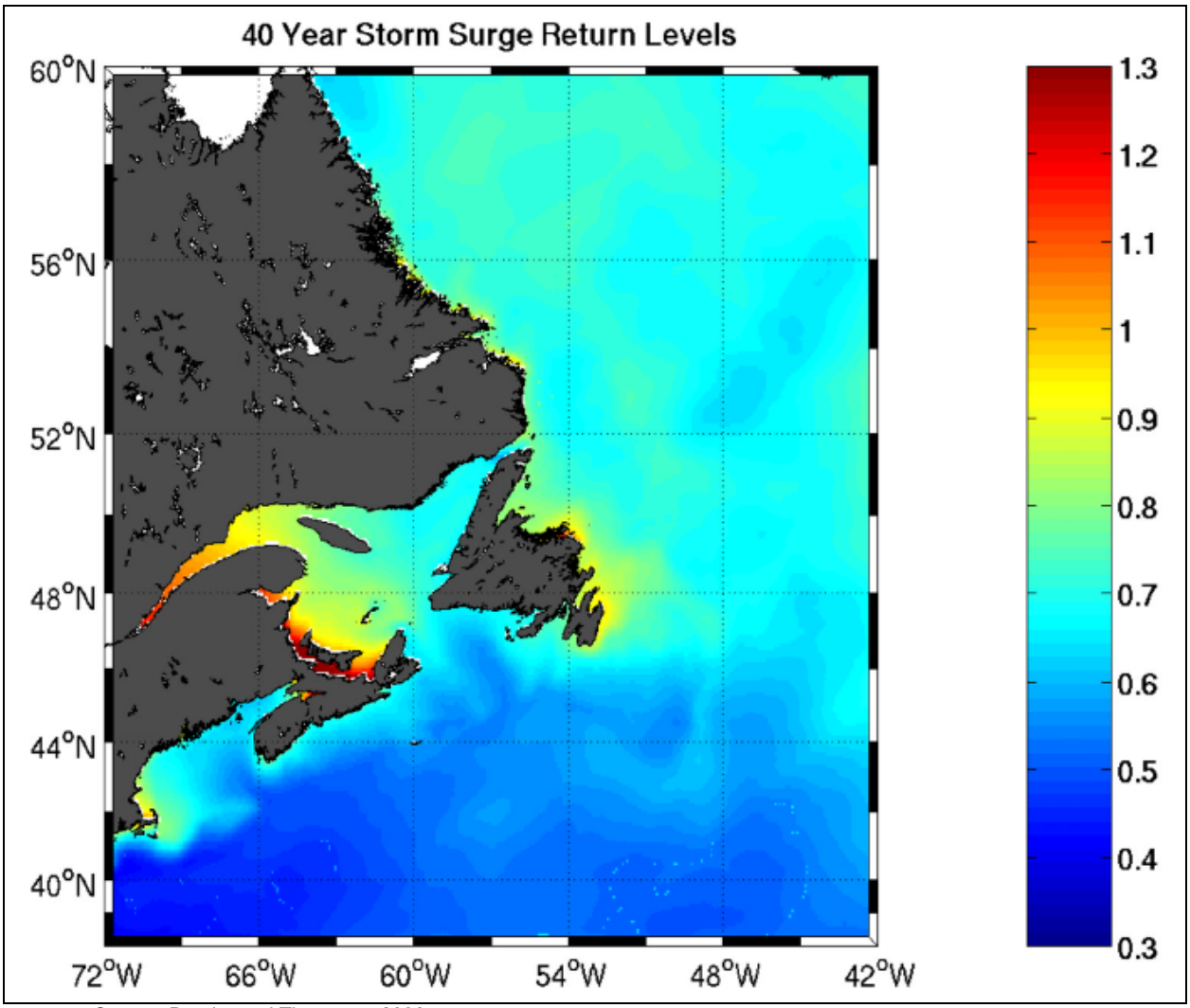

Source: Bernier and Thompson 2006

Figure 4-64 40-Year Return Level of Extreme Storm Surges, Atlantic Canada

An example of sudden and large changes in water levels associated with passage of a storm system is reported in the Guide to Marine Weather in Atlantic Canada (Bowyer 1995):

> On the morning of January 5, 1989, an intense low-pressure system crossed the Burin peninsula. Storm-force southerlies ahead of the low pushed very large seas in to Placentia Bay. It happened at high tide, when levels approached spring tide height. When this very high water was forced over the low-lying land near the town of Placentia, extensive flooding resulted. The tide gauge at the mouth of Argentia Harbour registered 3.17 m above the predicted tide – an all-time record.

Water levels at Argentia rose from low tide height values of approximately 1 m in the preceding days to a high of 2.62 m at 6 pm on January 4, dropping to a low of 1.67 m at 6 pm, and rising to a maximum height of 3.13 m at 6 am on January 5 (Figure 4-65). This is consistent with the HHW value of 3.4 m reported in Table 4-33.

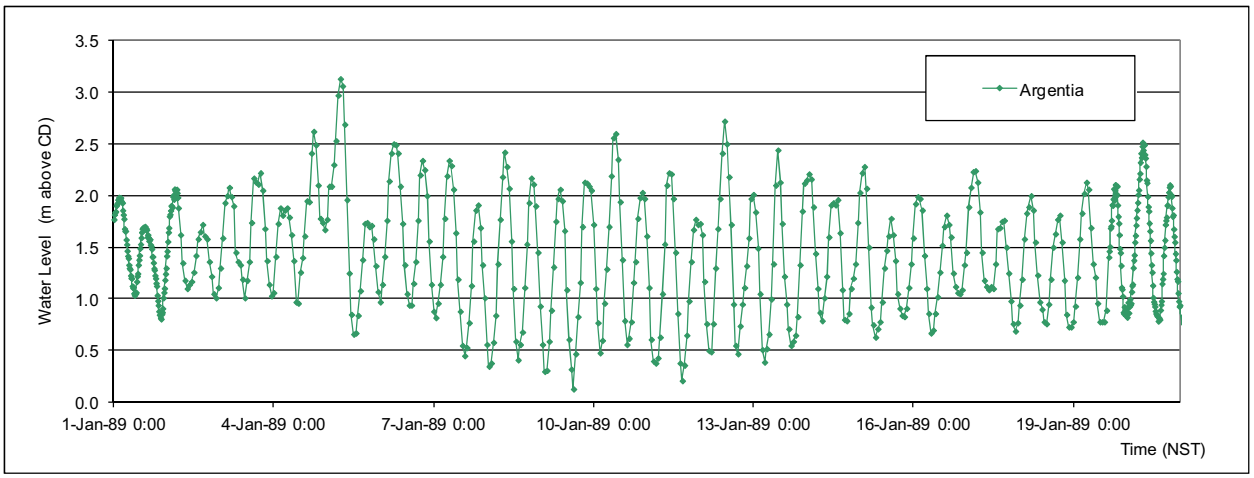

Source: DFO 2012b

Figure 4-65 Argentia Storm Surge Event, January 5, 1989

4.2.2.6 Physical and Chemical Properties

Temperature, salinity, and density data were extracted from the Bedford Institute of Oceanography (BIO) hydrographic database (BIO 2011). This database is a collection of temperature and salinity measurements for the area defined by 35° to 80° N and 42° to 100° W. The data come from a variety of sources, including hydrographic bottles, conductivity, temperature, depth (CTD) casts (either up or down casts), spatially and temporally averaged Batfish tows and expendable digital or mechanical bathythermographs. The database currently consists of approximately 850,000 profiles and 35 million individual observations from 1910 to the present and updates are made monthly. Data of the entire bay (47°N to 47.8°N and 54°W to 55.2°W) were acquired. Approximately 62,500 measurements were available and averaged on a monthly basis; the results are presented in Figures 4-66 to 4-68. The plots show monthly cross-sections of mean sea temperature, salinity, and water density vs. depth. For example, in January the mean sea temperature in the bay (Figure 4-66) is near-zero at all depths, whereas in August, with seasonal warming of the sea surface, sea temperature in the upper 20 m rises to 10 to 14°C. White patches in the figures indicate no data.

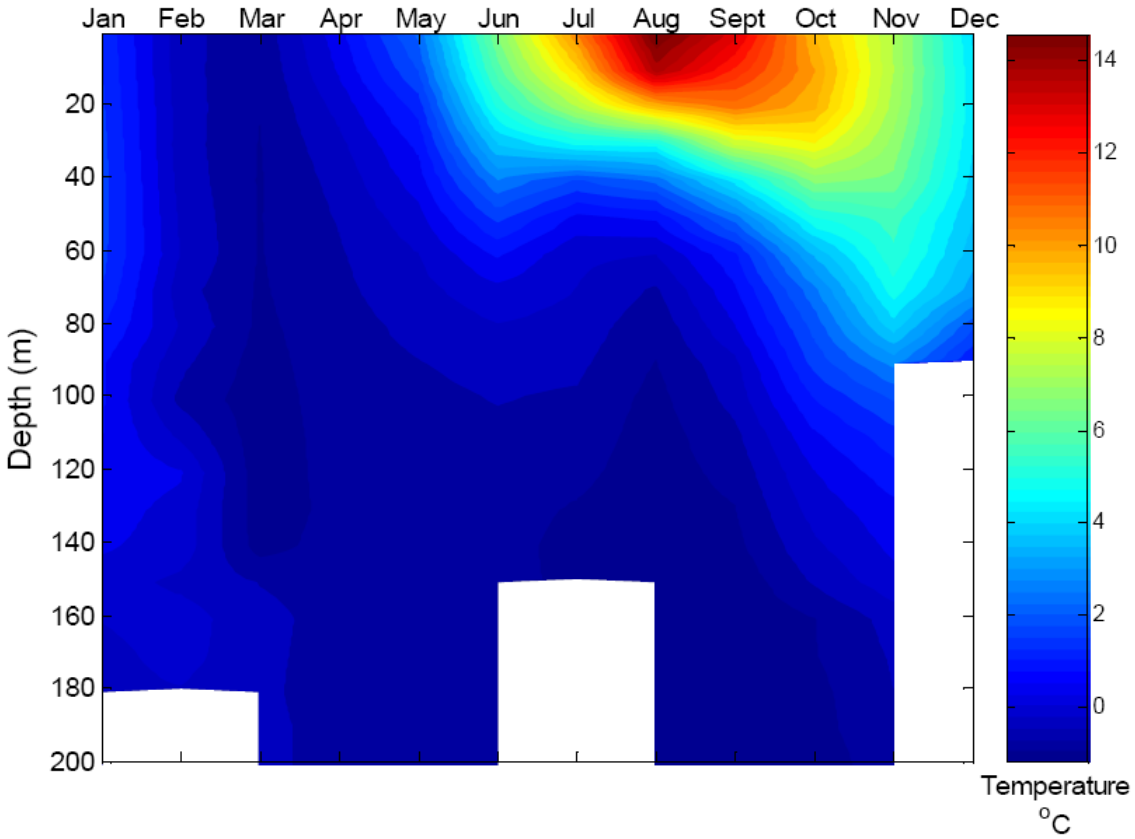

Source: BIO 2011

Figure 4-66 Monthly Mean Sea Temperature, Placentia Bay

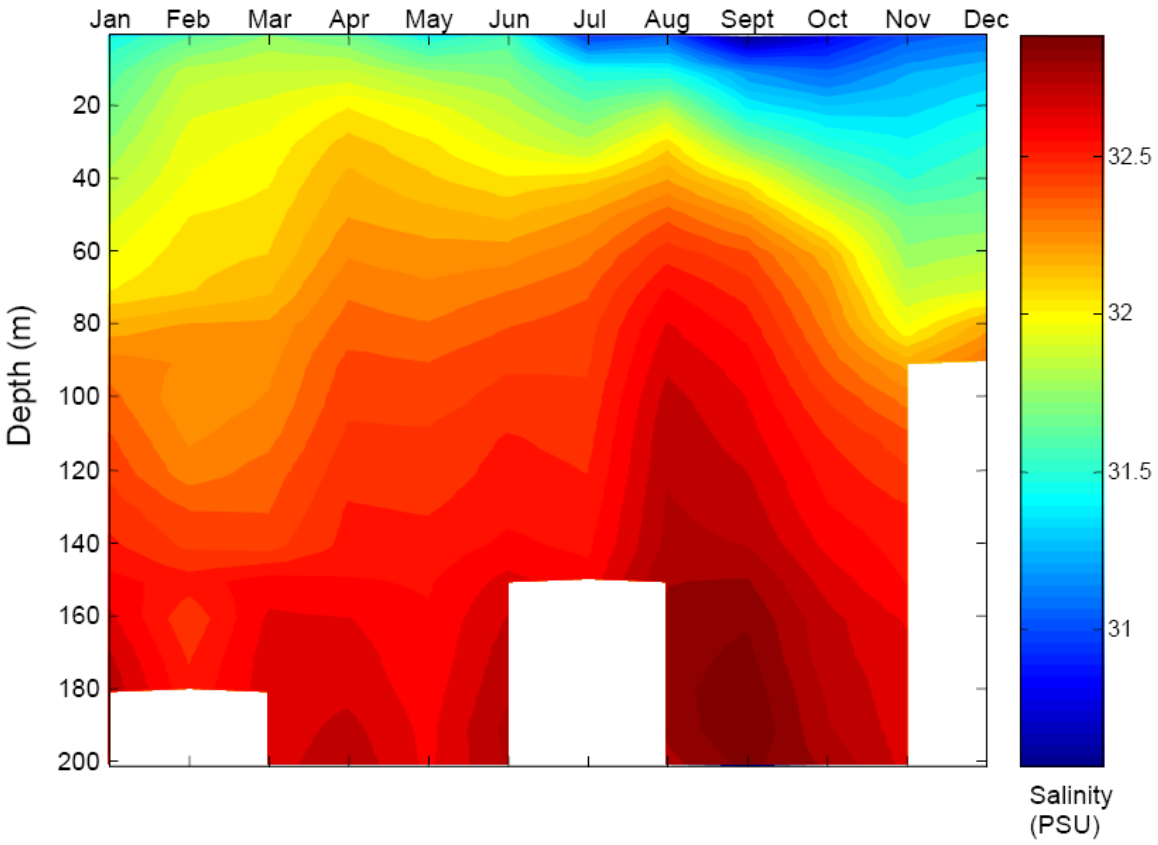

Source: BIO 2011

Figure 4-67 Monthly Mean Salinity, Placentia Bay

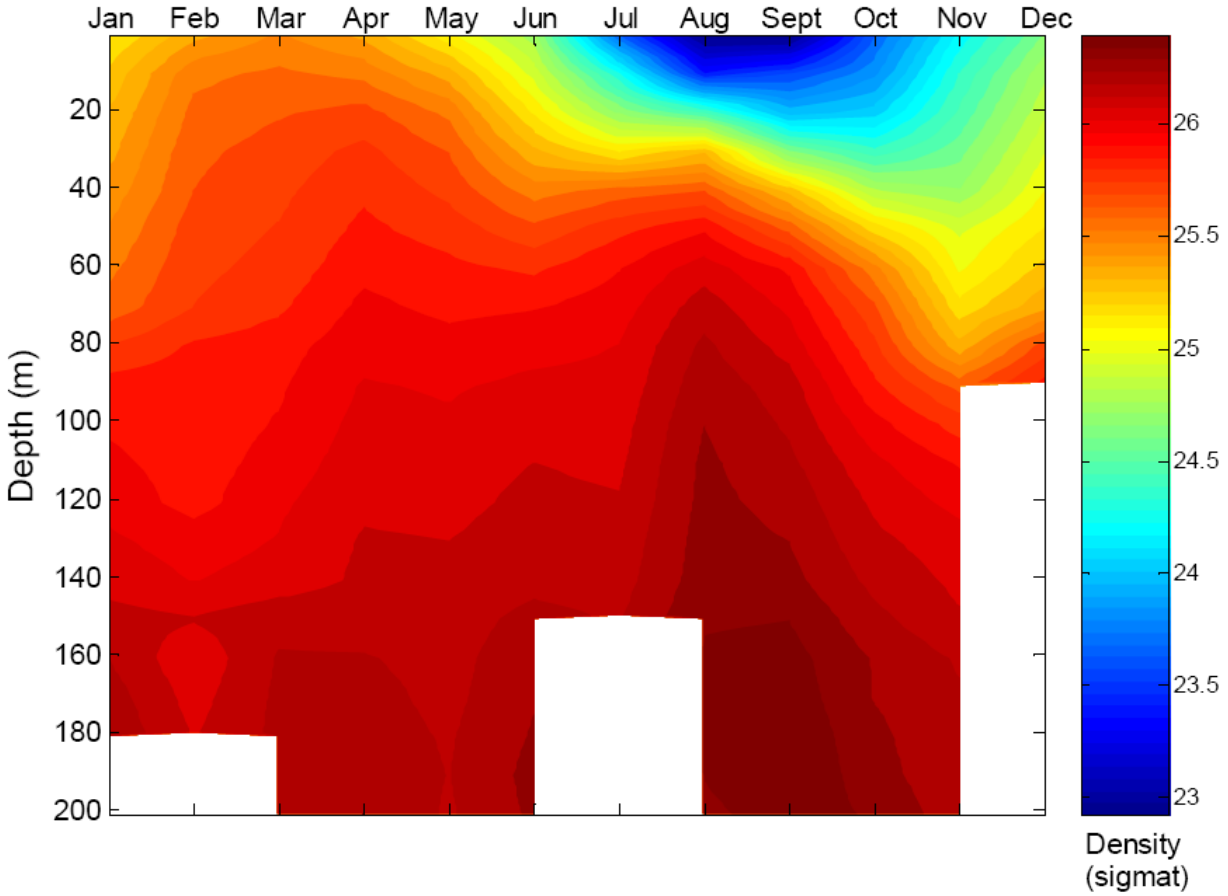

Source: BIO 2011

Figure 4-68 Monthly Mean Water Density, Placentia Bay

Placentia Bay shows a marked seasonal cycle with a strong stratification during the summer, with relatively warm and fresh water standing above colder and saltier waters, a more mixed system in fall and an almost completely mixed water column during the winter and spring. The summer period also shows a marked intrusion of deep and salty water entering in the bay and present from June through October.

Based on the density field (Figure 4-68) three different seasons can be identified:

- Summer (June to October), three-layer system with warm and fresh water on the upper 30 m (temperature approximately 14°C, salinity approximately 31 practical salinity units (psu)), an intermediate water between 30 to 150 m (temperature approximately 3°C, salinity approximately 32 psu) and a cold and salty water on the bottom final 50 m of the water column (temperature approximately -1°C, salinity approximately 32.5 psu)
- Fall (November to December), two-layer system with a mixed surface layer of 60 m (temperature approximately 8°C, salinity approximately 31 psu) and a bottom layer of 140 m (temperature approximately 2°C, salinity approximately 32.5 psu)
- Winter/Spring (January to May), quasi-uniform water column of constant temperature (approximately 2°C), with a large mixed surface layer 140 m thick (salinity 32 psu) and saltier bottom layer (32.5 psu).

4.2.3 Wind, Waves and Air Temperature Extremes

Extremal analysis was conducted on the MSC50 (MSC06min subset) wind and waves hindcast dataset (Swail et al. 2006; Environment Canada 2011; DFO 2012a) for annual extremes as well as seasonal extremes at the three following nodes:

- M6012169: Between Red Island and Argentia, water depth of 216 m
- M6012548: Between Isle Valen and Merasheen, water depth of 75 m
- M6011561: Mouth of Placentia Bay, water depth of 244 m.

Extremal analysis was conducted on the daily maximum and minimum air temperatures from the Environment Canada Argentia and Placentia records (Environment Canada 2012a).

4.2.3.1 Wind

Annual extreme winds for the three MSC50 nodes are presented in Table 4-34. There is very little difference between the extreme wind speeds at the three nodes.

Table 4-34 Annual Extreme Wind Speeds

Extreme Wind Speed (m/s)	Return Period (years)			
Node #	**1**	**10**	**50**	**100**
M6012169	22.9	26.3	29.1	30.2
M6012548	22.6	25.8	28.5	29.6
M6011561	23.6	26.9	29.6	30.7
Source: DFO 2012a				

Seasonal extremes are presented in Figures 4-69 to 4-71. The value for each month is determined from a three-month period centred on the month (e.g., for February, January to March). Highest extreme values are encountered from September to December and from January to March. Mid-summer (July) extremes are approximately 50 percent less than winter and fall extremes.

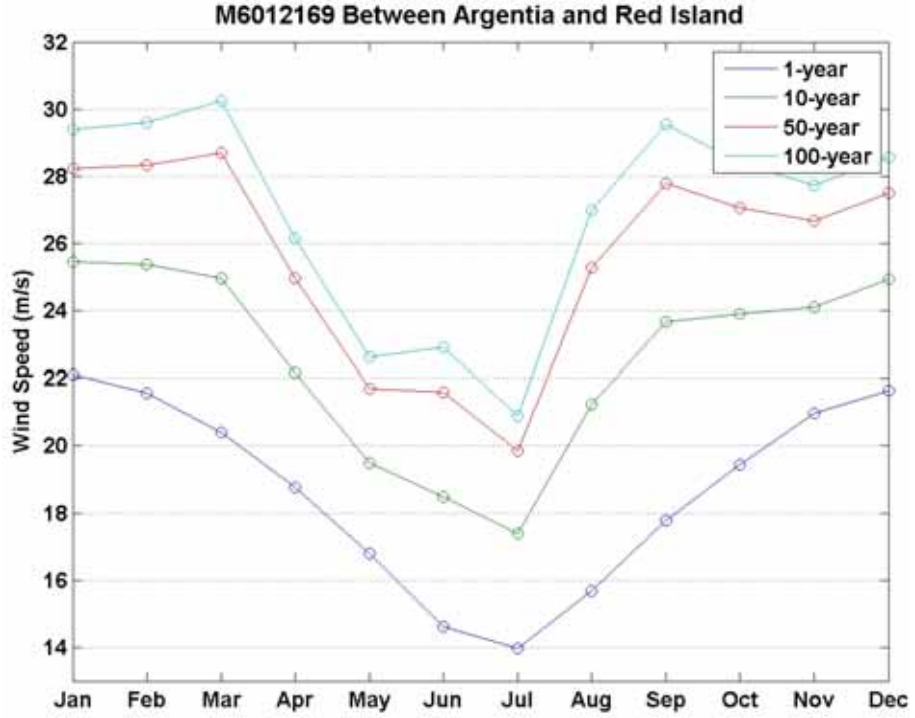

Source: DFO 2012a

Figure 4-69 Seasonal Extreme Wind Speed at MSC50 Node M6012169

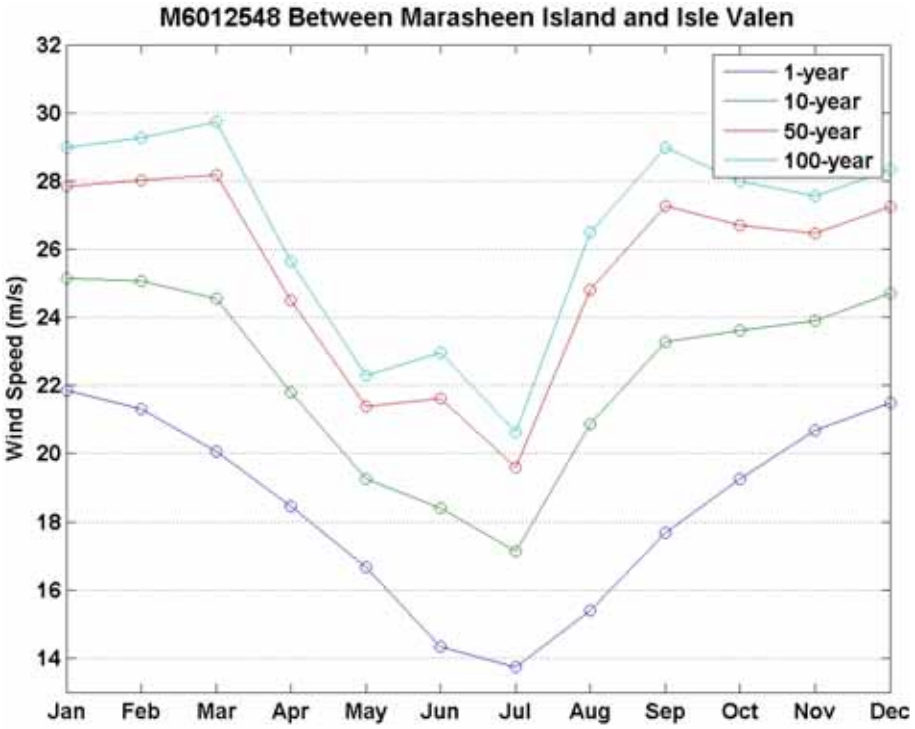

Source: DFO 2012a

Figure 4-70 Seasonal Extreme Wind Speed at MSC50 Node M6012548

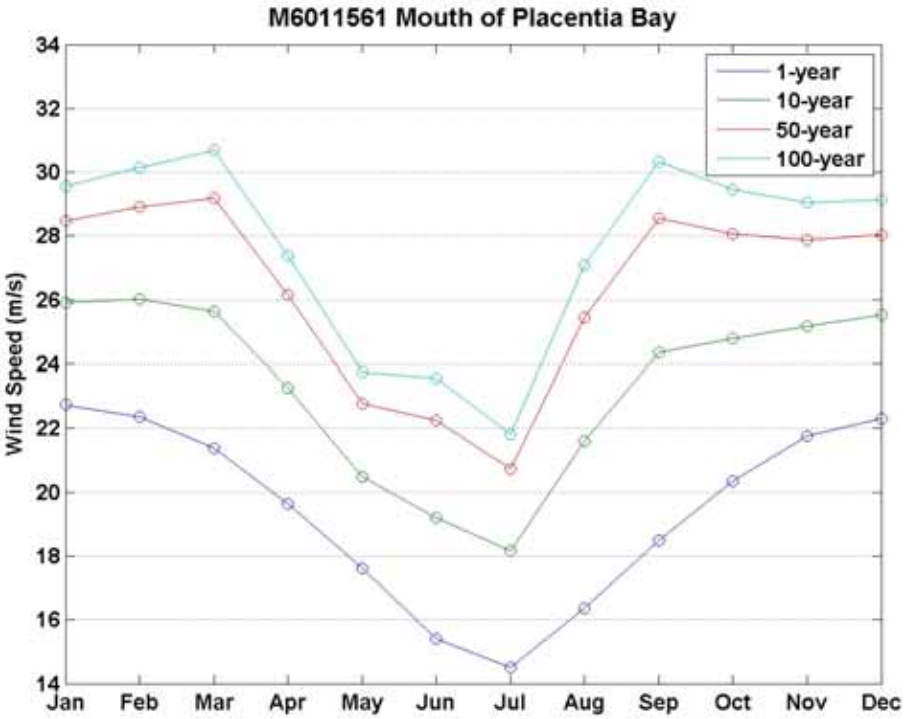

Source: DFO 2012a

Figure 4-71 Seasonal Extreme Wind Speed at MSC50 Node M6011561

4.2.3.2 Waves

Annual extreme significant wave heights and associated peak periods are presented in Table 4-35. As expected, the mouth of Placentia Bay is exposed to the most severe seas, with a 100-year significant wave height of 12 m. The site between the Argentia Peninsula and Red Island at the entrance of the channel leading to the head of the bay is still exposed to very severe seas, with a 100-year significant wave height of 9.2 m. The site between Marasheen Island and Isle Valen is quite sheltered from the most severe seas, with a 100-year significant wave height of only 2.3 m.

Table 4-35 Annual Extreme Significant Wave Height and associated Peak Period

	Return Period (years)							
	1		10		50		100	
Node #	Hs (m)	Tp (s)	Hs (m)	Tp(s)	Hs (m)	Tp(s)	Hs (m)	Tp(s)
M6012169	5.6	11.7	7.2	13.2	8.6	14.4	9.2	14.9
M6012548	1.6	9.1	1.9	7.4	2.2	7.9	2.3	8.1
M6011561	7.5	12.5	9.6	14.2	11.3	15.4	12.0	15.9
Source: DFO 2012a								

Seasonal extreme significant wave heights are presented in Figures 4-72 to 4-74. The value for each month is determined from a three-month period centred on the month.

Most severe extreme seas are in January and December. Mid-summer (July) extremes are almost half the winter extremes.

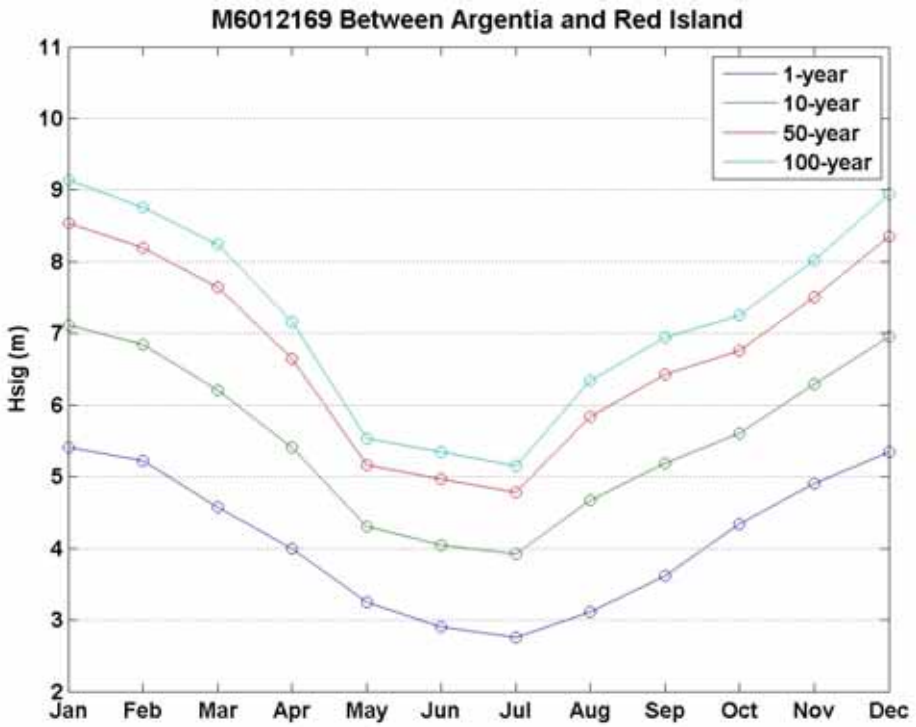

Source: DFO 2012a

Figure 4-72 Seasonal Extreme Significant Wave Height at MSC50 Node M6012169

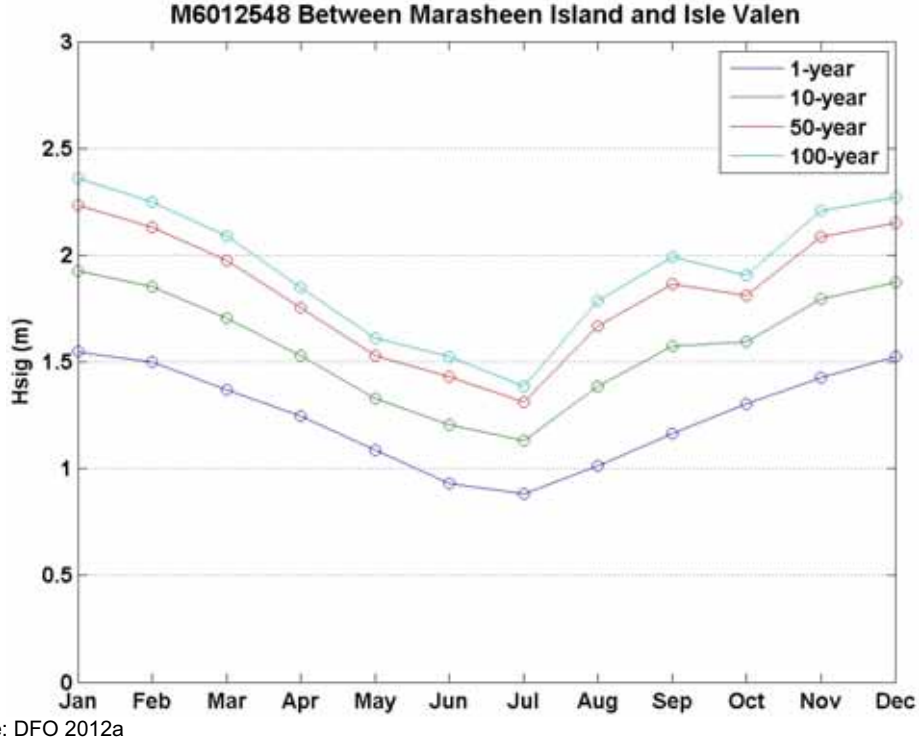

Source: DFO 2012a

Figure 4-73 Seasonal Extreme Significant Wave Height at MSC50 Node M60121548

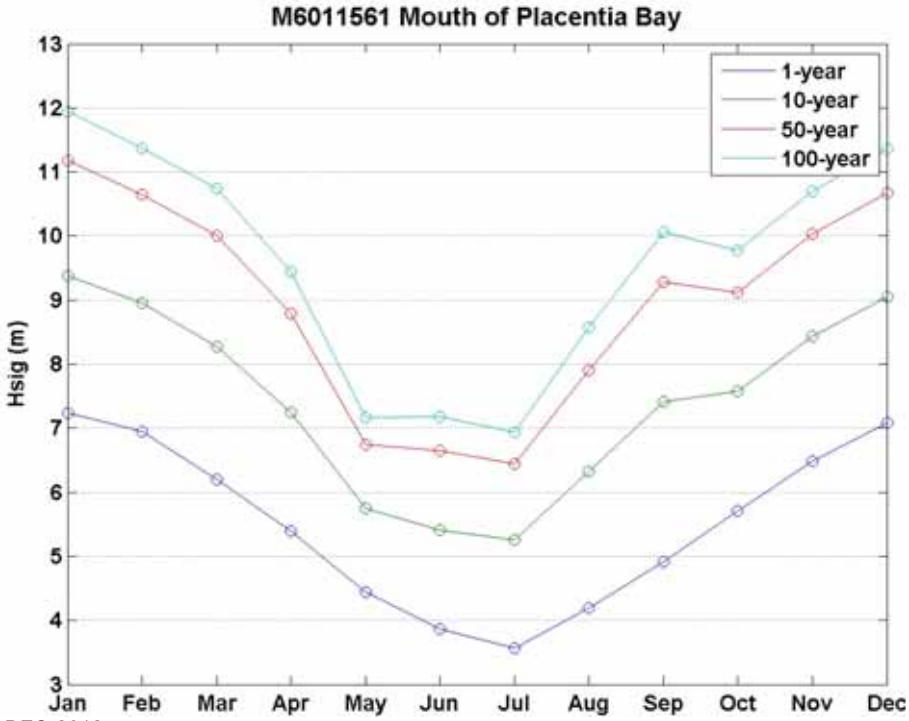

Source: DFO 2012a

Figure 4-74 Seasonal Extreme Significant Wave Height at MSC50 Node M6011561

4.2.3.3 Air Temperature

Extreme daily maximum and minimum temperatures at Argentia and Placentia[5] are presented in Table 4-36.

Table 4-36 Extreme Daily Maximum and Minimum Air Temperature at Argentia and Placentia

Extreme Temperature (°C)	Return Period (years)			
	1	10	50	100
Maximum	22.9	26.3	28.8	29.8
Minimum	-15.1	-19.4	-23.7	-25.5
Source: Environment Canada 2012a				

[5] Years of record for Argentia: 1953 to 1970, 1976 to 2011; Placentia: 1970 to 1975.

4.2.4 Sea Ice and Icebergs

Regional sea ice data are available from approximately 40 years of ice observations carried out by the Canadian government. Initially, these observations were obtained from aerial reconnaissance.

Beginning in the 1970s, satellite images supplemented aerial observations, eventually replacing them as the principal sources of data by the mid-1990s. These data appear in daily and (approximately) weekly composite ice charts produced by the Canadian Ice Service (CIS).

The charts and compilations by Sowden and Geddes (1980), Seaconsult Ltd. (1988), and Cote (1989) underlie the description of sea ice in this document. Supplementary information on ice movements, thicknesses and floe sizes and their linkages to environmental factors have been obtained from:

- Observations made by the offshore oil exploration industry from the 1970s to 2011
- Research programs carried out by DFO, Atmospheric Environment Service and by the Program on Energy Research and Development (PERD).

The sea ice database is more reliable than the iceberg database (described below). Rather, sea ice data support relatively unambiguous and detailed cross-comparisons dating back to the late 1950s and, with lesser precision, to the second decade of the twentieth century (Hill and Jones 1990).

Data on icebergs are available for an even longer period, dating back some 100 years. The formation of the International Ice Patrol (IIP) in 1913 led to the routine compilation of iceberg sightings in areas south of Labrador. Marine vessel reports were initially the basic data sources. Beginning in the 1950s, fixed-wing aircraft assumed the major responsibility of iceberg surveillance. Additional data have been obtained in the last three decades from observations made during oil exploration activities.

Over the years, the IIP has collated and cross-indexed sighting data from all sources to provide updated position maps and estimates of numbers of icebergs crossing 48°N for annual and shorter time frames. Additional coverage beyond the 52°N limits of IIP interest, and inshore areas, has been available from the CIS for more than two decades.

The IIP data have been used to quantify and understand iceberg behavior off eastern Canada. These analyses have included daily charts of iceberg positions prepared from recent sightings and radar target positions. Iceberg positions and sizes are deduced using simple models of iceberg drift and deterioration. This database may not be consistent because, over time, production procedures, detection technologies and levels of effort have changed. This has constrained analyses of iceberg spatial and temporal trends and their characteristic variations (Petro-Canada 1995).

Since 1989, iceberg survey data for the Canadian East Coast between 45°N and 55°N have been available from Provincial Aerospace Ltd. (PAL). These data are particularly notable because the icebergs are visually-confirmed after initial detection with radar. The methodology and sensors used have been consistent since the program's inception. The revisit time of these surveys is an average of three to five days, so iceberg numbers estimated in defined counting areas are simple sums of local counts obtained in all surveys during the period of interest.

The accuracies of such estimates depend on the drift and deterioration rates of all icebergs moving through the area. Average drift speeds of 20 km/day on the Grand Banks, and 30 km/day east of the Grand Banks, mean that icebergs move completely through the 110 km × 75 km areas defined on the daily ice charts within the three- to five-day revisit time. As a result, each new count in a grid block yields a new iceberg population.

Comparisons of annual total numbers of icebergs south of 48°N indicate that IIP estimates are larger than PAL iceberg counts (Figure 4-75). This difference is likely the result of different operating mandates, estimation procedures and uncertainties associated with each survey. The IIP mandate is to advise mariners of the extreme limit of all known icebergs. Under this mandate, any debate on what a particular radar target is will err on the side of caution and identify it as an iceberg.

Under a 1998/2008 PERD initiative, both the IIP database and those from offshore oil exploration have been combined into a single iceberg database. Some data formatting inconsistencies and obvious positional errors were improved, but this database provided no new insights into iceberg distributions. It has however proved useful in providing insight into iceberg size.

This document bases its description of the regional iceberg environment using the PAL data obtained for the years 2000 to 2011. The longer-term historic data is provided by the IIP database, and occasionally the PAL iceberg database from 1992 onward, for comparison purposes.

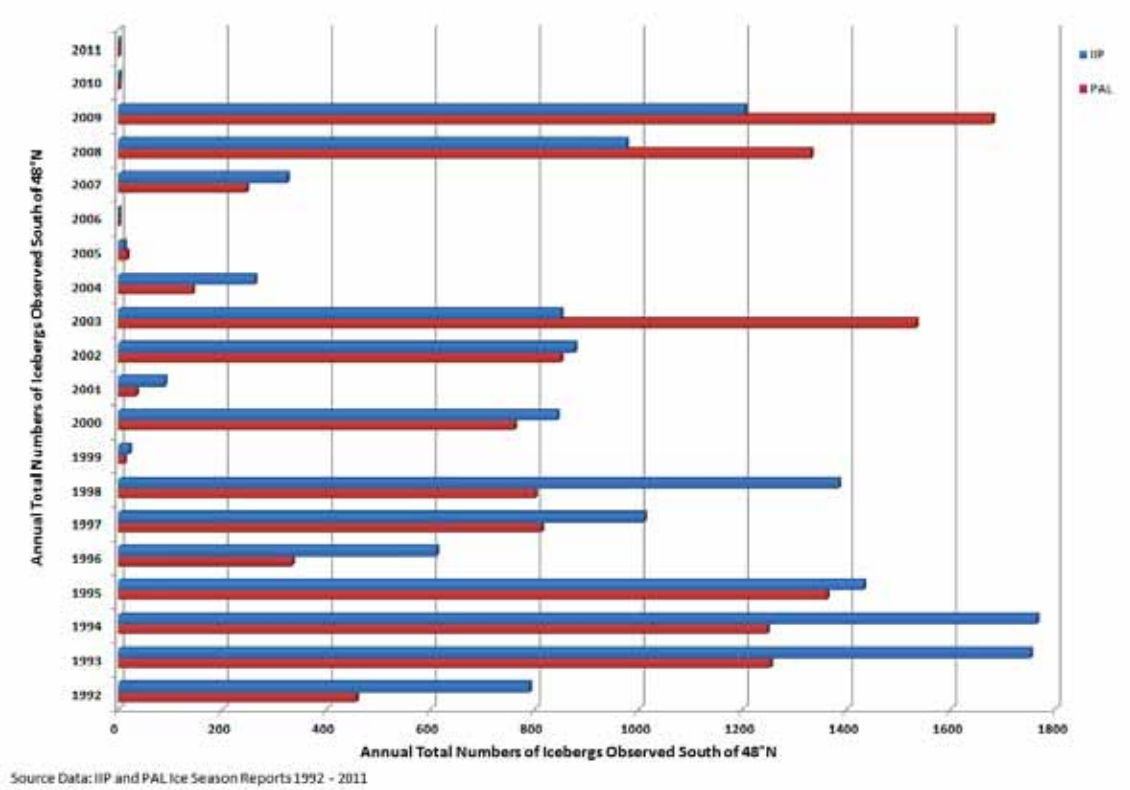

Figure 4-75 Comparison of International Ice Patrol and Provincial Airlines Limited Iceberg Databases 1992 to 2011

4.2.4.1 Sea Ice Conditions in Placentia Bay

Pack ice presence in Placentia Bay from year to year may be variable, based on a review of the weekly CIS charts from 1981 to 2010, inclusive (Environment Canada CIS 2010). Most sea ice within the bay is formed off southern Labrador and drifts south to enter the bay around the mid-February timeframe. From mid-February through mid to late-April, the bay experiences first year ice, which can range in thickness from 30 to 120 cm. The bay has been divided into two sections for analysis: the mouth and the bottom (Figure 4-76). The mouth of the Bay is more susceptible to incursions of the annual pack, while the bottom of the bay only fills with pack when there are sustained periods of onshore winds. The available data do not have the resolution to provide information on ice distribution in the various inlets and coves around the bay.

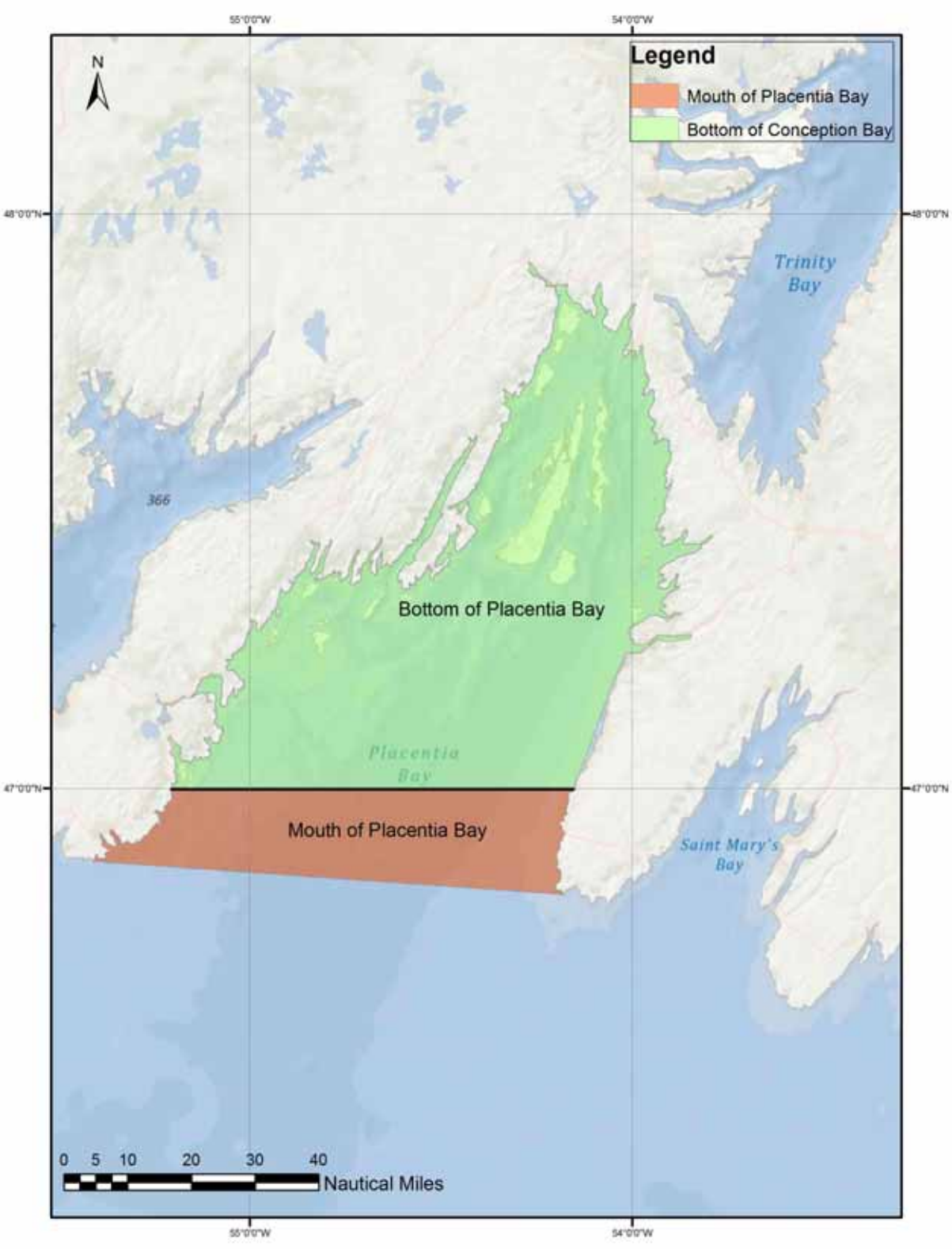

Figure 4-76 Division of Placentia Bay into the Mouth and Bottom of the Bay

The “Frequency of Presence of Sea Ice” is a term coined by the Canadian Ice Service that explains the likelihood of total concentration of greater than or equal to 1/10 at a given location at a specified date. The values can be interpreted as the probability of encountering sea ice for the appropriate date. Where 100% frequency of presence has been noted, there has always been sea ice reported in the specified time period. The frequency of presence of sea ice in Placentia Bay by week is shown in Figure 4-77. For this analysis, the frequency of sea ice in the mouth (most seaward point) of the bay and at the bottom (most landward point) of the bay over a 30-year period (1981 to 2010) was reviewed.

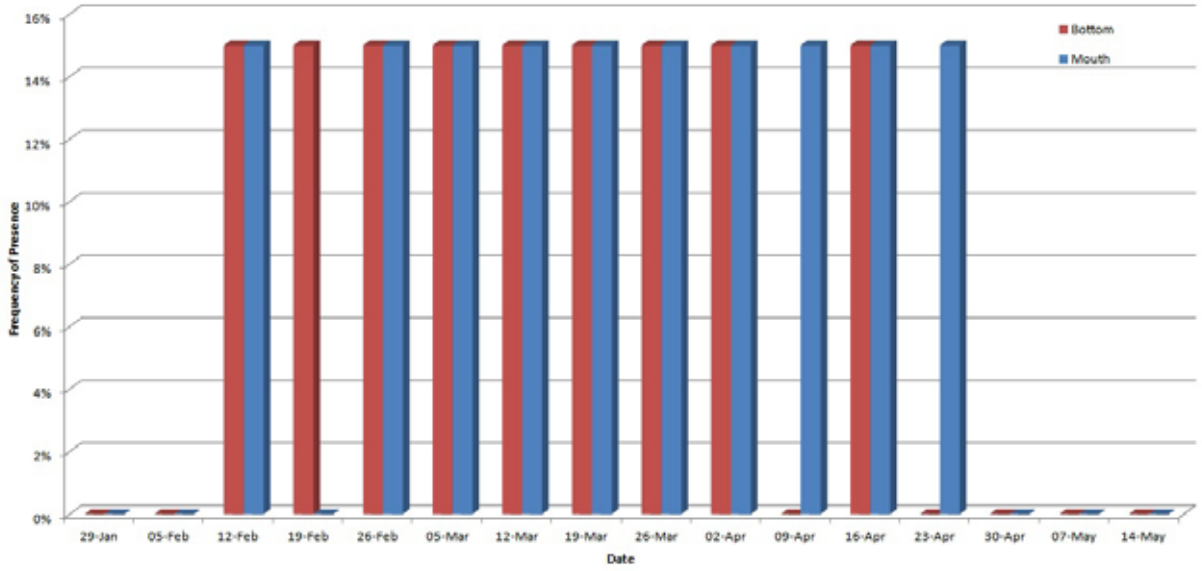

Source: CIS 2011

Figure 4-77 Frequency of Presence of Sea Ice in Placentia Bay (1981-2010)

There are few data on the exact thickness of the sea ice in Placentia Bay. As a result, the analysis uses the upper limit for the standard ice types to derive sea ice thickness. As with the offshore area (Section 4.3.4.1), the derived sea ice thickness (in centimeters, when ice is present) in Placentia Bay by week is shown in Figure 4-78. This analysis involves the sea ice at the mouth and bottom of the bay over the 30-year period of 1981 to 2010, inclusive.

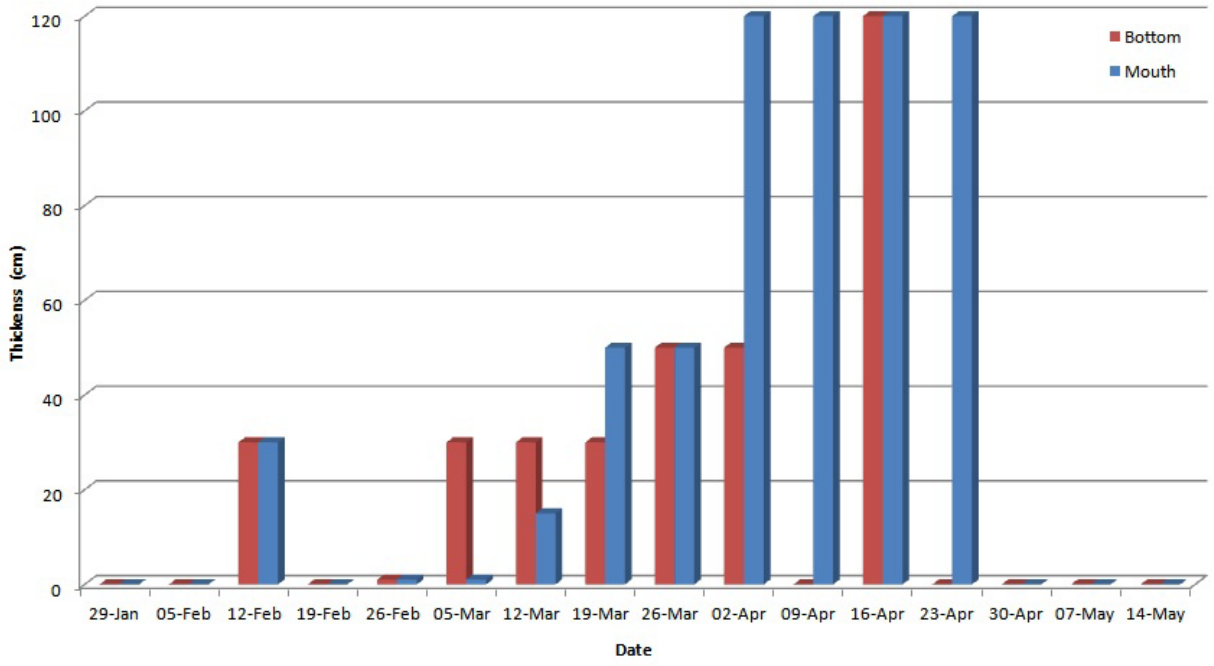

Source: CIS 2011

Figure 4-78 Derived Sea Ice Thickness at the Mouth and Bottom of Placentia Bay (30 year average for period from 1981-2010)

Ice thicker than 100 cm is uncommon at the bottom of Placentia Bay (Figure 4-4); average thicknesses between 30 and 50 cm are the most common.

4.2.4.2 Iceberg Conditions in Placentia Bay

The mean circulation in Placentia Bay is driven by westward currents from the inshore branch of the Labrador Current that flows into the bay on the eastern side, continues along the coastline, and flows out of the bay on the western side. As a coastal region, it tends to be less influenced by the cold component of the Labrador Current (deYoung et al. 1993). The average current velocity in Placentia Bay was about 0.22 m/s between January 2010 and December 2011 (SmartBay 2012).

The IIP has recorded icebergs in Placentia Bay. Icebergs were recorded in seven of the 30 years between 1974 and 2003.A total of 30 icebergs were recorded in this period. (Figure 4-79).

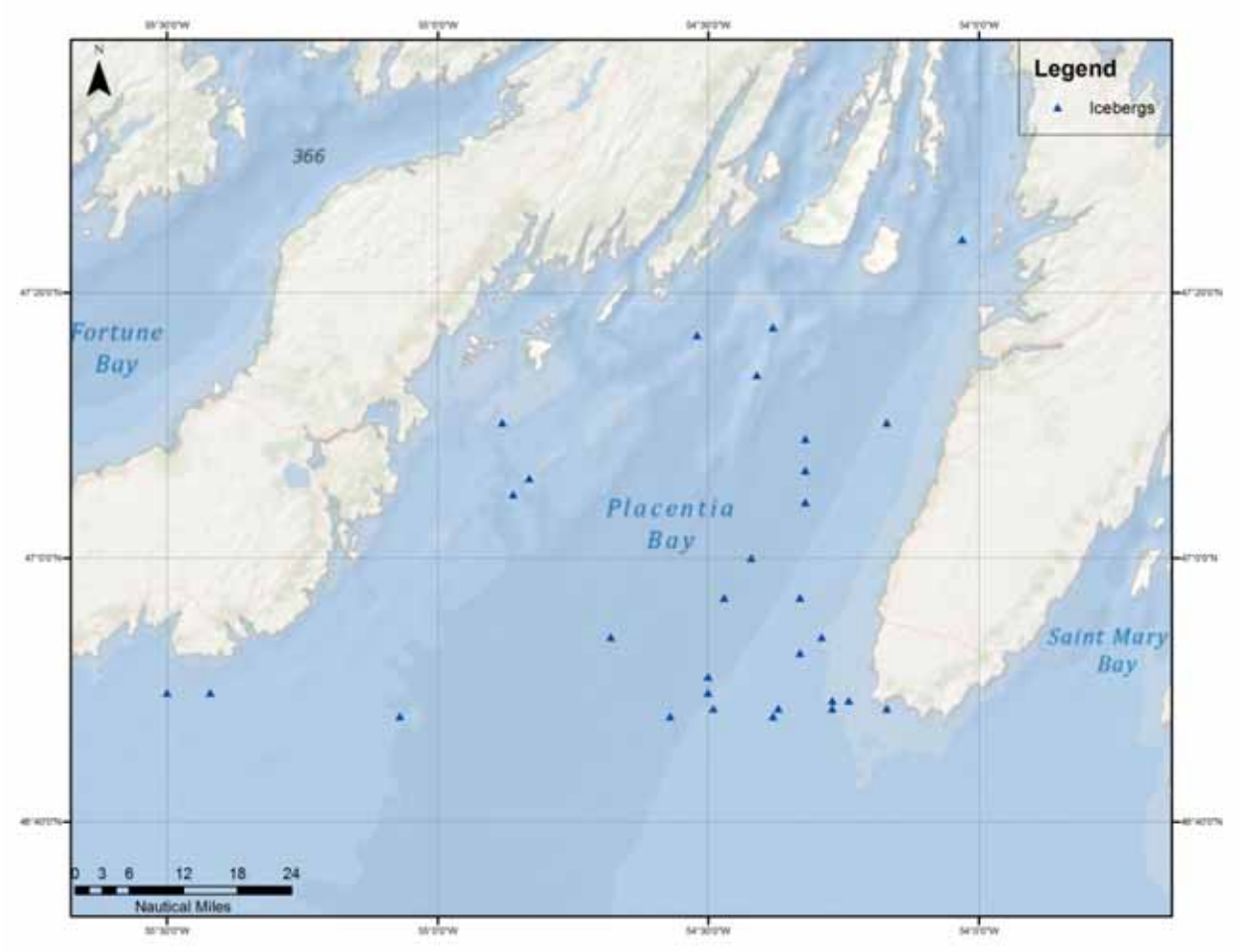

Source: Vale Inco 2008

Figure 4-79 Icebergs Recorded by International Ice Patrol in Placentia Bay (1974 to 2003)

4.2.5 Geological Setting – Placentia Bay and Argentia

Placentia Bay is located on the south coast of the island of Newfoundland. It is bounded on the west by the Burin Peninsula, on the east by the Avalon Peninsula and to the north by the isthmus of Avalon and occupies an area of approximately 5,000 km^2. The Bay is characterized by well-defined channels that can reach water depths of 430 m, and by islands, shoals, reefs and banks. Placentia Bay is a glacially-modified basin that has a complex glacial history, having been affected by ice draining from both the Burin and Avalon Peninsulas (Brushett et al. 2007).

Glacial ice history over the Avalon and Burin peninsulas has been interpreted largely from the relationship between cross-cutting bedrock striations (Brushett et al. 2007). Recent studies have resulted in a better understanding of ice-flow history on the west side of the Placentia Bay (e.g., Batterson et al. 2006; Brushett et al. 2007; Brushett 2008; Shaw et al. 2011). The most recent interpretation by Batterson et al. (2006) based on fresh, unweathered bedrock striations on the Burin Peninsula and northward on the main body of Newfoundland, suggests that the Peninsula underwent three phases of glacial flow during the Late Winconsinan Glaciation (Figure 4-80). Linear features

observed in multibeam imagery on the western side of Placentia Bay align with and agree in directionality with the ice-flow features seen on the Burin Peninsula (Figure 4-81; Brushett et al. 2007).

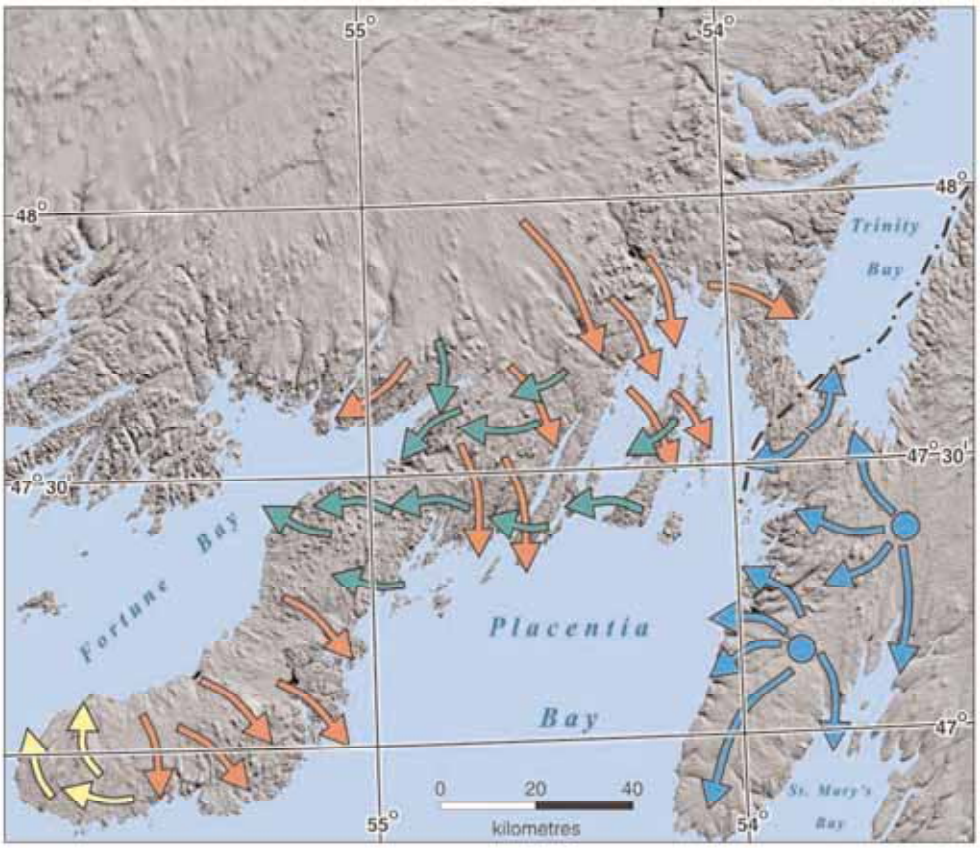

Souce: Image from Brushett et al. 2007
Note: Three flow phases on the Burin Peninsula (red, green and yellow arrows) have been interpreted as late Wisconsinan. The dashed black line represents the limit of the Newfoundland ice sheet and the blue arrows on the Avalon Peninsula delineate the local ice-dispersal centres.

Figure 4-80 Ice Flow Patterns on the Burin and Avalon Peninsulas

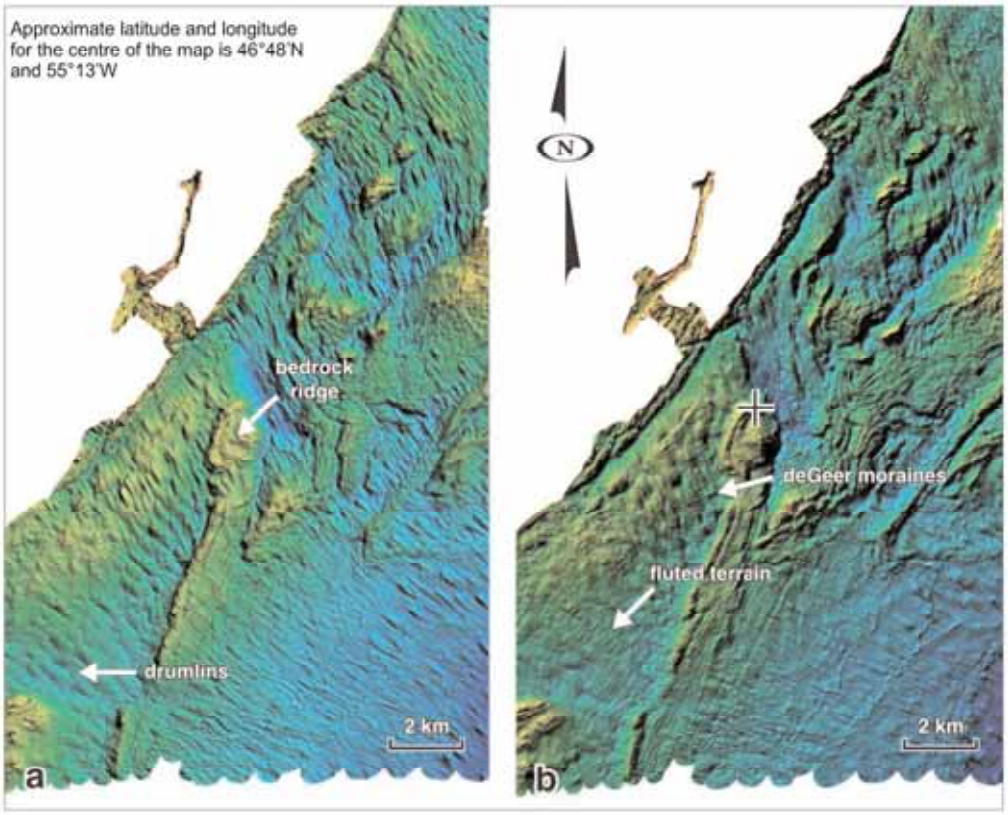

Source: Image from Brushett et al. 2007
Note: Two shaded-relief images illuminated from different angles from the same area in southwestern Placentia Bay. A) Subdued drumlins are visible when illuminated from the northeast. B) A series of small transverse flutes and deGeer moraines are superimposed on the surfaces of the drumlins when the surface is illuminated from the northwest

Figure 4-81 Geology of Placentia Bay

The glacial history on the Avalon Peninsula has been extensively studied since the late 1800s (e.g., Murray 1883; Chamberlin 1895; Coleman 1926; Henderson 1972; Catto 1998). Several glacial histories have been proposed. The suggestion that the Avalon Peninsula was once covered by an independent Wisconsinan ice cap (Chamberlin 1895) has been supported and accepted over the years. The Avalon ice cap was characterized by radial expansion and coalescence of local dispersal centres (Brushett et al. 2007) (Figure 4-79). As on the Burin Peninsula, interpreted ice-flow directions on the Avalon Peninsula are based on bedrock striations and glacially eroded landforms.

In the Argentia area, ice-flow appears to have been west-southwest originating from dispersal centres of a local ice divide located on the Placentia sub-peninsula (Figure 4-82). A connection between terrestrial ice-flow history and that of Placentia Bay is supported by trends delineated by seabed features on multibeam imagery. These features include flow-parallel landforms such as drumlins, mega-flutes, mega-lineations, crag-and-tail features and streamlined bedrock ridges that together indicate a southwest ice-flow direction (Figure 4-82; Brushett et al. 2007).

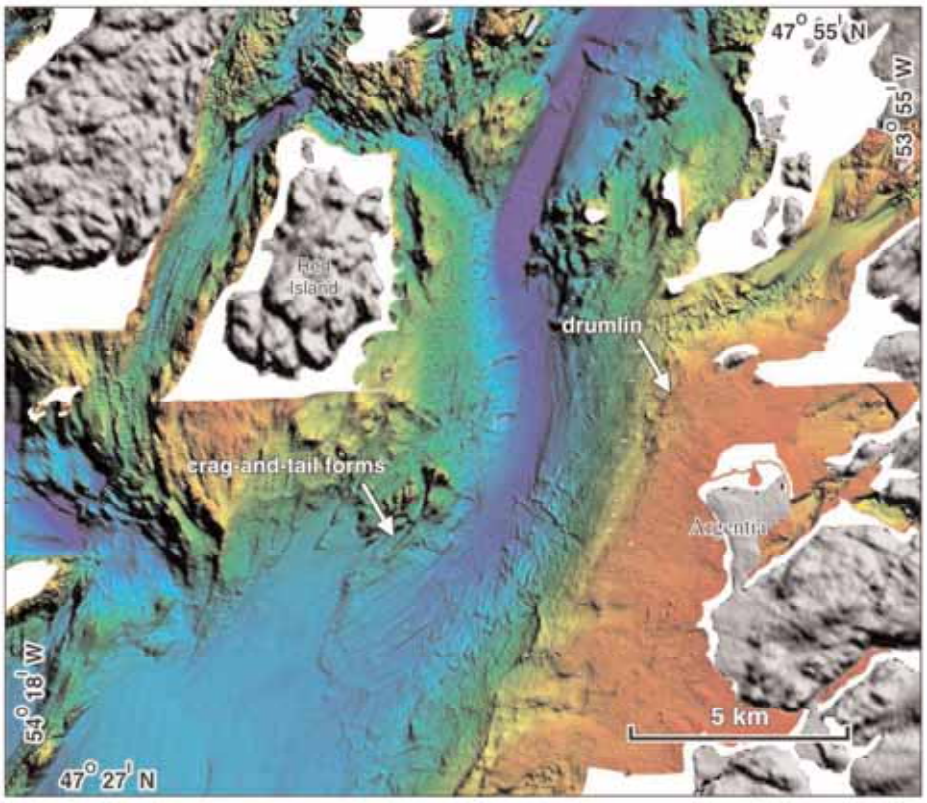

Source: Image from Brushett et al. 2007
Note: Illustrates flow features including elongated drumlins and streamlined bedrock forms (craig-and-tail features). These features indicate a southwest flow direction. Surface is illuminated from the northwest. White space represents areas of no multibeam data.

Figure 4-82 Multibeam Shaded-relief Image from East-central Placentia Bay

It has been suggested that the westward flow of ice from the Avalon Peninsula was confluent with ice flowing from the Newfoundland ice sheet southward into Placentia Bay (Catto 1998; Brushett 2008). Flow-parallel landforms on the seafloor of Placentia Bay also suggest convergent ice streams flowing parallel to the axis of the Bay.

4.2.5.1 Data Sets - Placentia Bay and Argentia

A number of datasets were used for this desktop study, including multibeam bathymetry, acoustic sub-bottom reflection profile, sediment core and grab samples and colour seabed photographs.

Multibeam Bathymetry: A regionally extensive multibeam dataset collected by Canadian Hydrographic Service (CHS) was used. Data, gridded at 5 m, cover Argentia Harbour, Placentia Sound, Ship Harbour and part of Placentia Bay (Attachment A). Small gaps in data coverage (white spaces) occur in the deeper part of Placentia Bay.

Additionally, a high-resolution multibeam bathymetry data set was provided through Husky and C-CORE. Data were collected during a recent cruise of the Marine Institute's *M/V Atlanticat*. These data are gridded to 0.5 m and cover the basins within Argentia

Harbour, and Ship Harbour (Attachment A). The higher resolution multibeam data were overlain on the regional CHS multibeam bathymetry to provide greater resolution within the Argentia area.

Sub-Bottom Reflection Profiles: Sub-bottom data from Argentia Harbour and Placentia Bay were acquired during Geological Survey of Canada-Atlantic (GSC-A) Expeditions in the late 1980s and 1990s. Data were collected within the Argentia Harbour and surrounding area during the 89026 and 99020 GSC-A expeditions (Attachment B).

Sub-bottom data surrounding the Argentia Peninsula were collected during the 89026 GSC-A cruise using both a Seistec system and Bubble Pulser system deployed from the stern of the vessel and fired in alternating order. The acquired data were of relatively good quality and flawed only by continuous ringing in the upper few metres of the Bubble Pulser record.

Cores, Grabs and Colour Photographs: Extensive groundtruthing was completed in Argentia Harbour, Placentia Sound and Ship Harbour by the GSC-A during the 89-026 and 99-020 expeditions. Locations of the grab samples and camera stations are illustrated on Attachment B. Sediment sample descriptions are provided in Table 4-37 (GSC Expedition 99-020) and Table 4-38 (GSC Expedition 89-026); samples were collected with a Van Veen grab at a sample depth of 0 m and a gravity corer at various depths.

Table 4-37 Geological Society of Canada-Atlantic Expedition 99-020 Grab and Core Sample Descriptions

Station Number	Description
Van Veen Grab (at 0 m sample depth)	
0027	Dark olive grey silty mud, numerous worm tubes, brown surface layer. Sea urchin
0028	Dark olive grey silty mud, closely packed worm tubes, brown surface layer
0029	Dark olive grey silty mud, closely packed worm tubes, brown surface layer
0030	Dark olive grey silty mud with brown mottles, closely packed worm tubes, brown surface layer
0031	Poorly sorted pea gravel with some sand and shell fragments
0032	Brown gravelly sand, coarse sand with granules, shell fragments
0033	Dark olive grey silty mud with brown mottles, closely packed worm tubes
0034	Dark olive grey silty mud with brown mottles, closely packed worm tubes
0035	Pebbles, cobbles, encrusted with branching read coral, some with branches on only one side
0036	Dark grey sandy mud, bivalve fragments throughout, a few small red worm tubes
0037	A cobble, diameter 20 cm, encrusted all over with red *Lithothamnion*
0038	Dark grey sandy mud, bivalve fragments throughout, worm tubes
0039	Dark olive grey silty mud with brown mottles, closely packed worm tubes, brown surface layer and a sea urchin

Station Number	Description
0040	Brownish-grey, well-sorted medium sand with numerous bivalve fragments and one rounded pebble with a thin coating of red coral
0041	Brownish-grey, well-sorted medium sand, shell fragments, several sand dollars
0042	Poorly sorted fine gravel, mostly pea size, with coarse sand and one cobble
0043	Two large pebbles encrusted with red coral all over
0044	A surface layer of gravel overlying coarse sand and pea size pebbles. Gravel is covered by red coral, except several large cobble-sized clasts, which have coral on the upper surface only
0045	A surface layer of gravel overlies a mixture of medium sand and pea size gravel. Small pebbles have red coral. Large clasts (small cobbles) have coral on the upper surface only, two sea urchins
0046	Well-sorted medium-fine sand with shell fragments. Surface layer several cm thick is brown; below, sand is black and smells of rotten eggs
0047	Pebbles and cobbles with no coral. Larger clasts have long strings of seaweed attached
0048	Dark grey muddy fine sand with shell fragments, a few worm tubes. Brownish-grey at surface
0049	Muddy fine sand, brown on surface, black below 1 cm. Many bivalves, one large crab
0050	Well-sorted fine-medium sand
0051	Well-sorted fine-medium sand. Brown on the surface, grey below
0052	Layer of rounded large pebbles with red coral on upper surfaces overlying muddy fine black sand
0053	Layer of rounded large pebbles with red coral on upper surfaces overlying muddy fine sand
0054	Very dark grey mud with some fine sand. Brown on surface, no worms
0055	Layer of pebbles and cobbles (subangular) with coral on upper side only, overlying dark grey sandy gravelly mud
0056	Grey silty mud, worm tubes, brown on surface
0057	Layer of angular pebbles and cobbles coated with red coral on upper surface, overlying muddy coarse poorly sorted sand
0058	Black mud, shell fragments throughout, brown surface layer
0059	Black mud, brown on surface
0060	Black mud, sulphur smell, brown surface layer, scattered shell fragments
0061	
0062	Clack mud, brown mottles, worm tubes
0063	Brown gravelly mud. Many angular gravel clasts in a matrix of clayey mud. A few clasts have seaweed attached
0064	Black silty mud, living bivalve, brown surface layer
0065	Black mud with brown patches, living buried bivalves, brown surface layer includes

Station Number	Description
	tangle of seaweed
0066	Black mud, living buried bivalves, brown surface
0067	Muddy gravelly sand – gravel mainly angular pebbles. Grey but brown on surface. Strings of seaweed and one small starfish
0068	Muddy gravelly sand
0069	Black mud, brown on surface, worm tubes, red worm
0070	Black mud, brown on surface, worm tubes, orange worm
0071	Black mud, brown on surface, worm tubes, orange worm
0072	Grey gravelly mud, large piece of wrack attached to a cobble. Large orange sandworm
0073	Black mud, brown on top
0074	Black mud, brown on top

Gravity Corer

Station Number	Sample Depth (m)	Description
0075	95	
0076	142	
0077	132	
0078	110	
0079	56	
0081	89	
0082	125	
0083	123	Approximately 19 cm lost from bottom of core
0084	148	
0085	148	
0086	103	
0087	93	

Table 4-38 Geological Society of Canada-Atlantic Expedition 89-026 Grab and Core Sample Descriptions

Station Number	Description
Van Veen Grab (at 0 m sample depth)	
3192	Soft dark grey mud with numerous worm tubes and a few shell fragments. Light brown surface layer
3000	Muddy gravel. Gravel with dark grey mud with some sand granules. A few worm tubes
3001	Black mud. Strong smell. Included a plastic bag fragment
3002	Mainly gravel with mud. Gravel is mostly subangular. Most coated with pink coral on the upper side only. Some sponges attached. Also a few shell fragments
3003	Olive-grey mud. Some worm tubes. One encrusted bolt
3004	Poorly sorted mixture of olive-grey mud, sand granules and gravel. Some of the gravel is coated with coral
3006	Muddy gravel. Predominantly fine gravel (subangular), small amount of grey sand, two large (20 cm) scallop shells – one alive and one dead
3007	Black smelly mud. Scattered single-valve shells
3008	Black mud with strong smell. Light brown surface layer. Some worm tubes. Because of the two failed attempts and strong winds, this sample was off the original location. Jammed locking ping cause two failed attempts
3009	Muddy gravel. Mainly gravel with seaweed attached; grey mud with some fine sand
3010	Dark olive-grey with light brown surface layer. Some worm tubes
3011	Dark olive-grey mud. Very shelly. Light brown surface layer. Some worm tubes
3012	Dark olive-grey mud with a light brown surface layer. Worm tubes and shell fragments
3193	Dark olive-grey muddy sand with few pebbles. Some worm tubes and shell fragments. One piece of wood (30 X 2 cm)
3013	Dark grey mud with a light brown surface layer. Very numerous worm tubes
3014	Dark grey mud with a light brown surface layer. Some worm tubes
3015	Dark grey fine sand with some mud. A few worm tubes and shell fragments
3016	Dark grey/brown medium/fine sand. A few worm tubes and numerous pairs of clam shells (dead)
3017	Gravel and sand. Poorly sorted mixture of pebbles, some cobbles and coarse sand. Four sand dollars. Slight coral coating on one pebble
3019	Medium/fine brown/grey sand. Sand dollar and seaweed fragments
Gravity Corer	

Station Number	Sample Depth (m)	Description
2997	113	Dark grey mud in core and catcher. Worm tubes

Station Number	Description	
2998	87	Catcher was blackish-grey mud. Core was blackish-grey mud
2999	44	Olive grey mud in catcher with some worm tubes. Black pebbly mud on the outside of the weights. Core was dark olive grey gravelly mud. Some shell fragments. Core was disturbed during recovery
3020	103	Core was mostly olive/grey mud. Worm tubes on the outside around the weights. The core was disturbed during recovery. Catcher was empty
3022	85.5	Smelly olive-grey mud. Core was disturbed during recovery. Catcher sample bagged in a bucket
3023	82	Core was olive-grey mud. Stiff mud in the catcher. Catcher sample bagged in a bucket. Valve was removed for this attempt and a double catcher inserted

4.2.5.2 Surficial Geology – Placentia Bay and Argentia

Placentia Bay

The bathymetry of Placentia Bay is characterized by northeast-southwest-trending bedrock ridges (Figure 4-83). The ridges are dissected by deep structural channels that reach depths greater than 400 m. The northeast-southwest structural trend is the result of tectonic compression during the formation of the Appalachian Orogen (Brushett et al. 2007; Brushett 2008). High-relief bedrock ridges, ledges and pinnacles are located throughout the western and northern regions of the bay (Shaw et al. 2011).

As previously mentioned, glacial landforms indicating flow direction are observed on the seabed throughout Placentia Bay. Features located on the western side of the Bay have been studied by Brushett et al. (2007) and Brushett (2008) and indicate a southwesterly ice-flow direction. Flow-parallel landforms, such as drumlins, megaflutes, flutes and crag-and-tail features are found in conjunction with ice-marginal landforms such as De Geer moraines and grounding-line moraines. Drumlins observed on the west side of the bay exhibit average lengths of 795 m, widths of 230 m and heights of 10 m (Brushett 2008).

Seabed features on the eastern side of Placentia Bay also include landforms indicative of glacially-modified terrain. Drumlins and mega-flutes are common. Elongated spindle-shaped drumlins grade into low, long ridges (mega-flutes) in deeper water. Drumlins have average lengths of 1,040 m, widths of 320 m and heights of 10 m (Brushett 2008). These seabed features, streamlined bedrock ridges and crag-and-tail features located south of Red Island indicate a southwest direction of ice-flow (Brushett et al. 2007).

Seafloor surficial sediments vary from coarse-grained glacial deposits in the nearshore regions to fine-grained sediments near the centre of Placentia Bay. Shaw et al. (2011) mapped 14 surficial geological "seascapes" within Placentia Bay using multibeam sonar bathymetry and geophysical seismic profile data. Boundaries between seascape units are inferred and may be gradational in nature. Seascape units are described in Table 4-39.

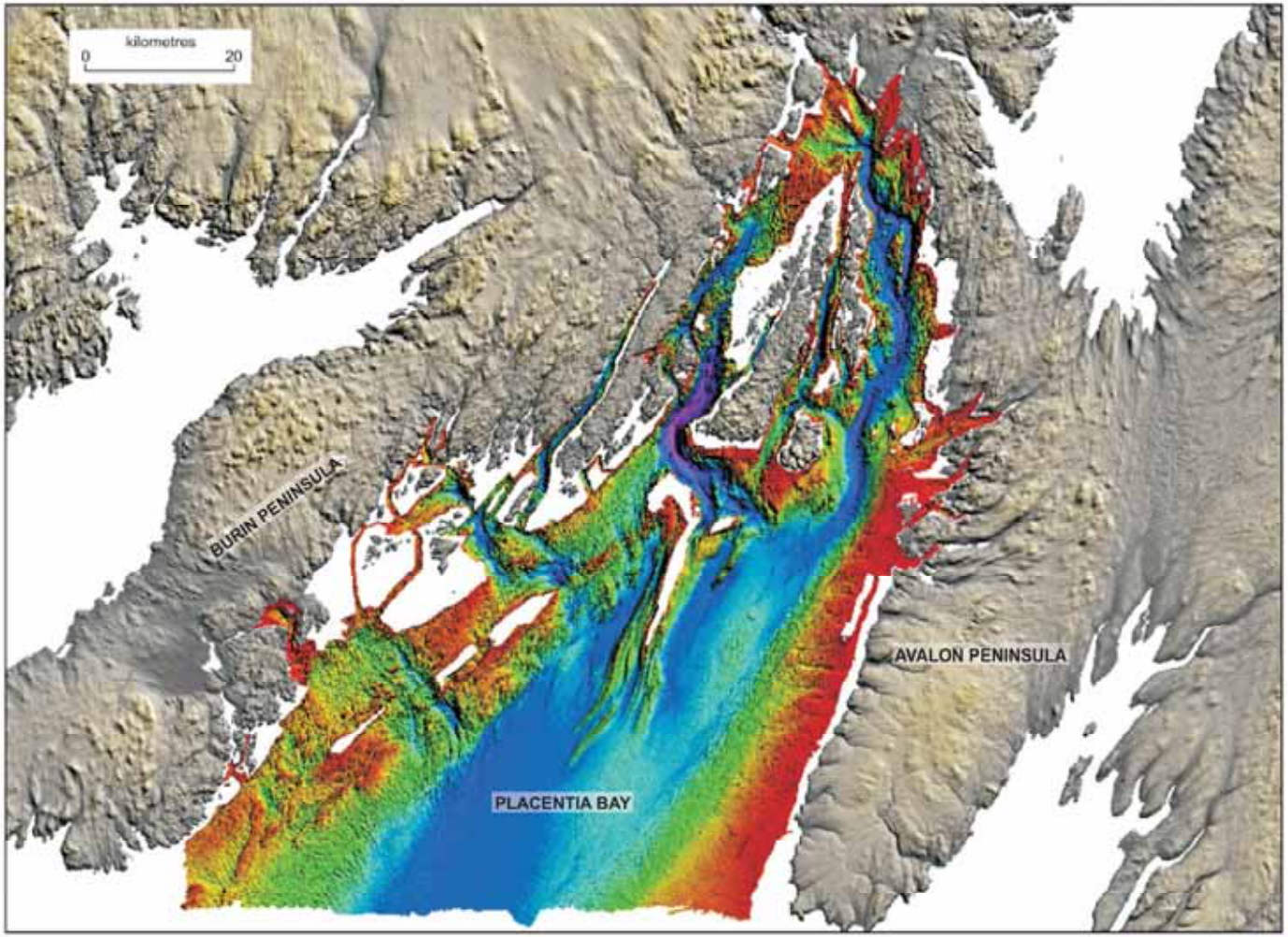

Source: Image from Shaw et al. 2011
Note: Water depths are indicated by colour ranging from shallow (red) to deep (blue)

Figure 4-83 Multibeam Shaded-relief Image Illustrating Placentia Bay Northeast-southwest Trending Bedrock Ridges

Table 4-39 Sublittoral Seascapes

Unit	Morphology	Texture
1. Sub-littoral Muddy Seascapes	Low or flat relief	Mud, silty mud, sandy mud
2. Sub-littoral Mobile Sediment Seascapes	Low relief bodies of sediment with ripples, etc. Includes tidal deltas at Placentia and spillover at Argentia.	Sand and muddy sand; poorly sorted sandy gravel
3. Sub-littoral Glacial/Paraglacial Seascapes	High relief, irregular ridges, mounds of glacial material (3a); submerged paraglacial deltas (3b); low relief platform (3c)	Boulder gravel veneer over glacial sediments. Patches of rippled, poorly sorted sandy gravel (3a); muddy gravel on old deltas (3b); boulder gravel and patches of coarse sand and poorly sorted gravel (3c)
4. Sub-littoral Bedrock Seascapes	High relief ridges, ledges, and pinnacles.	Rock and gravel
5. Deep-water Muddy Seascapes	Little-no relief except on banks within the eastern channel.	Mud, silty mud, sandy mud
6. Deep-water Winnowed Muddy Seascapes	Very low relief except in pockmarks.	Mud, sandy mud, muddy sand
7. Deep-water Glaciomarine Seascapes	Smooth, low relief seafloor	Angular fine gravel, sandy gravel, and muddy gravel as a veneer overlying glaciomarine mud
8. Deep-water Glacial Seascapes	High and irregular relief.	Veneer of bouldery sandy gravel over glacial landforms
9. Deep-water Bedrock Seascapes	High relief ridges, ledges, pinnacles. Subdued compared to outcrops in shallower water.	Rock, muddy gravel and gravelly mud
10. Deep-water Fluted Seascapes	Low relief in vicinity of flutes; individual flutes or coalesced flutes.	Mud, sandy mud
11. Deep-water ‘Current-stressed’ Seascapes	Gently undulating seabed	Muddy gravel, muddy sand
12. Deep-water Sandy Seascapes	Flat seabed with ripples	Sandy with shell hash
13. Dredged Areas	Parallel grooves (several metres high)	Commonly gravel
14. Debris	Mounds, blocks	Gravel, concrete
Source: defined by Shaw et al. 2011		

Argentia Harbour

Argentia Harbour is located on the eastern shore of Placentia Bay, on the Avalon Peninsula (Figure 4-83). The harbour comprises two basins, the inner Argentia Harbour basin and the outer Argentia Harbour basin. These basins reach maximum water depths of 30 and 58 m, respectively, and are separated by a shoal, with a minimum water depth of approximately 15 m, that extends eastward into the harbour (Shaw et al. 1996, 2011). Glacial sediments of the shoal are overlain by a mid-Holocene wave-formed spit composed of pebble-cobble gravel (Shaw et al. 1996, 2011). The spit, located in Figure 4-84 (labelled "13" next to the red aircraft symbol) and on Attachment A, has been dredged to a water depth of approximately 8.5 m. Spoils from the dredging of the spit are presumed to have been dumped on the southern side of the harbour (Shaw et al. 1996, 2011) (Figure 4-85).

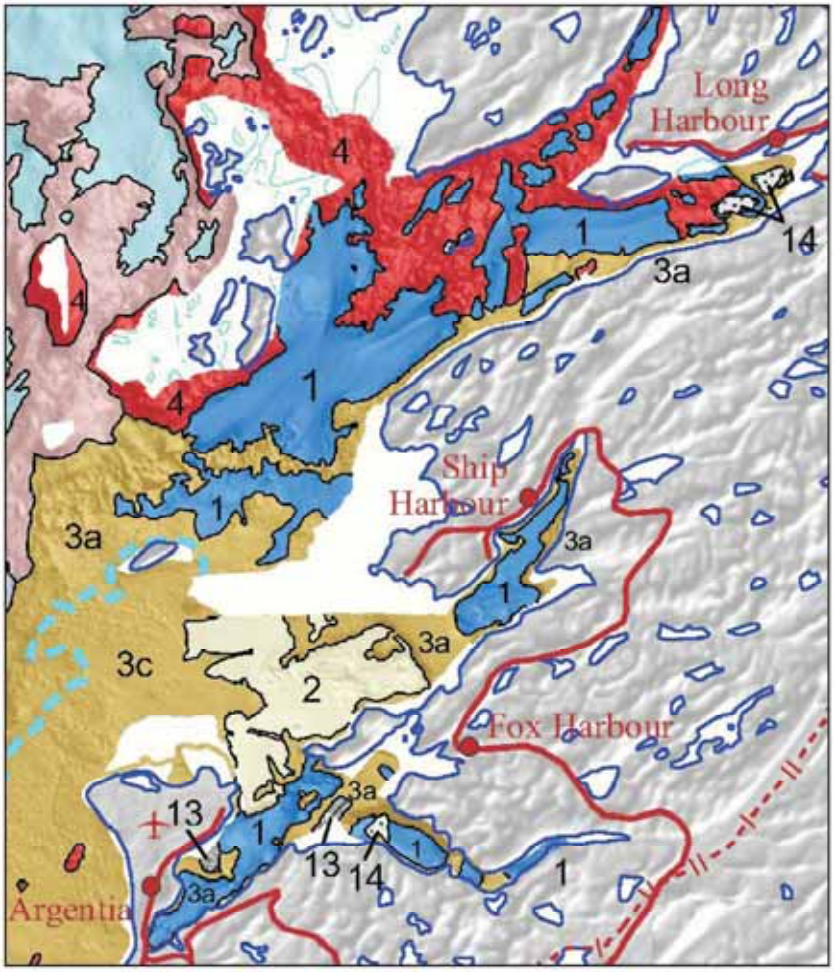

Source: Image from Shaw et al. 2011
Note: 1 – mud, silty mud, sandy mud; 2 – sand and muddy sand, poorly sorted sandy gravel; 3a – patches of rippled, poorly sorted sandy gravel; 3c – boulder gravel and patches of coarse sand and poorly sorted gravel; 4 – rock and gravel; 13 – gravel within dredged area; 14 – gravel, concrete debris. See Table 4-37 in text for full unit descriptions

Figure 4-84 Surficial Sediments within Eastern Placentia Bay, Surrounding the Argentia Peninsula

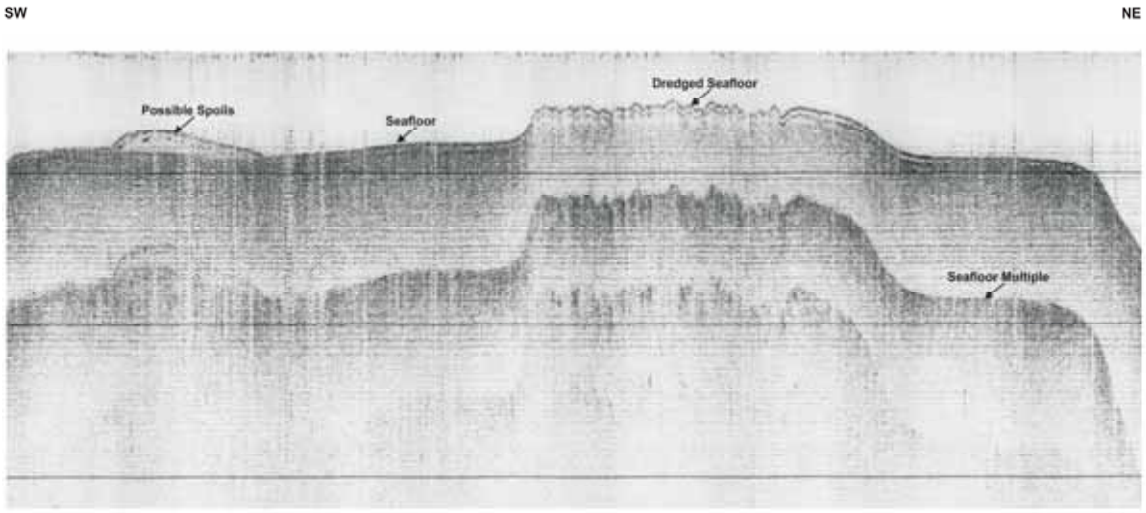

Source: GSC Expedition 89-026
Note: See Attachment B for location

Figure 4-85 Seistec Boomer Line (Scanned), Line 89026_ST_269_1945: Dredged Area - Argentia Harbour

Surficial sediments of Argentia Harbour are illustrated in Figure 4-84. Five units, defined by Shaw et al. (1996, 2011), occur within this area and include: the sub-littoral muddy sediments of Unit 1 within the basins; a region of sub-littoral mobile sandy sediments (Unit 2) northeast of the Argentia Peninsula towards Ship Harbour; and glacial/ paraglacial sediments (Unit 3; both 3a and 3c are present) on the topographic highs. Dredged areas and areas of debris (Units 13 and 14) are also mapped (see Table 4-39).

Groundtruth data collected in the area (Attachment B) are consistent with the surficial units mapped by Shaw et al. (2011) (Figure 4-84). Grab samples 0044 and 0045, and camera stations 0100 and 0101 from a channel 1.5 km to 2 km north of Argentia Peninsula, illustrate a mix of medium- to coarse-grained sand and poorly sorted gravel (Tables 4-37 and 4-38; Figure 4-86). Red coral encrusts the gravel-sized clasts, but only the tops of larger, partially buried clasts. This substrate is consistent with Unit 3c (see Table 4-38).

Towards the mouth of the harbour, sediment samples 047 and 050 (see Tables 4-37 and 4-38) and seabed imagery stations 0103 and 0105 (Figure 4-87) from a channel indicate a sandy substrate with concentrations of gravel to cobbles occurring seaward. Shaw et al. (2011) interpret this sandy unit (Unit 2) as mobile as it often exhibits ripples and other bedforms. Samples collected within this area are typically clean, well-sorted sands.

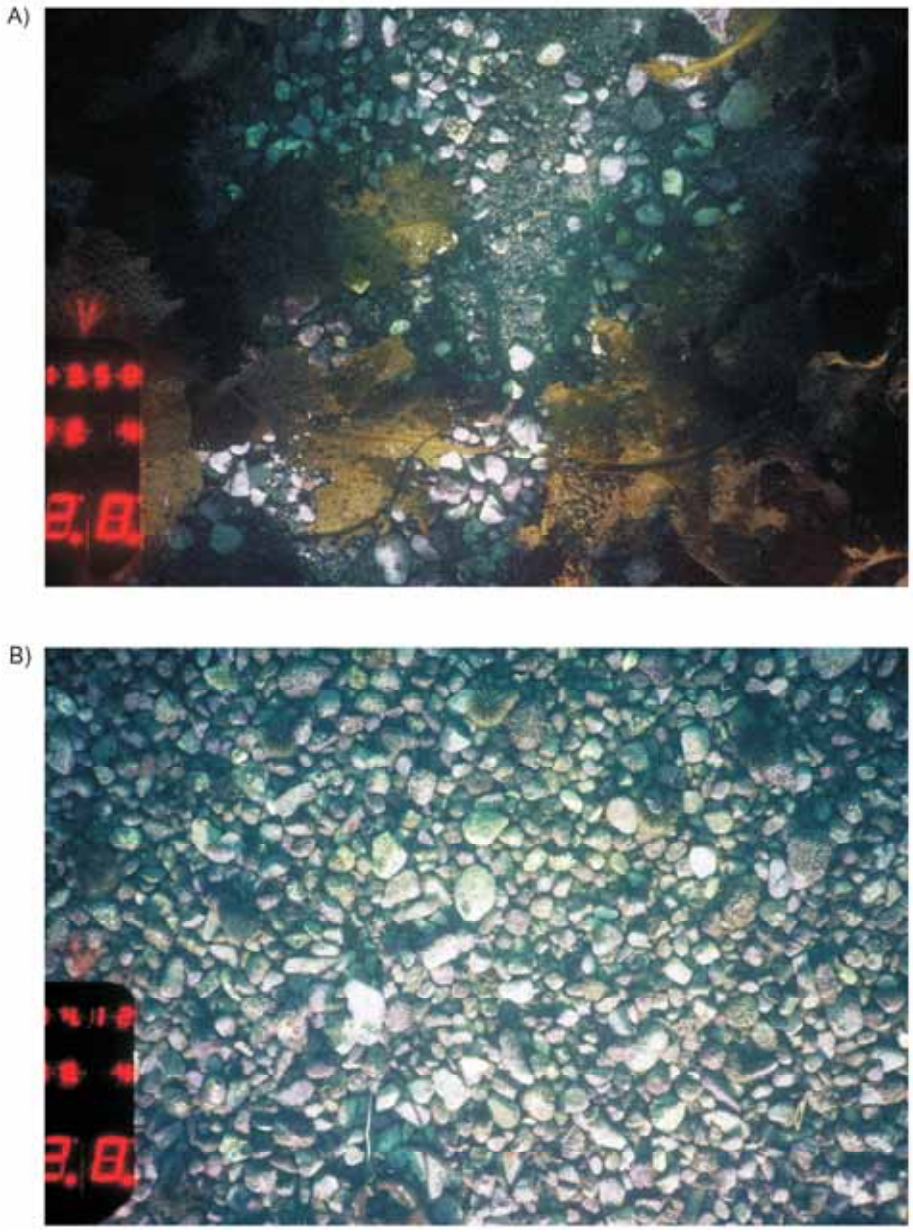

Note: A) Station 0100 illustrating coarse sand and gravel. B) Station 0101 illustrating poorly sorted gravel. Locations of the images are shown on Attachment B

Figure 4-86 Camera Images from GSC Expedition 99-020

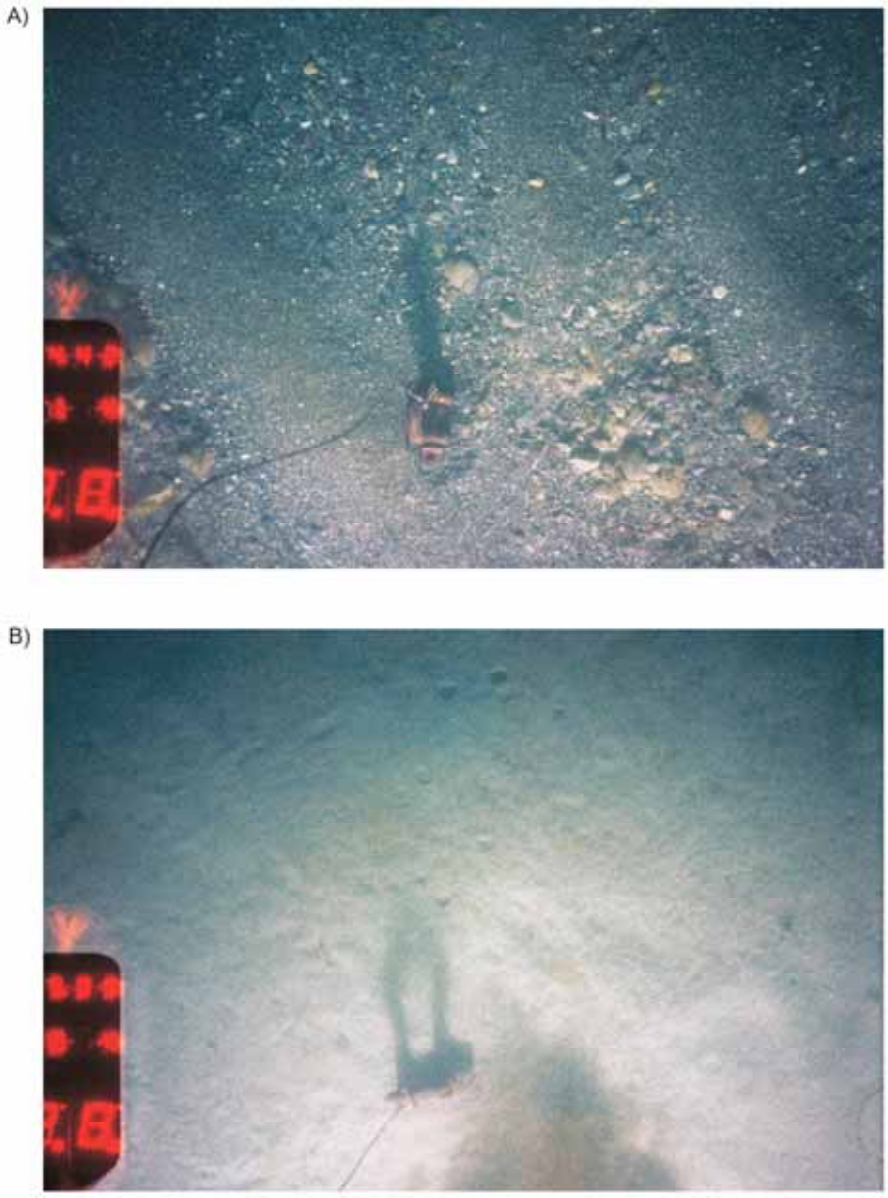

Note: A) Station 0103 illustrating coarse sand and gravel. B) Station 0105 illustrating a sandy substrate. Locations of the images are shown on Attachment B

Figure 4-87 Camera Images from GSC Expedition 99-020

Sediment samples collected from the outer basin, along the southeast shore, and the inner basin of Argentia Harbour, comprise black mud, typically with a brown surface and with worm tubes and abundant organism traces, as seen in seabed imagery from station 0125 (Figure 4-88). Samples 067, 068 and 3009 were collected on the shoal on the northeast side of the harbour, and are characteristic of glacial sediment, consisting of muddy gravel to muddy, gravelly sand, classified as Unit 3a of Shaw et al. (2011). The seabed in this shoal area has been dredged. Seabed image station 0124 shows the poorly sorted sand and gravel of the dredged zone (Tables 4-37 and 4-38; Figure 4-88).

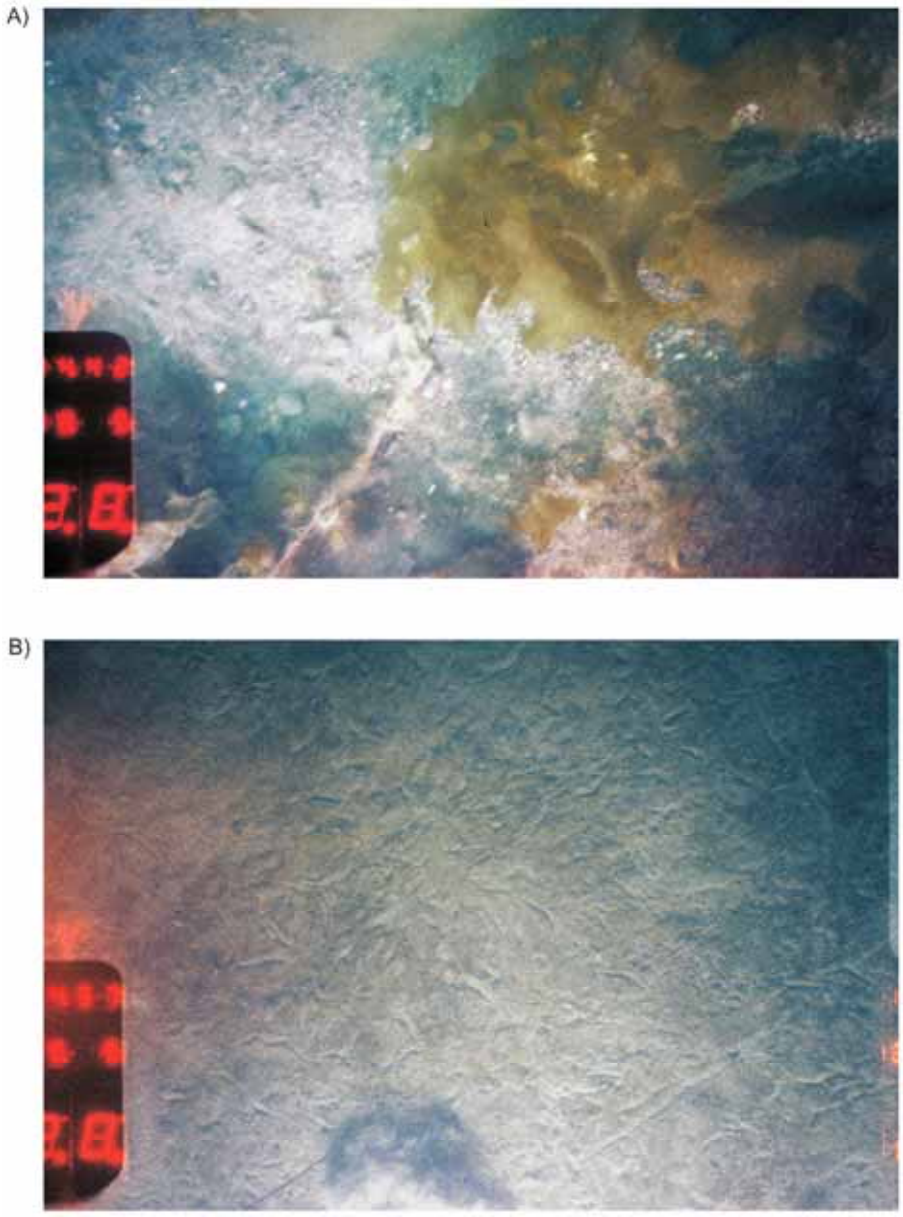

Note: A) Station 0124 illustrating coarse, poorly sorted sand and gravel of the dredged zone on the northeast side of Argentia Harbour. B) Station 0125 illustrating the muddy substrate of the basin within inner Argentia Harbour. Locations of the images are shown on Attachment B

Figure 4-88 Camera Images from GSC Expedition 99-020 – Argentia Harbour

During the late 1990s, the seabed surrounding the Argentia Peninsula was further modified by dredging, spoil dumping, cable-laying and anchor dragging. A variety of anthropogenic material and debris has been placed or deposited on the seabed since World War II, associated with the military base on the Argentia Peninsula, including wharves, piers, seaplane slipways and ammunitions handling berths (Shaw et al. 1996). Dredging locations are illustrated on Figure 4-84.

4.2.5.3 Subsurface Geology – Placentia Bay and Argentia

Placentia Bay

The subsurface geology of Placentia Bay has previously been studied and interpreted from seismic records and core samples (e.g., Fader et al. 1982). Late Proterozoic Hadrynian and Carboniferous bedrock has been mapped from previous surveys (Brushett 2008). The oldest bedrock beneath Placentia Bay and on the surrounding land forms part of the Avalon Zone stratigraphy, as defined by Coleman-Sadd et al. (1990), consisting of Late Proterozoic submarine and non-marine volcanic, sedimentary, metamorphic and granitic rocks. Proterozic bedrock has minimal acoustic penetration when imaged with sub-bottom profilers, and occurs as seafloor outcrops in the northern region of Placentia Bay. These rocks are unconformably overlain by acoustically stratified Carboniferous shallow marine conglomerate, sandstone, siltstone and limestone. The Proterozic and Carboniferous stratigraphic sequence defines a syncline with its axis sub-parallel to the bathymetric axis of Placentia Bay (Brushett et al. 2007; Brushett 2008).

Argentia Harbour

Seismic reflection profiles collected in Argentia Harbour, Placentia Sound and Ship Harbour delineate two seismostratigraphic units. The lowest acoustic unit is defined by a dense, chaotic acoustic signature and is interpreted to be possible glacial diamicton (Shaw et al. 1989) (Figure 4-89). This unit is continuous throughout the inlets and appears to form several broad ridges located between the basins.

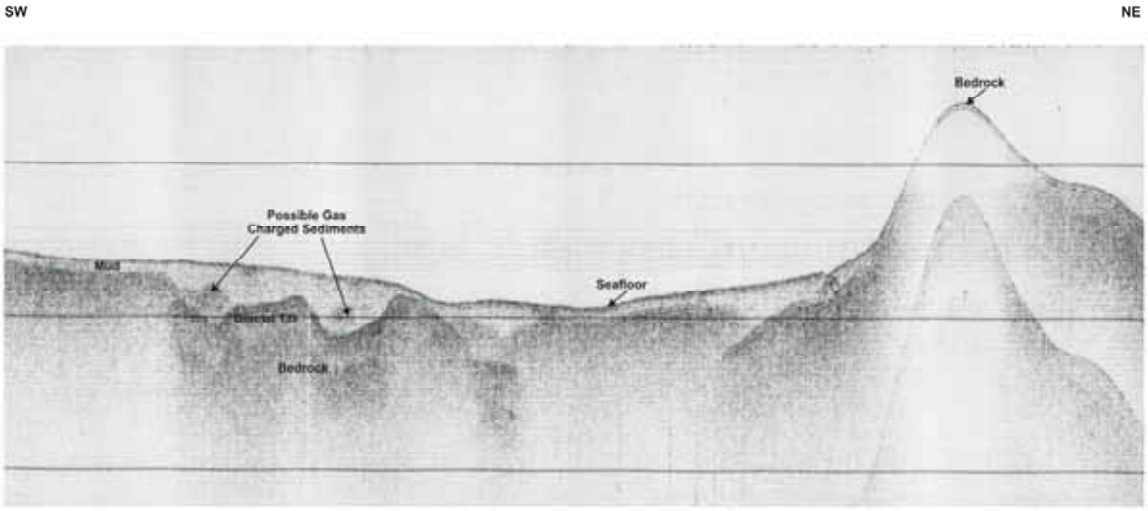

Note: see Attachment B for location

Figure 4-89 Seistec Boomer Line (scanned), Line 89026_ST_269_1945, GSC Expedition 89-026, Argentia Harbour

Within the basins, acoustically transparent mud overlies the inferred diamicton. This upper unit is interpreted to be of postglacial Holocene age, and exhibits a depositional style characteristic of onlapping, basin-fill sedimentation. In some locations, this unit

reaches thicknesses over 5 m. Acoustic stratigraphy in the thicker zones of the Holocene muds is often masked by shallow gas (Shaw et al. 1989, 1996).

Terraces between the basins are typically covered with a thin veneer of coarse gravel and boulders that is not distinguishable from underlying glacial sediments on sub-bottom profiles acquired during the 89026 expedition. North of the Argentia Peninsula the glacial till is covered by sand and fine gravel (Shaw et al. 1989).

4.3 Offshore

4.3.1 Atmospheric Environment

The White Rose field experiences weather conditions typical of a marine environment, with the surrounding waters having a moderating effect on temperature. In general, marine climates experience cooler summers and milder winters than continental climates and have a much smaller annual temperature range. Furthermore, a marine climate tends to be fairly humid, resulting in reduced visibilities, low cloud heights and substantial precipitation.

The climate of the White Rose field is very dynamic, largely governed by the passage of high and low pressure circulation systems. These circulation systems are embedded in, and steered by, the prevailing westerly flow that typifies the upper levels of the atmosphere in the mid-latitudes, which arises because of the normal tropical to polar temperature gradient. The mean strength of the westerly flow is a function of the intensity of this gradient and as a consequence, this flow is considerably stronger in the winter months than during the summer months, due to an increase in the south to north temperature gradient (note: meteorological convention defines seasons by quarters; (e.g., winter is December, January, February)).

At any given time, the upper level flow is a wave-like pattern of large and small amplitude ridges and troughs. These ridges and troughs tend to act as a steering mechanism for surface features and, therefore, their positions in the upper atmosphere determine the weather at the Earth's surface. Upper ridges tend to support areas of high pressure at the surface, while upper troughs lend support to low pressure developments. The amplitude of the upper flow pattern tends to be higher in winter than summer, which is conducive to the development of more intense storm systems.

During the winter months, an upper level trough tends to lie over central Canada and an upper ridge over the North Atlantic, resulting in three main storm tracks affecting the region: from the Great Lakes Basin; from Cape Hatteras, North Carolina; and from the Gulf of Mexico. These storm tracks, on average, bring eight low pressure systems per month over the area. The intensity of these systems ranges from relatively weak features to major winter storms. Recent studies (Archer and Caldeira 2008) have shown that there is a poleward shift of the jet stream and, consequently, storm tracks, at a rate of 0.17 to 0.19 degrees/decade in the northern hemisphere. This shift has been related to an increase in the equator-to-pole temperature gradient. McCabe (2001) obtained similar results, finding that there has been a decrease in mid-latitude cyclone frequency and an increase in high-latitude cyclone frequency. In addition, McCabe (2001) found that storm intensity has increased in both the high and mid-latitudes.

In the case where the upper level long wave trough lies well west of the region, the main storm track will lie through the Gulf of St. Lawrence or the Island of Newfoundland. Under this regime, an east to southeast flow ahead of a warm front associated with a low will give way to winds from the south in the warm sector of the system. Typically, the periods of southerly winds and mild conditions will be of relatively long duration and, in general, the incidence of extended storm conditions is likely to be relatively infrequent. Strong frictional effects in the stable flow from the south results in a marked shear in the surface boundary layer and relatively lower winds at the sea surface. As a consequence, local wind and wave development tends to be inhibited under such conditions. Precipitation types are more likely to be in the form of rain or drizzle, with relatively infrequent periods of continuous snow; although periods of snow showers prevail in the unstable air in the wake of cold fronts associated with the lows. Visibility will be reduced at times in frontal and advection fogs, in snow and in snow shower activity.

With the upper long wave trough situated further to the east, the main storm track may lie through or to the east of the Grand Banks. With the lows passing closer to the site and a higher potential for storm development, the incidence of strong gale and storm conditions is greater. Longer bouts of cold, west to northwest winds behind cold fronts occur more frequently and, because the flow is colder than the surface water temperatures, the surface layer is unstable. The shear in the boundary layer is lower, resulting in relatively higher wind speeds near the surface and, consequently, relatively higher sea state conditions. With cold air and sea surface temperatures coupled with high winds, freezing spray will occur quite frequently. In this synoptic situation, a greater incidence of precipitation in the form of snow is likely to occur. Freezing precipitation, either as rain or drizzle, occurs rather infrequently on the Grand Banks. Visibility will be reduced in frontal and advection fogs, and relatively more frequently by snow.

Frequently, intense low pressure systems become ‘captured’ and slow down or stall off the coast of Newfoundland and Labrador. This may result in extended periods of unchanging conditions. Depending on the position, overall intensity and size of the system, these conditions may range from relatively benign to heavy weather conditions.

By summer, the main storm tracks have moved further north than in winter. Low pressure systems are less frequent and much weaker. With increasing solar radiation during spring, there is a general warming of the atmosphere, which is relatively greater at higher latitudes. This decreases the north-south temperature contrast, lowers the kinetic energy of the westerly flow aloft and decreases the potential energy available for storm development. Concurrently, there is a northward shift of the main band of westerly winds at upper levels and a marked development of the Bermuda-Azores sub-tropical high-pressure area to the south. This warm-core high-pressure cell extends from the surface through the entire troposphere. The main track of the weaker low-pressure systems typically lies through the Labrador region and tends to be oriented from the west-southwest to the east-northeast.

With low pressure systems normally passing to the north of the region, in combination with the northwest sector of the sub-tropical high to the south, the prevailing flow across the Grand Banks is from the southwest during the summer season. Wind speed is lower during the summer and the incidence of gale- or storm-force winds is relatively infrequent. There is also a corresponding decrease in significant wave heights.

The prevailing southwesterly flow during the late spring and early summer tends to be moist and it is relatively warmer than the underlying surface waters on the Grand Banks.

Rapidly deepening storms are problematic south of Newfoundland in the vicinity of the warm water of the Gulf Stream. Sometimes these explosively-deepening oceanic cyclones develop into a “weather bomb”, defined as a storm that undergoes central pressure falls greater than 24 mb over 24 hours. Hurricane-force winds near the centre, the outbreak of convective clouds to the north and east of the centre during the explosive stage, and the presence of a clear area near the centre in its mature stage (Rogers and Bosart 1986) are typical of weather bombs. After development, these systems will either move across Newfoundland or to the east of Newfoundland, producing gale- to storm-force winds from the southwest to south over the Grand Banks.

In addition to extratropical cyclones, tropical cyclones often retain their tropical characteristics as they enter the White Rose field. Tropical cyclones account for the strongest sustained surface winds observed anywhere on Earth. The hurricane season in the North Atlantic basin normally extends from June through November, although tropical storm systems occasionally occur outside this period. Once formed, a tropical storm or hurricane will maintain its energy as long as a sufficient supply of warm, moist air is available. Tropical storms and hurricanes obtain their energy from the latent heat of vapourization that is released during the condensation process. These systems typically move east to west over the warm water of the tropics; however, some of these systems turn northward and make their way toward Newfoundland. Since the capacity of the air to hold water vapour is dependent on temperature, as the hurricanes move northward over the colder ocean waters, they begin to lose their tropical characteristics. By the time these weakening cyclones reach Newfoundland, they are usually embedded into a mid-latitude low and their tropical characteristics are usually lost.

A substantial number of tropical cyclones that move into the mid-latitudes will undergo transition into extratropical cyclones. On average, 46 percent of tropical cyclones that form in the Atlantic transform into extratropical cyclones. During this transformation, the system loses tropical characteristics and becomes more extratropical in nature. These systems frequently produce large waves, gale- to hurricane-force winds and intense rainfall. The likelihood that a tropical cyclone will undergo transition increases toward the second half of the tropical season, with cyclones in October having the highest probability of transition. In the Atlantic, extratropical transition occurs at lower altitudes in the early and late hurricane season and at higher latitudes during the peak of the season (Hart and Evans 2001).

4.3.1.1 Data Sources

The data sources to describe the wind climatology at White Rose came from three main sources: ICOADS (Woodruff et al. 2011), Manual of Marine (MANMAR) Observations (rig) observations and the MSC50 North Atlantic wind and wave climatology database. The locations of the climate data sources are presented in Figure 4-90.

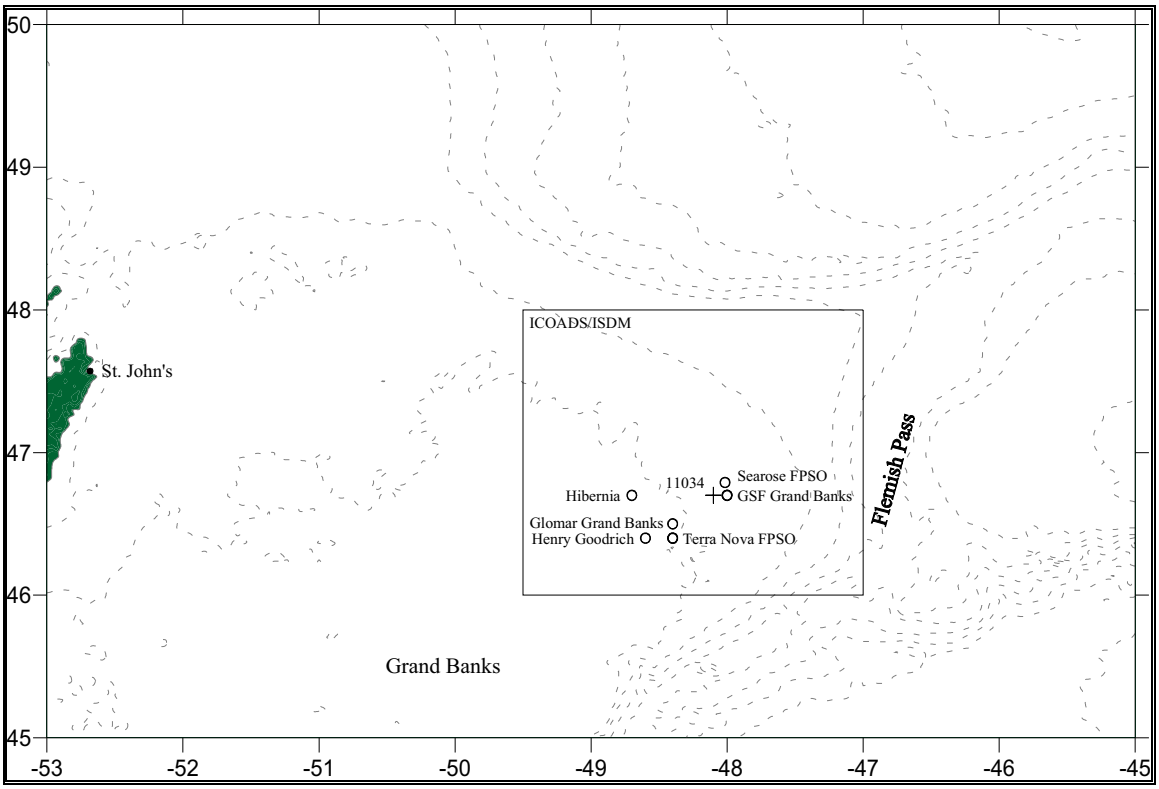

Figure 4-90 Locations of the Climate Data Sources

It should also be noted that wind speeds from the MSC50 data set and ICOADS are not directly comparable to each other due to their sampling period and the heights at which they were measured. Wind speed is dependent on height, since the wind speed increases at increasing heights above sea level. Methods to reduce wind speeds from anemometer level to 10 m to standardize the data sets have proven ineffective due to atmospheric stability issues. Winds in ICOADS were either estimated or measured by anemometers at various heights above sea level.

Wind speeds from each of the data sources have different averaging periods. The MSC50 winds are 1-hour averages, while ICOADS and MANMAR winds are 10-minute average winds.

International Comprehensive Ocean-Atmosphere Data Set

Wind, air temperature, sea surface temperature and visibility statistics for the area were compiled using data from ICOADS. A subset of global marine surface observations from ships, drilling rigs and buoys for the area from 46°00'N to 48°00'N, and 047°00'W to 049°30'W, covering the period from January 1980 to January 2011, was used in this report.

ICOADS has certain inherent limitations; the observations are not spatially-or temporally-consistent. In addition, the data set is somewhat prone to observation and coding errors, resulting in some erroneous observations within the data set. The errors were minimized by using an outlier trimming level of 5.5 standard deviations for wind speed and

3.5 standard deviations for air and sea surface temperatures. In an attempt not to exclude valid observations from the data set, any data greater than 4.5 standard deviations for wind speed and 2.8 standard deviations for air and sea surface temperature were flagged and subsequently analyzed for consistency with other data within the same region and same time. Despite this analysis, valid observations may still have been excluded from the data set. Conversely, invalid data that fell within the limits of the quality control analysis may have been included in the data set.

While the ship-based reports have been quality controlled to the extent possible, they are likely to contain some observation errors in addition to position report errors, particularly for the older reports. As well, the data set is known to contain a 'fair weather bias', which arises for the following reasons: ship captains may choose to avoid areas of heavy weather; and, since the reporting program is voluntary, fewer observations are likely to be taken under adverse weather and sea state conditions. This bias is more likely to be present during the winter season and over temperate and northern seas, where vessel traffic is light.

Kent et al. (1993) demonstrated various systematic inconsistencies in the meteorological observations from voluntary observing ships. These inconsistencies were mostly dependent on the method of estimation that was used. Sea surface temperature data from engine intake thermometers were found to be biased high by an average of 0.3°C. The dew point temperatures from fixed thermometer screens were biased high compared to psychrometer readings. The magnitude of the bias was on the order of 1°C and varied with dew point temperature. Wind speeds from anemometers were biased high compared to visual winds by approximately 1 m/s (2 knots) for winds up to approximately13 m/s (25 knots). It was unknown whether visual winds or anemometer winds were more accurate. Compared to daytime values, visual winds at night were underestimated by approximately 1 m/s at 15 m/s and 5 m/s at 25 m/s.

Rig Observations

Wind statistics were also compiled using MANMAR data from several offshore platforms located in the region. The location, period of observation and anemometer height for each of these stations is presented in Table 4-40. Note that the Glomar Grand Banks and the GSF Grand Banks are the same platform under different names at the time of the observations.

Table 4-40 Locations of Manual of Marine Observations

Location	Latitude	Longitude	Anemometer Height (m)	Period
Sea Rose FPSO	46.8°N	48.0°W	42	Nov 04, 2005 – Dec 31, 2011
Terra Nova FPSO	46.4°N	48.4°W	50	Aug 12, 2007 - Dec 31, 2011
Glomar Grand Banks	46.5°N	48.4°W	82.5	Dec 31, 1998 - Jul 02, 2000
GSF Grand Banks	46.7°N	48.0°W	82.5	July 16, 2003 – Dec 11, 2011
Henry Goodrich	46.4°N	48.6°W	95	Feb 23, 2000 - Jun 30, 2009
Hibernia	46.7°N	48.7°W	139	Jan 01, 1999 - Dec 31, 2011
Ocean Ranger	46.5°N	48.4°W	N/A	Dec 04, 1980 – Feb 09, 1982

MSC50 Data Set

Wind climate statistics for the area were extracted from the MSC50 North Atlantic wind and wave climatology database compiled by Oceanweather Inc., under contract to Environment Canada (Oceanweather Inc. and Environment Canada 2011). The MSC50 database consists of continuous wind and wave hindcast data in 1-hour time steps from January 1954 to December 2010, on a 0.1° latitude by 0.1° longitude grid. Winds from the MSC50 data set are 1-hour averages of the effective neutral wind at a height of 10 m (Harris 2007, pers. comm.). Grid Point 11034 was chosen to represent conditions within the area of interest.

The MSC50 project followed the same basic methodology as was applied in the AES40 hindcast, with notable improvements and upgrades. The temporal resolution was changed from a six-hour time base to a three-hour analysis. This increased resolution resulted in improved modelling of rapidly deepening winter storms that develop off the US Eastern Seaboard and track northeast across the Grand Banks.

4.3.1.2 Wind Climatology

The White Rose field experiences predominately southwest to west flow throughout the year. There is a strong annual cycle in the wind direction. West to northwest winds, which are prevalent during the winter months, begin to shift counter-clockwise during March and April, resulting in a predominant southwest wind by the summer months. As autumn approaches, the tropical-to-polar temperature gradient strengthens and the winds shift slightly, becoming predominately westerly again by late fall and into winter. Low pressure systems crossing the area are more intense during the winter months. As a result, mean wind speeds tend to peak during this season.

In addition to mid-latitude low pressure systems crossing the Grand Banks, tropical cyclones often move northward out of the influence of the warm waters of the Gulf Stream, passing near the Island of Newfoundland. Once the cyclones move over colder waters they lose their source of latent heat energy and often begin to transform into a fast-moving and rapidly developing extratropical cyclones producing large waves and sometimes hurricane force winds.

Low pressure systems crossing the area are more intense during the winter months. As a result, mean wind speeds tend to peak during this season. Wind speed typically increases with increasing heights above sea level. Statistics in Table 4-41 are presented in order of increasing height above sea level with the MSC50 data set being the lowest and the Hibernia Platform being the highest. The anemometer heights for each platform are found in Table 4-40. Statistics for each anemometer level are presented to give a better idea of winds at varying heights above sea level.

A wind rose of the annual wind speed for Grid Point 11034 is presented in Figure 4-91 and the associated histogram of the wind speed frequency in Figure 4-92. Percentage frequency of wind direction by month is presented in Table 4-42.

Table 4-41 Mean Wind Speed (m/s) Statistics

Month	MSC50 Grid Point 11034	ICOADS	Ocean Ranger	Sea Rose FPSO	Terra Nova FPSO	Glomar Grand Banks	GSF Grand Banks	Henry Goodrich	Hibernia
January	11.1	14.2	13.8	12.8	13.8	12.9	13.2	15.4	16.1
February	10.9	13.6	13.0	12.1	13.6	11.9	12.8	15.3	15.6
March	9.8	12.5	-	11.0	12.2	11.9	12.1	14.0	14.5
April	8.3	11.7	-	10.3	11.6	11.4	12.0	12.7	13.6
May	7.0	10.6	-	8.9	10.5	9.7	10.9	11.8	12.2
June	6.5	10.5	-	8.6	9.8	9.4	9.1	11.6	11.7
July	6.1	10.2	-	8.4	9.6	9.5	9.6	11.1	11.4
August	6.4	9.4	-	10.3	9.2	8.4	8.8	9.8	10.6
September	7.5	10.4	-	10.7	10.5	10.3	9.7	10.4	11.7
October	8.8	11.7	-	12.3	11.9	12.8	10.5	12.2	13.5
November	9.5	12.3	14.1	12.4	12.2	11.0	11.7	12.7	13.9
December	10.7	14.0	12.3	12.7	13.9	12.6	13.2	14.4	15.7

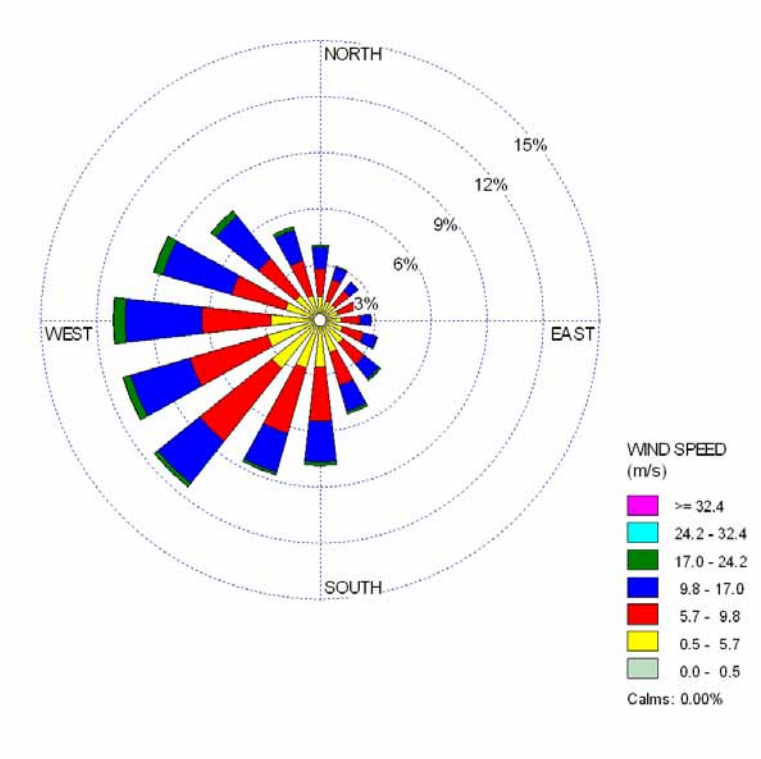

Figure 4-91 Annual Wind Rose for MSC50 Grid Point 11034 located near 46.7°N; 48.1°W, 1954 to 2010

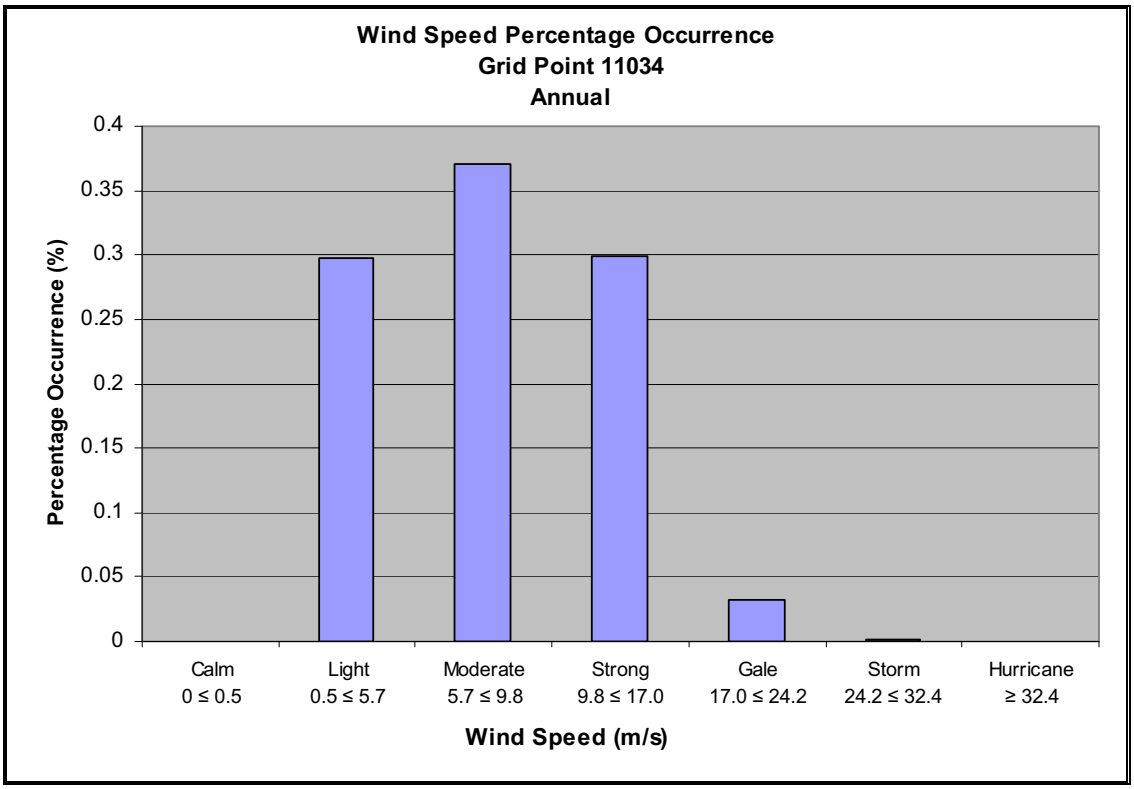

Figure 4-92 Annual Percentage Frequency of Wind Speeds for MSC50 Grid Point 11034 (located near 46.7°N; 48.1°W), 1954 to 2010

Table 4-42 Monthly and Annual Percentage Frequency of Wind Direction for MSC50 Grid Point 11034 (1954 to 2010)

Month	Direction							
	NE	E	SE	S	SW	W	NW	N
January	4.2	5.0	7.9	11.7	17.6	29.0	17.7	6.9
February	5.3	6.0	8.5	11.8	15.2	26.8	18.1	8.2
March	7.4	7.2	7.9	12.1	16.4	21.7	16.7	10.8
April	7.4	9.1	10.0	12.7	17.6	18.1	14.9	10.0
May	7.6	7.3	9.2	15.3	20.5	17.4	13.2	9.5
June	5.0	5.3	7.9	16.9	30.5	17.0	9.8	7.6
July	2.6	3.5	6.9	21.8	37.9	16.4	6.9	3.9
August	4.6	4.2	8.3	18.4	29.9	18.5	9.2	6.8
September	5.8	4.6	6.8	14.7	21.6	21.3	15.8	9.3
October	4.7	5.2	7.4	13.3	18.1	22.6	19.3	9.4
November	5.0	5.5	9.1	14.4	17.0	21.7	18.9	8.3
December	4.3	5.4	8.3	12.8	16.1	26.5	18.5	8.2
Annual	5.3	5.7	8.2	14.7	21.6	21.4	14.9	8.2

Wind speeds are much lower in the summer than in winter. The percentage exceedance of wind speeds at Grid Point 11034 is presented in Figure 4-93.

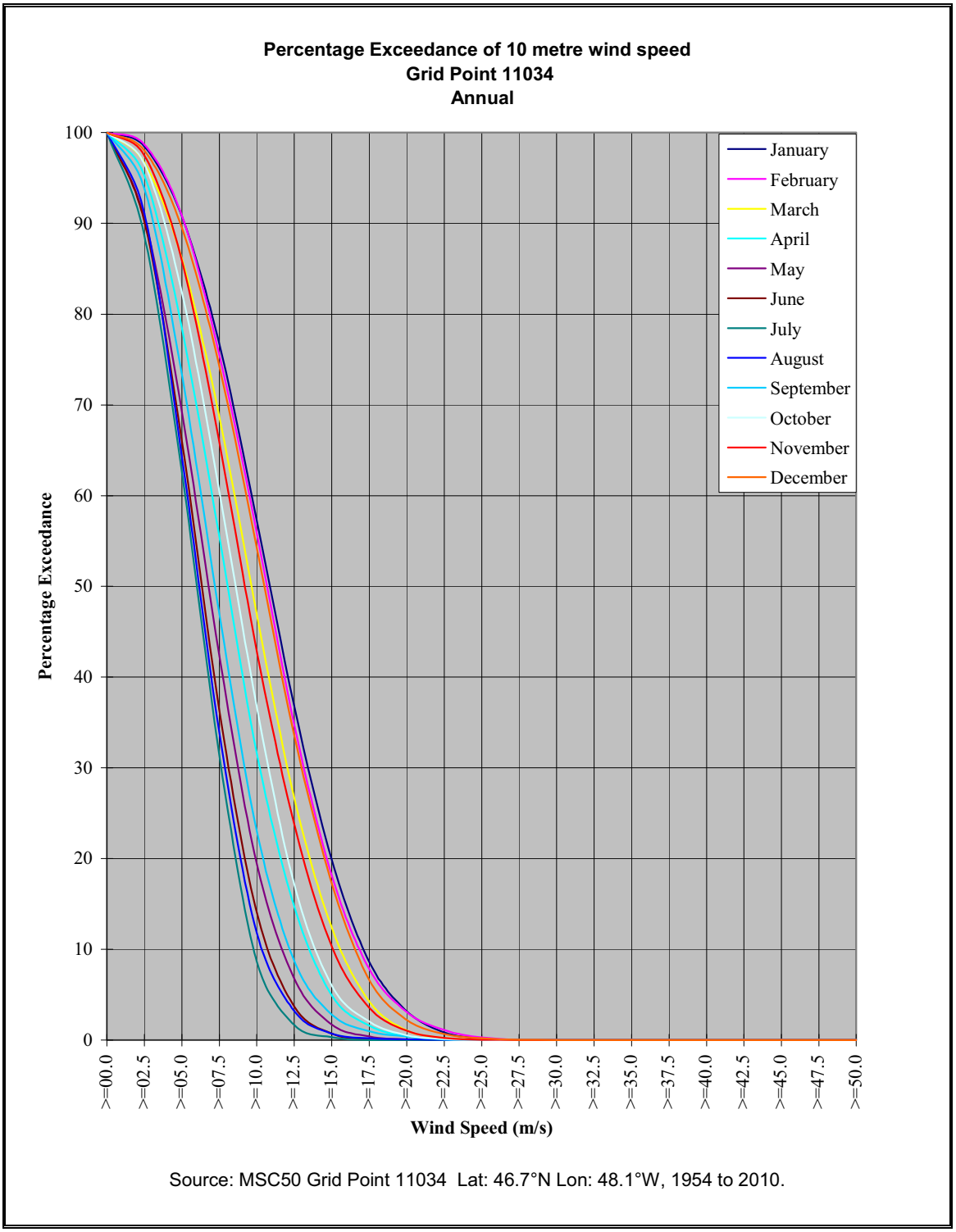

Figure 4-93 Percentage Exceedance of 10-m Wind Speed at Grid Point 11034 Located near 46.7°N; 48.1°W, 1954 to 2010

Monthly maximum wind speeds for each of the data sets is presented in Table 4-43 and the monthly maximum wind speed by direction from the MSC50 database in Table 4-44. Rapidly deepening storm systems known as weather bombs frequently cross the Grand Banks. These storm systems typically develop in the warm waters of Cape Hatteras and move northeast across the Grand Banks. At 00Z (Zulu time, aka UTC) on February 11, 2003, a 987 mb low pressure off Cape Hatteras deepened to 949 mb as it moved northeast, crossing eastern Newfoundland near 18Z. The low then began to weaken as it moved north of the forecast waters in the evening. There were no observations on the White Rose field during this event. Wind speeds of 49.4 and 50.9 m/s from the southwest were recorded by the Hibernia and the Henry Goodrich anemometers, respectively, as this system passed. The values from the Hibernia Platform do not give a true indication of the winds during this event, as the anemometer reached its maximum speed for a period of time. Furthermore, wind speeds reported in both the Henry Goodrich and Hibernia MANMARs are every three hours and, as such, probably did not capture the highest wind speeds measured during this event. The anemometers on all platforms on the Grand Banks; the Henry Goodrich, Terra Nova FPSO and Hibernia registered the maximum speeds the anemometers could record during gusts. While wind speeds at the surface were estimated to be high, the wind speeds measured at the anemometers were not related to the surface winds and therefore adjustment factors to adjust wind speeds from the anemometers to the surface are not valid. The extreme wind speeds measured during this event were due to a combination of a very low central pressure, which resulted in the surface boundary layer dropping to below anemometer heights. As a consequence, the anemometers were subject to a very strong low-level jet associated with the low pressure system.

Table 4-43 Maximum Wind Speed (m/s) Statistics

Month	MSC50 Grid Point 11034	ICOADS	Ocean Ranger	Sea Rose FPSO	Terra Nova FPSO	Glomar Grand Banks	GSF Grand Banks	Henry Goodrich	Hibernia
January	29.0	43.7	34.5	25.7	31.9	30.9	37.6	44.2	43.2
February	32.0	46.3	37.0	29.8	34.0	26.8	31.4	52.5	49.4
March	28.4	38.0	-	23.7	29.8	23.7	28.8	32.9	37.6
April	25.0	37.0	-	24.7	26.8	26.8	33.4	30.9	37.6
May	22.5	33.9	-	21.6	25.2	22.1	25.7	32.9	32.4
June	23.4	35.5	-	18.5	24.2	21.1	27.3	28.3	35.5
July	19.6	31.9	-	18.0	23.2	20.1	25.2	26.2	31.9
August	28.9	26.0	-	33.4	29.8	25.7	26.2	28.8	41.2
September	24.6	37.6	-	30.9	34.5	29.3	27.8	28.3	43.2
October	27.0	41.1	-	43.7	34.0	32.9	30.9	27.8	44.8
November	27.5	41.2	28.8	25.2	28.3	25.7	25.7	32.4	38.1
December	30.1	47.8	28.8	24.7	37.6	27.3	29.3	38.1	39.1

Table 4-44 Monthly Maximum Anemometer Wind Speed (m/s) by Direction, 1954 to 2010

Month	Direction								Monthly	
	NE	E	SE	S	SW	W	NW	N	Min	Max
January	21	23	24	26	29	28	27	25	21	29
February	23	22	25	30	30	30	32	24	22	32
March	22	25	24	22	25	28	28	25	22	28
April	22	20	21	25	24	23	24	24	20	25
May	16	18	18	19	20	19	23	19	16	23
June	16	17	21	18	18	22	23	15	15	23
July	14	16	17	20	17	17	18	15	14	20
August	17	18	19	29	28	23	29	24	17	29
September	21	21	24	24	25	23	21	21	21	25
October	22	22	24	27	27	27	25	23	22	27
November	21	23	23	27	23	27	28	26	21	28
December	22	22	25	23	28	28	30	25	22	30
Years Max	23	25	25	30	30	30	32	26		

A wind speed of 43.7 m/s was recorded by the *SeaRose FPSO* at 00Z and 03Z on October 15, 2009. This occurred as another storm following a similar track to the February 2003 storm passed over the area. During this event, the low pressure system deepened from 1,002 mb at 00Z on October 14, 2009, to 963 mb as the system passed northeast of the Avalon on October 15, 2009.

4.3.1.3 Air and Sea Temperature

The moderating influence of the ocean serves to limit both the diurnal and the annual temperature variation on the Grand Banks. Diurnal temperature variations due to the day/night cycles are very small. Short-term, random temperature changes are due mainly to a change of air mass following a warm or cold frontal passage. In general, air mass temperature contrasts across frontal zones are greater during the winter than during the summer season.

Air and sea surface temperatures for the area were extracted from ICOADS. A monthly plot of air temperature versus sea surface temperature is presented in Figure 4-95. Air and sea surface temperature statistics are presented in Figure 4-94 and Tables 4-45 and 4-46 show that the atmosphere is coldest in the month of February with a mean monthly air temperature of -0.4°C, and warmest in August with a mean monthly air temperature of 14.3°C. Similarly, sea surface temperature is warmest in August with a mean monthly temperature of 13.7°C and coldest in February and March with mean monthly temperatures of 0.3°C. The mean sea surface temperature is cooler than the mean air temperature from March to August, with the greatest difference occurring in the month of July. From September to February, sea surface temperatures are warmer than the mean air temperature. The colder sea surface temperatures from March to August have a

cooling effect on the atmosphere, while relatively warmer sea surface temperatures from September to February tend to warm the overlying atmosphere.

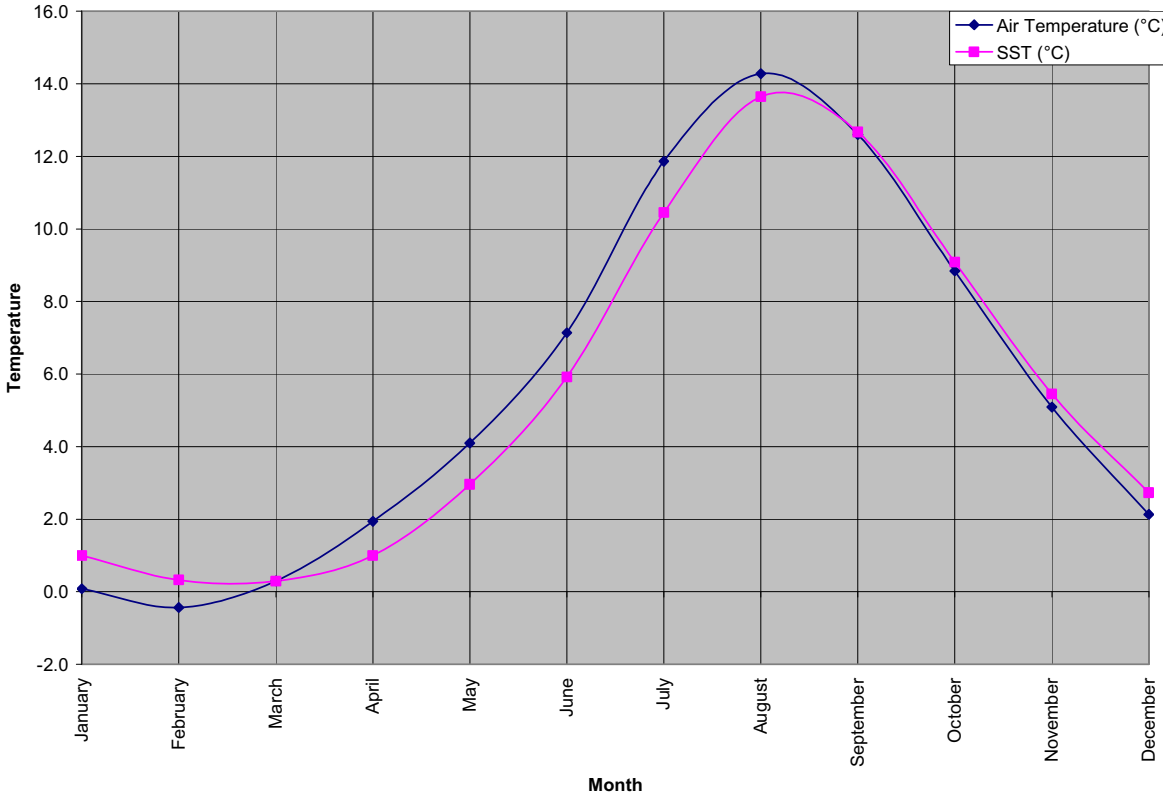

Figure 4-94 Monthly Mean Air and Sea Surface Temperature (°C) for the International Comprehensive Ocean-Atmosphere Data Set, 1980 to 2010

Table 4-45 International Comprehensive Ocean-Atmosphere Data Set Air Temperature (°C) Statistics

Month	Mean	Maximum	Minimum	Standard Deviation	Mean Daily Maximum	Mean Daily Minimum
January	0.1	12.0	-12.0	3.2	2.6	-2.2
February	-0.4	10.4	-12.1	3.1	1.9	-2.9
March	0.3	15.3	-17.3	2.8	2.5	-1.7
April	1.9	11.4	-7.3	2.4	4.1	0.1
May	4.1	13.0	-10.0	2.3	6.2	2.3
June	7.1	16.8	-1.2	2.4	9.3	5.3
July	11.9	25.3	-3.2	2.6	13.5	9.7
August	14.3	23.6	5.5	2.3	16.1	12.4
September	12.6	20.5	-4.0	2.5	14.7	10.7
October	8.8	18.4	-1.0	3.0	11.1	6.9
November	5.1	15.3	-4.6	3.0	7.5	3.2
December	2.1	12.8	-13.5	3.3	4.5	0.1

Table 4-46 International Comprehensive Ocean-Atmosphere Data Set Sea Surface Temperature (°C) Statistics

Month	Mean	Maximum	Minimum	Standard Deviation	Mean Daily Maximum	Mean Daily Minimum
January	1.0	7.0	-2.0	1.5	2.3	0.2
February	0.3	6.0	-2.0	1.7	1.6	-0.4
March	0.3	6	-2.0	1.4	1.5	-0.4
April	1.0	7.5	-2.0	1.6	2.0	0.2
May	3.0	9.6	-2.0	1.8	4.2	1.8
June	5.9	14.0	-2.0	2.4	7.1	4.4
July	10.5	19.0	2.3	2.5	11.4	8.8
August	13.7	20.5	6.0	2.2	14.7	11.9
September	12.7	20.0	4.0	2.4	13.9	10.8
October	9.1	17.0	1.0	2.7	10.8	7.2
November	5.5	13	-1.9	2.6	7.25	3.9
December	2.7	10.2	-2.0	2.11	4.3	1.6

Monthly mean daily maximum and minimum temperature statistics are also presented for ICOADS. Mean temperatures for each month are the mean of all temperatures recorded at the site during that month. The maximum and minimum temperatures are the highest and lowest temperatures, respectively, recorded during the month over the entire data set. The mean daily maximum is the average of all maximum temperatures recorded during the specified month, while the mean daily minimum is the average of all minimum temperatures recorded during the specified month.

4.3.1.4 Precipitation

Precipitation is classified as liquid, freezing or frozen. Included in the three classifications are:

- Liquid precipitation
  - Drizzle
  - Rain
- Freezing precipitation
  - Freezing drizzle
  - Freezing rain
- Frozen precipitation
  - Snow
  - Snow pellets
  - Snow grains
  - Ice pellets
  - Hail
  - Ice crystals.

The migratory high and low pressure systems transiting the temperate middle latitude of the Northern Hemisphere cause a variety of precipitation types in their paths. The frequency of precipitation type for the project area was calculated using data from ICOADS, with each occurrence counting as one event. Precipitation statistics for these regions may be low due to a fair weather bias. That is, ships tend to either avoid regions of inclement weather, or simply do not report during these events.

The percentage of occurrences of freezing precipitation data was also calculated from ICOADS. Freezing precipitation occurs when rain or drizzle aloft enters negative air temperatures near the surface and becomes super-cooled so that the droplets freeze upon impact with the surface. This situation typically arises ahead of a warm front extending from low pressure systems passing west of the area. The frequency of freezing precipitation was slightly higher in the winter months than during the spring.

The frequency of precipitation type (Table 4-47) shows that annually, precipitation occurs 22.1 percent of the time. Winter has the highest frequency of precipitation with 34.6 percent of the observations reporting precipitation. Snow accounts for the majority of precipitation during the winter months, accounting for 59.0 percent of the occurrences of winter precipitation. Summer has the lowest frequency of precipitation with a total

frequency of occurrence of only 12.9 percent. Snow has been reported in each month. However, this is probably due to coding errors rather than the actual presence of snow.

Table 4-47 Percentage Frequency (%) Distribution of Precipitation for International Comprehensive Ocean-Atmosphere Data Set

Month	Rain / Drizzle	Freezing Rain / Drizzle	Rain / Snow Mixed	Snow	Thunder storm	Hail	Total
January	12.7	0.5	0.6	23.3	0.0	0.2	37.3
February	10.1	0.8	0.4	22.5	0.0	0.0	33.9
March	11.8	0.9	0.3	14.5	0.0	0.0	27.6
April	13.2	0.2	0.2	5.0	0.0	0.0	18.7
May	14.1	0.0	0.1	1.1	0.0	0.0	15.3
June	13.1	0.0	0.0	0.1	0.1	0.0	13.3
July	10.9	0.0	0.0	0.0	0.1	0.0	11.0
August	14.2	0.0	0.0	0.1	0.2	0.0	14.5
September	15.5	0.0	0.0	0.1	0.1	0.0	15.7
October	20.2	0.0	0.1	1.1	0.1	0.1	21.6
November	19.3	0.0	0.4	5.9	0.0	0.2	25.8
December	15.9	0.1	0.6	15.4	0.1	0.3	32.4
Winter	13.0	0.5	0.5	20.4	0.0	0.2	34.6
Spring	13.1	0.4	0.2	6.6	0.0	0.0	20.2
Summer	12.7	0.0	0.0	0.1	0.1	0.0	12.9
Autumn	18.3	0.0	0.2	2.4	0.1	0.1	21.1
Total	14.3	0.2	0.2	7.3	0.1	0.1	22.1

Thunderstorms occur relatively infrequently over the project area though they may occur in any month of the year. It should be noted that hail only occurs in the presence of severe thunderstorms, yet Table 4-47 shows that the frequency of hail is higher than the frequency of thunderstorms during the months of November to January. This may be due to observer inexperience, classifying what should be ice pellets (formed through entirely different atmospheric processes) as hail or through coding error.

Freezing precipitation occurs when rain or drizzle aloft enters negative air temperatures near the surface and becomes super-cooled so that the droplets freeze upon impact with the surface. This situation typically arises ahead of a warm front extending from low pressure systems passing west of the area.

The percentage of occurrences of freezing precipitation (Table 4-47) was calculated using ICOADS. Since negative air temperatures are required for freezing precipitation, statistics show the frequency of freezing precipitation occurs only during the winter and spring months with winter having a slightly higher percentage occurrence than spring. On a monthly basis, the month of March has the highest frequency of freezing precipitation; however it occurs less than 1 percent of the time.

4.3.1.5 Icing

Spray icing can accumulate on vessels and shore structures when air temperatures are below the freezing temperature of water and there is potential for spray generation. In addition to air temperature, icing severity depends on water temperature, water salinity, wave conditions and wind speed, which influence the amount of spray and the cooling rate of droplets. A review of the spray icing hazard is provided by Minsk (1977). The frequency of potential icing conditions and its severity was estimated from the algorithm proposed by Overland et al. (1986) and subsequently updated by Overland (1990). These algorithms are based primarily on reports from vessels that were 20 to 75 m in length. The algorithm presented by Overland (1990) is:

$$PPR = \frac{V_a (T_f - T_a)}{1 + 0.3(T_w - T_f)}$$

where: PPR = Icing predictor ($m°Cs^{-1}$)

V_a = Wind Speed (ms^{-1})

T_f = Freezing point of seawater (usually -1.7°C or -1.8°C)

T_a = Air Temperature (°C)

T_w = Sea temperature (°C).

The algorithm generates an icing predictor based on air temperature, wind speed, and sea surface temperature, which was empirically related to observed icing rates of fishing vessels in the Gulf of Alaska. This method will provide conservative estimates of icing severity in the study region as winter sea surface temperatures are colder and wave conditions are lower in the study area compared to the Gulf of Alaska where the algorithm was calibrated (Makkonen et al. 1991). Based on the above algorithm, the terminology and associated vessel icing rates for freezing spray forecasts are shown in Table 4-48. These rates and terminology are used when forecasting freezing spray on the Grand Banks.

Table 4-48 Intensity of Freezing Spray

Intensity Term	Icing Rate (cm per hour)
Light	less than 0.7 cm/hr
Moderate	0.7 to 2.0 cm/hr inclusive
Heavy	2.0 – 4.0 cm/hr
Extreme	greater than 4.0 cm/hr

Potential icing rates were computed using wind speed and air sea surface temperature observations from the MANMAR data set. A total of 67197 observations were used to calculate the percentage frequency of icing occurrence and severity for area. Monthly, seasonal, and annual summaries are presented in Table 4-49.

Table 4-49 Frequency of Occurrence of Potential Spray Icing Conditions

Month	None (0 cm/hr)	Light (<0.7 cm/hr)	Moderate (0.7- 2.0 cm/hr)	Heavy (2.0-4.0 cm/hr)	Extreme (>4.0 cm/hr)
January	77.7	16.2	4.8	1.1	0.2
February	73.3	18.3	6.2	1.3	0.9
March	82.6	12.8	3.6	0.7	0.4
April	94.8	4.5	0.6	0.1	0.0
May	99.9	0.1	0.0	0.0	0.0
June	100.0	0.0	0.0	0.0	0.0
July	100.0	0.0	0.0	0.0	0.0
August	100.0	0.0	0.0	0.0	0.0
September	100.0	0.0	0.0	0.0	0.0
October	100.0	0.0	0.0	0.0	0.0
November	99.8	0.2	0.0	0.0	0.0
December	91.6	7.6	0.8	0.0	0.0
Winter	80.9	14.0	3.9	0.8	0.3
Spring	92.4	5.8	1.4	0.3	0.1
Summer	100.0	0.0	0.0	0.0	0.0
Autumn	99.9	0.1	0.0	0.0	0.0
Annual	93.3	5.0	1.3	0.3	0.1

Potential sea spray icing conditions start during the month of November with a frequency of icing potential of just 0.2 percent. As temperatures cool throughout the winter, the frequency of icing potential increases to a maximum of 26.7 percent of the time in February. Extreme sea spray icing conditions were calculated to occur 0.9 percent of the time during February. Icing potential decreases rapidly after February in response to warming air and sea surface temperatures.By May, the frequency of icing conditions is only 0.1 percent (Figure 4-95).

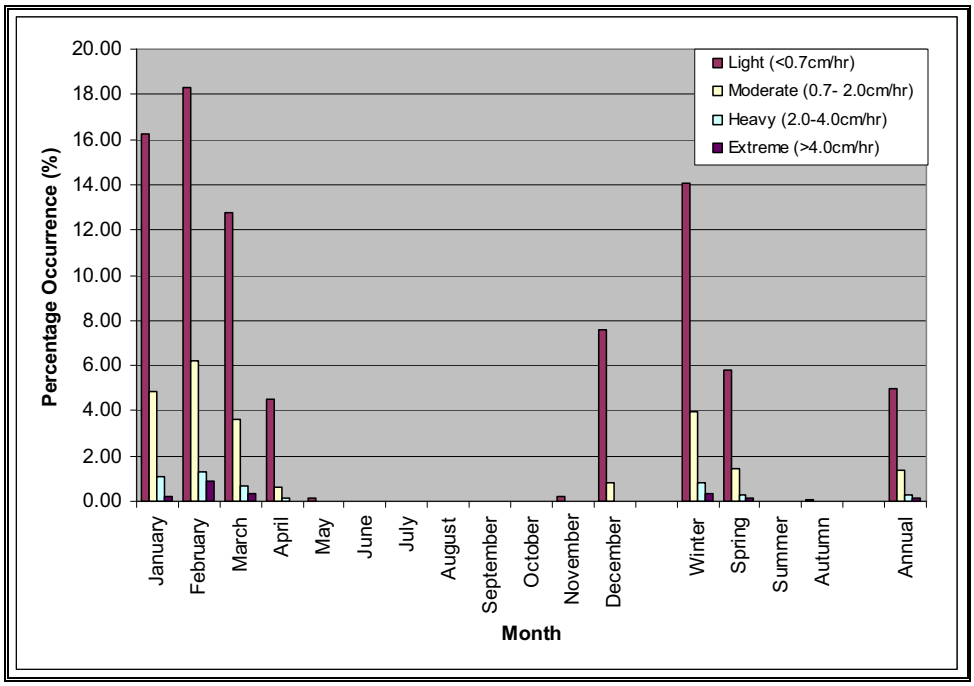

Figure 4-95 Percentage Frequency of Occurrence of Potential Spray Icing Conditions, 1980 to 2010

4.3.1.6 Visibility

Visibility is defined as the greatest distance at which objects of suitable dimensions can be seen and identified. Horizontal visibility may be reduced by any of the following phenomena, either alone or in combination:

- Fog (visibility less than 1 km)
- Mist (visibility less than 10 km)
- Haze
- Smoke
- Liquid precipitation (e.g., drizzle)
- Freezing precipitation (e.g., freezing rain)
- Frozen precipitation (e.g., snow)
- Blowing snow.

During the winter months, the main obstruction is snow; however, mist and fog may also reduce visibilities at times. As spring approaches, incidences of visibility reduction attributed to snow decreases. As the air temperature increases, so does the occurrence of advection fog. Advection fog forms when warm moist air moves over cooler waters. By April, the sea surface temperature south of Newfoundland is cooler than the surrounding air. As warm moist air from the south moves over the colder sea surface, the air cools and its ability to hold moisture decreases. The air continues to cool until it becomes saturated and the moisture condenses to form fog. The presence of advection fog increases from April through July. The month of July has the highest percentage of

obscuration of visibility, most of which is in the form of advection fog; although frontal fog can also contribute to the reduction in visibility. In August, the temperature difference between the air and the sea begins to decrease and by September, the air temperature begins to fall below the sea surface temperature. As the air temperature drops, the occurrence of fog decreases. Reduction in visibility during autumn and winter is relatively low and is mainly attributed to the passage of low-pressure systems. Fog is the main cause of reduced visibility in autumn, and snow is the main cause of reduced visibility in the winter. September and October have the lowest occurrence of reduced visibility since the air temperature has, on average, decreased below the sea surface temperature and it is not yet cold enough for snow.

Fog also occurs at White Rose as relatively warm rain falls through cooler air beneath a frontal surface. Typically, the base of the cloud layer lowers as the air becomes saturated and condensation occurs. If the cloud base reaches the surface, frontal fog occurs. Most frequently, frontal fog occurs ahead of a warm front associated with a frontal disturbance. As the front moves through, clearing of the fog may occur. However, frequently frontal fog gives way to advection fog in the warm sector of a low pressure system. Typically, fog clears as drier air is advected into the region from continental source regions to the west.

A plot of the frequency distribution of visibility from ICOADS is presented in Figure 4-96. This figure shows that obstructions to vision can occur in any month. Annually, 47.8 percent of the observations had reduced visibilities less than 10 km. The percent frequency of visibilities is shown in Figure 4-96.

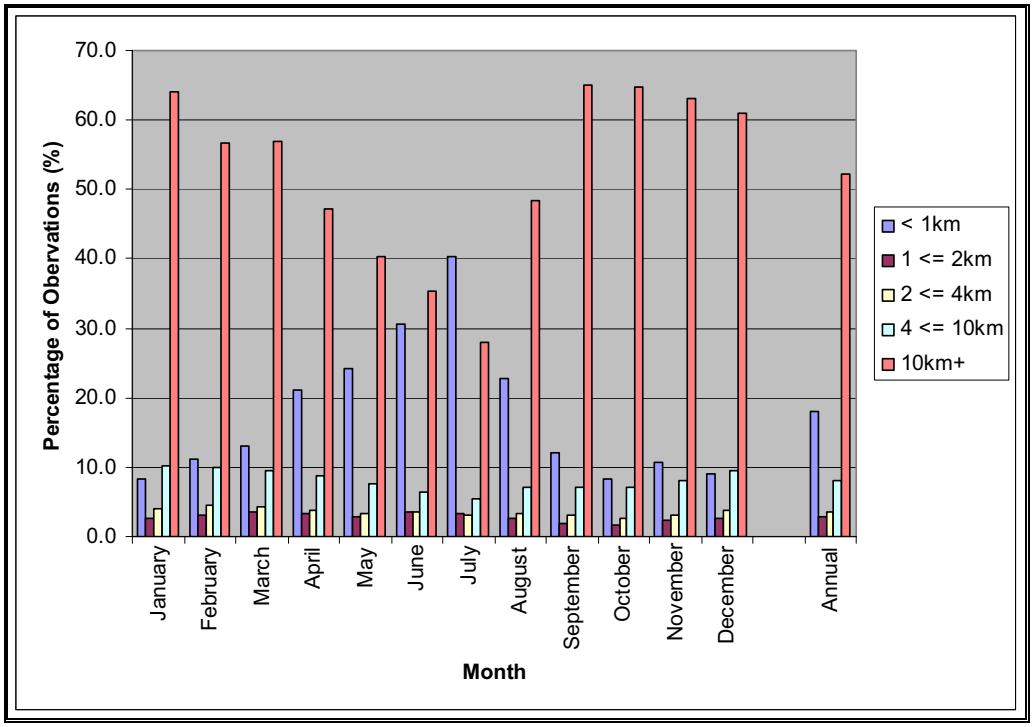

Figure 4-96 Monthly and Annual Percentage Occurrence of Visibility Distances from the International Comprehensive Ocean-Atmosphere Data Set, 1980 to 2010

4.3.1.7 Tropical Systems

The hurricane season in the North Atlantic basin normally extends from June through November, although tropical storm systems occasionally occur outside this period. While the strongest winds typically occur during the winter months and are associated with mid-latitude low pressure systems, storm force winds may occur at any time of the year as a result of tropical systems. Once formed, a tropical storm or hurricane will maintain its energy as long as a sufficient supply of warm, moist air is available.

Tropical storms and hurricanes obtain their energy from the latent heat of vapourization that is released during the condensation process. These systems typically move east to west over the warm water of the tropics. However, some of these systems turn northward and make their way toward Newfoundland and the project area. Since the capacity of the air to hold water vapour is dependent on temperature, the hurricanes begin to lose their tropical characteristics as they move northward over the colder ocean waters. By the time these weakening cyclones reach Newfoundland, they are usually embedded into a mid-latitude low and their tropical characteristics are usually lost.

There has been a substantial increase in the number of hurricanes that have developed within the Atlantic Basin during the last 15 years. The five-year average of tropical storms that have developed within the Atlantic Basin since 1961 is shown in Figure 4-97. This increase in activity has been attributed to naturally-occurring cycles in tropical climate patterns near the equator called the tropical multi-decadal signal (Bell and Chelliah 2006). As a result of the increase in tropical activity in the Atlantic Basin, there has also been an increase in tropical storms or their remnants entering the Canadian Hurricane Centre Response Zone. There is little change in the five-year trend for hurricanes entering the project area. It should be noted that the unusually high number of tropical storms in 2005 may be skewing the results for the 2001 to 2005 season.

A substantial number of tropical cyclones that move into the mid-latitudes transform into extratropical cyclones. On average, 46 percent of tropical cyclones that form in the Atlantic transform into extratropical cyclones. During this transformation, the system loses tropical characteristics and becomes more extratropical in nature. This results in an increase in system size, which produces large waves, gale to hurricane force winds and intense rainfall. The likelihood that a tropical cyclone will undergo transition increases toward the second half of the tropical season; with October having the highest probability of transition. In the Atlantic, extratropical transition occurs at lower latitudes in the early and late hurricane season and at higher latitudes during the peak of the season (Hart and Evans 2001).

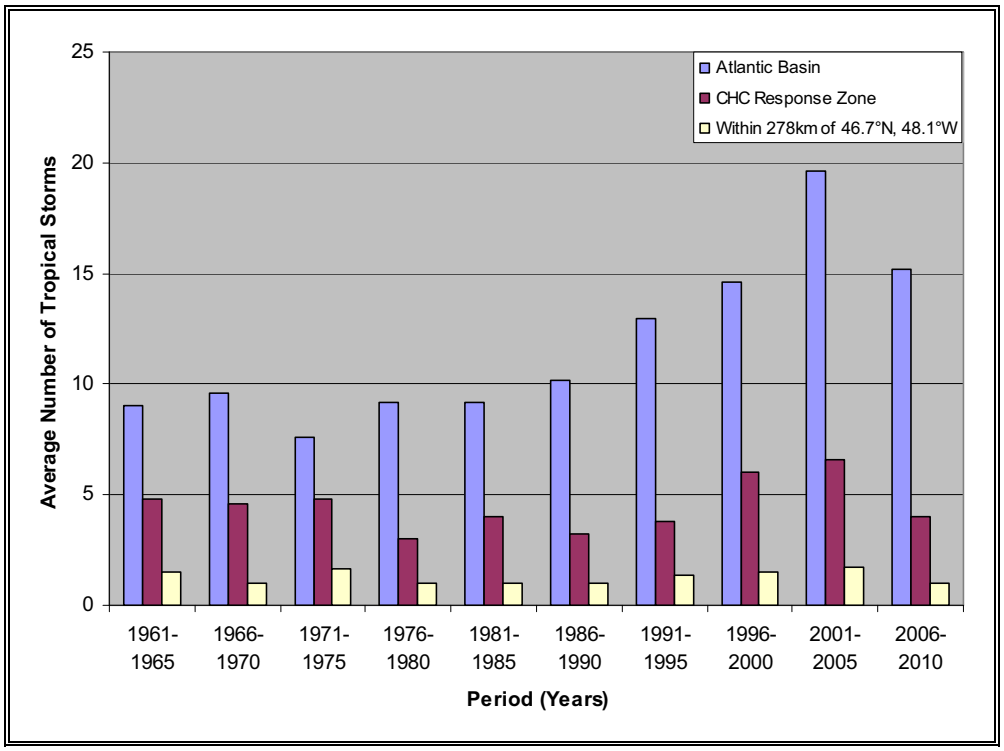

Figure 4-97 Five-year Average of the Number of Tropical Storms which formed in the Atlantic Basin since 1961

Between 1960 and 2010, 32 tropical systems passed within 278 km of 46.7°N; 48.1°W. The names are given in Table 4-50 and the tracks are shown in Figure 4-98. It should be noted that the values are the maximum 1-minute mean wind speeds occurring within the tropical system at the 10-m reference level as it passed within 278 km of the location.

Table 4-50 Tropical Systems Passing within 278 km of 46.7ºN, 48.1ºW (1960 to 2010)

Year	Month	Day	Hour	Name	Latitude	Longitude	Wind (m/s)	Pressure (mb)	Category
1963	8	28	0000	Beulah	45.8	-48.3	36.0	N/A	Category 1
1963	10	12	1800	Flora	45.2	-47.5	38.6	N/A	Extratropical
1964	9	4	1800	Cleo	46.9	-49.8	36.0	N/A	Category 1
1967	9	4	0600	Arlene	45.8	-48.6	30.9	N/A	Tropical Storm
1969	8	13	0000	Blanche	47.1	-49.0	25.7	N/A	Extratropical
1971	7	7	1800	Arlene	46.5	-53.0	23.1	N/A	Extratropical
1971	8	6	1200	Unnamed	55.7	-43.8	36.0	974	Category 1
1974	7	20	0600	Subtrop 2	46.7	-48.0	20.6	N/A	Extratropical
1975	7	4	0600	Amy	44.5	-51.6	25.7	986	Tropical Storm
1975	10	3	1200	Gladys	46.6	-50.6	43.7	960	Category 2
1976	8	24	0000	Candice	45.9	-48.7	33.4	N/A	Category 1
1978	9	5	0600	Ella	47.2	-50.2	41.2	975	Category 1
1979	8	6	0600	Unnamed	48.2	-50.6	12.9	N/A	Tropical Depression
1980	9	8	1200	Georges	45.6	-51.1	34.5	993	Category 1
1982	9	19	0600	Debby	47.0	-50.5	38.6	979	Category 1
1984	9	2	1984	Cesar	46.0	-50.4	25.7	994	Tropical Storm
1990	9	3	0000	Gustav	46.0	-46.5	28.3	993	Tropical Storm
1992	10	26	1800	Frances	46.0	-46.9	28.3	988	Tropical Storm
1993	9	10	0600	Floyd	45.4	-48.3	33.4	990	Category 1
1995	7	20	1200	Chantal	45.4	-48.8	25.7	1000	Extratropical
1995	8	22	1200	Felix	46.8	-50.8	25.7	985	Tropical Storm
1999	10	19	1200	Irene	48.0	-48.0	41.2	968	Extratropical
2000	9	25	1200	Helene	44.0	-55.5	28.3	988	Tropical Storm
2001	8	29	0000	Dean	47.0	-48.5	23.1	999	Extratropical
2001	9	20	0000	Gabrielle	48.5	-48.5	30.9	988	Extratropical
2001	11	6	1200	Noal	43.0	-48.5	25.7	996	Extratropical
2003	10	7	1800	Kate	47.5	-47.2	30.9	980	Tropical Storm
2004	8	6	0000	Alex	44.5	-49.3	38.6	978	Category 1
2004	9	2	0000	Gaston	47.0	-50.0	23.1	997	Extratropical
2005	7	30	1800	Franklin	46.4	-48.8	20.6	1006	Extratropical
2008	10	1	1800	Laura	47.5	-46.3	20.6	995	Extratropical
2009	8	24	0900	Bill	48.6	-50.2	36.0	980	Tropical Storm

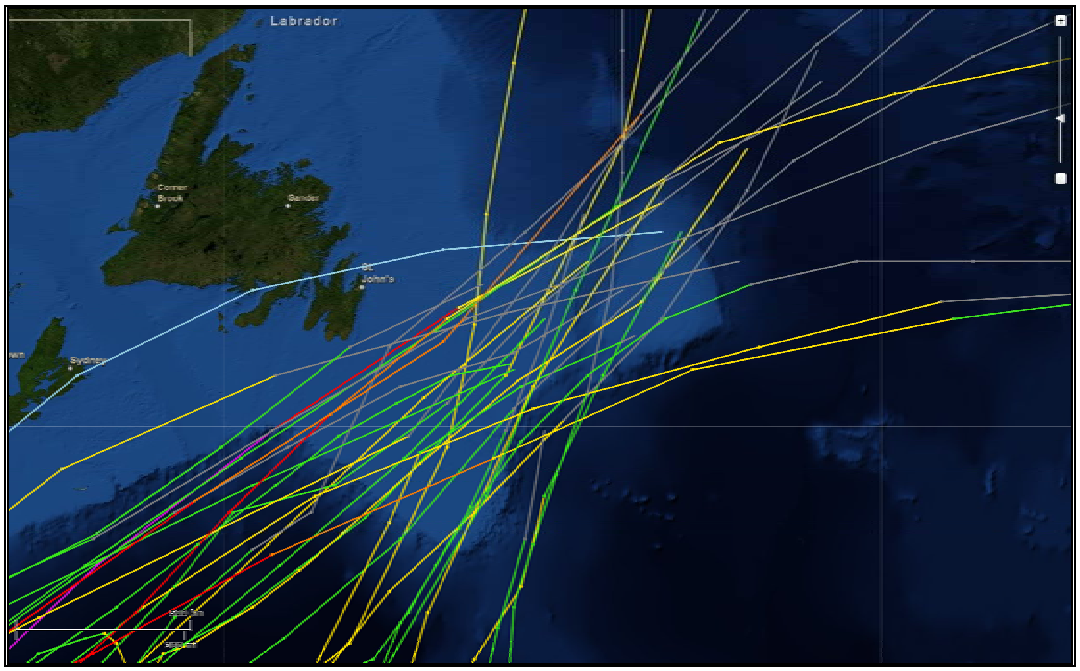

Source: NOAA Historical Hurricane Tracks Website

Figure 4-98 Storm Tracks of Tropical Systems Passing within 278 km of 46.7°N, 48.1°W, 1960 to 2010

On occasion, these systems still maintain their tropical characteristics when they reach Newfoundland. Nine Category 1 and one Category 2 hurricanes crossed within 278 km during the period from 1958 to 2008. The most intense of these storms was Hurricane Gladys, which crossed at 12Z on October 3, 1975, with maximum sustained wind speeds of 43.7 m/s and a central pressure of 960 mb. Hurricane Gladys underwent extratropical transition over the following hours and moved northeast of the area as an extratropical storm with wind speeds of 38 m/s.

4.3.2 Oceanic Environment

4.3.2.1 Bathymetry

White Rose is situated near the Continental Shelf break on the northeast Grand Banks in approximately 120 m of water. The main bathymetric features are the Grand Banks, Flemish Pass and Sackville Spur. The Grand Banks are shallow, with the majority of the area having a depth less than 100 m. Flemish Pass is a deep trough of 1,200 m depth between the Grand Banks and Flemish Cap. The Sackville Spur is a bathymetric feature that protrudes to the northeast between the Orphan Basin and Flemish Pass (Figure 4-99).

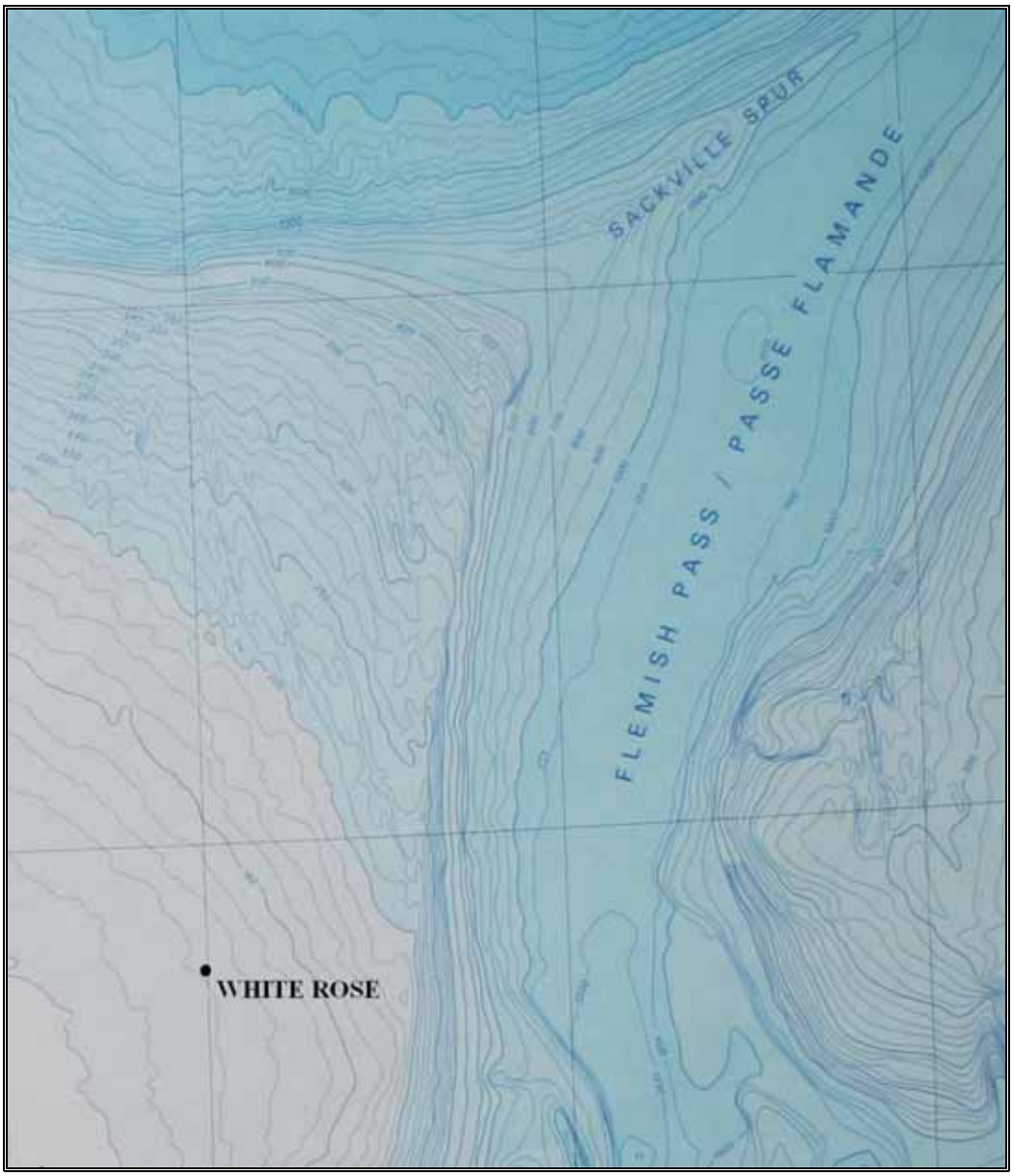

Source: Canadian Hydrographic Services bathymetry chart

Figure 4-99 Bathymetry in the Vicinity of White Rose

The offshore branch of the Labrador Current follows the Continental Slope until it reaches the Sackville Spur where the current divides; one component flows northeast along the northern side of the Sackville Spur and the other flows across the Sackville Spur and then south through Flemish Pass. White Rose is located just inside the offshore branch of the Labrador Current. The currents at White Rose exhibit a lot of variability as a result of the bathymetry of the region such as: variations in the mass transport from the current division process; influence of periodic intrusions of warmer water from the North Atlantic Current to the south; sea level changes from the passage of low pressure systems; and from oscillations along the shelf break.

The majority of icebergs at White Rose are transported to the region by the component of the current that flows across the Sackville Spur; following the bathymetric contours to the northeast of White Rose.

4.3.2.2 Waves

The main parameters for describing wave conditions are significant wave height, maximum wave height, peak spectral period, and characteristic period. Significant wave height is defined as the average height of the highest one third of waves, and its value roughly approximates the characteristic height observed visually. Maximum height is the greatest vertical distance between a wave crest and adjacent trough. Spectral peak period is the period of the waves with the largest energy levels. The characteristic period is the period of the highest one third of waves. The characteristic period is the wave period reported in ship observations, and the spectral peak period is reported in the MSC50 data set.

A sea state may be composed of the wind wave alone, swell alone, or the wind wave in combination with one or more swell groups. A swell is a wave system not produced by the local wind blowing at the time of observation and may have been generated within the local weather system, or from within distant weather systems. The former situation typically arises when a front, trough, or ridge crosses region, resulting in a marked shift in wind direction. Swells generated in this manner are usually of low period. Swells generated by distant weather systems may propagate in the direction of the winds that originally produced the waves to the vicinity of the White Rose field. These swells may travel for thousands of miles before dying away. As the swell advances, its crest becomes rounded and its surface smooth. Swell energy may propagate through a point from more than one direction at a particular time.

The wave climate of the Grand Banks is dominated by extra-tropical storms, primarily during October through March. Severe storms may, on occasion, occur outside of these months. Storms of tropical origin may occur during the early summer and early winter, but most often from late August through October. Hurricanes are usually reduced to tropical storm strength or evolve into extra-tropical storms by the time they reach the area but they are still capable of producing storm force winds and high waves.

During autumn and winter, the dominant direction of the combined significant wave height is from the west. This corresponds with a higher frequency of occurrence of the wind wave during these months, which suggests that during the late fall and winter, the wind wave is the main contributor to the combined significant wave height. During the months of March and April, the wind wave remains predominantly westerly while the swell begins to come from a southerly direction, resulting in the vector mean direction of the combined significant wave heights being southwesterly. A mean south-westerly direction for the combined significant wave heights during the summer months is a result of a mainly southwesterly wind wave and a southwesterly swell. During the months of September and October, the wind wave will veer to the west and become the more dominant component of the combined significant wave height. This will result in the dominant direction of the combined significant wave heights being westerly once again.

Wave statistics were also compiled from wave data measured in and near the project area. The White Rose data set from October 2003 to December 2010 has been split due to the change in measuring equipment from a TRYAXIS directional waverider buoy to a

Datawell directional waverider buoy. A non-directional Datawell waverider buoy was used on the White Rose field for the period of March 31, 1999, to June 25, 2000. The location and observation period of these stations is presented in Table 4-51.

Table 4-51 Locations of wave observations

Location	Latitude	Longitude	Period
Terra Nova	46.4°N	48.4°W	July 13, 1999 – September 30, 2009
White Rose	46.8°N	48.0°W	March 31, 1999 – June 25, 2000
White Rose	46.8°N	48.0°W	October 06, 2003 – August 18, 2007
White Rose	46.8°N	48.0°W	August 15, 2007 – December 31, 2010
Ocean Ranger	46.5°N	48.4°W	December 04, 1980 – February 09, 1982

The data sources to describe the wave climatology at White Rose came from the Integrated Science Data Management (ISDM) data base and the MSC50 North Atlantic wind and wave climatology data base. Locations of wave observations from buoys located on the Grand Banks are presented in Table 4-51.

MSC50 Data Set

Wave climate statistics for the White Rose field were extracted from the MSC50 North Atlantic wind and wave climatology data base compiled by Oceanweather Inc. under contract to Environment Canada (Oceanweather Inc. and Environment Canada 2011). The MSC50 data base consists of continuous wind and wave hindcast data in 1-hour time steps from January 1954 to December 2010, on a 0.1° latitude by 0.1° longitude grid. Grid Point 11034 was chosen to represent conditions within the area of interest. Wave heights and periods in the MSC50 data base are computed using a Pierson Moskowitz spectrum.

Prior to 1962, mean monthly ice statistics were used when calculating the wave heights in the MSC50 data set. As a result, if the mean monthly ice coverage for a particular grid point was greater than 50 percent for a particular month, the whole month (from the 1st to the 31st) was “iced out”; meaning that no forecast wave data was generated for that month. This sometimes results in gaps in the wave data. Since 1962, weekly ice data supplied by the Canadian Ice Service was used, allowing the MSC50 hindcast to better represent the changing ice conditions (Swail et al. 2006).

Integrated Science Data Management Data Base

While drilling operations are being conducted, a wave buoy is normally deployed within the region. Wave buoys provide real-time measured wave data, which are incorporated into the marine weather reports. Normally, the significant wave height and average period derived from the buoy data are archived for use in determining wave climate statistics for the area. The Integrated Science Data Management (ISDM) has been collecting, archiving and providing spectral wave data since 1970 and archives over six million observed wave spectra from 500 locations. ISDM performs a quality inspection of each observed wave spectra prior to uploading into the database. Flags are assigned to the observed and derived parameters reflecting data quality. Quality control is performed by ISDM by examining the energy distribution of the power

spectrum and comparing relative values of significant wave height and peak period between neighbouring buoys.

The annual wave rose from the MSC50 Grid Point 11034 is presented in Figure 4-100. The wave rose shows that the majority of wave energy comes from the west-southwest to south-southwest, which accounts for 36.0 percent of the waves. Waves were “iced out” for 1.34 percent of the time at Grid Point 11034 over the 57-year record.

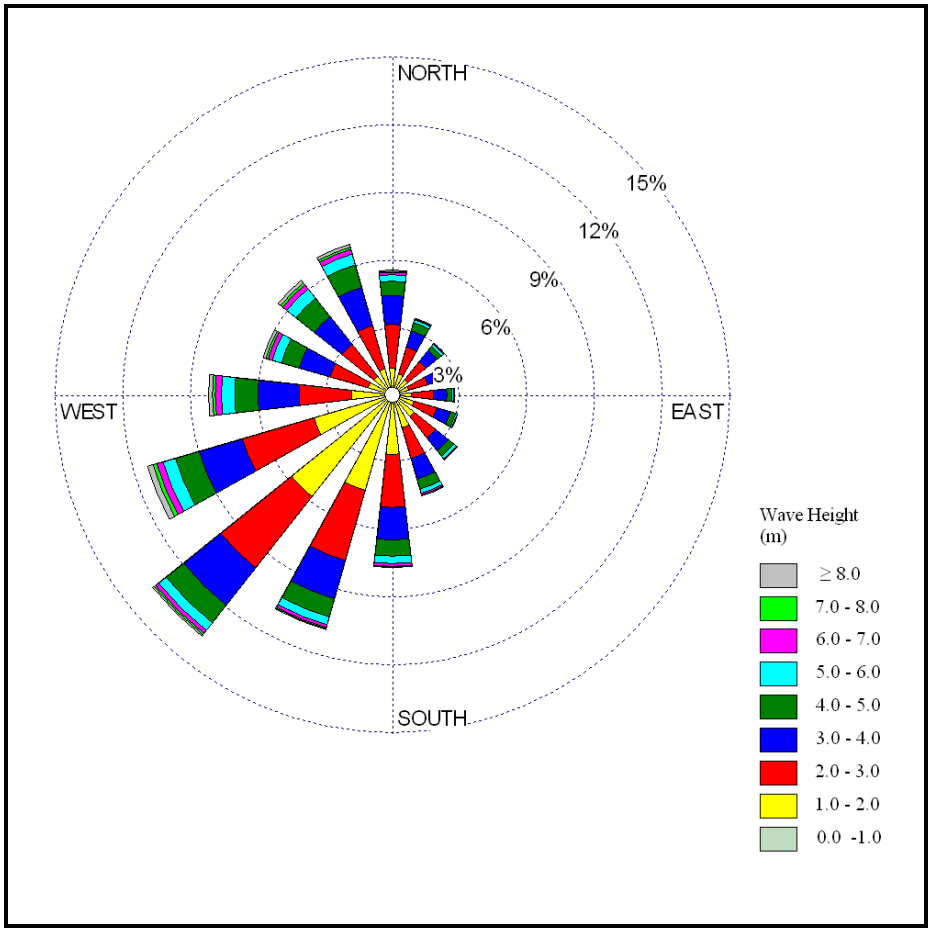

Figure 4-100 Annual Wave Rose for MSC50 Grid Point 11034 Located near 46.7°N; 48.1°W, 1954 to 2010

The annual percentage frequency of significant wave heights is presented in Figure 4-101. This figure shows that the majority of significant wave heights are between 1.0 and 3.0 m. There is a gradual decrease in frequency of wave heights above 3.0 m and only a small percentage of the wave heights exceed 7.0 m.

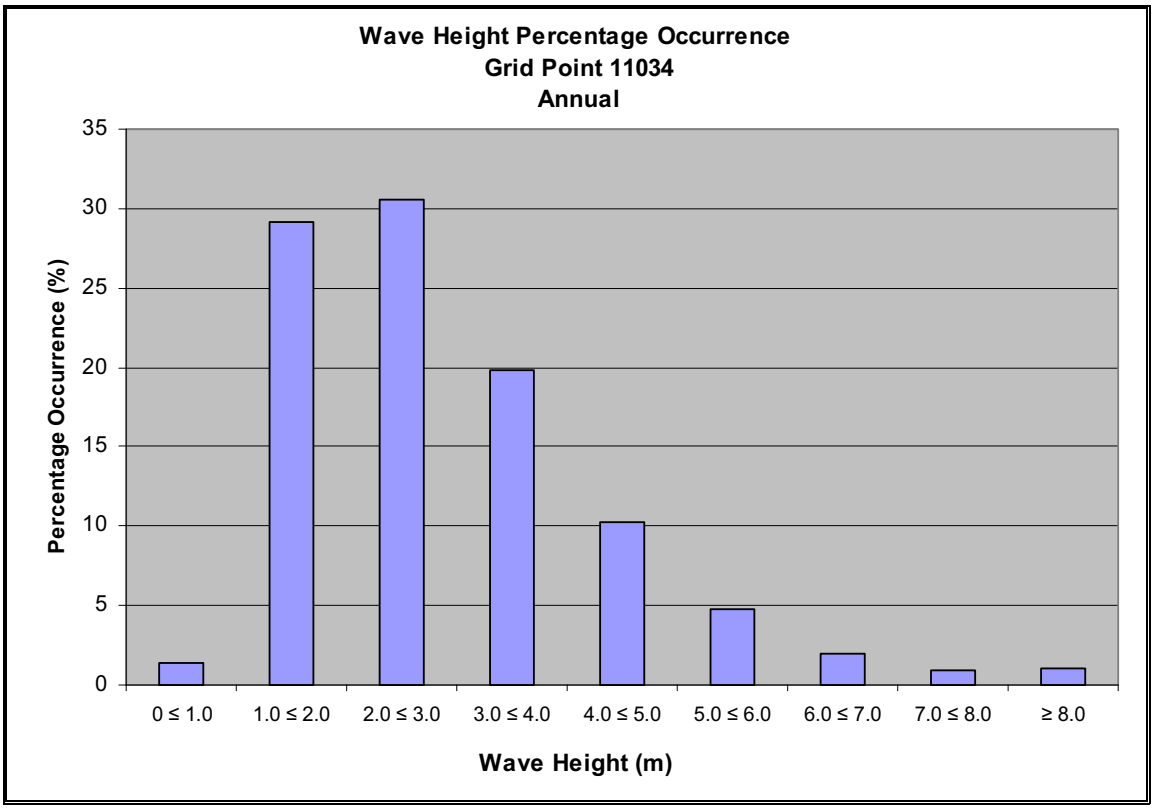

Figure 4-101 Annual Percentage Frequency of Wave Height for MSC50 Grid Point 11034 Located near 46.7°N; 48.1°W, 1954 to 2010

Significant wave heights on the Grand Banks peak during the winter months with Grid Point 11034 having a mean monthly significant wave height of 4.2 m in January. The lowest significant wave heights occur in the summer with July having a mean monthly significant wave height of only 1.7 m (Table 4-52).

Combined significant wave heights of 10.5 m or more occurred in each month between September and April in the MSC50 data, with the highest waves occurring during the month of February (Table 4-53). The highest significant wave height of 14.8 m in the MSC50 data set occurred on February 15, 1982. The highest combined significant wave heights of 14.6 and 13.8 m in the Terra Nova and Hibernia data sets, respectively, occurred during the February 11, 2003 storm event previously mentioned. While the maximum significant wave heights tend to peak during the winter months, a tropical system could pass through the area and produce high wave heights during any month.

The percentage exceedance curves of significant wave heights for Grid Point 11034 are shown in Figure 4-102. Percentage exceedance curves for the months of January through April show that the curves do not reach 100 percent because of the presence of ice during these months.

Table 4-52 Mean Significant Wave Height Statistics (m)

Month	MSC50 Grid Point 11034	Ocean Ranger	Terra Nova	White Rose (2003-2007)	White Rose (2007- 2010)
January	4.1	5.2	4.1	4.9	4.2
February	3.8	4.4	3.8	4.5	3.8
March	3.2	4.7	3.3	4.3	3.2
April	2.7	3.7	2.6	2.7	2.5
May	2.2	1.7	2.2	2.6	2.4
June	1.9	1.5	1.8	2.6	1.9
July	1.7	1.8	1.5	2.4	1.6
August	1.8	1.8	1.8	2.3	1.9
September	2.4	3.8	2.3	2.8	2.3
October	3.0	3.0	3.0	3.8	3.1
November	3.4	4.8	3.1	3.8	3.0
December	4.0	4.6	3.8	4.2	4.2

Table 4-53 Maximum Combined Significant Wave Height Statistics (m)

Month	MSC50 Grid Point 11034	Ocean Ranger	Terra Nova	White Rose (2003-2007)	White Rose (2007- 2010)
January	13.0	10.6	12.5	12.2	11.8
February	14.8	8.3	14.6	11.9	10.2
March	11.4	7.2	9.4	12.8	8.8
April	10.8	7.8	7.1	11.0	5.7
May	10.3	3.8	6.3	10.9	6.6
June	10.0	3.0	6.5	9.2	5.6
July	6.2	4.2	4.1	8.5	3.5
August	9.4	3.3	8.0	9.3	7.3
September	11.7	8.4	10.4	11.1	12.9
October	12.1	5.8	10.4	12.2	9.5
November	11.5	7.0	10.2	11.2	9.4
December	13.8	8.1	11.7	11.1	11.1

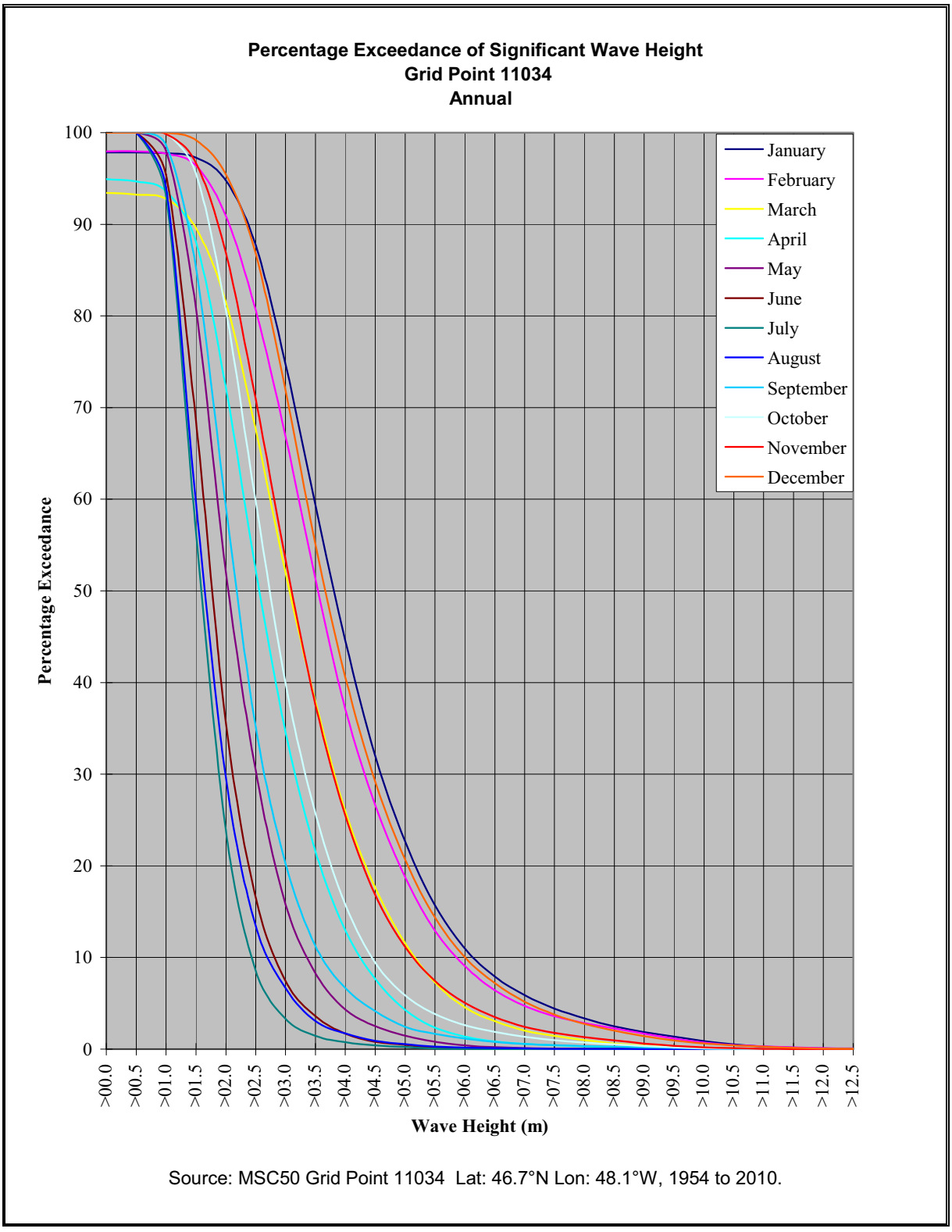

Figure 4-102 Percentage Exceedance of Significant Wave Height at Grid Point 11034 Located near 46.7°N; 48.1°W, 1954 to 2010

The spectral peak period of waves varies seasonally with the most common period varying from 7 seconds during summer to 11 seconds in winter. Annually, the most common spectral peak period is 9 seconds, occurring 18.4 percent of the time at Grid Point 11034. The percentage occurrence of spectral peak period for each month is shown in Table 4-54 and Figure 4-103.

Table 4-54 Percentage Occurrence of Peak Spectral Period of the Total Spectrum at Grid Point 11034 Located near 46.7°N; 48.1°W, 1954 to 2010

Month	Peak Spectral Period (seconds)															
	1	2	3	4	5	6	7	8	9	10	11	12	13	14	15	16
January	0.0	0.0	0.0	0.0	0.2	1.2	4.6	8.6	14.6	18.6	**22.3**	12.7	11.5	5.0	0.6	0.1
February	0.0	0.0	0.0	0.1	0.8	2.4	6.6	9.9	15.7	18.2	**20.1**	12.6	8.4	4.2	0.7	0.3
March	0.0	0.0	0.0	0.3	1.1	3.2	8.5	11.5	17.1	**18.9**	18.0	11.2	5.9	3.7	0.2	0.3
April	0.0	0.0	0.0	0.2	1.3	4.2	9.1	14.7	**23.6**	20.3	14.1	7.5	3.1	1.6	0.2	0.1
May	0.0	0.0	0.0	0.1	1.5	7.0	15.7	**25.2**	23.3	14.8	6.2	4.4	1.4	0.4	0.0	0.0
June	0.0	0.0	0.0	0.2	3.5	10.5	24.6	**27.4**	19.7	8.7	2.2	1.4	1.5	0.2	0.0	0.0
July	0.0	0.0	0.0	0.3	4.2	14.3	**29.2**	27.8	14.0	5.6	1.4	0.8	1.8	0.2	0.1	0.2
August	0.0	0.0	0.0	0.4	4.8	12.7	**29.0**	26.2	14.5	5.4	2.7	2.1	1.6	0.4	0.1	0.1
September	0.0	0.0	0.0	0.1	1.7	6.4	17.0	**21.6**	20.5	10.5	8.4	7.3	4.5	1.4	0.4	0.3
October	0.0	0.0	0.0	0.0	0.9	3.4	10.8	17.4	**22.4**	16.5	12.1	9.0	5.2	1.9	0.2	0.2
November	0.0	0.0	0.0	0.0	0.6	2.6	8.2	12.2	19.9	**20.3**	16.1	9.7	7.5	2.7	0.2	0.2
December	0.0	0.0	0.0	0.0	0.2	1.3	4.7	9.0	15.6	**21.1**	20.9	12.8	9.9	3.9	0.4	0.2
Winter	0.0	0.0	0.0	0.1	0.4	1.6	5.3	9.2	15.3	19.3	**21.1**	12.7	10.0	4.4	0.6	0.2
Spring	0.0	0.0	0.0	0.2	1.3	4.8	11.1	17.1	**21.4**	18.0	12.8	7.7	3.5	1.9	0.1	0.1
Summer	0.0	0.0	0.0	0.3	4.2	12.5	27.6	**27.1**	16.1	6.6	2.1	1.4	1.6	0.3	0.1	0.1
Autumn	0.0	0.0	0.0	0.1	1.1	4.1	12.0	17.1	**20.9**	15.8	12.2	8.7	5.7	2.0	0.3	0.2
Annual	0.0	0.0	0.0	0.2	1.7	5.8	14.0	17.6	**18.4**	14.9	12.0	7.6	5.2	2.1	0.3	0.2
Note: The highest percentage for each month is bolded																

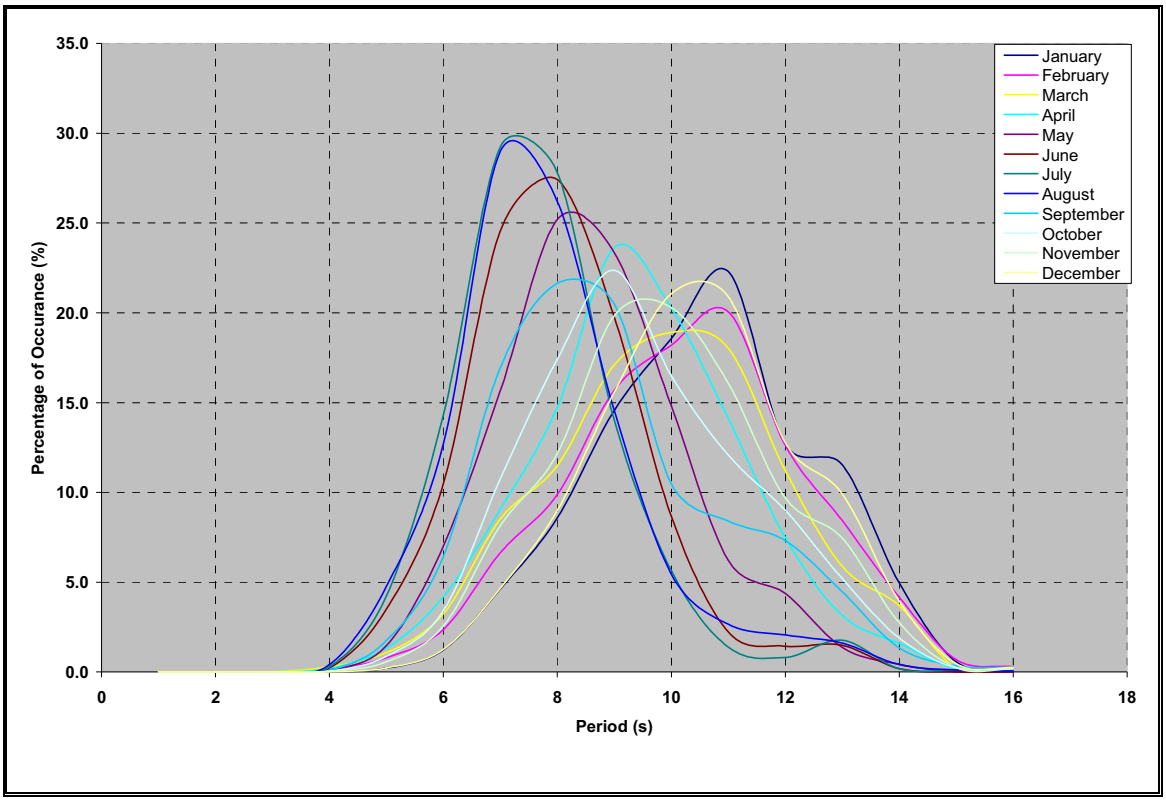

Figure 4-103 Percentage of Occurrence of Peak Wave Period at Grid Point 11034 Located near 46.7°N; 48.1°W, 1954 to 2010

A scatter diagram of the significant wave height versus spectral peak period is presented in Table 4-55. From this table it can be seen that the most common wave at Grid Point 11034 is 2 m with a peak spectral period of 9 seconds. Note that wave heights in these tables have been rounded to the nearest whole number. Therefore, the 1 m wave bin would include all waves from 0.51 to 1.50 m.

Table 4-55 Percent Frequency of Occurrence of Significant Combined Wave Height and Peak Spectral Period at Grid Point 11034 located near 46.7°N; 48.1°W

		Wave Height (m)														Total
		<1	1	2	3	4	5	6	7	8	9	10	11	12	13	
Period (s)	0	1.32														1.32
	1	0.00														0.00
	2	0.00														0.00
	3	0.00	0.00													0.00
	4	0.00	0.12	0.03												0.16
	5	0.00	0.96	0.73	0.04	0.00										1.73
	6	0.00	1.58	3.77	0.38	0.02	0.00									5.75
	7	0.00	4.29	5.90	3.43	0.28	0.01									13.93
	8	0.01	4.43	6.47	4.46	1.98	0.15	0.00								17.51

		Wave Height (m)														Total
		<1	1	2	3	4	5	6	7	8	9	10	11	12	13	
	9	0.00	1.54	8.03	3.99	3.45	1.06	0.07	0.00							18.15
	10	0.00	0.61	4.42	4.30	2.47	2.19	0.58	0.04	0.00						14.62
	11	0.00	0.20	1.99	4.15	2.34	1.41	1.17	0.43	0.07	0.00					11.76
	12	0.00	0.22	1.42	2.12	1.47	0.73	0.53	0.48	0.33	0.15	0.02	0.00			7.46
	13	0.00	0.23	0.70	1.14	1.23	0.69	0.34	0.20	0.19	0.20	0.15	0.03	0.00		5.10
	14		0.04	0.14	0.41	0.58	0.41	0.17	0.08	0.05	0.04	0.07	0.06	0.02	0.00	2.08
	15		0.01	0.02	0.04	0.06	0.07	0.03	0.01	0.00	0.00	0.00	0.01	0.01	0.01	0.26
	16		0.02	0.02	0.03	0.04	0.02	0.01	0.00	0.00	0.00			0.00	0.00	0.15
	17		0.01	0.02	0.01	0.00	0.00	0.00	0.00							0.04
	18		0.00				0.00	0.00								0.00
Total		1.35	14.26	33.66	24.50	13.92	6.75	2.91	1.24	0.64	0.40	0.24	0.09	0.03	0.01	100.00
Note: The incidence of 0 wave height and <1 wave period is due to the presence of sea ice																

4.3.2.3 Tsunamis

Tsunamis are long, surface gravity waves in the ocean produced by earthquakes, submarine landslides and volcanic island explosions. Tsunami amplitudes are usually less than 2 m in height in the open ocean. Since the associated currents have nearly uniform speed from the water surface to bottom, they can induce large forces.

Not all earthquakes generate tsunamis, since an earthquake must be of sufficient magnitude and accompanied by an appropriate deformation of the sea floor to produce tsunamis. Amplitude magnitudes depend primarily on the mass displaced, but also on the depth of submergence, the water depth and other characteristics of the generation (Murty 1977). Information from Japanese tsunamis shows that apart from rare exceptions, the limiting earthquake magnitude (M) for a tsunami-producing earthquake is $M = 6.3 + 0.0005D$, where D is the focal depth in kilometres. An alternate form for M (and the one used by Terra Nova) is $M = 5.6 + 0.01D$ (Adams 1986). In the Terra Nova analysis, D was taken as 0 so that $M = 5.6$ was a conservative estimate for the limiting magnitude to produce a tsunami. The tsunami of 1929 that occurred offshore southern Newfoundland had a Richter Scale $M = 7.2$. This was the largest earthquake along the US/Canadian Atlantic in the last 100 years (Whitmore et al. 2009). This earthquake produced a tsunami that caused deaths and extensive property damage. The absence of a tsunami for the 1951 ($A = 5.0$) and the two in 1954 ($M = 5.2$ and 5.3) earthquakes in this area confirm the presence of a lower threshold (Adams 1986).

Whitmore et al. (2009) compared earthquake magnitudes with tsunami generation for earthquakes along the US West Coast, Alaska and British Columbia coasts. The results presented in Table 4-56 show that offshore earthquakes less than $M = 6.5$ have a very small probability of generating a tsunami.

The earthquakes that have occurred within 500 km of White Rose over the last 22 years are shown in Figure 4-104. The list of these earthquakes is shown in Table 4-57. The largest earthquake in this time period had a magnitude of 4.2. This magnitude is too low to produce a tsunami.

Table 4-56 Earthquakes Producing Tsunamis

Magnitude	Total no. of earthquakes (US west of coast, BC and Alaska) in potential tsunami generation areas (1900 to 2004)	No. of events which produced a tsunami ≥0.5 amp.	Percentage of occurrence
5.0 to 5.9	3,549	1	0.28%
6.0 to 6.4	422	0	0%
6.5 to 7.0	266	2	0.75%
7.1 to 7.5	55	3	5.5%
7.6 to 7.8	10	2	20%
7.9+	13	7	59%

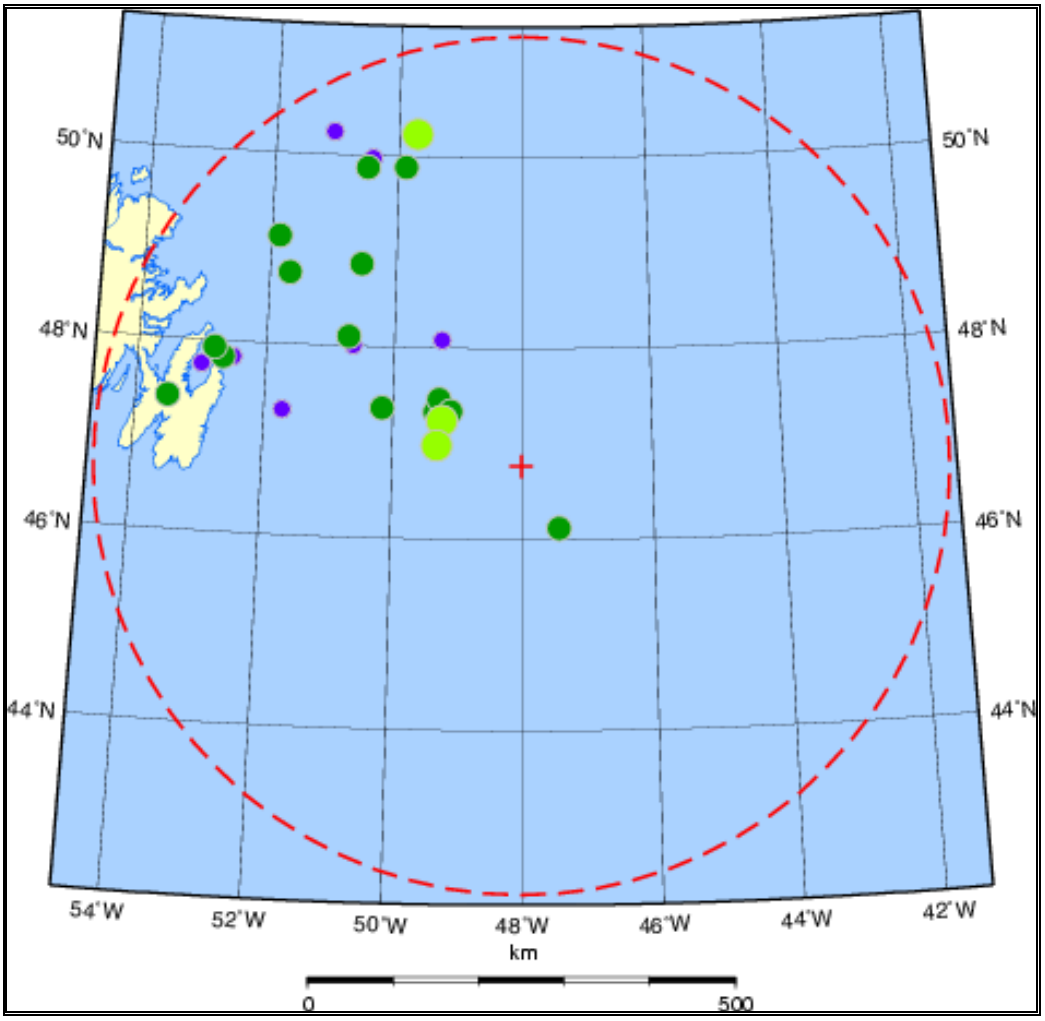

Source: Earthquakes Canada 2012
Note: All earthquakes between M2 (small dark blue circle) to M4 (large light green circle)

Figure 4-104 Earthquakes within 500 km of White Rose between 1988 and 2010

Table 4-57 Earthquakes within 500 km of White Rose 1988 to 2010

Date	Time(UT)	Lat	Long	Depth	Mag	Region and Comment
2010/12/01	03:35:32	48.86	-50.55	18.0g (A)	3.3ML (B)	190 km E from Bonavista
2010/01/12	22:47:18	48.01	-50.65	18.0g	2.7MN (B)	164 km E from St. John's
2009/04/29	01:26:03	47.40	-53.50	18.0g	3.3MN	28 km SW from Bay Roberts
2008/12/17	07:20:22	47.93	-52.81	18.0g	3.2MN	37 km NE from Carbonear
2008/11/18	00:15:29	50.23	-49.70	18.0g	4.2ML	Offshore Newfoundland.
2008/10/30	05:34:37	49.97	-50.42	18.0g	2.9ML	245 km NE from Bonavista
2008/06/12	12:34:51	48.10	-50.72	18.0g	3.1MN	162 km E from St. John's
2007/02/06	01:27:51	48.08	-49.25	18.0g	2.9MN	Grand Banks
2005/04/05	15:07:13	49.87	-50.50	18.0g	3.3ML	234 km NE from Bonavista
2003/04/20	10:30:25	50.24	-51.06	18.0g	2.6MN	320 km N from St. John's
2002/03/02	07:37:39	49.13	-51.87	18.0g	3.1MN	185 km N from St. John's
2001/04/06	21:09:48	48.75	-51.69	18.0g	3.1MN	150 km NE from St. John's
1996/03/13	23:55:07	47.75	-53.00	18.0g	2.4MN	Conception Bay
1995/01/22	06:46:20	47.84	-52.52	18.0g	2.4MN	34 km NE from St. John’s
1994/12/01	09:32:25	47.31	-51.72	18.0g	2.6MN	Offshore Newfoundland
1994/08/11	18:13:49	47.83	-52.67	0.0g	3.1MN	St. John’s Newfoundland
1992/08/10	11:31:52	47.34	-49.11	18.0g	3.4MN	Grand Banks
1992/07/17	04:20:22	46.12	-47.44	18.0g	3.9MN	Eastern Margin of Grand Banks
1992/07/06	16:58:16	47.33	-49.35	18.0g	3.0ML	Grand Banks
1992/01/13	06:07:28	47.24	-49.24	18.0g	4.0MN	Southern Grand Banks
1991/07/23	11:23:01	47.36	-50.17	18.0g	3.2MN	Grand Banks
1989/12/03	05:15:40	46.98	-49.32	18.0g	4.2ML	Offshore Newfoundland
1988/08/09	00:16:45	47.46	-49.29	18.0g	3.1ML	Grand Banks
1988/01/09	07:15:43	49.88	-49.88	18.0g	3.5ML	Offshore Newfoundland

(A) g = Peak ground acceleration

(B) ML refers to `local magnitude` which was originally defined for California by Charles Richter. However, this does not apply to eastern North America, where seismic waves attenuate differently. Otto Nuttli developed a formula for measuring seismicity of eastern Canada, Nuttli Magnitude or MN

The most seismically active portion of the Continental Slope occurs at the mouth of the Laurentian Channel. It was at this location, in 1929, that the Grand Banks earthquake, with a M7.2, initiated a tsunami that devastated the southern end of the Burin Peninsula. Aftershocks that followed reached magnitudes as high as M6. Subsequent earthquakes in the same area that occurred in 1951, 1954 and 1987 recorded magnitudes on the order of 5 (Basham and Adams 1982).

The revised locations of offshore earthquakes determined by Wahlström and Adams (Adams 1986) are shown in Figure 4-105. Magnitudes of the earthquakes are not

distinguished in the figure, only localities. The box marked LSP (Laurentian Slope) encloses a cluster of earthquake epicentres on the that includes the 1929 Grand Banks earthquake.

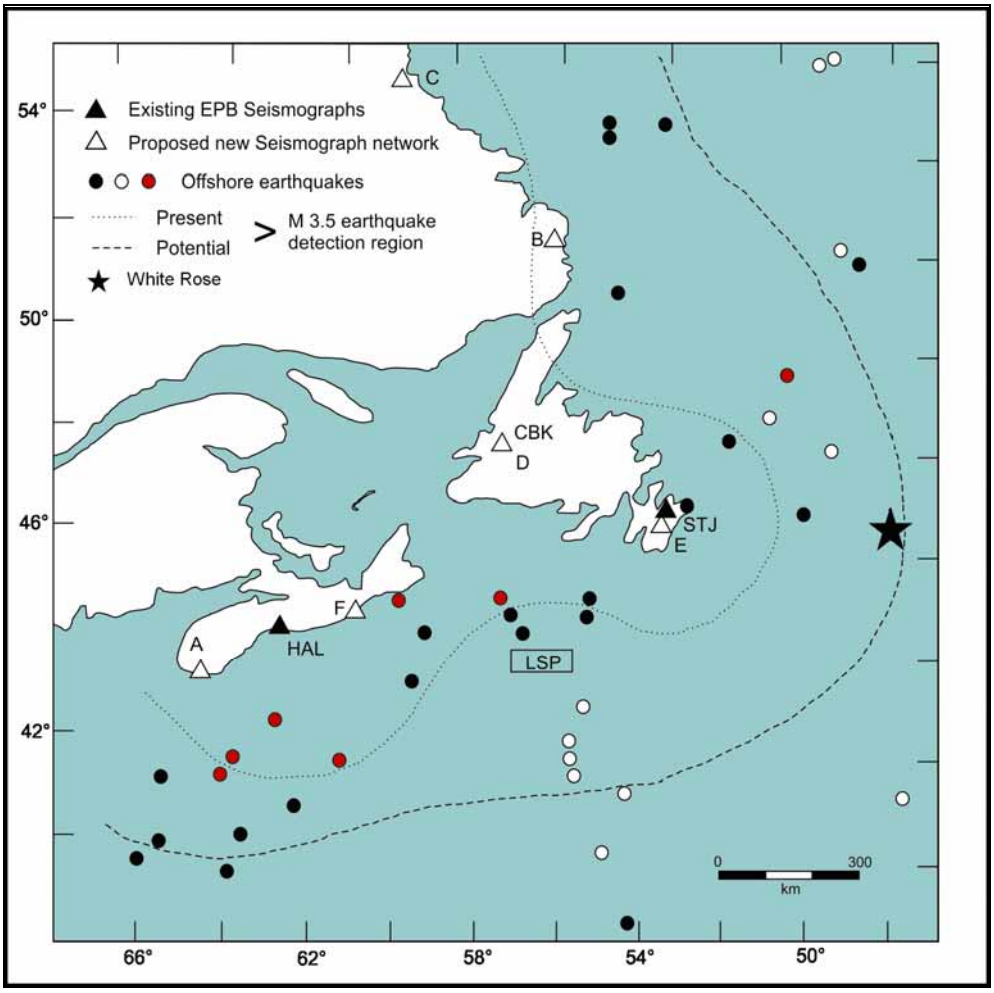

Source: modified from Adams 1986

Figure 4-105 Map of earthquakes off Canada's Southeastern Margin

4.3.2.4 Currents

General Circulation

The regional oceanic circulation on the Grand Banks and surrounding areas is governed by the bathymetric features of the Continental Shelf. A major characteristic of ocean currents is their tendency to follow local and regional underwater bathymetry.

The Grand Banks-Flemish Cap bathymetric features (Figure 4-106) exert a major influence on the regional oceanic circulation. The shape of the banks and channels steers the flow of the Labrador Current. The Labrador Current is comprised of two main branches; an inshore stream near the coast, and a more intense offshore stream over

the shelf break between the 400 and 1,200 m isobaths (Lazier and Wright 1993). There is some exchange between these two streams, which occurs in the channels and saddles that separate the banks offshore of Labrador and Newfoundland. The inshore branch of the Labrador Current flows through the Avalon Channel, while the offshore branch flows along the northern slope of the Grand Banks (Figure 4-106). This offshore branch of the Labrador Current divides east of 48°W, resulting in part of the branch flowing to the east around Flemish Cap and the other flowing south across the Sackville Spur and through Flemish Pass.

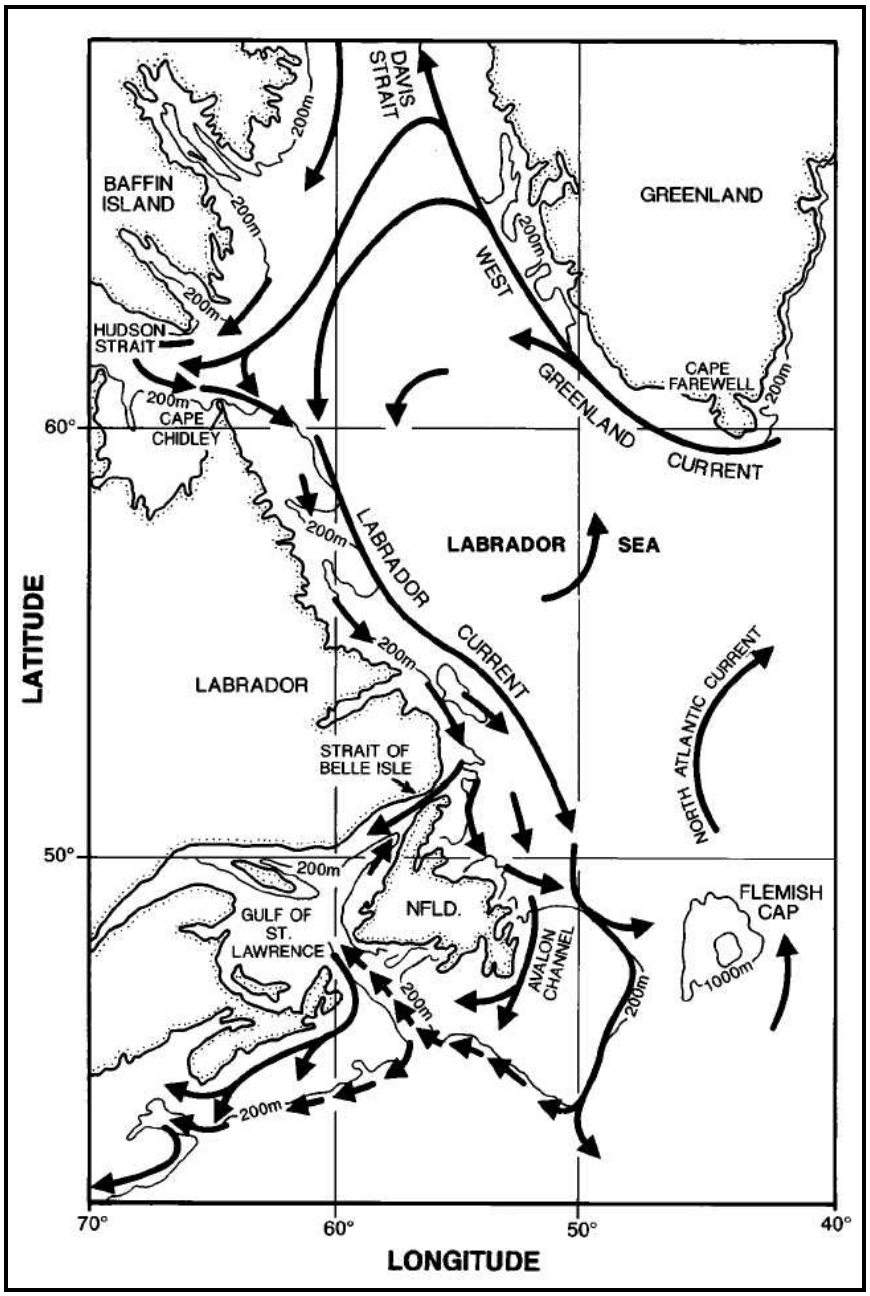

Source: Colbourne 1997

Figure 4-106 Major Ocean Circulation Features in the Northeast Atlantic

The volume transport of the Labrador Current is variable from year to year. Han et al. (2010) found that the transport decreased by 6.3 Sv (a unit of measure of volume transport; the sverdrup Is 106 m^3/s.) from the early to late 1990s and increased by 3.2 Sv from the late 1990s to the early 2000s. They found that the multi-year changes in the Labrador Current transport appeared to be primarily barotopic and positively correlated with the North Atlantic Oscillation (NAO) at zero lag, implying a fast response of the regional circulation to the atmospheric forcing variability.

Another major current system is situated to the south of the Grand Banks. The Gulf Stream, a major western boundary current, departs the shelf break near Cape Hatteras, NC, at approximately 75°W, flowing northeast. In the area of the Southeast Newfoundland Rise, which runs from the tail of the Grand Banks toward the Mid-Atlantic Ridge, the Gulf Stream branches into two streams. The southern branch continues east at approximately 40°N. The northern branch, known as the North Atlantic Current, turns north and runs along the east side of the Grand Banks and Flemish Cap, and then turns east following approximately 50°N latitude across the Atlantic. Krauss (1990) found the North Atlantic Current to be approximately 300 km wide. Near the ail of the Grand Banks, the North Atlantic Current comes into contact with the Continental Slope and follows it northeast around Flemish Cap (Figure 4-107). In this area, it also meets the Labrador Current flowing south. The entire area of the southeastern Grand Banks is a massive mixing area between two water masses with very different temperature and salinity characteristics. A secondary eastward current also flows inshore of the Atlantic Current along the Continental Slope, sometimes referred to as the Slope Current, with characteristics of Slope Water (McLellan 1957). Slope Water is formed from Atlantic Current Water and Coastal Water. The North Atlantic Current and Slope Current transport warmer, high salinity water to the northeast along the southeast slope of the Grand Banks and Flemish Cap.

White Rose is located in the northeast sector of the Grand Banks and is located in a water depth of approximately 120 m. In the immediate area, the bottom relief is relatively featureless, but steep slopes occur to the north and east at the edge of the Grand Banks. White Rose is located inshore of the Labrador Current where, most of the time, the flow is weak, with variable mean flows, compared to the strength of the two major current systems in the vicinity. At times, the variability in the mixing and interactions created by these two major current systems can have an effect on the current flow at White Rose.

The general circulation and mean currents on the Grand Banks are well understood from geostrophic calculations, drifter data, current modelling, and direct measurements. The variability is becoming more understood as the quantity of data collected at White Rose increases.

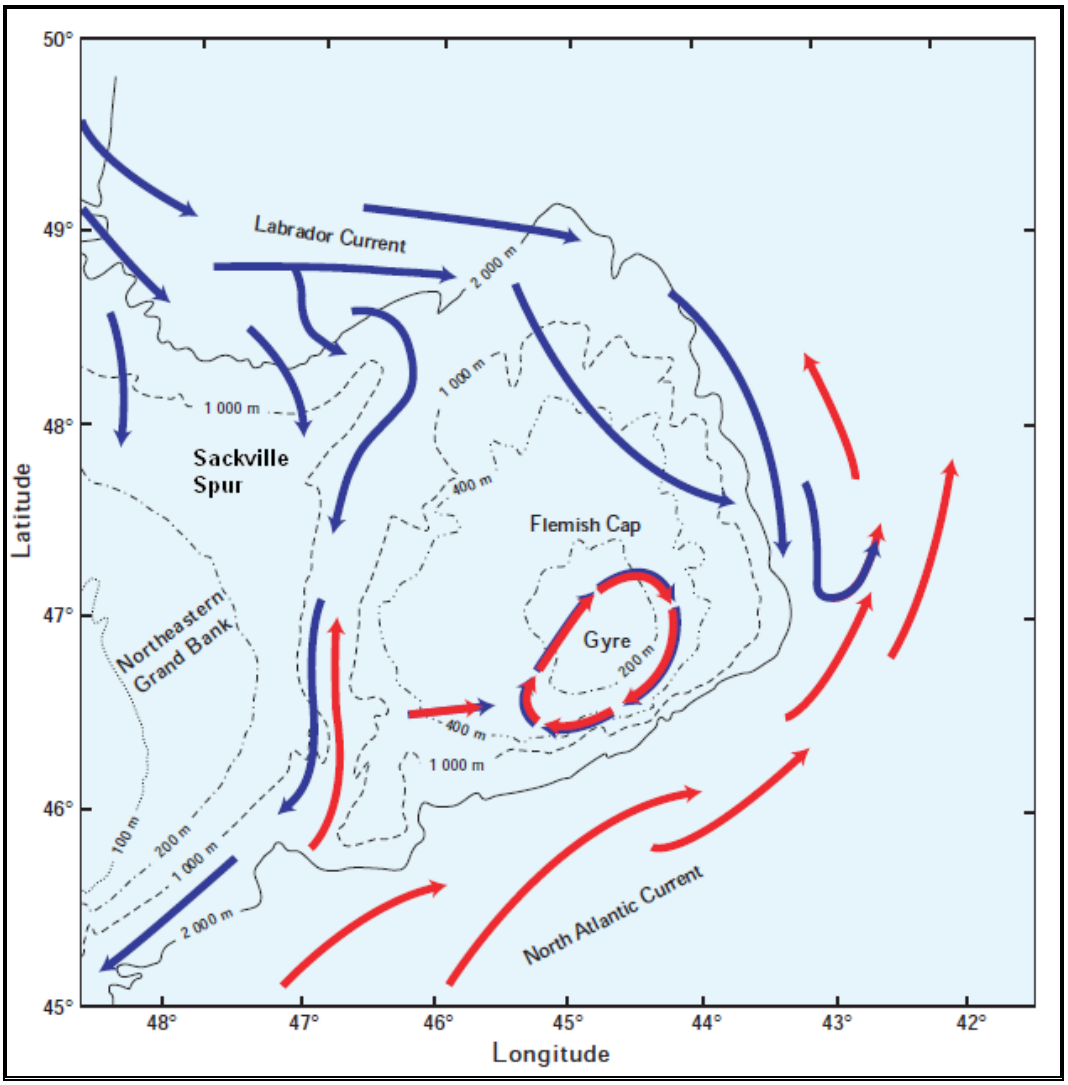

Source: modified from Colbourne and Foote 2000

Figure 4-107 Major Circulation Features around the Flemish Cap and Sackville Spur

Moored Current Meter Data

In the White Rose area, moored current meter data was collected over short intervals (a few months per site) during the early exploration period between 1984 and 1988 and for the period between 1999 and 2002. These data sets and statistical information are listed in Tables 4-58 to 4-60. At mid-depth and near-bottom, continuous data exists from August 2007 to December 2010. Since January 2008, there has been continuous near-surface current data measured at White Rose.

Table 4-58 Currents (intermittent data) at Near-surface at White Rose

Well Site	Period	Max. Speed (cm/s)	Mean Speed (cm/s)	Mean Velocity (cm/s)	Direction
Gros Morne C-17	Sep 4 to Sep 18, 2002	41.0	14.7	6.9	South
Trepassey J-91	Jul 25 to Aug 27, 2002	33.0	11.7	6.8	South
White Rose H-20	May 15 to Jul 8, 2000	67.0	12.5	0.5	Southeast
White Rose N-30	Aug 19 to Sep 29, 1999	89.9	27.0	5.0	Southeast
White Rose A-17	Jun 23 to Aug 6, 1999	42.1	11.4	8.4	Northeast
White Rose L-08	Mar 31 to Jun 22, 1999	45.7	10.4	2.7	Northwest
White Rose E-09	May 14 to Jul 5, 1988	45.2	15.7	7.5	Southeast
White Rose J-49	Aug 10 to Nov 19, 1985	61.7	14.7	4.9	South
White Rose L-61	Dec 19 to Feb 15, 1986	36.0	13.0	6.4	Northeast
White Rose N-22	Jul 5 to Oct 16, 1984	82.0	19.6	19.0	Southwest
Trave E-87	Nov 15 to Jan 14, 1984	55.0	19.5	8.1	South
Trave E-87	Feb 1 to Mar 11, 1984	40.0	16.9	11.1	Southeast

Table 4-59 Currents (intermittent data) at Mid-depth at White Rose

Well Site	Period	Max. Speed (cm/s)	Mean Speed (cm/s)	Mean Velocity (cm/s)	Direction
Gros Morne C-17	Sep 4 to Sep 18, 2002	24.0	11.4	2.6	South
Trepassey J-91	Jul 25 to Aug 27, 2002	31.0	9.0	3.0	South
White Rose H-20	May 15 to Jul 8, 2000	25.0	9.3	0.5	South
White Rose N-30	Aug 19 to Oct 14, 1999	40.8	11.2	10.6	Northeast
White Rose L-08	Mar 31 to Jun 22, 1999	29.4	12.1	3.8	South
White Rose A-90	Jul 13 to Aug 11, 1988	24.7	8.9	3.4	Southeast
White Rose E-09	May 14 to Jul 5, 1988	39.0	12.3	5.9	Southeast
White Rose E-09	Jan 19 to Feb 20, 1988	35.0	10.4	3.5	Southeast
Whites Rose E-09	Sep 1 to Oct 22, 1987	32.6	10.0	9.0	Southwest
White Rose J-49	Aug 10 to Nov 19, 1985	43.7	11.8	2.6	Southeast
White Rose N-22	Jul 5 to Nov 10, 1984	31.0	9.6	1.8	Southeast
Trave E-87	Feb 1 to Mar 12, 1984	31.0	12.2	7.5	South
Trave E-87	Nov 14 to Jan 15, 1984	46.0	13.7	5.0	Southeast

Table 4-60 Currents (intermittent data) Near-bottom at White Rose

Well Site	Period	Max. Speed (cm/s)	Mean Speed (cm/s)	Mean Velocity (cm/s)	Direction
Gros Morn C-17	Sep 4 to Sep 18, 2002	30.0	10.2	1.2	Southwest
Trepassey J-91	Jul 25 to Aug 27, 2002	30.0	8.7	1.3	South
White Rose H-20	May 11 to Jul 8, 2000	25.0	9.1	1.8	Southeast
White Rose L-08	Mar 31 to Jun 22, 1999	27.6	9.5	2.8	Southeast
White Rose A-90	Jul 13 to Aug 11, 1988	25.2	8.9	4.1	Southeast
White Rose E-09	May 14 to Jul 5, 1988	32.6	10.8	3.7	Southeast
White Rose E-09	Jan 19 to Feb 20, 1988	34.5	13.0	3.7	Southeast
White Rose E-09	Sep 1 to Nov 19, 1987	36.2	10.9	2.7	Southeast
White Rose J-49	Aug 10 to Nov 19, 1985	50.6	10.7	2.0	Southeast
White Rose N-22	Jul 5 to Nov 10, 1984	18.0	5.9	--	No Direction
Trave E-87	Nov 14 to Jan 21, 1984	39.0	13.1	6.6	Southeast
Trave E-87	Feb 1 to Mar 11, 1984	32.0	10.1	5.9	Southeast

Statistics from the continuous data collected since August 2007 are listed in Tables 4-61 to 4-63. Current measurements at White Rose are now being measured on an ongoing basis. Since January 2008, measurements are available in 4 m bins throughout the water column. The data collection periods, the maximum speeds, mean speeds and mean velocities are listed in Tables 4-61 to 4-63. At 20 m (near-surface), the maximum speed that was measured was 89.9 cm/s in September 1999 at White Rose N-30 (Table 4-58). During the same event, current speeds of 40.8 cm/s were measured at mid-depth. These strong currents were due to the passage of Hurricane Gert. At mid-depth, the maximum current speed of 55.6 cm/s (Table 4-62) occurred in December 2007 during a winter storm. During the same event the currents near bottom were 36.1 cm/s. The maximum speed near bottom occurred in November 1985 at White Rose J-49 with a speed of 50.6 cm/s (Table 4-63). During the same event near-surface speed was 61.7 cm/s (Table 4-58).

Table 4-61 Currents (continuous data) at Near-surface at White Rose (January 2008 to December 2010)

Year	Max Speed (cm/s)	Mean Speed (cm/s)	Mean Velocity (cm/s)	Direction
2008	60.7	15.3	3.2	South
2009	56.0	14.4	2.9	South
2010	52.8	13.5	1.9	Southwest

Table 4-62 Currents (continuous data) Mid-depth at White Rose (August 2007 to December 2010)

Year	Max Speed (cm/s)	Mean Speed (cm/s)	Mean Velocity (cm/s)	Direction
2007	55.6	13.4	1.7	Southeast
2008	39.3	10.7	1.5	Southeast
2009	37.8	11.8	1.6	South
2010	40.5	11.1	0.9	Southwest

Table 4-63 Currents (continuous data) Near-bottom at White Rose (August 2007 to December 2010)

Year	Max Speed (cm/s)	Mean Speed (cm/s)	Mean Velocity (cm/s)	Direction
2007	36.1	11.9	2.6	Southeast
2008	36.4	11.7	1.5	Southeast
2009	34.5	11.4	1.6	Southeast
2010	41.6	11.2	1.1	Southeast

Current Variability

The most notable characteristic of the currents at White Rose is the amount of variability in the current flow. The residual flow over a year time period is in a southerly direction, anywhere from southwest to southeast. This is illustrated in Figure 4-108, which shows the progressive vector diagrams for 2010 at depths of 20, 64 and 112 m. The current at White Rose can flow in any direction for days at a time. This high degree of variability is illustrated in Figure 4-109, which presents progressive vector diagrams for February 2010 for the same three depths. The current direction during any month is also variable from year to year, as illustrated in Figure 4-110, which shows the progressive vector diagrams at 20 m for the month of July for years 2008 to 2010.

There are many contributing factors to the variability in current flow at White Rose. The largest contributing factor is the sea surface slope produced by atmospheric pressure systems as they pass through the area. Other contributing factors to the variability at White Rose include the surface wind stress, tidal forces, buoyancy fluxes, and the large-scale circulation and interactions associated with the Labrador Current and the North Atlantic Current. Wind stress influences the flow in two time scales; synoptic periods on the order of 2 to 10 days associated with severe storms, and the inertial period of 16.4 hours. Wind stress provides a major driving force of currents on the Continental Shelf, with a distinct annual cycle of comparatively strong winds in fall and winter and weaker, more variable winds in spring and summer.

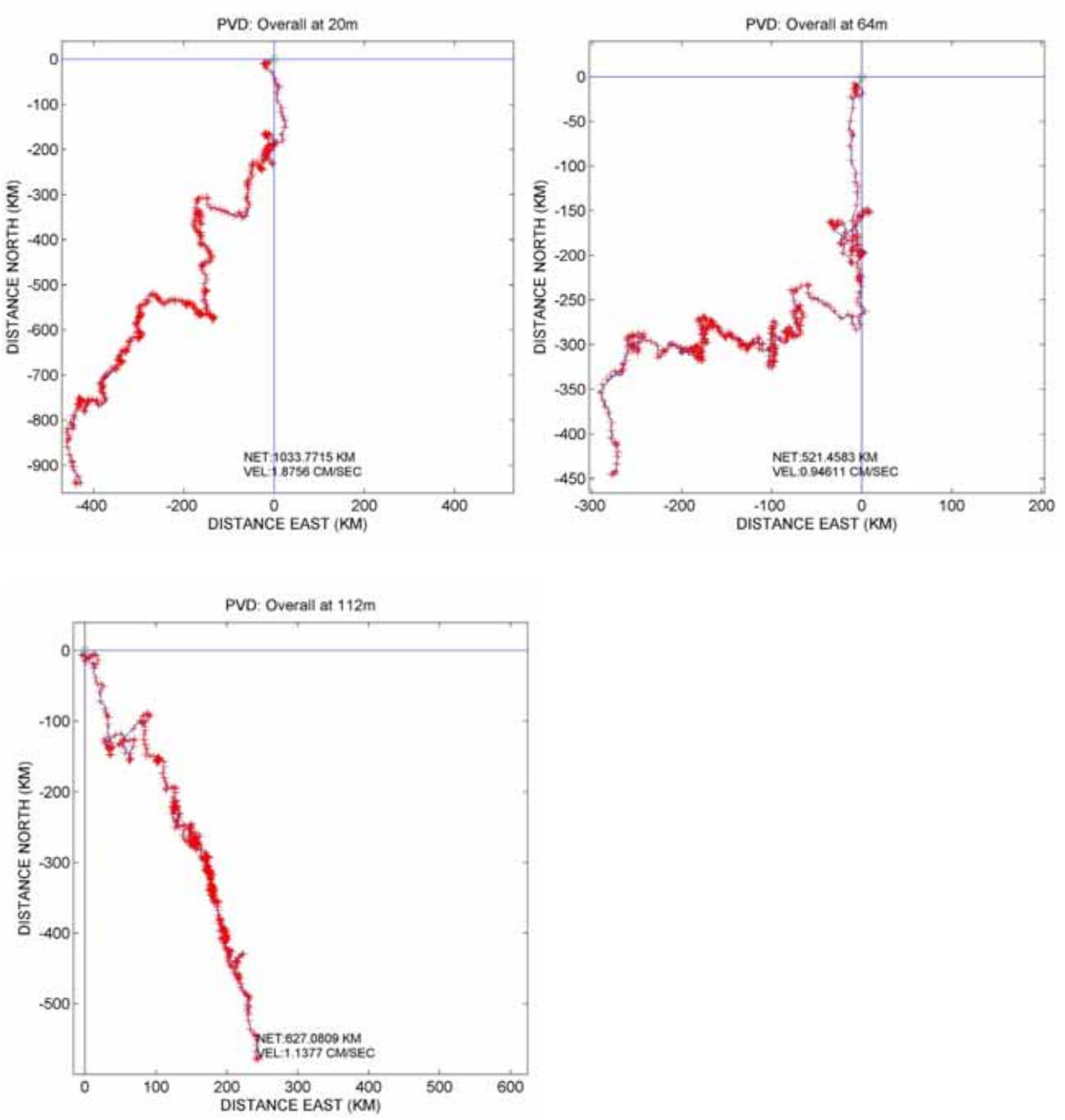

Figure 4-108 Annual Progressive Vector Diagrams for 2010 at Depths of 20, 64 and 112 m at White Rose

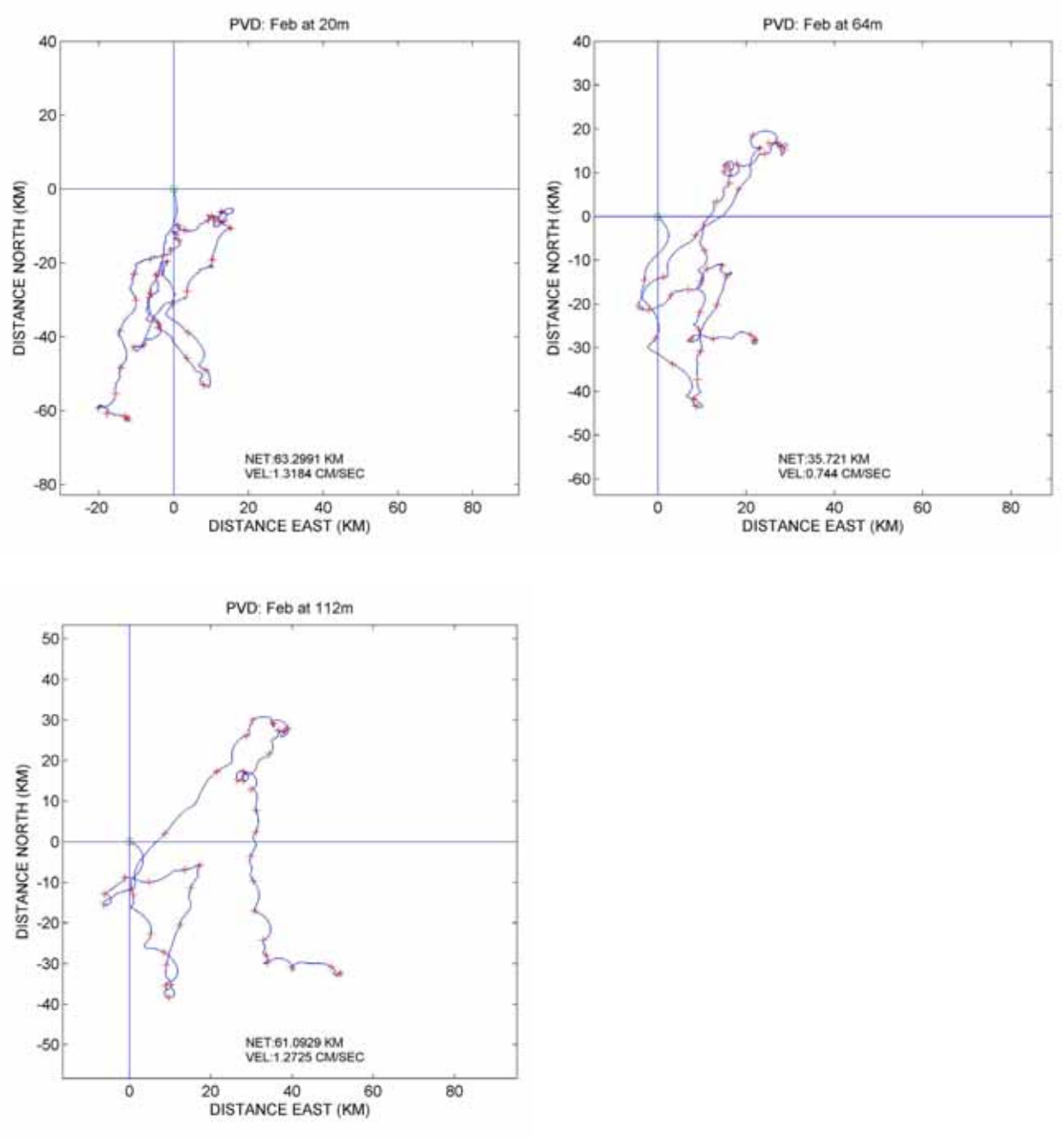

Figure 4-109 Progressive Vector Diagrams for February 2010 at Depths of 20, 64 and 112 m at White Rose

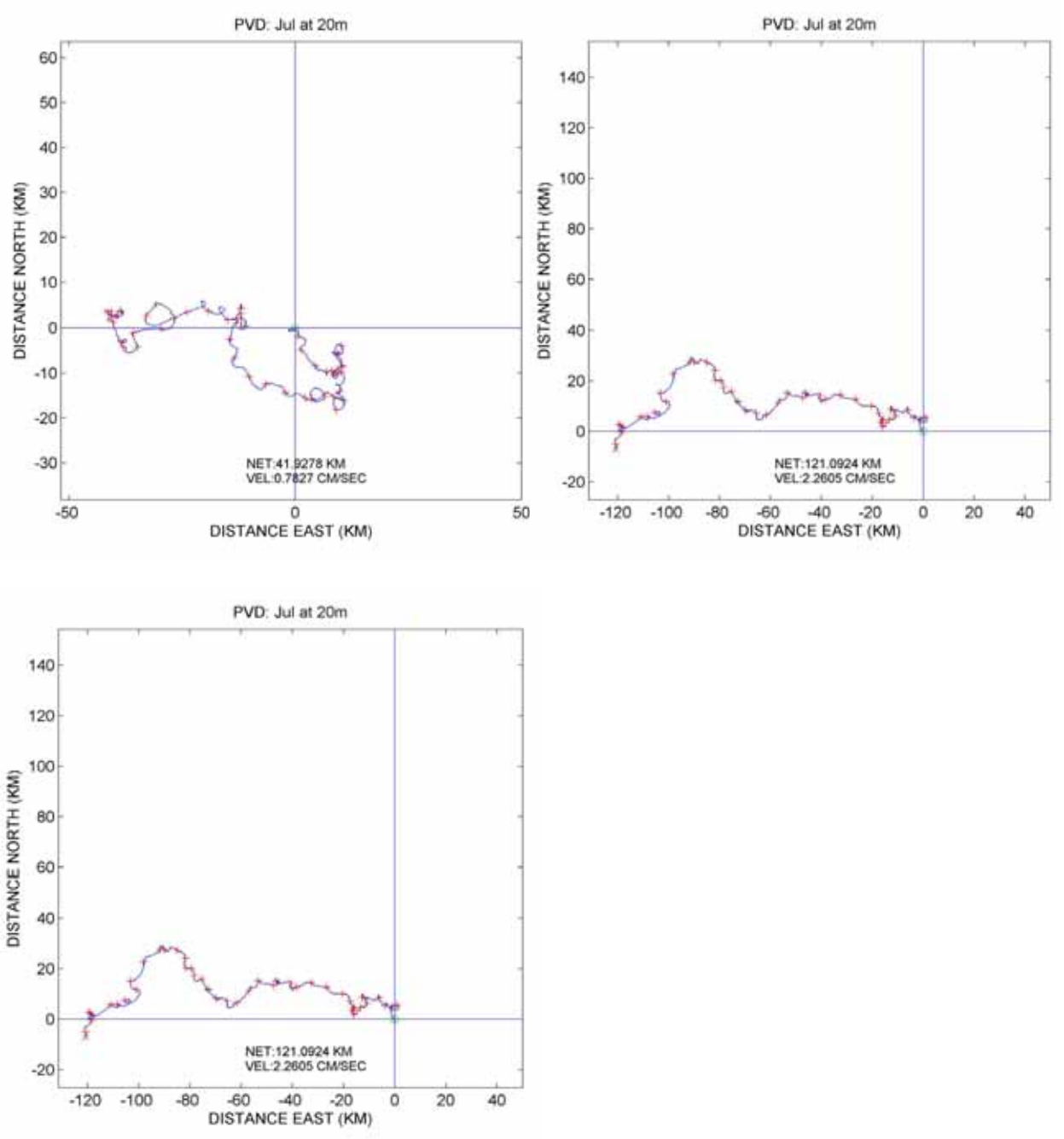

Figure 4-110 Progressive Vector Diagrams for July at 20 m, for Years 2008 to 2010 at White Rose

An analysis of the measured currents prior to 2007 showed that tides accounted for approximately 20 percent of the variability at White Rose. Buoyancy fluxes associated with large freshwater inputs produce strong density gradients leading to pressure gradients that drive alongshore currents. The outer branch of the Labrador Current exhibits a distinct seasonal variation in flow speeds (Lazier and Wright 1993) in which the mean flows from September to October are nearly twice as large as the mean flows in March and April. The large variation in density on the shelf results from increased

freshwater input from melting ice and freshwater runoff occurring upstream in the spring and summer.

Offshore eddies and rings have an important influence on circulation over the Continental Slope. Interactions between the Labrador Current and eddies of the North Atlantic Current system will influence the flow along the southeastern section of the Grand Banks. When a Gulf Stream ring encounters a sloping bottom, it radiates low-frequency energy in the form of topographic Rossby waves with characteristic periods of 10 to 30 days (Louis et al. 1982). On approach to the shelf, the wave energy is strongly reflected by the Continental Slope and scattered into baroclinic modes trapped to the shelf edge such that little energy penetrates onto the shelf (Smith and Schwing 1991). However, the resulting redistribution of the density field may have an influence on the currents near the shelf edge. Voorheis et al. (1973) have identified over 30 eddies on the central part of the Continental Slope along the eastern margin of the Grand Banks from an analysis of historical oceanographic data sets going back to the 1920s. The eddies were mostly counter-clockwise, with typical speed of 25 to 30 cm/s and with an average size of 102 km in diameter. Meanders had typical lengths of 275 km in the along-stream direction, and about half this distance in the cross-stream direction.

White Rose is situated far enough north on the Grand Banks to avoid any direct effects from the eddies and meanders on the southern part of the banks. The years when the northern boundary of the North Atlantic Current is further north than usual there is a potential for some indirect effects.

4.3.2.5 Tides and Storm Surges

Astronomical tides are highly predictable. From an extended measurement at any selected site, the major astronomical constituents can be determined and used to accurately predict tidal heights. Over the Grand Banks, the largest tidal constituent is the lunar semidiurnal (M2) with amplitude of approximately 40 cm. The other major semidiurnal (S2) and diurnal constituents (01, K1) are lower in amplitude; each constituent has a value of approximately 10 to 15 cm (Godin 1980).

The tides on the Grand Banks are mixed, mainly semidiurnal with two high tides and two low tides occurring each day. The successive highs (and lows) are usually not the same height. A typical tidal range is 1 m.

Tidal information for the Grand Banks comes from a tidal study carried out by the BIO in 1983-84, and tidal data collected by Husky for two periods; August 6 to December 10, 1985, and December 28, 1985 to February 13, 1986. BIO collected data at eight sites over a period of six months on the Grand Banks, and along its edge (Petrie et al. 1987). From the BIO data, Petrie et al. (1987) prepared co-range and co-phase charts for the Grand Banks for constituents M2, S2 and K1. These charts are presented in Figure 4-111. Co-range lines are lines of equal amplitude and co-phase lines are lines of equal phase. The co-range lines show that the M2 constituent is approximately 25 cm at White Rose and S2 and K1 are approximately 10 and 17 cm, respectively.

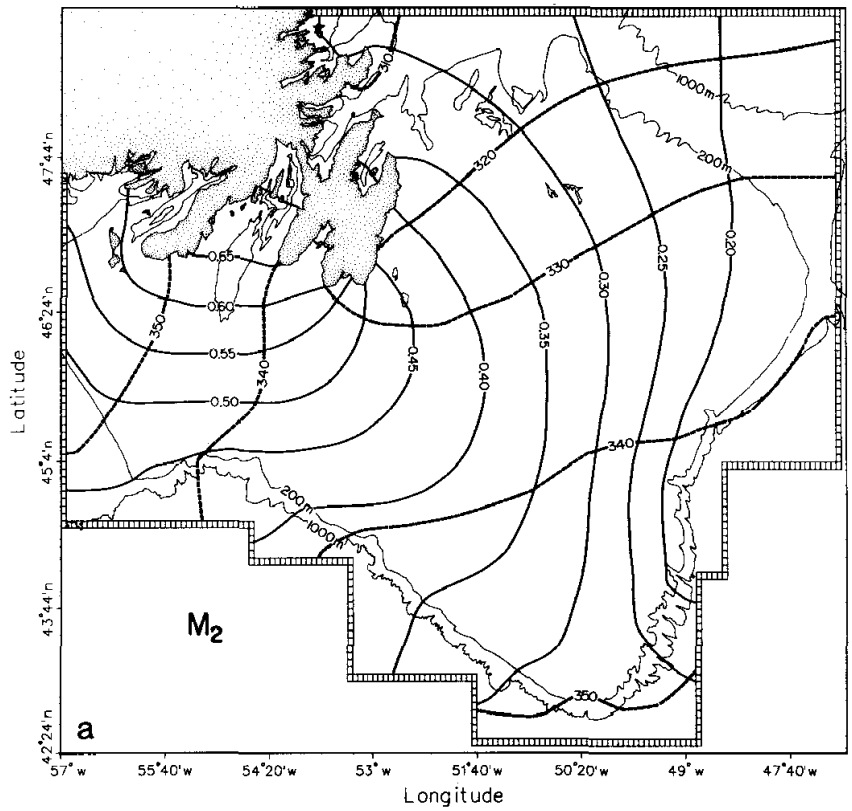
M2
a
Latitude
Longitude
47°44'n
46°24'n
45°4'n
43°44'n
42°24'n
57° w
55°40'w
54°20'w
53° w
51°40'w
50°20'w
49° w
47°40'w
1000m
200m
320
330
340
350
0.65
0.60
0.55
0.50
0.45
0.40
0.35
0.30
0.25
0.20

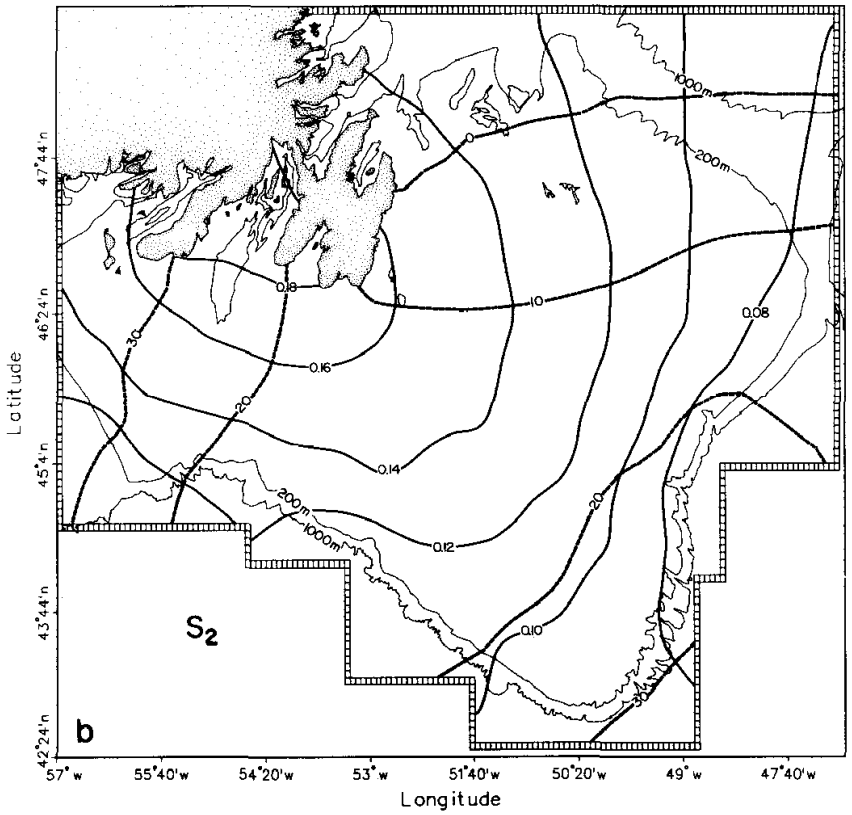
S2
b
Latitude
Longitude
47°44'n
46°24'n
45°4'n
43°44'n
42°24'n
57° w
55°40'w
54°20'w
53° w
51°40'w
50°20'w
49° w
47°40'w
1000m
200m
0.18
0.16
0.14
0.12
0.10
0.08
10
20
30

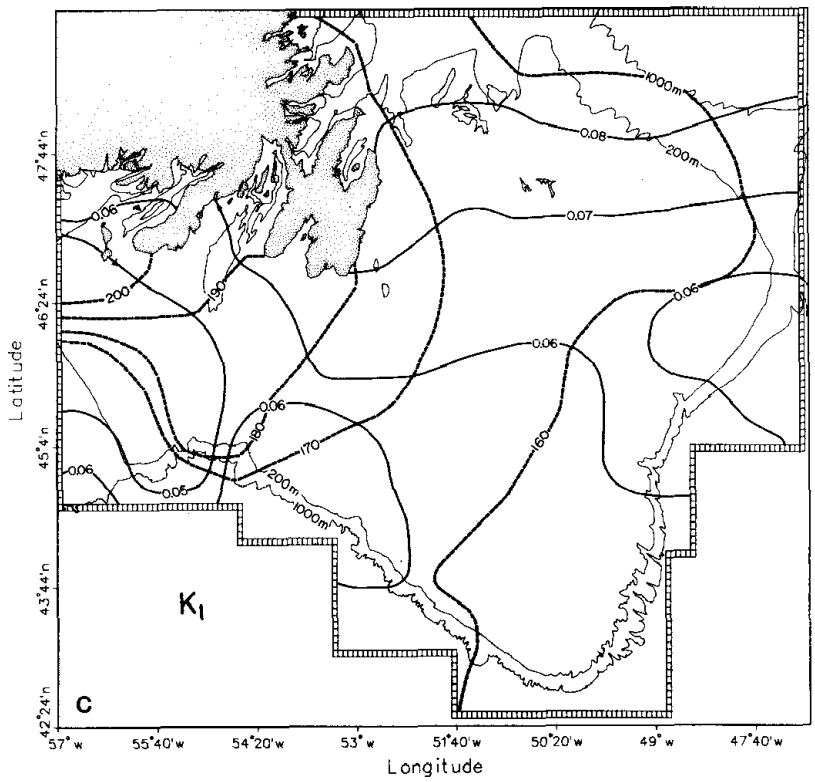

Source: Petrie et al., 1987
Note: Co-range is solid line (in metres) and Co-phase is broken line

Figure 4-111 Co-range and Co-phase Charts for the Grand Banks

Tidal data was collected between November 6, 2009 and February 28, 2010 in the White Rose field with an Aanderaa water level recorder. The water level difference between the lowest low water and highest high water was 1.44 m. The tidal constituents are presented in Table 4-64. The values for the largest constituents M2, S2, K1 and O1 are 0.177, 0.076, 0.073 and 0.056 m, respectively. Note that these values represent one half of the tidal constituent amplitude.

Table 4-64 Tidal Constituents from Husky Water Level Data (November 2009 to February 2010)

Name	Frequency (cph)	Amplitude (m)	Phase (o)
MM	0.001512	0.072224	144.2981
MSF	0.002822	0.034239	111.6555
ALP1	0.034397	0.011391	136.7266
2Q1	0.035706	0.007278	303.1457
Q1	0.037219	0.004892	87.79878
O1	0.038731	0.05575	127.3923
NO1	0.040269	0.010553	191.5029

Name	Frequency (cph)	Amplitude (m)	Phase (o)
K1	0.041781	0.072579	171.2435
J1	0.043293	0.010472	234.6508
OO1	0.044831	0.004553	196.534
UPS1	0.046343	0.006569	239.454
EPS2	0.076177	0.008509	341.3757
MU2	0.077689	0.010182	325.0568
N2	0.078999	0.038217	297.1987
M2	0.080511	0.177036	318.2682
L2	0.082024	0.002987	255.5125
S2	0.083333	0.076496	11.217
ETA2	0.085074	0.006589	296.0131
MO3	0.119242	0.008784	301.2988
M3	0.120767	0.004968	17.19392
MK3	0.122292	0.008286	97.04533
SK3	0.125114	0.00985	305.0364
MN4	0.159511	0.011279	110.979
M4	0.161023	0.013567	147.5201
SN4	0.162333	0.008624	331.5436
MS4	0.163845	0.007564	10.27288
S4	0.166667	0.006295	243.3306
2MK5	0.202804	0.008836	5.287672
2SK5	0.208447	0.007707	74.58054
2MN6	0.240022	0.011561	23.54241
M6	0.241534	0.013034	67.6537
2MS6	0.244356	0.010059	247.7408
2SM6	0.247178	0.008403	129.7494
3MK7	0.283315	0.007977	258.7407
M8	0.322046	0.006795	307.5446

Storm surges cause sea level to rise as a result of wind stress on the surface of the ocean. Severe storm surges can cause the ocean to rise by a few metres in coastal regions, but away from the coast the effect of wind stress is much smaller in the absence of a boundary. Therefore, the effect of storm surges at White Rose is expected to be negligible.

4.3.2.6 Physical and Chemical Properties

The water structure on the north-eastern edge of the Grand Banks of Newfoundland is characterized by the presence of three identifiable features.

The first identifiable feature is the surface layer, which is exposed to interaction with the atmosphere and experiences temperature variations from sub-zero values in January and February to above 15°C in summer and early fall. Salinity in this layer is strongly affected by wave action and local precipitation. During the summer, the stratified surface layer can extend to a depth of 40 m or more. In winter, the stratification in the surface layer disappears and becomes well mixed due to atmospheric cooling and intense mixing processes from wave action.

A second element of the water structure on the Grand Banks is the Cold Intermediate Layer (Petrie et al. 1988). In areas where the water is deep enough, this layer of cold water is trapped during summer between the seasonally-heated upper layer and warmer slope water near the seabed (Colbourne 2002). Its temperatures range from less than -1.5°C to 0°C (Petrie al. 1988; Colbourne et al. 1996) and salinities vary within 32 and 33 psu. It can reach a maximum vertical extent of over 200 m (Colbourne 2004). The Cold Intermediate Layer is the residual cold layer that occurs from late spring to fall and is composed of cold waters formed during the previous winter season. It becomes isolated from the sea surface by the formation of the warm surface layer during summer, and disappears again during late fall and winter due to the intense mixing processes that take place in the surface layer from strong winds, high waves and atmospheric cooling. In winter, the two layer structure is replaced by a mixed cold body of water that occupies the entire water column.

A third element of the water structure is the Labrador Sea water, which is formed in the Labrador Sea as a result of the deep convection processes that take place during severe winters. The Labrador Sea water has temperatures between 2°C to 4°C and salinities between 34.8 to 35 psu. The Labrador Sea water is separated from the Intermediate Cold Layer by a frontal region denoted by a strong temperature and salinity gradient near the edge of the Continental Shelf (Colbourne 2004; Stein 2007).

The sea surface temperatures in the study area are presented in Figure 4-112, which shows the geographical location and average temperatures, by season, of the frontal region east of the Grand Banks. The spatial distribution of water properties offshore Newfoundland at 20 m and 75 m is presented for July and January in Figures 4-113 and 4-114, respectively (Colbourne and Foote 1994). The warmer, high-salinity slope water is evident to the south and east of the Grand Banks at both 20 and 75 m depths. The large horizontal gradients mark the boundaries (oceanic fronts) between the cold low salinity water of the Labrador Current and coastal waters, and the warm high salinity slope and Atlantic current waters.

The spatial variability of temperature and salinity in the northeast sector of the Grand Banks is routinely sampled each year by DFO. During 2010, this hydrographic section was sampled in April, July and December. The temperature and salinity contours across the Flemish Cap section in 2010 are shown in Figures 4-115 to 4-117. The temperature distribution is characterized by an area of strong vertical gradients located above the Grand Banks in July (Figure 4-116). This vertical temperature structure breaks down during the winter season, as shown in Figures 4-115 and 4-117.

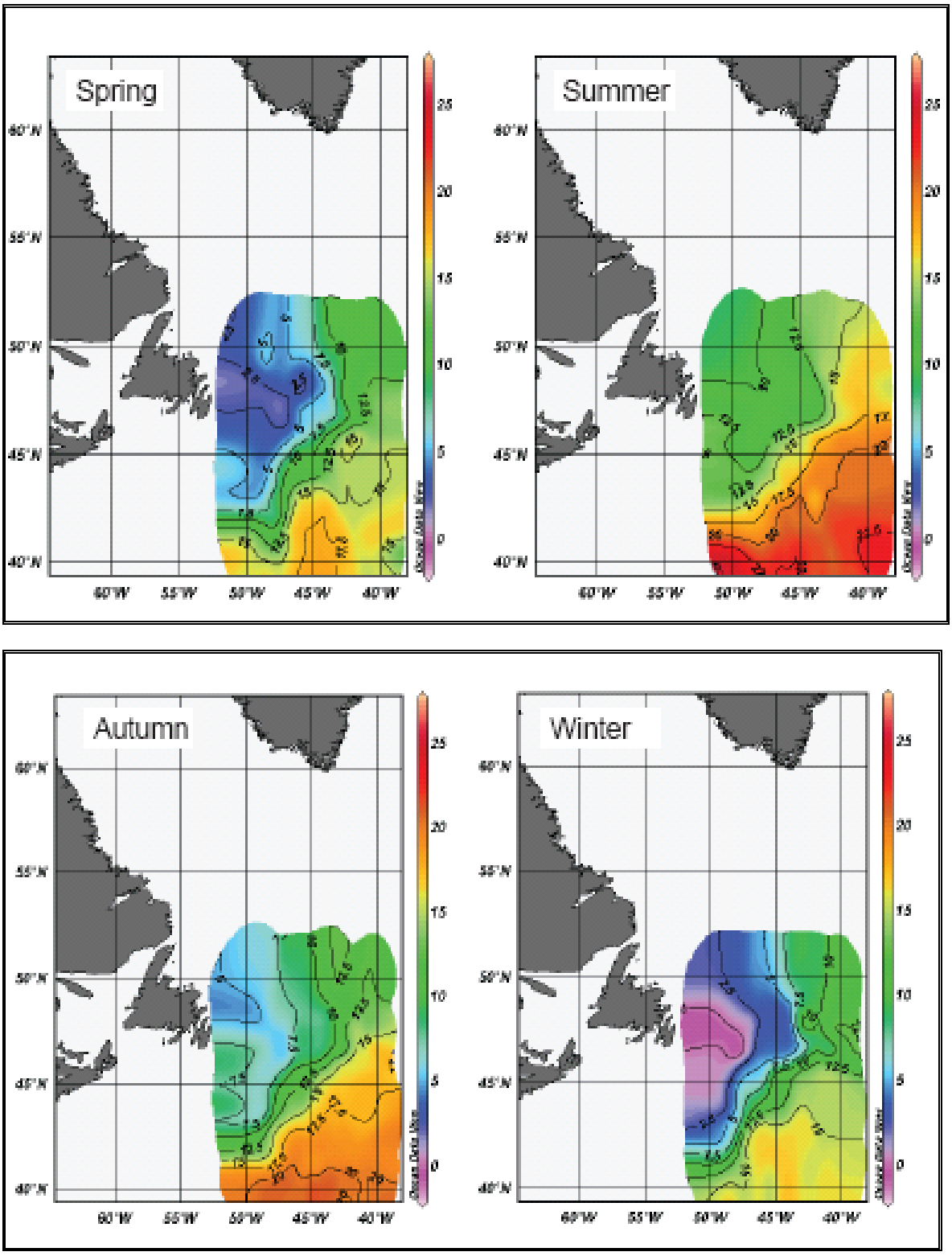

Source: from Stein 2007

Figure 4-112 Sea Surface Temperatures for each Season (produced from the World Oceans Database 2001)

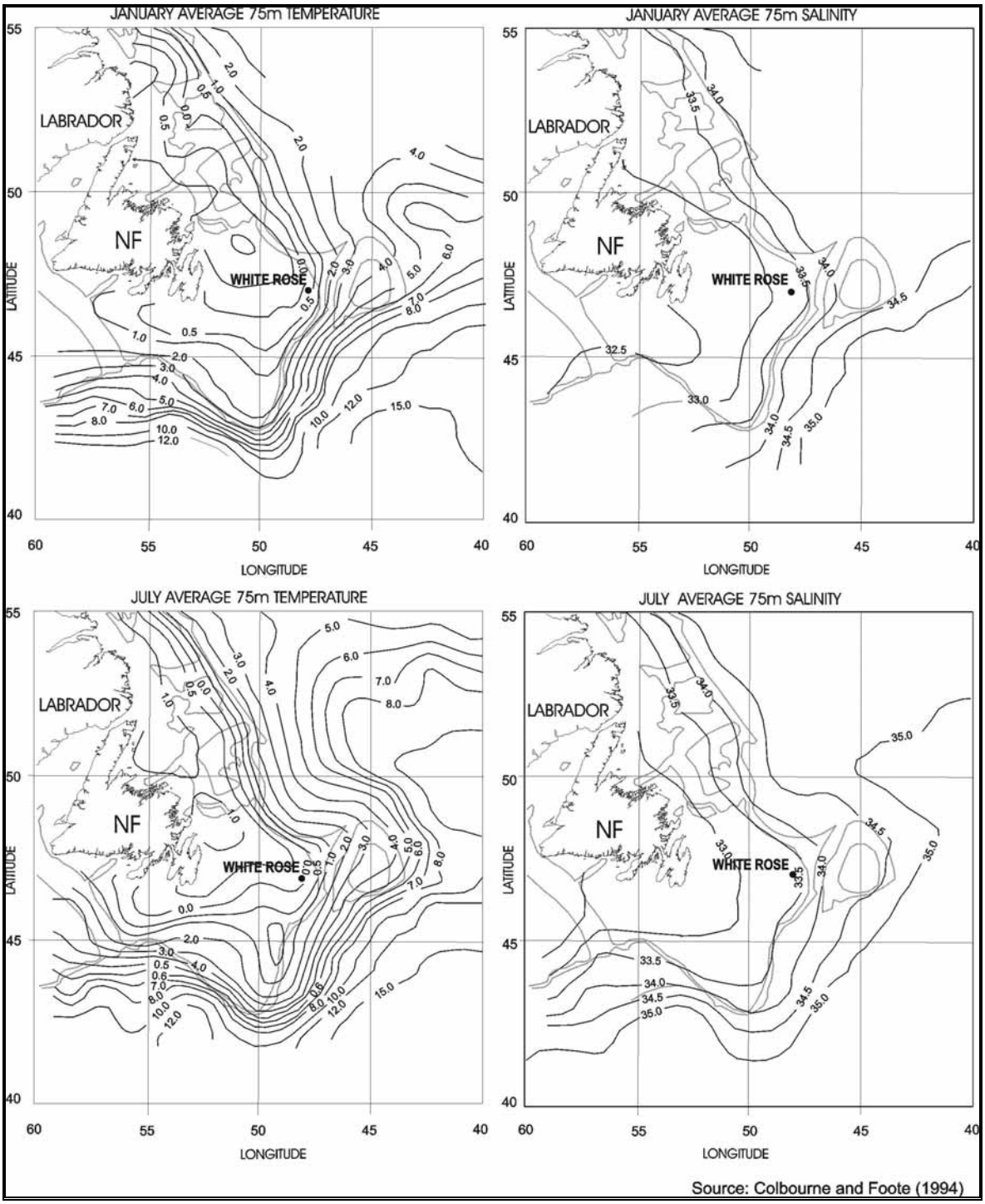

Source: Colbourne and Foote 1994

Figure 4-113 Average Spatial Distribution of Temperatures and Salinity at 75 m depth in January and July for many Years

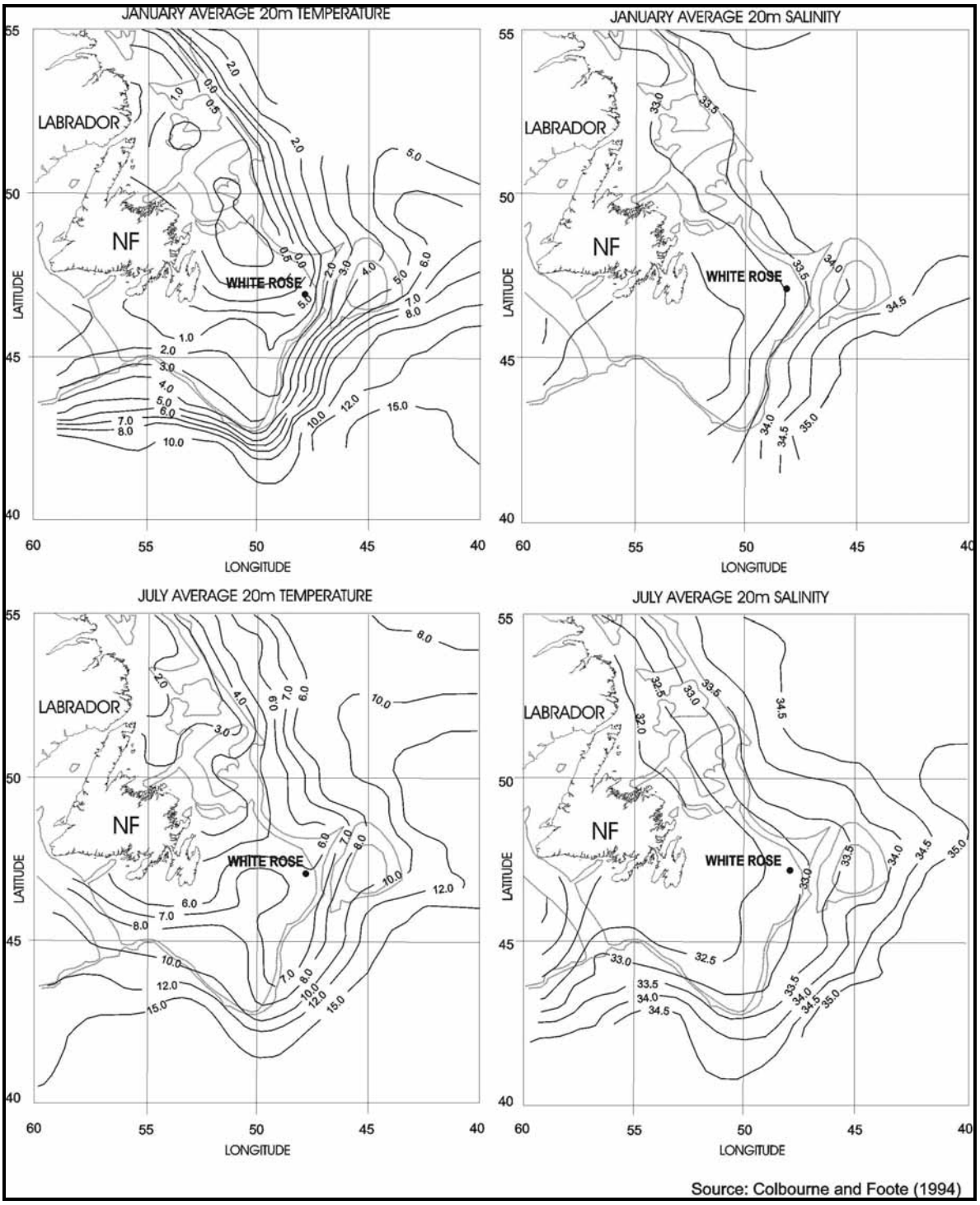

Figure 4-114 Average Spatial Distribution of Temperature and Salinity at 20 m in January and July

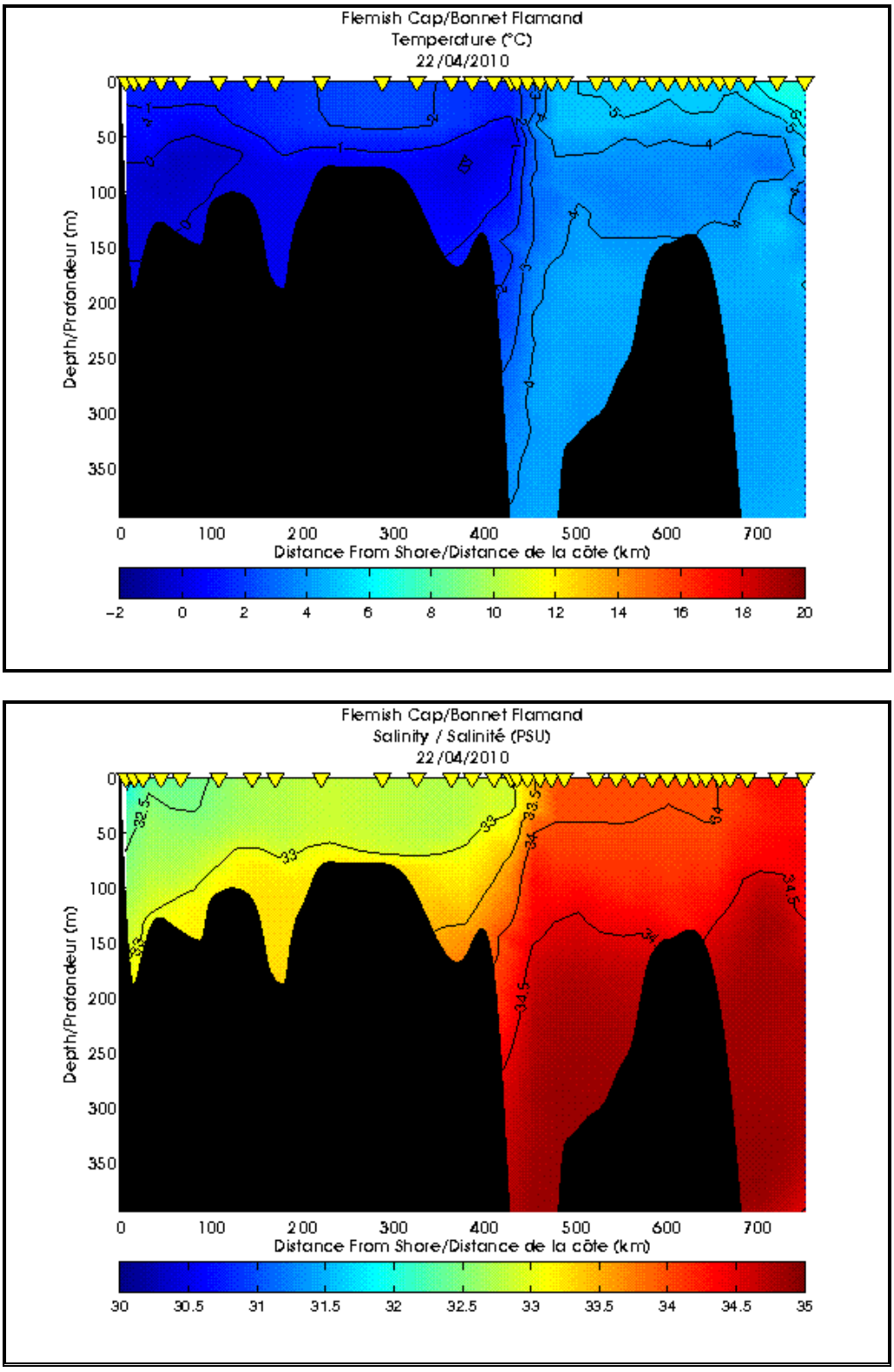

Source: from DFO 2012b (Marine Environmental Data Service Website)

Figure 4-115 Hydrographic Contours across the Flemish Cap Section during April 2010

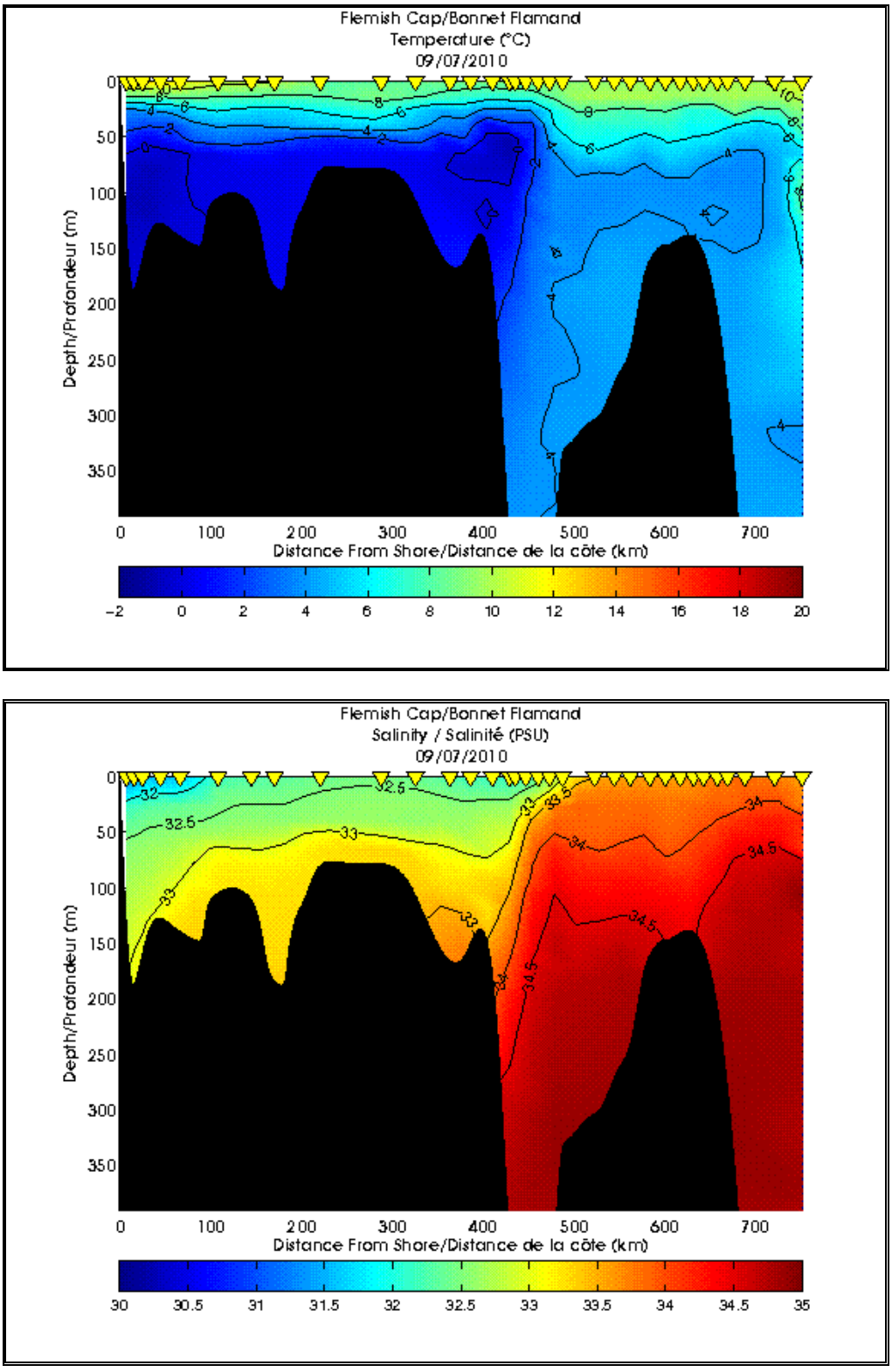

Source: from DFO 2012b (Marine Environmental Data Service Website)

Figure 4-116 Hydrographic Contours across the Flemish Cap section during July 2010

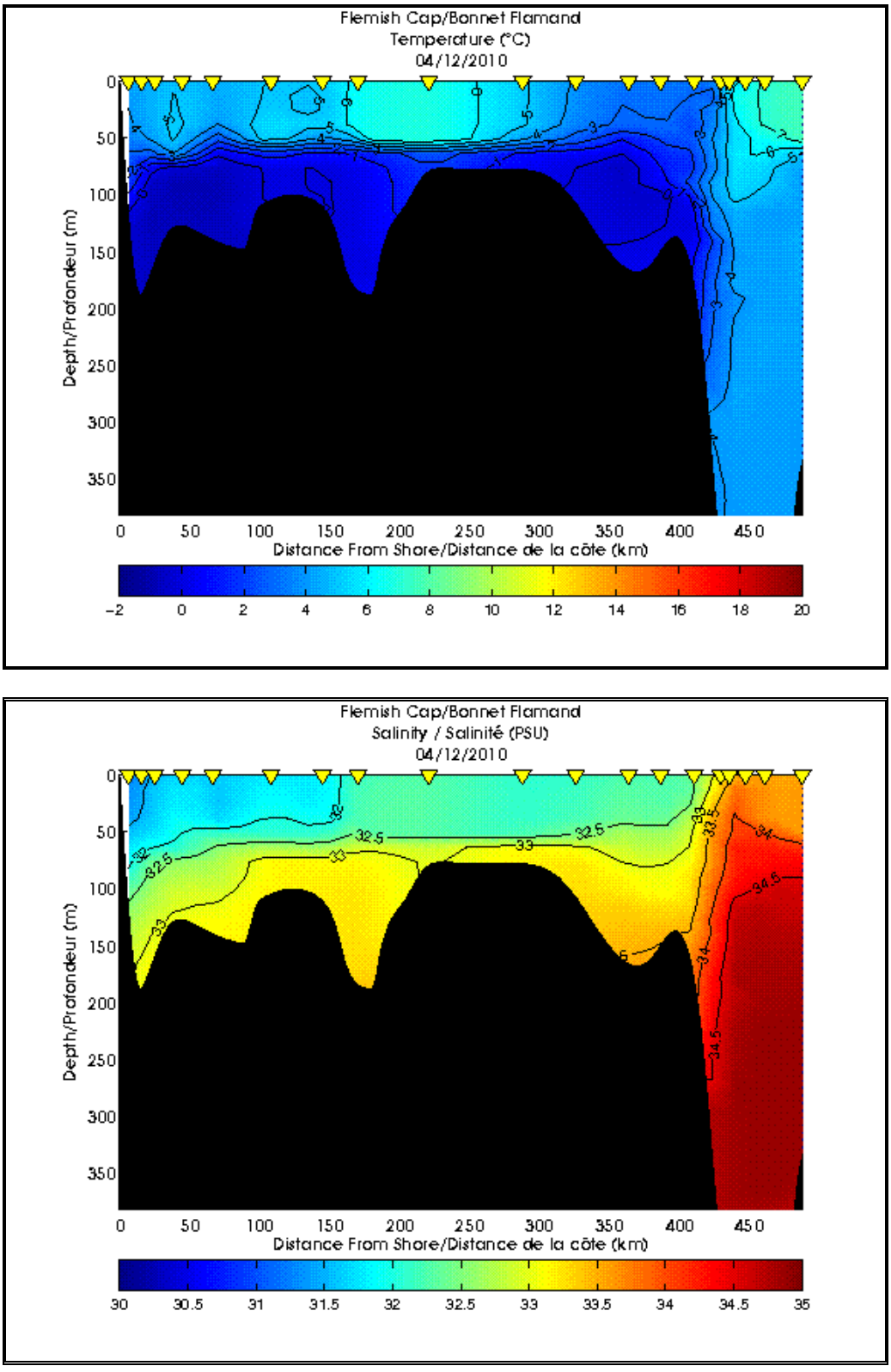

Source: from DFO 2012b (Marine Environmental Data Service Website)

Figure 4-117 Hydrographic Contour across the Flemish Cap Section during December 2010

The most noticeable feature is the high horizontal gradient in the area over the shelf break that separates the relatively fresh low salinity waters of the Grand Banks from the warmer, higher salinity waters in Flemish Pass (Figure 4-116). The offshore branch of the Labrador Current flows along the shelf break in the region of the strong density gradients shown in Figures 4-115 to 4-117. The majority of the water in the offshore branch of the Labrador Current has been known to have temperatures between 3°C and 4°C and salinities of 34.88 to 34.92 psu (Lazier 1982).

Historical temperature and salinity data were obtained from the BIO archives for the area between the 100 m and 200 m isobaths on the Northeast Grand Bank. The temperature and salinity data by month at the surface and at 75 m are presented in Tables 4-65 and 4-66, respectively. The information in the tables shows that the surface waters were warmest during the months of July to September, with mean temperatures ranging from 9.08° to 11.28°C. The coldest temperatures were in February and March with mean temperatures of -0.61°C and -0.75°C, respectively. The main salinities ranged between a low of 31.59 psu in August and a high of 32.94 psu in February.

Table 4-65 Monthly Temperature and Salinity Statistics for the Surface Water from Historical CTD Data for a Water Depth between 100 m and 200 m

Month	# Observations	Mean	Min	Max	STD
Surface temperature (0 m) on the outer edge of the Grand Banks					
January	15	0.10	-1.40	1.40	0.90
February	23	-0.61	-1.81	0.55	0.80
March	33	-0.75	-1.77	0.50	0.78
April	235	-0.16	-1.50	2.53	0.77
May	303	1.52	-1.10	5.08	1.33
June	422	4.15	0.64	10.34	1.70
July	249	9.08	4.15	13.7	1.86
August	72	11.28	6.37	16.08	2.08
September	87	9.98	4.23	17.1	2.61
October	60	7.13	3.54	11.54	1.97
November	184	4.19	0.83	9.74	1.72
December	53	2.44	-1.00	6.06	1.37
Surface salinity (0 m) on the outer edge of the Grand Banks					
January	15	32.77	32.19	33.30	0.31
February	23	32.94	32.61	33.29	0.21
March	33	32.91	32.41	33.37	0.18
April	235	32.86	32.23	33.33	0.19
May	303	32.72	31.82	33.19	0.22
June	422	32.56	31.62	33.50	0.24
July	249	32.23	31.08	32.77	0.27

Month	# Observations	Mean	Min	Max	STD
August	72	31.59	30.62	32.65	0.53
September	87	31.87	31.16	32.68	0.32
October	60	32.10	31.32	33.21	0.44
November	184	32.39	31.45	33.77	0.36
December	53	32.51	31.91	33.08	0.27

Table 4-66 Monthly Temperature and Salinity Statistics for 75 m Depth from Historical CTD Data for Water Depth between 100 m and 200 m

Month	# Observations	Mean	Min	Max	STD
Temperature 75 m depth on the outer edge of the Grand Banks					
January	16	-0.38	-1.40	0.55	0.54
February	19	-0.71	-1.73	0.96	0.79
March	29	-0.88	-1.76	0.57	0.76
April	384	-1.11	-1.78	1.62	0.55
May	285	-0.88	-1.76	1.48	0.71
June	391	-0.99	-1.80	1.49	0.55
July	244	-0.84	-1.81	5.90	0.79
August	130	-1.50	-1.70	-0.21	0.31
September	71	-1.25	-1.68	-0.05	0.37
October	133	-1.01	-1.65	0.05	0.33
November	178	-0.25	-1.50	3.30	1.10
December	55	-0.27	-1.44	2.13	0.98
Salinity 75 m depth on the outer edge of the Grand Banks					
January	16	33.03	32.69	33.33	0.20
February	19	33.18	32.66	33.55	0.22
March	29	33.11	32.77	33.68	0.23
April	384	32.94	32.53	33.8	0.29
May	285	33.09	32.65	34.11	0.19
June	391	33.06	32.53	33.66	0.18
July	244	33.05	32.56	34.00	0.15
August	130	33.08	32.75	33.52	0.11
September	71	33.16	32.79	33.79	0.25
October	133	33.16	32.81	33.69	0.19
November	178	33.17	32.48	33.98	0.24
December	55	33.14	32.75	33.69	0.20

At a depth of 75 m, the mean temperatures were always negative, ranging between -1.50°C in August to -0.25°C in November. The mean salinities ranged between 32.94 psu in April and 33.18 psu in February.

The colder waters in this area indicate that the water in this area is experiencing advection from the north by the Labrador Current rather than by vertical mixing through local cooling.

In recent years CTD water structure profiling was conducted on the White Rose field using the Sippican CTD system. Some of these profiles are presented in Figures 4-118 and 4-119. Three of the six profiles shown in the figures were carried out in the months of November for the years 2008 to 2010. The temperature profiles in Figure 4-118 show that the surface waters (top 20 m) were approximately five degrees warmer in November 2008 and 2010 than in 2009. In 2008 and 2009, the water temperature reached approximately 0°C just below a depth of 40 m, but in 2010 the water did not reach 0°C until 100 m depth. This unusually warm water was probably due to the prevalent westward flowing currents between March and October transporting warmer water onto the shelf. The water salinity indicated that the source of the warmer water was from the north rather than the south.

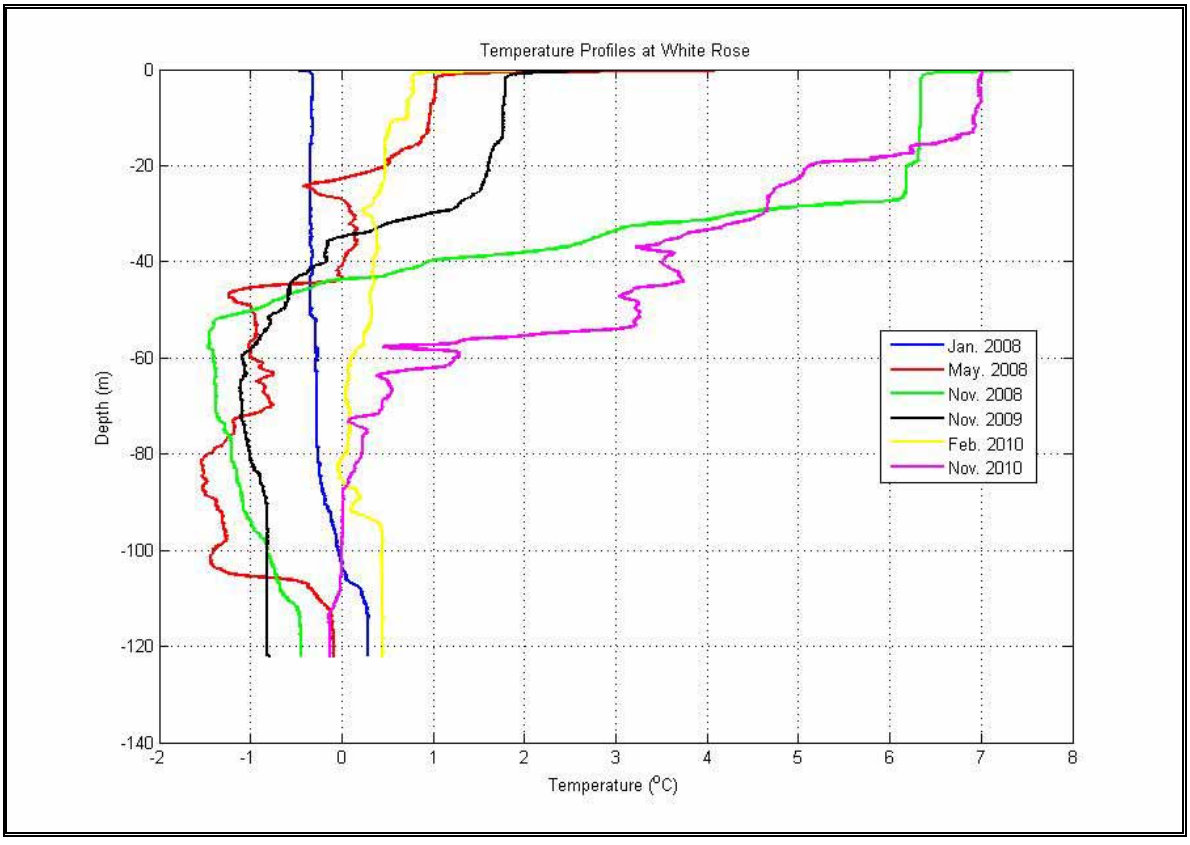

Figure 4-118 Water Temperature Profiles at White Rose (2008 to 2010)

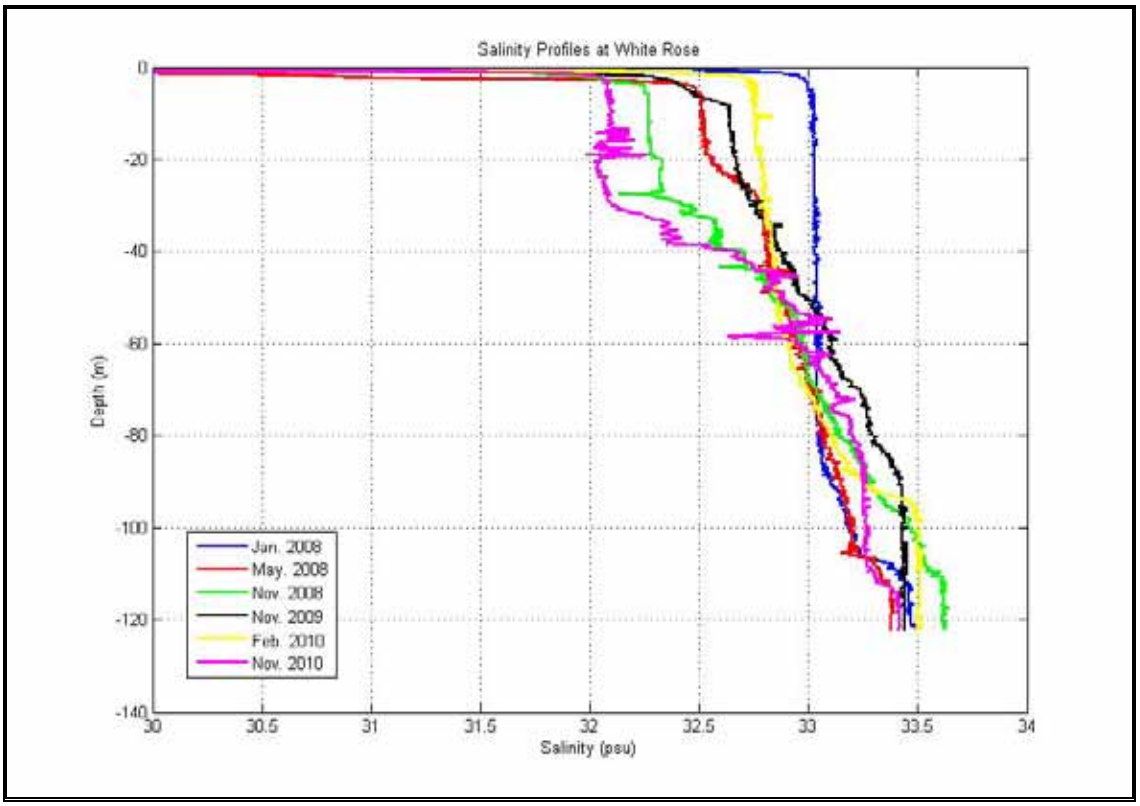

Figure 4-119 Salinity Profiles at White Rose

The temperature profiles show that the water structure is practically isothermal (i.e., temperature does not change with depth) during winter. During May, the 2008 profile shows an influx of colder water as compared to that present during winter between 45 and 105 m depths. This is the Cold Intermediate Layer, characteristic of the water on the Grand Banks during the summer months. The January salinity profile shows that the salinity is approximately 35 psu in the top 60 m of the water column in January and then on a gradient between 33 and 33.5 psu between 60 m and bottom.

Concentrations of the major ions in seawater are directly proportional to the salinity of seawater. Using salinities of 32.5, 33.0 and 33.5 psu for surface, mid-depth and bottom, respectively, the chemical properties at White Rose were calculated to have the values presented in Table 4-67.

Table 4-67 Chemical Composition of Seawater at White Rose

Parameter	Unit	Surface	Mid-depth	Bottom
Chemical Composition		Calculated	Calculated	Calculated
Sodium	(mg/L)	9,995	10,149	10,300
Potassium	(mg/L)	360	365	371
Calcium	(mg/L)	379	385	390
Magnesium	(mg/L)	1,204	1,223	1,241
Chloride	(mg/L)	17,989	18,266	18,540
Bicarbonate	(mg/L)	132	134	136
Sulphate	(mg/L)	2,508	2,546	2,584

4.3.3 Wind and Waves Extremes

Extreme wind and waves were calculated for the White Rose field using the MSC50 hindcast data set. This data set was determined to be the most representative of the available data sets, as it provides a continuous 57-year period of 1 hourly data for the site. All extremes are specified for return periods of 1-year, 10-years, 50-years and 100-years. All wind speeds are referenced to a height of 10 m.

The extreme value analysis for wind speeds was carried out using the peak-over-threshold method. For the extreme wave analysis, two methods were used; the peak-over-threshold method and the joint probability method.

After considering four different distributions, the Gumbel distribution was chosen to be the most representative for the peak-over-threshold method as it provided the best fit to the data. Since extreme values can vary depending on how well the data fits the distribution, a sensitivity analysis was carried out to determine the number of storms to use. The number of storms, the 100-year extreme value, the correlation coefficient and storm threshold were all compared on an annual and monthly basis. The number of storms determined to provide the best fit annually and monthly for each grid point are presented in Table 4-68.

Table 4-68 Number of Storms Providing Best Fit for Extreme Value Analysis of Winds and Waves

		Annually	Monthly
Grid Point 11034	Wind	305	112
	Wave	248	70

4.3.3.1 Wind

The extreme value estimates for wind were calculated using Oceanweather's OSMOSIS software program for the return periods of 1-year, 10-years, 25-years, 50-years and 100-years. The analysis used hourly wind values for the reference height of 10 m above sea level. These values were converted to 10-minute and 1-minute wind values using a constant ratio of 1.06 and 1.22, respectively (US Geological Survey 1979).

A comparison of these values, with actual values measured by platforms in the Grand Banks, was not possible. Logarithmic profiles for adjusting wind speeds from anemometer height to the surface are valid only in neutral or unstable conditions. Observations from platforms on the Grand Banks over the past ten years frequently show stable conditions in which the surface layer wind speed profiles are not valid. Using a logarithmic profile to adjust wind speeds between the 10 m and anemometer level would therefore introduce an unnecessary source of error in the results.

The maximum individual wave heights were calculated within Oceanweather's OSMOSIS software by evaluating the Borgman integral (Borgman 1973), which was derived from a Raleigh distribution function. The variant of this equation used in the software has the following form (Forristall 1978):

$$\Pr\{H > h\} = \exp\left[-1.08311\left(\frac{h^2}{8M_0}\right)^{1.063}\right]; T = \frac{M_0}{M_1}$$

Where: h is the significant wave height,

T is the wave period

M_0 and M_1 are the first and second spectral moments of the total spectrum.

The associated peak periods are calculated by plotting the peak periods of the chosen storm peak values versus the corresponding significant wave heights. This plot is fitted to a power function (y = axb), and the resulting equation is used to calculate the peak periods associated with the extreme values of significant wave height.

The calculated annual and monthly values for 1-hour, 10-minutes and 1-minute are presented in Tables 4-69 to 4-71. The annual 100-year extreme 1-hour wind speed was determined to be 32.0 m/s at Grid Point 11034. Monthly, the highest extreme winds occur during February with a 100-year extreme wind estimate of 31.3 m/s.

Table 4-69 One-hour Extreme Wind Speed Estimates for Return Periods of 1, 10, 25, 50 and 100 Years

Period	Wind Speed 1-hr (m/s)				
	1	10	25	50	100
January	22.6	26.2	27.5	28.5	29.4
February	22.2	27.0	28.7	30.0	31.3
March	20.3	24.5	26.0	27.1	28.2
April	18.0	22.3	23.8	24.9	26.0
May	15.6	19.4	20.8	21.8	22.9
June	14.5	18.3	19.6	20.6	21.6
July	13.4	16.8	18.0	18.9	19.8
August	14.7	21.0	23.3	25.0	26.7
September	17.1	22.3	24.1	25.5	26.9
October	18.4	23.3	25.0	26.3	27.6
November	19.9	24.8	25.7	26.9	28.0
December	21.8	26.3	27.9	29.1	30.3
Annual	25.0	28.6	29.9	31.0	32.0

Table 4-70 Ten-minute Extreme Wind Speed Estimates for Return Periods of 1, 10, 25, 50 and 100 Years

Period	Wind Speed 10-min (m/s)				
	1	10	25	50	100
January	23.9	27.8	29.1	30.2	31.2
February	23.6	28.6	30.5	31.8	33.2
March	21.6	26.0	27.5	28.7	29.9
April	19.1	23.6	25.2	26.4	27.6
May	16.5	20.6	22.0	23.1	24.2
June	15.4	19.4	20.8	21.8	22.9
July	14.2	17.8	19.1	20.1	21.0
August	15.6	22.3	24.7	26.5	28.2
September	18.1	23.6	25.6	27.1	28.5
October	19.5	24.7	26.5	27.9	29.3
November	21.1	26.3	27.3	28.5	29.7
December	23.1	27.9	29.6	30.8	32.1
Annual	26.5	30.3	31.7	32.8	33.9

Table 4-71 One-minute Extreme Wind Speed Estimates for Return Periods of 1, 10, 25, 50 and 100 Years

Period	Wind Speed 1-min (m/s)				
	1	10	25	50	100
January	27.5	32.0	33.5	34.7	35.9
February	27.1	33.0	35.1	36.6	38.2
March	24.8	29.9	31.7	33.1	34.4
April	22.0	27.1	29.0	30.4	31.7
May	19.0	23.7	25.4	26.6	27.9
June	17.7	22.3	23.9	25.1	26.3
July	16.3	20.5	22.0	23.1	24.2
August	17.9	25.6	28.4	30.5	32.5
September	20.8	27.2	29.4	31.1	32.8
October	22.5	28.4	30.5	32.1	33.7
November	24.2	30.3	31.4	32.8	34.2
December	26.6	32.1	34.0	35.5	37.0
Annual	30.5	34.9	36.5	37.8	39.0

4.3.3.2 Waves

The annual and monthly extreme value estimates for significant wave height for return periods of 1-year, 10-years, 25-years, 50-years and 100-years are provided in Table 4-72. The annual 100-year extreme significant wave height is 15.0 m for Grid Point 11034. Monthly, the highest extreme significant wave height occurs during the month of February with an extreme height of 15.0 m.

Table 4-72 Extreme Significant Wave Height Estimates (m) for Return Periods of 1, 10, 25, 50 and 100 Years

Period	Significant Wave Height (m)				
	1	10	25	50	100
January	9.1	12.0	12.9	13.5	14.2
February	8.4	12.1	13.3	14.2	15.0
March	7.1	10.2	11.1	11.9	12.6
April	5.6	8.6	9.6	10.3	11.1
May	4.5	7.1	8.0	8.6	9.2
June	3.7	6.1	6.9	7.4	8.0
July	3.3	5.3	5.9	6.4	6.8
August	3.7	6.8	7.8	8.5	9.3

Period	Significant Wave Height (m)				
	1	10	25	50	100
September	5.1	9.1	10.4	11.4	12.3
October	6.1	9.9	11.1	12.0	12.9
November	7.3	10.5	11.5	12.2	12.9
December	8.8	11.7	12.6	13.3	14.0
Annual	10.8	12.9	13.7	14.4	15.0

During a storm event on January 8, 2007 a maximum individual wave height of 22.6 m was recorded by a waverider in the Terra Nova field. This is greater than the January maximum 10-year return period estimate of 21.8 m for Grid Point 11034, but less than the 25-year return period estimate of 23.5 m. The significant wave height during this event was 9.72 m.

The maximum individual wave heights and extreme associated peak periods are presented in Tables 4-73 and 4-74, respectively. Maximum individual wave heights and the extreme associated peak periods are highest during the month of February.

Table 4-73 Extreme Maximum Wave Height Estimates (m) for Return Periods of 1, 10, 25, 50 and 100 Years

Period	Maximum Wave Height (m)				
	1	10	25	50	100
January	16.7	22.0	23.6	24.9	26.1
February	15.7	22.4	24.5	26.1	27.7
March	13.1	18.9	20.7	22.0	23.4
April	10.3	15.9	17.6	18.9	20.2
May	8.4	14.3	16.2	17.6	19.0
June	7.2	11.5	12.9	13.9	14.9
July	6.3	9.9	11.0	11.8	12.7
August	6.9	12.4	14.2	15.5	16.8
September	9.6	16.7	19.0	20.7	22.3
October	11.5	18.4	20.5	22.2	23.8
November	13.5	19.3	21.2	22.5	23.9
December	16.2	21.7	23.4	24.7	26.0
Annual	19.9	23.7	25.2	26.3	27.4

Table 4-74 Associated Peak Period (s) Estimates for Return Periods of 1, 10, 25, 50 and 100 Years

Period	Associated Peak Period (s)				
	1	10	25	50	100
January	12.7	14.4	14.9	15.2	15.6
February	12.2	14.4	15.0	15.5	15.9
March	11.8	13.3	13.7	14.0	14.2
April	10.8	12.2	12.6	12.9	13.1
May	10.0	11.9	12.4	12.7	13.1
June	8.7	10.9	11.5	11.9	12.3
July	8.3	10.7	11.3	11.8	12.2
August	8.9	11.9	12.7	13.2	13.7
September	10.7	13.3	13.9	14.3	14.8
October	11.4	13.4	13.9	14.3	14.7
November	12.1	13.4	13.7	14.0	14.2
December	12.7	14.3	14.7	15.0	15.3
Annual	13.7	14.9	15.4	15.7	16.0

The annual values for the significant wave height estimates and the associated spectral peak periods are given in Table 4-75. A contour plot depicting these values for return periods of 1-year, 10-years, 25-years, 50-years, and 100-years is presented in Figure 4-120. The extreme wave height for all return periods was higher using the Weibull distribution when compared to the Gumbel distribution.

Table 4-75 Annual Extreme Significant Wave Estimates and Spectral Peak Periods for Return Periods of 1, 10, 25, 50 and 100 Years

	Return Period (years)	Significant Wave Height (m)	Spectral Peak Period Median Value (s)
Grid Point 11034	1	11.5	14.3
	10	13.9	15.6
	25	14.8	16.1
	50	15.5	16.4
	100	16.1	16.8

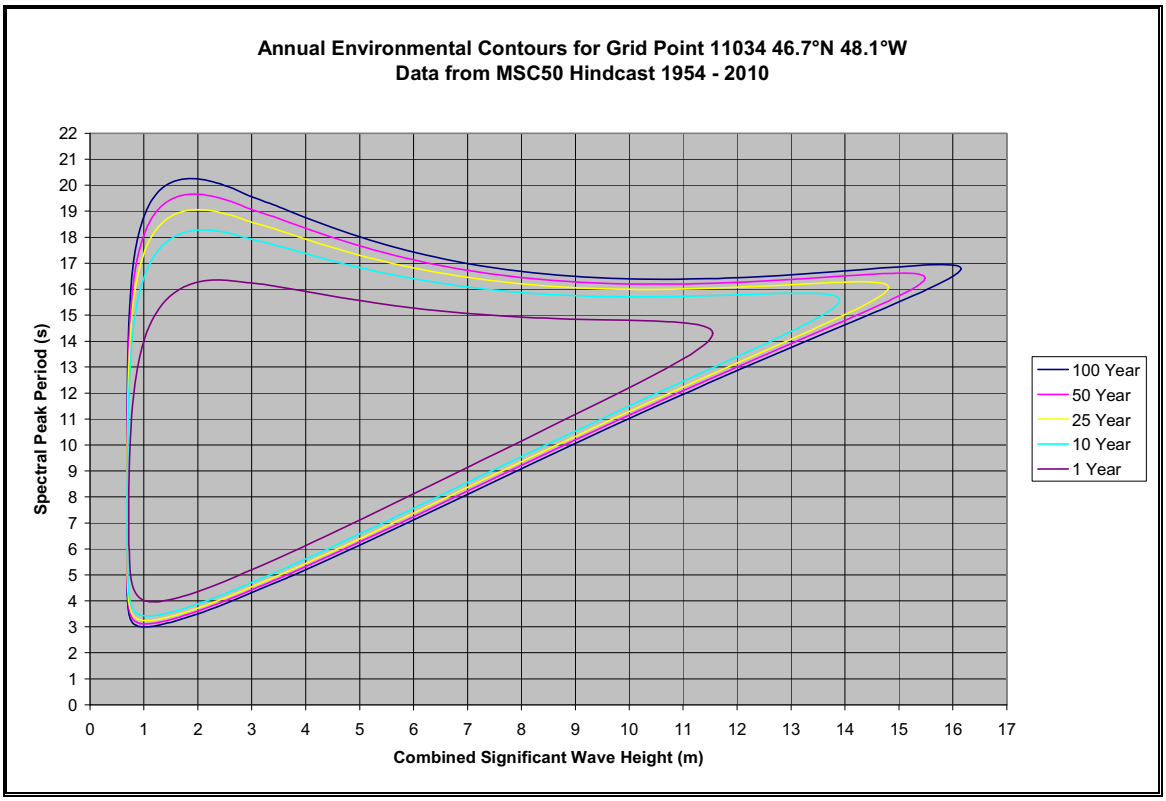

Figure 4-120 Environmental Contour Plot of 1, 10, 25, 50 and 100-year Return Periods for Grid Point 11034 located near 46.3°N; 48.0°W (1954 to 2010)

4.3.3.3 Extreme Temperature Analysis

ICOADS was analyzed to determine the number of days each year that specified thresholds were met. The results are presented in Table 4-76. There were 544 days when the minimum daily temperature decreased below -5°C. Of these, 224 days occurred during the 1980s, 142 occurred during the 1990s and 178 during the 2000s. The temperature decreased below -10°C on only 36 days; half of which occurred during the 1980s. The temperature decreased to below -15°C on only two days. The two days when the temperature decreased below -15°C occurred on March 10 to 11, 1986 when temperatures dropped to -17.3°C. This cold temperature occurred because of pack ice in the area (Figure 4-121) and winds from the northwest.

The extreme temperature analysis was carried out using ICOADS.

Table 4-76 Number of Days below Threshold

Year	Days ≤-5°C	Days ≤-10°C	Days ≤-15°C	Minimum Temperature (°C)
1980	15	1	0	-11.5
1981	6	1	0	-10.0
1982	30	0	0	-9.5
1983	22	1	0	-10.0
1984	27	5	0	-13.5
1985	30	4	0	-11.8
1986	29	3	2	-17.3
1987	12	0	0	-7.2
1988	23	2	0	-10.5
1989	30	2	0	-12.0
1990	32	2	0	-11.0
1991	30	5	0	-11.0
1992	22	1	0	-10.0
1993	15	2	0	-11.2
1994	11	0	0	-7.5
1995	5	0	0	-7.0
1996	6	0	0	-8.0
1997	6	0	0	-8.3
1998	11	0	0	-8.4
1999	4	0	0	-8.0
2000	10	0	0	-8.2
2001	15	1	0	-10.1
2002	27	2	0	-11.5
2003	37	4	0	-12.0
2004	6	0	0	-7.9
2005	12	0	0	-7.9
2006	6	0	0	-9.2
2007	19	0	0	-8.3
2008	22	0	0	-8.8
2009	17	0	0	-8.1
2010	7	0	0	-8.7

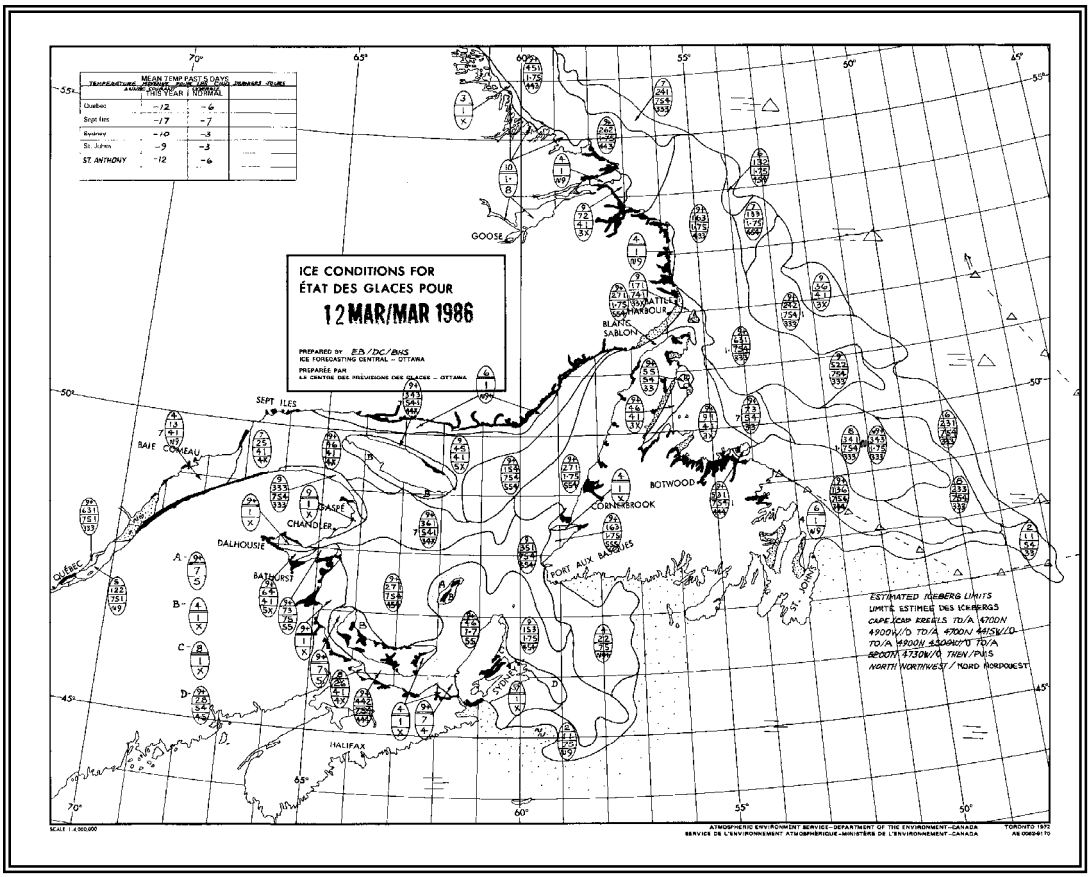

Minimum Temperature

For the minimum temperature analysis, the daily minimum temperature was found for each day in the data set. The 30 lowest minimum temperature events were then chosen with one restriction; no event could occur within five days of another. This restriction ensured that all the chosen events were independent of each other. The lowest minimum temperature event chosen was -17.3°C, which occurred on March 10, 1986. These temperature events were fitted to a Gumbel distribution and extreme value estimates for minimum temperature were calculated for return periods of 2-years, 10-years, 25-years, 50-years and 100-years. These values are given in Table 4-77, together with the 95 percent confidence intervals.

Table 4-77 Extreme Minimum Temperature Estimates for Return Periods of 2, 10, 25, 50 and 100 Years

Return Period (years)	Annual Probability of Exceedance	Extreme Minimum Temperature (°C)	95% Lower Confidence Bound (°C)	95% Upper Confidence Bound (°C)
2	0.5	-11.8	-12.4	-11.3
10	0.1	-14.8	-16.2	-13.3
25	0.04	-16.3	-18.3	-14.3
50	0.02	-17.4	-19.8	-15.0
100	0.01	-18.5	-21.3	-15.7

Maximum Temperature

For the maximum temperature analysis, the daily maximum temperature was found for each day in the data set. The 30 highest maximum temperature events were then chosen with one restriction; no event could occur within five days of another. This restriction ensured that all the chosen events were independent of each other. The highest maximum temperature event chosen was 22.5°C, which occurred on August 29, 2005. These temperature events were fitted to a Gumbel distribution and extreme value estimates for maximum temperature were calculated for return periods of 2-years, 10-years, 25-years, 50-years and 100-years. These values are given in Table 4-78 together with the 95 percent confidence intervals.

Table 4-78 Extreme Maximum Temperature Estimates for Return Periods of 2, 10, 25, 50 and 100 Years

Return Period (years)	Extreme Maximum Temperature (°C)	95% Lower Confidence Bound (°C)	95% Upper Confidence Bound (°C)
2	20.71	20.33	21.09
10	22.65	21.70	23.60
25	23.63	22.33	24.93
50	24.35	22.79	25.92
100	25.07	23.24	26.90

4.3.4 Sea Ice and Icebergs

The following sections provide a description of the ice environment surrounding the White Rose field. This description uses as its foundation, data from the Provincial Aerospace (PAL) and IIP iceberg databases, Environment Canada CIS Ice Atlas and MANICE publications. These data have been supplemented with subsequent data and reports from 2000 to 2011. A reworking of the site-specific information was undertaken to account for the different ice regime at the White Rose field.

The White Rose field lies approximately 363 km southeast of St. John's, on the eastern slope of the continental shelf, making it susceptible to seasonal incursions of ice. Two different forms of floating ice, sea ice and icebergs, are present in this marine environment. Sea ice is produced when the ocean's surface layer freezes. On the White Rose field, sea ice is loosely-packed and pressure-free. Floes are small and generally in advanced stages of deterioration, permitting easy vessel movement. Despite this, sea ice can interfere with iceberg detection and management operations.

Icebergs are freshwater ice made from snow compacted in a glacier. When the leading edge of a glacier reaches the sea, slabs of ice fall from it, creating icebergs. Grand Banks icebergs originate primarily from the glaciers of West Greenland. Ice management efforts in this area focus on icebergs, as they pose a potential hazard to offshore production facilities.

A summary of the characteristics of sea ice cover and a description of icebergs is provided in the following sections. Extreme conditions are included because they illustrate how the ice regime varies over time and space. Such variability is important when assessing the effect of ice on offshore development. This section of the report concludes with a summary of current ice management practices by operators in the offshore production fields.

4.3.4.1 Sea Ice

Formation and growth

Seawater, when cooled through atmospheric heat exchange, increases in density. It then sinks to a depth determined largely by the salinity of the upper ocean. In polar and sub-polar regions, this process eventually produces a relatively well-defined surface layer of water at its freezing temperature. Further loss of heat to the atmosphere causes ice growth. Ice growth is governed by:

- Air temperature
- Wind speed
- Sea state
- Levels of snow accumulation
- Magnitudes of heat fluxes from deeper, warmer ocean layers
- Ice deformation driven by winds and currents.

Major categories of sea ice age and thickness are listed in Table 4-79. Almost all of the ice occurring near White Rose is either young or first-year ice between 30 and 100 cm thickness. Some thicker first-year ice also occurs. Ice thicknesses that are greater than 100 cm are usually only associated with deformed first-year ice. Old ice, which is ice that has survived one or more summer melt seasons, appears very rarely in the White Rose area. It is denser and harder than regular sea ice because it has been refrozen many times and much of its brine has leached out. Old ice is difficult to detect within the ice pack but, in practical terms, poses the same threat to vessels as growler and bergy bit-sized iceberg fragments.

Table 4-79 Characterization of Sea Ice by Type, Thickness and Age

Ice Type/Stage of Development	Thickness (cm)	Age/Period of Formation
New Ice	<10	Seasonal ice: Earliest stage of development
Young (Grey) Ice	10 to 15	Seasonal ice: Generally early season
Young (Grey-White) Ice	15 to 30	Seasonal ice: Generally early to mid-season
Thin First-Year (White) Ice	30 to 70	Seasonal ice: Generally mid- to late season
Medium First-Year Ice	70 to 120	Seasonal ice: Generally late season
Thick First-Year Ice	>120	Seasonal ice: Generally late season
Second-Year/Multi-Year/Old Ice	>120	Perennial ice
Source: Meteorological Service of Canada CIS MANICE 2005		

Spatial Distribution

The White Rose field lies close to the extreme southern limit of the regional ice pack. In this area, relatively high water temperatures dissipate the last remnants of ice that have drifted south from original ice growth areas in Baffin Bay, Davis Strait and the Labrador Sea.

The annual regional ice cycle begins in September with the growth of new ice in Northwest Baffin Bay. In October, sea ice accumulates and drifts southward with help from the prevailing northerly winds and the Baffin Current. By December, the leading edge of the advancing ice pack lies off northern Labrador. Simple modeling estimates (Marko et al. 1994a) suggest that in April, 60 to 80 percent of the ice south of 55°N was grown in areas north of 60°N.

In typical years, the ice edge reaches the northern tip of Newfoundland in early January and the Grand Banks in mid-February (National Climate Data Center 1986). The pack ice off Newfoundland generally reaches annual peak coverage in March, but can remain at high levels through May. Thicker first-year or white ice becomes the dominant ice form in areas off Newfoundland beginning in March, just before water temperatures rise above the freezing level.

By the end of July, the ice pack retreats rapidly northward, with substantial ice concentrations confined to north of Labrador. Occasionally, first-year ice remnants linger at the end of the summer season off the east coast of Baffin Island, near 70°N. These remnants, together with late discharges of first-year and older ice from Lancaster, Jones and Smith sounds, are the source of the old ice that can appear off Labrador the following ice season (Markham 1980).

Seasonal frequency of presence of sea ice coverage in Newfoundland and Labrador waters is shown for mid-months of January through May in Figures 122 to 4-126. The charts show the likelihood, in a given month, of ice greater than or equal to 1/10 concentrations. The 100 percent line represents the minimum extent of sea ice; within it there has always been ice reported in the period. On the charts, 1 to 33 percent depicts an above-normal extent, 34 to 66 percent depicts near-normal and 67 to 99 percent conveys a below-normal extent. Beyond the one percent line, no ice data were reported in the dataset (CIS 2011).

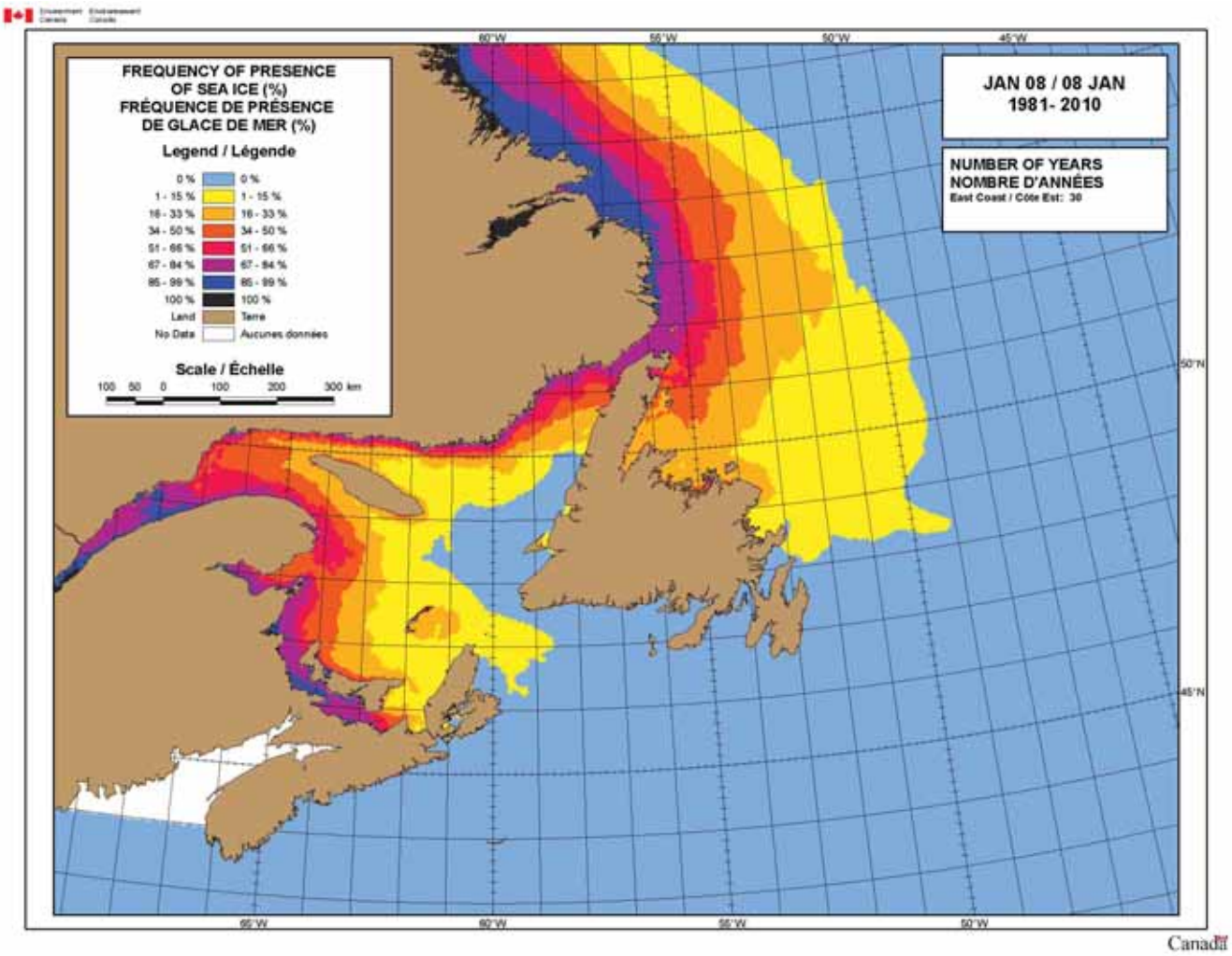

Source: Environment Canada CIS 2011

Figure 4-122 Frequency of Pack Ice Cover: Week of January 8 (1981 to 2010)

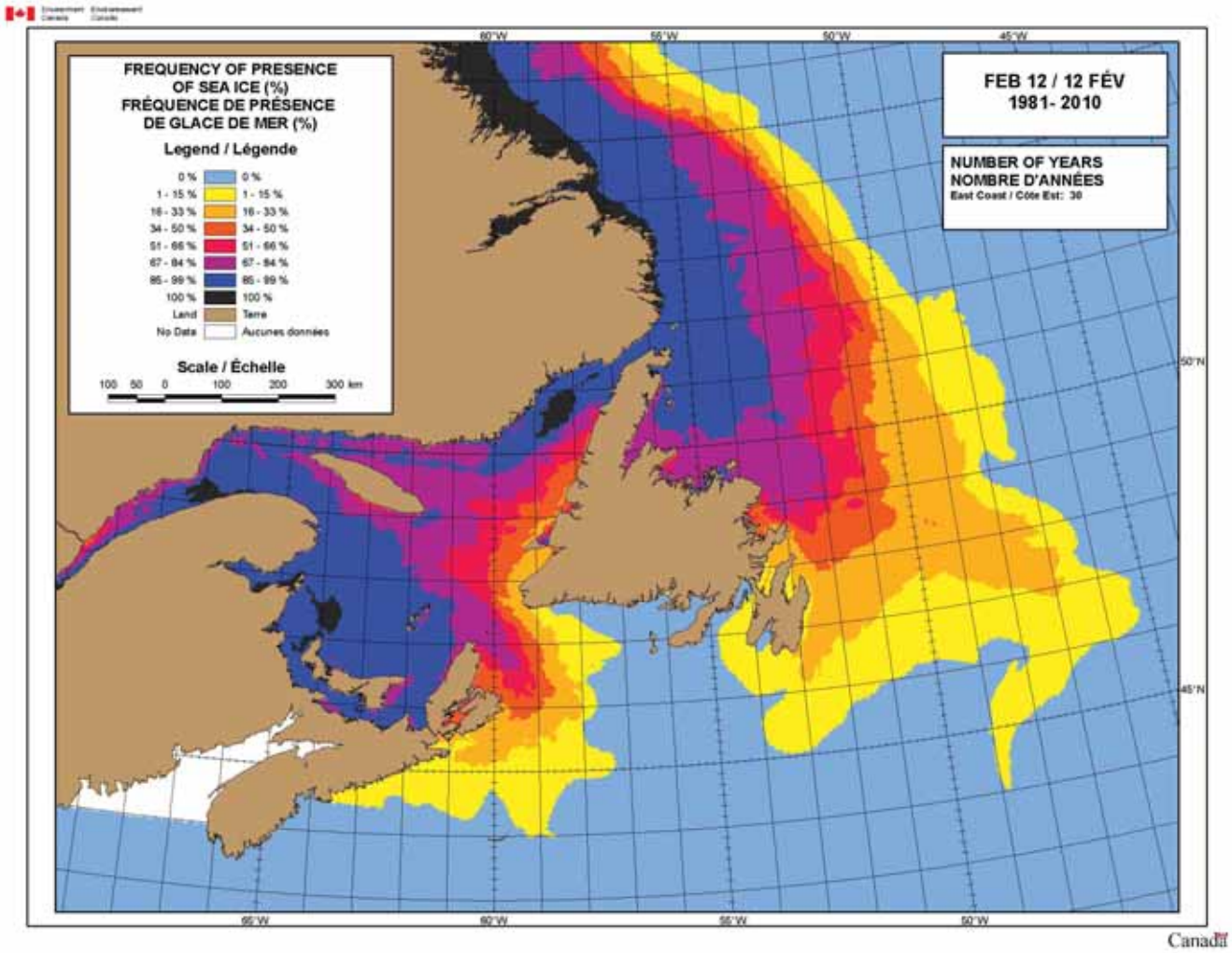

Source: Environment Canada CIS 2011

Figure 4-123 Frequency of Pack Ice Cover: Week of February 12 (1981 to 2010)

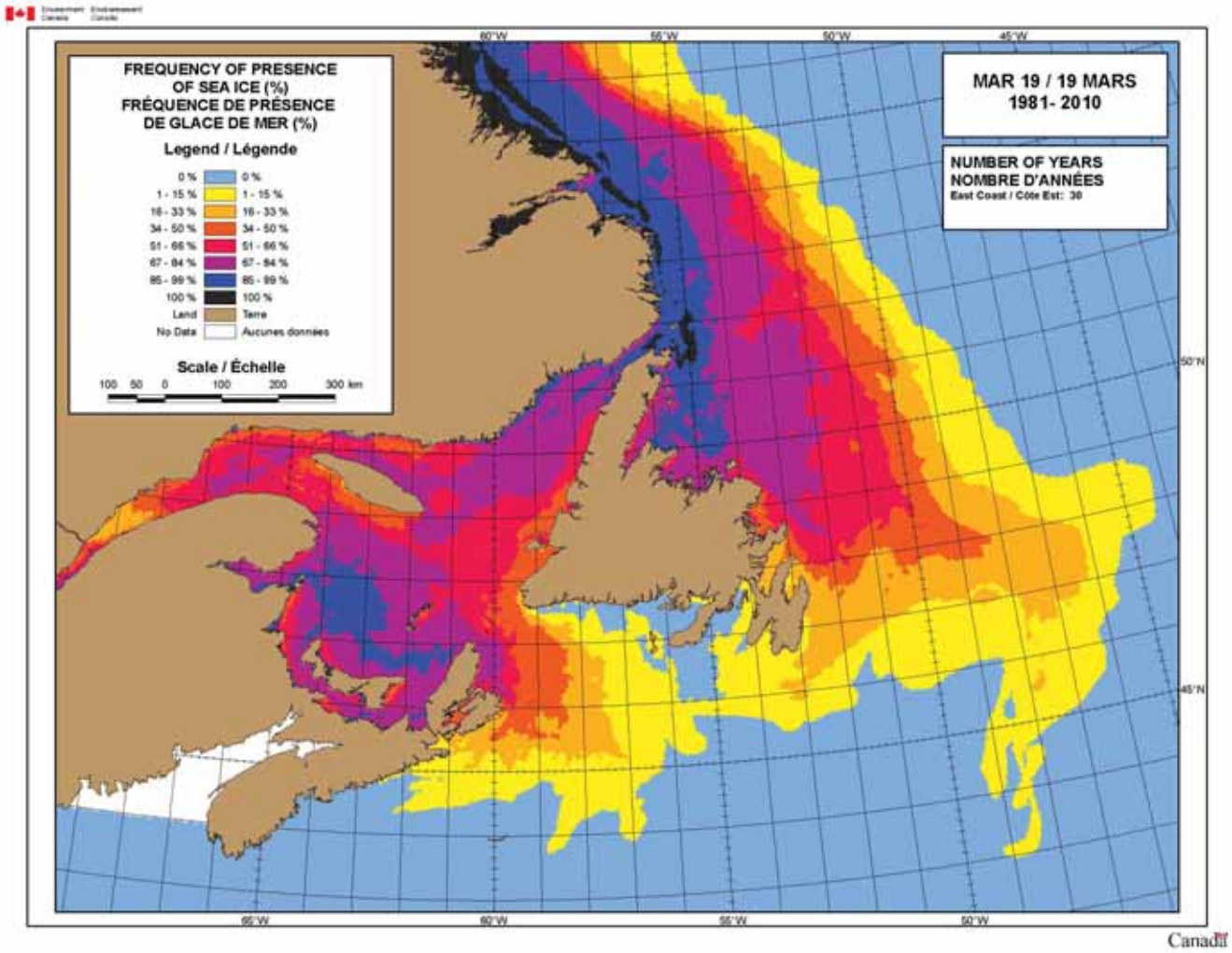

Source: Environment Canada CIS 2011

Figure 4-124 Frequency of Pack Ice Cover: Week of March 19 (1981 to 2010)

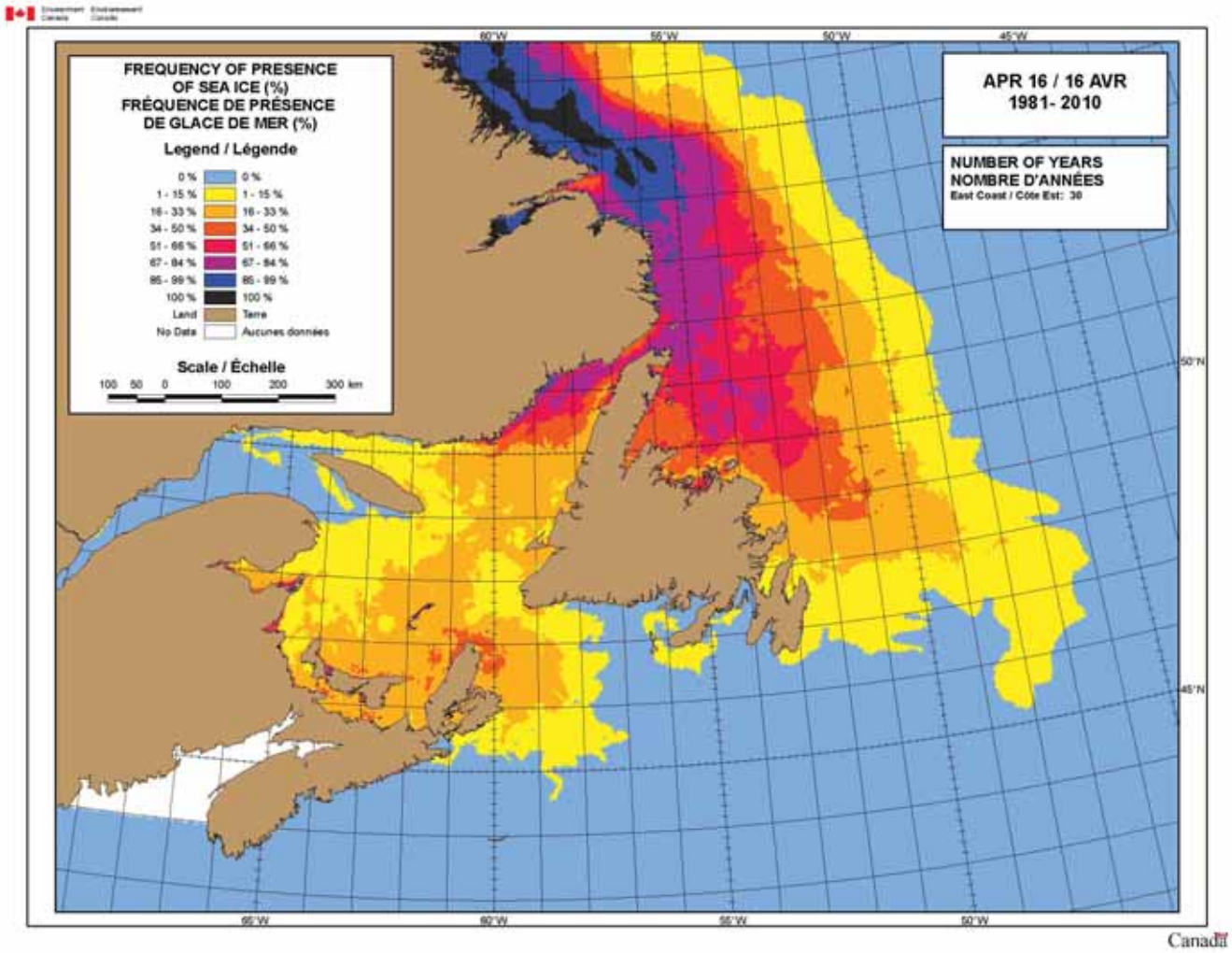

Source: Environment Canada CIS 2011

Figure 4-125 Frequency of Pack Ice Cover: Week of April 16 (1981 to 2010)

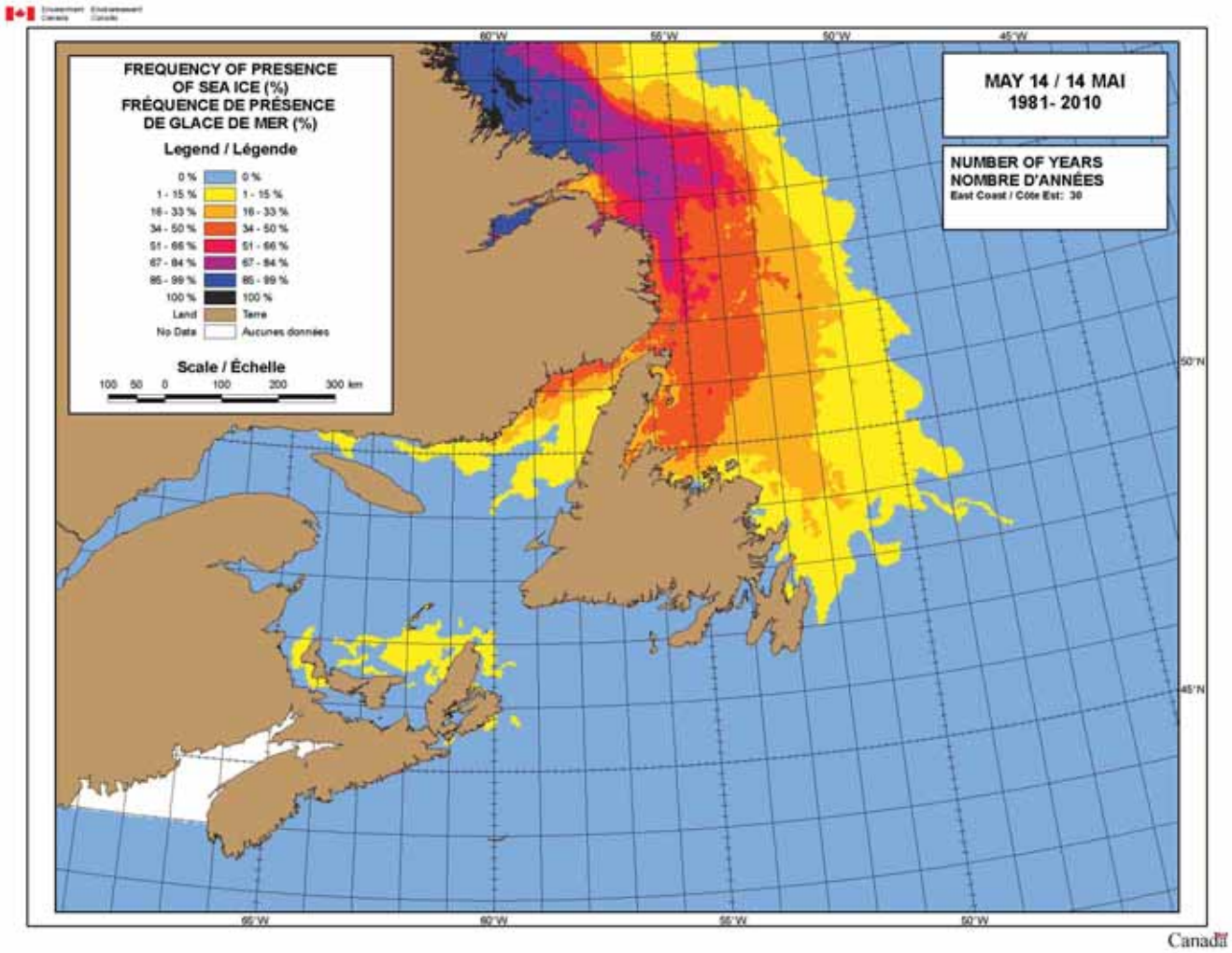

Source: Environment Canada CIS 2011

Figure 4-126 Frequency of Pack Ice Cover: Week of May 14 (1981 to 2010)

The annual timing of all ice incursions near the White Rose field, from 1980 to 2012, is shown in Figure 4-127. These data show the years of higher-than-average incursion (1983 to 1995, 2000 and 2008). The maximum recorded incursion of sea ice for east Newfoundland waters occurred in 1993 and is illustrated in Figure 4-128.

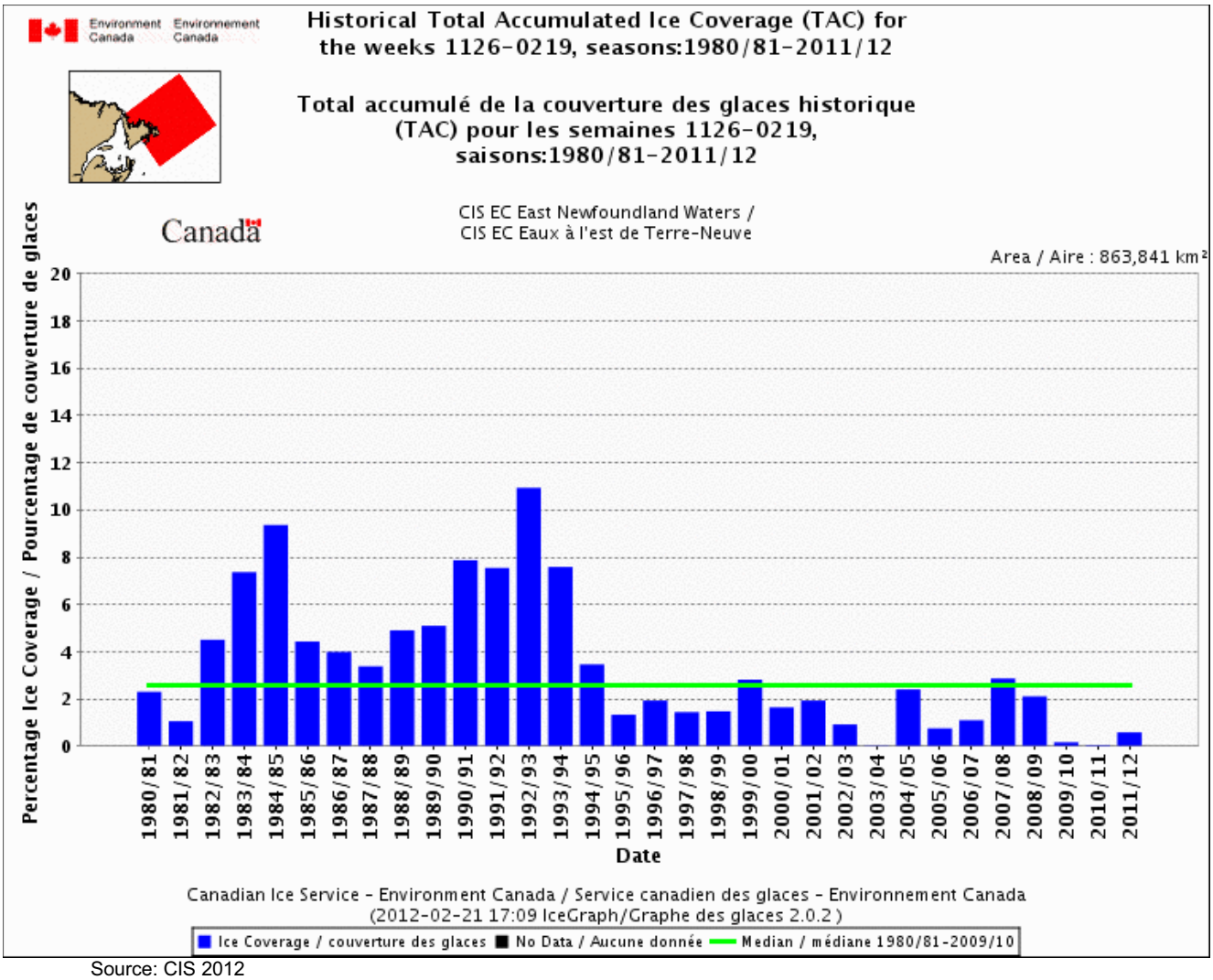

Source: CIS 2012

Figure 4-127 Historical Total Accumulated Ice Cover by Season (1980 to 2012)

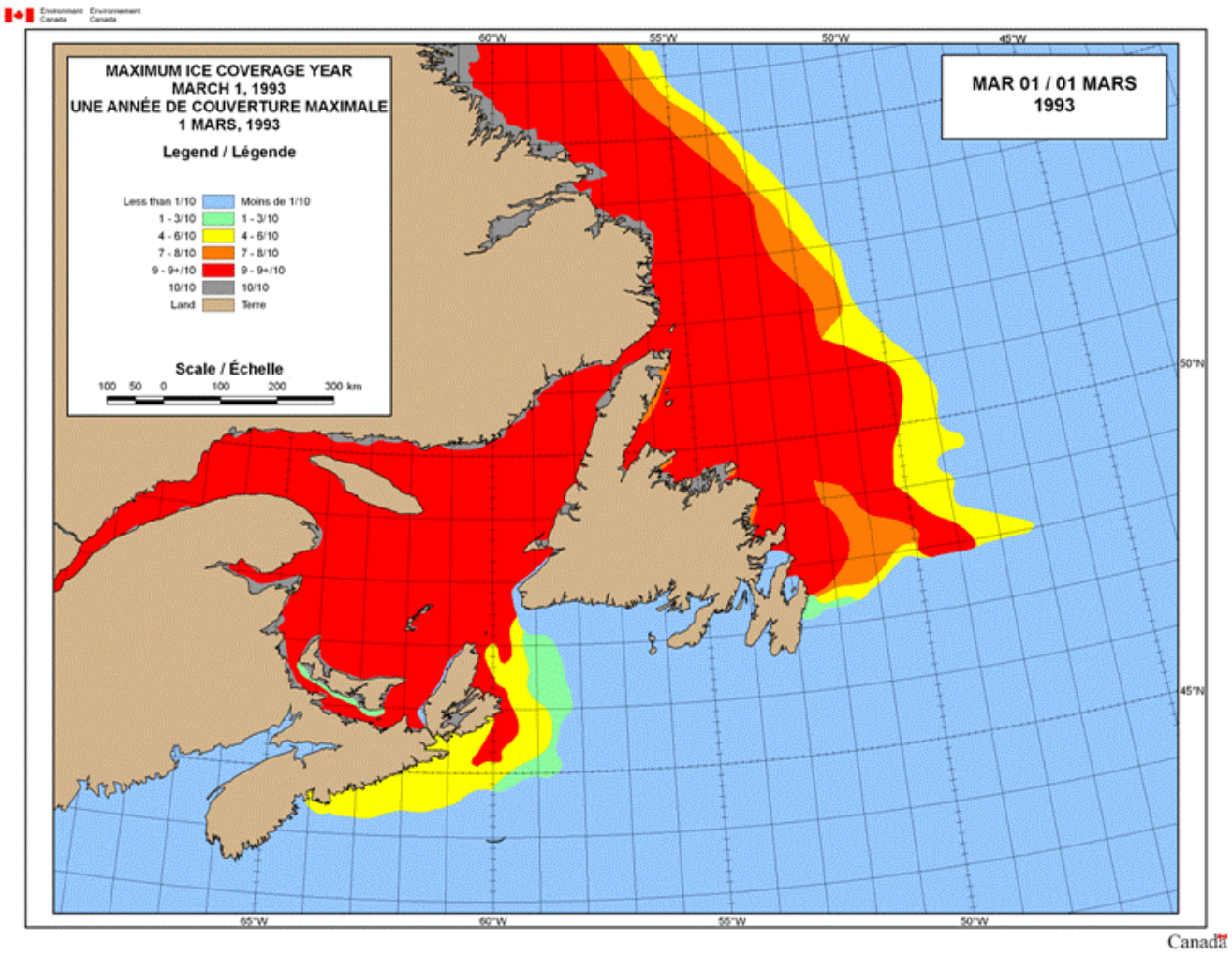

Source: CIS 2011

Figure 4-128 Maximum Recorded Incursion of Sea Ice for East Newfoundland Waters

Sea Ice Movement

While the position of White Rose is at the extreme southern limit of the regional ice pack, it does lie just to the west of the path of the ice tongue that is formed by the loose pack ice being swept around the Grand Banks by the offshore branch of the Labrador Current.

The principal circulation features of the region include:

- Strong easterly and southerly movements associated with the offshore branch of the Labrador Current on the northern and eastern slopes of the Grand Banks.
- A weaker southerly drift, evident in the Avalon Channel, associated with a continuation of the inner branch of the Labrador Current.
- Over the body of the Grand Banks, a mean flow that is weaker and less definitive in direction.

- Extreme variability of velocities of ice and surface currents. Their standard deviations are comparable to or larger than their corresponding long term temporal averages.

Concentrations

The median sea ice concentrations for the Grand Banks south of 49°N are usually between 4/10 and 6/10 by early February and persist at this concentration through early April, after which they slowly decrease to 1/10th to 4/10ths coverage and recede to above 49°N, as illustrated in Figure 4-129 (the term “Central Value” was determined by averaging the minimum and maximum median concentrations of sea ice found below 49°N in each given week over the 30-year period between 1981 and 2010).

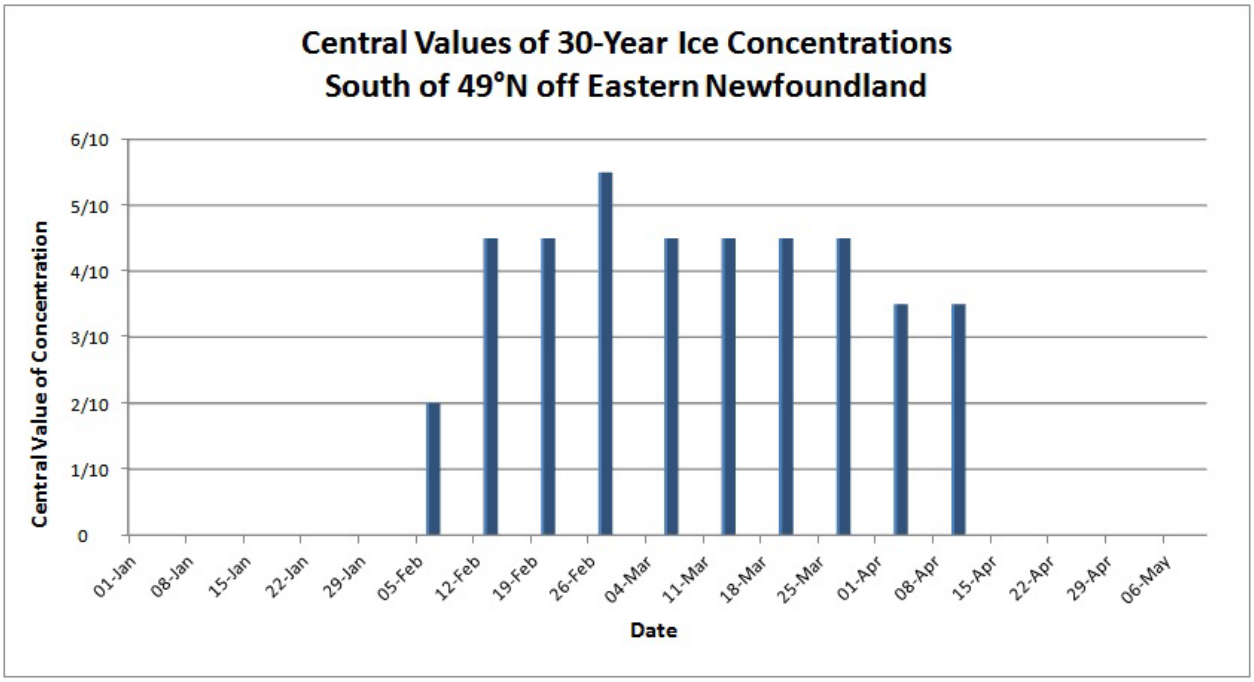

Source: CIS 2011

Figure 4-129 Central Values of 30-Year Median Ice Concentrations South of 49°N on the Grand Banks (1981 to 2010)

The White Rose field can be affected by the seasonal ice tongue. Current patterns are largely dictated by bathymetry, and since the White Rose field is located near the 200 m depth contour, it is subject to incursions of the seasonal ice tongue. Ice concentrations in the tongue vary from 2/10 in light years to 9/10 in extreme years.

Floe Size

An ice floe is any relatively flat piece of ice 20 m or more across. They can be broken into size categories of small (20 to 100 m), medium (100 to 500 m), big (500 to 2000 m), vast (2 to 10 km) and giant (greater than 10 km). The horizontal dimensions of individual ice floes are influenced by:

- Ice history
- Ice concentration
- Thickness
- Water temperature
- Sea state
- Proximity to land.

In Newfoundland waters, a distinction is made between the size of floes located within approximately 100 km of the coastline (inshore area) and those in areas north and south of the 49°N boundary of the Grand Banks (offshore areas). Large floes occur more often in the inshore area because of:

- Physical confinement
- Colder air
- Colder water temperatures
- Damping of wave amplitudes by seaward ice.

In both offshore areas, floe sizes are smaller south of 49°N because of:

- Melting
- Fracturing
- Higher water temperatures
- Sea states.

In both offshore regimes, floe size decreases from west to east because of progressive increases in wave amplitudes propagating into the pack ice from the open ocean.

The Meteorological Service of Canada supports the CIS, which compiles composite ice chart data. Estimates made in several earlier studies (Blenkarn and Knapp 1969; Nolte and Trethart 1971; LeDrew and Culshaw 1977; Dobrocky Seatech 1985) indicate that mean floe diameters in offshore areas south of 49°N are less than 30 m. Only a few floes with diameters larger than 60 m were observed.

A northwest-to-southeast size gradient was also identified (Dobrocky Seatech 1985). In the vicinity of White Rose, the mean floe diameter decreased from 8 m to 1m at 49°N and 51°W.Maximum floe diameter decreased from 37 m to 3 m. These values were determined from reviews of research between 1971 and 1985 (Seaconsult Ltd. 1988). Mean and maximum diameters may be an order of magnitude larger (Seaconsult Ltd. 1988) when the ice extent is close to its seasonal maximum in years of exceptionally severe ice conditions.

There is evidence that many of the larger floes recorded in the cited studies were observed on coarse resolution (1 km) satellite images. It is likely that these floes are conglomerates of smaller floes bound at their peripheries by newly grown, thinner ice (Petro-Canada 1995).

Thickness

Physical growth of sea ice on the Grand Banks primarily occurs south of the main pack edge and in leads and open patches within the pack. This is 'new ice' (Table 4-79), and is usually formed in calm wind conditions. It tends to be short-lived as a distinct entity. Wave action tends to disperse it and it melts in later warmer periods. Often it is incorporated into adjacent floes and deformed ice structures.

Most of the sea ice found on the Grand Banks is formed in upstream areas and increases in thickness during subsequent southward drift during the ice season. Most of the ice coverage within 15 km of the White Rose field ranges from 25 to 120 cm in thickness. Average thickness of undeformed sea ice near the White Rose field is illustrated in Figure 4-130. These data were derived subjectively from CIS 1981 to 2010 ice chart data for periods of ice coverage that exceeded four weeks in duration.

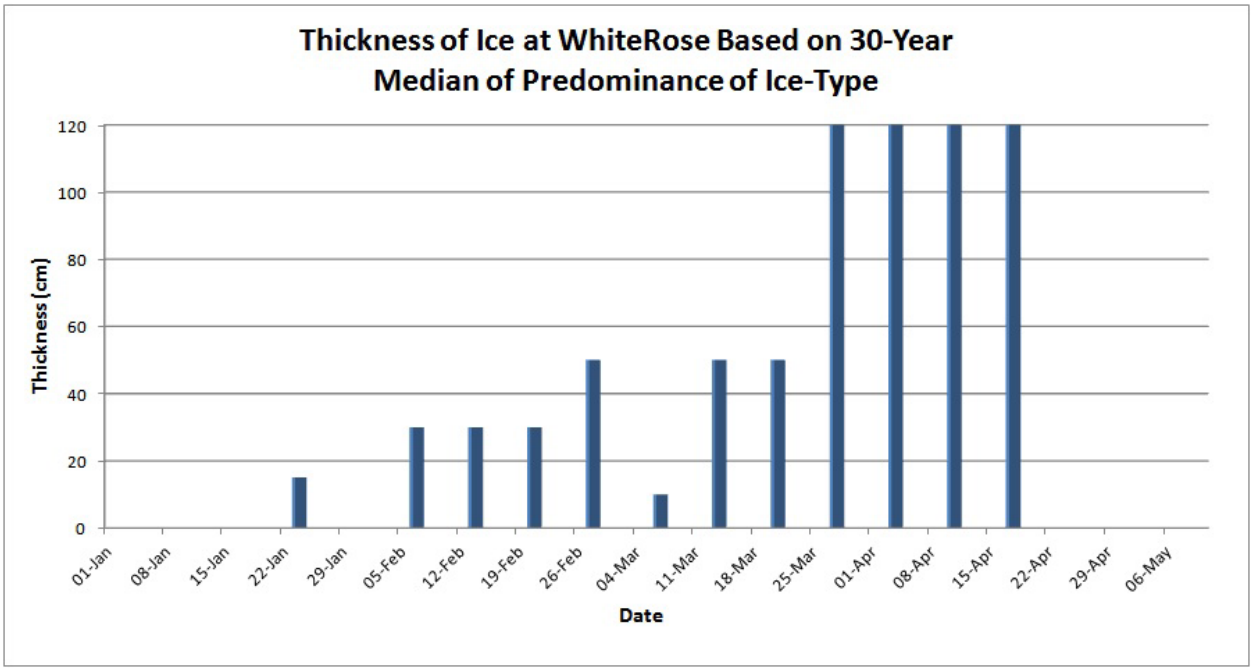

Source: CIS 2011

Figure 4-130 Average Ice Thickness at the White Rose Field (1981-2010)

Deformation

The maximum thickness of undeformed sea ice is largely determined by:

- Heat flow from the ocean at the under-surface of the ice
- Rate of heat loss at the ice surface.

Ice on the northern Grand Banks that is thicker than approximately 50 cm has drifted from colder, more northern areas, as noted earlier, or is present through ice deformation.

Most types of sea ice deformation occur in highly-concentrated (approximately 10/10 concentration) pack ice, typically near land. Deformations are classified as rafting, ridging or hummocking (Figure 4-131). Rafting occurs when one sheet of ice overrides an adjacent sheet. Ridging is produced by repeated local failures at a common boundary between two sections of relatively undeformed ice. The third category, hummocking, refers to a much wider spatial distribution of randomly scattered broken and upturned ice blocks, generally in a piled formation resulting from excess pressure and heaping.

Quantitative data on deformed ice are usually confined to ridge type deformations because they can be easily characterized by:

- Frequency (number of ridges/km)
- Length
- Width
- Maximum top-to-bottom thickness (sail height plus keel depth).

Few quantitative data are available for the Grand Banks region, in part because linear ridge formations of the type commonly observed in Arctic areas are relatively rare. Instead, the deformed pack ice consists of fields of confused jumbles of uplifted and broken floes (Petro-Canada 1995). Observations indicate that maximum sail heights, corresponding to local peak heights in such fields, are approximately 2 m (Dobrocky Seatech 1985). Nolte and Trethart (1971) calculated average ridge heights of approximately 1 m. These estimates are reasonably consistent with airborne electromagnetic sensor measurements in Newfoundland areas farther inshore (Prinsenberg et al. 1993).

Ridge thicknesses for the Grand Banks have also been estimated from data gathered off southern Labrador during February and early March and extrapolated to the Grand Banks (Seaconsult Ltd. 1988). These estimates indicate that ridges or rubble fields with sails as large as 3.5 m could form on the Grand Banks (Bradford 1972; NORDCO Ltd. 1977). However, these estimates are offset by the fact that the farther south the ice deformations occur, the faster the rafted and upturned floes, as well as the thin binding ice between the floes, will melt. As the melting occurs, structural fragility and ice porosity increase. This reduces the operational hazards of any ridge or rubble field fragments surviving to well below those associated with smaller pieces of old or glacial ice.

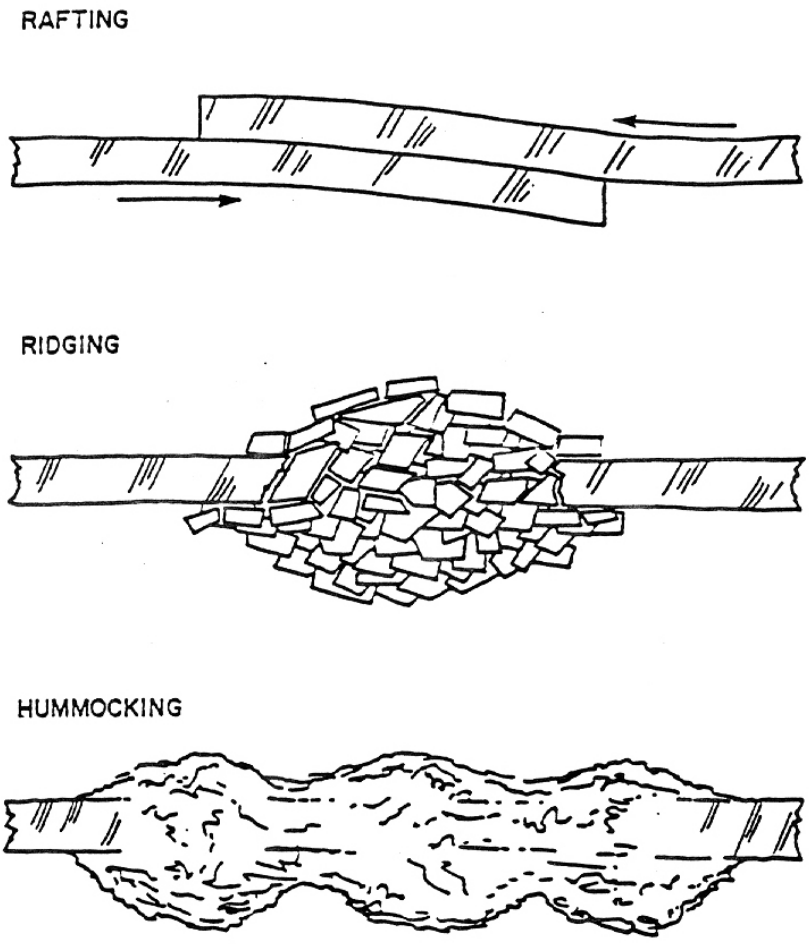

(b) Typical Strucure of Marginal Pack Ice

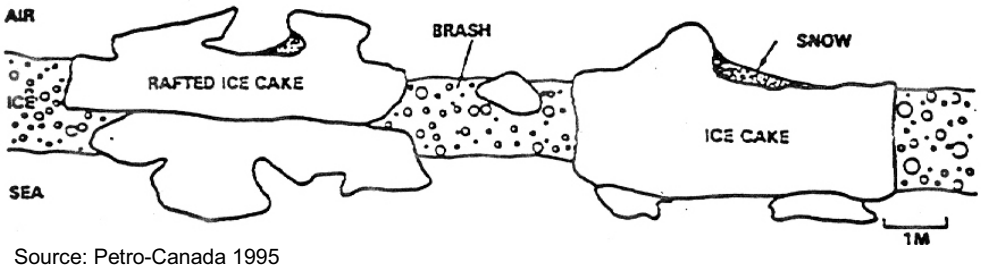

Source: Petro-Canada 1995

Figure 4-131 Sea Ice Deformation Types

4.3.4.2 Icebergs

Origins and Controlling Factors

Glacial ice is formed from the accumulation of snow, which gradually changes form as it is compressed into a solid mass of large granular ice. This process produces a structure quite different from pack ice. The principal origins of the icebergs that reach the White Rose field location are the tidewater glaciers of West Greenland. Between 10,000 and 15,000 icebergs are calved each year, primarily from 20 major glaciers between the Jacobshaven and Humboldt glaciers. These glaciers account for 85 percent of the icebergs that reach the Grand Banks. Of the remaining icebergs, 10 percent come from the East Greenland glaciers and 5 percent from the glaciers and ice shelves of Ellesmere Island.

The basic regional circulation pattern shown in Figure 4-132 reflects the predominant strong cyclonic ocean currents centred on the continental slopes. Most icebergs reaching Newfoundland and Labrador initially move northward, taking a year or so to reach northwestern Baffin Bay. In the interim, the icebergs melt, fracture and subdivide, reducing their size by a factor of approximately two, on average. Many icebergs never reach northwestern Baffin Bay because of long term or repeated groundings accompanied by melting in shallow waters off West Greenland. Similar iceberg losses occur in waters adjacent to Baffin Island and Labrador during the warm ice-free months.

There is considerable evidence that most icebergs reaching offshore Newfoundland each spring and summer have drifted southward across 75°N between September and November of the previous year (Marko et al. 1994b). These icebergs avoid substantial depletion during subsequent winter drift past the Baffin Island and Labrador coastlines.

Deterioration of icebergs during subsequent southward drift determines seasonal iceberg severities in offshore Newfoundland. The number of icebergs that survive to reach the Grand Banks each spring has been shown to have a direct relationship to the pack ice extent off Labrador in the winter and early spring (Marko et al. 1994b). In other words, when the pack ice covers the core of the Labrador Current, iceberg counts for the Grand Banks increase markedly per unit increase in pack ice cover.

According to the IIP and PAL, the number of icebergs reaching the Grand Banks (48 degrees latitude) each year varied from a low of zero in 1966, 2006 and 2011, to a high of 2,202 in 1984 (Figure 4-133). Of these, only a small portion will pass through the White Rose field.

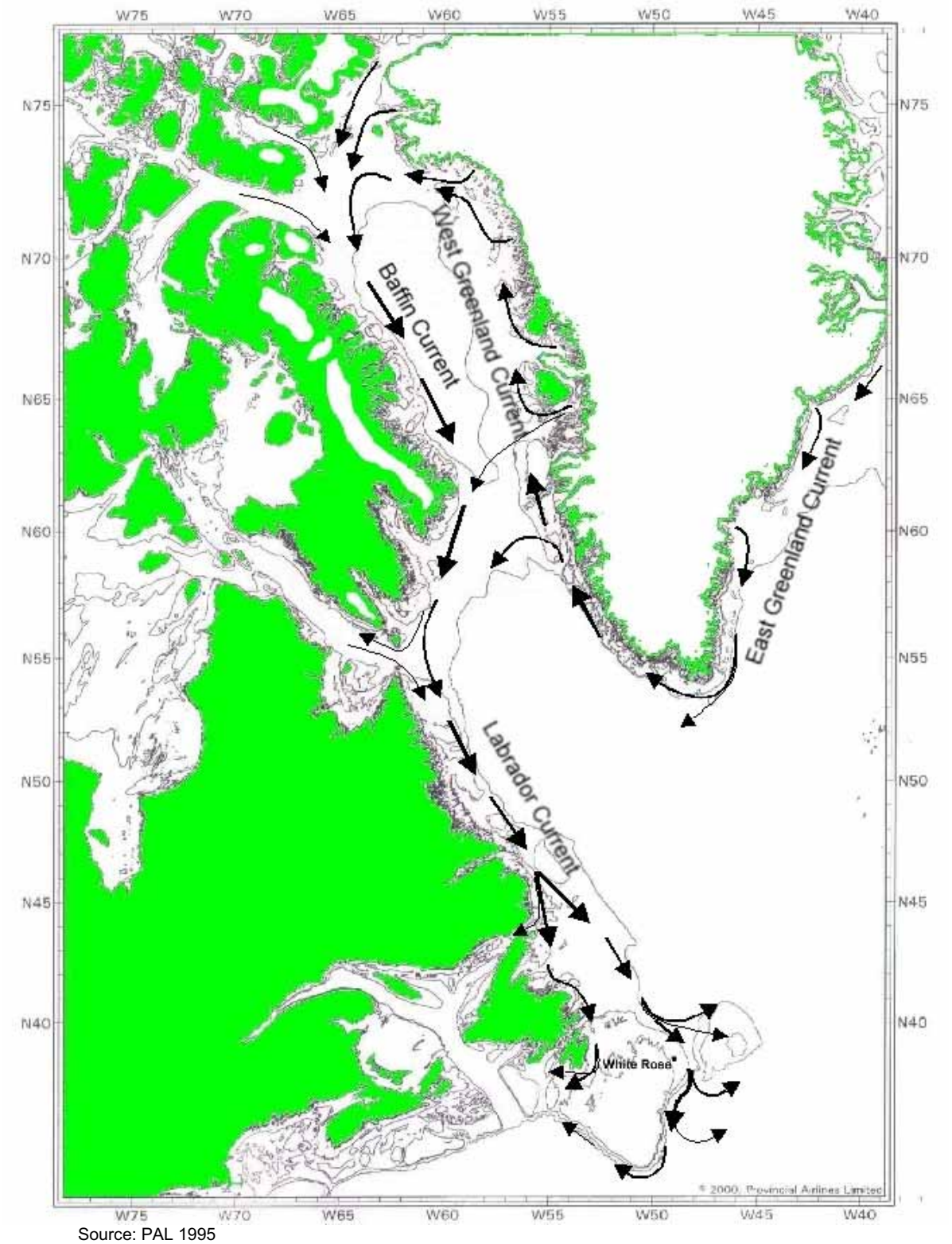

Source: PAL 1995

Figure 4-132 Iceberg Circulation

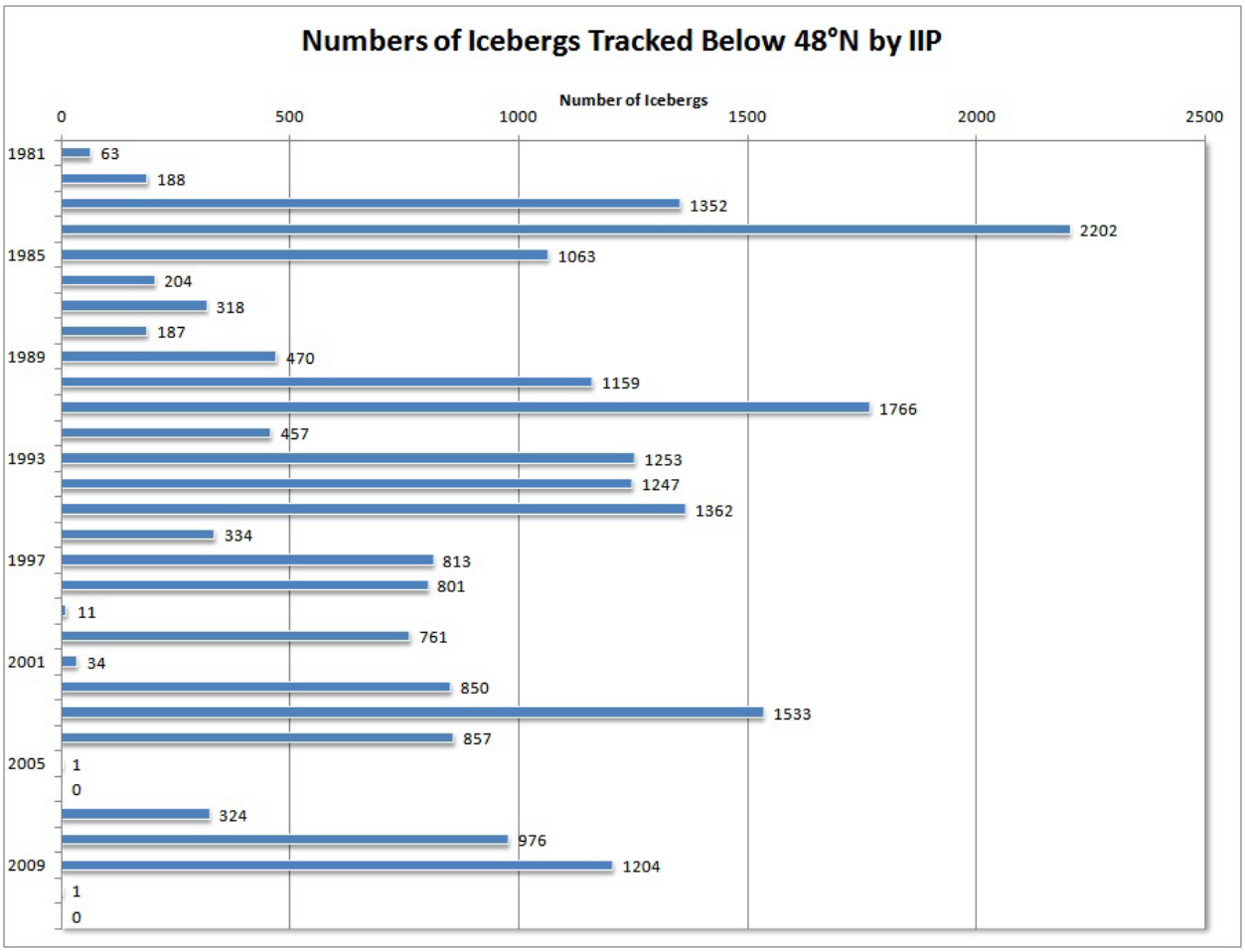

Source: IIP 2011

Figure 4-133 International Ice Patrol Annual Count of Icebergs Crossing 48°N

Variations in Local and Regional Iceberg Numbers

The number of icebergs off eastern Canada varies considerably both annually and monthly; the number of icebergs on the Grand Banks peaks in mid-April to late-May and their approach to 48°N varies. Extremes in iceberg distributions between March and May of two years; 2009 and 2010, are illustrated in Figures 4-134 and 4-135. These years were selected as 2009 was a particularly heavy year for icebergs on the Grand Banks, while 2010 was an exceptionally light year. Typically, icebergs and pack ice begin drifting south of 48°N around March, signaling the start of the “ice season” on the Grand Banks. In 2009 the ice season started on February 16 (earlier than average) and closed on July 31. In the 2010 season did not officially open as no icebergs or pack ice were confirmed as having crossing 48°N.

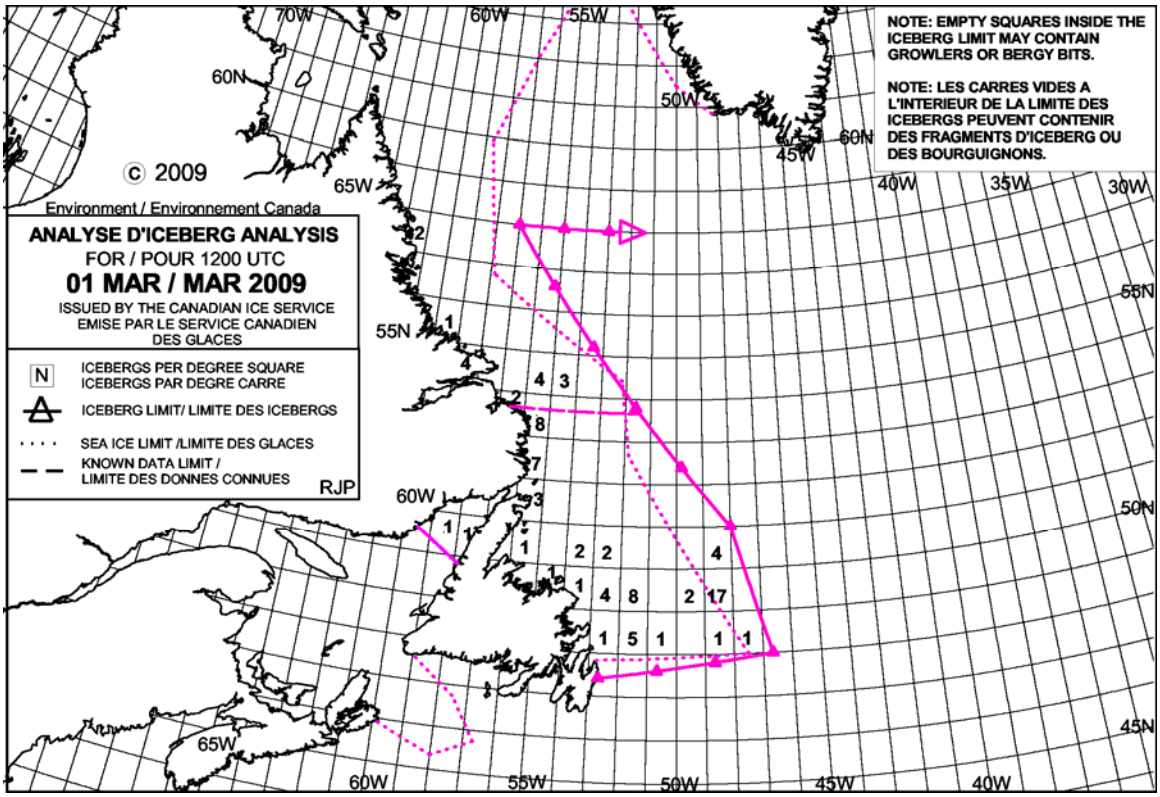

Figure 4-134a Minimum Extent of Icebergs in 2009

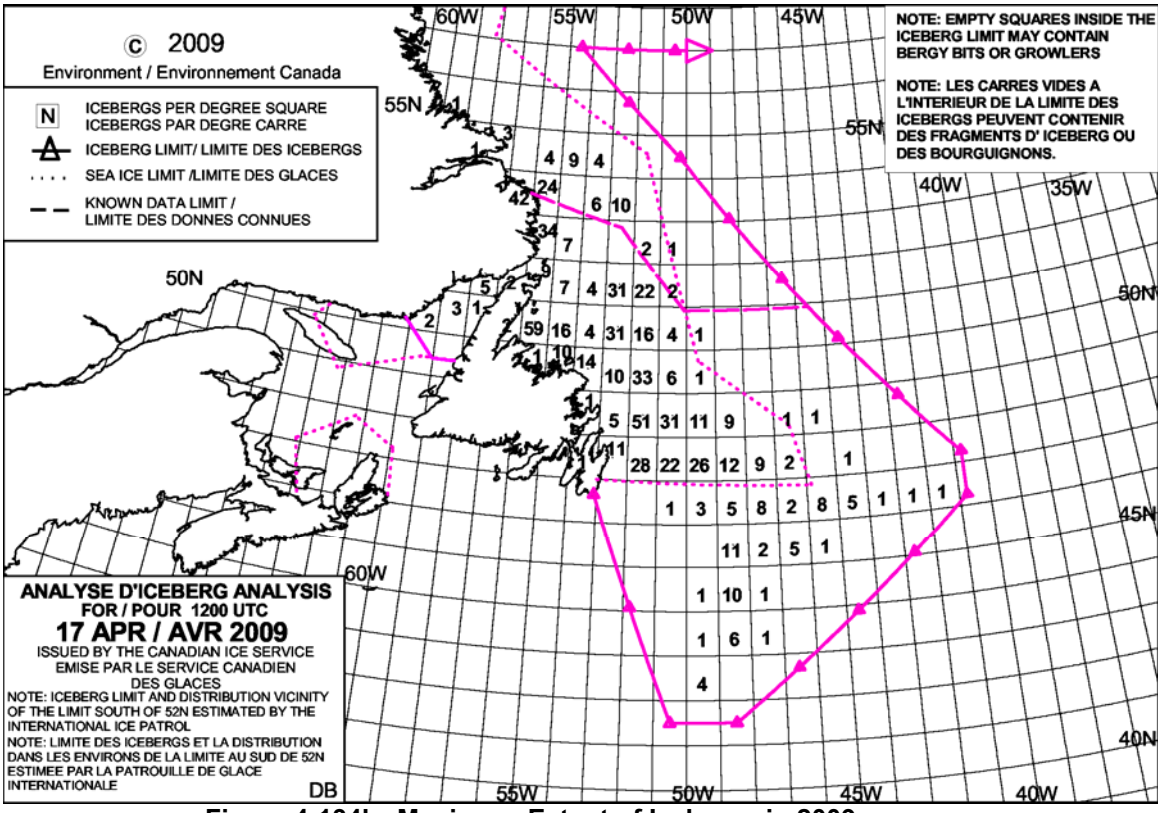

Figure 4-134b Maximum Extent of Icebergs in 2009

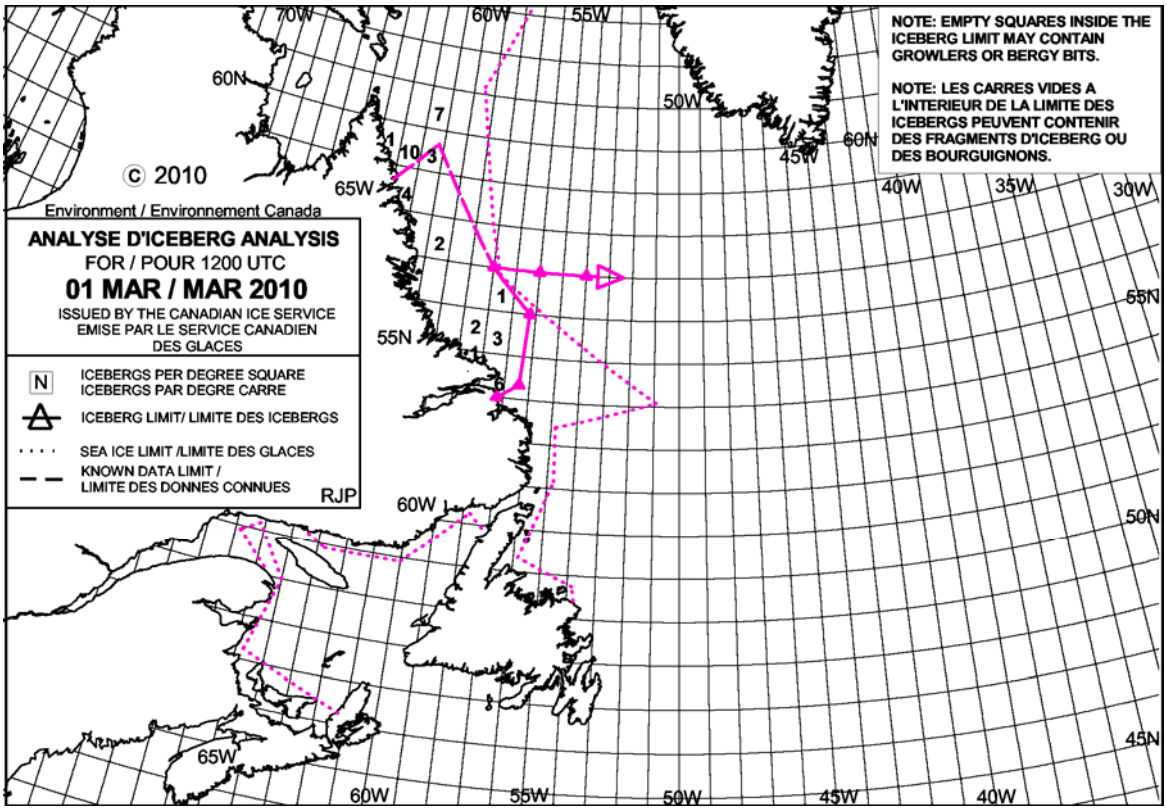

Figure 4-135a Minimum Extent of Icebergs in 2010

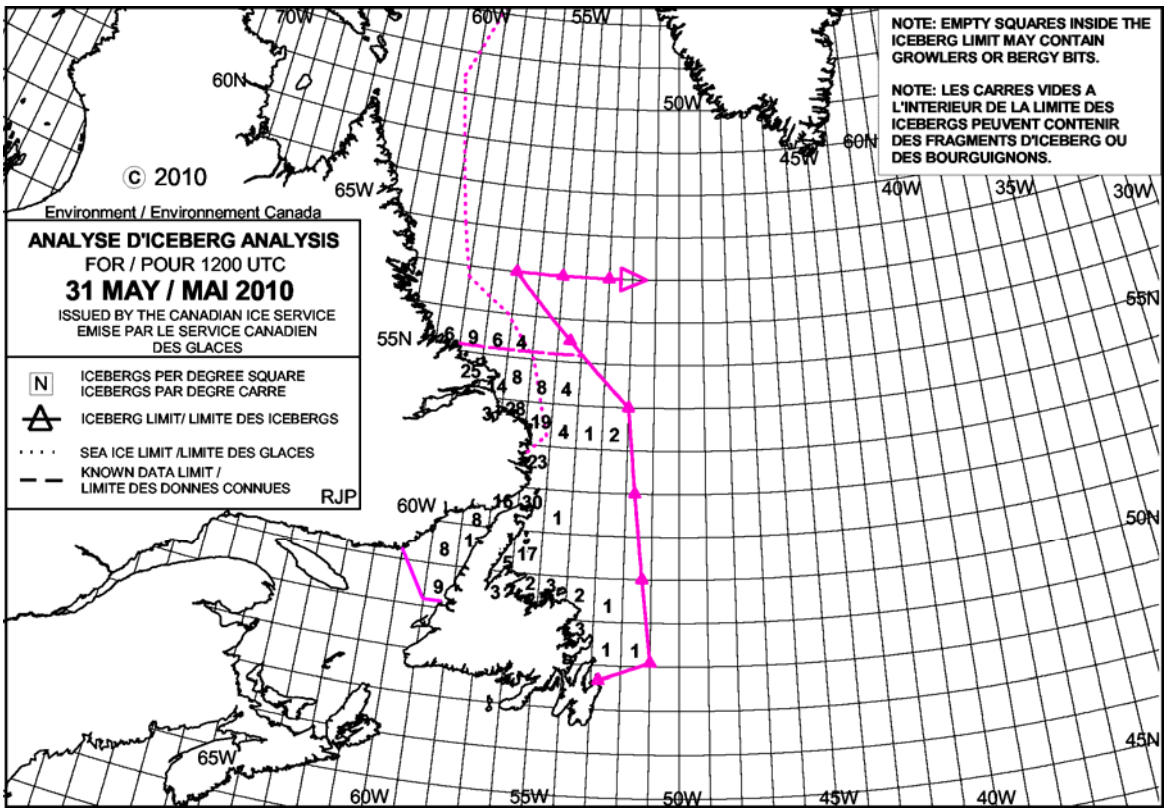

Figure 4-135b Maximum Extent of Icebergs in 2010

There has been much variation in the number of icebergs to pass south of 48°N each year during the past decade. Prior to 1999, the long-term record indicated a trend towards a larger number. However, there was a severe drop in the number of icebergs appearing south of 48°N just before 2000. These low numbers were attributed to a combination of higher than normal water temperatures on the Grand Banks, very light sea ice coverage and prolonged periods of onshore easterly winds during the spring months, which drove the icebergs onto the Labrador Coast, where they grounded. As a result, ice was not free to drift south into Newfoundland offshore waters. This trend for light iceberg distribution south of 48°N ended with the 2008 season, which saw large numbers and the trend continued into 2009. The years 2010 and 2011 were exceptionally light again.

It is worth noting that, while the major iceberg influx falls into the March to June period, iceberg sightings on the approaches to the White Rose field have been made at least once in each month of the year (Figure 4-136).

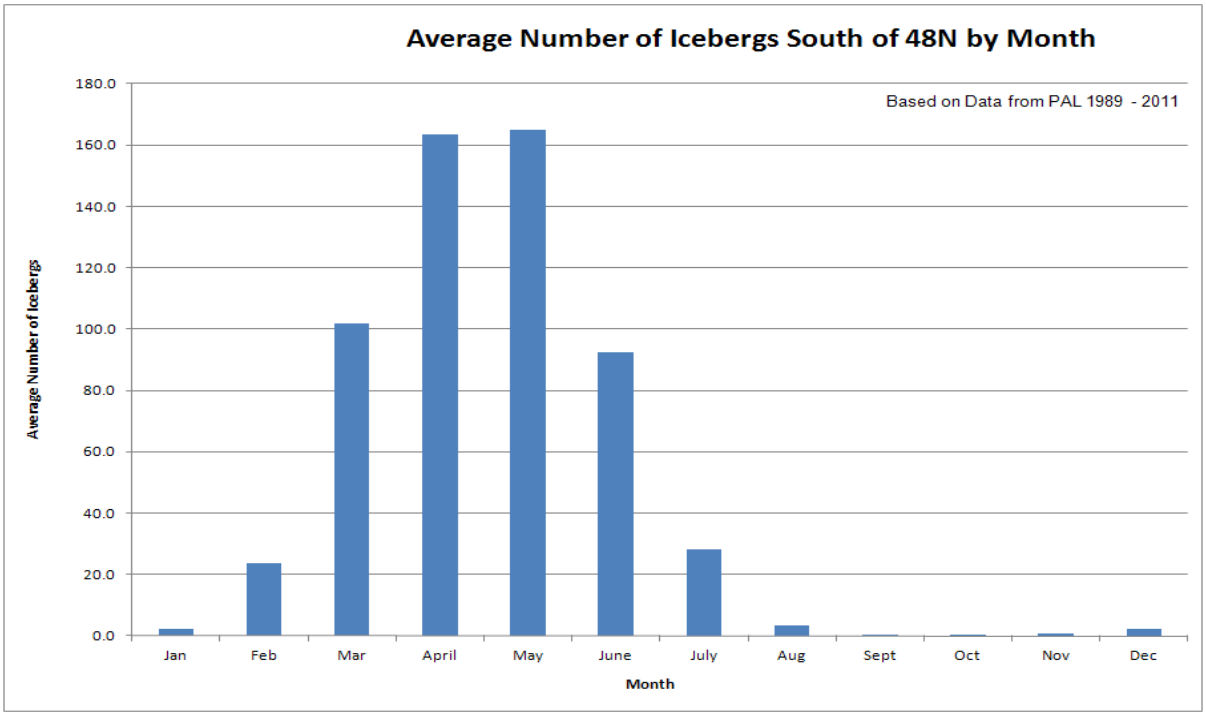

Source: Based on data from PAL 1989 to 2011 (PAL 2011a)

Figure 4-136 Average Number of Icebergs South of 48°N by Month (1989 to 2011)

Variations in the timing of iceberg influxes reflect annual differences in southward-moving ice, iceberg drift rates and wind fields. Winds, along with the offshore position and extent of the ice pack, heavily influence iceberg drift rates.

It should be noted that very low (less than 12) to iceberg-free conditions are present 30 percent of the time when looking at only the past 10 years. Whether this is a result of climate change or simply seasonal variation is unknown, as sightings south of 48°N over the 2008-2009 ice seasons returned those seen in the early 1990s.

A plot of annual iceberg numbers in a 0.25° grid (using 2000 to 2011 PAL data) shows the regional iceberg distribution (Figure 4-137) in the region during that 11 year timeframe. The PAL iceberg database contains over 700 visually-confirmed iceberg sightings and more than 21,000 observations made between 45°N and 62°N in 11 years. Of these, approximately 94 percent were observed south of 48°N.

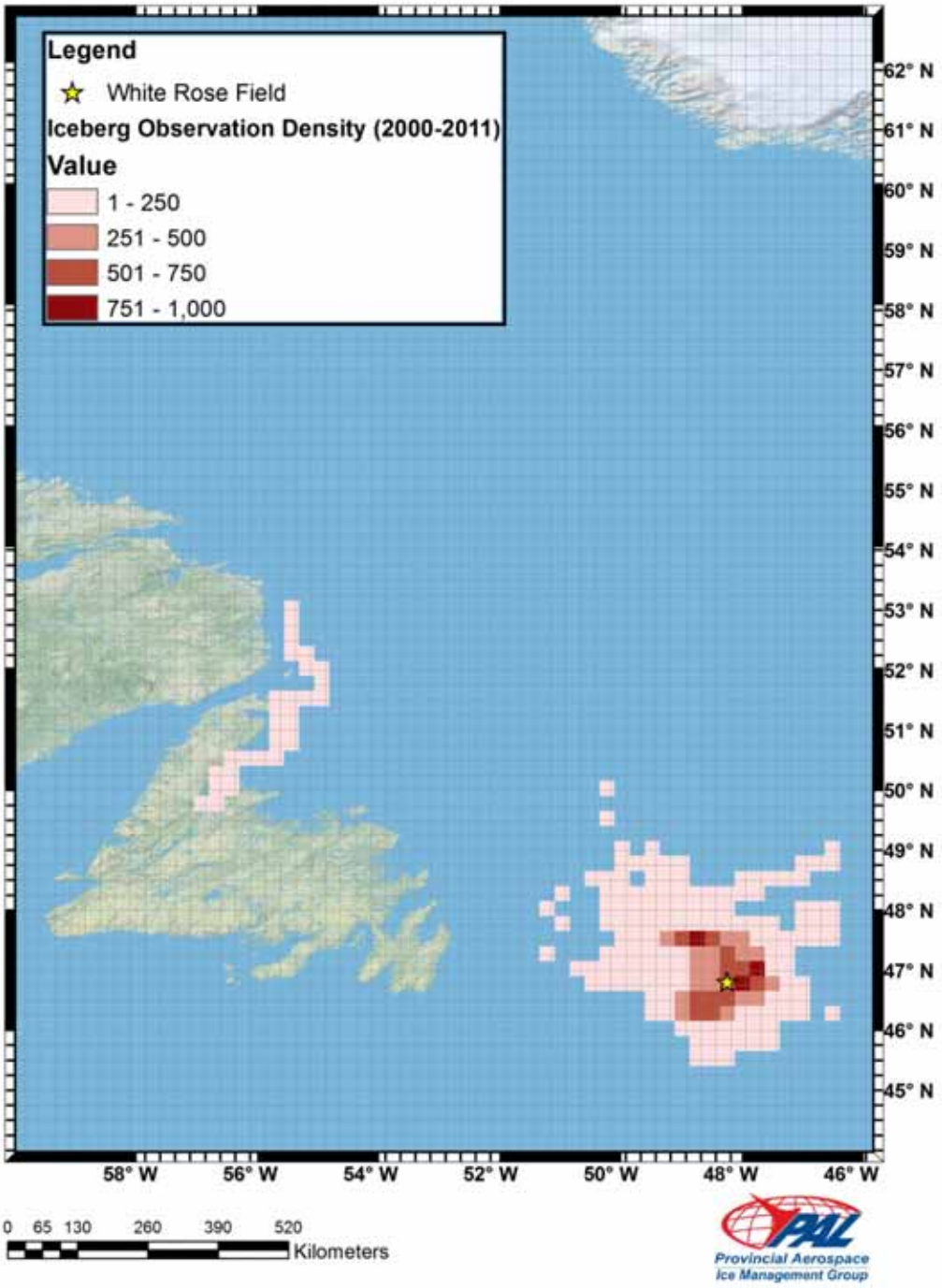

Source: PAL Iceberg Sighting Database 2000 to 2011

Figure 4-137 Iceberg Observation Density (2000 to 2011)

The maximum number of iceberg sightings (214) near the White Rose Location was observed in 1990. This number, though high, is substantiated by the iceberg tracking records from Petro-Canada's King's Cove A-26 well site (PAL 1990), located just north of White Rose.

The largest numbers of icebergs immediately adjacent to the White Rose field tend to appear in the 1° grid immediately to the northeast. This area is traversed by the 200 m contour, which is associated with the approximate inshore edge of the outer branch of the Labrador Current.

Drift

Local winds and currents largely determine the movements of free floating icebergs (i.e., ungrounded icebergs in open water or in low concentrations of sea ice). When embedded in extensive fields of first-year or older sea ice, iceberg movements follow those of the adjacent ice, except when such ice is in an advanced state of decay. In the vicinity of the White Rose field, an area generally characterized by low-to-moderate concentrations of relatively thin sea ice, icebergs tend to move independently of the sea ice, reflecting the influence of deeper currents.

Iceberg speeds and drift directions observed on the Grand Banks from oil platforms and vessel sightings (Figure 4-138), as measured over one- to three-hour time intervals in the years 2000 to 2011 (PAL 2011b), are qualitatively similar to mean sea ice velocity fields. Approximately 50 percent of the measured speeds were less than 30 km/day and mostly with a southeasterly component being the most prevalent (18.2 percent). For drift speeds, the exceedance plot represents the percentage of values a specified speed value is met or exceeded. For drift direction, the bar chart shows the percentage of observations in each drift direction.

Size Distributions

Icebergs are categorized by size, as defined in Table 4-80. These general size classifications have been in use for the past 30 years by all collectors of iceberg data (IIP, CIS and PAL). However, the accuracy of size distributions extracted from the various databases is questionable, because most data are based on visual estimations and unspecified selection criteria.

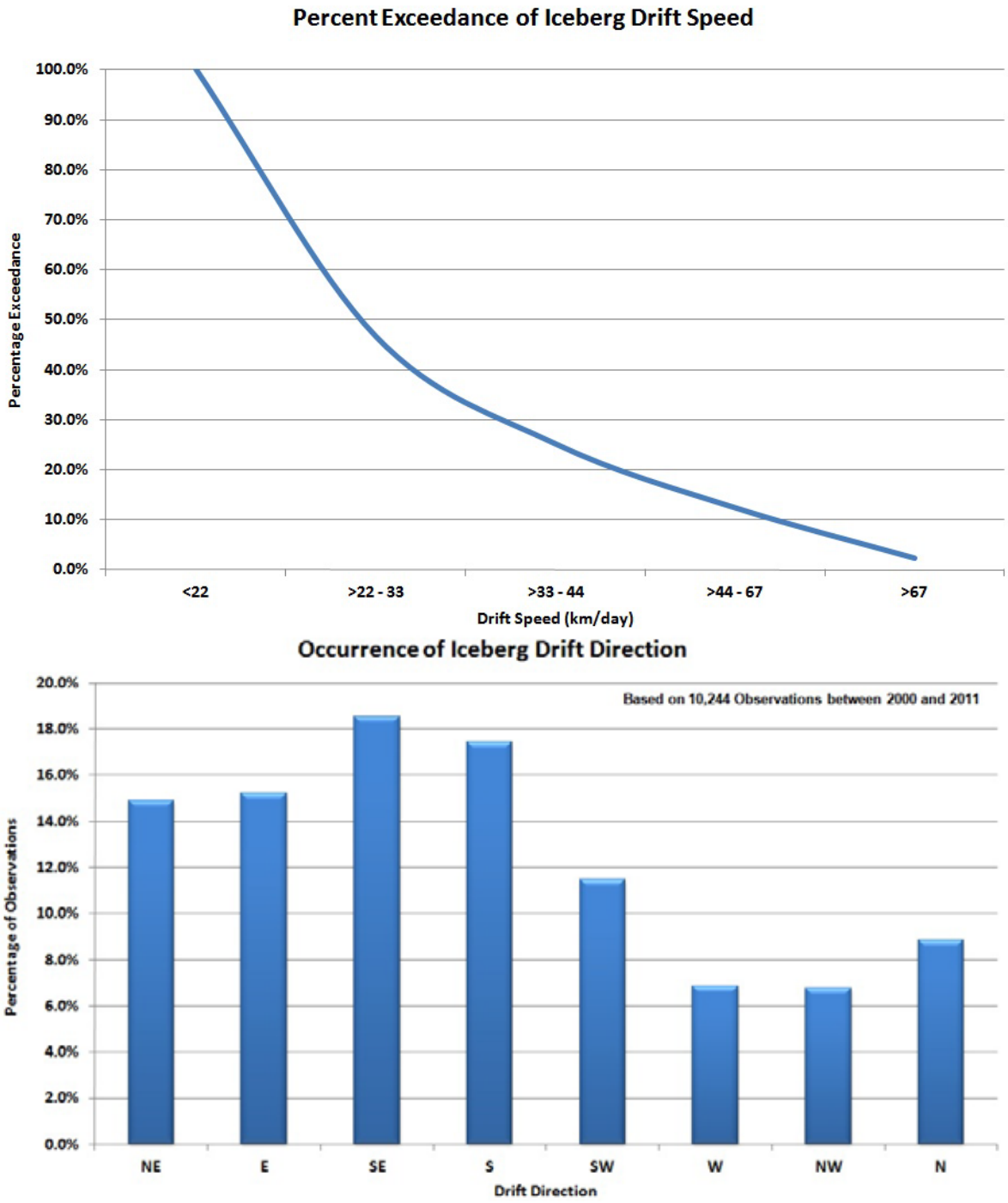

Source: PAL Iceberg Sighting Database 2000 to 2011

Figure 4-138 Speed Exceedance and Distribution of Drift Directions

Table 4-80 Iceberg Size

Category	Height (m)	Length (m)	Approx. Mass (t)
Very Large	>75	>200	>10 Million
Large	45 to 75	120 to 200	2 to 10 Million
Medium	15 to45	60 to 120	100,000 to <2 Million
Small	5 to 15	15 to 60	100,000
Bergy Bit	1.0 to 5	5 to 15	10,000
Growler	<1.0	<5	1,000
Source: Meteorological Service of Canada CIS MANICE (2002)			

A PERD study conducted using data from the 1970s to 1980s (CANATEC Consultants Ltd. 1999) lists dimensions for 872 icebergs measured on the Grand Banks and off Labrador, along with several three-dimensional iceberg profiles. This database provides extensive measurement data (both above and below water) on icebergs. However, statistical plots of these data showed no significant differences compared to results obtained from earlier analysis (Seaconsult Ltd. 1988) of industry data. The PAL database of visually-confirmed iceberg sightings over the past 20 years was also analyzed to extract iceberg size distributions and again was found to be consistent with other studies. The 2000 to 2011 PAL iceberg dataset shows that the majority (75 percent) of the icebergs south of 48°N fall within the small to medium categories (Figure 4-139).

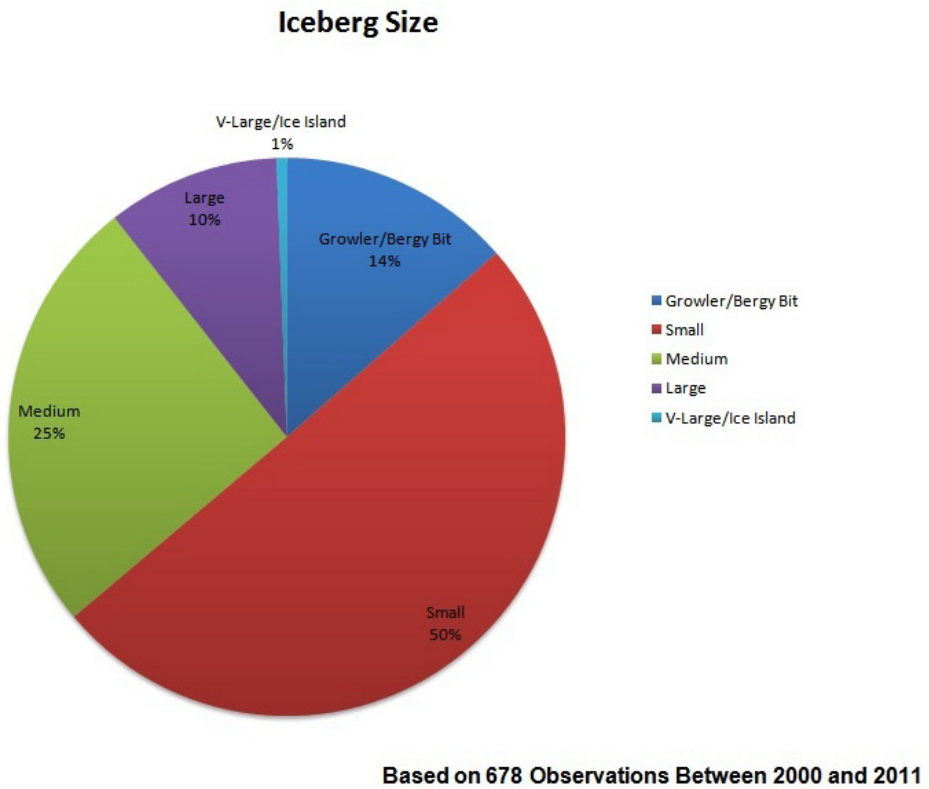

Source: PAL Iceberg Sighting Database 2000 to 2011

Figure 4-139 Iceberg Size Distribution

Iceberg Length

The exceedance percentages for the waterline lengths of icebergs, based on data collected since 2000, as well as the percentage of iceberg mean lengths in divisions of 25 m, are illustrated in Figure 4-140. Most iceberg (23.8 percent) lengths were between 25 and 50 m. Only six percent of observations have had lengths exceeding 150 m.

The mean iceberg length, based on observations since 2000, is 60 m (Figure 4-140). This is consistent with observations obtained from visual iceberg sightings made from aerial surveillance, 1989 to 2011.

Of note are several ice island fragments or very large icebergs sighted in the 2002, 2003, 2004 and 2011 ice seasons. Several of these fragments were detected from facilities on the Grand Banks, and were thus within 20 Nautical Miles of the locations. In 2011; however, the fragments deteriorated prior to making it south of 48°N. These icebergs, while having very large surface area, had drafts of 50 m or less. Based on several studies (Stoermer and Rudkin 2003; Rudkin et al. 2005; PERD 2004) these ice island fragments were the result of a significant calving event on the Petermann Glacier.

Iceberg Draft

The draft of icebergs (the depth of the iceberg below the water) as derived from observations and measurements made from 2000 to 2012 on the Grand Banks is illustrated in Figure 4-141. The mean iceberg draft was 44.5 m. Almost half (49.2 percent) of draft observations fall into the 25 to 50 m category. Less than 1 percent (0.8 percent) of observed icebergs have drafts which exceed 125 m.

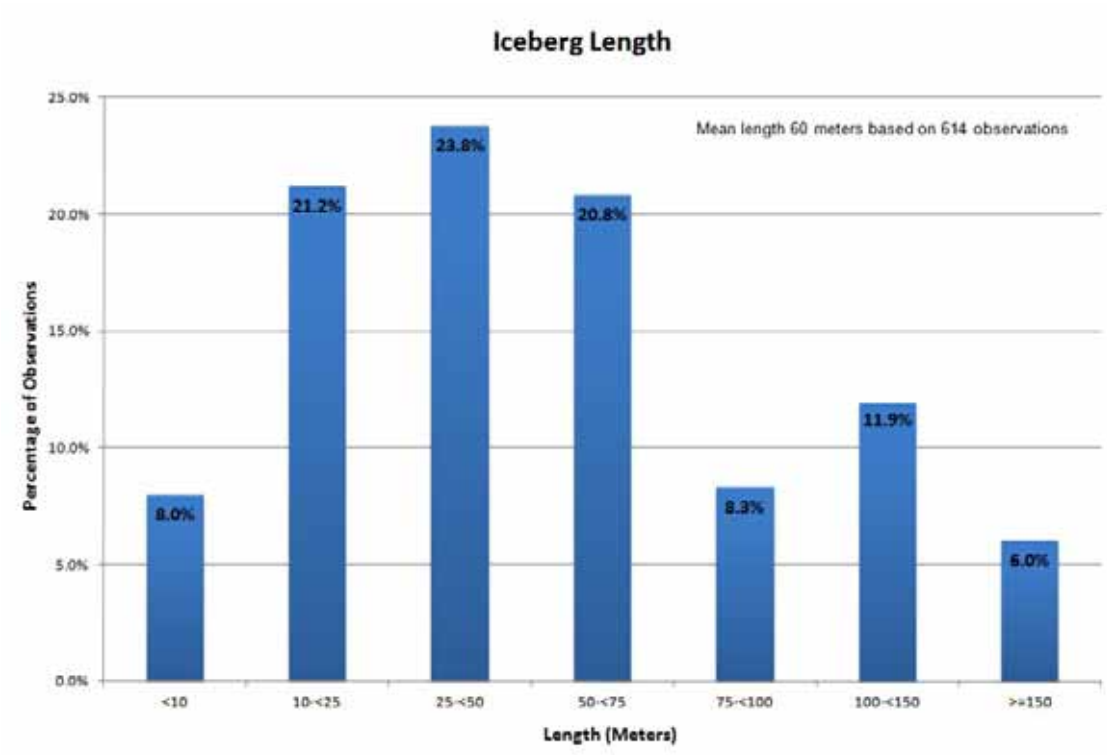

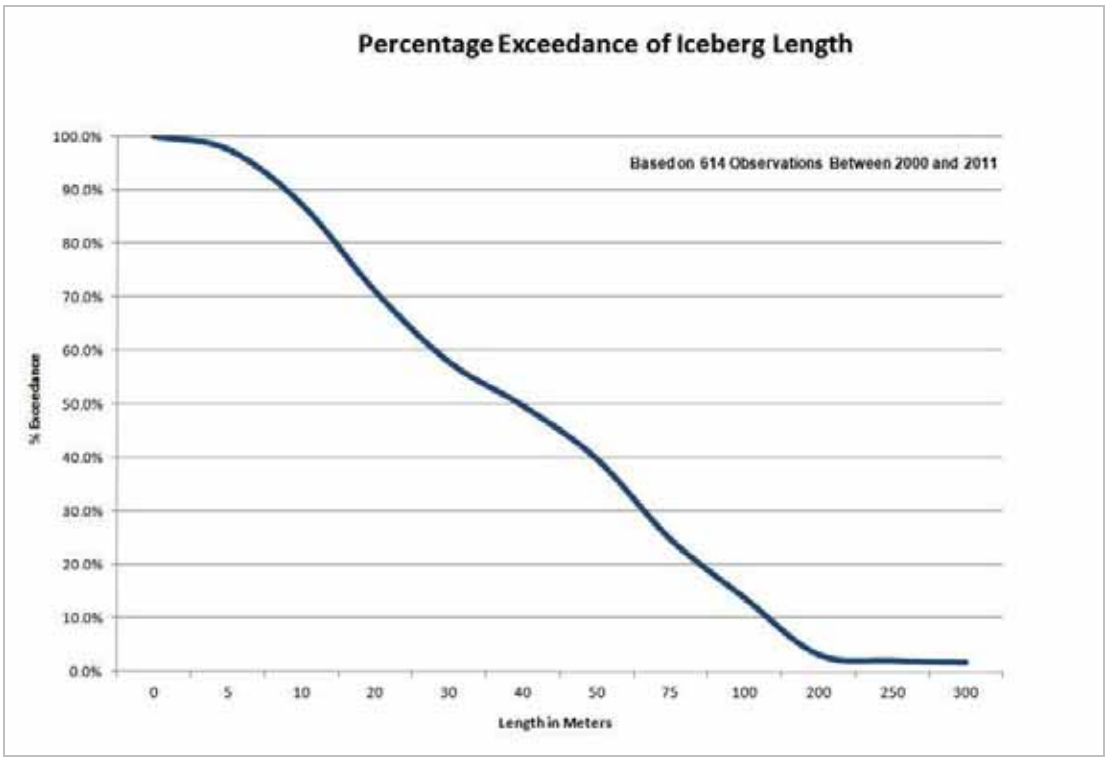

Source: PAL Iceberg Sighting Database 2000 to 2011

Figure 4-140 Iceberg Length and Percent Exceedance of Iceberg Length on the Grand Banks

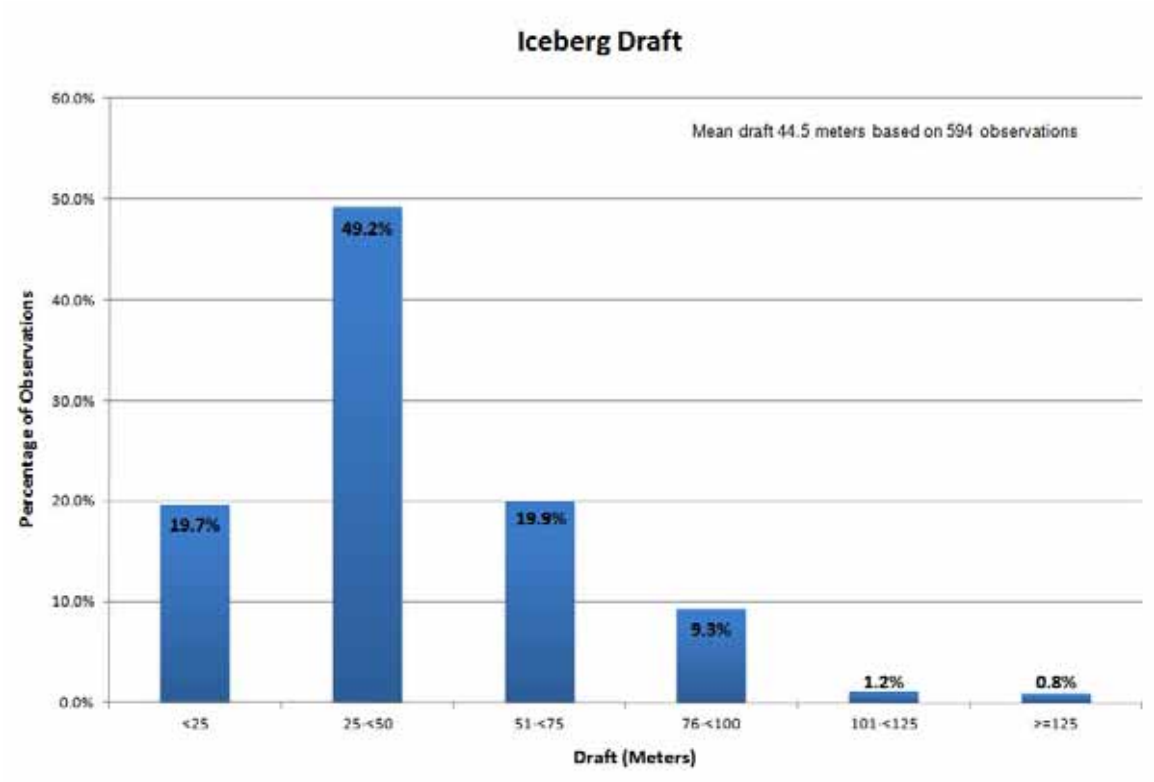

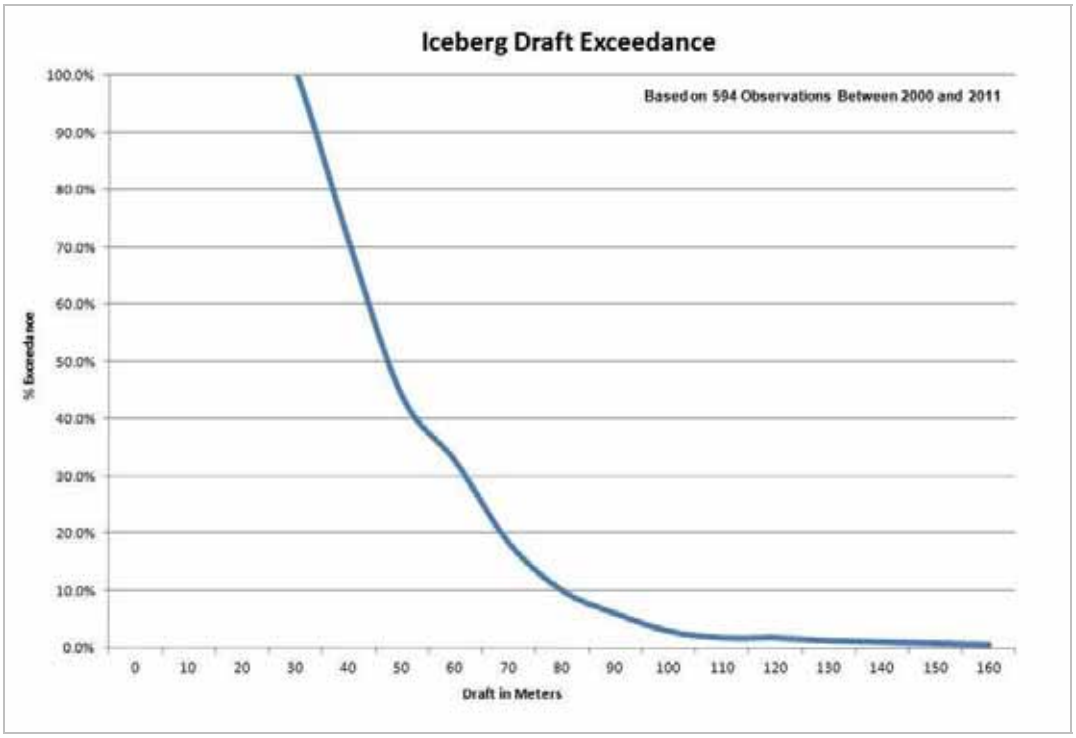

Source: PAL Iceberg Sighting Database 2000 to 2011

Figure 4-141 Iceberg Draft and Exceedance of Iceberg Draft for Icebergs on the Grand Banks

Iceberg Height

Data are available on above-water iceberg heights (sail height) and on the overall masses of Grand Banks icebergs. Measurements of 113 icebergs on the Northern Grand Banks (Ice Engineering Ltd. 1981a, 1981b, 1982, 1983) (Figure 4-142) show median heights of approximately 20 m. Only 4 percent of the icebergs had heights in excess of 50 m, while 20 percent were less than 10 m. More recently, the PERD (Singh et al. 1999) database provides 468 individual iceberg measurement sets. These data were compared to the results from the Ice Engineering Ltd. data (1981a, 1981b, 1982, 1983) and show identical mean values.

The data set that provided the most accurate information was that collected operationally on the Grand Banks over the past 11 years. These data show a mean sail height of 12.2 m based on 612 observations. The majority of observations icebergs (40.5 percent) had heights ranging from 10 to 25 m. Only 1.5 percent of icebergs had heights 50 m or greater.

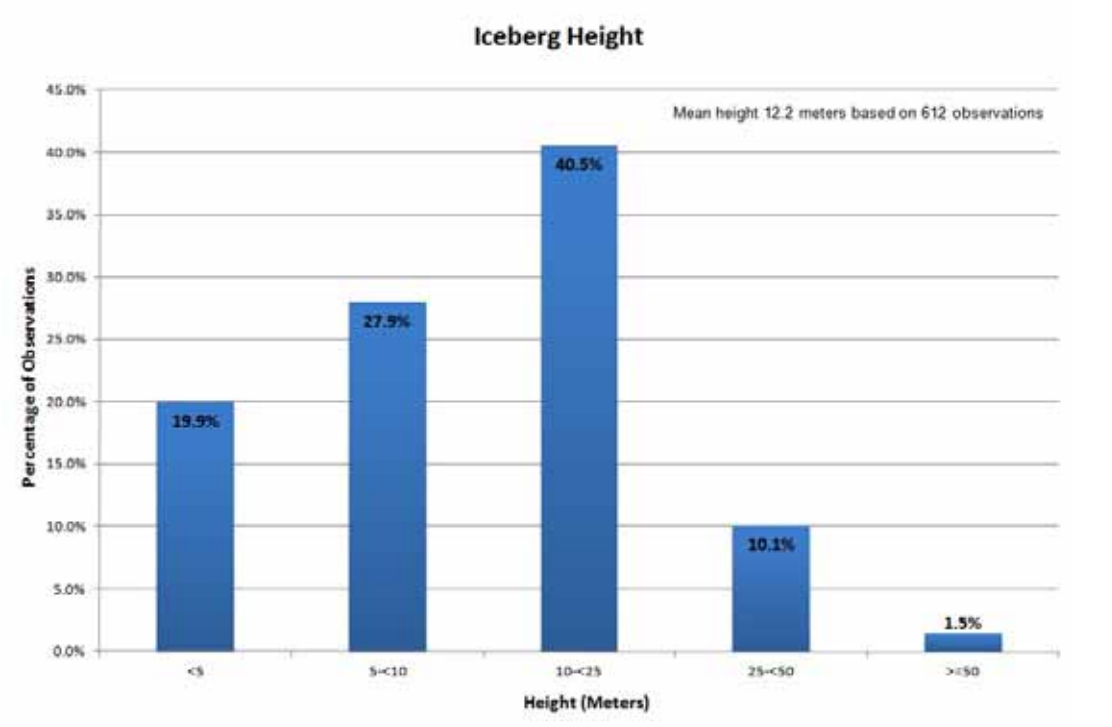

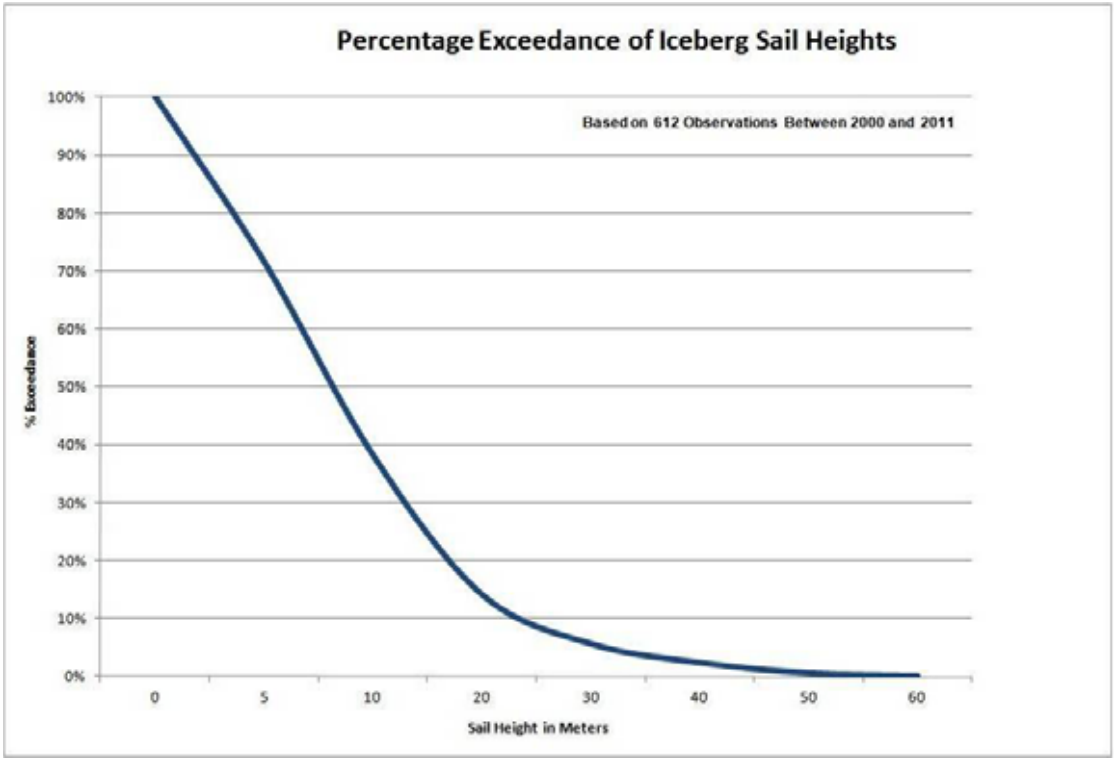

Source: PAL Iceberg Sighting Database 2000 to 2011

Figure 4-142 Iceberg Sail Height and Exceedance of Iceberg Sail Height

A representative mass distribution derived from calculations made from observations of 598 icebergs between the years 2000 and 2011, is shown in Figure 4-143. The mean mass from these data is 215,007 tonnes, with 4.3 percent exceeding 1,000,000 tonnes and 38 percent below 10,000 tonnes.

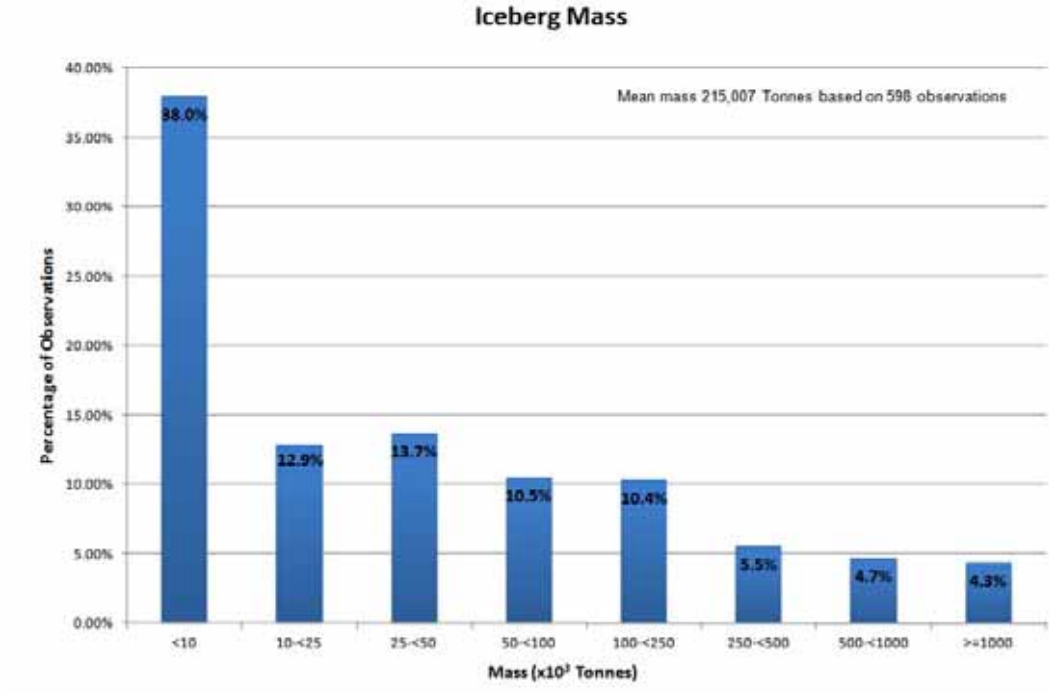

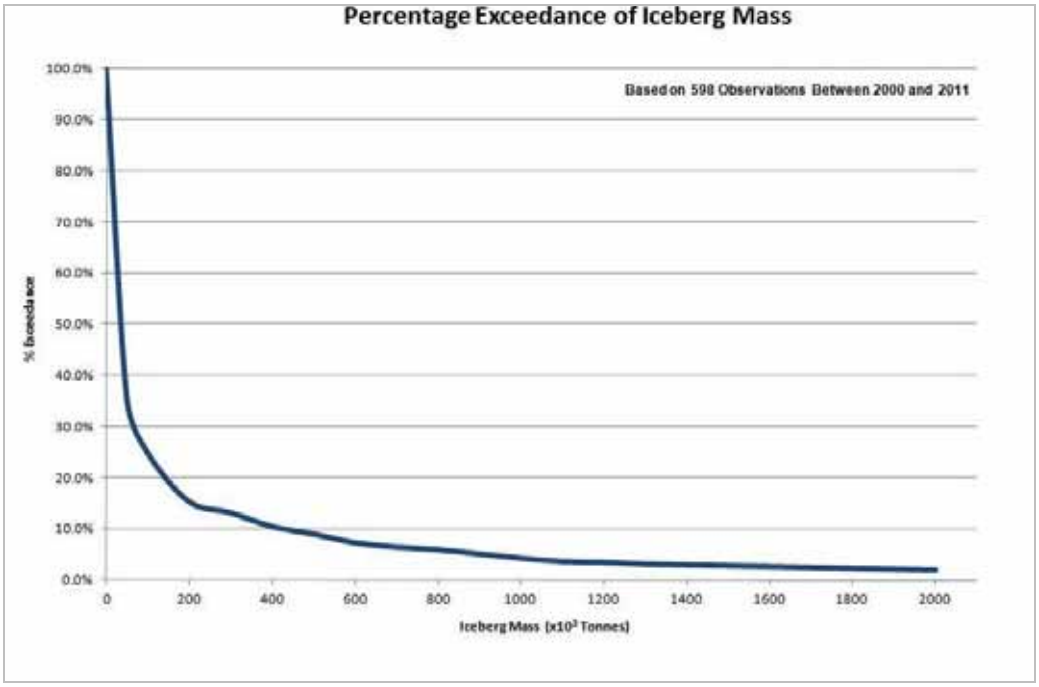

Source: PAL Iceberg Sighting Database 2000 to 2011

Figure 4-143 Iceberg Mass and Exceedance of Iceberg Mass

Only in recent years has substantial effort been directed to the systematic study of the bergy bits and growlers that comprise most of the smaller iceberg regime (lengths less than 20 m). Bergy bits and growlers must also be managed to ensure transport vessel and support vessel safety. Although they are the smallest icebergs, they are still of substantial size, and they are more difficult to detect, particularly in high seas.

The inclusion of more bergy bits and growlers in the dataset reduces the average mass.

4.3.5 Geological Setting – White Rose Field

The White Rose field is situated on the northeast margin of Grand Bank, offshore Newfoundland. Grand Bank is the largest of a series of shallow outer shelf banks that together form the Grand Banks of Newfoundland, an area of 100,000 km^2. The Grand Banks are separated from the Newfoundland coast by irregular inner shelf bathymetric lows of the Avalon and St. Pierre channels.

The surficial and shallow geology of Grand Bank reflects episodes of Pleistocene glaciation, relative sea level change and marine shelf sedimentation (Sonnichsen and King 2005; Shaw 2006; Shaw et al. 2006; King 2010). Ice-contact and ice-proximal deposits are known to occur on parts of the northeast Grand Banks (e.g., Fader and Miller 1986; Sonnichsen and King 2005). The extents of recent shelf glaciations are uncertain; however, the margins of the banks are known to have been affected by exposure and inundation during glacio-eustatic relative sea level changes.

Repeated advances and retreats of Laurentide and Newfoundland glacial ice across the Grand Banks to the edge of the continental shelf began at approximately 1 mega annum (Ma) before present (BP) (Piper 2005), as documented by the presence of prominent seafloor till ridges of the Sackville Moraine complex at the shelf margin (Huppertz and Piper 2009). Sedimentation on the Grand Banks substantially increased during these periods of widespread shelf-crossing glaciation (Piper 2005), at which time large volumes of suspended sediments were transported to the slope edge and reworked by storm waves and shallow ocean currents. Pro-glacial Quaternary sediments were deposited in Flemish Pass in the form of eastward-prograding muds of hemipelagic and proglacial plume origin, minor thin-bedded turbidite sands, and thick-bedded mass-transport deposits (Piper and Campbell 2005).

During the last glacial maximum, the ice margin probably only reached as far as the mid-shelf, before retreating from the area 15,000 years ago (Huppertz and Piper 2009). At this time much of the outer Grand Banks was exposed above sea level (Shaw 2006) (Figure 4-144).

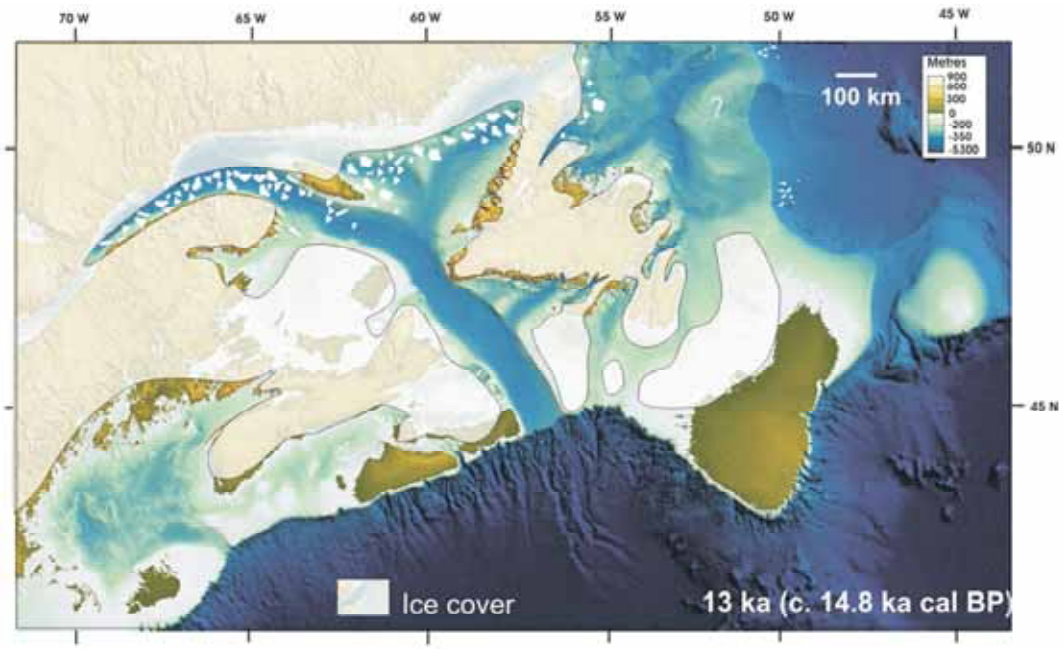

Source: from Shaw et al. 2006
Note: Approximately 15 kilo annum (ka) BP, showing large parts of the outer Grand Banks exposed above sea-level

Figure 4-144 Ice Extents during the Last Glacial Maximum

Mechanical reworking of seafloor and sub-seafloor shelf and upper slope sediments has been occurring throughout the Quaternary due to scouring and grounding icebergs produced from local calving along the Grand Banks ice margins, and more recently by icebergs carried southwards by the Labrador Current from Baffin Bay. Grounding and scouring icebergs created curvilinear scour marks and grounding pits that influenced buried topography. Icebergs still affect the modern seafloor.

The northeast Grand Banks is underlain by Tertiary fine-grained marine sediments and tectonically-structured strata of the Mesozoic Jeanne d'Arc Basin, which hosts Cretaceous reservoir sandstones. Reservoirs are highly compartmentalized and being exploited from a number of oil fields, including the White Rose field. The surficial and shallow and subsurface geology of the White Rose field are summarized below.

4.3.5.1 Surficial Geology – White Rose

Sediment distribution on northeastern Grand Bank has been extensively studied by both the GSC-A and by private geophysical contractors over the past few decades. The regional surficial sediment distribution, interpreted by Sonnichsen and King (2005), is shown in Figure 4-145.

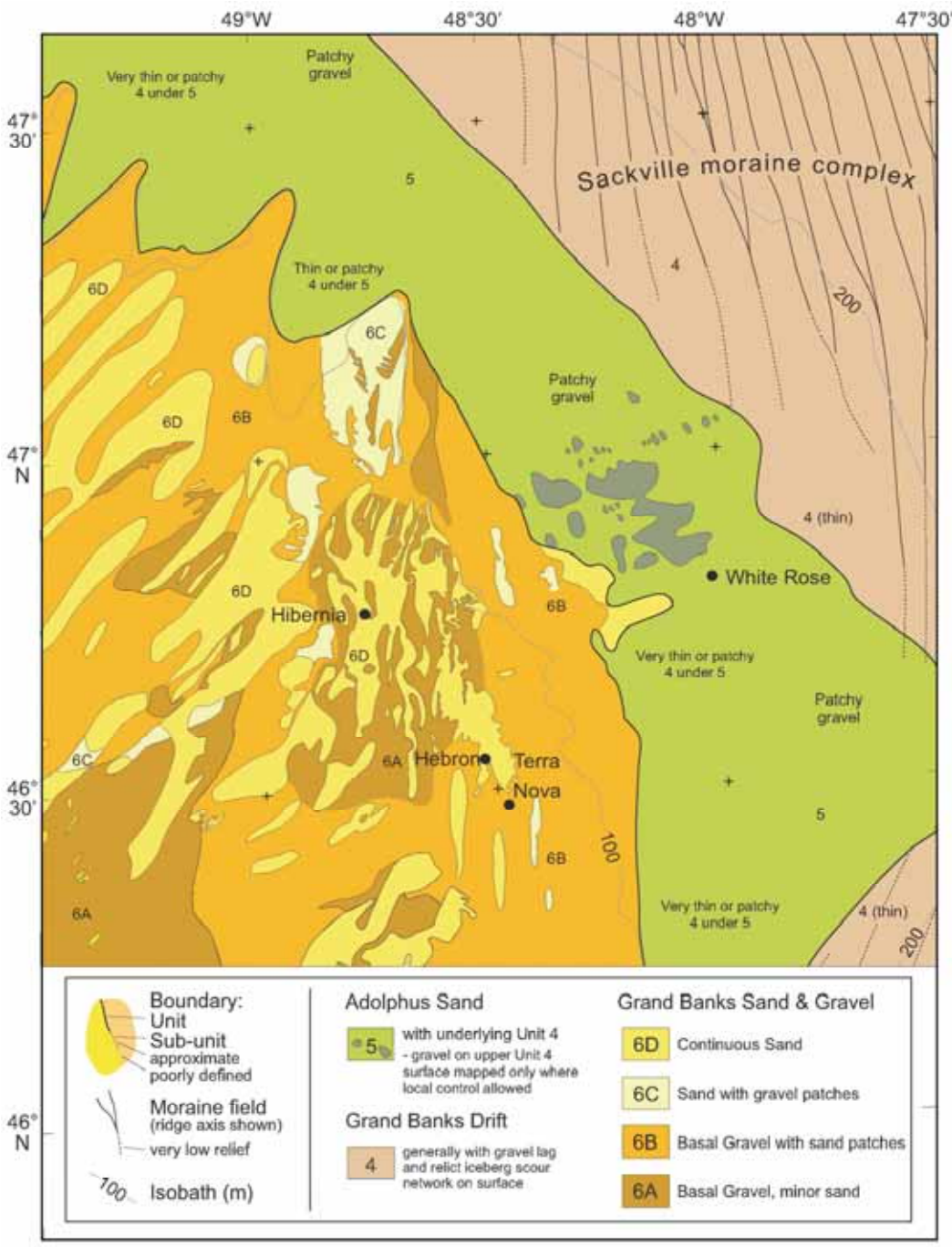

Source: from Sonnichsen and King, 2005
Note: The post-glacial relative sea level (RSL) low-stand was approximately 110 m below present, with the paleo-shoreline at the transition from sediment Unit 6A (dark brown) to Unit 5 (green). The present White Rose Field is situated in a former shallow-water shoreface environment at the RSL low-stand, which is blanketed by marine sands (Unit 5)

Figure 4-145 Distribution of Surficial Sediments for Northeastern Grand Bank

Regions of northeast Grand Bank that are shallower than the present approximately 110 m bathymetric contour were sub-aerially exposed during the late-Wisconsin sea level lowstand, approximately 15,000 years ago (Sonnichsen and King 2005). Sea level subsequently rose, the surficial sediments were reworked, and the result was a relatively thin (average 1 to 3 m) veneer of sand and gravel that overlies the truncated Tertiary Banquereau Formation (Fader and King 1981; Stoffyn-Egli et al. 1992), or glaciogenic sediment, where present (see Section 4.3.5.2). The reworked coarse-grained sediments comprise the Grand Banks Sand and Gravel. The overlying Adolphus Sand, which blankets the White Rose field, was derived from erosive transgression of the bank top, and deposited in a shallow shoreface environment. The White Rose field now lies in water depths greater than 115 m.

Surficial sediments at White Rose are comprised of a blanket of fine- to medium-grained Adolphus Sand, which overlies a coarser, irregular substrate of Grand Banks Sand and Gravel (McElhanney 1981, 1982; Nortech Jacques Whitford 1998; Fugro Jacques Geosurveys Inc. (FJGI) 1999a, 1999b, 2000a, 2000b, 2005a). The Adolphus Sand transitions westward into the reworked Grand Banks Sand and Gravel, and eastward into partially exposed glacial deposits of the Grand Banks Drift (Figure 4-145).

The Grand Banks Sand and Gravel (Unit 6) is the youngest sedimentary unit on outer Grand Bank (Sonnichsen and King 2005). The unit is composed of the Grand Banks Gravel, a gravel lag deposit that lies above a regional unconformity. Grand Banks gravel deposits consist of glacially transported gravel and boulders, and is distributed regionally as a thin continuous transgressive lag often beneath surficial sands. The Grand Banks Gravel is overlain by reworked surficial sands and fine gravels of the Grand Banks Sand. Four different sandy and gravelly facies (6A to 6D) can be recognized within the Grand Banks Sand and Gravel (Sonnichsen and King 2005) and are shown in Figure 4-145.

As defined by Sonnichsen and King (2005), Adolphus Sand (Unit 5) occurs at the seafloor and is composed of loose to compact, fine- to medium-grained sand covering a large area of northeastern Grand Bank. The unit rarely exceeds 2 to 3 m in thickness. This occasionally laminated unit often contains silt, shells and fine gravel. The unit thickens towards the deeper portions of the bank top, thinning again toward the upper slope, where it partially fills the relict iceberg scour marks preserved in the Grand Banks Drift. Adolphus Sand is interpreted to be a sublittoral deposit that formed seaward of the Late Wisconsinan lowstand of sea level.

The Grand Banks Drift (Unit 4) is a mixed glacial deposit typically occurring as a continuous cover of varying thickness and overlying a regional unconformity. This unit is composed of poorly sorted sand, silt and clay containing clasts ranging from granules to boulders. On the northeastern Grand Bank, Unit 4 primarily occurs as a thin blanket, 0.5 to 15 m thick, which thickens to 25 m in the Sackville Moraine complex and thins south and west beneath a veneer of sand (Sonnichsen and King 2005).

The seafloor in the White Rose field is relatively smooth and dips gently northeastward. The thickness of surficial Adolphus Sand appears to vary from 0 m to occasionally greater than 3 m, depending on the irregularity of the underlying surface. Side scan sonar mosaics display a mottled seafloor appearance, with some of the ‘outcrops’ of the underlying sands and gravels being suggestive of linear and circular patterns that are perhaps the surface expression of large, buried, relict ice scour marks.

Other seafloor features include marks made by the dragging of otter trawl doors during fishing activities, anchor chain marks and well sites from previous drilling activities. Otterboard trawl marks were well defined during surveys in 1981 and 1982 (McElhanney 1981, 1982). Previous interpretations of biota identified from seafloor photographs have suggested that the seafloor is stable, with relatively little sediment transport occurring in the region (McElhanney 1982). This conclusion is supported by the results of site surveys (FJGI 1999a, 1999b, 2000a, 2000b), which clearly display anchor marks from old drilling programs, preserved in sand after 15 to 20 years (e.g., at the E-09 well site). Seafloor imagery from the White Rose field displays variable concentrations of benthic organisms (such as starfish, brittle stars, bivalves).

4.3.5.2 Subsurface Geology – White Rose

The near-surface stratigraphy (less than 15 m sub-seafloor) at White Rose reflects episodes of Quaternary glaciation, as well as associated relative sea level changes, and varying degrees of reworking by scouring icebergs. Near-surface deposits comprise thin Adolphus Sand (Unit 5) overlying proglacial and glacial sediments of the Grand Banks Drift (Unit 4; Figure 4-145). Geotechnical borehole investigations have characterized the near-surface glaciogenic deposits as highly heterogeneous, and consisting variously of dense to very dense sand and gravel (with cobbles), silty sand and sandy silt, and stiff clay (e.g., FJGI 2001, 2005a). The buried surface of the Grand Banks Drift is highly irregular, suggestive of numerous iceberg scour marks formed perhaps by periods of frequent and heavy ice grounding during phases of lower relative sea level. It is also possible that the irregular topography reflects channel erosion. The near-surface deposits are characterized by high lateral variability of soil properties. Partially cemented sands have been encountered in places, potentially resulting from consolidation, desiccation and cementation by meteoric groundwater diagenesis during phases of sub-aerial exposure (e.g., Sonnichsen and King 2005).

Below the Grand Banks Drift lie Late Tertiary, dominantly marine sediments that dip gently to the northeast. A shallow stratigraphic sub-division for Tertiary deposits on the northeastern margin of Grand Bank has been developed on the basis of geophysical profiles and geotechnical borehole correlations (Taylor et al. 1993; Sonnichsen et al. 1994; Terraquest Associates 1995, 1996; Sonnichsen and Cumming 1996; Sonnichsen and King 2005; King 2010) (Figures 4-146 and 4-147). The identification of three main Late Tertiary stratigraphic units is based upon the recognition of well-defined progradational sequences of clinoform reflections (including the Hibernia Delta; Unit 2), and the gently dipping, near-parallel sequences, that over and underlie them (the Upper and Lower Parallel Reflection Sequences; Units 3 and 1) (Figures 4-147 and 4-148).

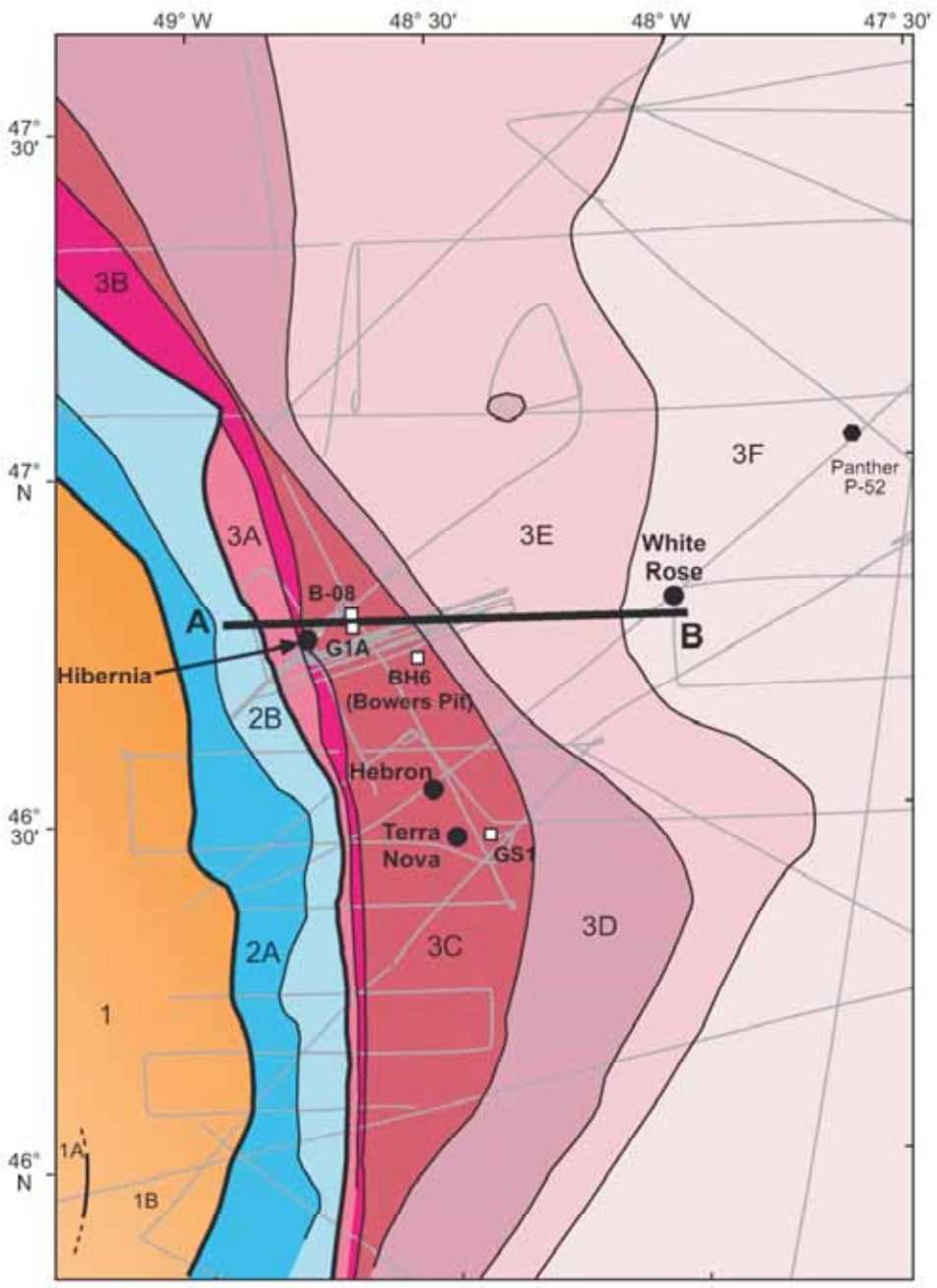

Source: From Sonnichsen and King 2005
Note: Legend is shown in Figure 4-150; also indicates location of profile in Figure 4-151

Figure 4-146 Geological Map Showing Distribution of Near-surface Seismo-stratigraphic Units

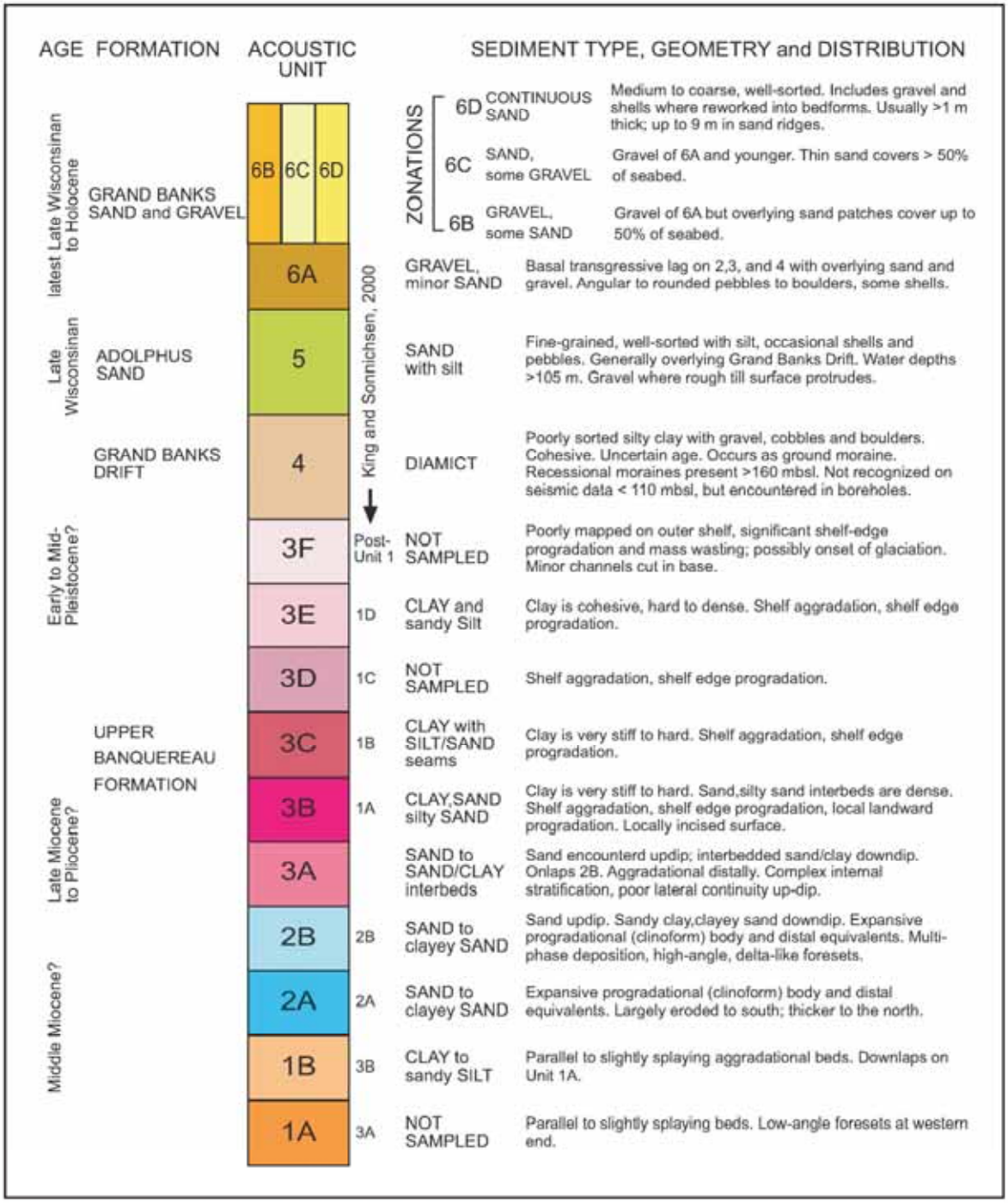

Source: From Sonnichsen and King 2005

Figure 4-147 Stratigraphic Column, Northeast Grand Bank

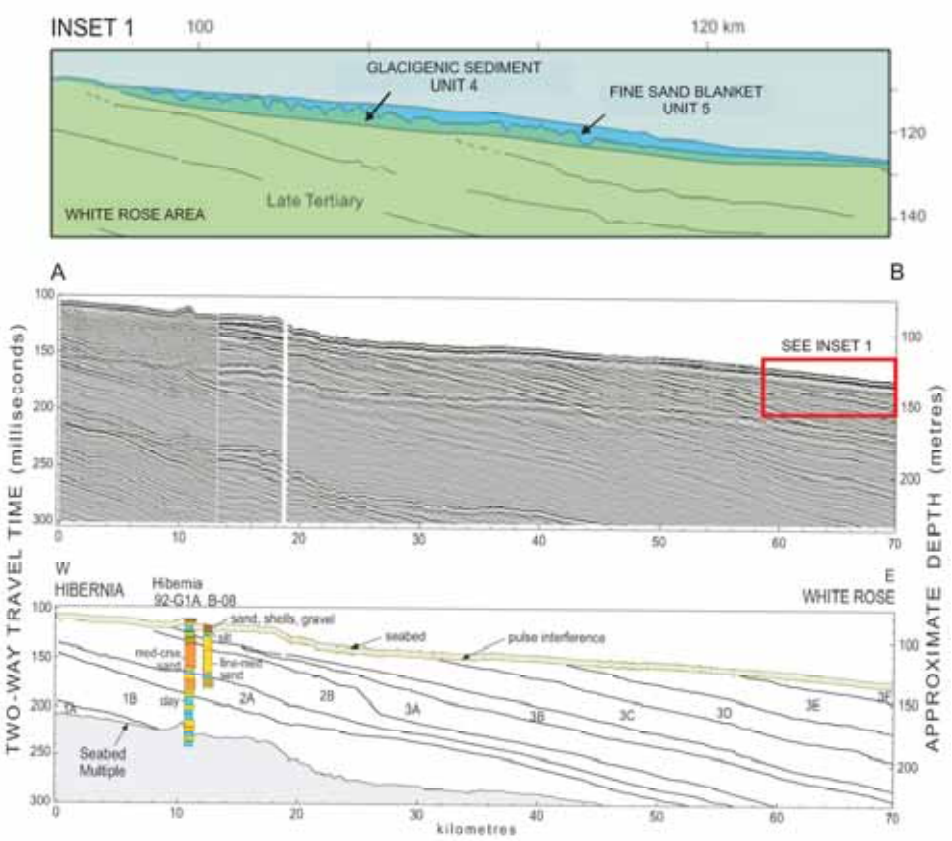

Source: From Sonnichsen and King 2005
Note: The shallow stratigraphy is comprised of the Upper Parallel Reflection Sequence (Unit 3), overlying the Clinoform Reflection Sequence (Unit 2) and Lower Parallel Reflection Sequence (Unit 1). In the White Rose field, Unit 3 strata are truncated near the seafloor, and overlain by glacial deposits (Unit 4) with a veneer of marine sand (Unit 5)

Figure 4-148 Near-surface Profile Schematic (INSET 1) and Geological Society of Canada Seismic Reflection Profile from Hibernia to White Rose with Stratigraphic Interpretation

Unit 3, the near-surface Upper Parallel Reflection Sequence, characterized by King and Sonnichsen (1999) and Sonnichsen and King (2005), displays regionally continuous medium- to high-amplitude reflectors with subtle unconformities. This unit is interpreted to consist of interlayered clays, silts and sands, and was deposited in an aggradational to progradational marine shelf environment. Unit 3 has been sub-divided into six unconformity-bounded sub-units, 3A to 3F, that thicken and become progressively more seafloor-parallel as they approach the paleoshelf break (Figure 4-148). The sub-units are truncated near the seafloor, and subcrop in a pattern of narrow, east-arcing bands below thin surficial deposits (Figure 4-146). The oldest sub-units of Unit 3 (A, B and potentially C) are interpreted to occur in the Hibernia region and eastward. The youngest sub-units (3D to 3F; Pliocene-Pleistocene) are present beneath the more distal White Rose field (Figure 4-148). Sub-units 3E and 3F thicken substantially at the shelf break (King and Sonnichsen 1999; Sonnichsen and King 2005).

Unit 2, underlying Unit 3, is the Clinoform Reflection Sequence, which is defined by internal clinoform reflectors and parallel, low-angle reflections. This unit (also informally known as the Hibernia Delta) sub-crops in a wide band west of Hibernia, and thins with a transition from foresets to bottomsets in the Terra Nova-Hebron region. Unit 2 is further sub-divided into two unconformity-bounded sub-units, units 2A and 2B, which are sand-dominant with minor clay, silt and gravel interbeds. The fine-grained sediment content increases distally. These deposits have been interpreted as pro-glacial outwash delta deposits or, alternately, as bank-spillover deposits of Late Tertiary (Miocene-Pliocene) age (Sonnichsen and King 2005). Unit 2 subcrops at the foundation zone at Hibernia and has been extensively sampled. A coarsening upward sequence of dense sands has been observed in these samples and has been interpreted to represent a shallow prograding shelf deposition (King and Sonnichsen 1999; Sonnichsen and King 2005).

The underlying Lower Parallel Reflection Sequence (Unit 1) is characterized by sub-parallel, high amplitude reflections that are closely spaced. An unconformity divides this unit into subunits 1A and 1B. The top of Unit 1 is bounded by a distinct, locally-incised unconformity. This unit outcrops west of the Hibernia and Terra Nova fields, and dips towards the east-northeast. Unit 1 consists mainly of clays, with sand interbeds interpreted to represent conformable marine aggradation (Sonnichsen and Cumming 1996; King and Sonnichsen 1999; Miller 1999; Sonnichsen and King 2005).

The dipping Unit 1 and 2 strata are below the depth of interest for foundation zone assessment in the White Rose field. Tentative correlations between the published regional shallow stratigraphy and White Rose geophysical data are discussed in Section 4.3.5.3.

In the Hibernia field, the Upper Parallel Reflection Sequence (Unit 3) is partially eroded and overlain by reworked surficial Grand Banks Sand and Gravel (Unit 6; Figure 4-145). West of Hibernia, the Clinoform Reflection Sequence (Unit 2) rises to the seafloor (Figure 4-146) and has been reworked to form part of the Grand Banks Sand and Gravel (Figure 4-145).

Further offshore in the White Rose field, the truncated, dipping marine strata of the Upper Parallel Reflection Sequence are overlain by undifferentiated glacial till deposits of the Grand Banks Drift (Unit 4) and a thin surficial blanket of marine Adolphus Sand (Unit 5) (Figure 4-145).

4.3.5.3 Site Stratigraphy and Soil Profile – White Rose

A preliminary interpretation of the site stratigraphy and a preliminary design soil profile at the proposed WREP location was presented in a site characterization report (Fugro Geosurveys Inc. (FGI) 2011), based on the correlation of available nearby geotechnical data, high-resolution geophysical data and published regional studies (e.g., Sonnichsen and King 2005; King 2010). The stratigraphic profile is presented in Table 4-81 and shows the proposed correlation with geotechnical strata. The depth of interpretation is to 120 m below seafloor (bsf).

Table 4-81 Preliminary White Rose Extension Project Location Stratigraphy and Correlation with Geotechnical Strata

Seismo-Strat Unit	Geotech Stratum	Approx. Depth (m)	Soil Description	Stratigraphic Interpretation
5	I	0 to 3	Compact to dense fine to medium SAND	Holocene marine sand veneer
4/3F	II III IV	3 to 11	Dense GRAVEL with Cobbles Interbedded dense grey GRAVELLY SAND, occasionally with SILT and/or clay Hard olive grey SANDY CLAY	Pleistocene proglacial and glacial deposits
3E	V	11 to 28	INTERBEDDED: Very dense SILT Very dense SAND Very stiff to hard olive grey CLAY with SAND Dense to very dense fine to medium SAND; Hard olive grey SANDY CLAY Possible GRAVEL at base	Plio-Pleistocene shelf deposits (progradational)
3D	VI (upper 8m)	28 to 55	Upper 8m (only) sampled at White Rose. Not sampled in adjacent Fields. Very stiff to hard CLAY with SAND. Dense SANDY SILT	Late Miocene - Pliocene shelf deposits (aggradational)
3C	N/A	55 to 75	Not sampled at White Rose. Lower section (only) sampled in adjacent Fields. Inferred silty sand and sand (GSC)	Late Miocene - Pliocene shelf deposits (aggradational)
3B	N/A	75 to 90	Not sampled at White Rose. Inferred interbedded silty and clayey sand (GSC)	Late Miocene shelf deposits (aggradational)
3A	N/A	>90	Not sampled at White Rose. Inferred clayey sands and silty sands (GSC)	Mid-Miocene shelf deposits (progradational)
Note: The stratigraphy based on White Rose geotechnical borehole data and approximate correlations with regional seismo-stratigraphy of Sonnichsen and King (2005)				

High-resolution near-surface profiles were acquired during previous surveys within the present WREP area with a Huntec Deep Tow System sub-bottom system (FJGI 2005a, 2007). Near-surface conditions at the approximate WHP location are illustrated in Figure 4-149. The sub-bottom profile shows the upper 12 m of vertical section (using an assumed sound velocity of 1,600 m/s). Vertical resolution is approximately 0.3 m. The near-surface and deeper stratigraphy are illustrated in Figure 4-150, which is a 2D high-resolution seismic profile between the proposed WHP location and existing O-28 well (see Figure 4-151 for location). The section extends to approximately 130 m bsf. Vertical resolution is approximately 4 m. Tentative correlations to regional seismo-stratigraphic units of Sonnichsen and King (2005) are indicated on the 2-D high-resolution section.

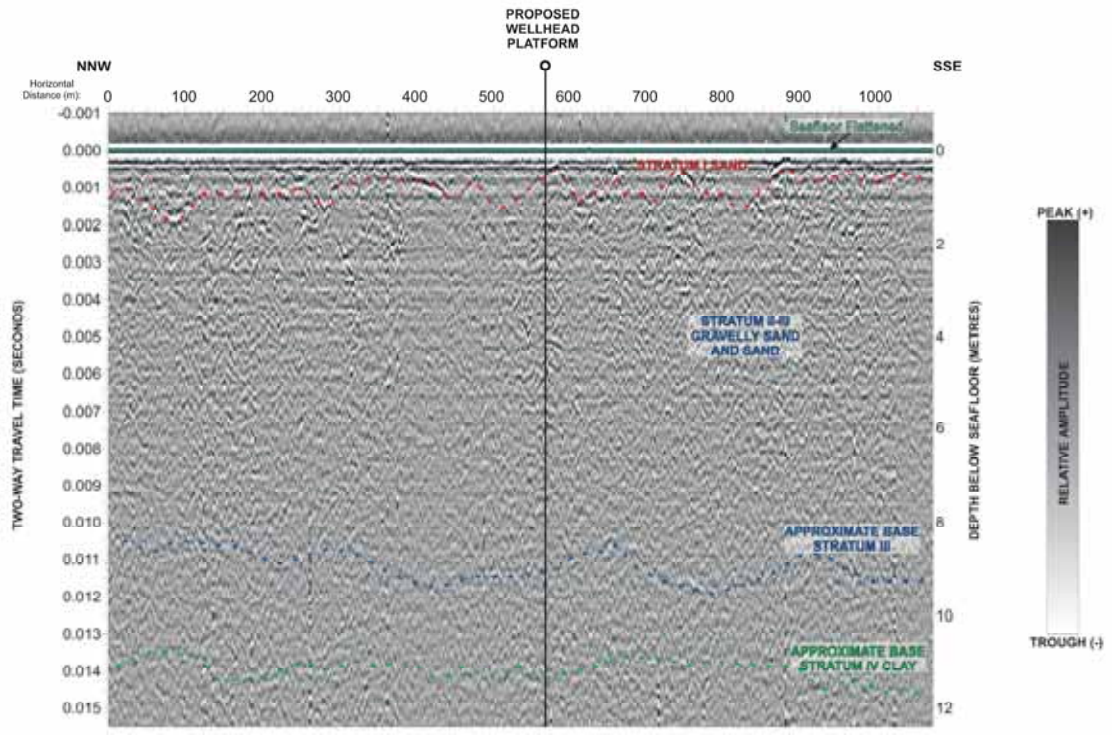

Note: Sub-bottom Profile, Line WRC05508

Figure 4-149 Near-surface Conditions at the Approximate Wellhead Platform Location

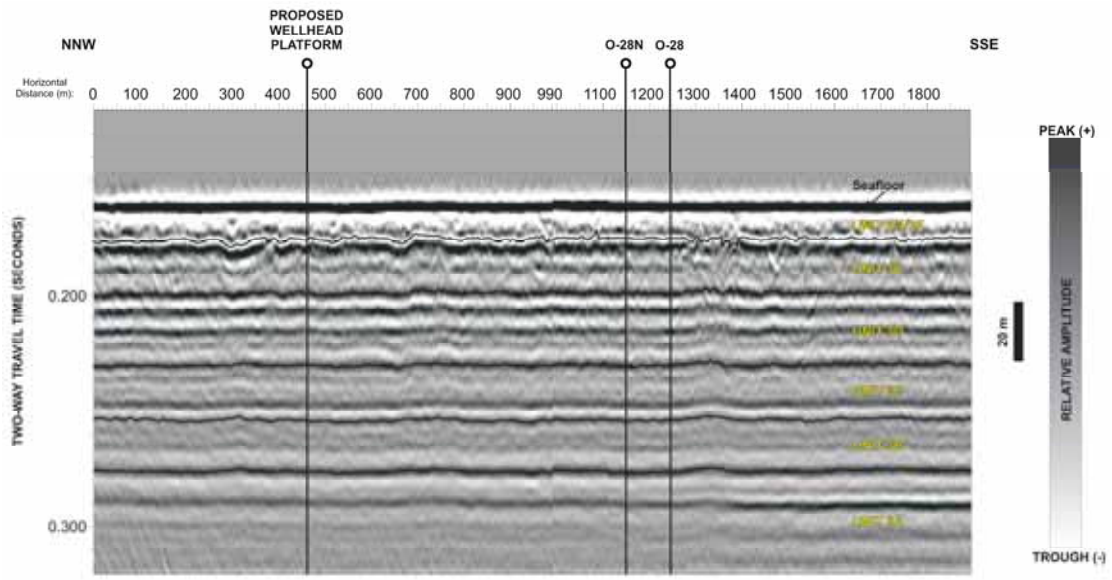

Note: see Figure 4-154 for location

Figure 4-150 2-D High-resolution Seismic Section, Arbitrary Tie Line, Linking the Proposed Wellhead Platform Location and Existing O-28 Well

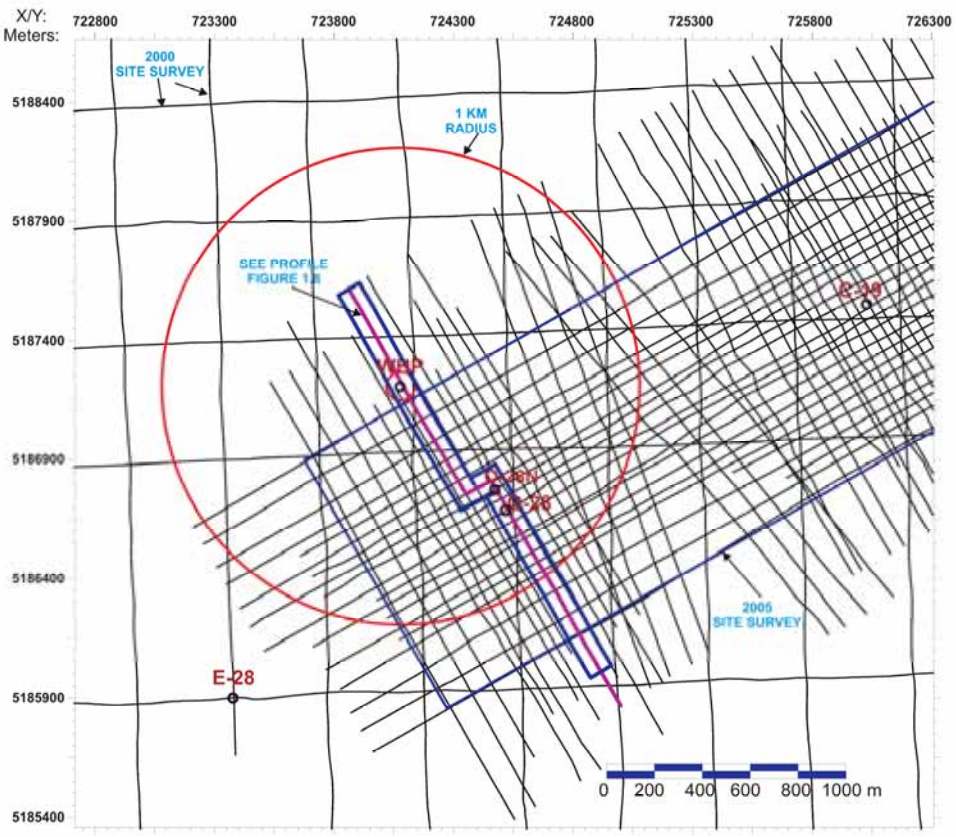

Note: Location of seismic profile in Figure 4-153 is illustrated

Figure 4-151 2-D High-resolution Seismic Post-Plot Base Map, Proposed Wellhead Platform Location

On the basis of the geophysical survey results reviewed for this report, it is concluded that the soil stratigraphy at well site O-28 can be used as a basis for a generalized geotechnical site stratigraphy and soil profile for the proposed WHP area.

A preliminary interpretation of the foundation zone stratigraphy of the proposed WHP location is described below and summarized in Table 4-81. The geological units have been correlated with geotechnical stratum nomenclature used in the reports referenced in Section 4.3.6.

Unit 5: Late Pleistocene – Holocene Surficial Marine Sand (Stratum I)

Seafloor sediments consist mainly of compact to dense fine- to medium-grained sands that blanket and fill an underlying, irregular ice-scoured surface. Coarse sand, gravel and occasional shell fragments are noted in some offset White Rose geotechnical boreholes. Sand thickness varies from near-zero to 2 to 3 m over short horizontal distances. The sand appears to form a generally thin surficial veneer (less than 2 m) in the vicinity of the proposed WREP surface location (Figure 4-147).

Unit 4/3F: Pleistocene-proglacial and Glacial Deposits (Strata II to IV)

The surficial sand is underlain by coarse-grained Stratum II and Stratum III, consisting of dense gravel with cobbles (II) and interbedded dense gravelly sand with occasional silt and clay (III), extending to variable depths of approximately 6 to 9 m bsf. The upper part of this interval displays intermittently high seismic amplitudes in sub-bottom profiles, suggesting variability in soil density and possible localized cemented hard-ground and/or coarse materials.

The dominantly coarse-grained near-surface sediments of Strata II and III are underlain by the very stiff to hard sandy clay of Stratum IV. Geotechnical boreholes show this sandy clay ranges in thickness from approximately 2 to 5 m.

The base of Stratum 4 appears to be an irregular erosion surface, interpreted across the WREP area in 2D high-resolution seismic data (Figure 4-150). The erosion surface varies in depth from approximately 10 to 12 m bsf seafloor in the WHP area. The Strata II IV sediments overlying this surface are interpreted to comprise undifferentiated proglacial and glacial deposits of regional seismo-stratigraphic Units 4 and 3F (Sonnichsen and King 2005; King 2010; Table 4-80).

Unit 3E: Plio-Pleistocene Shelf Deposits (Stratum V)

This interval is tentatively correlated with regional seismo-stratigraphic Unit 3E, which encompasses the geotechnical layers of Stratum V in the depth range 11 to 28 m at the O-28 wellsite. Stratum V consists of interbedded very dense silt, dense to very dense sand and sandy clay. The base of the geological Unit 3E lies at approximately 28 to 29 m bsf within the WREP area. It is expressed as a continuous high-amplitude event in 2D high-resolution seismic data (Figure 4-148), and occurs at consistent depth in geotechnical boreholes. A gravel horizon was intersected at the base of Unit 3E in borehole B-19_NW, indicating a possible erosion surface. Lateral variability of bedding and soil properties is likely, as indicated by seismic reflection character and the offset geotechnical borehole data.

Unit 3E displays generally low to moderate amplitude, semi-continuous, undulating seismic reflections, and is interpreted to have been deposited during a Plio-Pleistocene phase of shelf progradation (Sonnichsen and King 2005; King 2010).

Unit 3D: Late Miocene - Pliocene Shelf Deposits (Stratum VI)

Unit 3D is characterized by moderate to high-amplitude, continuous, conformable seismic reflections in 2D high-resolution seismic data (Figure 4-150). There are limited geotechnical data for this interval; White Rose boreholes O_28_N and B-19_NW penetrated 1 to 2 m into Unit 3D, and offset boreholes at the northwest and southwest anchor pile locations sampled the upper 5 to 8 m of 3D. The borehole data consistently characterize the upper part of the Unit as very stiff to hard clay with sand and occasional sand partings. These sediments are referred to as Stratum VI. Dense sandy silt was encountered below the clay within this stratum at the bottom of the deepest White Rose borehole (southwest anchor pile; 35.8 to 37.5 m).

The lower part of Unit 3D has not been sampled at White Rose or in other Grand Banks fields, but is interpreted to extend to an approximate depth of 55 m bsf within the WHP investigation area. The northeast-dipping strata are truncated at or near the seafloor west of White Rose, and are absent in adjacent fields.

Unit 3D is interpreted to have been deposited during a Late Miocene-Pliocene phase of shelf aggradation (Sonnichsen and King 2005; King 2010).

Unit 3C: Late Miocene – Pliocene Shelf Deposits

Unit 3C lies below the maximum penetration depth of White Rose area geotechnical boreholes, and is characterized by low to moderate amplitude semi-continuous reflections in 2D high-resolution seismic data (Figure 4-150). It extends to an approximate depth of 75 m bsf in the proposed WHP location. Similar to overlying Unit 3D, the Unit 3C strata rise to the SW and are partially truncated at or near seafloor in neighbouring fields (e.g., Terra Nova). Far offset boreholes from adjacent fields may have sampled the preserved lower part of 3C, which the GSC-A describes generally as silty sand and sand (Sonnichsen and King 2005). Lateral variability of soil properties is likely. Unit 3C is inferred to have been deposited during a Late Miocene-Pliocene phase of shelf aggradation (Sonnichsen and King 2005; King 2010).

Unit 3B: Late Miocene Shelf Deposits

Unit 3B is deeper than all of the White Rose boreholes, but is inferred to be interbedded silty and clayey sand, based on far-offset borehole sampling from adjacent fields (Sonnichsen and King 2005; King 2010). The Unit displays low to moderate amplitude, discordant to semi-continuous reflections in 2D high-resolution seismic data (Figure 4-150). Unit 3B was possibly deposited during a Late Miocene phase of concurrent shelf aggradation and shelf edge progradation. Lateral variability of soil types and characteristics is probable. The Unit is anticipated to be approximately 15 m thick, and lies at a depth of approximately 75 m bsf.

Unit 3A: Mid-Miocene Shelf Deposits

Unit 3A is characterized by moderate to high amplitude continuous reflections in the upper part, tending to lower amplitudes with depth in 2D high-resolution seismic data (Figure 4-150). It is greater than 50 m deeper than existing White Rose boreholes. Unit 3A is interpreted to have been deposited during a Mid-Miocene phase of shelf progradation. In distal, offshore areas such as White Rose; the GSC-A infers the Unit 3A strata to consist of clayey sands and silty sands (Sonnichsen and King 2005; King 2010). Unit 3A appears to extend below 120 m bsf at the proposed WHP location.

4.3.6 Near-surface Geotechnics – White Rose

Geotechnical investigations at White Rose show the soil stratigraphy in that area to consist of surficial granular strata (including surficial sands) to a typical depth of 7 to 8 m and as deep as 17 m, underlain by a complex of over-consolidated clay, interbedded over-consolidated sandy clay and silty sand, and clay to a depth of 36 m. The surficial granular soils consist of varying proportions of sands and gravels, with occasional pockets of cobbles and boulders. The proposed WHP soil profile is given in Table 4-82.

Geotechnical site investigations were conducted on Husky's behalf in the White Rose field by Fugro in 2001 and 2005. Details of the workscopes, equipment and results are provided in the following sections.

4.3.6.1 2005 White Rose Development Jack-up Rig Foundation Analyses

A geotechnical field program consisting of cone penetration tests (CPTs) and boreholes was conducted by Fugro at several proposed White Rose well site and drill centre locations in June 2005, using the drill ship *M/V Bucentaur* (FJGI 2005b). Soil conditions encountered at the proposed well site locations vary considerably across the White Rose field and also between boreholes at each well site location. However, in general terms, the soil stratigraphy can be described as 6 to 15 m of compact to very dense sands with gravel, overlying layers of very stiff to hard sandy clays and clays, interbedded with very dense sandy silts and sands to depths of at least 30 m.

Two boreholes were completed near each of the well site O-28 and B-19 surface locations, to penetration depths of 6 to 32 m. The deeper boreholes were offset from planned jack-up rig locations by approximately 80 m. A minimum offset distance of 50 m was specified by the client for deep geotechnical boreholes in order to limit seafloor disturbance at the planned rig location, and also to minimize any potential for shallow fluid/gas migration that might affect foundation integrity. Shallow (less than 10 m) boreholes were acquired at the centre of each proposed rig footprint, to obtain representative sampling of seafloor conditions at the site.

4.3.6.2 2001 White Rose Offshore Geotechnical Investigation

A previous geotechnical investigation was conducted in May 2001 at the White Rose field, and consisted of CPTs and soil sampling in boreholes put down at the proposed locations for the North, Central and Southern drill centres, as well as at the locations for the three planned anchor pile groups for the *SeaRose FPSO*. The investigation also included shallow borehole sampling and CPTs along the flowline routes between the drill centres (FJGI 2001).

Boreholes were drilled at two to three locations to depths ranging from 11 to 15 m within each of the proposed footprints for the three drill centres, with the deepest borehole at each location in the approximate centre. At the *SeaRose FPSO* anchor pile locations (east, northwest and southwest), primary boreholes were drilled to depths of approximately 35 to 37.5 m. Secondary boreholes were also drilled for each anchor pile at a location offset radially (from the proposed centre of the anchor pattern) approximately 200 m outward to depths of 7 to 14 m.

Table 4-82 Proposed Wellhead Platform Soil Profile

Stratum	Approximate Depth (m)	Soil Description	Su (kPa)	ϕ' (Degrees)	γ' (kN/m^3)	Wc (%)	Wp (%)	WL (%)	Dr (%)	Ko
I	0 to 3.0	Medium dense to very dense fine to medium SAND	n/a	40 to 45	10.0	20	n/a	n/a	80 to100	4
II	3.0 to 4.0	Very Dense GRAVEL to Silty Gravelly SAND and with occasional cobbles and boulders	n/a	42 to 45	10.0	10	n/a	n/a	100	4
III	4.0 to 9.0	INTERBEDDED: Very Dense clayey SAND, silty SAND Very Stiff to Hard Sandy CLAY	 n/a 200 to 300	 40 to 42 n/a	 10.0 10.0	 16 20	 n/a 24	 n/a 40	 100 n/a	1.5 to 2
IV	9.0 to 11	Hard CLAY to Sandy CLAY	270 to 300	n/a	10.2	22	16	45	n/a	n/a
V	11 to 28	INTERBEDDED: Dense to very dense fine to medium SAND Hard Sandy CLAY	 n/a 140 to 180	 42 n/a	 10 9	 20 25	 n/a -	 n/a -	 80-90 n/a	 1.5 -
VI	28 to 37	Very Stiff to Hard Sandy Clay	200 to 250	n/a	9	30	23	86	n/a	-
	37 to 55	Very Stiff to Hard Sandy Clay	250	n/a	9	30	23	86	n/a	-
VII	55 to 75	Possible Dense Silty SAND to SAND	n/a	36 to 38	10	-	n/a	n/a	60-80	
VIII	75 to 90	Possible Interbedded Dense Silty SAND and Clayey SAND	n/a	30 to 34	10	-	n/a	n/a	-	
IX	90 to >120	Possible Medium Dense to Dense Clayey SAND and Silty SAND	n/a	28 to 32	9	-	n/a	n/a	50-80	

Source: Adapted from FGI 2011

Note: Strata properties below dashed line (at 37 m bsf) are estimates only, and are based on regional geological interpretations and site-specific geophysical interpretations

A reinterpretation and simplification of the soil strata shows that there are similarities in soil types and consistent sequences across the White Rose field, although there are substantial differences in strata thicknesses. Other borehole locations considered to be relevant for a compilation of soil properties at the WHP area are: B-19 (from FJGI 2005c); and northwest anchor pile location, CGH and southwest anchor pile (from FJGI 2001). Boreholes O-28 and B-19 are closer to the proposed WHP location and within the most recent detailed geophysical survey (FJGI 2005a, 2007) - for this reason, these have been examined more closely than the other boreholes. Boreholes at the northwest and southwest anchor pile locations, and CGH were studied to compare variability and observe trends in soil stratum and soil properties. An extensive geotechnical program is scheduled for the summer of 2012 in the vicinity of the proposed WHP location.

4.3.7 Ice Scour Distribution - White Rose

The northern Newfoundland Shelf is subject to iceberg grounding and scouring. Iceberg scour marks and grounding pits are common features on the margins of Grand Bank, including the White Rose field. Scour marks occur as curved or linear furrows, with or without berms at the sides, and as elliptical or circular grounding pits. Scour marks observed in water depths of less than 110 m are considered to have formed since the exposure and transgression of the bank top, less than 15,000 years ago (e.g., Sonnichsen et al. 1994; Huppertz and Piper 2009). An older population of relict scour marks is present in deeper water. These are occasionally buried, and/or overprinted by more recent scour marks. Such features are evident on side scan sonar and swath bathymetry images in the White Rose field, as well as on sub-bottom profiler records.

Substantial efforts have been made to quantify the rate of present-day scouring. Repetitive mapping surveys and comparisons have been conducted with the aim of identifying new scour events that can be used to estimate the frequency of modern scouring events. Some of this work has been conducted within the White Rose field, using observed iceberg scouring events. A scour event, named 88-01, was inferred to have occurred between April 2 and 13, 1988, to the north-northeast of the E-09 well site at White Rose. The resultant scour mark was imaged with side scan sonar and studied in detail. Scour mark depth ranged from 0.5 to 1.1 m, with widths of 20 to 35 m (Banke 1988; Woodworth-Lynas 1989). Since that exercise, repetitive mapping surveys have been conducted over portions of the seafloor within the region (e.g., Terraquest Associates 1998), which attempted to identify new scour marks formed during the interval between surveys. However, repetitive mapping efforts have been complicated by poor positioning of older data sets, and inconsistencies in data quality, survey systems and survey conditions.

Regional estimates of the minimum scouring frequency are on the order of 2×10^{-4} scour events/km^2/year (Banke 1989), but this estimate does not consider short-term grounding events or scouring icebergs. Sonnichsen et al. (2005) estimate the scour frequency on the Grand Banks to be 2.7×10^{-4} scour events/km^2/year. The GSC-A-, C-CORE- and FJGI-derived scour frequency estimates based on comparisons of recent site survey and repetitive mapping data (including multibeam sonar) with older side scan datasets (C-CORE 2001a; FJGI 2004). Estimates reported by C-CORE (2001b) related specifically to the White Rose field are on the order of 1×10^{-3} scours/km^2/year.

4.3.8 Seismicity

The description of seismicity in the Offshore Project Area is limited to a review of available data, including: peer reviewed literature; published geologic maps; topographic maps; GSC publications; in-house Fugro proprietary data; and satellite imagery. These data were analyzed to characterize the seismotectonic setting of the region and seismic hazard in the White Rose field to provide a qualitative seismic hazard review of the White Rose field for the purposes of an environmental assessment. This data review did not include a detailed seismotectonic characterization or a site-specific probabilistic seismic hazard assessment (PSHA). Reviewed reports included:

- White Rose Oil Field Comprehensive Study (Husky Oil 2000)
- Hebron Project Comprehensive Study (ExxonMobil Canada Properties (EMCP) 2011)
- White Rose Oil Field Comprehensive Study: Responses to Comments from Canada-Newfoundland Offshore Petroleum Board, DFO, Environment Canada, Natural responses Canada, and Canadian Environmental Assessment Agency (Husky Oil 2001).

4.3.8.1 Seismotectonic Setting

The White Rose field is located on the margin of the Jeanne d'Arc Basin within the Grand Banks, 355 km offshore of Newfoundland (Figures 4-152 and 4-153). The Grand Banks is a broad continental shelf extending approximately 450 km eastward from Newfoundland (Tankard and Welsink 1987) (Figures 4-153 and 4-154). The northern and southern boundaries of the Grand Banks are bound by the Charlie Gibbs fracture zone and the Newfoundland fracture zone, respectively (Figure 4-153) (Mackay and Tankard 1990). These fracture zones represent transform faults that were active in the late Triassic and early Jurassic; they became dormant during later stages of rifting (Tankard and Welsink 1987). Geologic structure within the Grand Banks is defined by a complex suite of half-grabens that formed over approximately 225 Ma (Tankard and Welsink 1987). These developed as a part of Mesozoic-aged rifting as Pangea split, during inception of the mid-Atlantic rift (Tankard and Welsink 1987). One of the more substantial half-grabens formed during this rifting includes the Jeanne d' Arc Basin, in which the White Rose site is located (Figures 4-152 and 4-155).

Tectonic stress acting on the stable continental crust of the shelf (Figures 4-153 and 4-154) includes compression as the North American plate is being 'pushed' away from the mid-Atlantic ridge and being resisted by asthenospheric drag (Basham and Adams 1983). Other stresses acting on the region include ongoing post-glacial isostatic rebound and increasing weight of sedimentary deposits within the basins (Basham and Adams 1983). The principal seismic zones offshore of Newfoundland broadly correlate to Mesozoic structural features formed during rifting events; these may act to control the spatial distribution of earthquakes (Adams et al. 1995; Mazzotti and Adams 2005).

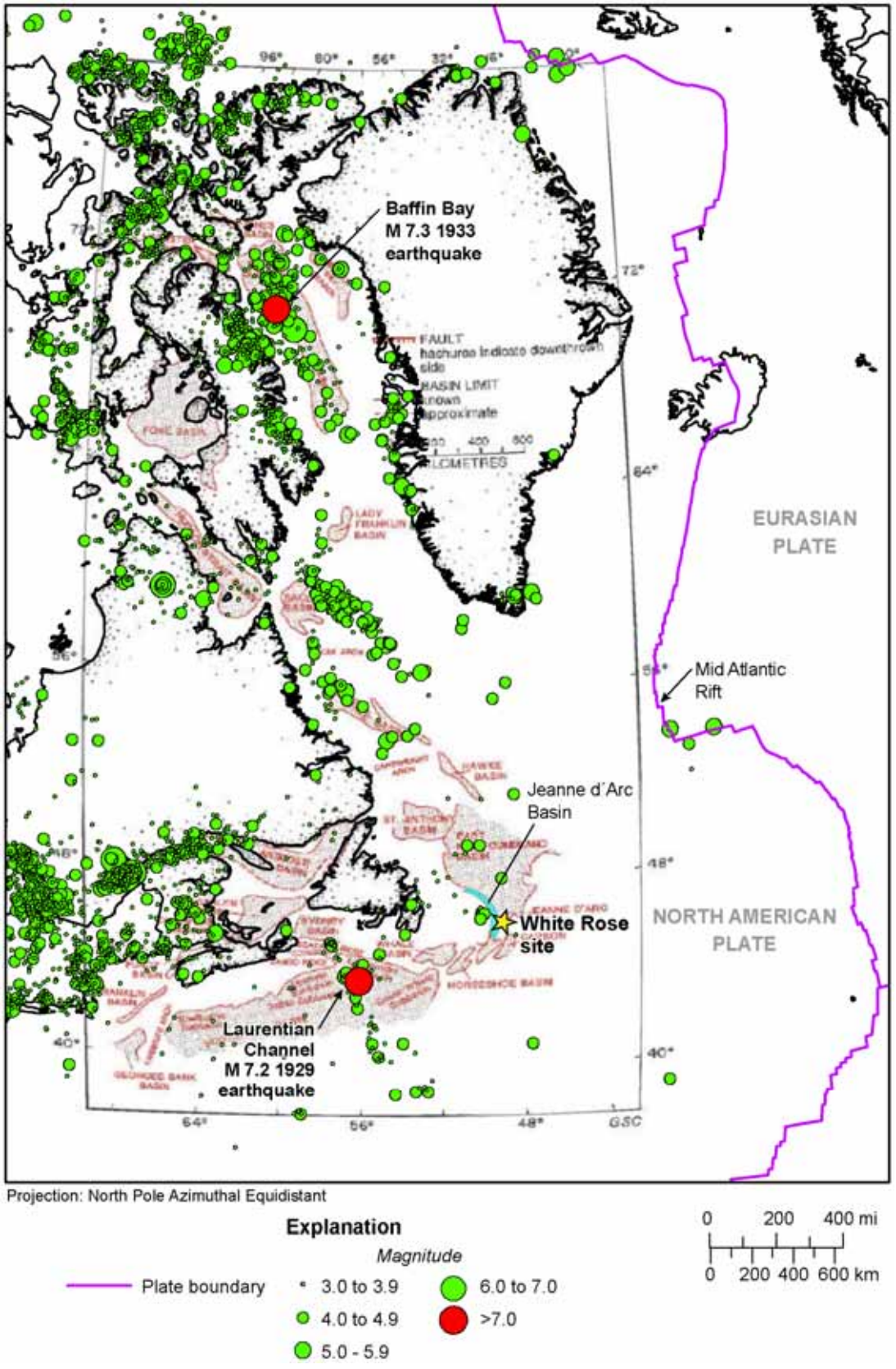

Figure 4-152 Regional Seismicity and Mesozoic Basin

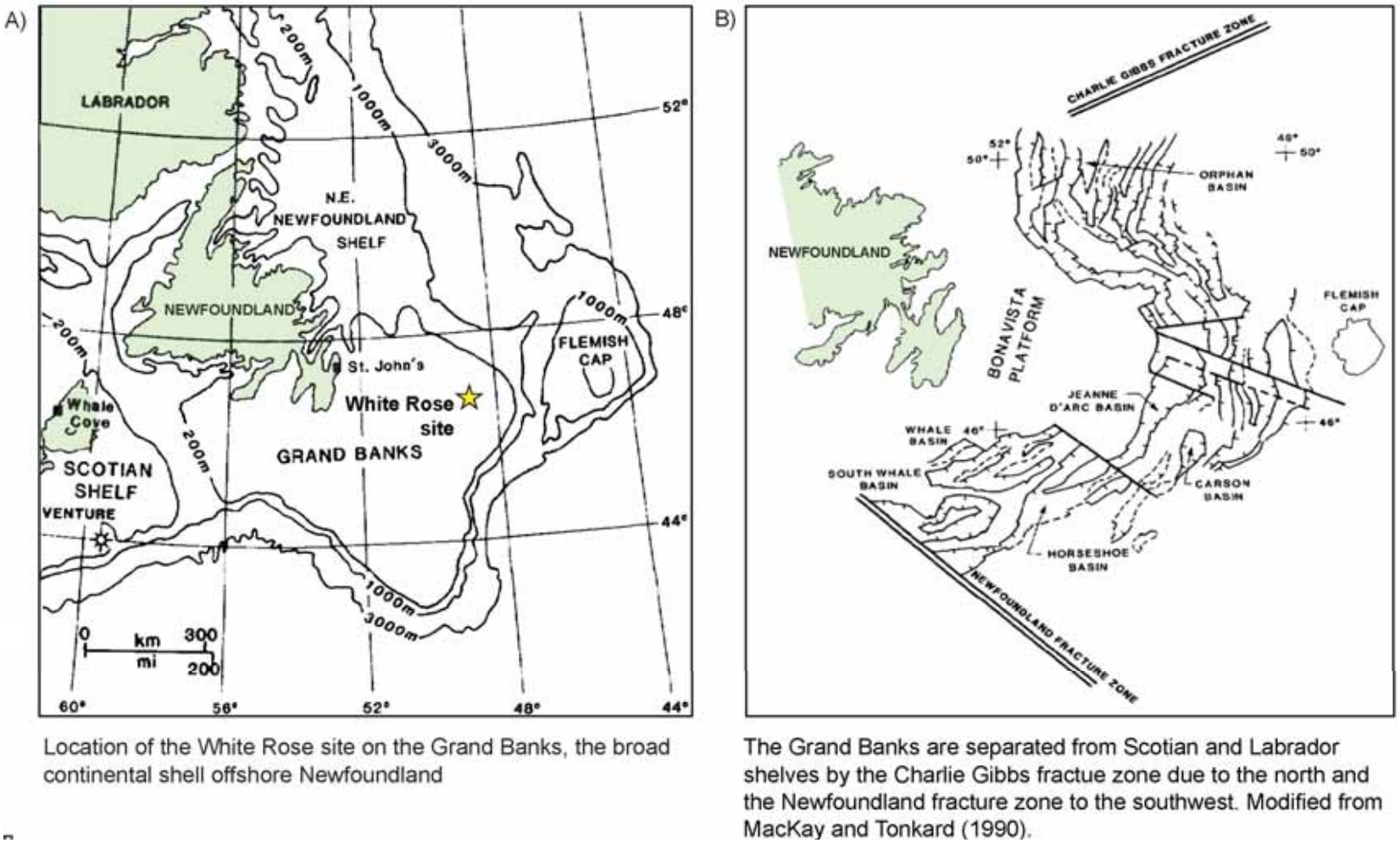

Location of the White Rose site on the Grand Banks, the broad continental shell offshore Newfoundland

The Grand Banks are separated from Scotian and Labrador shelves by the Charlie Gibbs fractue zone due to the north and the Newfoundland fracture zone to the southwest. Modified from MacKay and Tonkard (1990).

Figure 4-153 Location and Structure of Jeanne d'Arc Basin

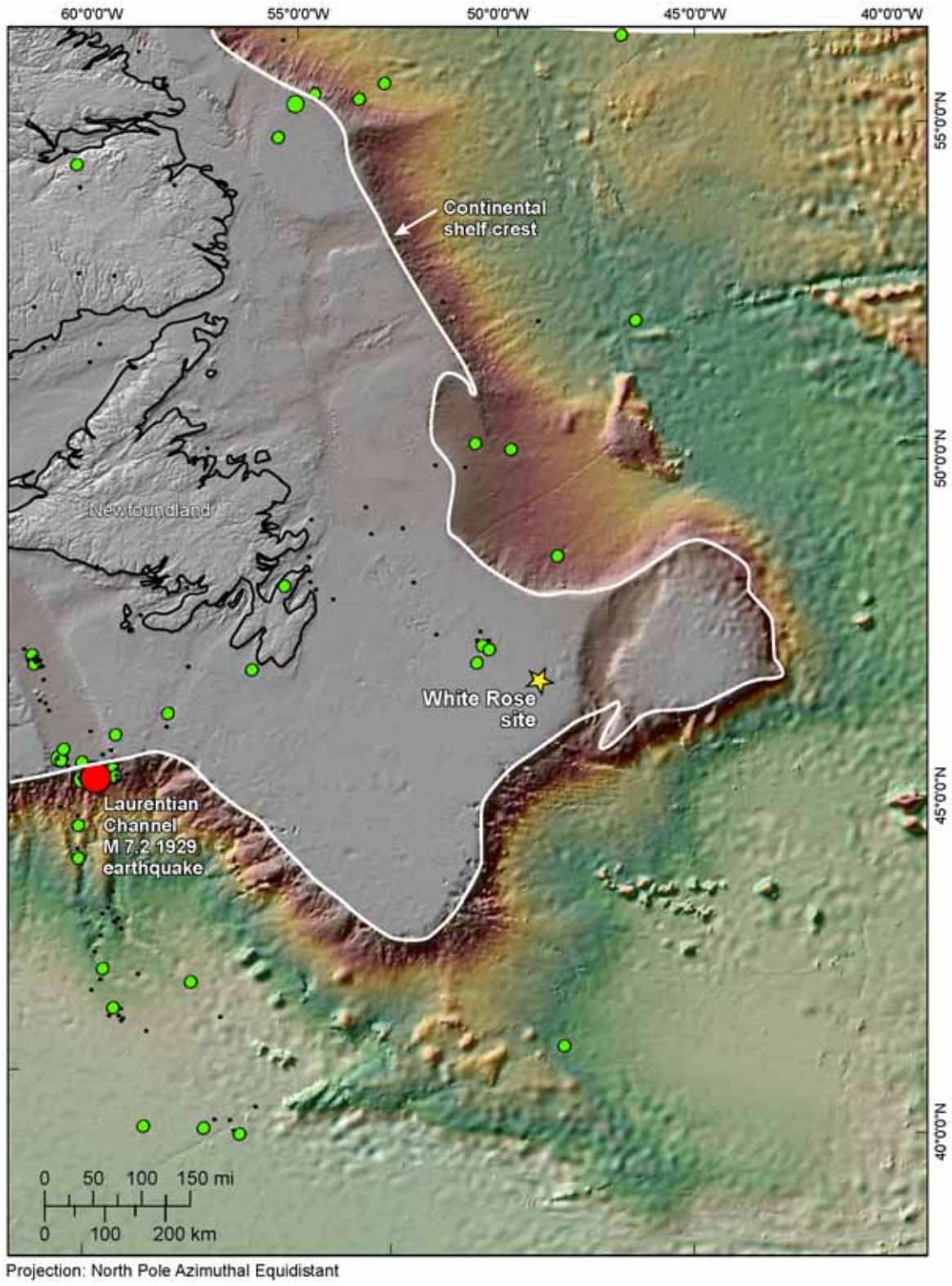

Note: See Figure 4-152 for magnitude legend

Figure 4-154 Eastern Boundary of Stable Continental Shelf Offshore Newfoundland

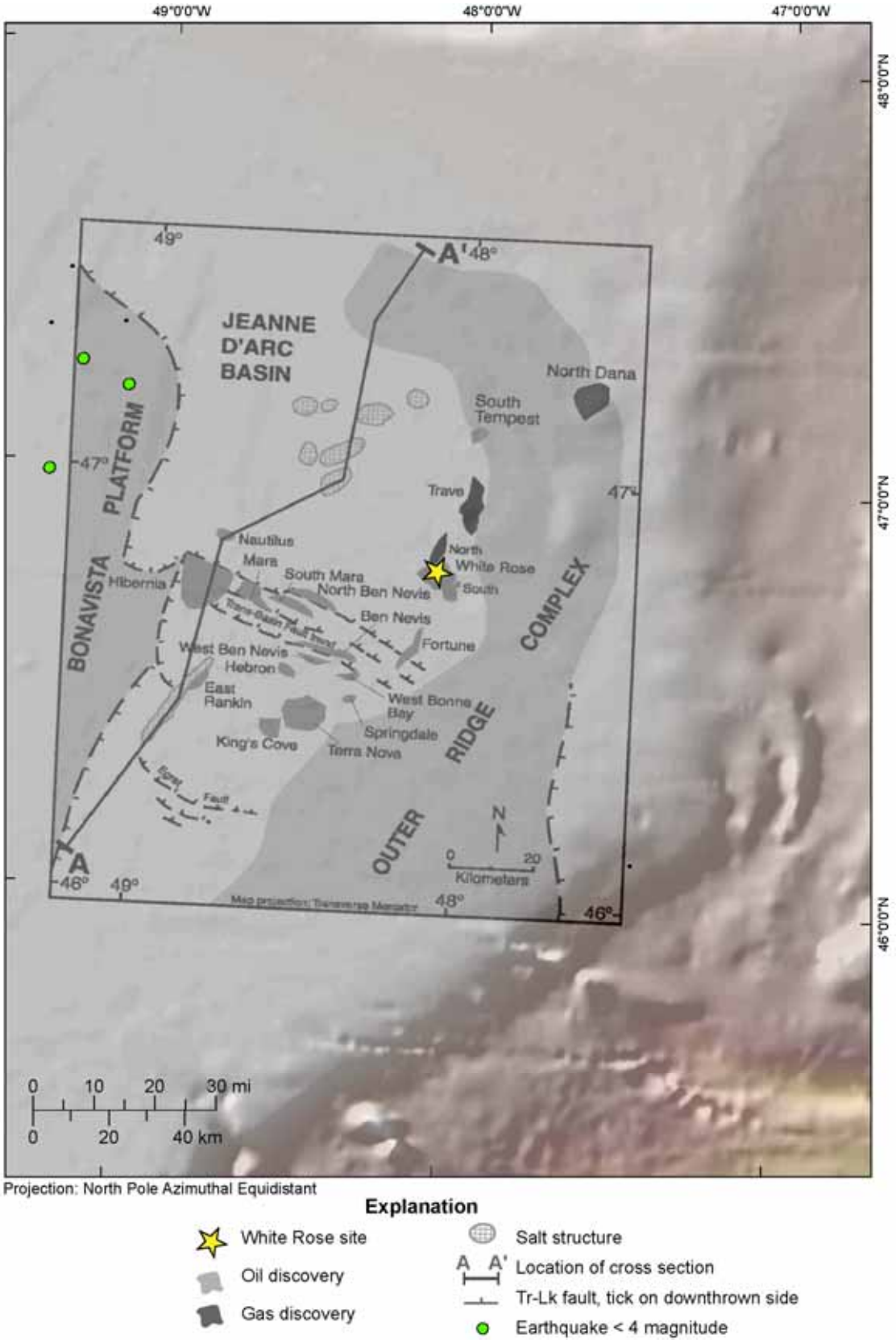

Figure 4-155 Local Jeanne d'Arc Basin Structural Features

Local Geologic Setting

The Jeanne d' Arc Basin is a narrow and elongate basin formed by normal movement on the listric Murre fault, which soles out towards the east at approximately 26 km depth (Tankard and Welsink 1987; Hurley et al. 1992). This fault bounds the basin on its west side and separates pre-Mesozoic metamorphosed Precambrian and Paleozoic basement rocks from Mesozoic strata within the basin (Hurley et al. 1992). Northwest-southeast intra-basin trans-basin faulting splits the basin and the Egret fault bounds it to the south (Figure 4-155) (Tankard and Welsink 1987; Magoon et al. 2005). Other major tectonic features of the Jeanne d' Arc Basin include the Bonavista platform to the west, the Avalon uplift to the south and the Central Ridge Complex to the east (Figure 4-155) (Hurley et al. 1992).

Stratigraphically, the Jeanne d' Arc Basin contains large-scale, unconformity-bounded sequences deposited during multiple rifting events beginning in the Triassic (Tankard and Welsink 1987). The strata represent Late Triassic to Early Jurassic rift valley sedimentation including (in ascending order) conglomerates, red beds, evaporites, carbonates and calcareous mudstones and sandstones (Jansa and Wade 1975; Hurley et al. 1992).

Historical Seismicity

Historically, the continental margin of eastern Canada has experienced low seismicity. However, two M7 earthquakes have occurred; one on the continental slope of Newfoundland in 1929 and the other in Baffin Bay in 1933 (Figure 4-155) (Basham and Adams 1983; GSC 2010).

The GSC compiled a Seismic Hazard Earthquake Epicenter File (SHEEF) in the early 1990s and has subsequently revised and updated this catalog three times (Halchuk 2009). SHEEF was the earthquake database the GSC used to develop a new seismic hazard model and a suite of new seismic hazard maps for Canada (Adams and Halchuk 2003; Halchuk 2009). Earthquakes from this catalog are plotted in Figures 4-152 and 4-154, showing the catalogued seismicity in the Grand Banks region of the continental shelf.

In historic times, earthquake activity has been concentrated north of the Jeanne d' Arc Basin, in Baffin Bay and the Labrador Sea and southwest of the basin at the mouth of the Laurentian Channel (Figure 4-153) (Basham and Adams 1983). The largest historic earthquake in the region was an M7.3 in Baffin Bay in 1933; following this, there have been three M6 and many smaller events in Baffin Bay (Basham and Adams 1983). Although there is evidence for a failed rift system in Baffin Bay (Jackson et al. 1979), the M6 and smaller events are not associated with this extinct spreading centre (Basham and Adams 1983). The second largest event was an M7.2 that ruptured the slope within the Laurentian Channel, causing a 200-km long slump of slope deposits, a turbidity current that destroyed numerous telegraph cables and a tsunami that led to 27 deaths in southern Newfoundland (Basham and Adams 1983). Seismic reflection surveys have located young faulting in the Laurentian Channel, but offsets in the uppermost layers of sediments are not definitive (King 1979).

4.3.8.2 Regional Seismic Hazard Assessments

The following sections provide a review of the regional and site-specific seismic hazard assessments that have been completed for the region. These studies include the GSC's ground motion estimates (Halchuk and Adams 2008) and a site-specific PSHA study for the Hebron platform site located 30 km southwest of the White Rose field (URS 2006).

Geological Survey of Canada

The Canadian government developed four generations of national seismic hazard maps for Canada (Basham et al. 1985; Adams et al. 1999; Adams and Halchuk 2003; Halchuk and Adams 2008; Halchuk 2009), which suggest the White Rose site region has moderate seismic hazard despite relatively limited seismicity (described in Section 4.3.8.1). The most recent published maps were developed to be used with the 2005 National Building Code of Canada (Halchuk and Adams 2008).

The original overall methodology and base source model were developed in the 1980s and have been updated three times since the original maps were generated (Halchuck and Adams 2008). These probabilistic seismic hazard maps were generated using the "Cornell-McGuire" method (which remains the current standard of practice) and included 32 earthquake source zones that cover the nation of Canada (Basham et al. 1985). In the White Rose field region, the Canadian model included two different geometries for aerial seismic sources, which are intended to capture the uncertainty in characterizing earthquakes in this region. The "H" model uses small source zones that encompass historical seismicity clusters and the "R" model uses larger source zones that encompass regions with a similar seismotectonic setting or feature (Halchuk and Adams 2008). These two methods were then combined using the "Robust" method of conservatively choosing the higher of the two ground-motion estimates at each grid point (Adams et al. 1995).

The "R" model and "H" model source zones within the White Rose site region (Figure 4-156) include:

- Atlantic offshore background (AOBH) – This source geometry surrounds most of onshore and offshore Newfoundland ("H" model).
- Laurentian Slope (LSP) – This small source geometry surrounds the 1929 Grand Banks earthquake and associated seismicity ("H" model).
- Atlantic offshore background (AOBR) – This source geometry surrounds most of eastern onshore and offshore Newfoundland following the eastern continental margin closely ("R" model).
- Eastern Continental Margin (ECM) – This source geometry (as the name suggests) encompasses the continental margin-including the 1929 Grand Banks earthquake and the 1933 M7.3 Baffin Bay earthquake. This geometry indicates a similar seismotectonic setting for the Eastern Continental Margin with an elevated potential for larger magnitude quakes.

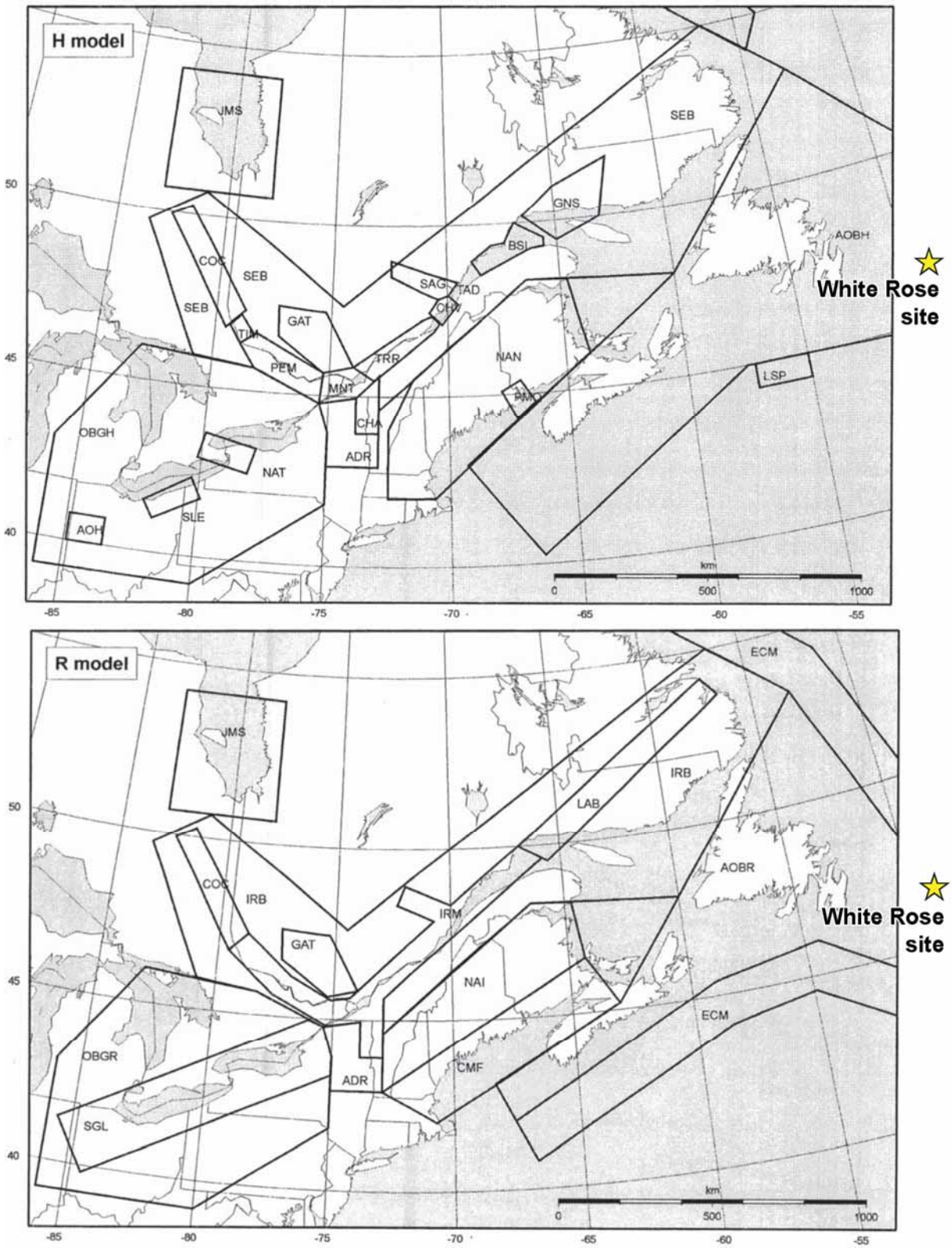

Source: from Halchuk and Adams 2003

Figure 4-156 Geological Survey of Canada Aerial Seismic Source Models "H" and "R"

These source geometries are clearly reflected in the predicted Site Class C ground motions for the latest (2010) generation of the seismic hazard maps of Canada (Figure 4-157) (Natural Resources Canada 2011).

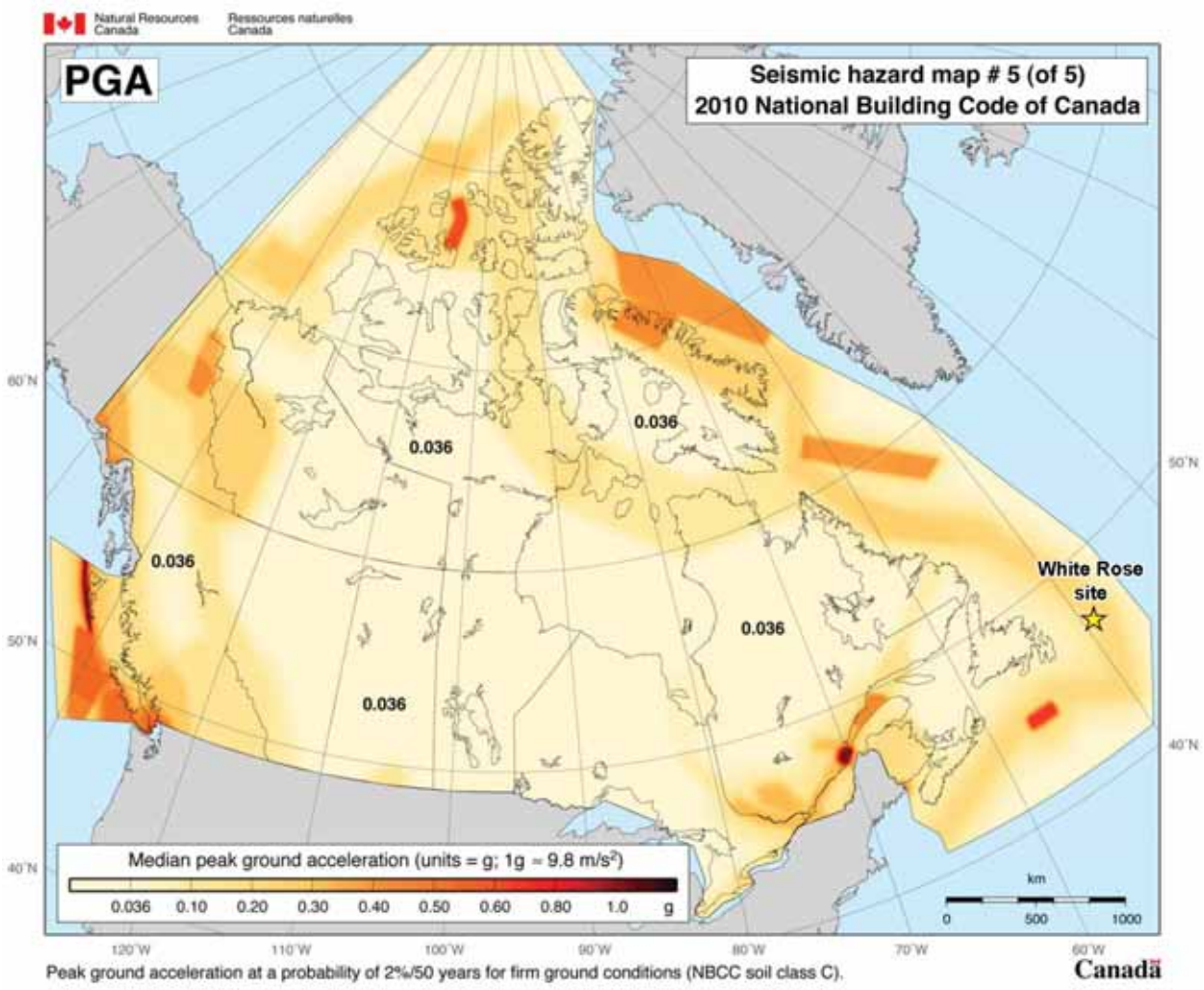

Figure 4-157 Geological Survey of Canada 2010 Seismic Hazard Map

As shown in Figure 4-157, the peak ground acceleration (PGA) for the White Rose field is estimated to be approximately 0.2 g to 0.3 g based on GSC, for a probability of exceedance of 2 percent in 50 years (GSC 2010). The National Building Code of Canada seismic hazard calculator (GSC 2010) does not extend to the White Rose site. Thus, to estimate spectral acceleration at the White Rose site, coordinates of 46.8°N, 49.0°W (approximately 64 km from the site) were used. Examination of the hazard shading shown in Figure 4-160 shows lower hazard just west of the White Rose field; thus, the accelerations of the GSC website may under-predict ground motions. Based on this observation and using the National Building Code of Canada seismic hazard calculator (GSC 2010) for coordinates 46.8°N, 49.0°W, the minimum spectral acceleration at the White Rose field is predicted to be 0.213 g, 0.448 g, 0.243 g, 0.122 g and 0.037 for PGA, and at 0.2, 0.5, 1.0 and 2.0 seconds, respectively (GSC 2010), for a 2 percent in 50-year probability of exceedence. Similar calculations can be done for a

2,500-year return period based on the GSC calculator. Examination of the hazard shading shown in Figure 4-157 shows lower hazard just west of the White Rose field; thus, the spectral accelerations at the White Rose site may be higher than those obtained from the GSC calculator.

URS Probabilistic Seismic Hazard Analysis Study for the Hebron Platform

URS conducted a PSHA for the Hebron platform site in 2006. This site is located approximately 30 km southwest of the White Rose field (Figure 4-154). The report evaluated the potential for active faulting immediately adjacent to the Hebron platform and considered uncertainties for seismic source characterizations and attenuation models available at that time.

The base seismic source models used for the Hebron platform PSHA were similar to those used by the GSC. Two models were considered to capture the uncertainty in characterizing earthquakes in this region: (1) large earthquakes would be expected only near unique geologic structures; recurrence rates would be higher near these and very small away from them; and (2) large earthquakes could occur anywhere along the continental margin; low recurrence rates everywhere (URS 2006). The probabilistic seismic hazard analyses were generated using the "Cornell-McGuire" method and the ground-motion attenuation models of Atkinson and Boore (1995) and those of Toro et al. (1997).

PGAs predicted at the Hebron site are 0.32 g at a period of 0.2 second and 0.12 g at a period of 1.0 second for a 2 percent probability of exceedence in 50 years (URS 2006). Spectral acceleration at the Hebron Stiff Soil (Site Class C) site conditions when Model 1 (described above) was used are 0.128 g, 0.075 g, 0.049 g and 0.030 g, at 0.2, 0.5, 1.0 and 2.0 seconds, respectively, at a 2 percent in 50-year probability of exceedence (URS 2006). The Hebron Stiff Soil (Site Class C) site conditions spectral acceleration when Model 2 (described above) was used are 0.323 g, 0.187 g, 0.121 g and 0.063 g, at 0.2, 0.5, 1.0 and 2.0 seconds, respectively, at a 2 percent in 50-year probability of exceedence (URS 2006).

4.3.8.3 Discussion

The review of literature reveals that while the region around the White Rose field does have relatively low seismicity based on the existing regional seismic catalogue, large magnitude (M7 and above) earthquakes have occurred in the region. The stresses driving these events are not well understood and the probable locations of future large earthquakes cannot be robustly forecast.

Husky Oil (2001) presented a PGA of 0.03 for a return period of 200 years, based on the findings of Foo and Crouse (1986). Foo and Crouse suggested that this PGA was appropriate for the Hibernia site (located approximately 64 km west of White Rose).

Independent seismic hazard analyses that have been recently conducted for the region of the White Rose field (URS 2006; GSC 2010) indicate much higher PGAs. PGAs calculated for a 2,500-year return period are an order of magnitude higher (Table 4-83). PGA calculated for a 200-year return period is more than double the 0.03 PGA presented in Table 4-84.

Table 4-83 Peak Ground Acceleration and Spectral Acceleration Estimates for an Exceedence Probability of 2 Percent in 50 years (2,500 year Return Period)

	PGA	Spectral Acceleration			
		(0.2 sec)	(0.5 sec)	(1.0 sec)	(2.0 sec)
GSC model [A]	0.213	0.448	0.243	0.122	0.037
URS [B]	0.323	0.244	0.141	0.090	0.048

(A) Calculated for a site approximately 64 km from the White Rose field at a Site Class C (GSC 2010)

(B) Calculated for a site approximately 32 km from the White Rose field at a Site Class C. Mean of Model 1 and Model 2 used for Sa values (URS 2006)

Table 4-84 Peak Ground Acceleration and Spectral Acceleration Estimates for an Exceedence Probability of 25 Percent in 50 years (200 year Return Period)

	PGA	Spectral Acceleration			
		(0.2 sec)	(0.5 sec)	(1.0 sec)	(2.0 sec)
URS [A]	0.069	0.048	0.029	0.018	0.008
Husky Oil [B]	0.03	Not Calculated	Not Calculated	Not Calculated	Not Calculated

(A) Calculated for a site approximately 32 km from the White Rose field at a Site Class C. Mean of Model 1 and Model 2 used for Sa values (URS 2006)

(B) From Foo and Crouse (1986) for the Hibernia Operating Level Earthquake

4.3.9 Climate Change

Climate is naturally variable and can change over a range of time scales from the very short term, to seasonally, and to longer time periods in response to small and large-scale changes of atmospheric circulation patterns. Short term meteorological variations are largely a consequence of the passage of synoptic scale weather systems: low pressure systems, high pressure systems, troughs and ridges. The energetics of these features varies seasonally in accordance with the changes in the strength of the mean tropical-polar temperature gradient. Long-term changes occur in response to small and large-scale changes of atmospheric circulation patterns, which in the past in the Northern Hemisphere were mainly the result of changes in the NAO. While the NAO still has an effect on climate patterns, there is a general consensus amongst the scientific community that greenhouse gas emissions have played an important role in the climate during the last 50 years. However, the high degree of climate variation naturally experienced makes it difficult to identify, with any degree of certainty, trends that are a direct result of climate change (Environment Canada 1997).

The dominant features of the mean sea level pressure pattern in the North Atlantic Ocean are the semi-permanent area of relatively low pressure in the vicinity of Iceland and the sub-tropical high pressure region near the Azores. The relative strengths of these two systems control the strength and direction of westerly winds and storm tracks

in the North Atlantic and, therefore, play an important role in the climate of the North Atlantic. The fluctuating pressure difference between these two features is known as the NAO, measured as the NAO Index, which is the normalized difference in pressure between the Icelandic low and the Azores high. A large difference in pressure results in a positive NAO Index and can be the result of a stronger than normal subtropical high, a deeper than normal sub-polar low, or a combination of both. The positive phase of the NAO Index results in: more and stronger winter storms crossing the North Atlantic on a more northerly track; and cold dry winters in northern Canada and Greenland. The negative phase results in fewer and weaker storms crossing on a more west-east track. A time-series of the winter (December, January, February) NAO Index during the period of 1950 to 2011 is presented in Figure 4-158.

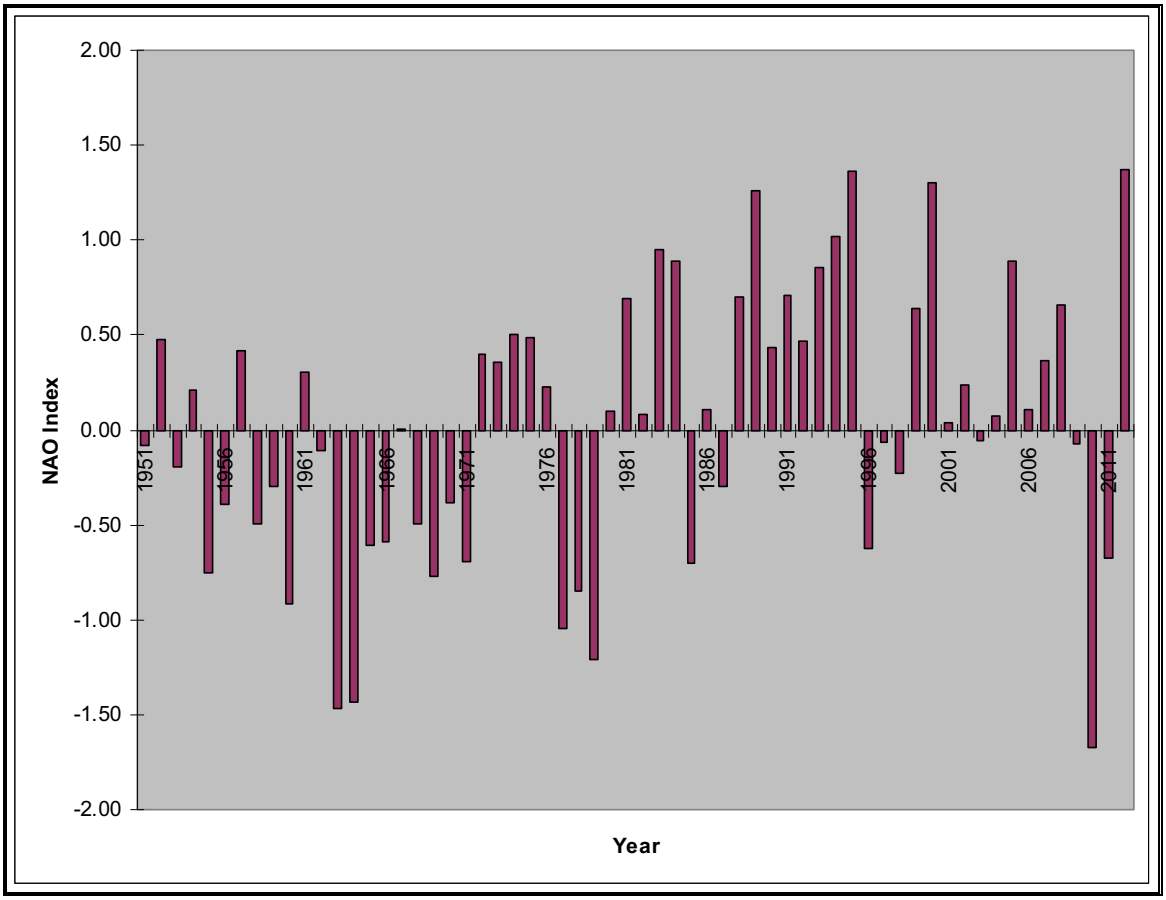

Figure 4-158 Winter North Atlantic Oscillation Index, 1950 to 2012

The negative phase of the NAO Index dominated from the mid- to late-1950s until the early 1970s. There was a five-year period of positive phase in the 1970s, then another shift back to a negative phase for three years from 1977 to 1979. From 1979/80 until the late 2000s, the NAO Index remained in a generally positive mode, with only six deviations into the negative mode during this 29-year period. The NAO Index has been in a negative phase from 2009 to 2011, with 2010 being the strongest negative phase since 1950. In 2012, the NAO Index completely reversed, with the strongest positive phase of the NAO Index in the last 61 years.

In general, over the Northwest Atlantic during the winter season, a positive NAO Index brings with it an increase in frequency and strength of westerly winds in the upper atmosphere, which tends to steer storm systems in a more west to east direction. As a result, a positive NAO Index results in an increase in storm systems coming off of the continent, resulting in colder temperatures, increased precipitation and relatively stronger winds. Due to the weaker trend in NAO Index and other atmospheric patterns, conclusions could not be drawn about correlations between NAO indices and temperature, precipitation and winds during the summer months.

A number of studies have been conducted recently to assess whether climate change and global warming would have an effect on storm tracks, frequency and intensity. Archer and Caldeira (2008) found that, during the period of 1979 to 2001, there was a poleward shift in the jet stream of 0.17 to 0.19 degrees/decade and a substantial pressure decrease, which would imply an increase in jet stream altitude in the Northern Hemisphere. These results were consistent with an increase in mean temperature from equator to pole. Changes in jet-stream latitude, altitude and strength have the potential to affect the formation and evolution of storms in the mid-latitudes and of hurricanes in the sub-tropical regions. These results are consistent with a study by McCabe et al. (2001), which showed that, from the period of 1959 to 1997, there has been a substantial decrease in mid-latitude cyclone frequency and a substantial increase in high-latitude cyclone frequency, consistent with increases in winter Northern Hemisphere temperatures.

During the summer months, the NAO Index has a less direct effect on the climate of eastern Canada; however, studies have shown that the NAO has an effect on the track of hurricanes in the North Atlantic. During seasons with a negative NAO Index, hurricanes tend to favour a track that parallels lines of latitude often ending up in the Gulf of Mexico and the Caribbean (Elsner 2003). During seasons with a positive NAO Index, hurricanes tend to curve northward (Elsner and Bosak 2004) along the US Eastern Seaboard. However, an analysis of the number of tropical storms entering the Canadian Hurricane Centre Response Zone shows no correlation between tropical cyclone frequency and NAO Index.

4.3.9.1 Sea-Level Rise

Annual mean sea level can vary considerably from year to year as a response to various meteorological and oceanographic variables. Higher-than-normal sea level pressure (negative NAO Index) would result in lower sea levels, while lower sea level pressure would result in higher-than-normal sea levels (positive NAO Index). Changes in ocean circulation can also have an effect on the regional scale.

Sea levels are rising and expected to continue to rise into the foreseeable future. There are many factors contributing to this rise, with the most important being thermal expansion due to increased ocean temperature. Other contributions come from the melting of glaciers and major sheet ice, such as that covering Greenland and Antarctica (Church 2011). Using satellite altimeter data, as well as sea level measurements, Church (2011) estimates the rise in global average sea level to be 1.7±0.2 mm/year from 1900 to 2009 and 1.9±0.4 mm/year from 1961 to 2009. A plot of global mean sea level rise from 1880 to 2010 is presented in Figure 4-159.

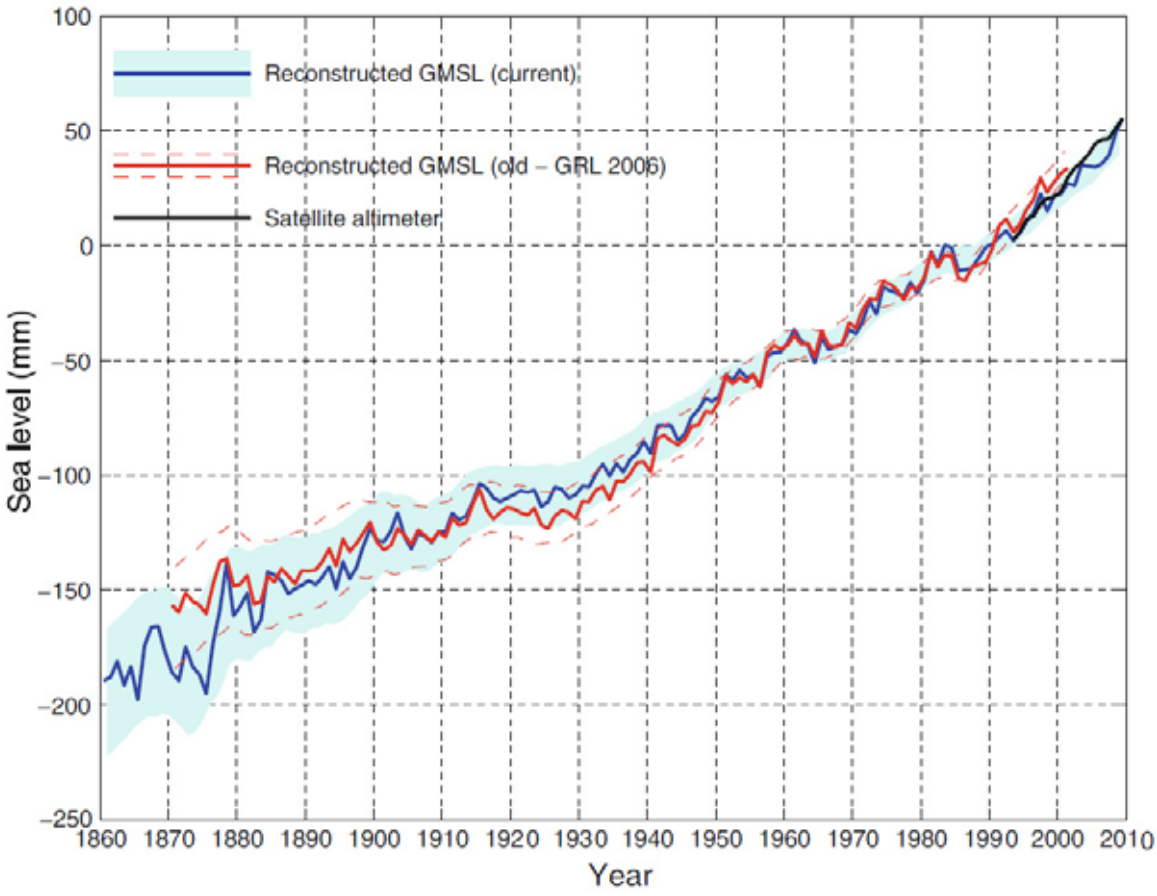

Source: Church 2011

Figure 4-159 Historical Global Mean Sea Level Rise

Global sea level is expected to rise at a greater rate during the 21st century than it has in the past. Thermal expansion is projected to contribute to more than half of the average rise, but melting of land ice will also play an important role. Melting of sea ice is expected to play less of a role since it is already in the ocean; however it is still expected to contribute to the total sea level rise.

A time series displaying historical and projected sea level rise is presented in Figure 4-160. The range of sea level rise projections represents the range of model projections for the SRES A1B scenario for the 21st century. Under this scenario, global sea level rises at a rate of about 4 mm/year and reaches 0.22 to 0.44 m above the 1990 levels by the mid-2090s (Solomon et al. 2007).

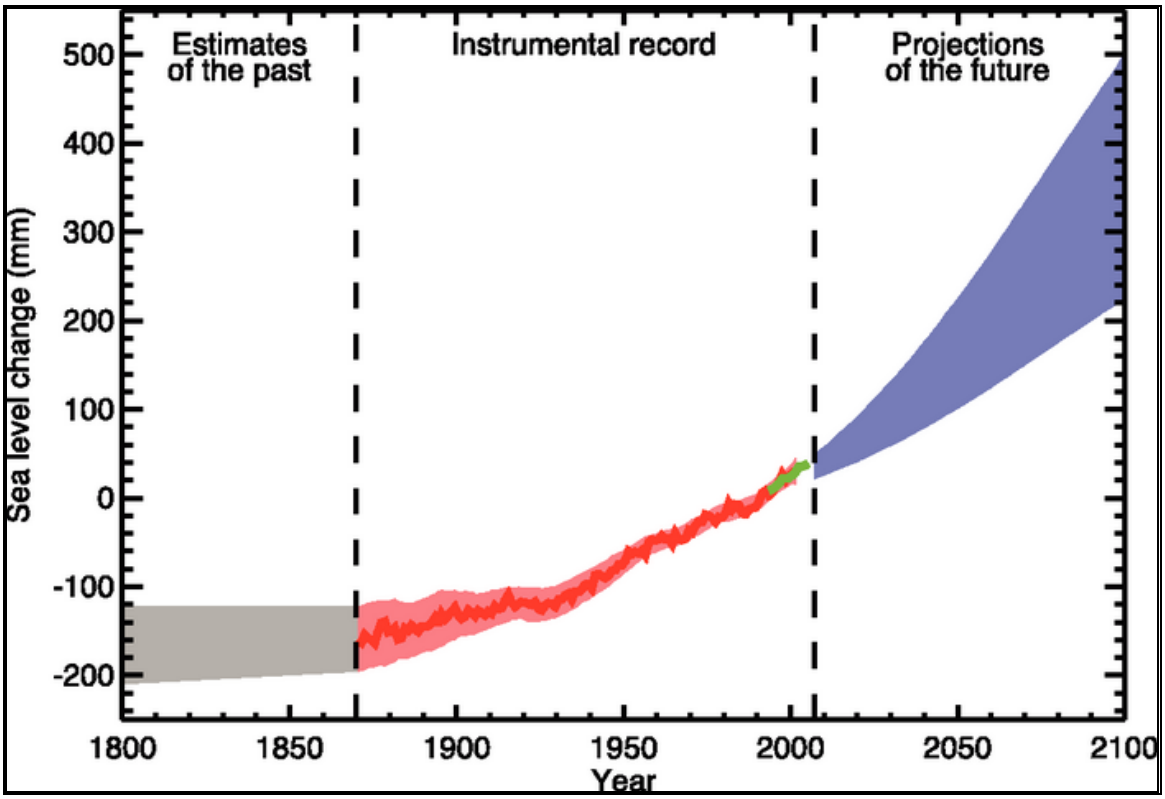

Source: Intergovernmental Panel on Climate Change (IPCC) 2007

Figure 4-160 Time Series of Historical and Projected Sea Level Rise

4.3.9.2 Waves

The mean significant wave height at Grid Point 11034 from the MSC50 data set shows an increasing trend (Figure 4-161) from 1954 to 2010, with significant wave heights increasing at a rate of 0.0042 m/year over the entire period.

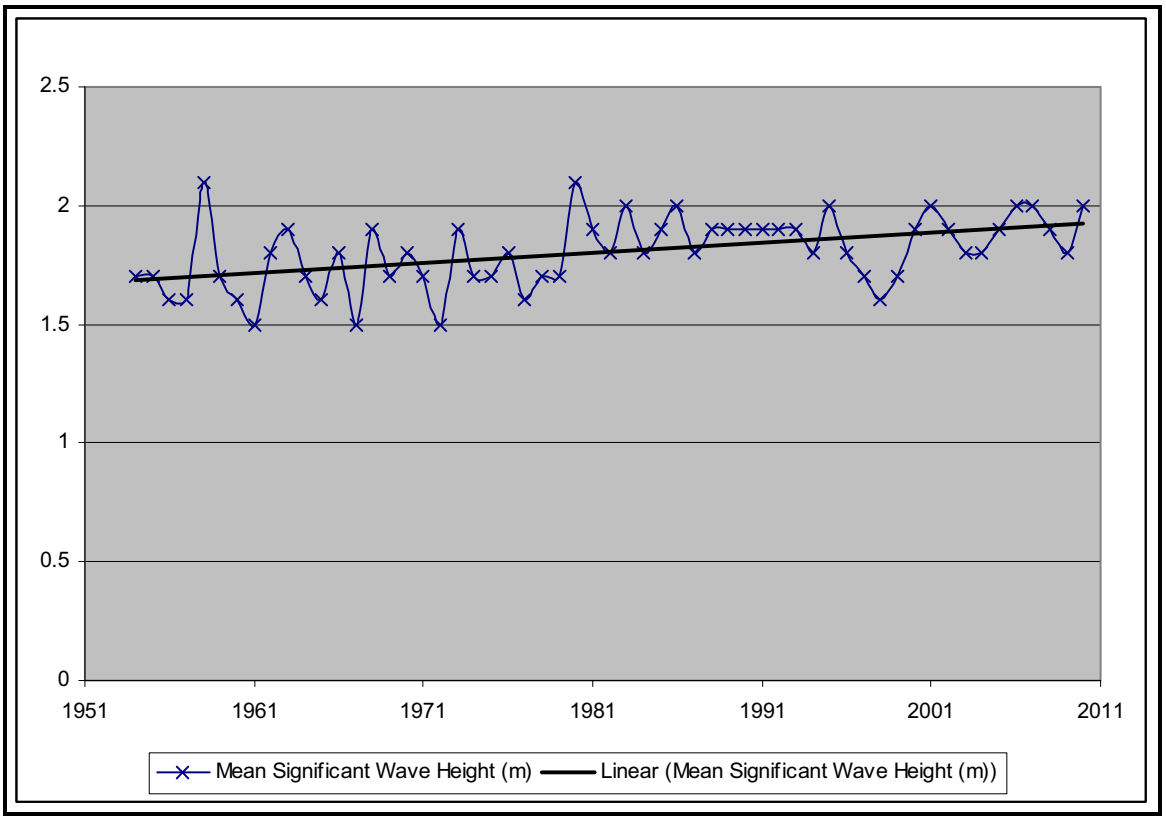

Figure 4-161 Annual Mean significant Wave Height (Grid Point 11034)

A scatterplot of seasonally averaged NAO Index against wave height (Figure 4-162) shows a positive correlation between the mean significant wave height and the winter NAO Index. An examination of the trendline shows that the r-squared between the NAO Index and wave height is low and as a result, there is little or no correlation between the two.

These results are typical of other studies done in the waters surrounding Newfoundland (Swail 1996; Swail et al. 1999). Swail et al. (1999) suggested that the increase seen in the MSC50 data set was the result of “creeping inhomogeneities” resulting from increased observational densities.

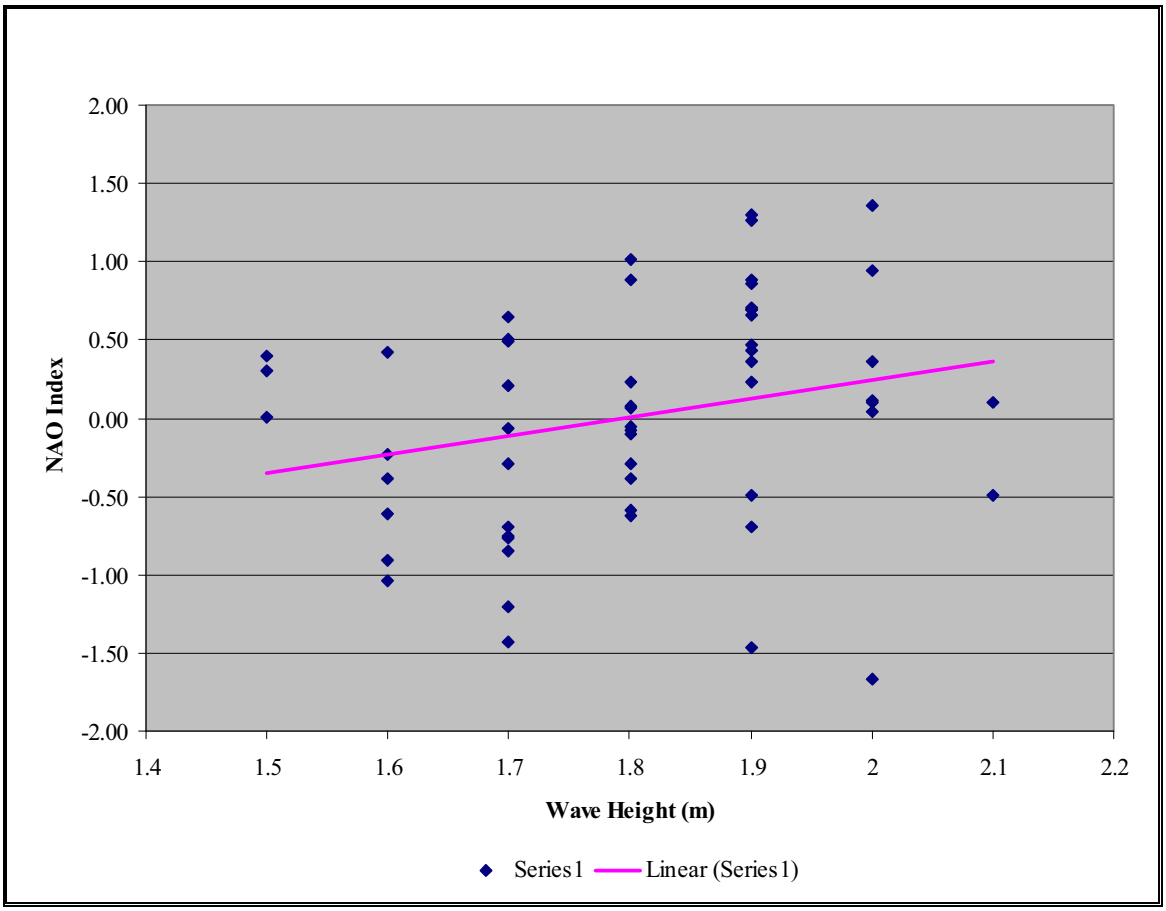

Figure 4-162 Scatterplot of Seasonally Averaged North Atlantic Oscillation Index against Wave Height at Grid Point 11034, Winter 1954 to 2010

Future climate trends are difficult to predict and the IPCC has developed a number of plausible future climate scenarios. The Canadian Global Climate Model Version 2 (CGCM2) running the IPCC SRES B2 forcing scenarios was examined for this report. The B2 scenario envisions a global population growth of 10.4 billion people by 2100. A rapidly-evolving economy and more emphasis on environmental protection would produce lower emissions and less future warming than other scenarios. This model produces output on a coarse grid and may not necessarily be representative of what would be seen on a site-specific scale.

Mean wind speeds for the 30-year period centred on 2020, 2050 and 2080 from the CGCM2 model are presented in Table 4-85. There is an increase in wind speeds predicted by this model, most of which occurs during the period centred on 2020. Since future significant wave height climate depends on future wind speeds, the frequency and intensity of storms would have a direct impact on significant wave heights on the Grand Banks.

Table 4-85 Mean Wind Speeds from the Canadian Global Climate Model

Month	Decade			
	1980s	2020s	2050s	2080s
January	8.38	9.3	8.6	9.15
February	8.37	8.7	8.69	8.67
March	6.78	8.31	8.11	8.03
April	6.57	7.04	6.85	6.41
May	5.7	5.76	5.33	5.34
June	4.83	4.53	4.51	4.68
July	4.21	4.06	4.22	4.19
August	4.66	4.54	4.54	4.42
September	4.39	4.76	4.82	4.43
October	6.13	6.3	6.53	6.33
November	6.7	7.44	7.29	7.64
December	7.99	8.75	8.51	8.56

4.3.9.3 Sea Surface Temperatures

The mean daily maximum and mean daily minimum sea surface temperatures from ICOADS were calculated for each winter and summer season from 1980 to 2010. The difference about the mean over the entire period is plotted against the NAO Index in Figures 4-163 and 4-164. These plots show that there is no discernible trend associating sea surface temperature with the NAO Index for the White Rose field.

An analysis of sea surface trends over the past 30 years indicates a gradual rise in sea surface temperatures. On average, the winter mean daily maximum sea surface temperature rose by 0.014°C (Figure 4-165) per year, while the winter mean daily minimum sea surface temperature rose by 0.0487°C per year. During the summer months, the mean daily maximum sea surface temperature rose by 0.0263°C, while the mean daily minimum sea surface temperature rose by 0.0782°C. Both the winter and summer values indicate that the spread between the mean daily maximum and mean daily minimum is narrowing.

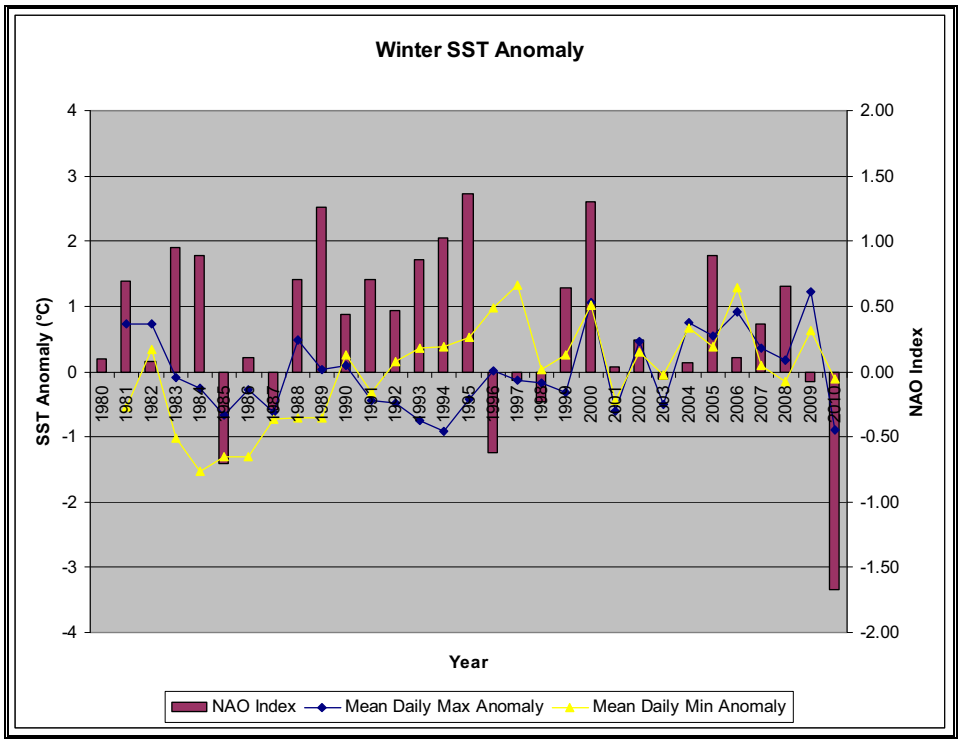

Figure 4-163 Winter North Atlantic Oscillation Index and Sea Surface Temperature, 1981 to 2010

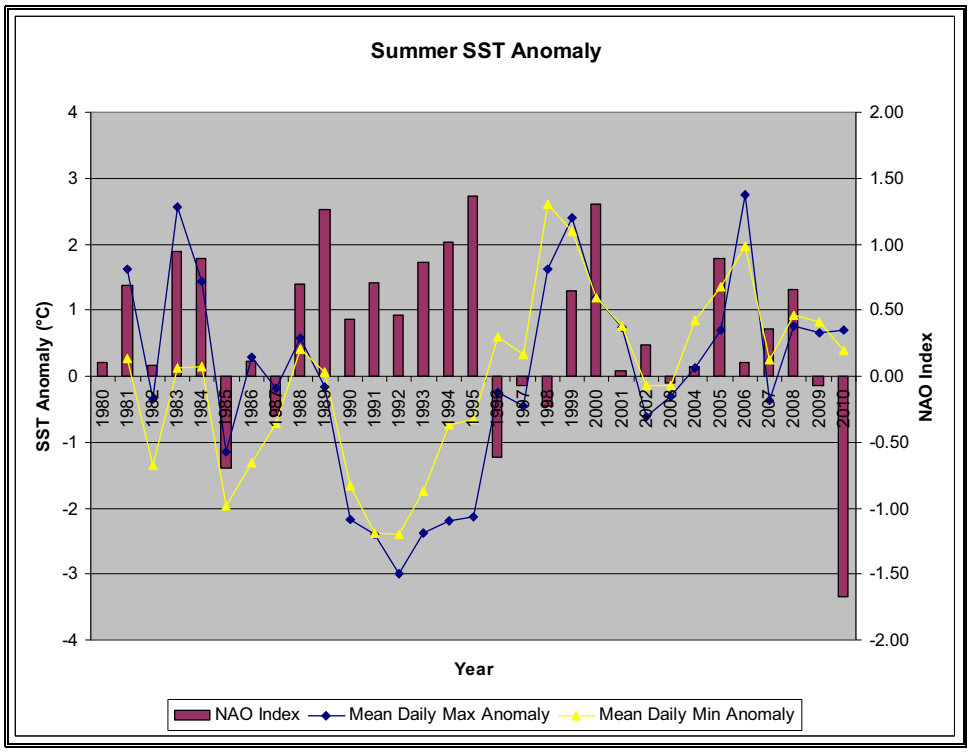

Figure 4-164 Summer North Atlantic Oscillation Index and Sea Surface Temperature, 1981 to 2010

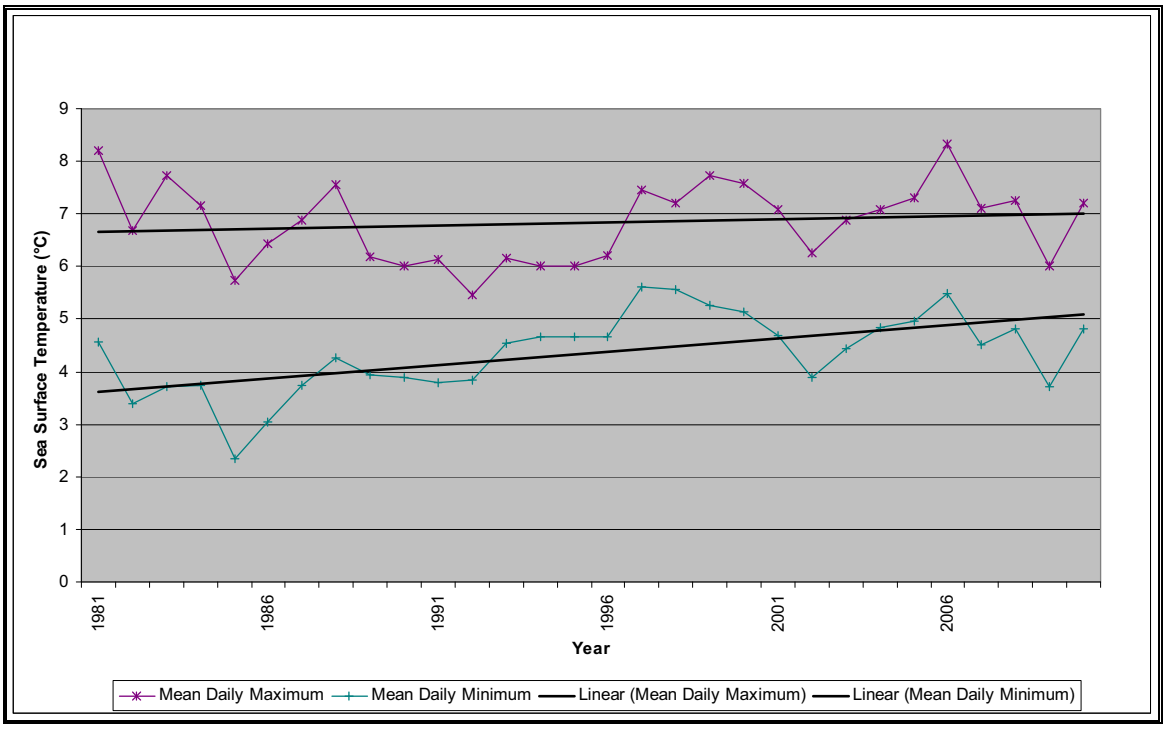

Figure 4-165 Annual Mean Daily Maximum and Minimum Sea Surface Temperatures, ICOADS 1981 to 2010

The annual mean daily maximum sea surface temperature over the 30-year period has risen at a rate of 0.0123°C, while the annual mean daily minimum sea surface temperature has risen at a rate of 0.05°C.

4.3.9.4 Icebergs

Since the early 2000s, the number of observed icebergs has increased in the North Atlantic Ocean (Rudkin et al. 2005). This may be a result of increased sea and air temperatures, but may also be a product of improved technologies for observing glacial sources. Should sea and air temperatures increase north of the Grand Banks, the number of icebergs entering a production area would likely increase, initially due to increased calving of glaciers and ice islands. The size and presence of the icebergs would eventually decrease due to melt as the icebergs drifted into warmer waters. Similarly, the number of icebergs could decrease as the lack of pack ice that helps carry and sustain the icebergs on the Grand Banks would decrease, providing no insulation for the icebergs in warmer waters.

Whether this effect would be cyclical or permanent, or if it will transpire at all, is unknown. There is currently no reliable way of predicting the future occurrence and movement of sea ice and icebergs.